GEOMAR REPORTS

1 GEOMAR FORSCHUNGSZENTRUM FÜR MARINE GEOWISSENSCHFTEN DER CHRISTIAN-ALBRECHTS-UNIVERSITÄT ZU KIEL. BERICHT FÜR DIE JAHRE 1987 UND 1988. 1989. 71 + 6 pp. In German

2 GEOMAR FORSCHUNGSZENTRUM FÜR MARINE GEOWISSENSCHAFTEN DER CHRISTIAN-ALBRECHTS-UNIVERSITÄT ZU KIEL. JAHRESBERICHT/ANNUAL REPORT 1989. 1990. 96 pp. In German and English

3 GEOMAR FORSCHUNGSZENTRUM FÜR MARINE GEOWISSENSCHAFTEN DER CHRISTIAN-ALBRECHTS-UNIVERSITÄT ZU KIEL. JAHRESBERICHT/ANNUAL REPORT 1990. 1991. 212 pp. In German and English

4 ROBERT F. SPIELHAGEN
DIE EISDRIFT IN DER FRAMSTRASSE WÄHREND DER LETZTEN 200.000 JAHRE. 1991. 133 pp.
In German with English summary

5 THOMAS C. W. WOLF
PALÄO-OZEANOGRAPHISCH-KLIMATISCHE ENTWICKLUNG DES NÖRDLICHEN NORDATLANTIKS SEIT DEM SPÄTEN NEOGEN (ODP LEGS 105 UND 104, DSDP LEG 81). 1991. 92 pp. In German with English summary

6 SEISMIC STUDIES OF LATERALLY HETEROGENOUS STRUCTURES – INTERPRETATION AND MODELLING OF SEISMIC DATA. Ed. by ERNST R. FLUEH
Commission on Controlled Source Seismology (CCSS), Proceedings of the 8th Workshop Meeting, held at Kiel – Fellhorst (Germany), August 27-31, 1990. 1991. 359 pp. In English

7 JENS MATTHIESSEN
DINOFLAGELLATEN-ZYSTEN IM SPÄQUARTÄR DES EUROPÄISCHEN NORDMEERES: PALÖKOLOGIE UND PALÄO-OZEANOGRAPHIE. 1991. 104 pp. In German with English summary. Out of print

8 DIRK NÜRNGERG
HAUPT- UND SPURENELEMENTE IN FORAMINIFERENGEHÄUSEN – HINWEISE AUF KLIMATISCHE UND OZEANOGRAPHISCHE ÄNDERUNGEN IM NÖRDLICHEN NORDATLANTIK WÄHREND DES SPÄTQUARTÄRS. 1991. 117 pp. In German with English summary. Out of print

9 KLAS S. LACKSCHEWITZ
SEDIMENTATIONSPROZESSE AM AKTIVEN MITTELOZEANISCHEN KOLBEINSEY RÜCKEN (NÖRDLICH VON ISLAND). 1991. 133 pp. In German with English summary. Out of print

10 UWE PAGELS
SEDIMENTOLOGISCHE UNTERSUCHUNGEN UND BESTIMMUNG DER KARBONATLÖSUNG IN SPÄTQUARTÄREN SEDIMENTEN DES ÖSTLICHEN ARKTISCHEN OZEANS. 1991. 106 pp.
In German with English summary

11 FS POSEIDON. EXPEDITION 175 (9.10.-1.11.1990)
175/1:OSTGRÖNLÄNDISCHER KONTINENTALRAND (65°N)
175/2: SEDIMENTATION AM KOLBEINSEYRÜCKEN (NÖRDLICH VON ISLAND).
Hrsg. von J. MIENERT und H.-J. WALLRABE-ADAMS. 1992. 56 pp. + app. In German with some English chapters

12 GEOMAR FORSCHUNGSZENTRUM FÜR MARINE GEOWISSENSCHAFTEN DER CHRISTIAN-ALBRECHTS-UNIVERSITÄT ZU KIEL. JAHRESBERICHT/ANNUAL REPORT 1991. 1992. 152 pp. In German and English.
Out of print

13 SABINE E. I. KÖHLER
SPÄTQUARTÄRE PALÄO-OZEANOGRAPHISCHE ENTWICKLUNG DES NORDPOLARMEERES UND EUROPÄISCHEN NORDMEERES ANHAND VON SAUERSTOFF- UND KOHLENSTOFF-ISOTOPENVERHÄLTNISSEN DER PLANKTISCHEN FORAMINIFERE *Neogloboquadrina pachyderma* (sin.).
1992. 104 pp. In German with English summary

14 FS SONNE. FAHRTBERICHT SO78 PERUVENT: BALBOA, PANAMA - BALBOA, PANAMA, 28.2.1992-16.4.1992
Hrsg. von ERWIN SUESS. 1992. 120 pp. In German with some English chapters. Out of print

15 FOURTH INTERNATIONAL CONFERENCE ON PALEOCEANOGRAPHY (ICP IV): SHORT- AND LONG-TERM GLOBAL CHANGE: RECORDS AND MODELLING. 21-25 SEPTEMBER 1992, KIEL/GERMANY.
PROGRAM & ABSTRACTS. 1992. 351 pp. In English

16 MICHAELA KUBISCH
DIE EISDRIFT IM ARKTISCHEN OZEAN WÄHREND DER LETZTEN 250.000 JAHRE. 1992. 100 pp.
In German with English summary

17 PERSISCHER GOLF: UMWELTGEFÄHRDUNG, SCHADENSERKENNUNG, SCHADENSBEWERTUNG AM BEISPIEL DES MEERRESBODENS; ERKENNEN EINER ÖKOSYSTEMVERÄNDERUNG NACH ÖLEINTRÄGEN.
Schlußbericht zu den beiden BMFT-Forschungsvorhaben 03F0055 A + B. 1993. 108 pp. In German with English summary

18 TEKTONISCHE ENTWÄSSERUNG AN KONVERGENTEN PLATTENRÄNDERN / DEWATERING AT CONTINENTAL MARGINS. Hrsg. von/ed. by ERWIN SUESS. 1993. 196 + 32 + 68 + 16 + 22 + 38 + 4 + 19 pp.
Some chapters in English, some in German

19 THOMAS DICKMANN
DAS KONZEPT DER POLARISATIONSMETHODE UND SEINE ANWENDUNGEN AUF DAS SEIMISCHE VEKTORWELLENFELD IM WEITWINKELBEREICH. 1993. 121 pp. In German with English summary

20 GEOMAR FORSCHUNGSZENTRUM FÜR MARINE GEOWISSENSCHAFTEN DER CHRISTIAN-ALBRECHTS-UNIVERSITÄT ZU KIEL. JAHRESBERICHT/ANNUAL REPORT 1992. 1993. 139 pp. In German and English

21 KAI UWE SCHMIDT
PALYNOMORPHE IM NEOGENEN NORDATLANTIK - HINWEISE ZUR PALÄO-OZEANOGRAPHIE UND PALÄOKLIMATOLOGIE. 1993. 104 + 7 + 41 pp. In German with English summary

22 UWE JÜRGEN GRÜTZMACHER
DIE VERÄNDERUNGEN DER PALÄOGEOGRAPHISCHEN VERBREITUNG VON *Bolboforma* - EIN BEITRAG ZUR REKONSTRUKTION UND DEFINITION VON WASSERMASSEN IM TERTÄR. 1993. 104 pp.
In German with English summary

23 RV PROFESSOR LOGACHEV. Research Cruise 09 (August 30 - September 17, 1993): SEDIMENT DISTRIBUTION ON THE REYKJANES RIDGE NEAR 59°N. Ed. by H.-J. WALLRABE-ADAMS & K.S. LACKSCHEWITZ. 1993. 66 + 30 pp.
In English

24 ANDREAS DETTMER
DIATOMEEN-TAPHOZÖNOSEN ALS ANZEIGER PALÄO-OZEANOGRAPHISCHER ENTWICKLUNGEN IM PLIOZÄNEN UND QUARTÄREN NORDATLANTIK. 1993. 113 + 10 + 25 pp. In German with English summary

25 GEOMAR FORSCHUNGSZENTRUM FÜR MARINE GEOWISSENSCHAFTEN DER CHRISTIAN-ALBRECHTS-UNIVERSITÄT ZU KIEL. JAHRESBERICHT/ANNUAL REPORT 1993. 1994. 69 pp. In German and English

26 JÖRG BIALAS
SEISMISCHE MESSUNGEN UND WEITERE GEOPHYSIKALISCHE UNTERSUCHUNGEN AM SÜD-SHETLAND TRENCH UND IN DER BRANSFIELD STRASSE - ANTARKTISCHE HALBINSEL. 1994. 113 pp.
In German with English summary

27 JANET MARGARET SUMNER
THE TRANSPORT AND DEPOSITIONAL MECHANISM OF HIGH GRADE MIXED-MAGMA IGNIMBRITE TL, GRAN CANARIA: THE MORPHOLOGY OF A LAVA-LIKE FLOW. 1994. 224 pp. In English with German summary. Out of print

28 GEOMAR LITHOTHEK. Ed. by JÜRGEN MIENERT. 1994. 12 pp + app. In English. Out of print

29 FS SONNE. FAHRTBERICHT SO 97 KODIAK-VENT: KODIAK - DUTCH HARBOR - TOKYO - SINGAPUR, 27.7.-19.9.1994. Hrsg. von ERWIN SUESS. 1994. Some chapters in English, some in German. Out of print

30 CRUISE REPORTS:
RV LIVONIA CRUISE 92, KIEL-KIEL, 21.8.-17.9.1992: GLORIA STUDIES OF THE EAST GREENLAND CONTINENTAL MARGIN BETWEEN 70°AND 80°N
RV POSEIDON PO200/10, LISBON-BREST-BREMERHAVEN, 7.-23.8.1993: EUROPEAN NORTH ATLANTIC MARGIN: SEDIMENT PATHWAYS, PROCESSES AND FLUXES
RV AKADEMIK ALEKSANDR KARPINSKIY, KIEL-TROMSÖ, 5.-25.7.1994: GAS HYDRATES ON THE NORTHERN EUROPEAN CONTINENTAL MARGIN
Edited by JÜRGEN MIENERT. 1994. 186 pp.
In English; report of RV AKADEMIK ALEKSANDR KARPINSKIY cruise in English and Russian

31 MARTIN WEINELT
BECKENENTWICKLUNG DES NÖRDLICHEN WIKING-GRABENS IM KÄNOZOIKUM - VERSENKUNGSGESCHICHTE, SEQUENZSTRATIGRAPHIE, SEDIMENTZUSAMMENSETZUNG. 1994. 85 pp.
In German with English summary

32 GEORG A. HEISS
CORAL REEFS IN THE RED SEA: GROWTH, PRODUCTION AND STABLE ISOTOPES. 1994. 141 pp.
In English with German summary

33 JENS A. HÖLEMANN
AKKUMULATION VON AUTOCHTHONEM UND ALLOCHTHONEM ORGANISCHEM MATERIAL IN DEN KÄNOZOISCHEN SEDIMENTEN DER NORWEGISCHEN SEE (ODP LEG 104). 1994. 78 pp.
In German with English summary

34 CHRISTIAN HASS
SEDIMENTOLOGISCHE UND MIKROPALÄONTOLOGISCHE UNTERSUCHUNGEN ZUR ENTWICKLUNG DES SKAGERRAKS (NE NORDSEE) IM SPÄTHOLOZÄN. 1994. 115 pp. In German with English summary

35 BRITTA JÜNGER
TIEFENWASSERERNEUERUNG IN DER GRÖNLANDSEE WÄHREND DER LETZTEN 340.000 JAHRE / DEEP WATER RENEWAL IN THE GREENLAND SEA DURING THE PAST 340,000 YEARS. 1994. 6 + 109 pp.
In German with English summary

36 JÖRG KUNERT
UNTERSUCHUJNGEN ZU MASSEN- UND FLUIDTRANSPORT ANHAND DER BEARBEITUNG REFLEXIONSSEISMISCHER DATEN AUS DER KODIAK-SUBDUKTIONSZONE, ALASKA. 1995. 129 pp.
In German with English summary

37 CHARLOTTE M. KRAWCZYK
DETACHMENT TECTONICS DURING CONTINENTAL RIFTING OFF THE WEST IBERIA MARGIN: SEISMIC REFLECTION AND DRILLING CONSTRAINTS.1995. 133 pp. In English with German summary

38 CHRISTINE CAROLINE NÜRNBERG
BARIUMFLUSS UND SEDIMENTATION IM SÜDLICHEN SÜDATLANTIK - HINWEISE AUF PRODUKTIVITÄTSÄNDERUNGEN IM QUARTÄR. 1995. 6 + 108 pp. In German with English summary

39 JÜRGEN FRÜHN
TEKTONIK UND ENTWÄSSERUNG DES AKTIVEN KONTINENTALRANDES SÜDÖSTLICH DER KENAI-HALBINSEL, ALASKA. 1995. 93 pp. In German with English summary

40 GEOMAR FORSCHUNGSZENTRUM FÜR MARINE GEOWISSENSCHAFTEN DER CHRISTIAN-ALBRECHTS-UNIVERSITÄT ZU KIEL. JAHRESBERICHT/ANNUAL REPORT 1994. 1995. 125 pp. In German and English.
Out of print

41 FS SONNE. FAHRTBERICHT / CRUISE REPORT SO 103 CONDOR 1 B: VALPARAISO-VALPARAISO, 2-21.7.1995. Hrsg. von ERNST R. FLUEH. 1995. 140 pp. Some chapters in German, some in English

42 RV PROFESSOR BOGOROV CRUISE 37: CRUISE REPORT "POSETIV": VLADIVOSTOK-VLADIVOSTOK, September 23 - October 22, 1994. Edited by CHRISTOPH GAEDICKE, BORIS BARANOV, and EVGENY LELIKOV. 1995. 49 + 33 pp. In English

43 CHRISTOPH GAEDICKE
DEFORMATION VON SEDIMENTEN IM NANKAI-AKKRETIONSKEIL, JAPAN. BILANZIERUNG TEKTONISCHER VORGÄNGE ANHAND VON SEISMISCHEN PROFILEN UND ERGEBNISSEN DER ODP-BOHRUNG 808. II + 89 pp. In German with English summary

44 MARTIN ANTONOW
SEDIMENTATIONSMUSTER UM DEN VESTERIS SEAMOUNT (ZENTRALE GRÖNLANDSEE) IN DEN LETZTEN 250.000 JAHREN. 1995. 121 pp. In German with English summary

45 INTERNATIONAL CONGRESS: CORING FOR GLOBAL CHANGE - ICGC '95. KIEL, 28 - 30 June, 1995. Edited by JÜRGEN MIENERT and GEROLD WEFER. 1996. 83 pp. In English

46 JENS GRÜTZNER
ZUR PHYSIKALISCHEN ENTWICKLUNG VON DIAGENETISCHEN HORIZONTEN IN DEN SEDIMENTBECKEN DES ATLANTIKS. 1995. 96 pp. In German with English summary

47 INGO A. PECHER
SEISMIC STUDIES OF BOTTOM SIMULATING REFLECTORS AT THE CONVERGENT MARGINS OFFSHORE PERU AND COSTA RICA. 1996. 159 pp. In English with German summary

48 XIN SU
DEVELOPMENT OF LATE TERTIARY AND QUATERNARY COCCOLITH ASSEMBLAGES IN THE NORTHEAST ATLANTIC. 1996. 120 pp. +7 pl. In English with German summary

49 FS SONNE - FAHRTBERICHT/CRUISE REPORT SO108 ORWELL: SAN FRANCISCO - ASTORIA, 14.4. - 23.5.1996 Edited by ERNST R. FLUEH and MICHAEL A. FISHER. 1996. 252 pp. + app. In English with German summary

50 GEOMAR FORSCHUNGSZENTRUM FÜR MARINE GEOWISSENSCHAFTEN DER CHRISTIAN-ALBRECHTS-UNIVERSITÄT ZU KIEL. JAHRESBERICHT/ANNUAL REPORT 1995. 1996. 93 pp. In German and English

51 THOMAS FUNCK
STRUCTURE OF THE VOLCANIC APRON NORTH OF GRAN CANARIA DEDUCED FOM REFLECTION SEISMIC, BATHYMETRIC AND BOREHOLE DATA. 1996.VI, 144 pp. In English with German summary

52 PETER BRUNS
GEOCHEMISCHE UND SEDIMENTOLOGISCHE UNTERSUCHUNGEN ÜBER DAS SEDIMENTATIONSVERHALTEN IM BEREICH BIOSTRATIGRAPHISCHER DISKONTINUITÄTEN IM NEOGEN DES NORDATLANTIK, ODP LEG 104, SITES 642B UND 643A. 1996. V, 73 pp. In German with Engllish summary

53 CHRISTIANE C. WAGNER
COLD SEEPS AN KONVERGENTEN PLATTENRÄNDERN VOR OREGON UND PERU: BIOGEOCHEMISCHE BESTANDSAUFNAHME. 1996. 108, XXXVI pp. In German with English summary

54 FRAUKE KLINGELHÖFER
MODEL CALCULATIONS ON THE SPREADING OF SUBMARINE LAVA FLOWS. 1996. 98 pp. In English with German summary

55 HANS-JÜRGEN HOFFMANN
OBJEKTORIENTIERTE ANALYSE UND MIGRATION DIFFRAKTIERTER WELLENFELDER UNTER VERWENDUNG DER STRAHLENMETHODE UND DER EDGE-WAVE-THEORIE. 1996. XXI, 153 pp. In German with English summary

56 DIRK KLÄSCHEN
STRAHLENSEISMISCHE MODELLIERUNG UNTER BERÜCKSICHTGUNG VON MEHRFACHDIFFRAKTIONEN MIT HILFE DER EDGE-WAVES: THEORIE UND ANWENDUNGSBEISPIELE 1996. X, 159 pp. In German with English summary

57 NICOLE BIEBOW
DINOFLAGELLATENZYSTEN ALS INIKATOREN DER SPÄT- UND POSTGLAZIALEN ENTWICKLUNG DES AUFTRIEBSGESCHEHENS VOR PERU. 1996. IV, 100, 17, 14 (7 pl.) pp. In German with English summary

58 RV SONNE. CRUISE REPORT SO109: HYDROTRACE ASTORIA-VICTORIA-ASTORIA-VICTORIA. MAY 23 - JULY 8, 1996. Ed. by PETER HERZIG, ERWIN SUESS, and PETER LINKE. 1997. 249 pp. In English

59 RV SONNE. CRUISE REPORT SO110: SO - RO (SONNE - ROPOS). VICTORIA-KODIAK-VICTORIA. JULY 9 - AUGUST 19, 1996. Ed. by ERWIN SUESS and GERHARD BOHRMANN. 1997. 181 pp. In English

60 RV AKADEMIK M. A. LAVRENTYEV CRUISE 27. CRUISE REPORT: GREGORY. VLADIVOSTOK-PUSAN-OKHOTSK SEA-PUSAN-VLADIVOSTOK. SEPTEMBER 7 - OCTOBER 12, 1996. Ed. by DIRK NÜRNBERG, BORIS BARANOV, and BORIS KARP.1997. 143 pp. In English

61 GEOMAR FORSCHUNGSZENTRUM FÜR MARINE GEOWISSENSCHAFTEN DER CHRISTIAN-ALBRECHTS-UNIVERSITÄT ZU KIEL. JAHRESBERICHT / ANNUAL REPORT 1996. 1997. 169 pp. In German and English

62 FS SONNE. FAHRTBERICHT/CRUISE REPORT SO123: MAMUT (MAKRAN MURRAY TRAVERSE - GEOPHYSIK PLATTENTEKTONISCHER EXTREMFÄLLE). Maskat - Maskat, 07.09 - 03.10.1997. Ed. by ERNST R. FLUEH, NINA KUKOWSKI, and CHRISTIAN REICHERT. 1997. 292 pp. In English with German summary

63 RAINER ZAHN
NORTH ATLANTIC THERMOHALINE CIRCULATION DURING THE LAST GLACIAL PERIOD: EVIDENCE FOR COUPLING BETWEEN MELTWATER EVENTS AND CONVECTIVE INSTABILITY. 1997. 133 pp. In English

64 FS SONNE. FAHRTBERICHT/CRUISE REPORT SO112 HIRESBAT (HIGH RESOLUTION BATHYMETRY). Victoria, B.C., Canada - Apra Harbor, Guam. 17.09 - 08.10.1996. Hrsg. von WILHELM WEINREBE. 1997. 90 pp. Some chapters in German, some in English

65 NIELS NØRGAARD-PEDERSEN
LATE QUATERNARY ARCTIC OCEAN SEDIMENT RECORDS: SURFACE OCEAN CONDITIONS AND PROVENANCE OF ICE-RAFTED DEBRIS. 1997. 115 pp. In English with German summary

66 THOMAS NÄHR
AUTHIGENER KLINOPTILOLITH IN MARINEN SEDIMENTEN - MINERALCHEMIE, GENESE UND MÖGLICHE ANWENDUNG ALS GEOTHERMOMETER. 1997. 119, 43 pp. In German with English summary

67 MATTIAS KREUTZ
STOFFTRANSPORT DURCH DIE BODENGRENZSCHICHT: REGIONALISIERUNG UND BILANZIERUNG FÜR DEN NORDATLANTIK UND DAS EUROPÄISCHE NORDMEER. 1998. IV, 166 pp. In German with English summary

68 AMIT GULATI
BENTHIC PRIMARY PRODUCTION IN TWO DIFFERENT SEDIMENT TYPES OF THE KIEL FJORD (WESTERN BALTIC SEA). 1998. 139 pp. In English with German summary

69 RÜDIGER SCHACHT
DIE SPÄT- UND POSTGLAZIALE ENTWICKLUNG DER WOOD- UND LIEFDEFJORDREGION NORDSPITZBERGENS. 1999. 123 pp. + app. In German with English summary

70 GEOMAR FORSCHUNGSZENTRUM FÜR MARINE GEOWISSENSCHAFTEN DER CHRISTIAN-ALBRECHTS-UNIVERSITÄT ZU KIEL. JAHRESBERICHT/ANNUAL REPORT 1997. 1998. 155 pp. In German and English

71 FS SONNE. FAHRTBERICHT/CRUISE REPORT SO118 BIGSET (BIOGEOCHEMICAL TRANSPORT OF MATTER AND ENERGY IN THE DEEP SEA). MUSCAT (OMAN) - MUSCAT (OMAN). 31.03.-11.05.1997. Ed. by OLAF PFANNKUCHE and CHRISTINE UTECHT. 1998. 188 pp. In English

72 FS SONNE. FAHRTBERICHT/CRUISE REPORT SO131 SINUS (SEISMIC INVESTIGATIONS AT THE NINETY EAST RIDGE OBSERVATORY USING SONNE AND JOIDES RESOLUTION DURING ODP LEG 179). KARACHI - SINGAPORE. 04.05-16.06.1998. Ed. by ERNST R. FLUEH and CHRISTIAN REICHERT. 1998. 337 pp. In English

73 THOMAS RICHTER
SEDIMENTARY FLUXES AT THE MID-ATLANTIC RIDGE: SEDIMENT SOURCES, ACCUMULATION RATES, AND GEOCHEMICAL CHARACTERISATION. 1998. IV, 173 + 29 pp. In English with German summary

74 BARBARA MARIA SPRINGER
MODIFIKATION DES BODENNAHEN STRÖMUNGSREGIMES UND DIE DEPOSITION VON SUSPENDIERTEM MATERIAL DURCH MAKROFAUNA. 1999. 112 pp. In German

75 SABINE JÄHMLICH
UNTERSUCHUNGEN ZUR PARTIKELDYNAMIK IN DER BODENGRENZSCHICHT DER MECKLENBURGER BUCHT. 1999. 139 pp. In German

76 WOLFRAM W. BRENNER
GRUNDLAGEN UND ANWENDUNGSMÖGLICHKEITEN DER MIKRO-ABSORPTIONSPHOTOMETRIE FÜR ORGANISCH-WANDIGE MIKROFOSSILIEN. 1999. 141 pp. In German with English summary

77 SUSAN KINSEY
TERTIARY BENTHIC FORAMINIFERAL BIOSTRATIGRAPHY AND PALAEOECOLOGY OF THE HALTEN TERRACE, NORWAY. 1999. VI, 145 pp. In English with German summary

78 HEIDI DOOSE
REKONSTRUKTION HYDROGRAPHISCHER VERHÄLTNISSE IM CALIFORNIENSTROM UND IM EUROPÄISCHEN MITTELMEER ZUR BILDUNGSZEIT ORGANISCH KOHLENSTOFFREICHER SEDIMENTE. 1999. IV, 111 pp. + app. In German with English summary

79 CLAUDIA WILLAMOWSKI
VERTEILUNGSMUSTER VON SPURENMETALLEN IM GLAZIALEN NORDATLANTIK: REKONSTRUKTION DER NÄHRSTOFFBILANZ ANHAND VON CADMIUMKONZENTRATIONEN IN KALKSCHALIGEN FORAMINIFEREN. 1999. 86, XXI pp. In German with English summary

80 FS SONNE. FAHRTBERICHT/CRUISE REPORT SO129. BIGSET (BIOGEOCHEMICAL TRANSPORT OF MATTER AND ENERGY IN THE DEEP SEA). PORT SULTAN QUABOOS - DUBAI. JANUARY 30 - MARCH 9, 1998. Ed. by OLAF PFANNKUCHE and CHRISTINE UTECHT. 1999. 107 pp. In English

81 FS SONNE. FAHRTBERICHT/CRUISE REPORT SO138. GINCO-2 (GEOSCIENTIFIC INVESTIGATIONS ON THE ACTIVE CONVERGENCE ZONE BETWEEN THE EAST EURASIAN AND AUSTRALIAN PLATES ALONG INDONESIA). JAKARTA - JAKARTA. 29.12.1998 - 28.01.1999. Ed. by ERNST R. FLUEH, BERND SCHRECKENBERGER, and JÖRG BIALAS. 1999. 333 pp. In English

82 CRUISE REPORTS: KOMEX I and II (KURILE OKHOTSK SEA MARINE EXPERIMENT)
RV PROFESSOR GAGARINSKY CRUISE 22
RV AKADEMIK M. A. LAVRENTYEV CRUISE 28
VLADIVOSTOK - PUSAN - OKHOTSK SEA - PUSAN - VLADIVOSTOK. 7 JULY - 12 SEPTEMBER 1998. Ed. by NICOLE BIEBOW and EDNA HÜTTEN. 1999. 188, 89 pp. In English

83 GREGOR REHDER
QUELLEN UND SENKEN MARINEN METHANS ZWISCHEN SCHELF UND OFFENEM OZEAN. REGIONALE VARIABILITÄT UND STEUERNDE PARAMETER DER METHANVERTEILUNG UND DER AUSTAUSCH MIT DER ATMOSPHÄRE. 1999. 161, 20 pp. In German with English summary

84 SVEN-OLIVER FRANZ
PLIOZÄNE ZEITREIHEN ZUR REKONSTRUKTION DER TIEFENWASSERZIRKULATION UND DER SILIZIKLASTISCHEN AMAZONASFRACHT IM ÄQUATORIALEN WESTATLANTIK (CEARA SCHWELLE, ODP LEG 154). 1999. 183 pp. In German with English summary

85 SYLKE HLAWATSCH
Mn-Fe-AKKUMULATE ALS INDIKATOR FÜR SCHAD- UND NÄHRSTOFFFLÜSSE IN DER WESTLICHEN OSTSEE. 1999. 132 pp. In German with English summary

86 BETTINA GEHRKE
ZUSAMMENSETZUNG UND VERTEILUNG DER LITHOGENEN FEINFRAKTION IN SPÄTQUARTÄREN SEDIMENTEN DES MITTELATLANTISCHEN REYKJANES RÜCKENS (59°N) - TONMINERALE ALS INDIKATOREN FÜR LIEFERGEBIETE, TRANSPORTMECHANISMEN UND ABLAGERUNGSPROZESSE. 1999. 102 pp.
In German with English summary

87 JENS GREINERT
REZENTE SUBMARINE MINERALBILDUNGEN: ABBILD GEOCHEMISCHER PROZESSE AN AKTIVEN FLUIDAUSTRITTSSTELLEN IM ALEUTEN- UND CASCADIA-AKKRETIONSKOMPLEX. 1999. 196, XX pp.
In German with English summary

88 CRUISE REPORTS: KOMEX V and VI (KURILE OKHOTSK SEA MARINE EXPERIMENT)
RV PROFESSOR GAGARINSKY CRUISE 26
MV MARSHAL GELOVANY CRUISE 1
VLADIVOSTOK - PUSAN - OKHOTSK SEA - PUSAN - VLADIVOSTOK. 30 JULY - 5 SEPTEMBER, 1999.
Ed. by NICOLE BIEBOW, THOMAS LÜDMANN, BORIS KARP, and RUSLAN KULINICH. 2000. 296 pp. In English

89 FS SONNE. FAHRTBERICHT/CRUISE REPORT SO136. TASQWA (QUATERNARY VARIABILITY OF WATER MASSES IN THE SOUTHERN TASMAN SEA AND THE SOUTHERN OCEAN, SW PACIFIC SECTOR). WELLINGTON - HOBART. OCTOBER 16 - NOVEMBER 12, 1998. Ed. by JÖRN THIEDE, STEFAN NEES et al. 1999. 78, 106 pp. In English

90 FS SONNE. FAHRTBERICHT/CRUISE REPORT SO142. HULA (INTERDISCIPLINARY INVESTIGATIONS ON THE TIMING OF THE HAWAII-EMPEROR BEND AND THE ORIGIN OF LITHOSPHERIC ANOMALIES ALONG THE MUSICIAN SEAMOUNT CHAIN. MIDWAY - HONOLULU. MAY 30 - JUNE 28, 1999. Ed. by ERNST R. FLUEH, JOHN O'CONNOR, JASON PHIPPS MORGAN, and JOCHEN WAGNER. 1999. 224 pp. In English

91 J. HAUSCHILD, T. GINDLER, D. RISTOW, A. BERHORST, C. BÖNNEMANN, K. HINZ
DFG-FORSCHUNGSPROJEKT *„KRUSTENSPLITTER“*. 3D-MAKRO-GESCHWINDIGKEITSBESTIMMUNGEN UND 3D-TIEFENMIGRATION DES SEISMISCHEN 3D-COSTA-RICA-DATENSATZES. 1999. 85 pp.
In German with English summary

92 FS AKADEMIK MSTISLAV KELDYSH. Fahrtbericht Reise Nr. 40: Norwegisch-Grönländische See, 27.6.-29.7.1998. Hrsg. von J. MIENERT, A. OMLIN, T. GÖLZ, D. LUKAS, J. POSEWANG. 1999. 65, 7 pp. In German

93 FS SONNE. FAHRTBERICHT/CRUISE REPORT SO143 TECFLUX. Ed. by GERHARD BOHRMANN, PETER LINKE, ERWIN SUESS, and OLAF PFANNKUCHE. 2000. 243 pp. In English

94 FS SONNE. FAHRTBERICHT/CRUISE REPORT SO144-1&2. PAGANINI (PANAMA BASIN AND GALAPAGOS "PLUME" - NEW INVESTIGATIONS OF INTRAPLATE MAGMATISM). SAN DIEGO - CALDERA. SEPTEMBER 7 - NOVEMBER 7, 1999. Ed. by JÖRG BIALAS, ERNST R. FLUEH, and GERHARD BOHRMANN. 1999. 437 pp. + app.
In English

95 CHRISTIAN MATTHIAS HÜLS
MILLENNIAL-SCALE SST VARIABILITY AS INFERRED FROM PLANKTONIC FORAMINIFERAL CENSUS COUNTS IN THE WESTERN SUBTROPICAL ATLANTIC. 2000. 81 pp. + app. In English with German summary

96 FS SONNE. FAHRTBERICHT/CRUISE REPORT SO146-1&2. GEOPECO (GEOPHYSICAL EXPERIMENTS AT THE PERUVIAN CONTINENTAL MARGIN - INVESTIGATIONS OF TECTONICS, MECHANICS, GASHYDRATES, AND FLUID TRANSPORT). ARICA - TALCAHUANO. MARCH 1 - MAY 4, 2000. Ed. by JÖRG BIALAS and NINA KUKOWSKI. 2000. 508 pp. In English

97 GEOMAR FORSCHUNGSZENTRUM FÜR MARINE GEOWISSENSCHAFTEN DER CHRISTIAN-ALBRECHTS-UNIVERSITÄT ZU KIEL. JAHRESBERICHT/ANNUAL REPORT 1998/1999. 2000. 261 pp. In German and English

98 RV SONNE. CRUISE REPORT SO148. TECFLUX-II-2000 (TECTONICALLY-INDUCED MATERIAL FLUXES. VICTORIA - VICTORIA - VICTORIA. 20.07.-15.08.2000. Ed. by PETER LINKE and ERWIN SUESS. 2001. 122 pp. In English

99 GEOMAR FORSCHUNGSZENTRUM FÜR MARINE GEOWISSENSCHAFTEN DER CHRISTIAN-ALBRECHTS-UNIVERSITÄT ZU KIEL. JAHRESBERICHT/ANNUAL REPORT 2000. 2001. 180 pp. In German and English

100 FS POSEIDON. FAHRTBERICHT/CRUISE REPORT POS 260 BIGSET (BIOGEOCHEMICAL TRANSPORT OF MATTER AND ENERGY IN THE DEEP SEA). LEIXOES/OPORTO (PORTUGAL) - GALWAY (IRELAND) - CORK (IRELAND). 26.04.-23.06.2000. Ed. by OLAF PFANNKUCHE and CHRISTINE UTECHT. 2001. 67 pp. In English

101 FS SONNE. FAHRTBERICHT/CRUISE REPORT SO159. SALIERI (SOUTH AMERICAN LITHOSPHERIC TRANSECTS ACROSS VOLCANIC RIDGES). GUAYAQUIL - GUAYAQUIL. AUGUST 21 - SEPTEMBER 17, 2001. Ed. by ERNST R. FLÜH, JÖRG BIALAS, and PHILIPPE CHARVIS. 2001. 256 pp. In English

102 FS SONNE. FAHRTBERICHT/CRUISE REPORT SO161-1&4. SPOC (SUBDUCTION PROCESSES OFF CHILE). ANTOFAGASTA - VALPARAISO. OCTOBER 9 - OCTOBER 15, 2001 &
VALPARAISO - VALPARAISO. NOVEMBER 30 - DECEMBER 23, 2001.
Ed. by ERNST R. FLÜH, HEIDRUN KOPP, and BERND SCHRECKENBERGER. 2002. 383 pp. In English

103 FS SONNE. FAHRTBERICHT/CRUISE REPORT SO162. INGGAS TEST (INTEGRATED GEOPHYSICAL CHARACTERISATION AND QUANTIFICATION OF GAS HYDRATES - INSTRUMENT TEST CRUISE). VALPARAISO - BALBOA. FEBRUARY 21 - MARCH 12, 2002.
Ed. by TIMOTHY JOHN RESTON and JÖRG BIALAS. 2002. In English

104 FS SONNE. FAHRTBERICHT/CRUISE REPORT SO158. MEGAPRINT (MULTIDISCIPLINARY EXAMINATION OF GALÁPAGOS PLUME RIDGE INTERACTION). ISLA DE PASCUA - GUAYAQUIL. JULY15 - AUGUST 20, 2001.
Ed. by REINHARD WERNER. 2002. 53 pp + app. In English

105 CRUISE REPORT: KOMEX (KURILE OKHOTSK SEA MARINE EXPERIMENT)
RV PROFESSOR GAGARINSKY CRUISE 32. SERENADE. SEISMO-STRATIGRAPHIC RESEARCH OFF NORTHERN SAKHALIN AND IN THE DERUGIN BASIN. VLADIVOSTOK - PUSAN - SEA OF OKHOTSK - PUSAN - VLADIVOSTOK. AUGUST 31 - SEPTEMBER 29, 2001.
Ed. by THOMAS LÜDMANN, BORIS BARANOV, and BORIS KARP. 2002. 42 pp. In English

106 FS SONNE. FAHRTBERICHT/CRUISE REPORT SO163. SUBDUCTION I. MULTI-SYSTEM ANALYSIS OF FLUID RECYCLING AND GEODYNAMICS AT THE CONTINENTAL MARGIN OFF COSTA RICA.
SO163-1. BALBOA- CALDERA. MARCH 13 - APRIL 20, 2002
SO163-2. CALDERA - BALBOA. APRIL 20 - MAY 21, 2002.
Ed. by WILLI WEINREBE and ERNST R. FLÜH. 2002. 534 pp. In English

107 GEOMAR FORSCHUNGSZENTRUM FÜR MARINE GEOWISSENSCHAFTEN DER CHRISTIAN-ALBRECHTS-UNIVERSITÄT ZU KIEL. JAHRESBERICHT/ANNUAL REPORT 2001. In prep. In German and English

108 RV METEOR. CRUISE REPORT M52/1: MARGASCH (MARINE GAS HYDRATES OF THE BLACK SEA). ISTANBUL - ISTANBUL. JANUARY 2 - FEBRUARY 1, 2002.
Ed. by GERHARD BOHRMANN and SILKE SCHENCK. 2002. 202 pp. In English

109 RV SONNE. CRUISE REPORT SO164. RASTA (Rapid Climate Changes in the Western Tropical Atlantic - Assessment of the biogenous and sedimentary record). BALBOA - BALBOA. MAY 22 - JUNE 2002. Ed. by DIRK NÜRNBERG, JOACHIM SCHÖNFELD, WOLF-CHRISTIAN DULLO, and MARCUS RÜHLEMANN. 2003. 151 pp. In English

110 CRUISE REPORT : KOMEX (KURILE OKHOTSK SEA MARINE EXPERIMENT)
RV AKADEMIK M.A. LAVRENTYEV CRUISE 29, LEG 1 and LEG 2. VLADIVOSTOK – PUSAN – OKHOTSK SEA – PUSAN – OKHOTSK SEA – PUSAN – VLADIVOSTOK. MAY 25 – AUGUST 05 2002. Ed. by NICOLE BIEBOW, RUSLAN KULINICH, and BORIS BARANOV. 2003. 190, 176 pp. In English

KOMEX II

KURILE OKHOTSK SEA MARINE EXPERIMENT

CRUISE REPORT

RV AKADEMIK M.A. LAVRENTYEV CRUISE 29 LEG 1 AND LEG 2

VLADIVOSTOK – PUSAN – OKHOTSK SEA – PUSAN – OKHOTSK SEA – PUSAN - VLADIVOSTOK

MAY 25 - AUGUST 05, 2002

110

GEOMAR REPORT

KOMEX II

KURILE OKHOTSK SEA MARINE EXPERIMENT

CRUISE REPORT

RV AKADEMIK M.A. LAVRENTYEV CRUISE 29
LEG 1 AND LEG 2

VLADIVOSTOK – PUSAN – OKHOTSK SEA – PUSAN – OKHOTSK SEA – PUSAN - VLADIVOSTOK

MAY 25 - AUGUST 05, 2002

Edited by
Nicole Biebow, Ruslan Kulinich and Boris Baranov
with contributions of cruise participants

The KOMEX marine expeditions were initialized on responsibility of
the P. P. Shirshov Institute of Oceanology, Moscow,
the Pacific Oceanological Institute (POI), Vladivostok,
and the GEOMAR Research Center for Marine Geosciences, Kiel

GEOMAR
Forschungszentrum
für marine Geowissenschaften
der Christian-Albrechts-Universität
zu Kiel

KIEL 2003

GEOMAR REPORT 110

GEOMAR
Research Center
for Marine Geosciences
Christian Albrechts University
in Kiel

Redaktion dieses Reports:
Nicole Biebow und Katharina Georgeleit

GEOMAR REPORT
ISSN 0936 - 5788

GEOMAR
Forschungszentrum
für marine Geowissenschaften
Wischhofstr. 1-3
D - 24148 Kiel
Tel. (0431) 600-2555, 600-2505

Editors of this issue:
Nicole Biebow and Katharina Georgeleit

GEOMAR REPORT
ISSN 0936 - 5788

GEOMAR
Research Center
for Marine Geosciences
Wischhofstr. 1-3
D - 24148 Kiel
Tel. (49) 431 / 600-2555, 600-2505

PART I:

RV AKADEMIK LAVRENTYEV CRUISE 29

LEG 1

VLADIVOSTOK - PUSAN - SEA OF OKHOTSK - PUSAN

MAY 25 - JUNE 27, 2002

Table of contents

INTRODUCTION

Ruslan Kulinich and Nicole Biebow

The 29th cruise of RV *Akademik Lavrentyev* was organized within the scope of the joint Russian - German KOMEX II project (2001 - 2004) which is a continuation of the first phase of joint research in the Okhotsk Sea (KOMEX I, 1998-2000). The expeditions carried out in KOMEX I made essential contributions to understand the geology, geochemistry, geophysics, paleoceanology and hydrology of this unique region, and their results have formed the basis for KOMEX II. As in KOMEX I, the main purpose of the KOMEX II project is to understand the mechanisms of the complex climate-controlling system 'Okhotsk Sea' and to study its influence on chemical distribution, chemical cycles, water mass formation, circulation and climate.
The main research topics of the joint project KOMEX II concentrate on the following problems:

- development of a plate tectonic model of the evolution of the Okhotsk Sea;
- characterization of the seismic facies and estimation of the influence of regional tectonics on sedimentation processes, distribution of the BSR and vent phenomena;
- record of material and temporal changes in magmatism and quantification of chemical and fluid cycles in the Kurile Kamchatka Subduction System;
- quantification of the trace element input into the atmosphere depending on seasonally changing hydrography and ice cover;
- quantification of gas and fluid expulsion rates and of the biogeochemical material and energy turnovers in vent areas;
- geochemical, mineralogical and isotopic characterization of the barite precipitates in the Derugin Basin to reconstruct the history, intensity and geochemical composition of the emanating fluids;
- quantification of the amount and type of gas hydrates, of their paleo-stability, temperature history and their influence on the recent as well as the paleo-environment;
- influence of Amur River on sea-ice formation, productivity and sedimentation processes during the last 50,000 years;
- paleoceanological significance of the Okhotsk Sea for water mass formation and climatic evolution in the Pacific Ocean.

On this basis and according to the results of previous expeditions, the research tasks and investigation areas for the LV29 cruise to the Okhotsk Sea were determined.
The first leg of the LV29 cruise focused on hydrochemical and geochemical investigations, video-controlled seafloor observations, sampling of vent sites and detailed mapping of the bottom relief by a swath bathymetry system. The main investigation areas comprise the shelf and slope of northeast Sakhalin and the "Barite Mounds" in the Derugin Basin.
In the second leg of the cruise, a coring program for paleoceanological purposes, plankton and water sampling, mapping of the seafloor with the sediment echosounder system SES-2000DS, dredging of volcanic rocks and reflexion seismics were the main targets. The investigation areas of the second leg covered the shelf and slope of Sakhalin and Kamchatka, the Sakhalin Gulf (Amur River mouth), the Derugin and Kurile Basins and La Perusa Strait.

The scientific objectives of cruise LV29 comprise and contribute to the following research topics of KOMEX:

1) One of the central scientific targets is to balance the geogenic and biogenic methane input into the atmosphere, as well as to find and to geochemically and geologically characterize the gas and fluid venting sites at the seafloor. The main component of these gas emanations off Sakhalin is methane which, alongside with CO_2, contributes to the so-called "greenhouse" effect causing global warming and as a consequence effecting the evolution of the planet`s climate. The following processes are responsible for the release of methane from the Okhotsk Sea into the atmosphere: degassing of methane from near-surface hydrocarbon deposits, degradation of gas hydrates in the sediments, and biologically derived methane. These processes are especially pronounced along the continental margin off Sakhalin and in the Derugin Basin, whereas along the Kurile Island Arc, tectonic and volcanic sources dominate.
Several expeditions within KOMEX I focused on these phenomena. A lot of earlier unknown gas emanation sources were discovered and sampled at the Sakhalin shelf and slope and in the Derugin Basin. The vent sites at the continental margin off NE Sakhalin are characterized by near-surface gas hydrate occurences, sulfide- and methane-rich pore waters, typical vent organisms, carbonate precipitates, methane bubbles forming flares and an enrichment of methane in the bottom waters. The investigations conducted within KOMEX I give the following scenario for methane venting off NE-Sakhalin: methane bubbles rise along faults from the sediment to the sediment surface. In the surface sediments, these bubbles are fixed as gas hydrates and - after microbiological oxidation- as carbonate precipitates. The remaining methane is converted at the sediment/water interface by vent organisms. Only a relatively small portion of the gas reaches the bottom water and the atmosphere.
During cruise LV29 these investigations were continued as follows: the stability of the gas venting sites, their venting intensity, and the hydrochemical characteristics of the surrounding waters were investigated, and a quantitative estimation of the gas bubbles` rising velocity was made. The hydrochemical work included the study of carbonate systems (pH, alkalinity, dissolved calcium), of dissolved oxygen and nutrients in the water columns above methane sources. The influence of methane venting on the carbonate system was the main target of these works. Apart from that, the geochemisty of pore waters was analyzed in order to study the formation processes of authigenic mineral precipitates.
The detection of new methane sources, the study of their spatial distribution and their connection with tectonics are other questions which were investigated in Leg 1 of RV *Akademik Lavrentyev* cruise LV29. For this purpose, mainly the 12 kHz hydroacoustic system ELAC was used. More than 100 flares were recorded, among which more than the half were earlier unknown. A generalization of all available data allowed us to suppose that the spatial extension of methane vents is controlled by a system of tectonic structures, mapped by geophysical methods during previous expeditions and verified on the present cruise by detailed mapping with the swath bathymetry system LOLA II.

2) A second main topic of previous expeditions within the framework of the KOMEX I project was the barite mineralization area in the Derugin Basin. This area is characterized by huge fields of barite precipitates, which cover the seafloor as massive rocks or chimneys. They even built a barite ridge with an elevation of ca. 50-100 m above the seafloor. These barites are associated with chemosynthetic organisms, which indicate a recent activity of fluid venting. Pore water analyzes show that extremly barium-rich fluids rise from the earth interior (>2 km sediment depth) to the sediment surface, react with the sulfate of sea water and form barite precipitates. Due to the high barium content of the very old bottom water of the Derugin Basin (ca. 1,600 years; Tiedemann, pers. com.) these precipitates are not dissolved.
Huge methane concentrations in the pore and bottom water of the barite mineralization area along with isotope studies on carbonate precipitates indicate that a large amount of methane is injected in the water column by the rising fluids. Sulfur and oxygen isotopes of the carbonate precipitates correspond to formation temperatures, which are certainly below 5°C (Greinert et

al., 2002), so that former theories of an hydrothermal origin could be revised within KOMEX I.
During the LV29 cruise, the investigations in the Derugin Basin concentrated on detailed mineralogical-petrographical investigations of carbonate and barite precipitates, determination of their distribution in the sediments and at the seafloor, and of their relationship with tectonic processes. Gas-geochemical and hydrochemical investigations were carried out at the "Barite Mounds" and in the surrounding areas, detailed mapping of the bottom relief by LOLA II, OFOS observations of the barite edifices and their environment and mapping of the barite mineralization area by the 12 kHz hydroacoustic system and OFOS accomplished these investigations. Additionally, the sediment and the precipitates were sampled by gravity corers and dredges.

3) The paleoceanological investigations carried out on previous expeditions to the Okhotsk Sea reveal the paleoceanographic potential of this NW-Pacific marginal basin. The carbonate-containing sediments allow to establish a continuous high-resolution oxygen isotope stratigraphy for the last approximately 350,000 years, which is outstanding in the Subarctic-Pacific area. The deposits facilitate insights into the closely coupled interplay between surface productivity, terrigenous supply and sea-ice coverage. This is of specific interest, since the interglacial high productivity in the N-Pacific and its marginal seas act as a sink of CO_2 that may counteract to the naturally induced atmospheric CO_2-increase during deglaciations and subsequent interglacials. The depositional environment of the Okhotsk Sea is dominated by terrigenous-siliciclastic material including high portions of ice-rafted material (IRD). The monotonous sequences are interrupted by short events of extremely high productivity, which characterize the end of glacial terminations and the subsequent interglacials. During glacials, surface productivity is reduced by a factor of 5 to 10. The productivity events exhibit a cyclicity of ca. 100 kyrs, and last typically for about 20 kyrs. Productivity maxima relate to changes in fluvial nutrient supply, sea-ice coverage and water mass stratification.
The cold deep-water masses of the Pacific Ocean originate from high-latitudinal marginal seas, among them the Okhotsk Sea. Insights into the scale of the influence on the global climate have not been reached yet. High-resolution studies of the sediments, especially in deep-water passages and in the influx area of the Kamchatka Current, were therefore one central question of Leg 2 of the LV29 cruise in order to paleoceanographically reconstruct the water masses. Another important objective is to study the influence of Amur River on sea-ice formation, circulation, productivity and sedimentation of the Okhotsk Sea. Amur River is the largest source for fresh water and sediment of the Okhotsk Sea and the 4th largest Siberian river. Apart from that, Amur River is the only of the large Siberian rivers which does not flow into the Arctic Ocean. Furthermore, the analysis of Amur sediments yield evidence about the development of the environment of the Siberian hinterland, for example by analyzing plant remains like spores and pollens which are transported by Amur waters into the Okhotsk Sea.

In order so solve the above-mentioned questions on cruise LV29, we took long gravity cores in the key areas of the Okhotsk Sea, e.g. the estuary of Amur River and along the straits into the Pacific Ocean. For the first time, we also deployed the sediment echosounder SES-2000DS from Rostock University with which we were able to survey and sample sediments which deposited without disturbance and continuously. This work was completed by multicorer, CTD and multinet deployments for plankton sampling. The plankton sampling on the LV29 cruise focused especially on the Kamchatka slope area, transects from the inner Kurile Basin towards the North Pacific and the Soya inflow area. The scientific goal of these investigations is to define the boundary conditions of the biological system between the

Okhotsk Sea and the North Pacific and the import of taxa via the Kamchatka Current (from the North Pacific) and the Soya Current (from the Japan Sea) into the Okhotsk Sea.

4) The main scientific objectives of the volcanological/petrological work within KOMEX I was to study interaction and dependencies between crustal and mantle sources, petrogenetic processes as well as the type and amount of volatiles in the eruptive products in different plate tectonic environments (e.g., rear arc/back-arc vs. volcanic front). Petrological work on previous cruises therefore aimed mainly to sample northern, central (Bussol Strait) and southern transects across the Kurile Island Arc as far as possible into the Kurile Basin. Extensive sampling of the Geophysicist seamount in the northeastern part of the Kurile Basin on the KOMEX I cruises and subsequent lab analyses of the dredged rocks also provided new informations on the structure and geodynamic evolution of the Kurile Basin (Baranov et al., 2002a; Werner et al., subm.).
The major goal of the volcanological, petrological, and geochemical studies of seamounts on the LV29 cruise was to make further contributions to a model for the geodynamic evolution of marginal basins by reconstruction of volcanic, magmatic and tectonic processes in the Kurile Basin. These objectives should be achieved by the reconstruction of the paleo-environment of the volcanoes at the time of their activity, age dating of the volcanoes, and characterization of tectonic setting of the volcanoes.
Accordingly, the planned dredge sites on RV *Akademik Lavrentyev* cruise did not primarily focus on submarine arc volcanoes but on volcanic structures in the Kurile Basin being probably not directly related to the Kurile Island Arc as, for example, the western foothills of Browton Ridge in the central Kurile Basin, Hydrographer Ridge west of Iturup Island, and Loskutov seamount in the southern Kurile Basin. These structures had been discovered on former Russian cruises but had not been mapped in detail, and the sampling of basement rocks failed since the volcanoes seem to be largely covered by marine sediment, ice-rafted debris (dropstones) and/or encrustations. Despite these difficulties we decided to focus on these volcanoes on cruise LV29 since we expected very interesting new results in case of successful sampling. To achieve the best possible results, approximately half of the time designated for petrological sampling was spent for detailed bathymetric and, at some places, additional seismic surveys. The hydroacoustic and seismic data gained on these surveys did not only enable us to select the most promising sites for dredge hauls, but also provided additional new informations on these volcanoes.
Apart from the Kurile Basin volcanoes, the dredging schedule included several structures in the Derugin Basin. The objectives of these dredging operations were sampling of basement rocks at the northern slope of the Derugin Basin (southern part of Kashevarov Bank) in order to get information on the basement structure of this area and sampling of tabular calcite and barite-calcite precipitates at the Barite Mounds in the northeastern part of the Derugin Basin.

5) The seismic survey on cruise LV29 in the central part of the Kurile Basin was carried out to study the nature of a specific basement rise, which separates two subbasins with a depth to the basement of up to 7 km. This basement rise in the central part of the basin was discovered during the Pacific expedition Souzmorgeo in 1976. The expedition showed that the rise has a complicated structure and consists of isometric basement highs. The depressions between them form fan-like, undulating systems that resemble river valleys. Over the top of the swell, the basement lies at a depth of about 5 km; in the depressions to the southwest and the northeast, it was found at depths of 8 and 7 km, respectively (Zhuravlev, 1982). The origin of the rise remained unknown. Much later they were supposed to represent shear/lateral fault

zones that defined an opening direction orthogonally to the general strike of the Kurile Basin (Gnibidenko et al., 1995).

For the second time, the rise was investigated during the SAKURA expedition in 1999 (Biebow et al., 2000). The data obtained showed that this rise (named Sakura Ridge) has a clear rift imprint. The morphology of its axial high suggests that it corresponds to a spreading axis. This axis (a spreading ridge) strikes N-S, i.e. in correspondence to the general strike of the Kurile Basin. Although this data is insufficient for a reliable identification of the spreading axis, it provides clear evidence for a SW-NE spreading direction, implying that the Kurile Basin opened along its general strike as a pull-apart basin (Baranov et al., 2002b). During the SAKURA expedition we mapped only one segment of it and the question how far the ridge continues to the north and south remained open. Obvious is only that it becomes wider to the north, and it was suggested that the ridge is apparently bounded near the northern slope of the Kurile Basin by a strike-slip or transform fault. On cruise LV29 the mapping of the ridge was therefore continued to the north.

1. CRUISE NARRATIVE

Nicole Biebow and Ruslan Kulinich

The research vessel *Akademik Lavrentyev* departed from Vladivostok on May 27th, 2002 with 17 Russian scientists and 35 crew members aboard. Modifications on the deck of the ship had been performed to accommodate a German self-contained mobile deep-sea winch system (MobiWinch) with a 20 mm conducting cable for work at sea. The MobiWinch was planned to be used for OFOS deployments, TV-grab sampling and coring. CTD castings and water sampling were planned to be carried out with the Russian hydrographical winch.
The vessel arrived in Pusan harbor on May 29th, 2002 in the morning. On the same day, 8 German, 2 Russian, 1 Italian and 1 Belgian scientist as well as their scientific equipment arrived and were transferred on board. At noon of May 30th RV *Akademik Lavrentyev* left Pusan harbor and made its way to the Sea of Okhotsk. The complete cruise track is shown in *Figure 1.1*; the working areas and stations are given in *Figure 1.2*.

Transit to the first area of investigations lasted about 4 days. This period was used for preparing and testing the equipment and laboratories for the upcoming work. At noon of June 1st we stopped for several hours in the Japan Sea to test the two winches. The Russian hydrographical winch had been equipped with a new cable and this had to be tested at 4,000 m water depth. The test of the cable was successful, but the test of the MobiWinch showed a malfunction of the spooling device, which seemed to be only a small problem at this time. During the stop, a Japanese reconnaissance plane several times overflew the vessel.

RV *Akademik Lavrentyev* reached the first area of investigations (Terpeniya Bay) in the afternoon of June 3rd, and the sampling program including CTD casts and hydrocorer deployment begun. We started with a CTD at a water depth of 80 m at one of the methane monitoring stations of the KOMEX I project. Again, we were able to detect very high methane concentrations, which were 200 times higher than the normal background values. The planned hydrocorer deployment had to be canceled due to a malfunction of the MobiWinch. Suddenly, we were not able to start the winch anymore, and both German technicians started to do whatever possible to repair the winch with the shipboard equipment. We finished this station with the calibration and a test of the swath bathymetry system called Lola II, which was successful. Then, RV *Akademik Lavrentyev* continued its way into the Derugin Basin.

We reached the Derugin Basin on June 5th at 4:00 p.m. local time and started our work in the area of the “Barite Mounds” known from the LV28 and GE99 cruises. Unfortunately, even with the help of specialists at home by e-mail and telephone we were up to then not able to repair the MobiWinch. Therefore, the period from June 7th to 11th was mainly devoted to CTD investigations along several profiles across the “Barite Mounds” area. For the first time, we were able to extensively map the methane plume and its extension in the barite area. Amazingly, our Russian colleagues were able to reproduce the concentration of methane in these plumes with the same values measured on cruises LV28 and GE99. This shows on the one hand that their method is very reliable and on the other hand that here methane venting is a continuous process over longer periods of time. The nights were used to map this area with the swath bathymetry system which worked very successful.
On June 10th, we thought for a short moment that we succeeded in repairing the MobiWinch, because we found and replaced a broken cable. But then, during trying to core sediments at 1,500 m water depth, it was found out that the winch had further defects which strongly hindered our work and because of which the deployment of cores and video equipment was impossible at water depths of more than 400 m. Nevertheless, the communication and

cooperation between the German and Russian teams and the vessels crew was excellent during this difficult time.

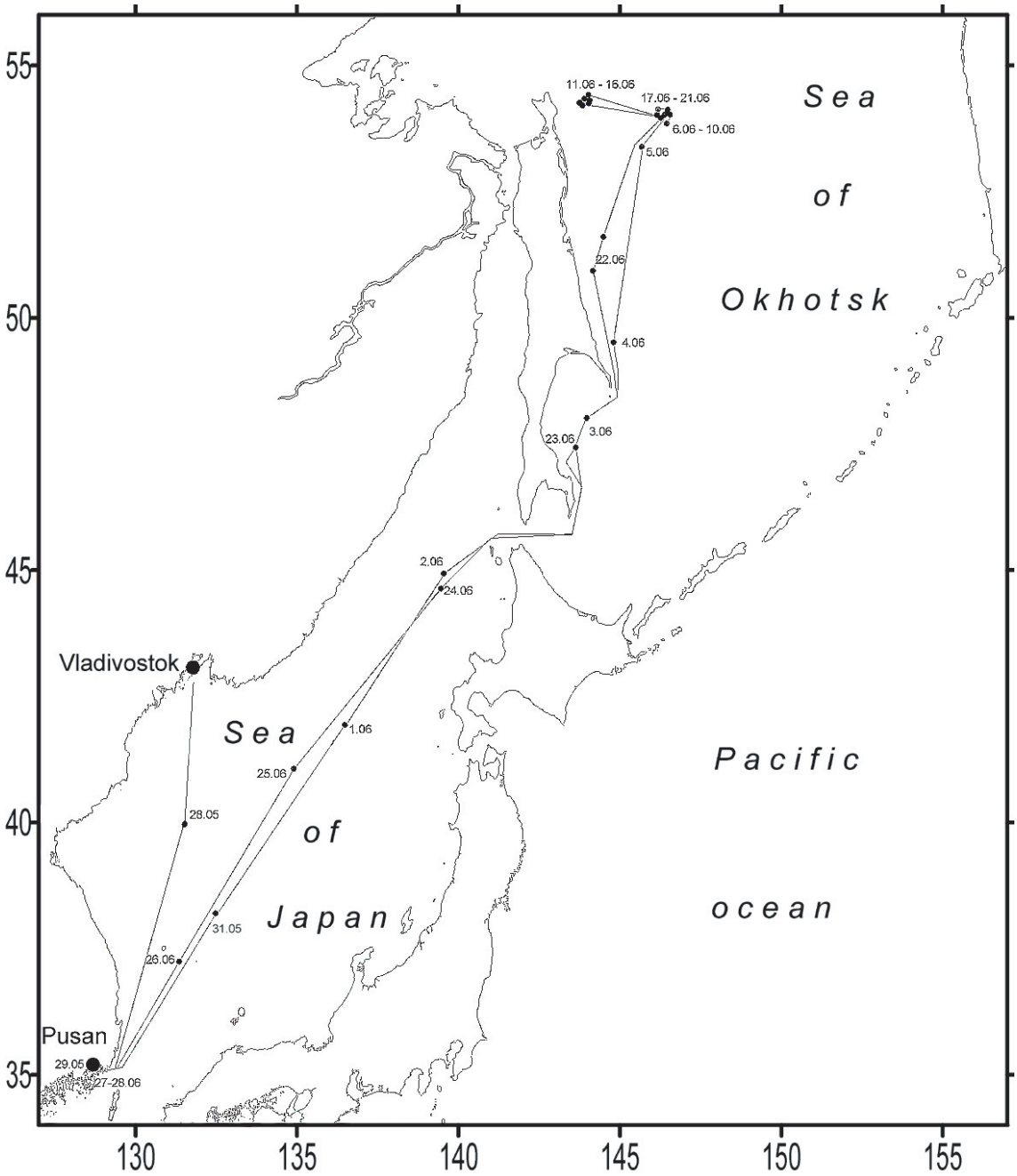

Fig.1.1: *Ships track of RV Akademik Lavrentyev 29th cruise, Leg 1, May - June 2002.*

In the evening of June 11th, we had to leave the Derugin Basin in direction of Sakhalin due to bad weather and bad performance of the MobiWinch. From the morning of June 12th on, we mapped and sampled the methane flares on the shelf and continental slope of Sakhalin. Apart from the flares already known from previous cruises, we discovered several so far unknown methane flares. We could record them now in more detail and also reconstruct the speed of the bubble rise by the improved echosounding system of our Russian colleagues. Methane flares from a water depth of 400 m ("Giselle flare") were visible up to the sea surface. This shows that methane produced here at the seafloor reaches the atmosphere.

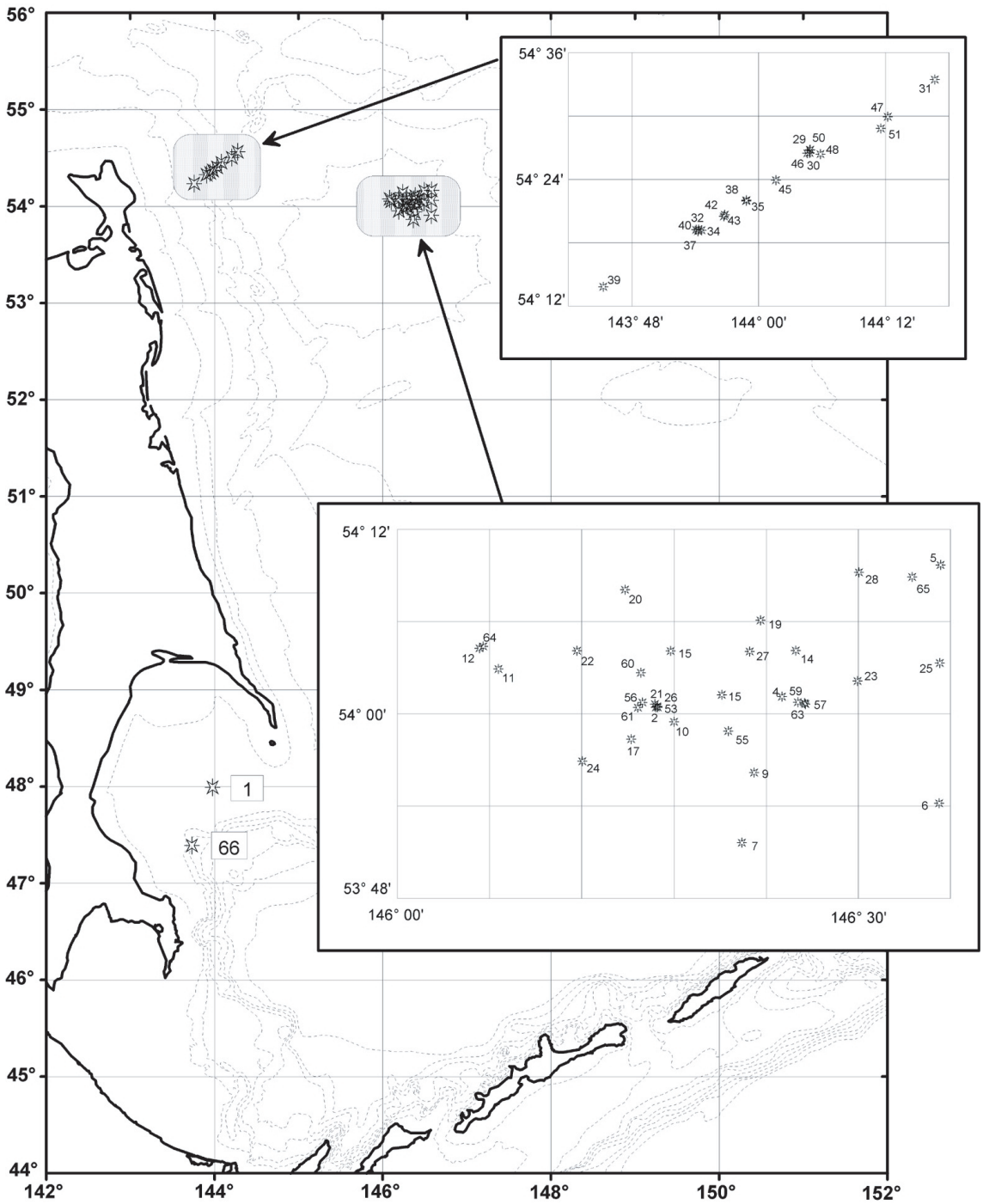

Fig. 1.2: *Map of the working areas (shaded rounded rectangles) and stations (asterisks) during 29th cruise, Leg 1 of RV Akademik Lavrentyev, May - June 2002.*

On June 12th, we were for the first time able to successfully deploy the gravity corer and twice the OFOS equipment on the shelf off Sakhalin at a water depth of 200 m in an area that is characterized by numerous methane flares. Apart from huge edible crabs, we also saw vent precipitates on the OFOS records. The attempt to sample the precipitates with the TV-grab on morning of June 13th failed due to problems with the MobiWinch: shortly after lowering the TV-grab into the water, we had to stop and were not able to get it out of the water again. Within several hours we picked it up meter by meter with the shipboard crane, and all of us were very glad that we did not loose the TV-grab and decided not to use it again.

On June 14th, our outstanding technicians succeeded in repairing the winch with only board devices to such an extent that most of our work could be carried out even in greater water

depths. Nevertheless, the winch had to be run by two persons during OFOS deployments, one person driving the winch and one person steering the spooling device. The whole group of Russian and German scientists we very enthusiastic to share the work with our technicians so that we could establish a dayround coring and OFOS program.

On June 15th, our patience was rewarded for the first time by a great success: we recovered gas hydrates in a sediment core from the Sakhalin slope (Obzhirov flare) at 4 m core depth. The core also contained large amounts of carbonate concretions and had a strong odor of hydrogen sulfide.
On June 16th we sampled a formerly unknown flare area at 800 m water depth by gravity corer and CTD.

On June 17th, we returned to the Derugin Basin in order to continue the work which we had to cancel on June 10th due to the defect winch and bad weather. From June 17th to June 21st, investigations were carried out mainly in the carbonate-barite mineralization area. Unfortunately, a lot of the cruise time had been wasted due to the malfunction of the MobiWinch, and our initial working plan had to be changed significantly. We therefore decided to shift additional coring and dredging program to the second leg of this cruise and started to extensively map the barite mineralization area by OFOS and swath bathymetry, which was very successful.
We observed huge vent sites with barite chimneys up to 10 m height and living *Calyptogena* clams. Thereby, it was found out that the Russian hydroacoustic system is able to detect the barite chimneys as individual reflectors. By comparing the hydroacoustic records with our OFOS profiles we were able to map these barite sites extensively. Apart from that, we discovered numerous smaller vent sites in the Derugin Basin which do not show such large barites, but are characterized by dense clusters of living *Calyptogena* clams.
We also recovered 4 sediment cores from the barite mineralization area which contain many barite and carbonate precipitates as well as shells of *Calyptogena* clams. The cores show typical degassing structures at their bases. This indicates that we sampled here the barite-forming fluids.

In the night of June 21st the works had to be finished and the vessel started to proceed towards Pusan. We shortly stopped on June 22nd in Terpeniya Bay to carry out one final CTD station in an area where we had observed a new methane flare at the beginning of the cruise. We passed La Perusa Strait in the evening of June 23rd and arrived in Pusan in the evening of June 26th. The next morning, a pilot was taken aboard and we proceeded into the port of Pusan and tied up at pier at 7:00 a.m. local time.

2. TECHNICAL SUPPORT OF THE HYDROACOUSTIC OBSERVATIONS

Alexander Salomatin

Acoustic observations were carried out using a hydroacoustic system created on the basis of the modernized shipboard echosounders Sargan-AM, ELAC, two sonars Sargan-GM and two multichannel systems of digital sonar signal registration.
The modernization of the shipboard echosounders included:

- making the operation of the echosounder Sargan-AM at two frequencies simultaneously possible;
- ping synchronization of all acoustic devices being in use;
- an exchange of a part of the receiver of the echosounder and the Sargan sonars;
- a change of the analog acoustic signal registration systems (by pen recorders on special paper) into multichannel systems of digital registration at personal computers with visualization in form of color echograms.

The hydroacoustic system provided the opportunity to simultaneously registrate acoustic signals by five independent channels at frequencies of 12, 19.7 and 135 kHz.

Tab. 2.1: *General properties of the different sonars*

Device	**ELAC**	**Sargan-AM**		**Sargan-GM**	
Operating frequency, kHz	12	19.7	135	19.7	135
Beam width, °	12	10	10	14	4
Impulse power, W	2000	-	-	-	-
Duration of sounding impulses, ms	0.8; 3; 10	0.5; 1; 3; 10	0.16; 0.3;1; 3	1; 3; 10; 30	0.16; 0.3;1; 3

2.1 Multichannel system of digital registration

The multichannel system of digital registration (SDR) is designed for acquisition, preprocessing, accumulation and visualization of hydroacoustic information by four channels simultaneously and comprises:

- an analog unit;
- two sound cards Creative Labs;
- a personal computer (Pentium-200 or better);
- an operating system Windows 2000;
- software for input, processing and visualization of echo signals – “Sonic”.

The acoustic signals are converted into digital form by using the four 16-bit analog-digital converters of the sound cards. The parameters of the acoustic signal registration (depth range, depth resolution, average sound speed and others) are determined by software. The digitized acoustic signals are written into data files on the computer’s harddisk, 700 acoustic signal samples in each file (the quantity of samples in the file is determined by the software).
The acoustic signals were visualized on a monitor screen in form of color echograms, in which each channel was plotted in two echograms with respective depth scales and color palettes. The software provided synchronous detection, filtration, registration and visualization of the acoustic signals throughout all depth ranges.

2.2 Scope of the acoustic survey

The main purpose of the work was to detect and investigate acoustic indications of underwater gas emission sources. For this purpose, the level of acoustic backscattering was collected simultaneously at frequencies of 12, 19.7 and 135 kHz in the water column and from the seafloor.
Calibration measurements were carried out to provide a valuable calibration for all sonars by the method of multiple reflections. This enables us to determine the absolute values of acoustic backscattering at different frequencies.
The received data can also be used for:

- evaluation of the magnitude of underwater gas emission sources;
- evaluation of the reflection coefficient and other seafloor characteristics;
- registration of frontal zones, internal waves and other oceanological processes;
- registration of the spatial distribution of fish, large and middle zooplankton and acoustic evaluation of their biomass.

Acoustic backscattering was recorded in all stations and, allowing for weather conditions (sea roughness and wind-force less than 4-5), on the tracks between them. The total time of acoustic observations amounted to 480 hours.

2.3 Preliminary results

In the first leg of cruise LV29, 114 hydroacoustic anomalies (HA) were registered, the coordinates of which are shown in Appendix 2. The map of HA (gas flares) of the eastern Sakhalin slope is shown in *Figure 6.3*, Chapter 6. HA were registered at best at frequencies 12 and 19.7 kHz with an elevation of the signal above the noise of minimum 20 dB. We divided the HA into deep-water (water depth >300 m) and shallow (water depth <300 m) ones. While the vessel is moving, the appearance of deep-sea HA is totally different from that of sound-scattering layers so that the HA are easy to detect. Another fact confirming that these HA are caused by emissions from the seafloor is the absolute constancy of the HA occurrence over an extended period of time. Some examples of HA recorded while the vessel was moving are shown in *Figure 2.1*.
HA 54 rises from the bottom to 200 m depth and ascents with a constant slope from the seafloor to a depth of 360 m, determined by the relation of the speed of the rising scatterers, causing the HA, and the current speed at the seafloor. In this case, these speeds are approximately the same and the real angle of slope is slightly less than 45°. Above 360 m, the current speed decreases and the HA runs nearly vertically. The acoustic signals reach maximum values at depths of 350-500 m. This shows that the vessel slightly passed the center of the HA source. The width of the HA source is, obviously, less than 100 m. The diameter of the area sounded by the ELAC echosounder is 150 m and 80 m for 700 m and 400 m depths, correspondingly, which hinders a more exact determination of the diameter of this HA.
HA 57 consists of two separate sources located in a distance of about 100 m from each other. The peculiarity of this HA is that its forming scatterers are observed up to a depth of 50 m below the sea surface. HA 41 (“Giselle flare”), composed of minimum three sources, has an even more complicated form. In *Figure 2.2*, several tracks in “Giselle flare” with different speeds and courses are shown. The records made at slow speed and while the vessel was drifting are of particular interest. They show that the scatterers causing the HA rise from the seafloor to the sea surface. Moreover, the individual scatterers are distinctly visible in the last record, which allows to evaluate their rising velocity. The evaluation of a group of scatterers running from 100 m to 75 m depth yields a rising velocity of 15 cm/s.

In many cases, deep-water HA are associated with particular forms of seafloor morphology. In *Figure 2.3*, an enlarged echogram fragment of the near-bottom part of HA 54 is shown. It is well visible that the HA source is a small elevation with a height of about 6 m and a width of about 300 m. Such elevations were observed near the bases of HA 72, 73 and 83, too.
This allows us to draw the conclusion that deep-water HA are very likely caused by emission of gas bubbles from the seafloor.
It is more difficult to make such well defined conclusions about the shallow HA, especially when recorded at maximum vessel speed, because of an increased density of fish schools in the shelf area, which can have various forms. Several somewhat doubtful HA are given at the end of Appendix 2 by letters a, b, c and d. Very interesting records of shallow HA were made at slow vessel speed. An example of such a record during drift is shown in *Figure 2.4*. Due to a higher spatial resolution it is obvious that HA 35 consists of scatterers rising with practically equal and constant speed. Here, the rising velocity is a little bit higher and amounts to 20 cm/s. But there were also several scatterers rising with a noticeably higher speed.
An interesting result was the discovery of deep-water HA 94 separately situated at a water depth of 1,200 m (*Fig. 2.5*).
Additionally, a survey of barite build-ups was carried out in the Derugin Basin. This became possible due to the fact that the initial parts of acoustic signals from a bottom area covered with barite build-ups and a bottom area without them significantly differ from each other (*Fig. 2.6*). The occurrence of barites results in the appearance of an additional signal directly at the bottom, the so-called “upper barite reflector”, the duration of which depends on the height of the build-ups and their amplitude. With correctly chosen registration parameters, bottom areas with barite build-ups are well defined on echograms. An example of such an echogram is given in *Figure 2.7*.

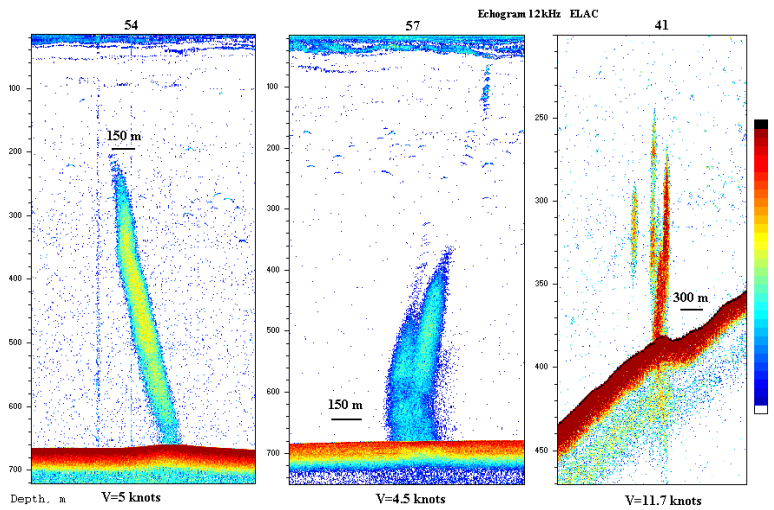

Fig. 2.1: *Echograms of deep-water HA made while vessel was moving.*

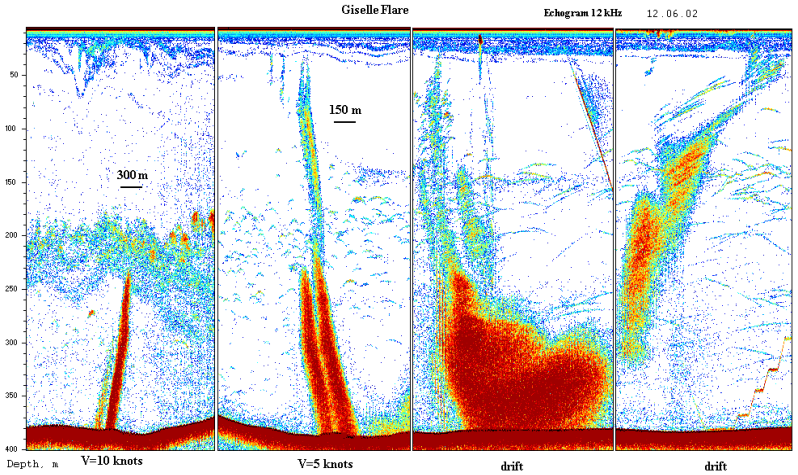

Fig. 2.2: *Echograms of deep-water HA made while vessel was slowly moving or drifting.*

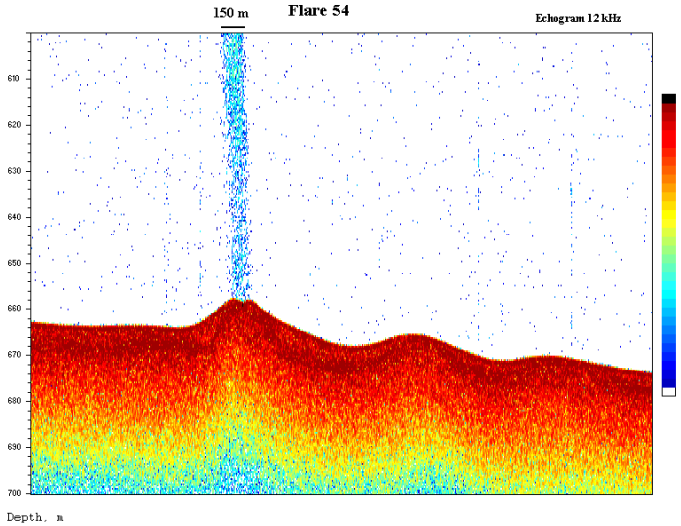

Fig. 2.3: *Echogram of the near-bottom part of HA 54.*

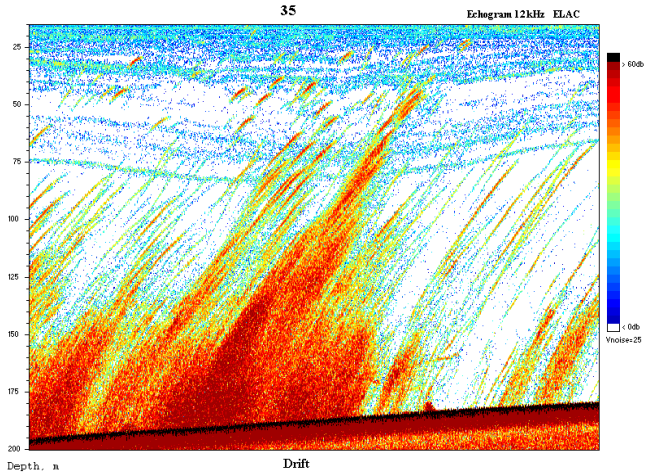

Fig. 2.4: *Echogram of the shallow HA 35 made while vessel was drifting.*

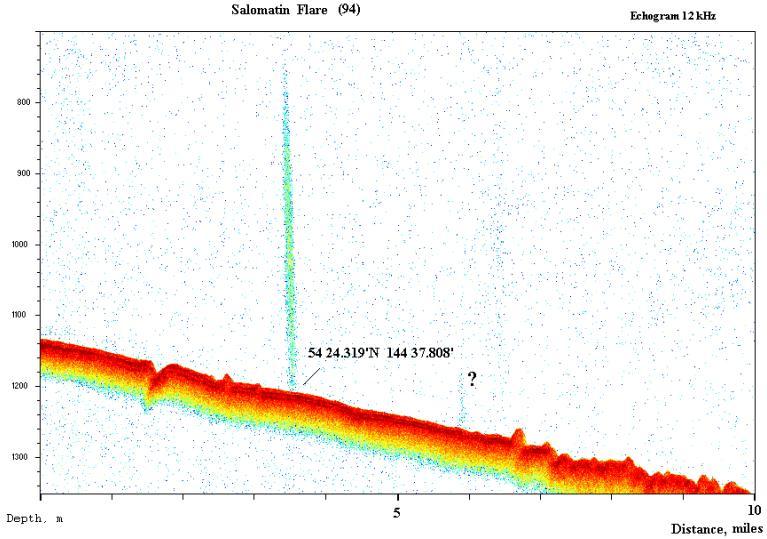

Fig. 2.5: *Echogram of the new deep-water HA 94 made while vessel was moving.*

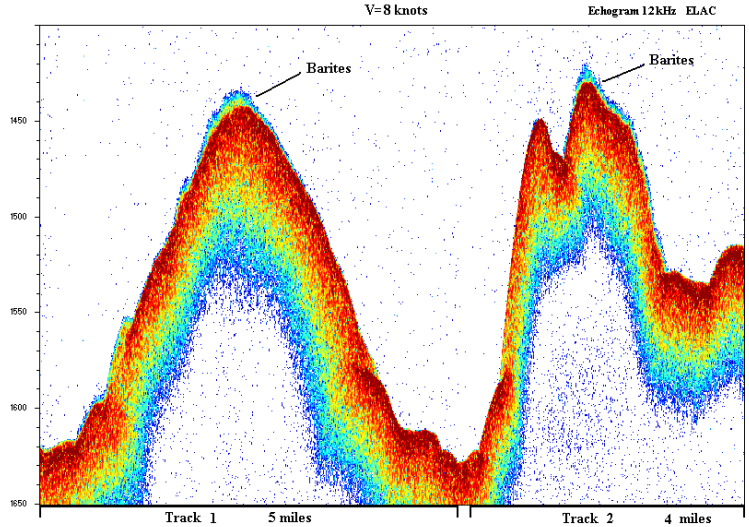

Fig. 2.7: *Echogram of barite build-ups in the Derugin Basin.*

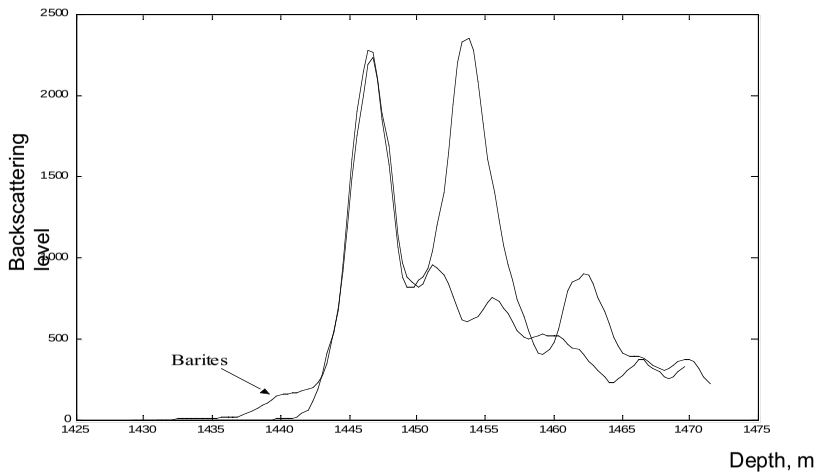

Fig. 2.6: *Initial parts of the reflected signals from a bottom covered with barite build-ups (solid line) and a bottom without them (dashed line).*

3. SWATH BATHYMETRY MAPPING

Hartmut Hein

A multibeam echosounder is a useful tool to get good bathymetric models and maps. Only with such a system it is possible to achieve full bottom coverage. These bathymetric models allow to map the real morphology of the seafloor for geodynamic interpretations and for planning detailed observations (coring, video-controlled records).
For the transducers/receiver arrays of the multibeam system, a special frame (called LOLA II) with 6 bouncy bodies was built at GEOMAR in Kiel. This construction was towed by a steel rope in a distance of 5 - 6 m to the ship's starboard side.
To get information about the heading and motion (hieve, rollangle, pitchangle) of LOLA II, a Gyrocompass (Octans3000 from iXSEA) with an integrated Motion Sensor was fixed in the middle of the frame. The used multibeam sytem was BOTTOM CHART MKII from ELAC-L3-Communications. *Hydrostar* software controlled the system and saved all rawdata with the position. The ship's GPS was used to get the positions in NMEA format. For postprocessing, we had to use *HPedit* and *HPpost* (ELAC).

Tab. 3.1: *Coordinates of swath bathymetry stations*

Station	*Investigation Area*				*Water Depths* [m]	*Remarks*
	SW Edge		*NE Edge*			
Derugin Basin						
3-1	53°57.3'	146°10.0'	53°58.9'	146°45.4'	1410-1580	
8-1	53°56.5'	146°12.0'	53°58.0'	146°45.5'	1420-1590	sometimes no GPS
13-1	53°55.5°	146°10.1'	53°56.6'	146°45.2'	1480-1600	no positions
18-1	53°52.1'	146°32.2'	54°10.4'	146°35.8'	1480-1600	
54-1	54°02.0'	146°10.6'	54°03.5'	146°31.7'	1480-1680	problems to detect bottom
58-1	53°58.8'	146°28.8'	54°10.1'	146°33.0'	1520-1620	
62-1	54°01.3'	146°04.2'	54°06.5'	146°09.7'	1450-1650	
Sakhalin Shelf						
33-1	54°19.2'	143°55.0'	54°28.0'	143°27.9'	650 - 790	
36-1	54°19.2'	143°58.2'	54°27.9'	144°03.1'	180 - 650	
41-1	54°19.2'	144°02.2'	54°28.0'	144°06.7'	160 - 230	
44-1	54°17.9'	143°54.0'	54°21.4'	143°56.2'	220 - 400	
49-1	54°27.9'	143°54.1'	54°21.2'	144°02.2'	390 - 670	
52-1	54°27.7'	144°02.4'	54°31.2	144°06.6'	650 - 720	

3.1 Testing and calibration

At the beginnig of the cruise the behavior of LOLA II in the water had to be tested (unfortunately, it was only possible to test in Kiel whether the construction floats). After testing LOLA II in Terpeniya Bay we decided to use only five bouncy bodies in order to get the frame a little bit deeper into the water.
Due to an offset between the real rollangle of each transducer and the rollangle measured by the Motion Sensor, the system has to be calibrated. This problem can be solved by an overlap of the adjacent tracks in shallow water. The sound velocity model from CTD measurements was used to calibrate the depth values.

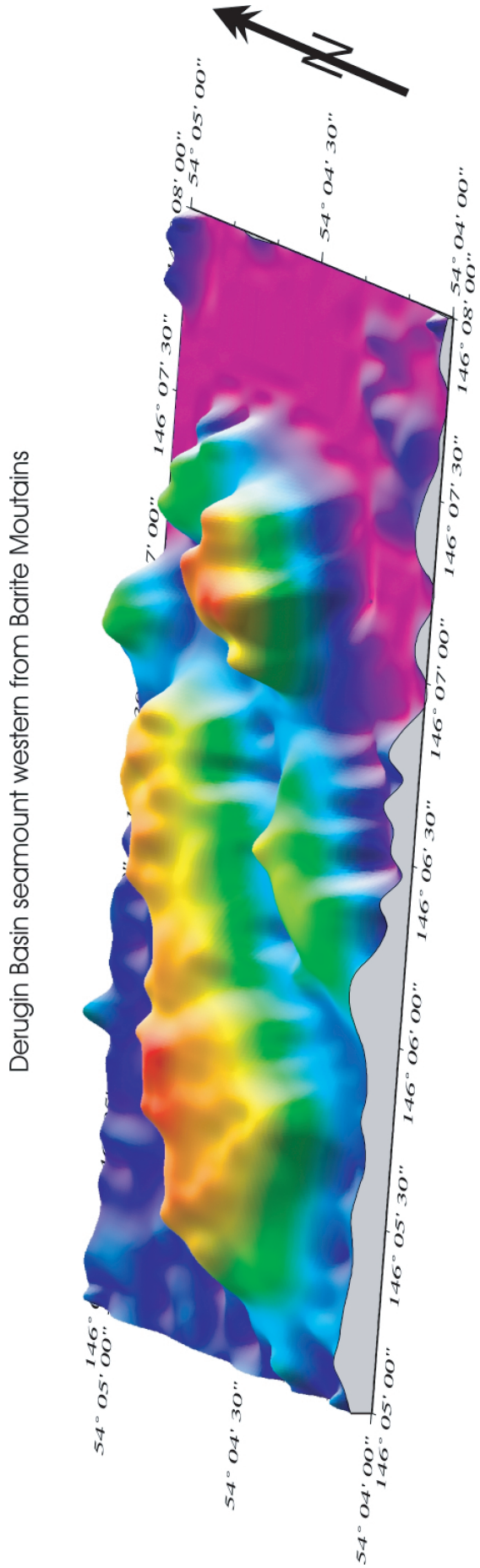

Fig. 3.1: *3D-image of the hills in the west of the "Barite Mounds" in the Derugin Basin.*

After the calculation of the offsets we were able to say that the accuracy of the depth error depending on a wrong calibration fits to the accuracy of the bathymetric model (min. 4 times better).

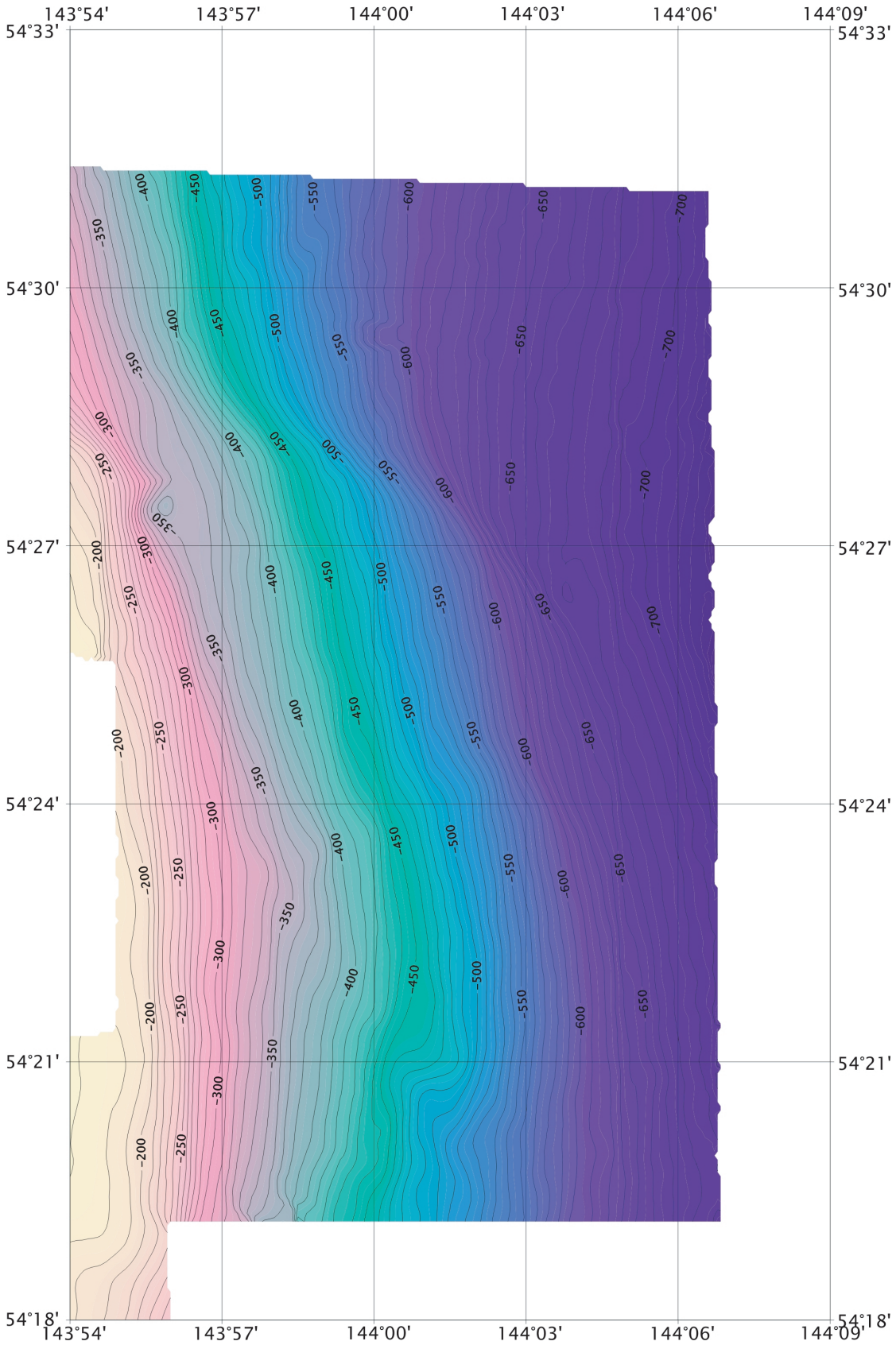

Fig. 3.2: *Bathymetric map of the northeastern Sakhalin shelf and slope.*

3.2 Investigation areas

The beam angle can be varied in discrete steps from 120° down to 18°. We decided to use beam angles from 60° up to 120° depending on the water depth: in shallow water, it is possible to use greater angles than in deeper water. The overlap of the tracks was defined as 20%. The ship's speed was 2 to 4 knots depending on water depth and weather conditions, which were quite well most of the time.

We were able to get a good coverage in the Derugin Basin and mapped areas in the south, in the north and in the east from the area mapped on cruise GE99 (see *Fig. 4.4*, Chapter 4). We also investigated hills west of this area (*Fig. 3.1)*, but we had not enough time to connect this with the bathymetric survey of cruise GE99.
On the Sakhalin shelf, the whole area between "Erwin flare" and "Obzhirov flare" (*Fig. 3.2*) was mapped as well.

3.3 Conclusions

The multibeam system worked quite well most of the time. A catamaran is not the optimal device for bathymetric mapping, because it is not easy to handle its movements. Probably, it would be a better solution to mount the transducers directly onto the ship`s body. For better measurement, it is important to get the transducers deeper into the water.
Sometimes, the positioning data of the ship`s GPS was not very well. An own GPS supported by the data from the Motion Sensor and the Gyrocompass would help to avoid such a problem. Additionally, the measurements from both systems could be connected with a Kalman filter to bridge the times with bad or no GPS data.

4. SEAFLOOR MORPHOLOGY OFF THE EASTERN OKHOTSK SEA COAST: RESULTS OF SINGLE- AND MULTIBEAM ECHOSOUNDER SURVEY

Boris Baranov, Hartmut Hein, Aleksander Salomatin, Aleksey Radyukin, and Gennady Nepomiluyev

4.1 Introduction

The bathymetric investigations conducted in the first leg of the 29th RV *Akademik Lavrentyev* cruise concentrate on two main targets:

1. Mapping of the seeping area along the eastern Sakhalin slope and the area of barite mineralization in the Derugin Basin in order to obtain an idea about specific bottom features connected with these phenomena;
2. Mapping of the major morphological features of these areas for tectonic purposes.

In addition to this, the obtained bathymetric maps served as a basis for sediment sampling, OFOS observations, dredging and hydrocasts. Two kinds of equipment were used for the bathymetric surveys: 1. single-beam echosounder ELAC (see Chapter 2 for technical details) and 2. multibeam echosounder LOLA II (see Chapter 3 for technical details).
The single-beam echosounder operated during the whole cruise, whereas the multibeam echosounder was used only in distinct areas which were chosen for detailed bathymetric investigations. There was no special track network for the single-beam survey except for the mapping of the "upper barite reflector" in the Derugin Basin (see Chapter 2). The space in between the multibeam tracks varied from 0.25 up to 1.1 nm depending on water depth and track direction. The total length of the LOLA II tracks was equal to 302 nm. In the first leg, one area was mapped on the eastern Sakhalin slope and two areas in the Derugin Basin (*Fig. 4.1*).

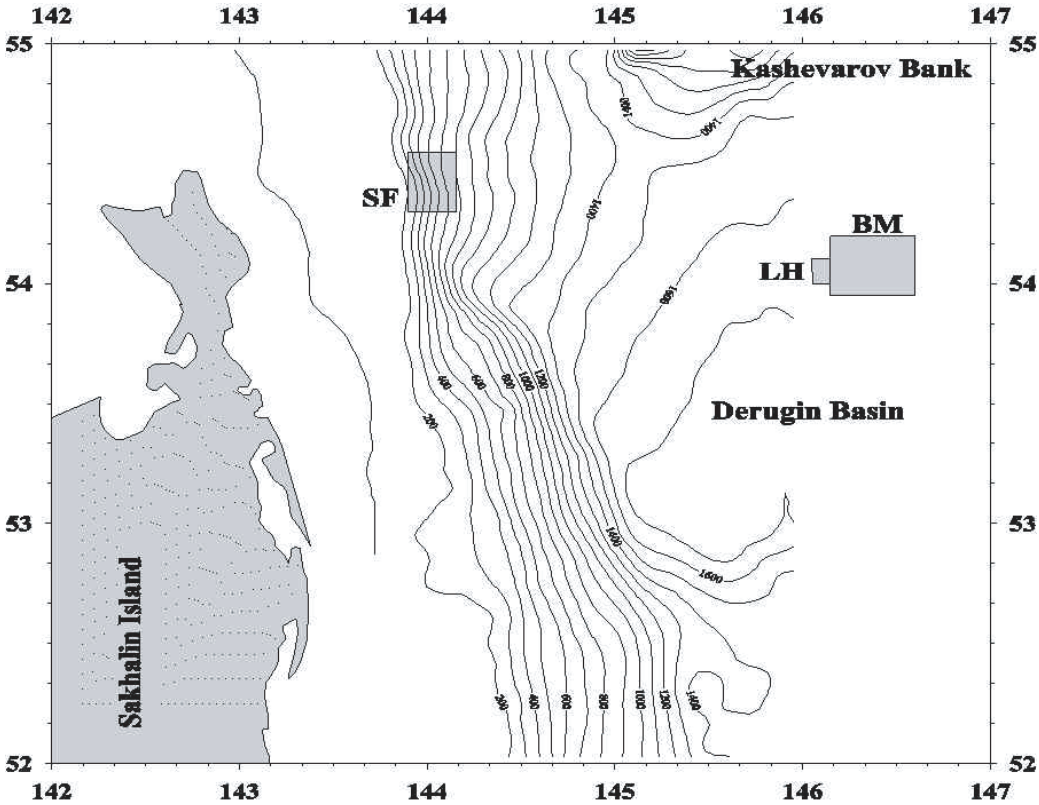

Fig. 4.1: *General location of the study areas (gray rectangular). SF = Sakhalin flares, BM = Barite Mounds, LH = Lola Hills. Contour interval is 100 m.*

4.2 Eastern Sakhalin slope

The morphology of the slope was investigated on the basis of a track network in a 180-700 m depth range. This network was regular and consisted of 30 N-S-striking tracks orientated along the general trend of the slope. The length of tracks varied from 3 up to 8 nm and the space between the tracks from 0.25 up to 0.8 nm. The total length of the survey was equal to 145 nm.

The bathymetric investigations along the Sakhalin slope show that the shelfbreak is very distinct and that it can be traced at depths between 180-190 m (*Figs. 4.2* and *4.3*, profile 1). Landwards of the shelfbreak lies the shelf which is represented by an eastward-sloping plain within a depth range of 50-180 m. The shelfbreak strikes generally in N-S direction except for the northernmost parts of the study area, where it slightly deflects to the west. Its contour is rather straight throughout the study area except for the southern part. Two small swells evident from the serpentine-shaped 190 m contour line and the shaded relief occur there. The larger one of them strikes in NW-SE direction and the smaller one trends to SW-NE. Another small swell is located at the northern shelfbreak (western margin of the study area) and has probably a SW-NE strike.

The slope has a slightly concave profile and can be divided into three parts: an upper (180-300 m), a middle (300-600 m) and a lower slope (600-650 m and below) which differ from each other in their forms and their angle of inclination (*Figs. 4.2* and *4.3*). The slope morphology is in general extremely simple and changes only slightly from south to north. The bathymetric maps (*Fig. 4.2*) of the study area show that the contour lines strike mainly in N-S direction with small deviations that occur in the northern part where the contour lines of the lower slope trend in NNE direction. Along the middle part of the slope the contour lines are clearly banded.
The upper slope has a maximal inclination angle of 2-3°. The shape of the upper slope is simple except for its northern part where a small asymmetric spur appears in depth interval 300-350 m. It has an asymmetric profile with its steep side trending to the northeast and facing to the southeast and is the most distinct feature of the whole slope (*Fig. 4.3*, profile 1). Two small spurs appear also on the southern boundary of the study area and strike in NW-SE direction.
The middle slope has the most remarkable structure. The contour lines in the northern part of the area show a sharp bend forming oblique steps, which are clearly visible as lineations of a NW-SE strike. Two more prominent lineations trending in NW-SE and NE-SW directions can be distinguished in the central part of area, as well (*Fig. 4.2*). These lineations restrict the small bulge that has a triangle shape and is slightly uplifted under the slope surface. In contrast to the general concave profile of the whole slope, its middle part has a convex form. Hummocks of a few meters height appear along both lineations and inside the bulge. Small hummocks occur also between the oblique steps and the northern edge of the bulge. They align in a more or less regular manner forming chains trending in SSW-NNE direction and are visible on the profile as a wavy surface (*Fig. 4.3*, profile 1). They occur also along the middle slope north of the oblique steps.
The lower slope is very shallow and has a simple morphology. Its characteristic feature is a divergence of the contour lines northward from the oblique step to the east, but not to the west. The seafloor of the lower slope is very smooth with occurrences of many small hummocks of a few meters height. These hummocks align in chains, which strike in two directions, namely SSW-NNE and NW-SE. The first direction corresponds to the strike of the lower slope contour in the northern part of the study area, and the second one coincides with the trend of the oblique step.

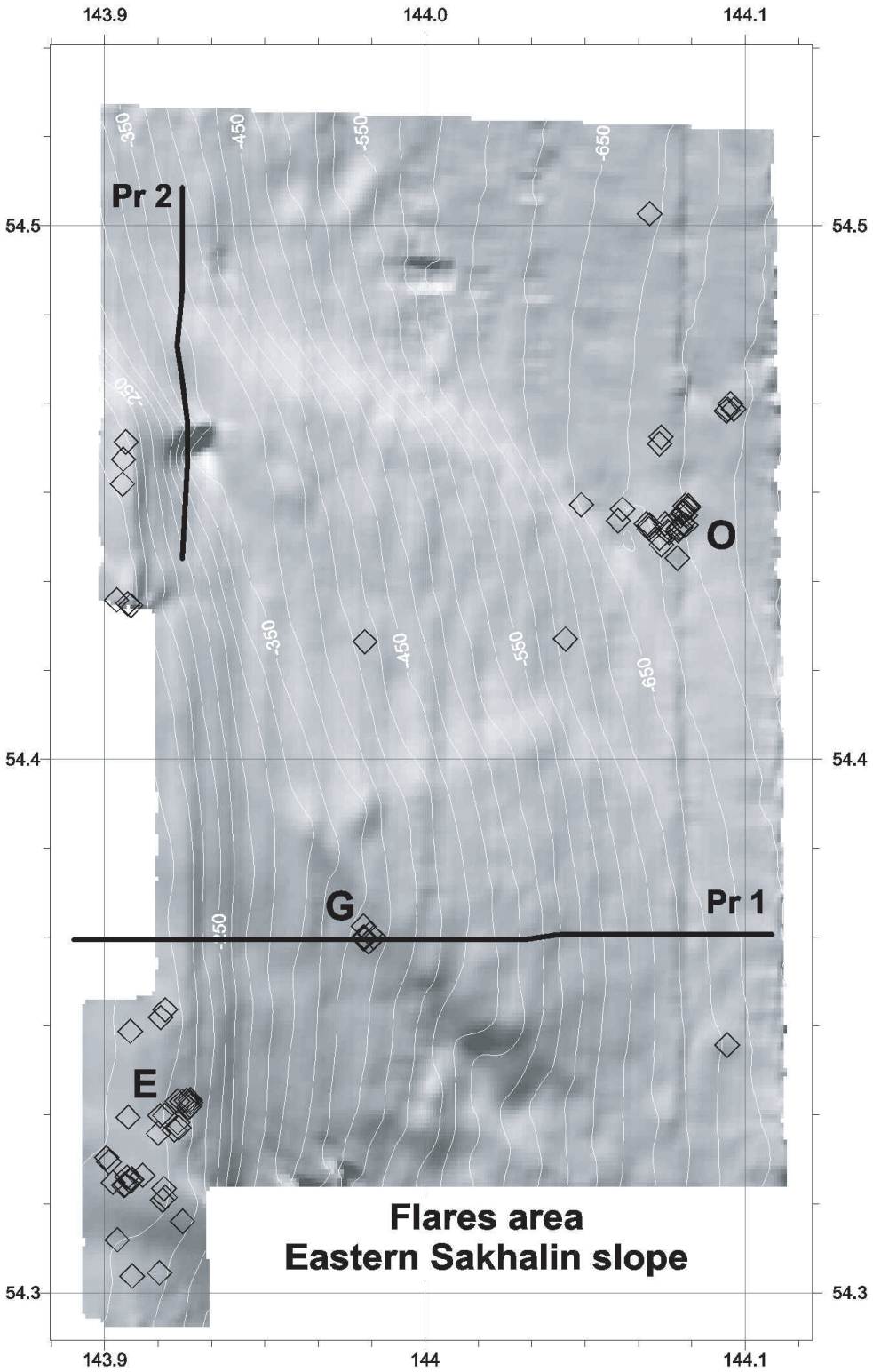

Fig. 4.2: *Shaded relief map of the Sakhalin flares area with overlapped contour lines. Contour interval is 20 m. Lines mark the location of the bathymetric profiles shown in Fig. 4.3. Diamonds indicate the positions of the hydroacoustic anomalies (gas flares). Flare fields: E = Erwin, G = Giselle, O = Obzhirov. Location of the map is shown in Fig. 4.1.*

The single-beam echosounder survey shows a good correlation between the observed hydroacoustic anomalies (flares) (see Chapter 2) and the morphological features. The detected flares concentrate in three locations: 1. near the shelfbreak, 2. in the middle part of the slope and 3. in the lower part of the slope.

Along the shelfbreak, the maximal concentration of flares was observed in the northern part of the area (the "Erwin flare" field) (*Fig. 4.2*). The flares line up in several zones, which have a NE and NW strike and are located in the small swells mentioned before or in flexures (sags) in between, which are trending in the same direction. The next two groups of flares are located in the northern part of the area and each one of them consists of three single flares. The flares of the first group concentrate more or less in single points and are located along the NE-striking swell. The flares of the second group trend in NS direction and occur at the beginning of the spur located in the middle slope.

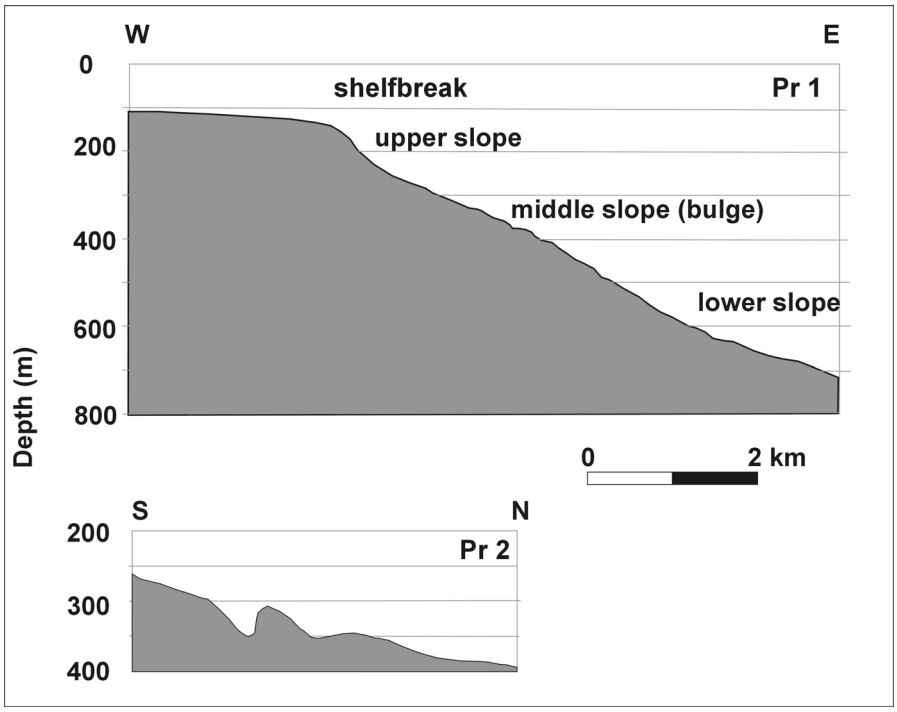

Fig. 4.3: *Bathymetric profiles showing the main morphological features of the eastern Sakhalin slope. Locations of profiles see in Fig. 4.2.*

Along the middle slope, maximum concentrations of flares were observed at the "Giselle flare" field (*Fig. 4.2*). This flare field is located on the slope of the hummock along the NW lineation, which limits the bulge from the south. The next two flares detected here appear on the slope of the hummocks.

Along the lower slope, maximum flare concentrations ("Obzhirov flare" field) occur at the southeastern end of the oblique step (*Fig. 4.2*). Similar to the shelfbreak, the flares concentrate here along two directions: SW-NE and NW-SE and occur on small swells consisting of separate hummocks.

Except for the "Obzhirov flare" field, several single flares or group of flares were detected on the lower slope as well. The deepest of them is located in a water depth of 800-900 m (outside the detailed bathymetric survey area). Most of these flares are concentrated on the slopes and less of them in the central parts of the hummocks. One of the deepest groups of them, consisting of five flares, trends in NW-SE direction.

4.3 Derugin Basin

Two areas were investigated in the Derugin Basin:

1. "Barite Mounds", and
2. "Lola Hills" (see *Fig. 4.1* for location).

The first area represents the extension of the map, which was prepared on the basis of a LOLA survey on the MV *Marshall Gelovany* cruise in 1999 (Biebow et al., 2000). This work intended to map the barite mineralization area.
On cruise LV29, the mapping area was extended to the south and to the east from the formerly mapped "Barite Mounds" (*Fig. 4.4*). The track lines for echosounding were carried out with a regular spacing. The lines strike in E-W direction for the southern part and in N-S direction for the eastern part of the study area. The maximum length of profiles was equal to 17.5 nm and the space between the tracks varied from 0.4 to 1.1 nm. The total length of the survey was 145 nm. The mapping of the second area was specially devoted to investigations of the small height, which was crossed on the GERDA cruise in 1995. This height looks like a diapir structure on the seismic profiles.

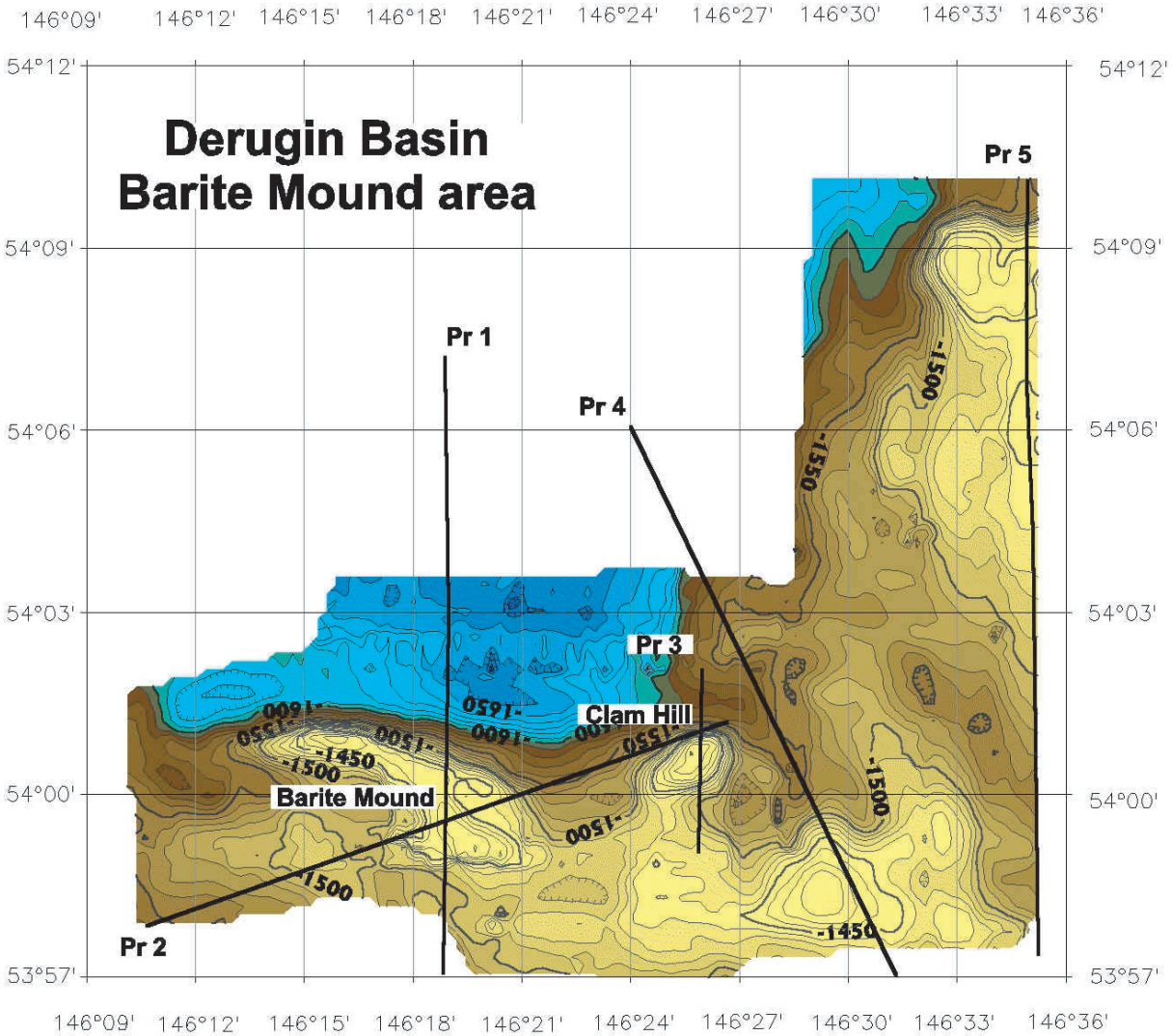

Fig. 4.4: *Bathymetric map of the "Barite Mounds" area. Contour interval is 10 m. Thick lines mark the location of the profiles shown in Fig. 4.5.*

4.3.1 "Barite Mounds" area

A basin with a water depth of up to 1,680 m occupies the central part of this area (*Fig. 4.4*). It is outlined along the south and east by a system of heights with a minimum depth of up to 1,420 m. As it was obtained before from seismic reflection investigations carried out in the framework of the KOMEX I project (Biebow et al., 2000), the basement of the Derugin Basin consists of tilted blocks. These tilted blocks have very characteristic forms. One side of the

block is steep and has a normal fault origin, and the second one is tilted. Sometimes, the tilted blocks are cut by normal faults from both sides forming a horst structure, but even in this case the surface of the horst is not plain, but tilted. Although the tilted blocks are covered by a blanket of sediments in the Derugin Basin, they appear in the seafloor morphology as small elongated ridges with one steep hillside and another slightly tilted hillside. Therefore, this structure can be determined even during the echosounder survey.

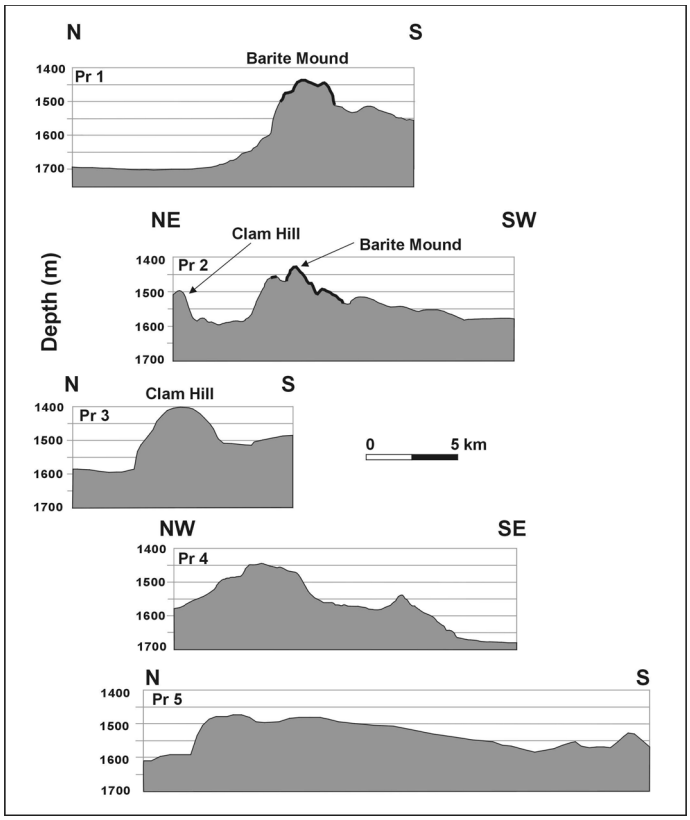

Fig. 4.5: *Bathymetric profiles showing different morphological features of the "Barite Mounds" area. Thick line indicates the area of barite mineralization. Location of the profiles is shown in Fig. 4.3. See text for discussion.*

Three tilted blocks with their tops outlined by contour line 1,450 m were distinguished in the investigation area. The eastern part of the area is occupied by a single block, which tilts to the south. The steep side of the block has a W-E strike and faces to the north (*Figs. 4.4* and *4.5*, profile 5). The top and southern slope of the block are smooth; its western side trends in NW-SE direction and has wandering outlines.

The second block is located in the southeastern corner of the map (*Fig. 4.4*) and separated from the previous one by a NW-SE-striking trough with a maximal depth of 1,550 m. This block has an E-W strike submerging from east to west. Its top tilts to the north and is cut from the north and the south by steep slopes forming a horst structure (see profile 4 in *Fig. 4.5*).

The third block yielding barite mineralization is located further to the west and strikes almost in W-E direction. Its northern slope is steep and faces to the basin. The top and the southern slope of the block are not plain like the blocks mentioned above, but are occupied by a mound. The mound can be subdivided into two parts: the western and eastern ones are arranged in an en-echelon pattern. Both parts strike in W-E direction. The northern and the southern sides of the mound are steep and probably have a fault origin. Exactly on this mound a giant field of barite chimneys was observed by OFOS on cruise LV28 in 1998 (Biebow & Hütten, 1999).

Due to the fact that the barite chimneys show a specific reflection on the echosounding profiles (see Chapter 2), a detailed single-beam echosounder survey was carried out on this mound in order to outline the area of barite mineralization (*Fig 9.3*, Chapter 9). This area roughly coincides with contour line 1,500 m (profiles 1 and 2 in *Fig. 4.5)* and strongly corresponds to the outlines of the mound.

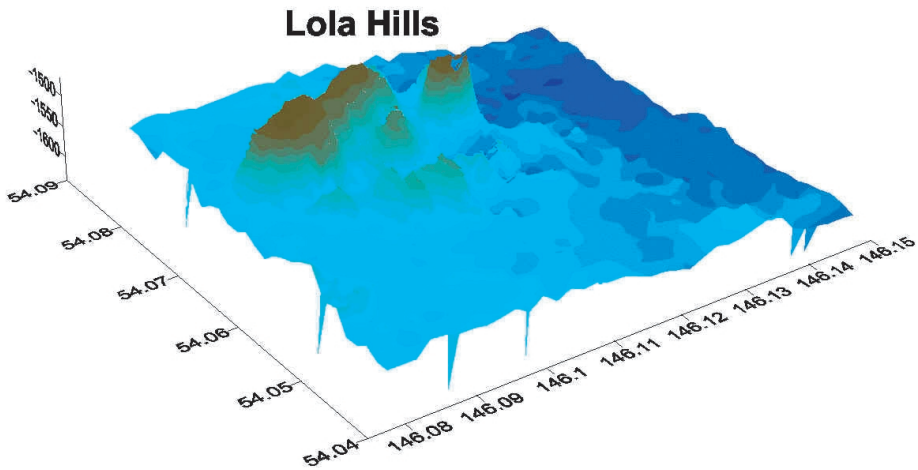

Fig. 4.6: *3D image of the "Lola Hills" area. This area consists of several hills and elongates in NE-ENE direction. See Fig. 4.1 for location.*

There are other morphological structures apart from the tilted blocks. The largest of them, called "Clam Hill" (due to the abundance of several *Calytogena* clams observed during OFOS survey), is located to the east from the "Barite Mounds". Its top is located in depths of a little more than 1,400 m (*Fig. 4.4*, profile 3), and the hill has rounded outlines slightly elongated in NNE direction. Another structure of such kind is located on the strike of the titled blocks and is orientated in WE or NW direction.

4.3.2 "Lola Hills" area

This area is connected to the "Barite Mounds" area in the west (*Fig. 4.1*) and was chosen for detailed investigations on the basis of seismic profiles carried out on the GERDA expedition (1995). The profile shows very amazing structures represented by a height which is elevated above the seafloor. It does represent neither an outcrop of bedrock's nor a volcanic edifice, but is more similar to an uplifted column of sedimentary cross-sections. A wipe-out structure was observed beneath this height that can be indicative of gas expulsions.
Because of the small size of the structure, only three tracks with a total length of 12 nm were run there. Our survey shows that several hills are located inside this area (we therefore named this place Lola Hills). They are situated on the shallow swell mentioned above, which limits the basin from the west. The hills have different sizes and altitudes. The minimal depth observed is a little less than 1,480 m, and the maximal dimension is about 1 nm. The sides of the hills are very steep (inclination is up to 30-40°); their altitudes reach 100 m. The total elevation of the highest hill above the flat basin floor is equal to approximately 150 m.

These hills are aligned in three groups from north to south. The northern group contains the largest hill striking in SW-NE (55°) direction (*Fig. 4.6*). This hill has a flat top outlined by the 1,480 m contour and seems to consist of four hills accreted each other. The middle group is represented by two large and one small hill of rounded outlines, which strike in the same direction. The southern group consists of five hills orientated in W-E direction.

4.4 Preliminary conclusions

1. Three directions of lineations were distinguished in the morphology of the eastern Sakhalin slope: NW-SE, NE-SW and NNE-SSW. The first two are the most pronounced. The hydroacoustic anomalies (flares) inside two flare fields ("Erwin flare" and "Obzhirov flare") concentrate along lines striking in NW-SE and NE-SW direction. This could be connected with the existence of fault systems.

2. Two directions are typical for the morphological features of the northeastern Derugin Basin: WE and NW-SE. The first of them is connected with fault scarps limiting the tilted blocks. The second direction is possibly connected with the existence of a second fault system.

3. The area of barite mineralization has a very good coincidence with the mound located on the top and the southern slope of the titled block. Due to the fact that it has very sharp northern and southern limits, we can suggest that its origin is connected with a fault system.

4. The origin of the "Lola Hills" remains unclear, and additional data is needed. However, the bathymetric survey shows that this structure consists of several hills, which align in NE-WE-striking lines, i.e. have more or less the same direction as the fault scarps of the "Barite Mounds" area. Therefore, we suggest that this structure can represent a diapir originating from compressional tectonics, which prevail recently in the Derugin Basin (Biebow et al., 2000).

5. WATER COLUMN STUDIES

Anatoly Salyuk, Valery Sosnin, Anatoly Obzhirov, Pavel Tishchenko, Galina Pavlova, Olga Vereshchagina, Natasha Khodorenko, Sergey Sagalayev, Nicole Biebow, Klaus Wallmann, and Bettina Domeyer

5.1 Introduction

The main objectives of the CTD observations in the first leg of cruise LV29 were water column investigations and water sampling in the methane venting area on the Northeast Sakhalin shelf and slope and in the barite mineralization area of the Derugin Basin. In the Derugin Basin, we concentrated our efforts on the mapping of a methane plume around the "Barite Mounds" in the central part of the basin. In the methane venting area we continued previous observations to compare methane concentrations in the well known vents like "Obzhirov flare", "Giselle flare", "Erwin flare" and searched for new ones.
Our observation demonstrated the importance of precise positioning of the ship during repeated observation of the same flare due to the high temporal and spatial variability of the flare orientation and its properties. For this purpose, we successfully used the shipboard echosounder.

5.2 CTD observations

Water column sampling was carried out using a rosette water sampling system consisting of a Sea-Bird-32 twelve position system with 10 liter Niskin-type bottles and a CTD probe Sea-Bird-911 with standard temperature, pressure, conductivity sensors and also sensors for oxygen light transmission, altimeter and bottom contact. The CTD was lowered up to 3 m above the seafloor at stations shallower than 100 m and to 8 m at deeper ones. Water sampling was started at maximum depths and the samples were taken during the upcasts. The interval of water sampling depended on the purpose of investigation, and the water depths varied during observations from 5 to 500 m.

5.2.1 Dissolved oxygen

The calibration of the CTD sensor for dissolved oxygen (DO) was done measuring DO in water samples by the modified Winkler method. DO concentrations in the water column at the moment of sampling were calculated from the DO sensor data taking into account the time deviation of the DO sensor for temperature.

5.2.2 CTD depth calibration

The depth of the seafloor was determined for each station by 3 different methods:

1) directly by CTD bottom contact. The depth at the moment of the bottom contact was calculated according to normal CTD formulas (UNESCO) using CTD pressure and station latitude;
2) calculated from the travel time of the acoustic signal measured by the ELAC echosounder and by the sound velocity, using the real temperature and salinity (TS) profile of the water column measured by CTD;
3) calculated from water compressibility, CTD pressure and TS data, using UNESCO formulas.

The calibrated ELAC echosounder depth data can be used also for depth calibration of historical depth data tracks crossed on this expedition, and for depth data obtained from other echosounding devices (LOLA II, SES-2000DS).
A total of 32 stations was carried out during the first leg of cruise LV29. Water samples were taken for pH and alkalinity, methane, oxygen concentration, oxygen isotopes, calcium, helium, and additionally 30 samples for investigations of the bacteria *Listeria monocytogena* were collected. All data is tabulated in Appendix 3.

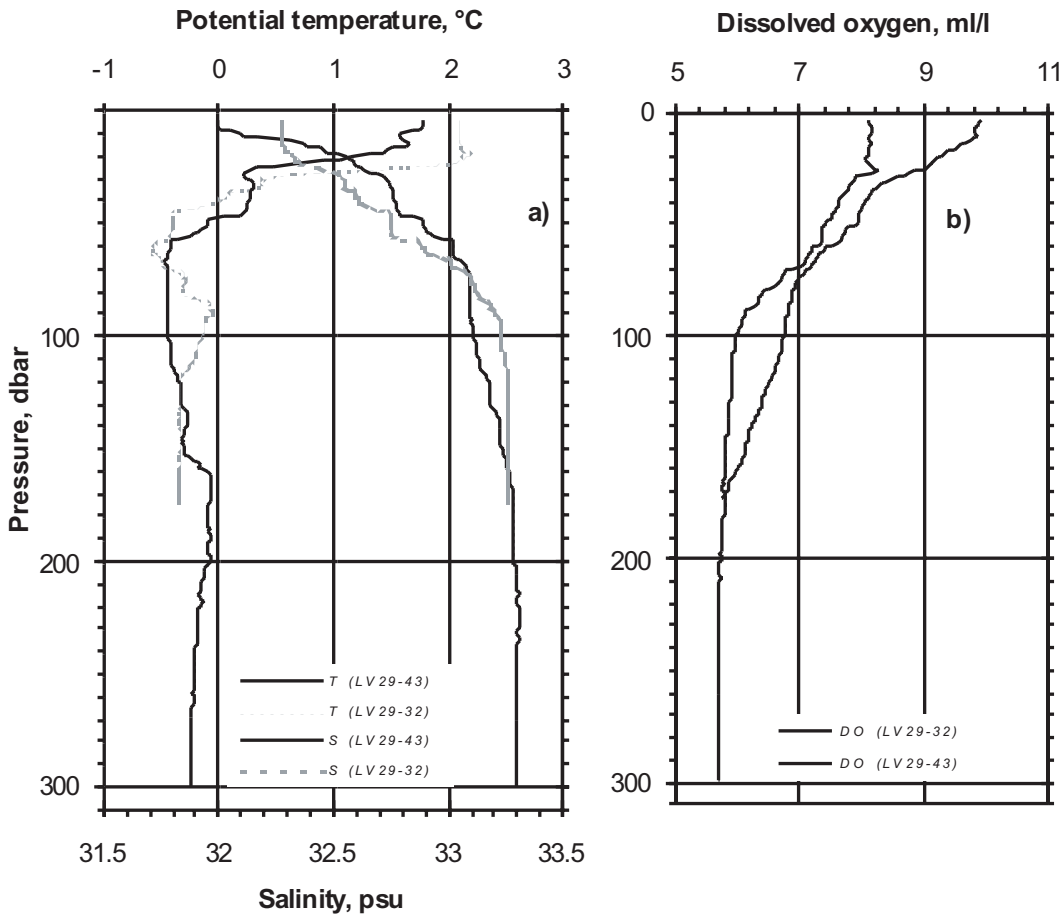

Fig. 5.1: *Vertical profiles of Potential temperature and Salinity (a) and Dissolved oxygen (b) at station LV29-43 and LV29-32.*

5.3 General hydrographic situation

The first leg of the LV29 cruise took place in spring subsequent to an anomalously warm winter season. In comparison with the analogous season of 1999, the properties of the sea water reflected warmer conditions indicated by higher water temperatures. The shelf waters had a temperature significantly above the freezing point. But winter conditions could still be observed in Terpeniya Bay. The hydrographic conditions of this area showed an anomalously intensive development of the dichothermal layer which is a product of winter cooling and of the specific circulation in this bay. The dichothermal layer was characterized by almost thermostad and halostad conditions at subsurface depths between 50-250 m.
Anticyclonic activity and meteorological conditions with calm weather dominating during Leg 1 were favorable for CTD and other observations. During the whole period of Leg 1 sea-ice fields were concentrated in the northern part of the sea as well as in the western part of the Tugur area and around northern Sakhalin. Sea-ice fields were observed on the eastern side of

Sakhalin towards 52°N. The average air temperature was 3-4°C. At the end of Leg 1, sea ice remained only in Tugur Bay.
All necessary information about the general water circulation in the Okhotsk Sea is given in the cruise reports of the KOMEX I expeditions (Biebow & Hütten, 1999; Biebow et al., 2000) and is therefore not repeated here.

5.4 Main hydrographic features

The CTD stations of Leg 1 were divided into two groups according to their purposes and geographical location: the Derugin Basin barite area and the gas hydrate and methane venting shelf and slope area. The total number of CTD stations was 32, 21 of which were carried out in the Derugin Basin and 9 in the slope area. The shipboard echosounder was used for more correct methane studies, for finding flares and for a precise positioning of the ship directly above the vent.

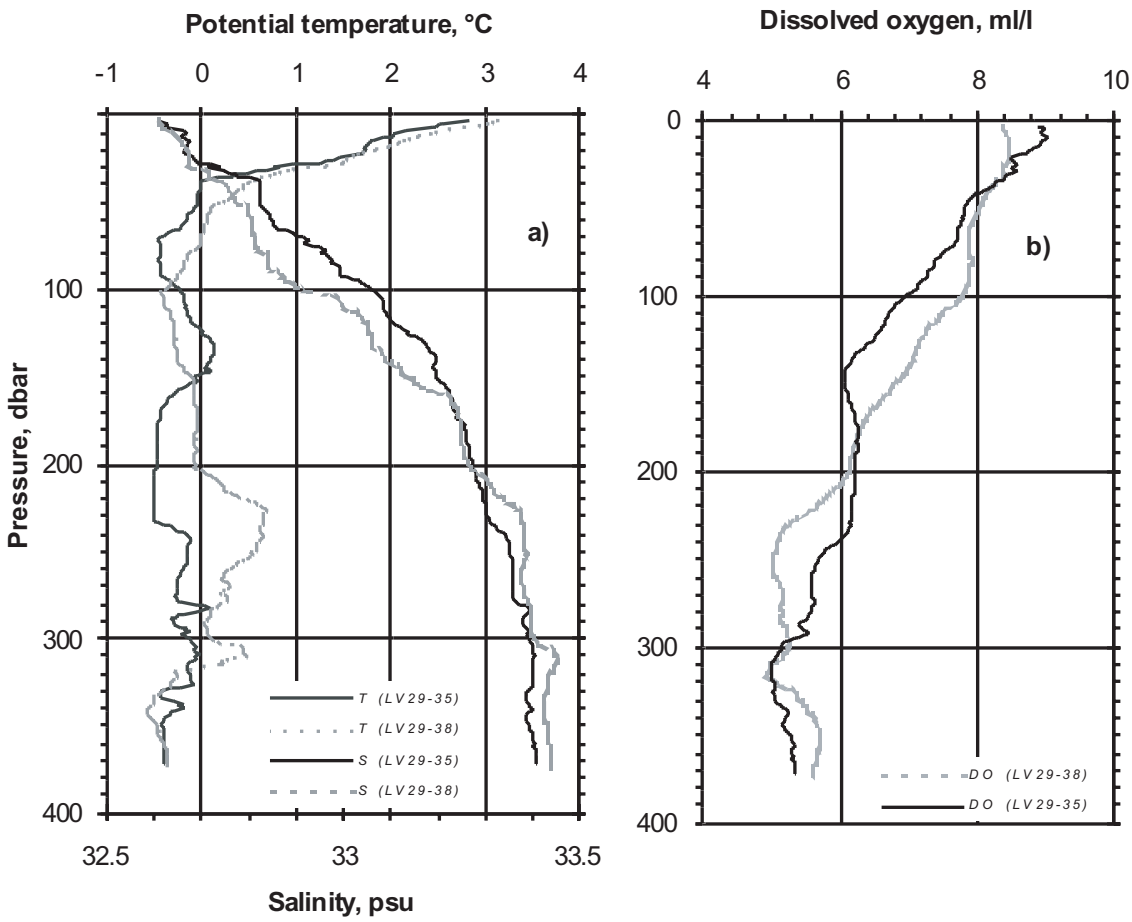

Fig. 5.2: *Vertical profiles of Potential temperature and Salinity (a) and Dissolved Oxygen (b) at stations LV29-35 and LV38.*

5.4.1 Shelf - slope area

The hydrological conditions on the shelf reflected the spring heating with positive (1.5°C) surface temperatures and negative temperatures in the homogeneous near-bottom layer (*Fig.* 5.1, station LV29-43).

Our new observations support previous conclusions from other KOMEX expeditions about an intensive mixing activity near the slope. Waters with different properties coming into this region from the northern and western shelf and from the deep sea mix and produce a lot of fine structural elements in the water column. The following comparison of two CTD stations serves as a good example for this:

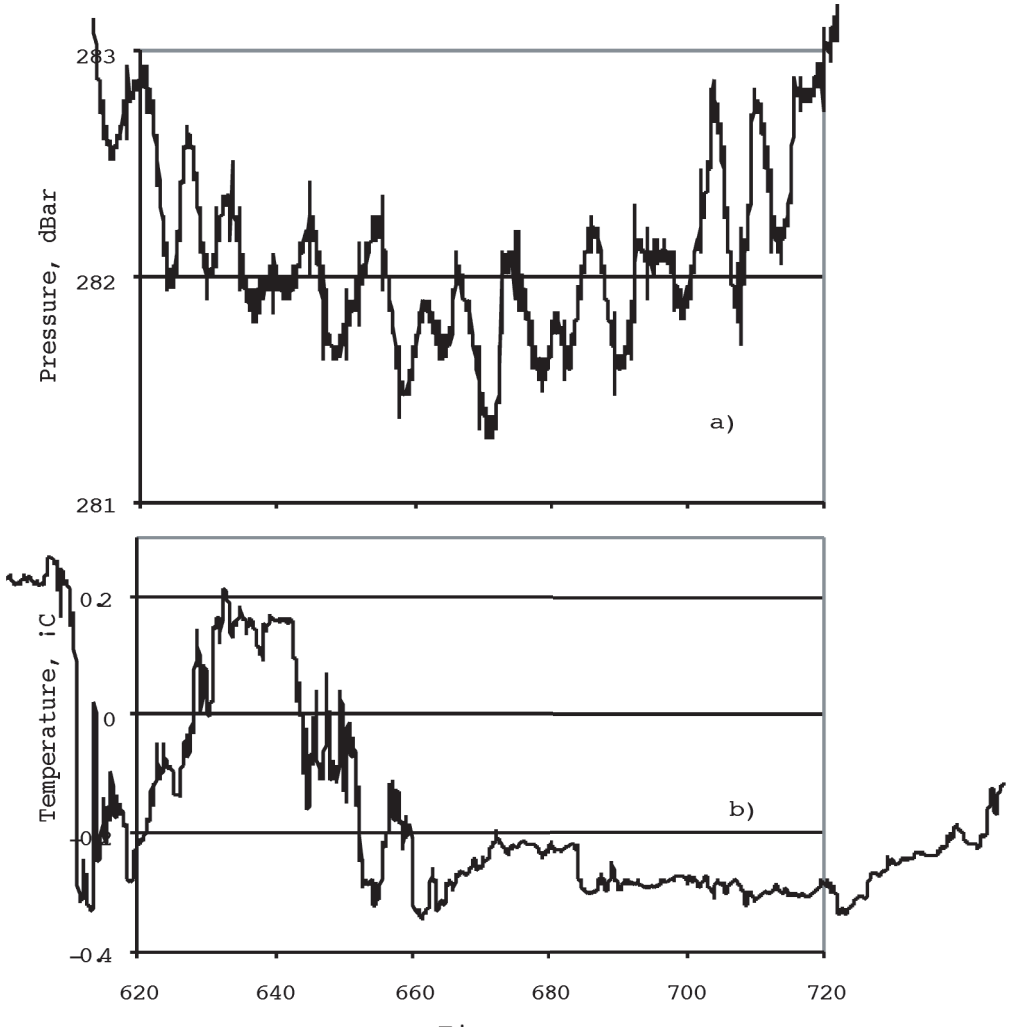

Fig. 5.3: *Temporal variability of pressure (a) and temperature (b) during a longer stop at station LV29-35, downcast.*

Two CTD deployments were carried out (station LV29-35 and -38) on the Sakhalin continental slope in the gas hydrate area ("Giselle flare"). Both stations were sampled nearly in the same location directly in the flare, but the observational results surprisingly differ from each other. Firstly, the echosounder showed different images of "Giselle flare" during the CTD casts, and significant differences in the hydrographic properties were measured. Both stations are characterized by an intense intrusion interleaving below 50 m depth. The whole water column reflects intense mixing processes (*Fig. 5.2*, stations LV29-35 and -38). The most outstanding feature was the appearance of a oxygen minimum layer at station LV29-38 at depths of 230-350 m. It is necessary to mention a very high temporal variability of the TS properties over a short time. Fortunately, we made urged temporal observations at approximately 300 m depth while waiting for the precise positioning of the ship above the vent. This record was made in the middle part of the warm intrusion at station LV29-35 (*Fig. 5.3*). During the observations the temperature values at this depth varied from -0.3°C to +0.2°C in a few seconds. The fine thermohaline structure of the warm intrusion supports the idea of an intensive mixing in the water column.

"Giselle flare" is situated in the conjunction point of two branches of the main current system of the Okhotsk Sea. One of them is the Northeast Sakhalin current along the Sakhalin coast and the other one is the northwestern periphery of the cyclonic circulation in the Derugin Basin. Additionally, tidal currents of diurnal type influence the mean flow. This is proved by the unstable character of the ship's drift during calm conditions.

Tab. 5.1: *Time of high and low sea level for place Moskalvo (53°36`N/143°30`E) nearest to cape Elizabeth (local time)*

Date	Time	Level
06/11	08:36	1.7 m
	23:31	**0.3 m**
06/12	09:12	1.8 m
	23:32	**0.2 m**
06/13	09:52	1.9 m
	23:32	**0.2 m**

Station LV29-35 was carried out on June 12th, 2002 at 22:52 p.m. local time and station LV29-38 on June 13th, 2002 at 15:07 p.m. According to *Table 5.1*, our observations were made in different phases of the tidal cycle: station LV29-35 was conducted during low water with minimum tidal currents, whereas station LV29-38 was carried out during maximum tidal currents.

The acoustic image of "Giselle flare" for the period of station LV29-35 demonstrated a straight vertical position of "Giselle flare" almost up to the surface. In contrast to this, the acoustic image of station LV29-38 demonstrated a strong inclination of the flare towards the south due to a reinforced mean flow. The flare lies almost horizontally along the bottom. By the way, this image represents the lowest inclination among all observed flares.

A possible explanation for the appearance of an oxygen minimum with regard to the temperature increase in the warm intrusion at station LV29-38 in comparison to LV29-35 might be the following: relatively warm waters with low oxygen values can be transported close to the slope from the western margin of the Derugin Basin during one tidal phase. This explanation is supported by the hydrographic properties of the offshore station LV29-47.

In order to understand these processes and their temporal variability, it would be necessary to carry out long-time observations at least in diurnal cycles.

5.4.2 Derugin Basin

A total of 21 CTD stations was carried out in the barite mineralization area in the vicinity of the "Barite Mounds". As in all parts of the sea during this time of the year, the vertical water column represented conditions of spring heating in the upper layer and a continuous ventilation (cooling) at intermediate depths. The vertical distribution of temperature and salinity indicates a well pronounced dichothermal subsurface layer. A more typical feature for all stations is the clearly expressed fine thermohaline structure (numerous intrusions of different vertical scales) in between the dichothermal layer and the intermediate temperature maximum (*Fig. 5.4*, station LV29-14). These features indicate internal interleaving, mixing and, in general, permanent ventilation and cooling of the water mass from cold surface (subsurface) layers. This means that the upper 500-600 m in the Derugin Basin do not represent a stagnant zone. Below these depths, the distribution of temperature and salinity is very monotonous up to the bottom.

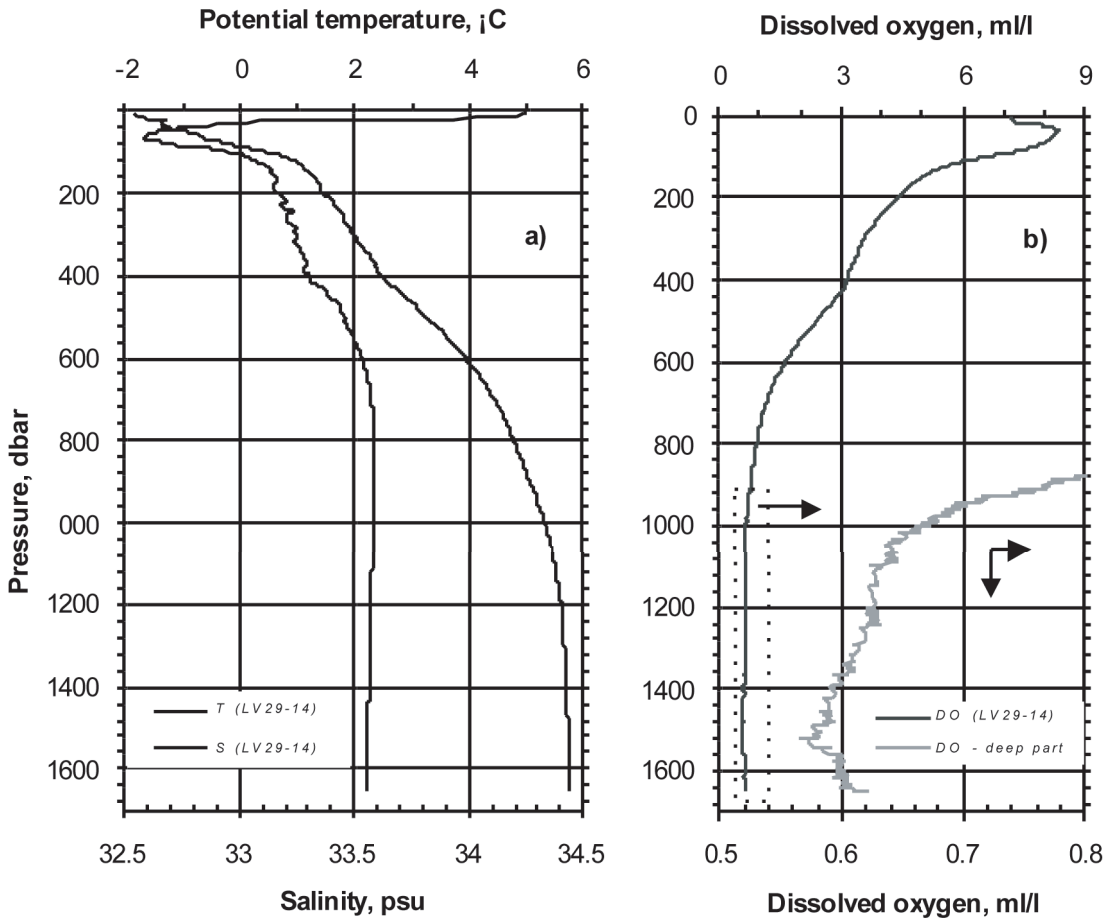

Fig. 5.4*: Vertical profiles of Potential temperature and Salinity (a) and Dissolved oxygen (b) at station LV29-14.*

Another important characteristic is the increasing oxygen concentration towards the bottom. Such features were found at almost all stations in the vicinity of the barite mineralization area. Of course, this data has to be confirmed by other chemical properties.

With regard to currents it should be mentioned that the good atmospheric conditions without wind during the observations resulted in a stable positioning of the ship without drifting.

Also, we would like to mention the phenomenon of the “red tide”, which took place during the observations. Obviously, it was caused by the spring bloom of dinoflagellates. This phenomenon was well pronounced and even led to a contamination of the CTD sensors and Niskin bottles.

6. METHANE INVESTIGATIONS

Anatoly Obzhirov and Olga Vereshchagina

6.1 Introduction

Methane was measured in the water column of the Okhotsk Sea on 6 expeditions within the KOMEX I project from 1998 to 2000 (Biebow & Hütten, 1999; Biebow et al., 2000). In this period, the following was discovered:

1. Several methane flares occur on the East Sakhalin slope and shelf. The water columns inside and near the flares contain methane concentrations from 1,000 to more than 20,000 nl/l. Methane bubbles emanate from the seafloor via fault zones rising up to 300-400 m in the slope area and up to the surface on the shelf.
2. The sources of methane are oil-gas-bearing sediments, dissociating gas hydrates and present bacteria-generating production.
3. Methane anomalies exceed the background concentration 10-10,000 times.
4. Especially in the shelf area, methane rises from the sediment via the water column and the sea surface into the atmosphere. This process intensifies in spring and autumn.
5. The flux of methane from the seafloor increases in periods of seismo-tectonic activity.
6. Water layers of the shelf containing methane anomalies intrude into water columns of the slope area.
7. Methane anomalies in the 70-100 m thick bottom water layer were found in the “Barite Mounds” area of the Derugin Basin and in other barite-bearing areas.

The main research targets of Leg 1 of RV *Akademik Lavrentyev* cruise LV29 were the following:

1. To study in detail the methane distribution in the water column in connection with methane flares on the Northeast Sakhalin shelf and slope.
2. To investigate formerly discovered flares and to find new flares on the Northeast Sakhalin shelf and slope.
3. To retrace the anomalous methane distribution of the bottom water layer (methane plume) in the “Barite Mounds” area of the Derugin Basin.
4. To compare the methane distribution in the water column with other chemical parameters.
5. To examine the source of methane in the “Barite Mounds” area.

6.2 Methods

Water samples for methane measurements were taken from Niskin bottles of the CTD-rosette without air contact. Gas was extracted from the water by a vacuum line and was analyzed by gas chromatography aboard the ship (Obzhirov, 1993). The accuracy of the hydrocarbon analyses is 0.00001%. To control the correctness of the analyses gas standards from the USA were used for calibration.

6.3 Methane distribution in the water column

6.3.1 Results

Methane concentrations in the water column of all stations are presented in Appendix 4. The stations were subdivided with respect to their location into the following groups: Terpeniya

Bay and the adjacent slope (2 stations), Northeast Sakhalin shelf and slope (8 stations), "Barite Mounds" area (21 stations).

6.3.1.1 Terpeniya Bay and slope

Station LV29-1 was carried out in an area about 20 nm to the east from stations monitored in KOMEX I. An anomalous high methane concentration was found here decreasing from the bottom water layer (1,605 nl/l, depth 74 m) to 636 nl/l at a depth of 11 m and to 99 nl/l at the surface. This is 2-3 times more than the usual methane content in Terpeniya Bay in spring except for the surface layer. At the sea surface, the methane distribution is similar to those measured during the KOMEX I investigations in this season.
Station LV29-66 is located on the slope near "Salyuk flare" about 40 nm in SW direction from station LV29-1. A high methane anomaly (2,791 nl/l) was found there at intermediate water depths (depth 137 m) and in the near-surface layer (963 nl/l, depth 50 m). Another, less high one was measured in the bottom waters (337 nl/l, depth 719 m). It is possible that the intermediate methane-containing water layer intruded from the Terpeniya Bay shelf into the water column of the slope area. As a result, a methane bubble flux formed in the bottom water of "Salyuk flare".

6.3.1.2 Northeast Sakhalin shelf and slope

The methane distribution in the water column is shown on the profile of stations LV29-39 – LV29-31 (*Fig. 6.1*).
Station LV29-31 is located on the slope at a greater depth (946 m) than the other stations of this profile. Here, the methane concentration almost equals the background concentration. Only the bottom waters (depth 946 m) contain a small methane anomaly of 192 nl/l. The methane concentration becomes less with decreasing depth and equals the background concentration at the sea surface (71 nl/l). At a water depth of 694-595 m, an intrusion was observed with a 2.5 times higher methane concentration (78 nl/l) than in the surrounding layers. It extends from the slope to the deeper part of the Derugin Basin.
Station LV29-47 was carried out at "Salomatin flare". This flare was firstly discovered during this cruise. Here, methane anomalies were found in the bottom water (1,013 nl/l, depth 863 m) and in the intermediate water layer (351 nl/l, depth 644 m). At the sea surface the methane concentration (93 nl/l) is about 20% higher than the background one.
Station LV29-29 is located in the area of "Obzhirov flare". Methane anomalies were measured here in the bottom water (468 nl/l, depth 683 m) and the near-bottom layer (3,726 nl/l, depth 674 m). Different layers from the bottom to a depth of 300 m with sharp variations in the methane concentrations from 1,300 nl/l to 35 nl/l occurred. This could be due to an irregular distribution of methane bubbles rising from the flare. In the surface layer, a background methane concentration (69 nl/l) was observed.
Station LV29-45 is located between "Giselle and Obzhirov flares". A slight anomaly of methane (269 nl/l, depth 504 m) was found here in the bottom water ascending up to a depth of 347 m. From this depth upwards, the methane concentration is at background level (60-80 nl/l), but at the surface it increases again to 129 nl/l.
Stations LV29-35 and -38 were carried out in the area of "Giselle flare": station LV29-35 almost inside the flare, station LV29-38 slightly outside. The methane anomaly of station LV29-35 is 3-10 times higher than that of station LV29-38. A maximum methane concentration was measured in both stations at a water depth of 288 m (9,338 nl/l and 2,784 nl/l, correspondingly). The methane concentrations in the bottom water (depth 372 m) strongly differ from each other 5,494 nl/l in LV29-35 and 359 nl/l in LV29-38, but in the surface water they are equal (83 nl/l).

Station LV29-43 is located between “Erwin and Giselle flares”. A methane anomaly was found in the water column from the seafloor (3,031 nl/l, depth 294 m) to a depth of 39 m (679 nl/l) and in the surface water (155 nl/l). It is likely that the observed anomalous methane concentrations in this area derived from both flares, but primarily from “Erwin flare” (from shelf to slope) and from the sediment via a fault zone.
Station LV29-32 is located almost inside “Erwin flare”. A methane maximum occurs in the bottom water (7,197 nl/l, depth 172 m). The methane concentration decreases slowly to 3,295 nl/l at 109 m depth and from this depth on sharply to 80 nl/l at 50 m depth.
Station LV29-39 was carried out in the shelf area. A methane anomaly was observed from the seafloor (3,942 nl/l, depth 123 m) to the surface (247 nl/l). Many little flares originating from oil-gas-bearing sediments are located in this area.

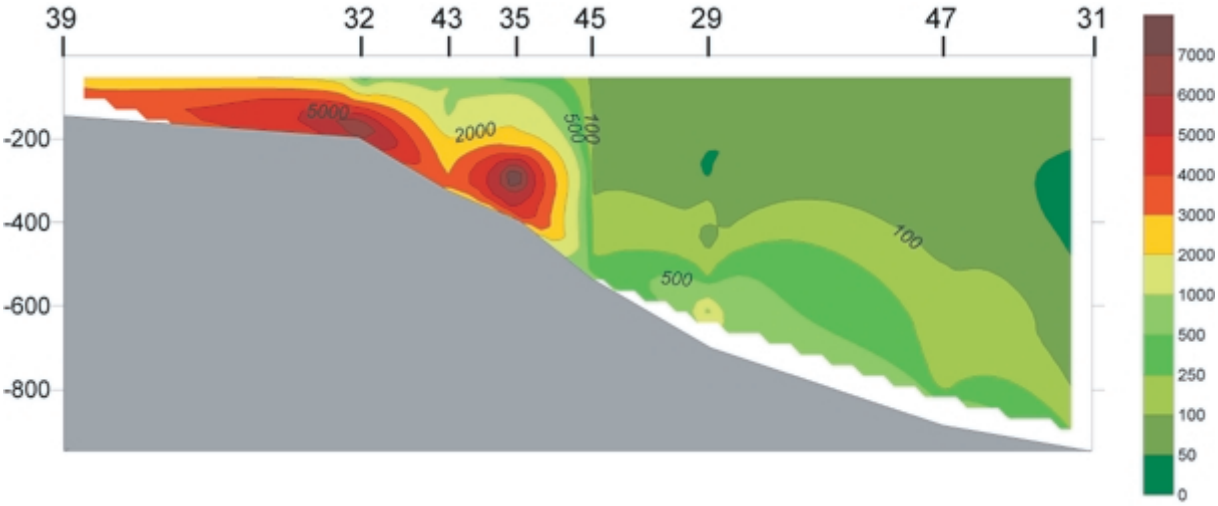

Fig. 6.1: *Methane distribution along the Sakhalin shelf and slope, stations LV29-31 - LV29-39.*

6.3.1.3 “Barite Mounds” of the Derugin Basin

In the “Barite Mounds” area, 21 stations were carried out. The methane distribution in the bottom water of this area is shown in *Figure 6.2*. A striking regularity in the methane distribution at all these stations is the presence of a thin bottom layer about 70-100 m thick with high methane concentrations of up to 1,000-6,000 nl/l. Stations LV29-2 and LV29-10 are located inside the barite-bearing area, and here, a methane anomaly was measured in the bottom water (1,213 nl/l, depth 1,478 m and 1,961 nl/l, depth 1,442 m, correspondingly). At all stations, the methane concentrations in the surface waters are almost at background level (60-80 nl/l).
During cruise GE99, a higher methane value (5,723 nl/l, depth 1,515 m) was measured in the bottom water near stations LV29-2 and LV29-10 (station GE99-32). Methane emanates via a fault zone from the sediment layers and basement rocks or from serpentine mantle rocks. Fluids enriched in barium and methane possibly rise from the earth interior to the seafloor. The change in the methane concentration of the bottom water from 1999 (GE99) to 2002 (LV29) may be caused by a changing activity of the fluid flow or by sampling in different points near the pathway of the fluid flow.
The methane investigations performed from 1998 to 2002 show that the methane plume is mostly distributed in a defined area above the barite-bearing hill which includes small sites of clams. The maxima in barite content and methane composition have an extension of about 10 x 5 nm (*Fig. 6.2*). On this cruise we investigated the area around the “Barite Mounds” in more detail. As a result, we found that the methane plume extends in N-E direction and that a new smaller plume centered in the area of station LV29-14 occurred. The methane

concentration in the bottom water of station LV29-14 amounts to 536 nl/l, and the number of barite fragments on the seafloor decreases in the aforementioned direction.

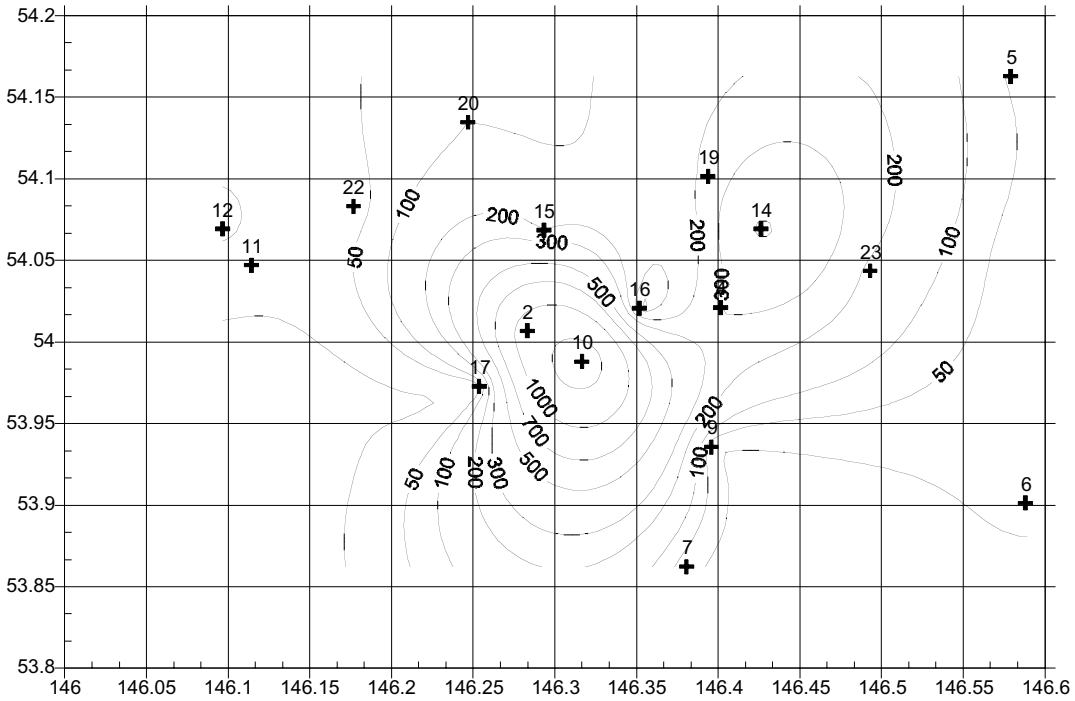

Fig. 6.2: *Methane distribution in the bottom waters of the "Barite Mound" area in the Derugin Basin.*

An unusual methane distribution in the water column was observed at station LV29-17. The methane concentration (10 nl/l, depth 1,516 m) in the bottom layer is at background level, but 100 m above the bottom the methane concentration increases to 955 nl/l (depth 1,417 m). This means that methane does not emanate from the seafloor, but is transported here by an intruded water layer possibly from the "Barite Mounds" area.
The methane distribution at station LV29-12 is different from the "Barite Mounds" plume area and therefore another small source of methane is supposed to exist in this area. There are two water layers (about 1,000 and about 500 m) with higher methane concentrations (70 nl/l, depth 990 m, and 49 nl/l, depth 495 m, respectively) than in the surrounding water column. This distribution pattern was observed at many stations in the "Barite Mounds" area, especially in its eastern part. It is possible that the two layers with higher methane concentrations intruded from the Derugin Basin. This means that methane emanates here from the seafloor and derives also from additional sources nearby.

6.3.2 Discussion

6.3.2.1 Sakhalin shelf and slope

The main objectives of these investigations are to determine the methane sources and how methane gets into the water column. There are three possible sources of methane: microbiological production, oil-gas-bearing sediments and dissociation of gas hydrates. The first one usually creates the background methane concentration in the water column – about 70-80 nl/l – in the surface as well as in the bottom water layer, if the sediment surface contains much organic matter (more than 1%), and 5-10 nl/l, if the content of organic matter is less. At the Sakhalin shelf and slope anomalous methane concentrations were found exceeding the background value 10-1,000 times (500-15,000 nl/l). Methane emanates from

oil-gas-bearing sediments and decomposing gas hydrates and migrates from the sediment into the water column mainly via fault zones.
Previous investigations (Obzhirov, 1993) and methane monitoring (Biebow & Hütten, 1999; Biebow et al., 2000) showed that the methane flux from the sediment into the water column increases in periods of seismo-tectonic activity during which the fault zones open and gas hydrates decompose. Thereby, methane gets into the water column and creates there sound-scattering flares (hydroacoustic anomalies) in the echogram. Inside the flares the methane concentration usually reaches 10,000-20,000 nl/l and more. In contrast, methane seeps from oil-gas-bearing sediment layers via fault zones into the water column without creating an hydroacoustic anomaly. In this case, a methane anomaly (500-2,500 nl/l) occurs in the bottom water and upper layers of the water column.
During Leg 1 of cruise LV29 many new flares were found. It is remarkable that they are located almost all in one line – a fault zone spreading in NE direction from the shelf to the slope and to the bottom of the Derugin Basin (*Fig. 6.3*). Some flares were observed in fissures which are crossed by the main fault. High methane contents (5,000-10,000 nl/l and more) were measured here. The methane distribution in the water column indicates that the sediment of this area is methane-enriched (oil and gas deposits and gas hydrates). Leg 1 of cruise LV29 was carried out during a period of seismic activity (June 2002) in which, for example, an earthquake happened on Sakhalin Island. Large amounts of methane rise from the sediment into the water column and the atmosphere at the Northeast Sakhalin shelf and slope. In the deeper part of the Derugin Basin the methane concentration in the water column decreases to the background level.

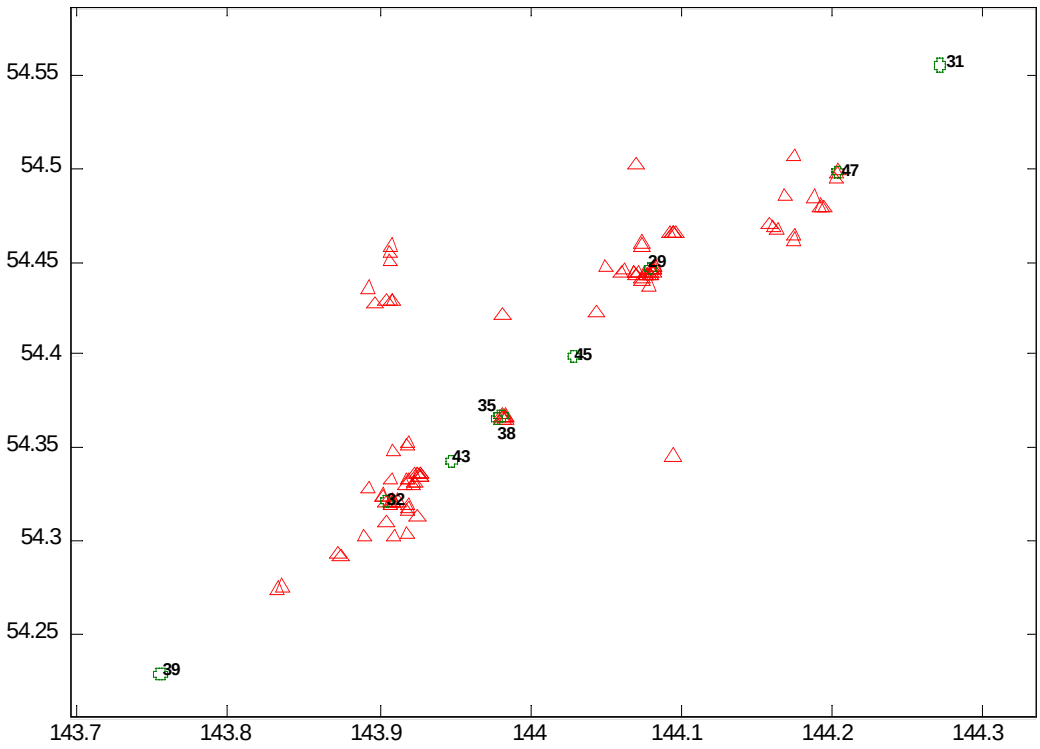

Fig. 6.3: *Map of the position of stations LV29-39 - LV29-31 and flares on the Sakhalin shelf and slope. Circles mark stations and station numbers; triangles mark flares.*

6.3.2.2 Barite area of the Derugin Basin

The source of methane in this area is yet unknown. It could be oil-gas-bearing sediment layers, metamorphic rocks of the basement, and methane derived from serpentinisation. The methane anomaly in the bottom water correlates well with the barite distribution. Therefore, it can be suggested that methane and barium rise together from the earth interior via fluid flow to the surface sediments. The area containing high barite and methane concentrations is located near a deep fault zone that goes down to the mantle (Gnibidenko, 1979). It represents the border between the Derugin Basin and the Kashevarov Rise. Stations LV29-2 and LV29-10 with methane anomalies in the bottom water are located in an area of the "Barite Mounds", where several faults extend from the interior to the sediment surface (see Chapter 4).
In this area, the top of a mantle diapir structure is located about 15-17 km below the seafloor (Gnibidenko, 1979). Several magnetic anomalies of about 3-5 nm in diameter were observed at the seafloor (see Chapter 12). There are traces of basaltic and (or) andesitic volcanic rocks near the sediment surface. The acoustic basement consists of basalt, andesite, tuff, green schists and other rocks (Gnibidenko, 1979). The green schists were formed when fluid containing methane and hydrogen passed through metamorphic rocks. In this process, barium is transported with the fluids from the metamorphic rocks and (or) from mantle rocks (basalt and andesite) to the surface thereby forming the barite chimneys. The hydrothermal processes including the barium and methane fluid flow took place several million years ago and have now ceased. Nowadays, barium is remobilized in the sediment and forms the barite crusts in the surface sediments. Clam fields are widespread in areas with methane seepage. Many dead clams were recorded by OFOS (see Chapter 9). The nowadays stable seismo-tectonic conditions in this area are possibly connected with the decreasing methane seepage.

6.3.3 Conclusions

The results of the methane investigation in Leg 1 of LV29 can be summarized as follows:

1. Many (more than 50) new flares were found in the area near "Giselle and Obzhirov flares". They create hydroacoustic anomalies at a water depth of 200-300 m above the seafloor. Inside the flares the methane concentrations amount to about 5,000-20,000 nl/l, whereas outside the flares they are about 500-3,000 nl/l.
2. The new flares are located mostly in the following line: "Erwin"-"Giselle"-"Obzhirov" from the shelf to the slope in NE direction (*Fig. 6.3*). This coincides with the orientation of a fault zone. Methane bubbles rise from oil-gas-bearing sediment layers via the fault zone and from decomposing gas hydrates into the water column and create a hydroacoustic anomaly like a flare.
3. The new flares seem to appear in the period of 2000-2002, because they were not observed in 1999 (Biebow et al., 2000). That means that this period was seismo-tectonically active. As a result, the fault zone has opened and methane emanates to the surface. The activity is confirmed by the earthquakes that happened in Sakhalin in 2000, 2001, and 2002.
4. A field with a high methane anomaly (5,000-10,000 nl/l and more) in the water column inside and outside the flares spreads from the shallow shelf to the slope at depths smaller than 400-500 m in the area of the northeast fault zone (line of stations LV29-39 – LV29-31, profiles 39-31, *Fig. 6.1*). The methane concentrations become less with increasing depth and increases only at the flares (methane vents).
5. There is a good correlation between the methane anomaly in the bottom water and the barite distribution in the "Barite Mounds" area of the Derugin Basin. Barium and methane are transported by fluid flow from the interior hydrothermal system via deep fault zones to the sediment surface. Today this area is tectonically stable, and only the methane flux continues to rise in the above-mentioned way.

6. An anomalous high methane concentration (500-2,500 nl/l) was found on the shelf and slope of Terpeniya Bay extending in SE direction. Its sources are oil-gas-bearing sediments on the shelf and possibly gas hydrates at the slope.

6.4 Methane distribution in sediment cores

The methane distribution in sediment cores was measured at 7 stations. Three stations (LV29-46, -50, -51) are located at the NE Sakhalin slope and four stations (LV29-53, -56, -59, -63) in the "Barite Mounds" area.
The main goal of this investigation was to study the methane concentration in sediment layers in areas inside and outside of gas hydrate deposits (Sakhalin slope) and inside and outside of areas with methane anomalies in the bottom water ("Barite Mounds" area).

6.4.1 Method

Two methods were used to extract the gas from the sediment: the Head Space method and the method of filling the sediment into impermeable plastic bags. Gas is taken from the bags by syringes. Gas analyzed in the gas chromatograph and methane extracted from the plastic bags are given in ppm; gas analyzed by Head Space is given in mM/kg or nl/kg. The sampling interval for gas measurement was 50 cm.

6.4.2 Results

The methane distribution in the sediment cores is presented in Appendix 4. Cores LV29-46 and LV29-50 were taken in "Obzhirov flare". Gas hydrates were sampled at station LV29-50 in the depth interval from 395 to 415 cm. The methane concentration in the upper layer from 0 to 150 cm is at background level (20-100 ppm). It sharply increases (35,000 ppm) in interval 200-250 cm and slightly decreases to the base of the core from 20,000 ppm (250 cm) to 4,000 ppm in layer 410 cm, where the gas hydrates were found. In core LV29-46 the methane concentration increases from background value (60 ppm) in interval 0-220 cm to 66,000 ppm at the base (510 cm). The methane distribution in both cores shows that the sediment in a gas hydrate area contains large amounts of methane at a depth of about 200 cm below the seafloor. Station LV29-51 is located outside "Obzhirov flare", but in an area with a new flare. The sediment in this area also has high methane contents (11,000 ppm), but less (from 400 cm) than in the gas hydrate area.
Cores LV29-53 and LV29-56 were recovered in an area with a high methane anomaly in the bottom water and a wide barite distribution at the seafloor. The sediments of these cores (especially of core LV29-56) have an anomalous high methane concentration. The concentration in the sediment of the upper layer 0-100 cm exceeds the background value about 10 times (0.004 mM/kg). The methane concentration in layer 150-250 cm is about 3.5 mM/kg. Down to the base of the core (300-600 cm) it decreases about 2-3 times. In this station sediment samples were taken by two methods: Head Space and plastic bags. A comparison of the methane distribution in the samples taken by the different methods shows that the two methods yield well correlating results.
Coring station LV29-59 is located outside the second area of barite distribution and LV29-63 inside of it. The methane anomaly (300-500 nl/l) in the bottom water is not very high, the barite crusts are thinner, and the surface sediment is stone-covered in this area. The methane concentration in all sediment cores outside station LV29-59 is at background level (0.0001-0.0003 mM/kg). The methane concentration at station LV29-63 increases from 0.0007 mM/kg (0 cm, seafloor) to 0.006 mM/kg (core base – 450 cm) and is 100 times less than at station

LV29-56 which is located in an area with a great methane anomaly in the bottom water and a wide barite distribution.

6.4.3 Conclusions

1. The methane distribution in sediment cores of the Sakhalin slope containing gas hydrates and of the “Barite Mounds” are nearly the same. The sediment cores of these areas yield high methane anomalies (about 1-3 mM/kg). It seems that the gas hydrate distribution in the sediments of the “Barite Mounds” area is the same as in the Sakhalin slope area.
2. Outside the gas hydrate and barite areas the sediment contains a background methane concentration (0.0001-0.0003 mM/kg).

7. HYDROCHEMICAL STUDIES OF THE WATER COLUMN ABOVE METHANE VENTS

Pavel Tishchenko, Galina Pavlova, Anatoly Salyuk, Valery Sosnin, Sergey Sagalayev, Natasha Khodorenko, Alexander Salomatin, Anatoly Obzhirov, Klaus Wallmann, Bettina Domeyer, and Janne Repschläger

7.1 Introduction

Currently, areas of the World Ocean in which gas hydrates occur are investigated intensively. These hydrate deposits contain enormous amounts of methane so that the upcoming shortage of fossil fuel might be overcome by the exploitation of gas hydrate reservoirs. Moreover, natural seeps increase the methane content in the atmosphere. Methane has a greenhouse effect; it therefore may play an important role in climate modulation. Monitoring of methane in the atmosphere and the study of natural sources of methane are thus necessary elements in the investigation of global warming processes. An additional interesting feature of methane venting areas are the authigenic mineral formations on the seafloor and its biological activity which develops in sediments around fluid vents.
On this cruise, we studied the carbonate system (pH, alkalinity, dissolved calcium), dissolved oxygen and nutrients in the water column above methane sources on the seafloor. The main goal of this study was to investigate the impact of methane venting on the carbonate system. Potential mechanisms, which may influence parameters of the carbonate system, are the following: a) microbiological oxidation of methane in the water column as shown by Valentine et al. (2001); b) transport of CO_2 by methane bubbles with subsequent dissolution in upper layers of the water column; c) water column mixing by a strong stream of methane bubbles.

7.2 Methods

pH measurements of sea water were carried out by means of a cell without liquid junction (Tishchenko et al., 2001; Tishchenko et al., 2002), composed of:

Glass-electrode-Na^+	test solution (standard solution)	H^+-glass-electrode

We used glass electrodes responding for hydrogen (ESL-43-G) and for sodium (ESL-51-G) ions which are manufactured by Gomel Plant (Belorussia). For the cell calibration a buffer solution of TRIS-TRIS·HCl-NaCl-H_2O (m_{TRIS}=$m_{TRISHCl}$=0.04, m_{NaCl}=0.4) was prepared. The pH values on “total” scale were calculated as:

$$pH_T = p(a_H/\gamma_{Na})_S + \frac{F\cdot(E_S - E_X)}{RT\ln(10)} + \log\left[\frac{(m_{Na})_S}{(m_{Na})_X}\right] - \log\gamma(_{Na})_X + \log\gamma(_H)_X$$

where E_S, E_X are electromotive forces of the cell in standard and test solution, respectively, and $(m_{Na})_S$ is the molality of sodium ions in standard solutions as defined in the recipe of the standard solution. The molality of sodium in test solutions (sea water) was calculated as:

$$(m_{Na})_X = \frac{13.872\cdot S}{1000 - 1.00511\cdot S}$$

Standard values of $p(a_H / \gamma_{Na})_S \equiv -\log(a_H / \gamma_{Na})_S$ in buffer solutions were tabulated previously (Tishchenko et al., 2001). The activity coefficients of sodium and hydrogen ions are also published (Tishchenko et al., 2001; Tishchenko et al., 2002). During the cruise, the formal standard potential of the usually daily calibrated cell was constant within −0.2 mV. Thereby, the error of pH_T measurements was about −0.003 pH unit.

Total Alkalinity (TA) in sea water was analyzed within 3 hours after sample retrieval by direct titration of 25 ml of sea water with 0.02 N HCl in an open cell. To remove carbon dioxide during titration the samples were flushed with a continuous stream of pure nitrogen. A mixture of methylene blue and methyle red was used as indicator, and the titration was completed when the green color of the solution turned to light pink (pH of the end point is equal to 5.4-5.5). This method is well-known as Bruyevich's method (Bruyevich, 1944) and recommended as standard operating procedure among oceanographers in Russia (Ivanenkov, 1978). The acid was standardized daily with Na_2CO_3 solution prepared from pre-weighted crystals dried at 280°C. The Brinkman/Dosimat 665 motor-driven piston burette reproducible to −0.001 ml in the delivered volume was applied for analysis. Based on analysis of sea water replicates, an analytical precision of −2.6 µM/kg (n=10) for TA was reached in this study.

Dissolved oxygen was determined by the modified Winkler method (Carpenter, 1965). Thereby, the end point was detected photometrically at a wave length of 350 nm. Automatic titration was carried out using a Dosimate burette, photometer and PC. Estimated from replicates, the precision of the oxygen analysis generally amounted to −1 µM.

Samples for *dissolved calcium* (Ca) in sea water were filled into 140 ml plastic flasks and preserved with hydrochloric acid to create pH = 2. These samples will be analyzed by complexometric titration of 10 g of sea water (Tsunogai, 1968) in the shore-based laboratory at POI. EGTA is used as titrant and GHA [glyoxal-bic (2hydroxyanil)], a sensitive reagent for calcium, is used as metal indicator at pH 11.7. Calcium is extracted into a small volume (4 ml) of organic solvent (n-Butanol) as its GHA-complex, and titrated with EGTA (9.714 mM/l). The end point is sharp and occurs when the red color of the organic layer vanishes. The EGTA is standardized daily with standard calcium solution prepared from 1.0309 g of highly pure calcium carbonate dissolved in hydrochloric acid and diluted to 1 liter after adding 13.114 g magnesium sulfate ($MgSO_4$ *7 H_2O) and 27.49 g sodium chloride. The solution is 10.30 mM in calcium, 53.20 mM in magnesium and 470 mM in sodium, as in sea water. A correction factor of 0.9946 is applied to account for Sr dissolved in sea water. The Brinkman/Dosimat 665 motor-driven piston burette reproducible to −0.001 ml in the delivered volume is applied for analysis. This method provides a precision of up to −0.1%.

Dissolved silicate was measured applying standard photometric procedures on a Perkin-Elmer Lambda 2 UV/VIS Spectrometer. A volume of 0.5 ml sample or standard was diluted to 5.0 ml with deionized Milli-Q water and 0.2 ml heptamolybdate solution. After 15 minutes, 0.2 ml oxalic acid solution and 0.2 ml ascorbic acid were added. After another 30 minutes, the blue-colored silicomolybdic complex developed and the absorbance was measured at 810 nm. A replicate analysis of the water column samples indicated a reproducibility of −3 %.

Dissolved phosphate and the sum of dissolved nitrate and nitrite (TNO) were measured using an auto-analyzer. Samples for TNO analysis were passed through a reductor column to convert nitrate into nitrite. Photometric reagents were added through plastic tubing's, and the adsorbance of the colored solutions was measured in flow-through photometric cells. A replicate analysis of the water column samples indicated a reproducibility of −10 % for both nutrients.

From each Niskin bottle, samples were analyzed for dissolved oxygen, pH, alkalinity and nutrients (silicate, TNO and phosphate). Dissolved inorganic carbon (DIC) and in situ pH were calculated using widely accepted procedures (Millero, 1995) and carbonic acid constants as suggested by Lucker et al. (2000).

7.3 Results and discussion

Hydrochemical data was collected along with hydrographic CTD data at 28 stations in three areas of the Okhotsk Sea. Two, seventeen and nine stations were conducted in Terpeniya Bay, the Derugin Basin and along the Sakhalin slope, respectively. All data is given in Appendix 3; the used abbreviations are listed in the table below.

Table 7.1: *Symbols, units, and abbreviations used in the figures and the table of hydrochemical properties.*

TA	Total alkalinity, mM/kg
NTA	Normalized total alkalinity, mM/kg (=TA*35/S)
$pH_t(15)$	PH_t measured at 15°C in "total" scale
$PH_{in\text{-}situ}$	pH at in situ temperature and pressure in "total" scale
DIC	Dissolved inorganic carbon, mM/kg
NDIC	Normalized dissolved inorganic carbon, mM/kg (=TCO_2*35/S)
pCO_2	Partial pressure of carbon dioxide, µatm
CO_3	Carbonate ion concentration, mM/kg
La	Aragonite saturation degree
Lc	Calcite saturation degree
O_2	Oxygen concentration, ml/l
AOU_b	Biological part of apparent oxygen utilization, µM/kg
SiO_2	Dissolved silica
PO_4	Dissolved phosphate (PO_4^{3-} + HPO_4^{2-} + $H_2PO_4^-$ + H_3PO_4)
TNO	Sum of dissolved nitrate and nitrite

7.3.1 Derugin Basin

The seventeen stations are situated very close to each other and from an oceanographic point of view it can be said that they are in one location (~54°N, 146.35°E). *Figure 7.1* presents the parameter profiles of the carbonate system and dissolved oxygen. The profile of normalized alkalinity shows that the consumption rate of dissolved $CaCO_3$ from sea water exceeds the rate of carbonate dissolution at water depths of 100-200 m due to biogenic $CaCO_3$ formation. Normalized alkalinity reaches a constant value (2.438 mmol/kg) at 1,430 m depth within experimental uncertainty. It is implied that biogenic $CaCO_3$ apparently does not reach the seafloor in the Derugin Basin. The saturation degree of calcite (Lc) is very low in deep water, and carbonate particles on the surface of the seafloor should dissolve. We tried to find a correlation between methane anomalies and carbonate parameters for deep-water samples but without success.

The nutrient distribution in the Derugin Basin is represented best by the dissolved nutrients measured at CTD stations LV29-11, -12, and -16 (*Fig. 7.2*). The concentrations of dissolved

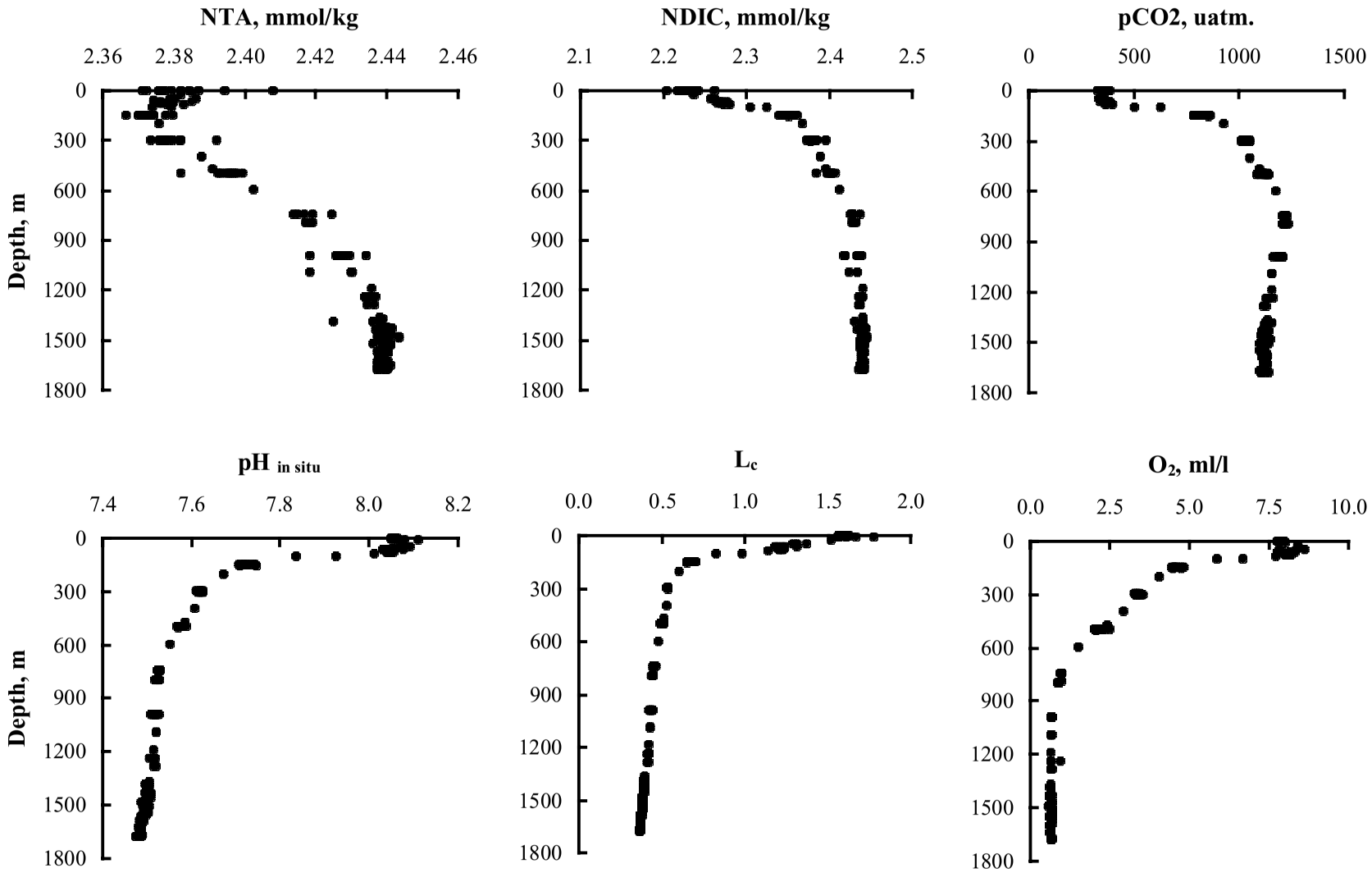

Fig. 7.1: *Profiles of normalized total alkalinity (NTA), normalized dissolved inorganic carbon (NDIC), CO_2 partial pressure (pCO_2), in-situ pH, saturation degree of calcite (L_c) and dissolved oxygen (O_2); all stations in the Derugin Basin.*

silicate decrease continuously with depth to values of up to 200 µM in the bottom waters. The concentrations of dissolved Ba in the sea water are tightly correlated with dissolved silica. Thus, the extremely high silica values also imply high concentrations of dissolved barium in bottom waters. Preliminary calculations of the saturation degree with respect to barite indicate that the bottom waters of the Derugin Basin are indeed close to saturation (Gramm-Osipov, pers. com.). Thus, the preservation of barite chimneys and precipitates in the "Barite Mounds" venting area seems to be favored by the unusually high concentrations of barium in the overlying bottom waters.

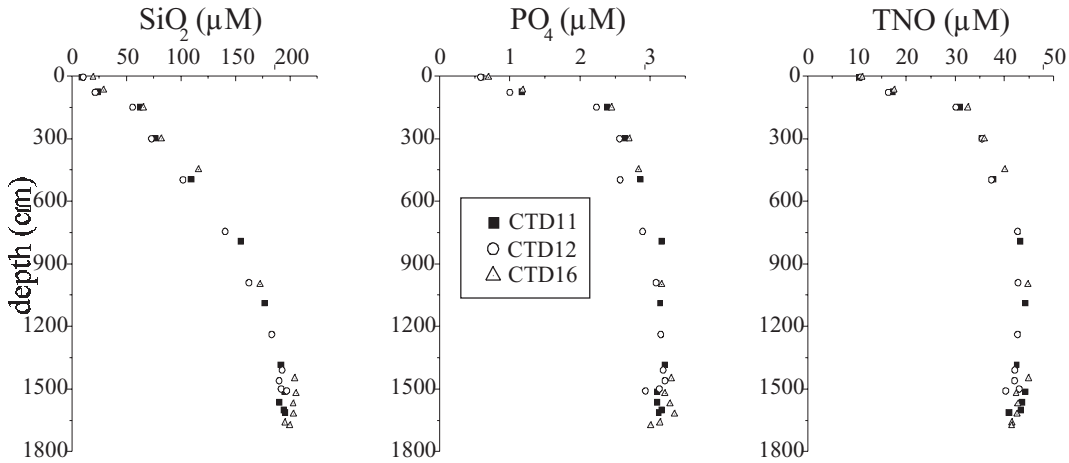

Fig. 7.2: *Profiles of dissolved silica (SiO_2), dissolved phosphate (PO_4) and the sum of dissolved nitrate and nitrite (TNO) at CTD stations LV29-11, -12 and -16 in the Derugin Basin.*

Dissolved phosphate reaches an almost constant level around 3.1 µM below a water depth of 1,000 m, whereas TNO shows a slight decrease below this depth (*Fig. 7.2*). The very low oxygen contents below 1,000 m (*Fig. 7.1*) suggest that TNO might by depleted by denitrification processes. A correlation plot of TNO versus phosphate taking into account the data of all measuring points in the Derugin Basin reveals that the average N : P ratio of the Derugin samples amounts to only 12.5 −0.3. This atomic ratio is significantly smaller than the average ratio observed in the World Ocean (15) confirming that the deep Derugin waters might have lost dissolved nitrate due to microbial denitrification. Surface waters contained rather high concentrations of dissolved silica (>10 µM), phosphate (>0.5 µM) and TNO (>10 µM) suggesting that primary production in the Derugin Basin was not limited by nutrient availability over the sampling period (June 2002).

7.3.2 Sakhalin slope

At the northeastern Sakhalin slope a field of flares is located at ~54°N. We tried to collect hydrochemical data inside "Erwin flare", "Giselle flare" and "Obzhirov flare". Additional samples were taken in between these flares, as well. The most unexpected results were obtained at stations LV29-35 and -38 situated nearest to "Giselle flare". Water samples were taken here within a lateral distance of only 160 m. The time lag between the sampling at the two stations was only 16 hours. *Figure 7.3* shows the profiles of pH and dissolved oxygen for these stations. Both parameters reveal a significant temporal variability which is also seen in the TA and dissolved silica profiles measured at the same stations (*Fig. 7.3*). Two hypotheses

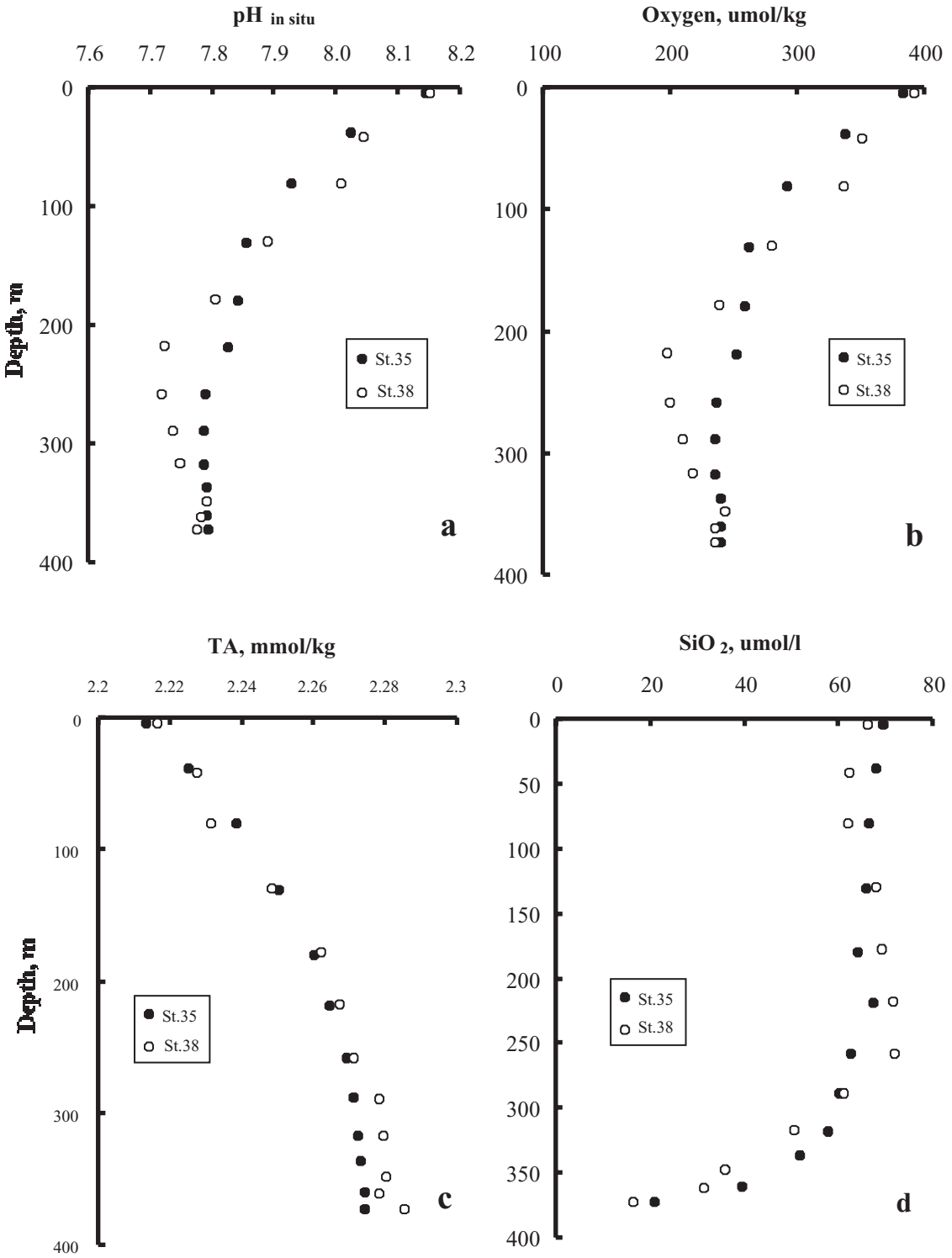

Fig. 7.3: *Profiles of pH (**a**), dissolved oxygen (**b**), alkalinity (**c**), dissolved silica (**d**) for stations LV29-35 and -38.*

have been made to explain this phenomenon. According to the first, a strong upward gas stream mixed the water column during sampling at station LV29-35. Hereafter, the water column was reconstructed so that an undisturbed water column was sampled at station LV29-38 16 hours later. The second hypothesis says that the variability is caused by other strong dynamic processes such as slope convection, tidal currents and eddy propagation. Sections of pH and dissolved oxygen show structures similar to that of the anticyclonic eddy situated near

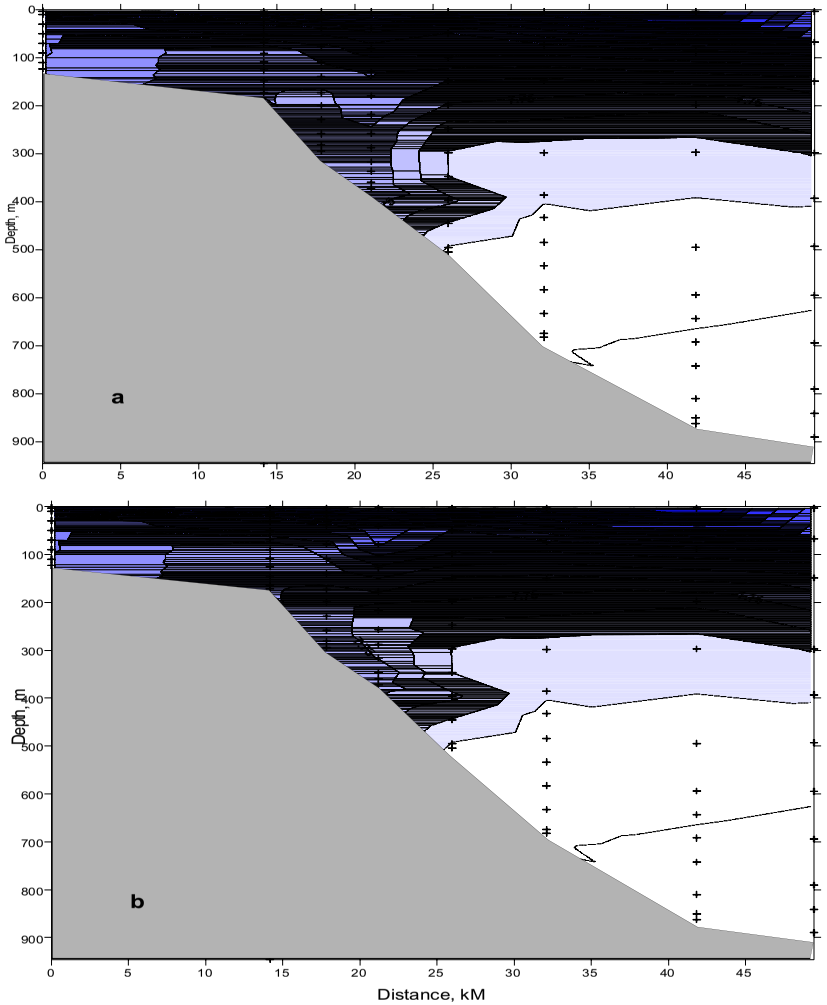

Fig. 7.4. *Sections of* $pH_{in\text{-}situ}$ *across stations LV29-29, -31, -32, -35, -39, -43, -45, -47 (**a**); and stations LV29-29, -31, -32, -38, -39, -43, -45, -47 (**b**). The deepening of isolines at central parts of the sections probably corresponds to anticyclonic mesoscale eddies*

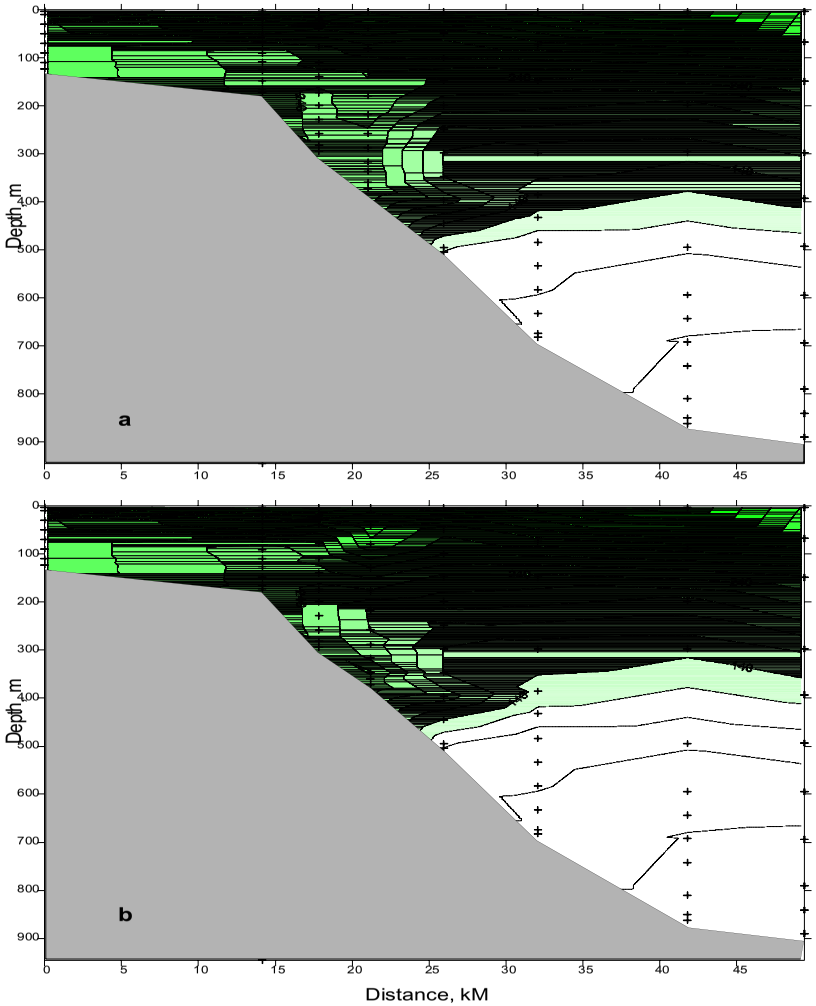

Fig. 7.5. *Sections of dissolved oxygen (µmol/kg) across stations LV29-29, -31, -32, -35, -39, -43, -45, -47 (**a**); and stations LV29-29, -31, -32, -38, -39, -43, -45, -47 (**b**).*

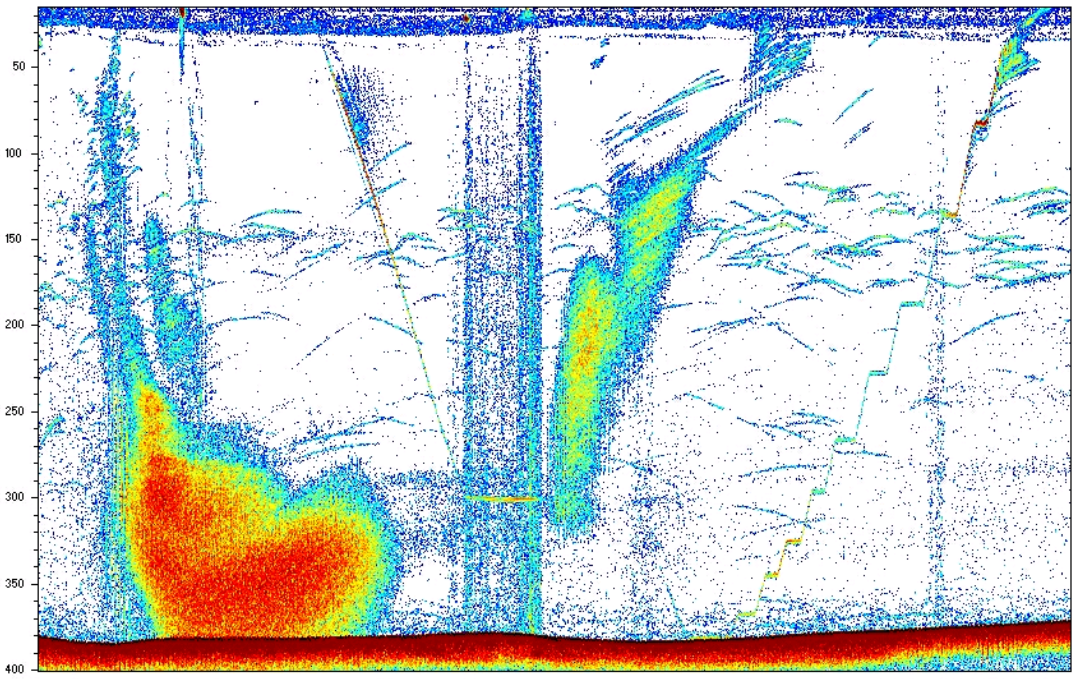

Fig. 7.6: *Acoustic images of "Giselle" Flare observed at station LV29-35.*

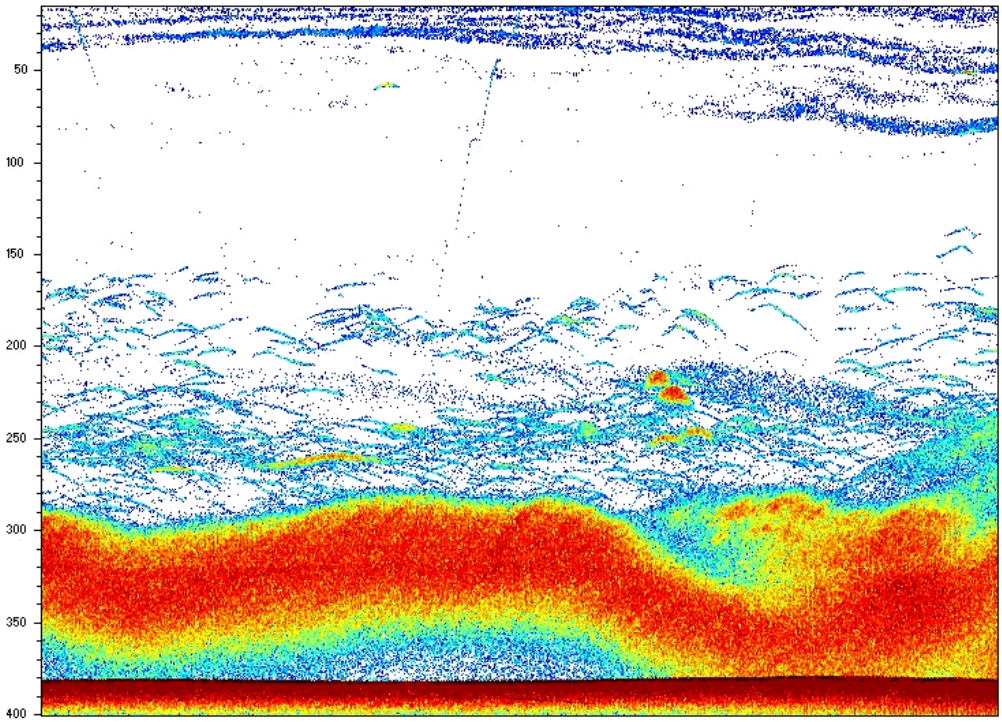

Fig. 7.7: *Acoustic images of "Giselle" Flare observed at station LV29-38.*

"Giselle flare" (*Figs. 7.4* and *7.5*). On the other hand, it is seen from *Figures 7.4* and *7.5* that fresh water penetrates along the slope near the bottom which might be regarded as an indication of slope convection. The tidal table for place Moskalvo (53°36'N/142°30'E) shows that our observations were made in different tidal phases. Station LV29-35 was conducted during low water when the tidal current is obviously nearly missing. This can be seen from hydroacoustic images of "Giselle flare" (*Fig. 7.6*). In contrast to this, station LV29-38 was carried out in the phase of maximum tidal current during which "Giselle flare" lies horizontally close to the bottom (*Fig. 7.7*). Future analyses are necessary for a final conclusion about which of the discussed processes governs the observed large temporal variability in hydrochemical parameters including the methane concentration on the Sakhalin slope.

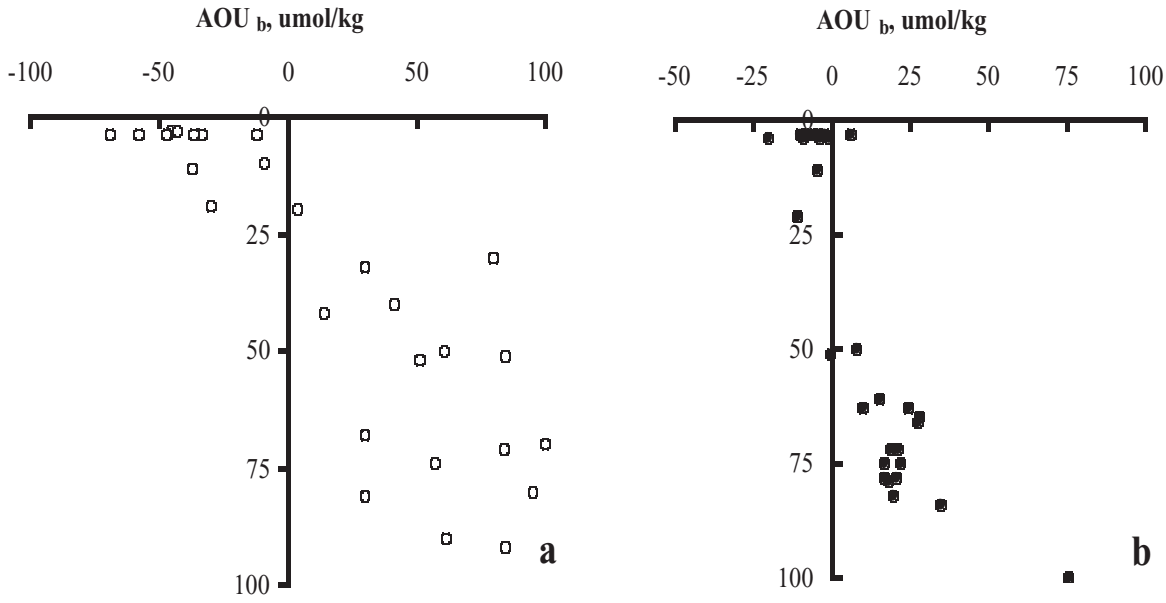

***Fig. 7.8**: Profiles of the "biological" term of apparent oxygen utilization (AOU_b) for the Sakhalin slope area (**a**) and Derugin Basin (**b**).*

The biological productivity in the upper water column is very important from a geochemical point of view, because in many cases, the main source of material for mineral formations is organic matter. There are different methods to estimate this productivity. The most simple quality estimation, the "biological" term of apparent oxygen utilization (AOU_b), was applied here (Tishchenko et al., 1998). A negative value of this parameter implies that the oxygen production by photosynthesis surpasses the oxygen consumption by respiration and oxidation of organic matter. AOU_b was calculated using data of dissolved oxygen and the measured parameters of the carbonate system. A comparison of the Sakhalin slope and Derugin Basin (*Fig. 7.8*) yields that the photosynthesis exceeds the decay of organic matter in the upper 25 m of the water column to a much greater extent on the Sakhalin slope than in the Derugin Basin. Obviously, the Sakhalin slope area is a much more productive region than the Derugin Basin.

7.4 Conclusions

Despite the high precision of our measurements, we did not find any effects of methane bubbles on the carbonate system parameters of the water column within the investigated

methane plumes. Only the exceptionally large temporal variability of hydrochemical properties of the water column in “Giselle flare” might be related to the mixing induced by gas bubbles. This variability will be subject to further investigations following this cruise.

The studied carbonate system of the water column provides useful information for the understanding of complex geochemical processes in the underlying sediments in form of the in situ pH near the bottom, the saturation degree of calcite in the water column, the character of the profile of normalized alkalinity, the estimation of the biological activity in the upper water column layer.

The nutrient data shows exceptionally high silica concentrations in the deep waters of the Derugin Basin suggesting that the bottom waters covering the “Barite Mounds” might be close to saturation with respect to barite, whereas the carbonate system data clearly demonstrate a strong undersaturation with respect to calcite and aragonite. It seems to be likely that these water properties exert a great influence on the chemical and mineralogical composition of the precipitates accumulating at the “Barite Mounds”. Moreover, the nutrient data shows that deep Derugin waters are subject to denitrification processes.

8. PORE WATER GEOCHEMISTRY

Klaus Wallmann, Pavel Tishchenko, Galina Pavlova, Bettina Domeyer, Janne Repschläger, Natasha Khodorenko, and Sergey Sagalayev

8.1 Pore water sampling and analysis

Sediment samples were squeezed in a cold room at 4°C temperature and 2-4 bar using a polypropylene apparatus pressurized by argon and equipped with 0.45 µm cellulose acetate membrane filters to separate the pore water from the sediment matrix.

Pore water samples were stored in the refrigerator at 4°C and sub-samples for sulfide determination, element analysis, and $\delta^{13}C$ measurements were taken and conserved within two hours after squeezing. Sulfide samples were conserved with 47.6 mM zinc-acetate solution, supra-pure HCl (50 µl of 30% HCl solution) was added to dissolved element sub-samples (4 ml), and $\delta^{13}C$ samples (1 ml) were given into gas-tight vials previously purged with nitrogen gas. All vials used for pore water storage were previously washed with acid and Milli-Q water to prevent sample contamination.

As pore water samples rapidly loose alkalinity and Ca during storage, these parameters were determined within some hours after sampling. The other nutrients and dissolved ions (phosphate, ammonia, silica, magnesium, and chloride) proved to be more stable and were thus analyzed during the following days.

8.1.1 Dissolved calcium

Samples for dissolved calcium (Ca) in pore water were analyzed 2-6 hours after squeezing by complexometric titration of 1 ml of pore water dispensed in 10 ml deionized water using the same procedure as with sea water analyses (Tsunogai, 1968). The correction factor concerning strontium (Sr) will be calculated after the analysis of pore water for Sr in the shore-based laboratory at GEOMAR. The Brinkman/Dosimat 665 motor-driven piston burette reproducible to ±0.001 ml in the delivered volume was applied for analysis. Based on the analysis in pore water replicates, an analytical precision of ±7 µmol/kg (n = 8) for calcium in pore water was achieved in this study.

8.1.2 Dissolved magnesium

The sea water of a salinity of 35 is approximately 0.055M in magnesium, 0.01M in calcium and 0.0001M in strontium, other divalent metals being present at the p.p.b. level. The concentration of magnesium can be derived from the total concentration of alkaline earth metals and determined calcium concentration. The total concentration of alkaline earth metals was determined by the photometric method with EDTA, with eriochrome black T as indicator. The procedure is the following: 1 ml of pore water, 5 ml of ammonium buffer, 0.1 ml indicator and 10 ml of pure water were added into a titration vessel, then a fiber optic cell was immersed into the titration vessel and the titration curve was recorded on a Brinkmann PC-2000 photometer at wave length 540 nm. The end point was calculated using the least square method for treatment of titration curve. IAPSO water with known concentrations of magnesium and calcium of 54 mM and 10.55 mM, respectively, is used as primary standard. Standard deviation of this method was found as 0.15%.

8.1.3 pH

pH is a master parameter in geochemical studies, because the solubility of minerals and the migration ability of different species are governed by this parameter. Therefore, precision and accurate measurements are highly desirable. Recently, we have shown that the main source of errors and thermodynamic uncertainty of pH measurements in the sea water is the liquid junction potential (Tishchenko et al., 2001), because commonly the cell with liquid junction is used

Ag,AgCl	Solution of KCl m≥3.5	test solution (standard solution)	H^+-glass-electrode	(A)

Owing to Pitzer's method (Pitzer, 1991) and the existence of highly stable and accurate ion selective electrodes, the cell without liquid junction has been proposed for pH measurements

glass-electrode-Na^+	test solution (standard solution)	H^+-glass-electrode	(B)

Thus, we executed Guggenheim's suggestions who wrote seventy years ago "... It must not be supposed that we mean in any way to disparage the many valuable results obtained by means of cells with liquid junctions of the type in general use for "p_H measurements". But these should be used only as a last resort and wherever possible discarded in favor of cells without liquid junctions. Thus cells of the type

$$H_2 \mid \text{solution} \mid HgCl \mid Hg\ ,$$

if the concentration of Cl^- in the solution is known, may be used to measure $C_{H^+} f_{\pm}^2$ while cells of type

$$H_2 \mid \text{solution} \mid Na\ (Hg)\ ,$$

if the concentration of Na^+ in solution is known, measure approximately C_{H+}..." (Guggenheim, 1930).

On this cruise, we measured pH in the sediments by means of cell (B). For minimizing the degassing process in the sediments, measurements were carried out in a cool room with an ambient temperature about 5°C. Sediments samples were thermostated at 5°C for stations LV29-34, -46 and at 10°C for others. The other details of pH measurements are described in Chapter 7. All pH data is listed in Appendix 5.

For discussing the quality of our pH measurements in the sediments, profiles of pH, saturation degree of calcite and alkalinity are given in *Figure 8.1*. There is a strong scatter in pH data which amounts to more than 0.5 pH unit. This scatter is not correlated with smooth profiles of alkalinity, dissolved calcium and magnesium. It is not caused by unstable work of the electrodes and pH-meter, because the same system has been used for pH measurement of sea water where the reproducibility of pH profiles in the water column in the Derugin Basin was better than 0.01 pH unit. We assumed that this scatter is caused by degassing. Station LV29-59 probably had the lowest gas content of the sediments and pH is about 7.5. For this station, the saturation degree of calcite is less than 1. But for station LV29-56 the saturation degree significantly exceeds 1 everywhere. This means that unreliable pH data has been obtained. Sediments of this core contained abundant gases. Therefore, degassing was more intensive at station LV29-56. As result of the degassing, pH shifts to the high side and pore water becomes supersaturated with regard to calcium carbonate. Apparently, the existence of some

scatters in the alkalinity profile of station LV29-56 might be caused by carbonate precipitation during core recovery.
Our final conclusion is that the pH data of the gray sediments measured aboard is unreliable. And the carbonate system of pore water might be studied only by modeling diagenesis processes using more reliable data as nutrients, alkalinity, calcium and magnesium concentrations.

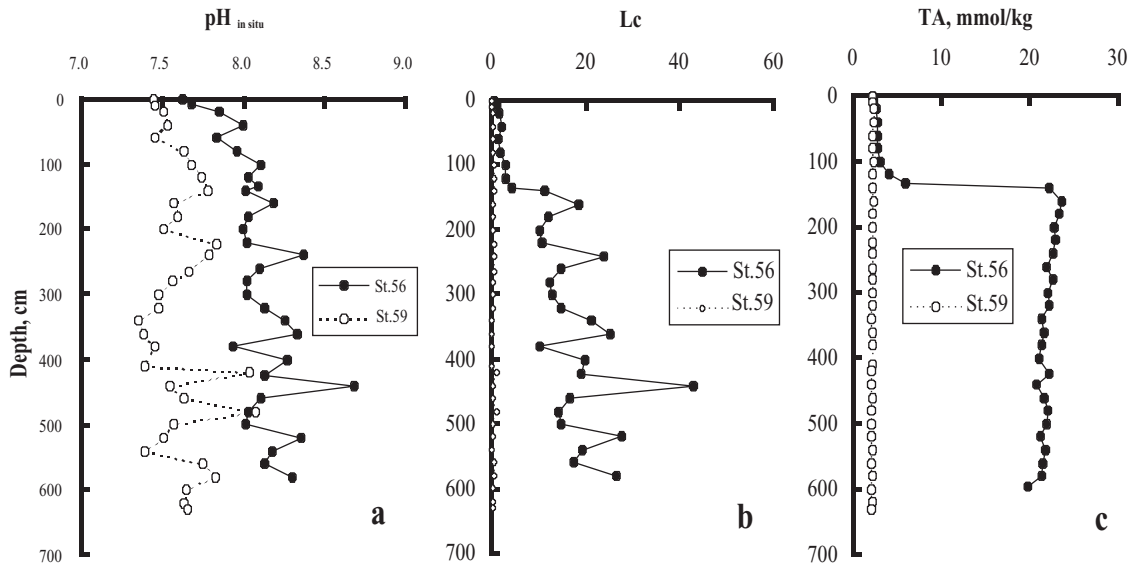

Fig 8.1: *Profiles of $pH_{in\ situ}$(**a**), saturation degree of calcite (**b**) and total alkalinity (**c**) for gravity corer stations (LV29-56-1, SL-R; LV29-59-1, SL-R).*

8.1.4 Total Alkalinity

Samples for Total Alkalinity (TA) in pore water were analyzed 2-3 hours after squeezing by direct titration of 1 ml of pore water dispensed in 10 ml deionized water with 0.02 N HCl in an open cell using the same procedure as with sea water titration (Bruyevich's method (Bruyevich, 1944)). Bruyevich's method is convenient to work with small volumes of the sample and allows to avoid the errors caused by H_2S oxidation during titration. The Brinkman/Dosimat 665 motor-driven piston burette reproducible to ±0.001 ml in the delivered volume was applied for analysis. Replicate measurements (n=8) indicated stable values, and an analytical precision of ±10 µmol/kg for TA in pore water was achieved in this study.

8.1.5 Total dissolved sulfide

Sulfide samples were conserved with zinc acetate gelatine solution (47.6 mM in Zn acetate) adding 0.1 ml solution to 1 ml oxic/suboxic pore water. For samples with intense H_2S odor, an aliquot of 0.5 ml was given into a solution composed of 4 ml Milli-Q water and 0.5 ml zinc acetate gelatine solution. The Zn-bearing solution was added to fix sulfide as colloidal zinc sulfide, whereas the water was used to inhibit ZnS precipitation. The resulting ZnS colloidal solution was mixed with 40 µl phenylen-diamin and 40 µl $FeCl_3*6H_2O$, and the absorbance was measured after 1 hour at 670 nm using a Perkin-Elmer Lambda 2 UV/VIS Spectrometer. A linear calibration curve was obtained in the concentration range of 0-57 µM $\sum H_2S$. The sulfide standard solution was titrated with sodium thiosulfate to determine the true concentration of the standard. Samples were diluted into calibration range before reagent addition.

8.1.6 Dissolved nutrients

Dissolved silicate, phosphate, and ammonia were measured applying standard photometric procedures on a Perkin-Elmer Lambda 2 UV/VIS Spectrometer. The analysis of nutrient concentrations was disturbed in anoxic samples with high ΣH_2S concentrations. Thus, sulfide-bearing samples were acidified with HCl (50 µl conc. HCl per ml sample) and stored in a cold room for two days prior to analysis. By this procedure sulfide was converted into hydrogen sulfide and transferred into the atmosphere.

Dissolved silica was determined diluting a volume of 0.5 ml sample (pore water and sea water) or standard to 5.0 ml with deionized Milli-Q water and 0.2 ml heptamolybdate solution. After 15 minutes 0.2 ml oxalic acid solution and ascorbic acid were added. The blue-colored silicomolybdic complex took an other 30 minutes to develop, before the absorbance could finally be measured at 810 nm.

For the analyses of phosphate, 2 ml of pore water sample or standard were diluted with 4 ml pure water; subsequently 0.1 ml ascorbic acid and 0.1 ml heptamolybdate reagent were added, and the absorbance was measured after 10 minutes at 880 nm.

To determine ammonia, 1 ml water sample or standard were made up to 5 ml using 4.8 ml Milli-Q water and 0.2 ml phenol solution. After 2 minutes 0.1 ml citrate buffer and 0.2 ml DTT reagent were added. After mixing, the samples were kept at room temperature protected from sunlight for about 24 hours, before the absorbance was measured at 630 nm.

Tab. 8.1*: Pore water sampling sites on cruise LV29*

Station	Location	Depth (m)	Working Area
34-1, HYC	54°19,202'N 143°54,576'E	182	Northern Sakhalin shelf, shelfbreak flare
46-1, HYC	54°26,492'N 144°04,600'E	684	Northern Sakhalin slope, “Obzhirov flare”
50-1, SL-R	54°26,811'N 144°04,870'E	695	Northern Sakhalin slope, “Obzhirov flare”
51-1, SL-R	54°28,812'N 144°11,561'E	825	Northern Sakhalin slope, deep flare
53-1, HYC	54°00,495'N 146°16,909'E	1493	Derugin Basin, “Barite Mounds”
56-1, SL-R	54°00,746'N 146°15,947'E	1470	Derugin Basin, “Barite Mounds”
59-1, SL-R	54°00,765'N 146°26,059'E	1425	Derugin Basin, “Clam Hill”
63-1, HYC	54°00,698'N 146°26,499'E	1431	Derugin Basin, “Clam Hill”

8.1.7 Chloride

Dissolved chloride was determined by titrating 0.1 ml sample dispensed in 5 ml Milli-Q water with $AgNO_3$ solution. As dissolved sulfide reacts with Ag^+ ions to form an Ag_2S precipitate, the chloride titration was performed only in aged samples with low sulfide content.

8.2 Results and discussion

Pore waters were separated from surface sediments recovered in 4 hydrocorer (HYC) and 4 gravity corer (SL(R)) deployments (*Tab. 8.1*). They were analyzed for dissolved nutrients (ammonia, phosphate, silica), alkalinity, sulfide, chloride, calcium, magnesium and pH as described in the methods section. A complete list of measured concentrations is given in Appendix 5.

8.2.1 Northern shelf and slope off Sakhalin Island

Sediments off North Sakhalin are sandy at water depths shallower than 300-400 m and silty at greater depths. They contain a terrigenous fraction delivered by Amur River and a biogenic fraction composed of biogenic opal and organic matter. Most of the fine-grained terrigenous particles delivered by Amur River are deposited at the mid-slope area inducing sedimentation rates of up to 100 cm kyr^{-1} (Tiedemann, pers. com.). Previously studied sediments from the mid-slope area (LV27-2-4, LV28-4-4, LV28-32-1, GE99 SL 24-2, GE99 SL 27-2, GE99 SL 29-3, GE99 SL 12-4, GE99 SL 26-2) have high particulate organic matter contents (1-2 wt-%) and high methane concentrations that document sulfate depletion and beginning methanogenesis at sediment depths of 3-6 m.

During cruise LV29, one sediment core was taken at the shelfbreak off northern Sakhalin within an area marked by an intense acoustic flare (HYC LV29-34-1). The core was very sandy and the pore water analysis revealed modestly reducing conditions at the core base. The low sulfide contents (<100 µM) and alkalinity values (<5 Eq. dm^{-3}) show that the sediments were not affected by gas or fluid venting at the coring site. Probably, the gas vents indicated by hydroacoustic data were missed during the coring operation.
Moreover, three sediment cores were retrieved in the northern mid-slope area (*Tab. 8.1*). Two of them were taken below “Obzhirov flare” (HYC LV29-46-1, SL LV29-50-1) where gas venting was documented on previous expeditions (Obzhirov, 1992; Biebow & Hütten, 1999; Biebow et al., 2000). One sediment core (SL LV29-50-1) contained gas hydrates that had previously been discovered at the same location by Ginsburg et al. (1993) and during the MV *Marshal Gelovany* expedition in 1999 (GE99). The top of the gas hydrate layer sampled in core LV29-50-1 was found in the core catcher at a sediment depth of 400 cm. In contrast, Ginsburg et al. (1993) found the gas hydrate top at a significantly shallower sediment depth of 30-120 cm, whereas gas hydrates were retrieved from a sediment depth of 300-320 cm during expedition GE99. The shift in the hydrate depth position is remarkable. It may either be due to a continuous deepening of the hydrate layer over the last 10 years or might be ascribed to lateral variability within the coring area. Continued hydroacoustic surveys suggest that gas venting first appeared in 1988 in the “Obzhirov flare” area (Obzhirov, pers. com.), whereas coring during GE99 recovered *Calyptogena* clam shells at various sediment depths documenting gas venting over extended periods of the Holocene. It might be envisioned that the historic venting re-started in 1988 and lost in intensity over the last decade inducing a continuous deepening of the hydrate deposition zone. Video-controlled coring and an enhanced positioning of the research vessel are needed to reveal the arial extend and structure of the venting area. Only with this enhanced data base and improved techniques, possible changes in the vent activity over time may be recorded.
One additional core (SL LV29-51-1) was taken at larger water depths north to the “Obzhirov flare” area. Here, hydroacoustic measurements showed a well developed flare and interesting seafloor structures suggesting strong venting activity. Nevertheless, the core contained no visible signs of venting such as massive carbonate crusts or gas hydrates. Thus, the venting site documented by the acoustic flare was again missed during coring.

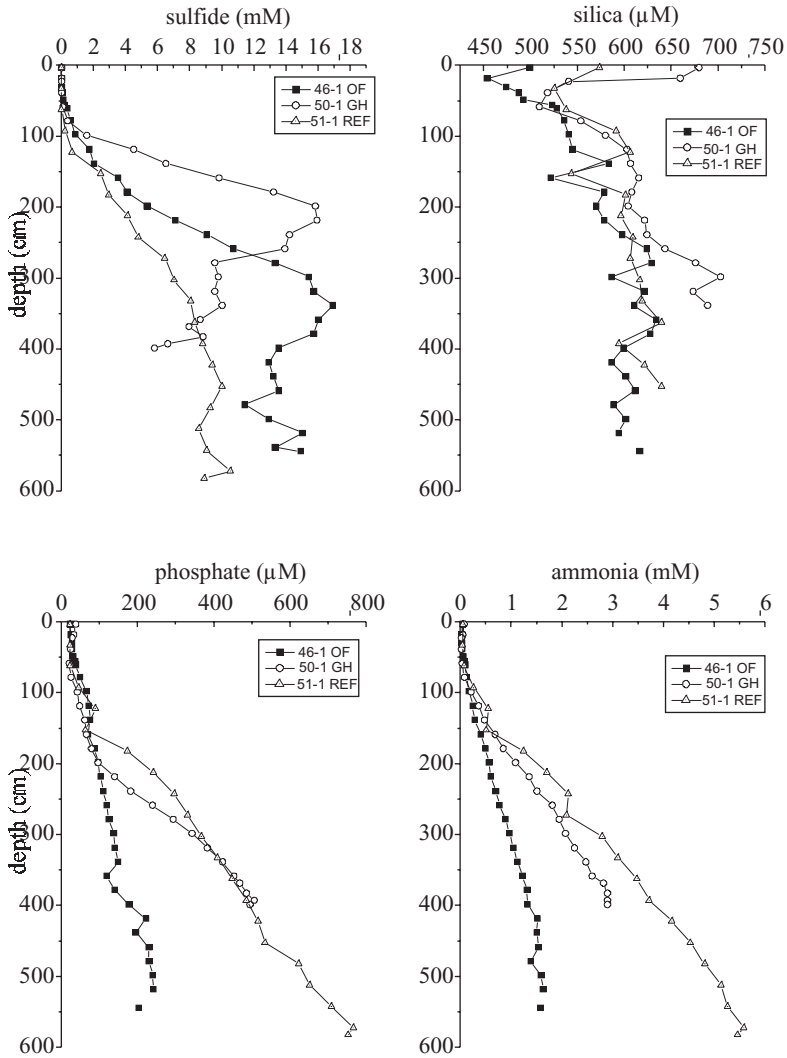

Fig. 8.2: *Concentrations of dissolved sulfide, silica, phosphate, and ammonia in Sakhalin slope sediments.*

Pore water data from the slope cores are summarized in *Figures 8.2* and *8.3*. The reference sediments taken to the north of "Obzhirov flare" (SL LV29-51-1) have high phosphate, ammonia, alkalinity, and sulfide values that document high rates of anaerobic organic matter degradation. The slope of the alkalinity profiles shows a distinct change at 400-450 cm depth that is accompanied by a sulfide maximum. This depth marks the lower boundary of the sulfate reduction zone and the upper boundary of the underlying methanogenic sediment column. Thus, methane production occurs at shallow depths in the northern mid-slope sediments as previously documented. Interestingly, the Mg concentrations begin to rise below a depth of 350 cm. The observation is surprising and might be related to de-sorption of Mg^{2+} ions from deep anoxic sediment layers caused by a change in solution composition.
In contrast to the reference core, sediments from "Obzhirov flare" (LV29-46-1, LV29-50-1) have enhanced sulfide concentrations and alkalinities in the upper 400 cm, whereas the nutrient values are generally diminished (*Figs. 8.2* and *8.3*). The hydrate-bearing core LV29-50-1 shows the highest alkalinity values accompanied by a strong sulfide maximum at shallow depth (200 cm) indicating high rates of anaerobic methane oxidation via sulfate reduction. The low Ca concentrations observed in the same core indicate intense carbonate precipitation processes.

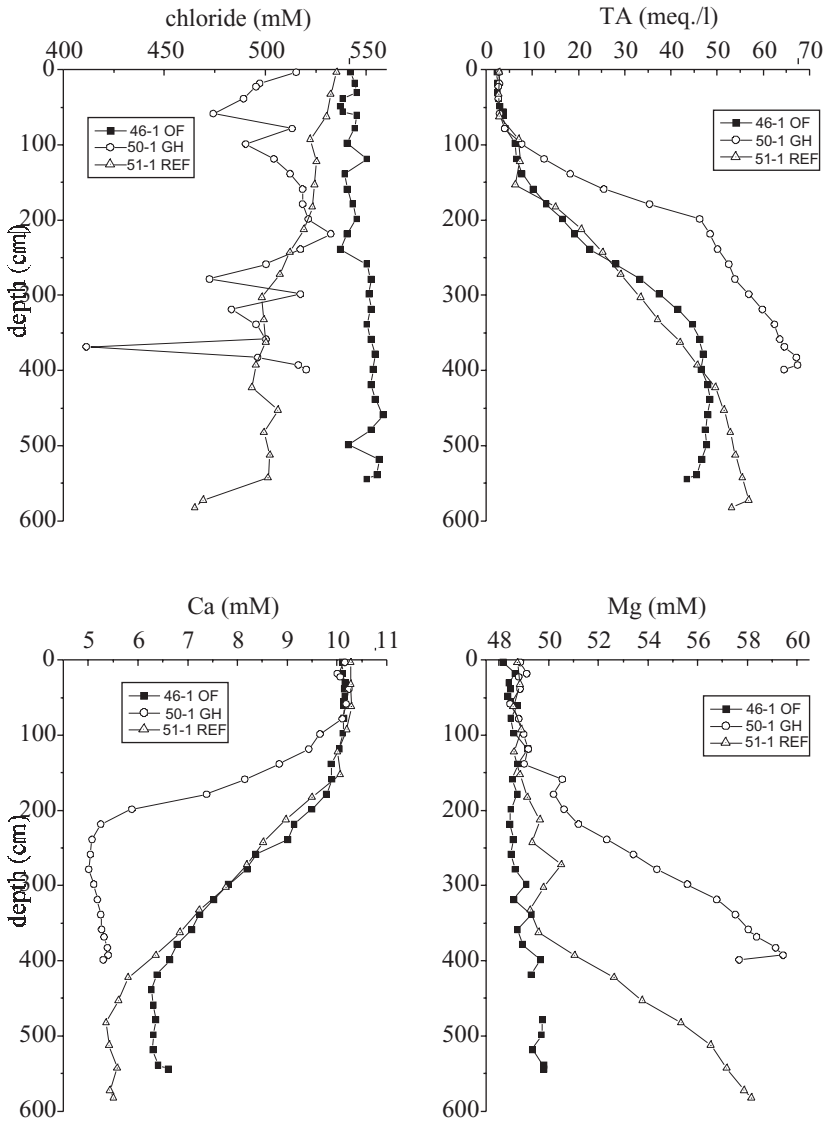

Fig. 8.3: *Concentrations of dissolved chloride, total alkalinity, calcium, and magnesium in Sakhalin slope sediments.*

A transport-reaction model was developed to simulate the processes occurring in the slope sediments. In this model, dissolved species are transported via bio-irrigation, molecular diffusion and burial, whereas solids are transported by burial only.

The model considers variable sediment porosity's as determined in cores taken during previous expeditions and depth-dependent transport coefficients. It simulates the distribution of two solid species (reactive POC, refractory POC) and six dissolved species (NH_4^+, SO_4^{2-}, CH_4, CO_2, HCO_3^-, Ca^{2+}) following the general approach outlined in Boudreau (1996), Luff et al. (2000), and Luff & Wallmann (subm.). The reactions and kinetic rate laws used in the model are summarized in *Table 8.2*. The model was implemented using MATHEMATICA Version 4.1. In this commercially available software, the system of coupled differential equation describing the depth profiles of solid and dissolved species is solved using the Method-of-Lines-Code, a finite difference procedure successfully used in previous models of early diagenesis (Boudreau, 1996; Luff et al., 2000).

Tab. 8.2: *Reactions and kinetic rate laws considered in the transport-reaction model for anoxic slope sediments.*

Degradation of particulate organic matter

via sulfate reduction: $2\ C(H_2O) + SO_4^{2-} \Rightarrow HCO_3^- + HS^- + CO_2 + H_2O$
via methanogenesis: $2\ C(H_2O) \Rightarrow CH_4 + CO_2$

Rate laws:
$R_{POC} = k_1 \times C_1 + k_2 \times C_2$
$R_{SO4} = 0.5 \times f_{POC} \times R_{POC} \times [SO_4^{2-}]/(M_{SO4} + [SO_4^{2-}])$
$R_{CH4} = 0.5 \times f_{POC} \times R_{POC} \times M_{SO4} /(M_{SO4} + [SO_4^{2-}])$
$R_{HS} = R_{SO4}$
$R_{CO2} = R_{SO4} + R_{CH4}$
$R_{HCO3} = R_{SO4}$
$R_{NH4} = (16/106) \times f_{POC} \times R_{POC}$

where R_{POC}, R_{SO4}, R_{CH4}, R_{HS}, R_{CO2}, R_{HCO3}, R_{NH4} are rates of POC degradation, SO_4^{2-} reduction, CH_4 formation, CO_2 formation, HS^- formation, HCO_3^- formation and NH_4^+ production, respectively. C_1 and C_2 are concentrations of reactive and refractory POC, k_1 and k_2 are the corresponding kinetic constants, f_{POC} is a function converting POC degradation rates from units wt-% POC yr^{-1} into units of µmol POC cm^{-3} yr^{-1}, $[SO_4]$ is the dissolved sulfate concentration, and M_{SO4} is a Monod constant (= 1 mM SO_4).

Anaerobic oxidation of methane

$CH_4 + SO_4^{2-} \Rightarrow HCO_3^- + HS^- + H_2O$

Rate law: $R_{SM} = k_{SM}\ [CH_4] \times [SO_4^{2-}]$

with k_{SM}: kinetic constant, []: concentrations in $mmol/dm^3$.

Carbonate precipitation

$Ca^{2+} + HCO_3^- \Rightarrow CaCO_3 + CO_2 + H_2O$

Rate law: $R_P = k_P \times (L_C - 1)$

with $L_C = [HCO_3]^2 \times [Ca]/([CO_2] \times K_{SP})$

where R_P is the carbonate precipitation rate, k_P is a kinetic constant, L_C is the saturation index with respect to calcite, and K_{SP} is the solubility product of calcite.

The model was first applied to sediment core LV29-51-1 to simulate the processes in slope sediments not affected by gas or fluid venting. The modeling procedure started with the simulation of POC and ammonia profiles. The kinetic constants of organic matter degradation (k_1 and k_2) and the penetration depth and intensity of non-local transport were varied until the resulting model curves fitted the available data. POC measurements in slope sediments cored during previous expeditions showed that the POC contents are close to 2 wt-% at the surface and decrease to 1.5 cm at 4-6 m sediment depth. These concentrations and the exponential decrease in POC concentrations observed in previous cores were taken as constraints to the model POC curve. Ammonia profiles were fitted to the data measured in core LV29-51-1 as

shown in *Figure 8.2*. Subsequently, the methane concentration at the base of the model column and the rate constant of anaerobic methane oxidation were varied until the calculated dissolved sulfide profile fitted the measured data. Finally, the rate constant for carbonate precipitation was varied to reproduce the measured Ca data. As a further control to the model results, the measured TA profiles were compared to the sum of HCO_3^- and HS^- concentrations calculated in the model.

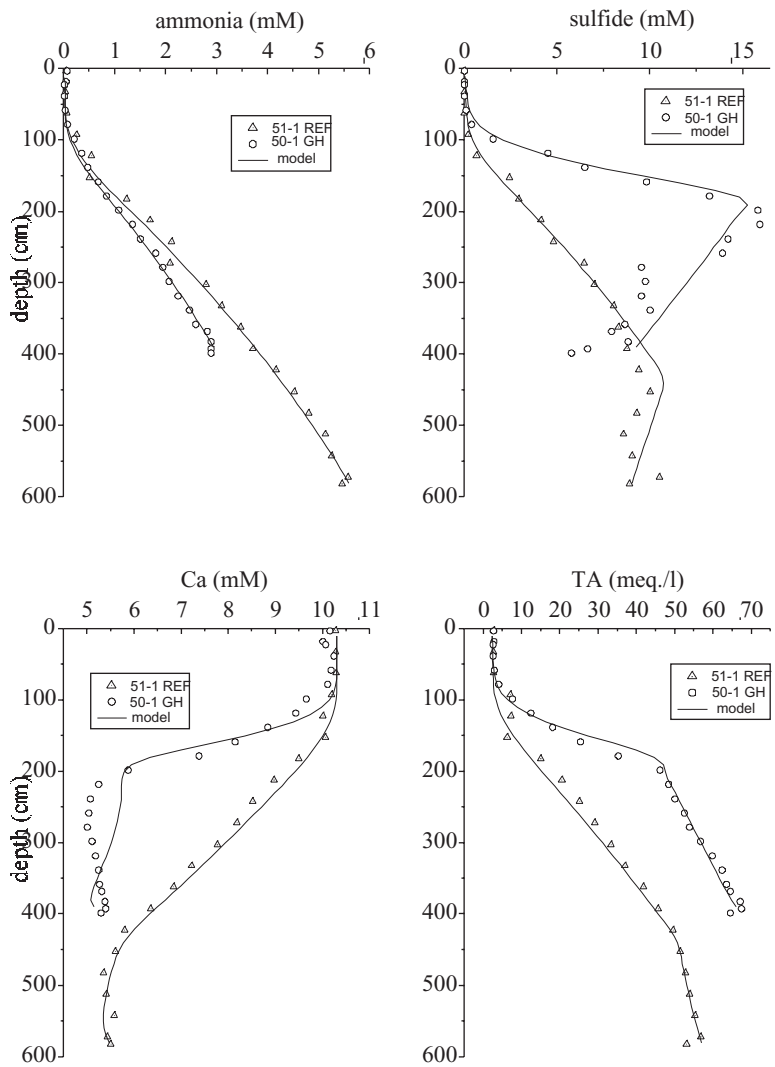

Fig. 8.4: *Dissolved ammonia, sulfide, calcium, and magnesium concentrations in sediment cores 51-1 and 50-1. Data versus model results.*

Figure 8.4 shows that the measured profiles were reproduced well by the model. The model results plotted in *Figure 8.5* indicate methane production below a sediment depth of 430 cm due to organic matter degradation and a methane concentration of 6 mM at the core base. The pore water data and the model thus confirm that methane is produced in sediments throughout the mid-slope area off North Sakhalin Island. Seismic measurements reveal a well developed BSR across the continental margin off North Sakhalin Island and thus demonstrate the presence of gas hydrates and free gas in the investigation area (Wong, 1999). Due to the extremely high input of organic matter and fast sedimentation, gas bubbles and gas hydrates are to be expected at shallow sediment depth. As the overlying sulfate reduction zone is rather thin (3-6 m), methane may escape into the bottom water throughout the northern mid-slope

area. The high methane background concentrations in bottom waters off North Sakhalin Island (Obzhirov, pers. com.) may be caused by an extended and diffuse input of methane from underlying sediments.

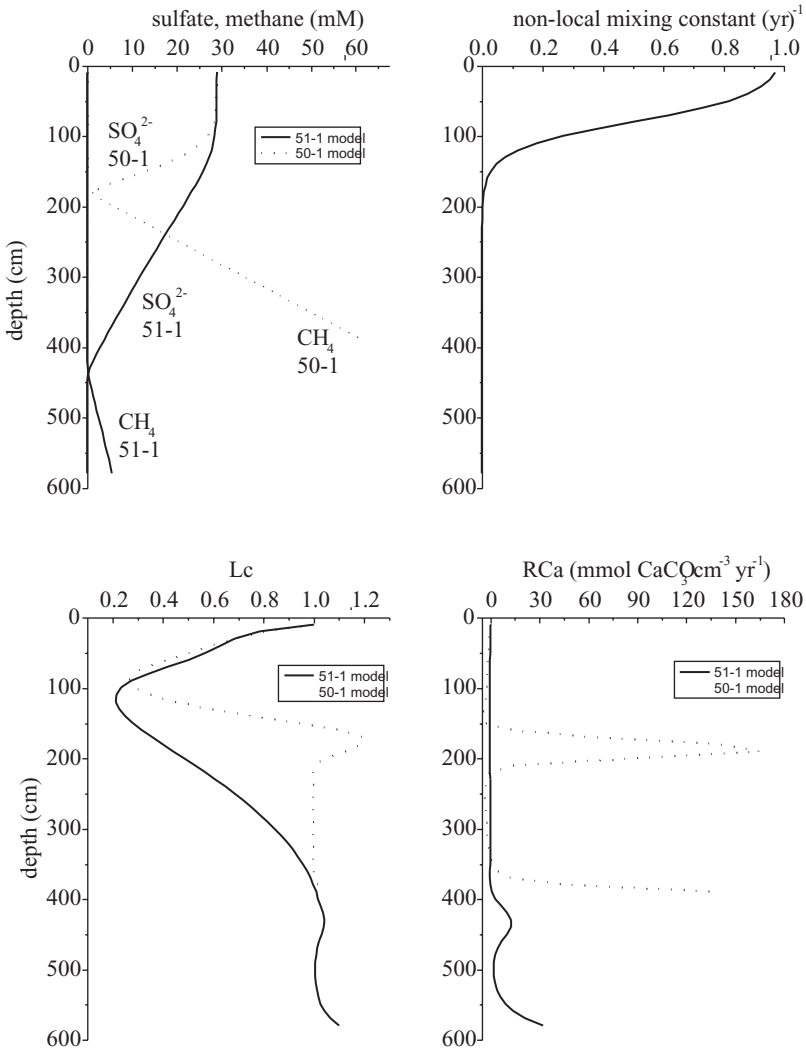

Fig. 8.5: *Results of the transport-reaction model applied to sediment cores LV29-51-1 and -50-1. Concentrations of sulfate and methane, depth-profile of the non-local mixing constant, saturation state with respect to calcite (Lc), and rate of calcite precipitation (RCa).*

Moreover, the model strongly suggests that the upper 150 cm of the sediment column were affected by non-local mixing processes (*Fig. 8.5*). The mechanisms responsible for this mixing are unknown. The mixing might be induced by deep-dwelling benthic infauna or might be caused by gas bubbles rising through the upper sediment layers. It induces a rapid exchange with the overlying bottom waters and thereby a strong nutrient depletion in the upper sediment horizons. Sediment cores from the Sakhalin slope retrieved during the previous LV28 and GE99 expeditions also had a depleted surface layer with unusually low nutrient contents overlying undisturbed and nutrient-rich sediments indicating that this distribution is a characteristic feature of the studied area.

According to the model, the pore fluids are close to saturation with respect to calcite (*Fig. 8.5*). The upper layers are undersaturated due to the CO_2 release upon microbial sulfate reduction and $CaCO_3$ precipitation, whereas the deeper layers are oversaturated due to the anaerobic oxidation of methane. The model result is also affected by the different molecular

diffusion coefficients of CO_2 and HCO_3^-. Thus, dissolved CO_2 diffuses much faster than HCO_3^- so that CO_2 escapes more rapidly towards the surface to induce undersaturation in the upper sediment horizons. The low saturation values produced by the model are more realistic than the extremely high values derived from pH measurements (*Fig. 8.1*). The rates of carbonate precipitation shown in *Figure 8.5* may thus be regarded as a realistic estimate even though the carbonate system implemented in the model has been strongly simplified to save computation time. A more sophisticated model (C.CANDI, Luff & Wallmann (subm.)) will be applied to the data during the shore-based analysis to derive well defined precipitation rates and pH values.
The model was also applied to the gas hydrate-bearing sediment core LV29-50-1 using the same parameter values as before. Only, the concentrations at the upper and lower boundaries of the model column were adjusted to reproduce the measured data. *Figure 8.4* shows that the model curves fitted the data very well even though no fluid advection was considered in the model. Thus, the model results confirm that the "Obzhirov flare" sediments are not affected by fluid venting but rather by gas venting. The resulting methane concentration at depth (62 mM, *Fig. 8.5*) is close to the theoretical concentration in equilibrium with gas hydrate for ambient pressure and temperature conditions again confirming the validity of the model approach. The model strongly suggests that the distribution of pore water species above the hydrate horizon is mainly controlled by the release of methane from hydrates and the diffusive transport of methane towards the sediment surface. Moreover, carbonate precipitation proceeds at a high rate where the upwards diffusing methane meets the sea-water sulfate infiltrating the sediments from above. The upper 150 cm of the sediment column are again affected by non-local mixing presumably induced by rising gas bubbles (Haeckel, pers. com.).

The vigorous gas venting at "Obzhirov flare" may be related to fractures that can serve as gas conduits and are reported to cut through the sedimentary deposits of the northern slope area. The source depth of the rising gas is currently unknown. The gas hydrates recovered by Ginsburg et al. (1993) are of biogenic origin (C_1/C_2 ratio 37 000, $\delta^{13}C$ = -64.3‰, δD = -207‰). Thus, it may be concluded that the oil and gas deposits off Sakhalin Island that are presumably of thermogenic origin are not the major source of the venting methane gas. It seems likely that the gas-bearing sediments below the BSR are the most important gas reservoir taped in the "Obzhirov flare" area. These sediments are located several hundreds of meters below the sediment surface but well above the deep gas deposits commercially exploited at the Sakhalin shelf and slope. Additional methane may be extracted from the extended Holocene sediment cover which generates methane at shallow depths.

8.2.2 Derugin Basin

Four sediment cores were recovered from the Derugin Basin on cruise LV29. Core LV29-53-1 was retrieved close to a site where barite- and fluid-bearing sediments were recovered during the previous GE99 expedition (core GE99-32-2). Core LV29-56-1 was taken at the base of the slope of the "Barite Mounds" where an OFOS survey revealed extended fields of *Calyptogena* and isolated barite build-ups. Both cores (LV29-53-1 and LV29-56-1) contained gas-rich sediments with a strong H_2S odor below sediment depths of 300 cm and 100 cm, respectively. The gas-rich sediments contained abundant crusts and authigenic precipitates of carbonate and barite. Cores LV29-59-1 and LV29-63-1 were taken at the slope of the "Clam Hill", an elevation situated east of the "Barite Mounds". Core LV29-59-1, which was taken further up the mound, showed no signs of venting and may thus be regarded as a reference sediment affected only by early diagenetic processes. Core LV29-63-1 was taken at the lower slope where a previous OFOS survey revealed dense and extended clusters of *Calyptogena*

clams. It contained sulfide-rich sediments at the base, again reflecting the upward flow of reducing fluids.

Core LV29-59-1 may be used to characterize the diagenetic processes prevailing in the Derugin Basin (*Figs. 8.6* and *8.7*). Previous studies showed that the Derugin Basin is the least productive area of the Okhotsk Sea and has sedimentation rates which are one magnitude order lower than at the Sakhalin shelf and slope (Biebow & Hütten, 1999). The nutrient and sulfide data confirms these results showing that organic matter degrades only very slowly within the sediment. Thus, ammonia, phosphate and sulfide concentrations are orders of magnitude lower than at the Sakhalin slope and are comparable to pore water data found in deep-sea environment. Chloride, alkalinity, Ca and Mg concentrations remain close to ambient sea-water values confirming the low diagenetic activity in these reference sediments (*Fig. 8.7*). The sulfide-bearing fluids at the bases of cores LV29-53-1, LV29-56-1, and LV29-63-1 are, thus, not formed in their present environment but at greater depths.

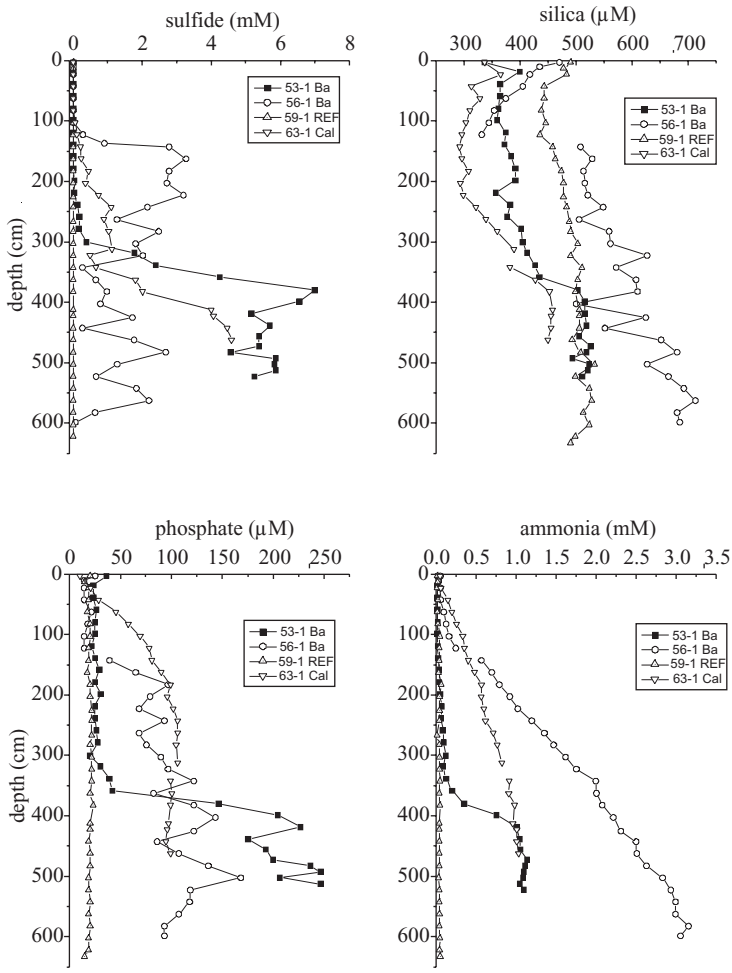

Fig. 8.6: *Concentrations of dissolved sulfide, silica, phosphate, and ammonia in sediment pore waters from the barite area.*

The most unusual concentrations and profiles were found in the gas-bearing sediment core LV29-56-1. Here, the chloride and magnesium concentrations were extremely low below sediment depths of 140 cm and increased sharply to sea-water values at 140-120 cm depth. The low concentrations indicate a deep origin of the fluids. They may be diluted with fresh water released from sediments by the diagenetic de-watering of biogenic opal and via

smectite-illit transformation. The chloride values were biased by a malfunction of a pipette, whereas the Mg data are of very high quality. The latter data shows little scatter and thus suggest that the freshening is not due to the dissociation of gas hydrates during core recovery. Hydrates were not found in the sediment core even though the presence of small amounts of micro-hydrates can not be discounted. The extreme gradients at 120-140 cm depth may again be caused by rapid non-local mixing in the surface sediments as already observed in the Sakhalin slope sediments. A rapid exchange with bottom waters is also suggested by the low dissolved-silica concentrations which are even more depleted than in the diagenetically almost inert reference core LV29-59-1.

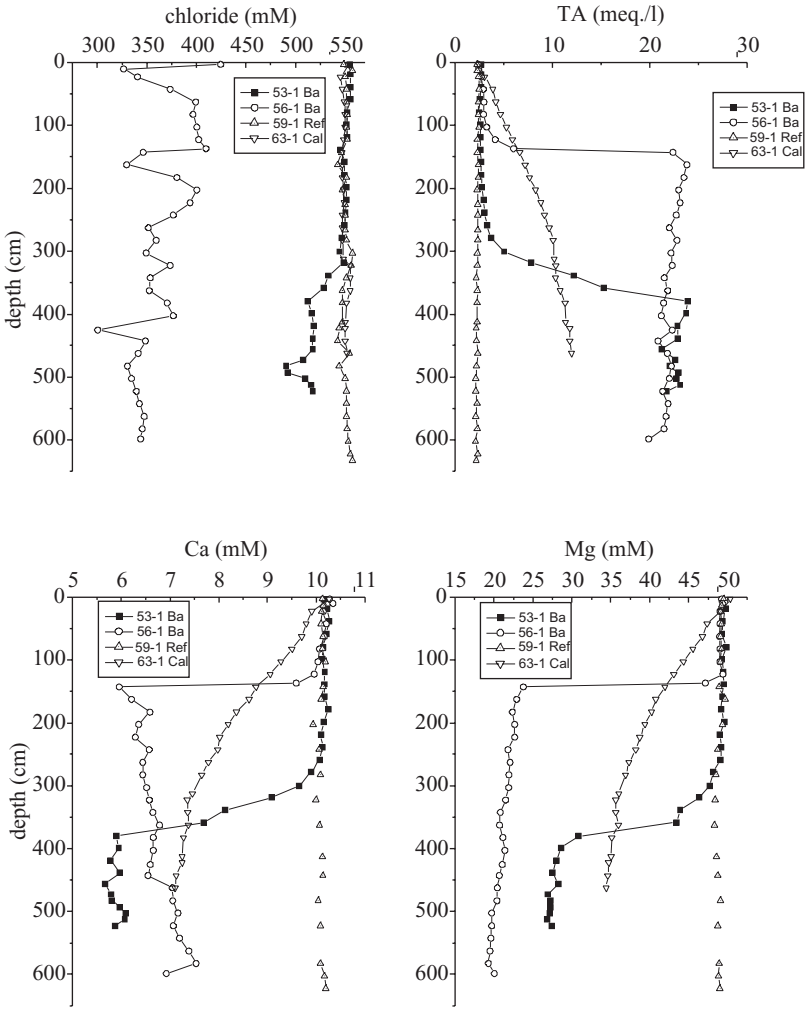

Fig. 8.7: *Concentrations of dissolved chloride, total alkalinity, calcium, and magnesium in sediment pore waters from the barite area.*

Sediment core LV29-56-1 had a similar signature even though the deep fluids seem to be more diluted with ambient pore waters and are only found in deeper sediment layers. Core LV29-63-1 taken at the “Clam Hill” shows increased sulfide and nutrient concentrations towards the base and decreasing Mg concentrations which again indicate a deep origin of the rising fluids. In contrast to the other fluid-bearing cores, the profiles were more continuous and showed no sharp gradients.

The cores taken during the expedition confirm that the barite area is affected and probably formed by deep fluids rising to the surface. Further shore-based analyses of the pore fluids will allow for a detailed exploration of fluid sources and hydrological processes prevailing in the barite area.

9. OFOS OBSERVATIONS

Giovanni Aloisi, Klaus Wallmann, Boris Baranov, Alexander Derkachev, Hartmut Hein, Harald Bohlmann, and Carl-Ulrich Noeske

9.1 Introduction

22 OFOS (Ocean Floor Observation System) lines were run on the Sakhalin shelf and slope and in the Derugin Basin area, looking for seafloor evidence of present or recent methane emission activity. In all but one of the explored areas, sound biological and/or geological evidence was observed in the form of benthic chemoautotrophic megafauna and/or authigenic mineral precipitates.
The position of OFOS lines was chosen based on the location of methane plumes, as mapped by echosounding and water column chemical surveys, and promising geological structures, identified during bathymetric and seismic surveys. For this, existing data collected during previous KOMEX cruises was integrated with data collected in newly explored areas during cruise LV29. OFOS lines were carried out drifting, taking advantage of the currents (0 to 1.4 knots) present both on the Sakhalin shelf and in the Derugin Basin. Currents are mostly along-coast on the Sakhalin shelf, (about N35 or N200, depending on the time of day); they are less predictable in the Derugin Basin area, where they may be affected by seafloor topography.
OFOS imaging confirmed to be a particularly effective method for the investigation of areas of cold seeps and provided a good intermediary between large-scale geophysical and geochemical surveys and bottom sampling operations. Biologists being absent aboard, considerations regarding the benthic macrofauna observed are limited in this report. A more accurate evaluation of the biological information collected during OFOS observations will be possible during land-based study of OFOS videos and photographs.

9.2 “Erwin flare”

6 OFOS lines were run across the newly discovered “Erwin flare”, located on the outer Sakhalin shelf (*Fig. 9.1*). These lines were aimed at crossing areas of methane emissions mapped during echosounder surveys earlier on the cruise.
The substrate in the “Erwin flare” area consists of coarse sand. Clouds of sediment, which form when the seafloor is hit by the OFOS frame, settle rapidly. The seafloor is littered with rounded cobbles, typical for this high-energy shelf environment. Less often, boulders a few decimeters across are present, possibly deriving, together with parts of the cobbles, from the shoreline of the Okhotsk Sea. Debris of this kind is typically trapped during winter time in ice forming at the shoreline of the Okhotsk Sea, is then transported by ice rafting to the shelf and beyond and is deposited as dropstones when the ice melts.
Benthic macrofauna is abundant. Amongst the most common organisms are crustaceans, starfish and anemones. Fish are also present. Shells are visible, although their abundance is difficult to appreciate, because scattered white debris is common on the seafloor and sometimes indistinguishable from shells.
In one part of the flare, white, massive, irregular build-ups up to 2 m high are present; several tens were seen in all but one of the OFOS lines. These build-ups protrude from the seafloor and sometimes have secondary, columnar bodies about 0.5 m long extending from them. A considerable amount of sediment is associated with these build-ups so that the overall appearance is of a massive, gray body covered by white decimetric patches. The seafloor around the build-ups is littered with white debris, forming an apron 2 to 3 m wide. The debris is composed of particles 5 to 10 cm across, presumably originating from the break-down of the build-ups.

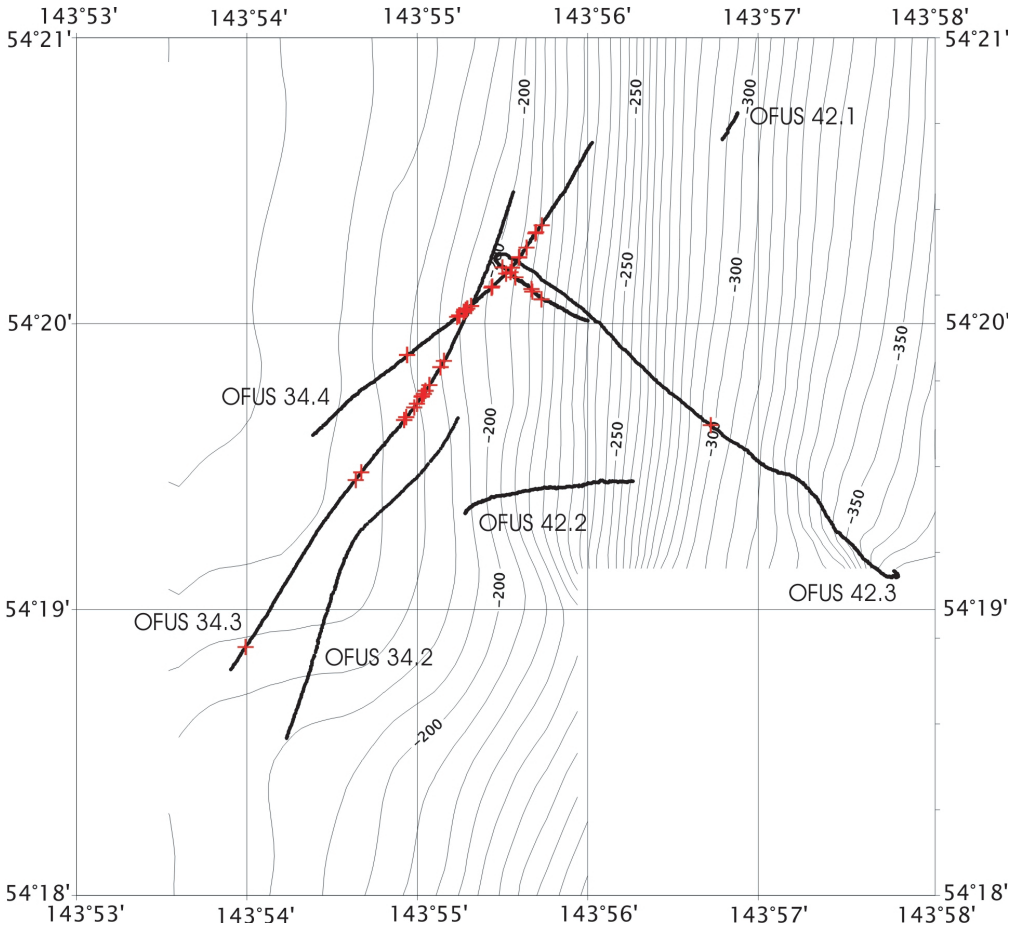

Fig. 9.1: *OFOS line run on the "Erwin flare" area. Crosses mark the occurrence of white, columnar build-ups.*

At present, the origin of the build-ups, biologic or abiotic, is not clear. One possibility is that they are built by colony-forming organisms bearing a calcareous shell. The recovery of aggregates of organisms composed of hard, calcareous, flower-shaped shells suggestive of a colonial mode of life are in favor of a biological origin. Alternatively, the build-ups are abiotic, and consist of authigenic carbonate precipitates. The fact that cold-seep authigenic carbonate formation is limited to anoxic pore waters, would require that build-ups form in the sediment and are subsequently exposed by erosion.
Bacterial mats, reported from another flare site on the outer Sakhalin shelf (Sahling et al., subm.), were not observed in the video recordings. In conclusion, no definitive evidence for methane emissions was seen during OFOS surveys of "Erwin flare".

9.3 "Obzhirov flare"

4 tracks run during the LV29 cruise in the "Obzhirov flare" area (*Fig. 9.2*) were aimed at expanding observations performed here during cruise LV28 (Biebow & Hütten, 1999). At "Obzhirov flare", situated on the intermediate continental slope, the substrate is fine-grained (silt-mud); rare debris, mainly cobbles, some of which are possibly ice-rafted, is present on the seafloor. The bottom waters are, however, turbid and the origin of some objects seen on the seafloor (e.g. black spots, which are common here) is uncertain.
Benthic macrofauna unrelated to fluid seepage is less abundant than at "Erwin flare". Fish, holothurians and crabs are the most commonly occurring large organisms. Infauna is thought

to be present too, and may be abundant, as suggested by the many centimeter-sized holes in the sediment.

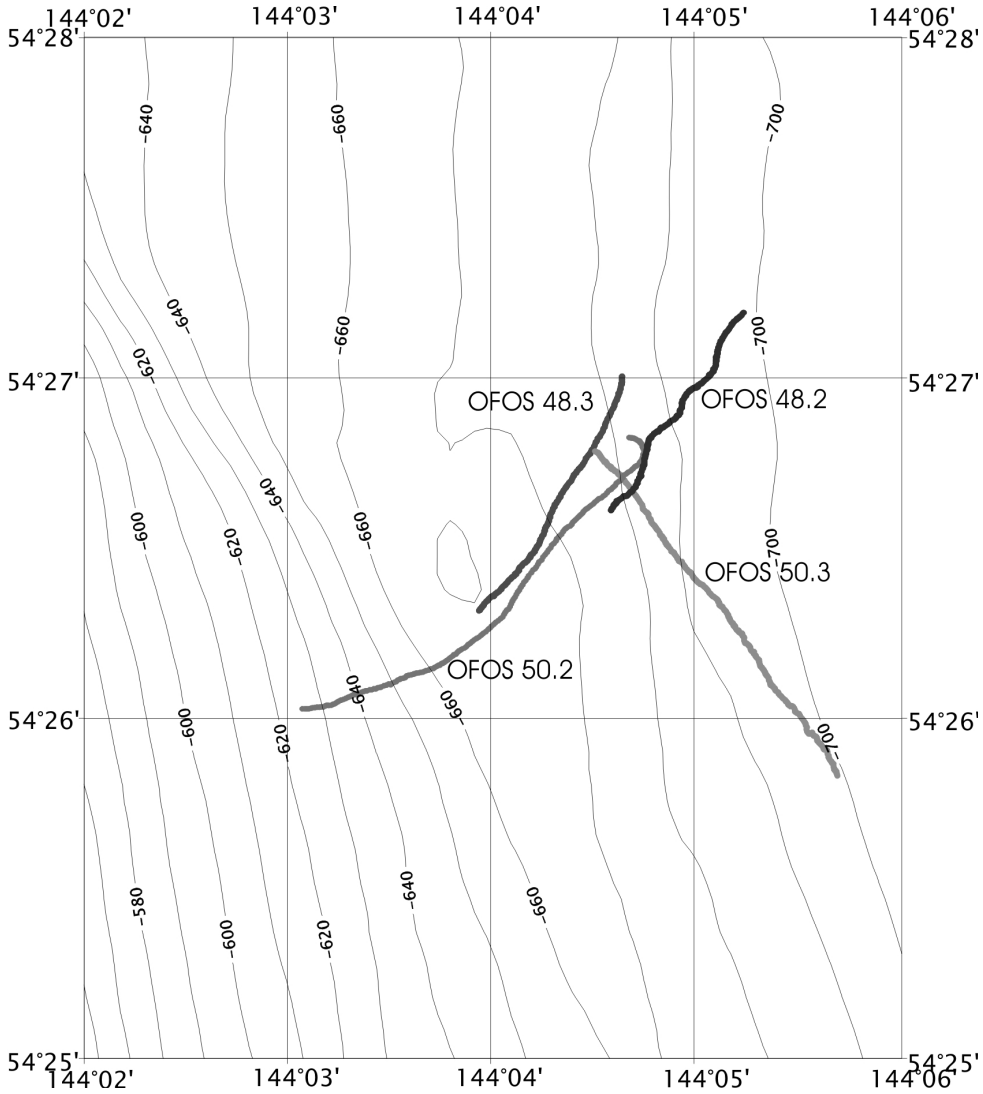

Fig. 9.2: *OFOS line run on the "Obzhirov flare" area.*

In addition to this fauna, extensive clam fields are present. These very likely consist of chemosynthesis-based species (*Calyptogena* and/or *Conchocele*?) which have been previously reported from this flare area (Sahling et al., submitted), and are indicative of active methane emission. Clam fields are up to 10 m across and can be very densely packed with clams which, in most cases, are partly buried in the sediment. Plenty bivalve shells lying on the seafloor are also present, single or in clusters, marking locations of recent methane emission. The areas of clam occurrence correlate nicely with flare images recorded with the echosounder.

In the areas most densely populated by clam colonies, a hard, irregular substrate is visible, covered by a few centimeters of soft sediment. It is not clear whether this is composed of sediment-covered clams or authigenic carbonate precipitates.

One area about 10-15 m wide, crossed on line LV29-50-3 (time on tape 3:05:00), is very densely covered by round, black and white patches of sediment. These occur next to what appears to be fields of living clams. Similar black patches in other areas of fluid seepage (e.g. the Mediterranean ridge) are composed of reduced sediments and represent single seeps; white patches, associated to the black ones, are bacterial mats. The examination of

photographs might reveal whether also the patches observed in “Obzhirov flare” are seep-related.

9.4 Derugin Basin

9.4.1 “Barite Mounds” area

The most spectacular evidence for the seepage of fluids was observed in the Derugin Basin. A ridge richly covered by authigenic barite that was first described on cruise LV28 (Greinert et al., 2002) was extensively mapped during cruise LV29. OFOS observations served to appreciate the extent of the authigenic barite, as well as that of the associated seep-related terrain. Altogether, 10 OFOS lines (*Fig. 9.3*) were run in this area; three types of terrain, described separately in this section, were defined by this survey: background seafloor, fringe areas of fluid seepage and areas of barite build-up. This OFOS survey is used to better constrain the extent of barite build-up deduced from the distribution of the “upper barite reflector” seen on the echosounder survey. Together, the echosounder and OFOS surveys are used to estimate the lateral extent and the volume of authigenic barite present at the “Barite Mounds”.

9.4.1.1 Background seafloor

The background seafloor in this part of the Derugin Basin consists of mud. 2-5 cm wide holes, often with a 10-15 cm rim of accumulated sediment particles surrounding them are very frequent. Often, the accumulated sediment surrounding the holes is white. The holes and the accumulated sediment are consistent in size throughout the whole investigated area. The most likely explanation is that these are holes made by burrowing organisms (clams, worms?). Sparse debris is also present on the seafloor and consists of brecciated particles of variable size, from centimeters to several decimeters across, to which benthic sessile organisms attach. These particles are probably of ice-rafted origin. Occasionally, trails several centimeters wide are seen. These are most probably traced by large (10 cm) gastropods which were observed at the end on some of such trails. Benthic macrofauna (crabs, starfish) are more rare here than in the shelf and slope areas.

9.4.1.2 Fringe areas of fluid seepage

These areas are similar to the background seafloor areas, except for the occurrence of seepage-related clams (*Calyptogena*?) that occur singularly and in clusters. Usually, approaching the fringe area of seepage from the background seafloor area, the first indication of fluid seepage is represented by clam shells. Moving towards the areas of barite build-up, living clams appear, and clusters become more frequent and contain a larger number of clams (typically from 3-4 to a few tens of individuals). The seafloor is often crossed by clam trails which lead to clusters of clams; these trails are narrower (2-3 cm) than those left by the passage of gastropods.
In the fringe area, barite debris can be seen on the seafloor. Sometimes it is hard to distinguish between barite debris and regional ice-rafted debris. However, debris increases considerably in abundance and size towards the barite build-ups (boulders of more than 1 m across are common) suggesting that considerable amounts originate from the break-down of authigenic barite constructions. The fringe area of fluid seepage is limited towards that of barite build-ups by the first occurrence of an in-place barite build-up.

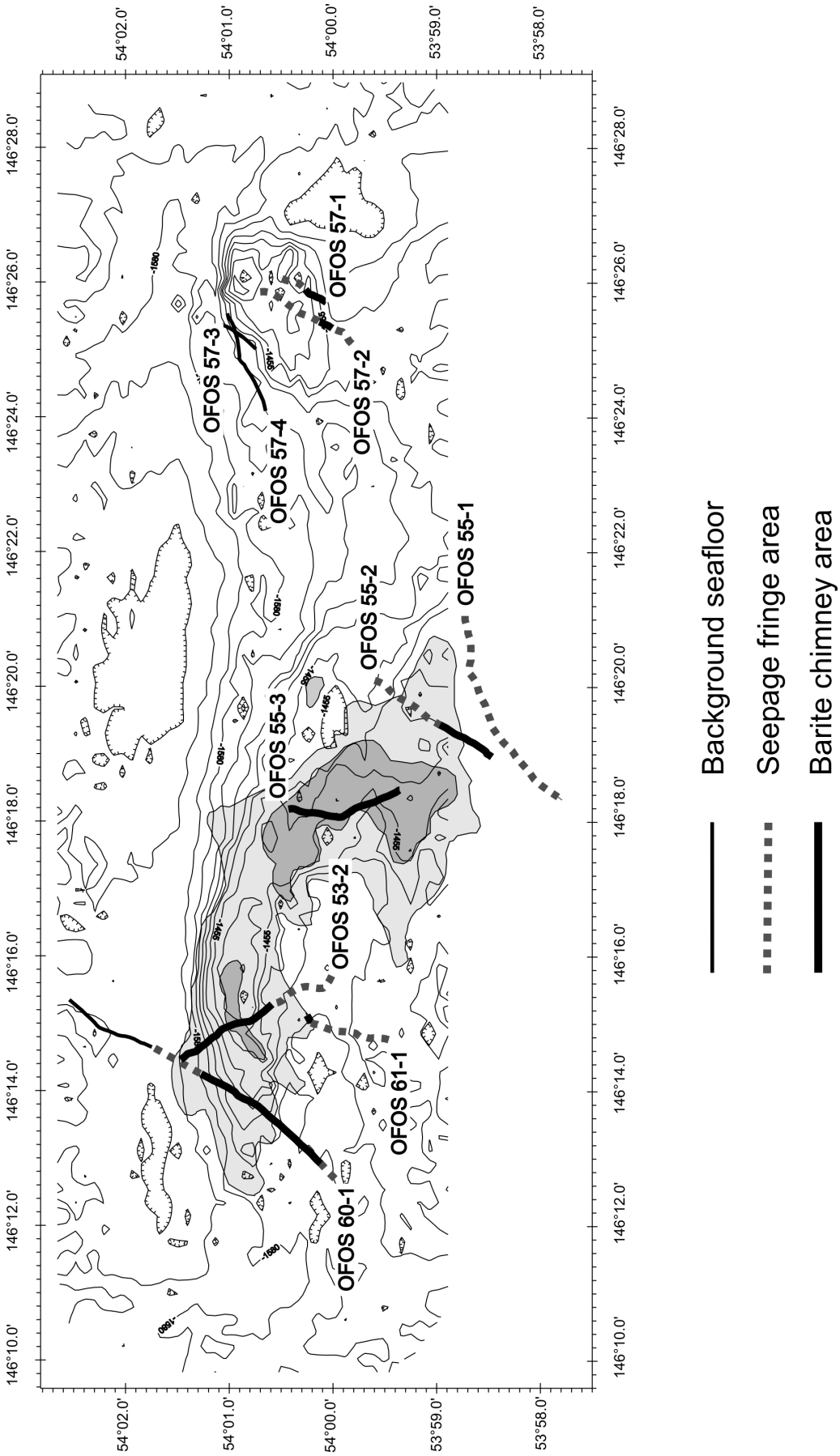

Fig. 9.3: *OFOS line run on the "Barite Mounds" area. Three types of terrain are distinguished based on OFOS observations. Shaded areas correspond to the extent of the barite build-ups as inferred by the distribution of the "upper barite reflector" seen on the 12 kHz echosounder.*

9.4.1.3 Area of barite build-up

In this area, massive barite build-ups (both massive and chimney-like) up to more than 20 m high dominate the landscape. They are separated by stretches of “fringe-type” seafloor (including the seep-associated macrofauna) a few to 40 m across. The alternation of flat, reflective seafloor with topographically rough areas of barite results in the presence of a secondary, weak reflector over the seafloor on echosounder tracks run in this area.
Often, authigenic barite build-ups are as wide at the base as they are high, giving the impression of a truncated pyramid construction (massive barites). Less often, they build vertically elongated, slim columnar structures (chimneys), a few meters in diameter and up to 20 m high. Commonly, the surface of the authigenic barite is dark due to an authigenic manganese oxide layer deposited on the barite. White patches of authigenic barite occur in decimetric to metric barite protrusions in the upper part of the barite chimneys and in cracks and fissures in the massive barites, showing that these are current locations of fluid seepage and authigenic barite precipitation. In patches of white barite, barite precipitation seems to occur in distinct centimeter-sized areas which give a mottled aspect to some parts of the chimneys, probably reflecting the highly porous nature of the barite fabric (Greinert et al., 2002) which offers a high number of distinct pathways the fluids can follow to reach sea water. Freshly built, recent barite deposits can thus be recognized on the basis of their white color.
The slope at the base of the barite build-ups is covered by a chaotic accumulation of barite blocks. Moving away from single build-ups, barite debris decrease in abundance and size.
The slope morphology in this area is strongly affected by the presence of barite precipitates. When going upslope, the OFOS often encounters vertical walls of barite up to 20 m high. Once the OFOS has risen over the top of these obstacles, it then descends typically half the distance it has risen, before touching the seafloor again. Terraces limited downslope by walls of barite are common and may be of tectonic origin. In this case, the barite walls develop on fault scarps which produce the terraces and which could be preferential pathways for the migration of fluids.
4 OFOS lines explored the mound to the east of the “Barite Mounds”, where a variant to the barite build-up terrain was observed. Although authigenic barite occurs as chimneys, the height of which does not exceed a few meters, most of the authigenic precipitate seems to occur as decimeter-thick crusts. This landscape is more similar to that of cold-seep areas worldwide, where carbonate precipitates more commonly form. In addition, the most impressive accumulation of dead clams occurs here. The seafloor between barite precipitates is often white due to the presence of a layer of shells.

The distribution of seafloor types according to the OFOS observations is plotted in *Figure 9.3*, along with the distribution of the “upper barite reflector” seen on the echosounder survey. The distribution of the barite build-ups as observed by OFOS is generally consistent with that inferred by the distribution of the “upper barite reflector”. Minor inconsistencies can, however, occur and are due to the different footprint of the OFOS video system (a few meters) and of the 12 kHz echosounder (about 200 m at 1,600 m water depth):

1) Barite chimneys were observed in OFOS lines which extend outside the “upper barite reflector” area (e.g. SW part of OFOS LV29-60-1). In these areas, barite chimneys are very rare in the OFOS record and likely are not abundant enough to produce a reflection in the echosounder signal. Similarly, in the eastern mound area explored during OFOS LV29-57-1 and LV29-57-2, although no reflector has been recorded, barites occur, mainly as crusts, but also as chimneys generally not higher than a few meters.

2) Parts of OFOS lines ascribed to the fringe area of fluid seepage (e.g. SE part of line LV29-53-2) fall within the area of barite chimney occurrence as inferred from the presence of the "upper barite reflector". Along these stretches of seafloor, no in-place barite chimneys were observed, but the seafloor is littered with large-scale debris of barite chimneys, indicating the presence of barite build-ups next to the track. The density of barite chimneys in these areas is very likely much greater than that in areas described in point 1, above.

In addition to better constraining the distribution of the barites, the OFOS surveys convey useful information on the extent of fluid seepage outside the "Barite Mounds" area. From OFOS lines LV29-61-1, LV29-53-2 and LV29-55-1, it is clear that the area of the seafloor affected by seepage of fluids is greater than that occupied by barite build-ups. It is difficult to estimate the extent of the fringe area of fluid seepage, since only OFOS line LV29-60-1 marks the border between this area and the background area. Large stretches of seafloor covered by the 'fringe-type' seafloor on lines LV29-61-1 and LV29-55-1 suggest, however, that it could be at least as big as the area of barite build-up.

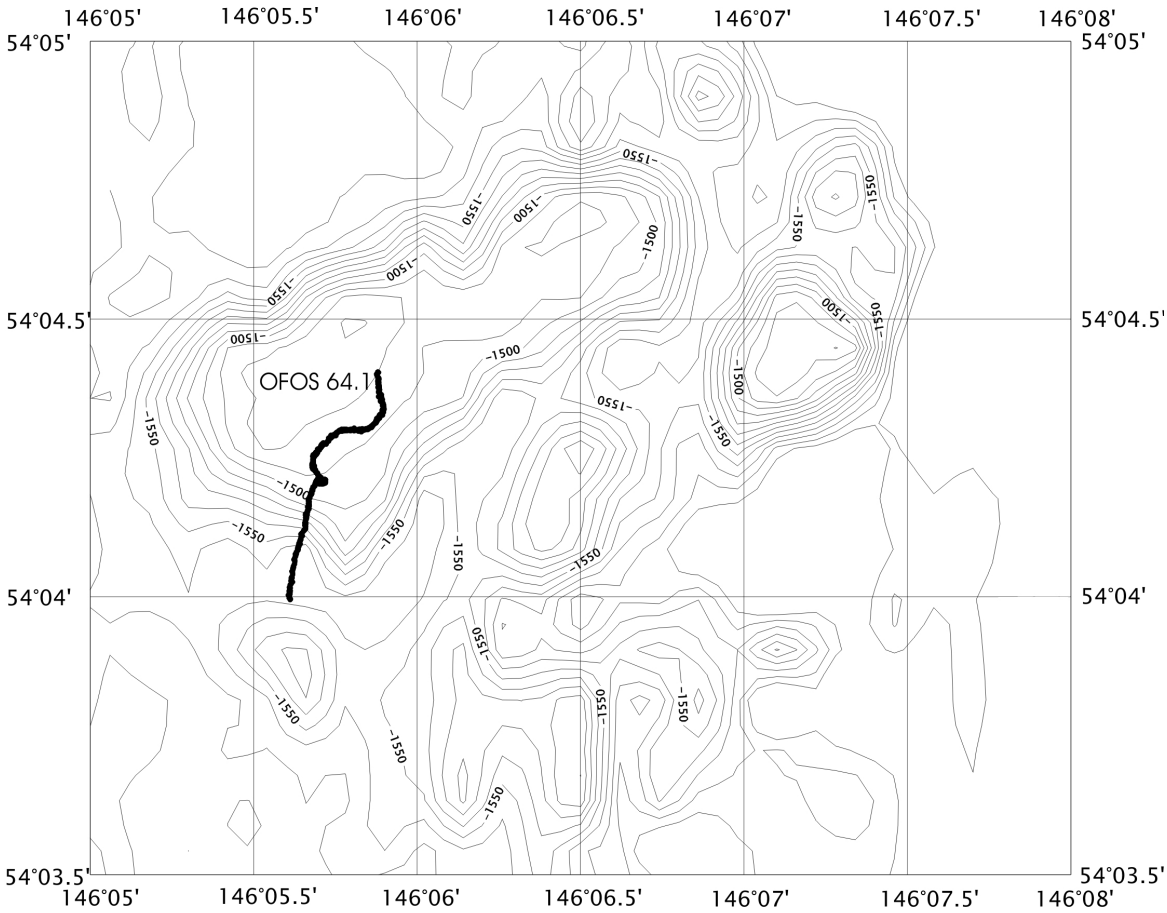

Fig. 9.4: *OFOS line run on the "Baranov high".*

9.4.2 "Baranov high"

One OFOS line explored the "Baranov high", a bathymetric high to the west of the "Barite Mounds" (*Fig. 9.4*) that shares its seismic and morphological characters, possibly indicative of active or recent seepage of fluids. The observed seafloor is of the 'fringe seepage type', confirming that the seepage of fluids is presently active. In addition, a considerable amount of debris (boulders up to 60 cm across occur), resembling fragments of barite chimneys were observed. No in-place barite precipitates were found, however, and it is not clear whether they

do occur, along with fluid venting, at this site. Evidence for fluid seepage decreased in the last part of the track towards the base of the southern slope.

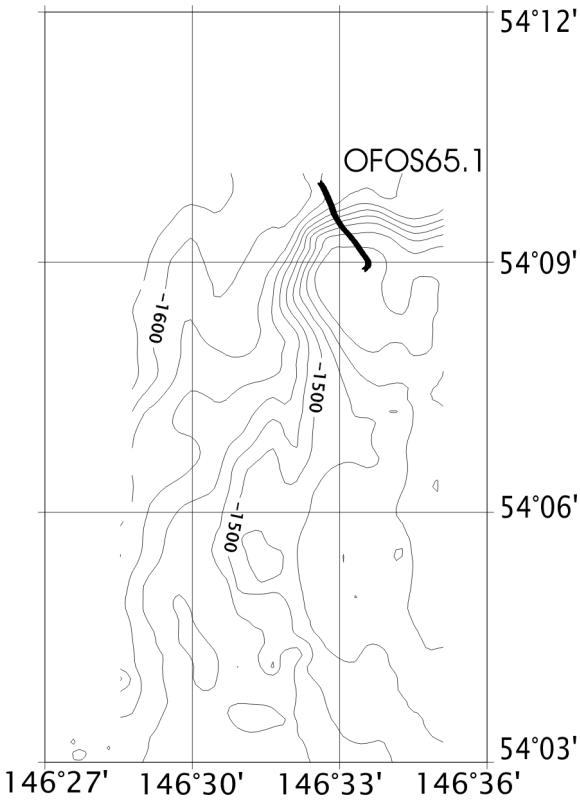

Fig. 9.5: *OFOS line run on the northeastern ridge.*

9.4.3 NE Ridge

This ridge culminates in a bathymetric high (*Fig. 9.5*) and is interpreted - on the basis of seismic data - as a tilted block. An OFOS line was run on this ridge to check the hypothesis that, in contrast to the other explored areas and as suggested by its distinct seismic character, this structure is devoid of fluid seepage. Seafloor typical of the background type was seen all along the OFOS line. Plenty debris occurs along this line, too.

10. SEDIMENTS AND AUTHIGENIC MINERALIZATION OF COLD-SEEP AREAS

Alexander Derkachev, Natasha Nikolayeva, Anatoly Botsul, and Giovanni Aloisi

10.1 Slope and shelf of Sakhalin Island

Five cores with a length from 55 to 580 cm and two dredges were taken on the shelf and slope of Sakhalin Island. For core descriptions see Appendix 6.
Coring stations LV29-34-1 and LV29-42-5 are located in a water depth of 182-191 m in the "Erwin flare" area. The cores recovered sediments of up to 100 cm in thickness, which consist of coarse-grained sand with an admixture of dropstones. In the lower part of core LV29-34-1 (interval 75-90 cm), the sediments are well sorted and contain a large amount of dropstones. Below 90 cm, they are suddenly replaced by silty clay, which probably is of lagoonal origin. In this core, a small fragment (about 1 cm in diameter) of sandstone with calcite cement was discovered at 20 cm. Carbonate debris probably of authigenic origin occurs in the entire core in minor quantities. The sediments of core LV29-42-5 are better sorted and contain more dropstones than core LV29-34-1. In the lower part of the core, they are replaced by gravel-pebble deposits with an admixture of sand and dark brown wood pieces.
Dredges LV29-40-1 and LV29-42-6 yielded sandy sediments with a large amount of dropstones. The bottom fauna is abundant and includes mollusks, crabs, starfish, and worms. One carbonate concretion of 6 x 1,5 cm in size consisting of dense massive calcite-cementing sandy particles was found. It has the same composition like the carbonate fragment from core LV29-34-1.

Two cores were taken in the "Obzhirov flare" area. One of them (core LV29-46-1 from 684 m water depth) recovered sediments typical for marginal areas of methane seeping. They are represented by terrigenous-diatomaceous silty clay and clayey silt of olive-green and greenish-gray color. The sediments are mottled and bioturbated; in sections 60-70 cm, 220-225 cm and 280 cm small shell fragments were discovered. For this core, small laminas and lenses of hydrotroilite and an H_2S odor are characteristic. From 430 cm on, the sediment becomes saturated with respect to gas and water and yields a typical lumpy-brecciated texture (Ginsburg & Soloviev, 1994; Derkachev et al., 2002). Fragments of *Calyptogena* and small (up to 1-1,5 cm in size) branchy carbonate concretions were discovered in the surface sediments.
Core LV29-50-1 was taken in direct proximity to a gas flare. It recovered sediment typical for areas of gas emanations (cold-seep areas): the sediments are bioturbated and contain lenses and laminas of hydrotroilite and carbonate concretions. Here, water-saturated and gas-saturated horizons with a characteristic lumpy-brecciated texture as well as fragments of *Calyptogena* and gas hydrate layers are significant. Carbonate concretions of different morphology and size were discovered at interval 148-320 cm. In the upper part of the horizon (148-200 cm), concretions of primary carbonate formation occur frequently. They are soft, slightly dense, and of 0.3-0.6 cm in diameter. Fragments of *Calyptogena* were discovered here, too.
Dense, massive concretions of flattened and branchy shape dominate in the lower part of the horizon. Besides, worm tubes with an empty or sediment-filled central channel were rarely observed here, as well. These up to 10 cm large concretions are located inside the sediments parallel to stratification. Concretions cementing shell fragments were found at 205 cm. A similar sedimentary section was discovered in this area on the MV *Marshal Gelovany* cruise in 1999 (Biebow et al., 2000; Derkachev et al., 2002) (*Fig. 10.1*).
Gas-saturated sediments were traced from 240 cm downwards, which turn into a gas hydrate-bearing horizon (395-405 cm). Gas hydrates are represented by thin interlayers and lenses of white color within massive sediments.

Station LV29-51-1 was conducted on the slope at a water depth of 825 m in a newly discovered area with a gas anomaly situated not far from “Obzhirov flare”. The core contained terrigenous-diatomaceous sediments from the marginal part of gas seeping, which is indicated by a characteristic pore water geochemistry (see Chapter 8).

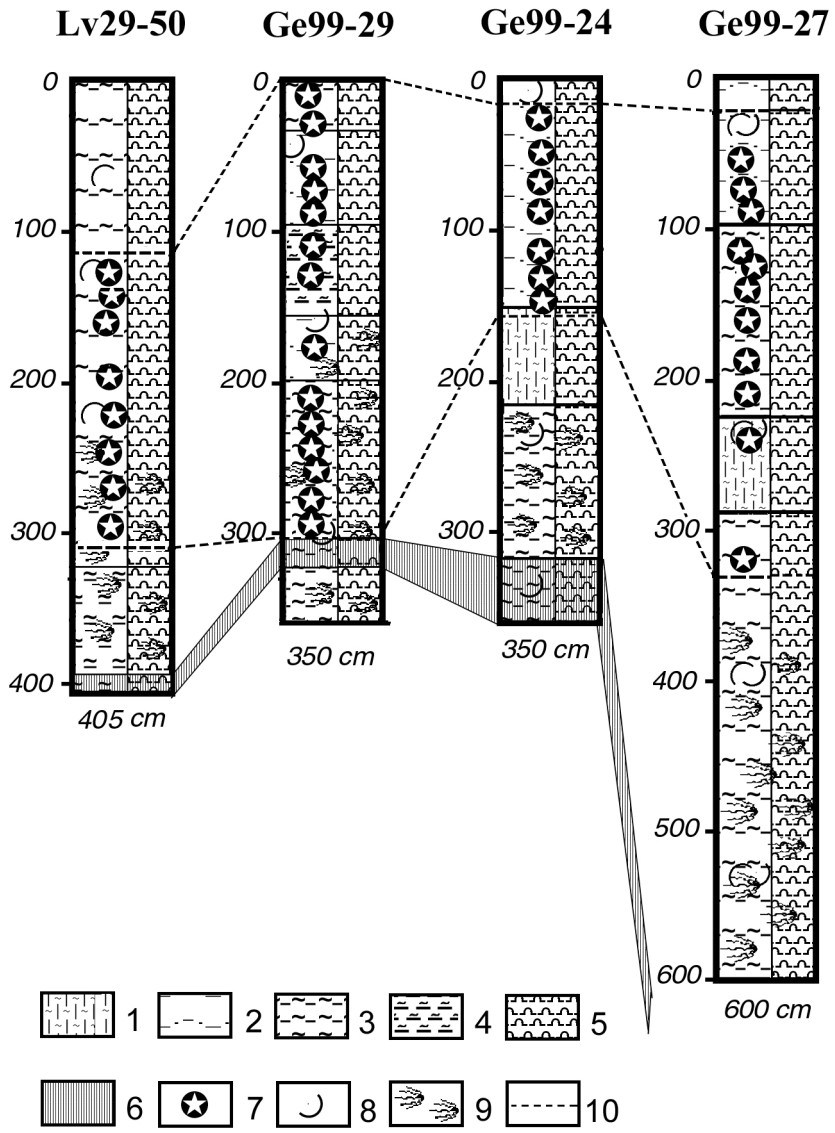

Fig. 10.1: *Distribution of carbonate concretions and gas hydrates in sediments from the area of active gas emanations on the Sakhalin slope (Obzhirov flare) and texture peculiarities of these sediments.*
1 - sand-silt-clay, 2 - sandy silt, 3 - clayey silt, 4 - silty clay, 5 - diatomaceous sediments, 6 - horizon with gas hydrates, 7 - carbonate concretions, 8 - shell fragments, 9 - texture of gas-saturated sediments, 10 - upper and lower boundaries of the distribution of carbonate concretions in the sediments.

10.2 Derugin Basin

Sediments and types of carbonate-barite precipitates, their mineral, chemical and isotopic composition were studied in detail on previous cruises in the Okhotsk Sea (Biebow & Hütten, 1999; Biebow et al., 2000; Derkachev et al., 2000, 2002; Greinert et al., 2002). These investigations allowed to conclude that carbonate and barite mineralization is widely

distributed not only at the sediment surface, but also inside the sediments of the "Barite Mounds" (Derugin Basin) covering an area of more than 10 km^2.
On GE99 cruise, an anomalous chemical composition of the pore waters connected with high barium concentrations was discovered (station GE99-32). The mineralogical and chemical composition of sediments and authigenic precipitates of core GE99-32 were studied, too (Derkachev et al., 2002). The obtained data allowed to suppose that the center of gas-fluid emanations with a marked flow of deep fluids is situated in the area of this station.

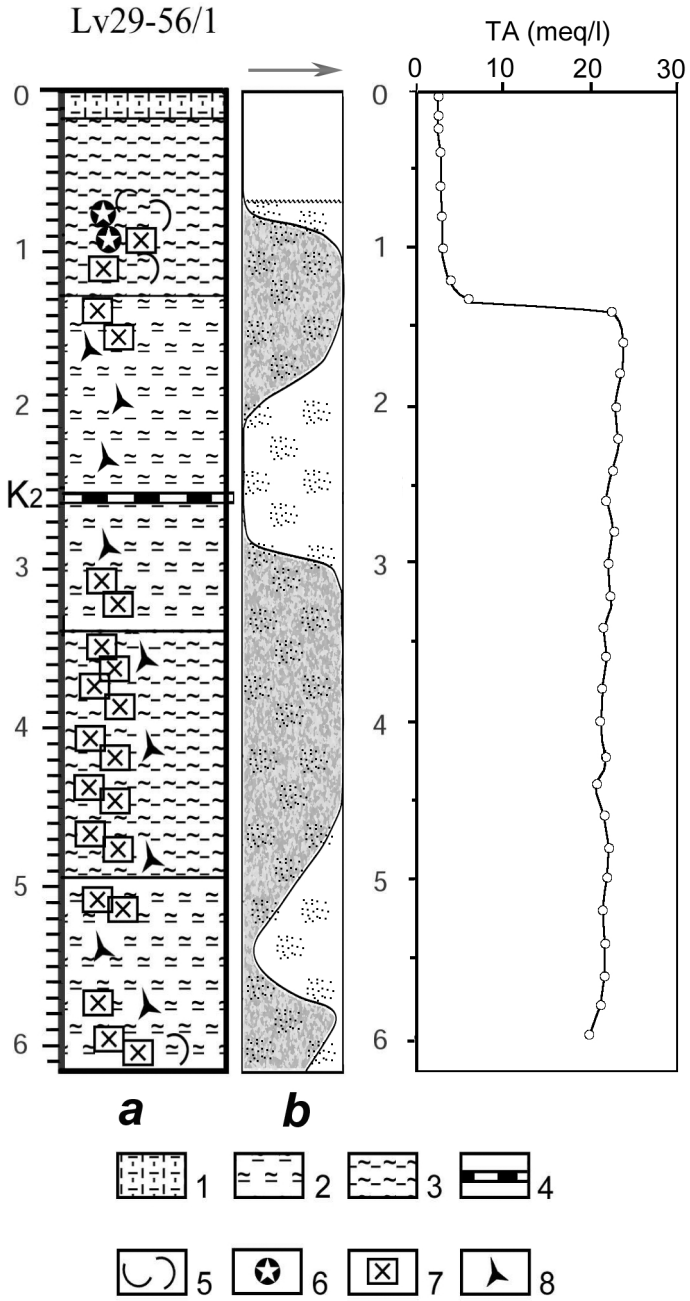

Fig. 10.2: *Manifestation of carbonate and barite mineralization in the sediments of core LV29-56.*
a - lithological column, b - distribution of carbonate (gray background) and barite (rare dots) mineralization in the core, TA - total alkalinity (see Chapter 8).
Wavy line shows upper boundary of authigenic barite distribution; arrow shows the trend of intensity increase for carbonate mineralization.
1 - sand-silt-clay, 2 - silty clay, 3 - clayey silt, 4 - volcanic ash layer, 5 - shell fragments (Calyptogena), 6 - carbonate concretions, 7 - barite-carbonate crusts, 8 - barite and carbonate tubular bodies.

For determining the origin and composition of fluids and their influence on processes of authigenic mineral formation, investigations were carried out close to the well known area of active seeping. Two cores (LV29-53-1 and LV29-56-1) taken here recovered a section of Holocene-Pleistocene sediments up to 615 cm thick, which contain a large quantity of varying carbonate and barite precipitates. Core LV29-100 was taken in Leg 2 of cruise LV29 in the southern part of the "Barite Mounds" and recovered sediment with authigenic carbonates and barites even at 10 cm depth.

Up to now, only core LV29-56-1 and partly core LV29-53-1 were analyzed in detail. Due to the fact that both cores are located relatively close to one another, their sediment composition is similar, but there are differences mainly expressed in the distribution of the mineral-morphological types of carbonates and barites.

The sediments consist mainly of terrigenous clayey silt and silty clay with a large sand admixture. Dropstones are common. Ash layer K2 discovered at 176-178 cm (LV29-53-1) and at 251-252 cm (LV29-56-1) is a good stratigraphic marker and consists mainly of volcanic glass, pumice fragments and crystalloclastics (crystals of plagioclase, pyroxenes and magnetite embedded in volcanic glass).

Two textural horizons of these cores can be divided: an upper horizon represented by soft or moderately dense sediments with slight bioturbation, and a lower horizon consisting of gas-saturated and water-saturated sediments with a typical lumpy-brecciated texture (at 382-530 cm in core LV29-53-1, at 115-615 cm in core LV29-56-1).

Authigenic carbonates and barites were observed throughout the entire cores except for the upper 60-70 cm (*Fig. 10.2*). In core LV29-53-1 the first carbonate concretions appear at 63 cm, they are represented by branchy bodies with smoothed edges (2 x 5 x 0,5 cm in size). Downcore, their content increases; horizons 290-305 cm and 373-385 cm are enriched by them. Their size varies from 1 to 10 cm. Many concretions have swells and tubes filled with authigenic barite. Below 380 cm, carbonate crusts of up to 5-10 cm in size occur frequently (especially at 400-425 and 450-480 cm). The upper part of the crusts usually has a flat rough surface; the lower part has cavities. They also contain barite worm tubes.

The first carbonate concretions in core LV29-56-1 appear at 76 cm (*Fig. 10.2*). These are small (up to 2-4 cm in diameter) precipitates oval in shape, which differ from the surrounding sediment by a lighter color. Authigenic bodies with an unusual morphology were discovered at interval 90-130 cm. They are represented by angular, very hard fragments of up to 10 cm in size consisting of an agglomerate from both highly bioturbated sediments and large fragments of *Calyptogena* and *Provanna.* The entire mass is impregnated with calcite and cryptocrystalline barite cement.

A predominance of carbonate crusts of different size and shape (individual fragments are 3-12 cm in size) is characteristic for core LV29-56-1. Branchy concretions with smoothed edges typical for core LV29-53-1 and other stations carried out in the "Barite Mounds" (Biebow & Hütten, 1999; Biebow et al., 2000; Derkachev et al., 2000) occur rarely. A lot of carbonate crusts were noticed at 370-510 cm. Usually, they have a flat, rough surface on one side (sometimes with an inclusion of dropstones) and cemented tubes filled with barite. Their other side is angular and contains numerous swells. The crusts are rather fragile; they easily crumble forming small angular fragments. Many fragments have a granular structure of carbonate cement consisting of numerous calcite, dumbbell-shaped aggregates. We previously observed similar aggregates in other cores (*Fig. 10.3*). Usually they are characteristic for bacterially induced carbonates (Buczynski & Chafetz, 1991; Gonzalez-Mucoz et al., 2000).

Some carbonate crusts contain shapeless and crustate precipitates of authigenic barite incrusting cavities in the sediment and worm tubes. Barites of this type are represented by aggregates of lamellar colorless or yellowish-brown crystals. There is also cryptocrystalline barite cement in the carbonate crusts, but for understanding its relation with carbonate mineralization special mineralogical investigations are required. Carbonate mineralization is distributed unequally. Even barite crusts without carbonate cement occur here.

The analysis of the distribution of different types of carbonates and barites showed that authigenic barite mineralization is pronounced within all recovered sediment layers except for the upper horizons (60-70 cm) (*Fig. 10.2*). The authigenic barites observed in core LV29-56-1 are of different morphological types: microconcretions with a rough surface and their aggregates, tubular bodies, crusts, cryptocrystalline cement in barite-calcite crusts. They formed apparently at the lower boundary of the sulfate reduction zone. The presence of authigenic barite in the entire core may indicate a long period of delivery of barium-saturated fluids from deep sediment horizons. The quantity and variety of the morphological types of barite precipitates depend on the intensity of gas-fluid flow. Barites are probably an earlier stage of authigenic mineral formation than calcite; numerous tubular bodies filled with barite and covered by a thin calcite coat prove this.

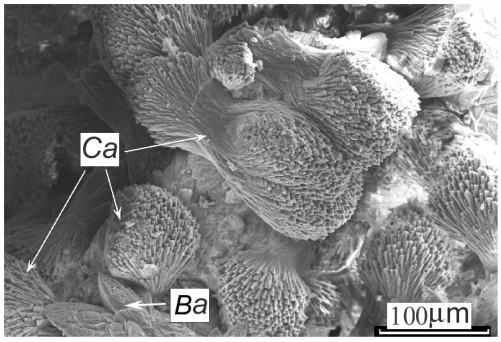

Fig. 10.3: *SEM-images of bacterially induced Mg-calcite (aggregates of dumbbell crystals) in the sediment of core GE99-32.*

If methane is the main source of carbon for the formation of carbonate concretions (Derkachev et al., 2000, 2002; Greinert et al., 2002), there was certainly a cyclicity in the delivery of methane by fluid flow. This periodicity of carbonate mineral formation was proven in core LV29-56-1 by the presence of horizons enriched with respect to carbonate precipitates (*Fig. 10.2*). One of them is horizon 80-210 cm containing carbonates and fragments of fauna (*Calyptogena, Provanna*) typical for areas of gas-fluid emanations.
The primary development of carbonate crusts can be observed in horizon 280-510 cm. The existence of carbonate crusts with a specific flat surface may provide evidence on their formation at the sediment surface close to the water-sediment boundary. Carbonate crusts are known in many areas of the World Ocean with active gas emanations (Kulm & Suess, 1990; Sakai et al., 1992; Jorgensen, 1992; Stakes et al., 1999; Aloisi et al., 2000; Greinert et al., 2001; etc.). Further analyses of the pore water geochemistry, sediment and authigenic precipitates will show to what extent our assumption about the cyclicity of carbonate mineral formation is correct.

On cruise GE99, an isolated submarine hill with an elevation of 150-170 m above the surrounding basin (Biebow et al., 2000) was mapped in a 5 km distance from the “Barite Mounds” close to the area with a prominent heat flow anomaly (Hayashi, 1997). As we believe that barite mineralization occurs at this structure as well, 4 OFOS profiles were run on this hill (“Clam Hill”). Two profiles (stations LV29-57-1 and LV29-57-2) crossed the southeastern slope of this structure, where large clusters of chemosynthetic fauna were discovered.
The dredging carried out in Leg 2 (station LV29-99) along the OFOS transect LV29-57-1 was very successful. Flat barite crusts, *Calyptogena* shells and their fragments of up to 10 cm size were recovered in large quantities as well as some living specimens of this specific fauna.
The size of the barite crusts varies from 8 to 22 cm. Besides, many small fragments (1-5 cm) were discovered. All these crusts are covered by a thin (0.1-0.2 mm) dark brown coat of both

iron and manganese hydroxides. Many of them have such a coat not only on the inner but on the outer surface too. This proves their prolonged exposure at the seafloor. Most likely, these crusts are fragments of build-ups and slabs which are more homogeneous in morphology and structure than those observed during OFOS records. Some crusts have a gray color and inclusions of soft sediments on the inner side showing their exposure on the sediment surface. All crusts are composed of barite, but it is possible to distinguish different morphological types:

1. Thin, flat lamellar fabrics of 1-2 mm in thickness and of 5-8 cm in length with a rough surface.
2. Crusts with a flattened surface complicated by tubular swells 0.7-2.0 cm thick. Their inner side is represented by numerous branching pillars and swells (*Fig. 10.4 c,d*). All of them consist of closely intergrown barite spherulites.
3. Multilayer crusts 1.5-3 cm thick and up to 15 cm long (*Fig. 10.4 b*). They consist of 2-3 flattened crusts of the first or second type; the space between them is filled with numerous compactly packed lamellar-globular aggregates of gray barite.
4. Crusts up to 2-2.5 cm thick. Their inner and outer surfaces represent dense interweaving of branchings and columnar barite fabrics some millimeters across and 0.5-2 cm high. On some of them, there are tubular fabrics of 0.5-0.8 cm in diameter with a pronounced channel, the walls of which are incrusted by brushes of lamellar yellow barite. These tubular fabrics are most likely remnants of barite-containing fluids filling up the channels in the surrounding sediments. The largest fragment (about 22 cm) recovered by dredging may be classified as this morphological crust type (*Fig. 10.4 a*). Among a dense network of branching, intergrown tubes and swells, it contains numerous holes not filled with barite.

Despite the considerable variety of crust morphology, the crust's composition and inner structure are relatively constant. It consists of barite represented by lamellar gray and yellow crystals; colorless crystals occur seldom. These crystals often form spherulitic aggregates and their growth products. The massive cryptocrystalline or spherulitic texture of closely intergrown barite aggregates is visible on fractures of thin crusts and swells; these aggregates cement the surrounding sediments. Often, the crusts contain inclusions of not only sandy clastic particles, but also both dropstones and shell fragments. The whole barite-containing mass is impregnated by numerous elongated tubes of about 0.1 mm diameter orientated in different planes, sometimes forming dense clusters. Their patterns are also visible on the surface of the crusts. Usually, the tubes are completely or partly filled with colorless lamellar and closely packed aggregates of barite. Most probably, these thin tubular fabrics are pseudomorphs of remnants of tubular worms or bacterial mats consisting of the filamentous bacteria *Beggeatoa*.

As shown by the OFOS observations at stations LV29-57-1 and LV29-57-2 and by dredging, an earlier unknown center of gas-fluid emanations was discovered in the southeastern part of "Clam Hill". The presence of mainly dead colonies of chemosynthetic fauna indicates a reduction of gas-fluid venting at present. The barite crusts here are covered by a coat of iron and manganese hydroxides showing their long exposure on the seafloor. It is remarkable that in contrast to the "Barite Mounds" neither fragments of barite chimneys nor carbonate crusts, concretions or carbonate-barite fabrics were observed (Derkachev et al., 2000, 2002; Biebow & Hütten, 1999; Biebow et al., 2000; Greinert et al., 2002). The different morphological types of barite crystals typical for barite chimneys are missing even in the fine sediment fractions.

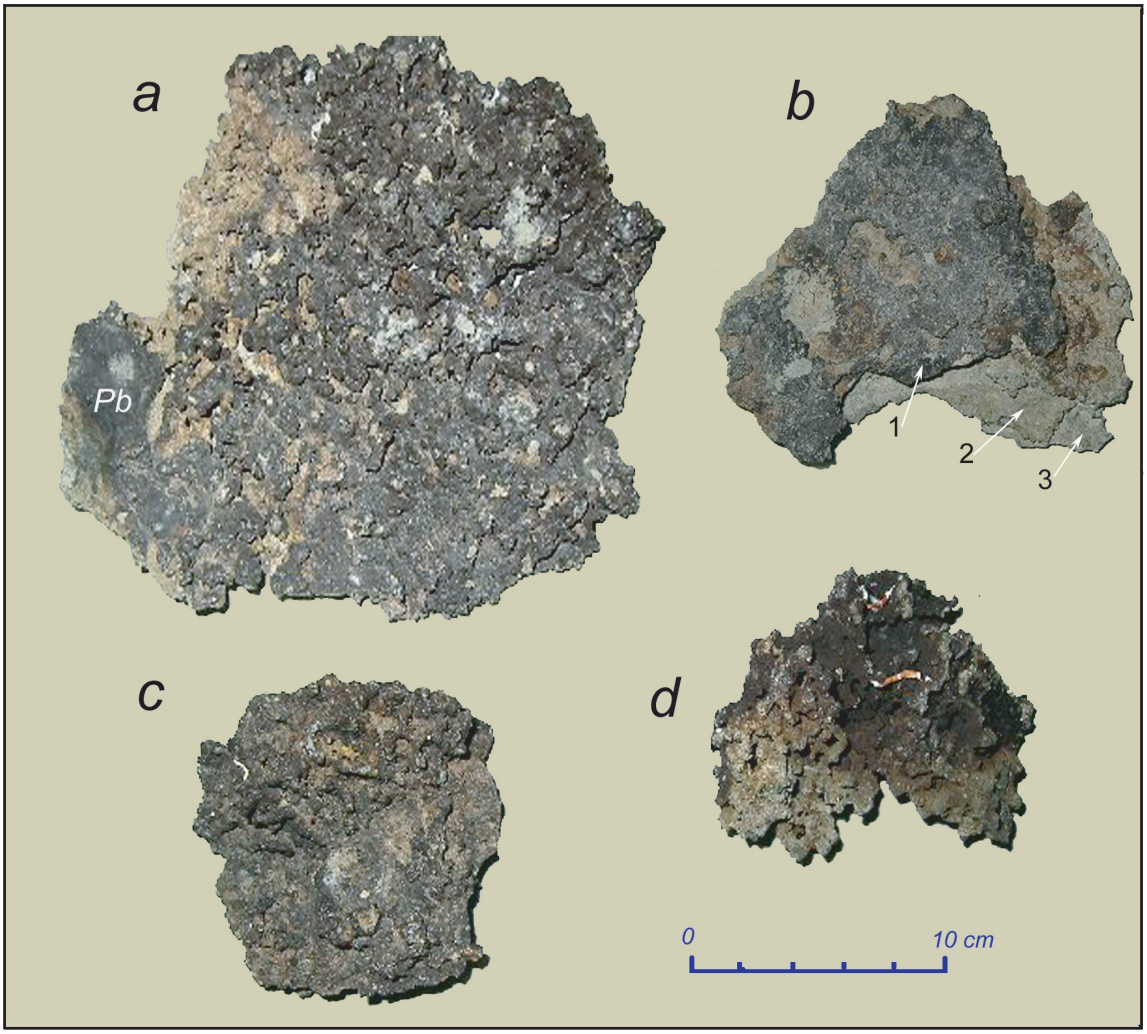

Fig. 10.4: *Photographs of barite crusts.*
a, c, d - fragments of flat barite crusts with numerous swells on their surface covered by a thin coat of iron and manganese hydroxides. These crusts cement enclosing sediment including gravel and pebble (Pb) of ice rafting; b - multilayer (laminas 1, 2, 3) barite crusts with a rough surface.

According to their morphology and inner structure, the barite crusts were formed near the sediment surface close to the water-sediment boundary. They were partly eroded by near-bottom currents, and later on, they formed slabs and crusts on the surface. Probably, barite crusts are formed in areas with a slow fluid flow, that is enriched with respect to barium and sulfide. In comparison to the gas-fluid expulsions of the “Barite Mounds”, the fluids of “Clam Hill” contain low methane concentrations, which is confirmed by the absence of carbonate mineralization.

Cores LV29-59-1 and LV29-63-1 taken in the “Clam Hill” area contain Late Pleistocene sediment typical for the Okhotsk Sea with large amounts of dropstones (sand, gravel, pebble). Core LV29-63-1 is located not far from the seeping area which can be seen from its pore water geochemistry.

It is likely that build-ups of barite chimneys occur also in the northern part of this hill. Rare findings of barite crystals, characteristic for chimney build-ups, in smear slides of the sediments from cores LV29-59-1 and LV29-63-1 are indicative of this.

Thus, summarizing all available information on the distribution of barites and carbonates in the studied area (Biebow & Hütten, 1999; Biebow et al., 2000; Suess et al., 1999; Derkachev et al., 2002; Greinert et al., 2002), we have convincing data that in the Derugin Basin ("Barite Mounds" and "Clam Hill" areas), a long-living and giant center of cold seeping exists. Similar vast manifestations of barite mineralization have not yet been found in other areas of the World Ocean.

11. CORE TEMPERATURE MEASUREMENTS AND PHYSICAL PROPERTIES OF SEDIMENTS

Jeffrey Poort, Tatyana Matveyeva, and Alexander Bosin

11.1 Objectives

The objectives of core temperature measurements were two-fold: to constrain the thermal conditions near venting systems off Sakhalin and in the Derugin Basin, and to detect temperature heterogeneities of sediments caused by dissociation of disseminated gas hydrates. In addition, thermal conductivity and magnetic susceptibility were measured on half cores providing us two important physical properties of the sediment column. Thermal conductivities further deliver us the information necessary to calculate heat flow from the thermal gradients. All data is listed in Appendix 7.

11.2 Core temperature measurements

11.2.1 Method

Temperatures were measured practically on all cores recovered by gravity and hydrocoring during Leg 1 of cruise LV29. Temperature measurements were performed within 10 min after core retrieval. Although complicated temperature paths may be induced during the core recovery process (generally 30-35 minutes from penetration to arrival on deck), the cold water and air temperatures provided optimal conditions with limited temperature changes. Because the process of core retrieval is fairly uniform, the temperature profiles at neighboring cores should be relatively consistent unless there are additional heat sources or sinks.
Temperature measurements were performed at intervals ranging from 20 cm to 100 cm. Needle thermometers were inserted in the sediments through holes in the polyethylene sediment core packing or on half cores (diameter of the cores: 10-14 cm). Temperature measurements were always started from the cores` upper interval downcore. Two different thermometers were used, both measuring temperatures using thermistor (semiconductor) sensors. The portable Japanese Technol Seven D617 with a resolution and accuracy of 0.01 and 0.1°C, respectively, allowed easy and quick handling. For more accurate measurement the LITOS device with an accuracy of 0.01°C was used. At several control points, the temperature was measured repeatedly to get an estimation of the temperature paths during the measurement procedure.

11.2.2 Preliminary results and discussion

11.2.2.1 Sakhalin slope

Core temperature measurements were performed on three cores from the Sakhalin slope area: LV29-46-1, LV29-50-1, LV29-51-1. The first two cores were taken in the “Obzhirov flare” area, a known site of near-surface hydrate occurrence located at a water depth of 690-700 m. The third core was recovered from a newly discovered acoustic flare situated northeast of “Obzhirov flare” at a water depth of 825 m. On these cores we used the portable thermometer and measured at small intervals of 20-25 cm (sometimes 50 cm) trying to detect zones where small pieces of hydrates left a cold thermal anomaly due to the endothermic dissociation process. The measured temperatures are shown in *Figure 11.1*. The corresponding near-bottom water temperature of 2.14°C taken from the nearby CTD station was plotted, too. The two cores from “Obzhirov flare” revealed near-vertical temperature profiles of 2.04°C and 2.06°C with overall thermal gradients of 5 mK/m and –19 mK/m for LV29-46-1 and LV29-50-1, respectively. In the latter, gas hydrates were recovered at the base of the core at 390 cm

subbottom depth. As the hydrates were immediately sampled for later laboratory measurement, no temperature measurements could be conducted here. A small negative anomaly of about 0.1°C in interval 30-50 cm above the hydrate-bearing sediments could indicate that some disseminated gas hydrate was present there, too. Core observation also suggested an increased gas content in this interval. In the first core a larger negative temperature anomaly was measured: the sediments there are up to 3.5°C colder than the over- and underlying ones. This is probably largely the result of sediment disturbance caused by pulling the sediment core out of the gravity corer on deck. However, near-bottom temperature variations could also have played a role. For hydrate dissociation, there were no indications.
Station LV29-51-1 at the new flare at 825 m water depth shows a linear temperature increase with depth of 50 mK/m up to 480 cm subbottom depth. From 480 cm up to the base of the core (580 cm) the thermal gradient suddenly increases to a highly anomalous value of 400 mK/m. Gas hydrates were not found in this core.

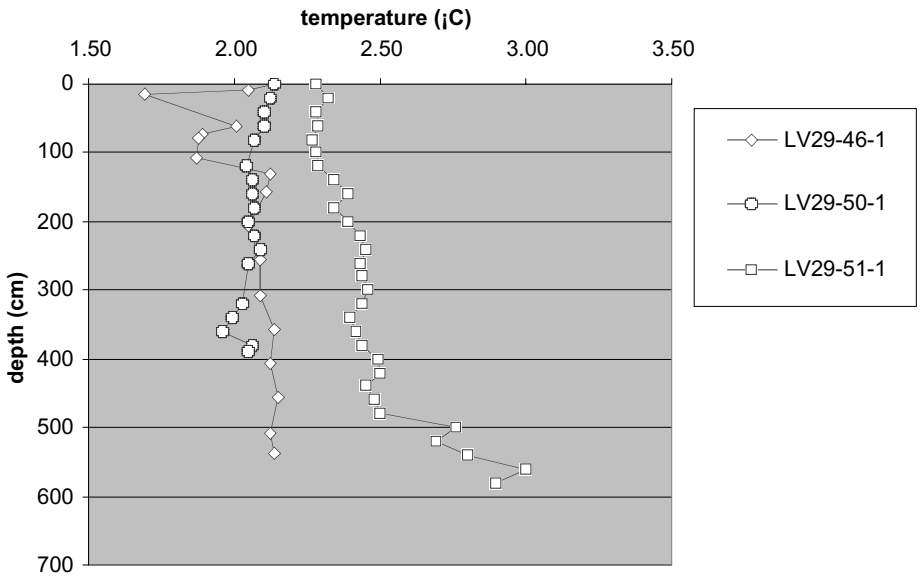

Fig. 11.1: *Temperatures measured on sediment cores from the Sakhalin slope.*

11.2.2.2 Derugin Basin

In the Derugin Basin 4 cores 450 to 600 cm long were recovered. Two cores were taken close to each other on the Barite Mounds at a water depth of about 1,500 m: LV29-53-1 and LV29-56-1. The other two cores were taken on the "Clam Hill" at water depths of 1,536-1,580 m: LV29-59-1 and LV29-63-1. Here, temperatures were measured at larger intervals of 50-100 cm with the LITOS thermometer in order to reduce the measuring time and get most accurate information on the thermal gradient and heat flow in this large venting area. Hydrate accumulations were previously not encountered here, but as the necessary stability conditions were given here, careful attention was paid to negative temperature anomalies. The measured subbottom temperatures are plotted in *Figure 11.2*. The near-bottom water temperatures measured by CTD were about 2.23°C.

All cores from the Derugin Basin show increased thermal gradients ranging from 142 to 243 mK/m for full core length averages. In all cores, and in particular in those of the "Barite Mounds", a general trend of higher gradients closer to the sediment surface was observed. The gradients in the upper intervals amount to such large values as 630-500 mK/m, whereas the gradients in the lowest intervals do not exceed 78-160 mK/m. This concave upward curving of geotherms is typical for areas with upward fluid flow.

Within this general trend, some intervals with colder temperatures can be recognized. The largest negative temperature anomaly (0.25°C) is expressed in the "Barite Mounds" core LV29-56-1 at a subbottom depth of 200 cm at which also anomalous high methane and water contents were found (see Chapter 6.4.2). All these indications suggest that disseminated gas hydrate was present in the interval of 150-350 cm and dissociated before the core was exposed for analysis. The core also appeared to have very low chlorinity values, but this information has to be confirmed by further analyses. Cold temperatures were also measured in cores LV29-63-1 and LV29-53-1 at subbottom depths of 250 and 300 m, respectively. These negative anomalies are, however, not larger than 0.1-0.15°C. Again, the dissociation of hydrates might have caused them, but this has to be confirmed by other proxies.

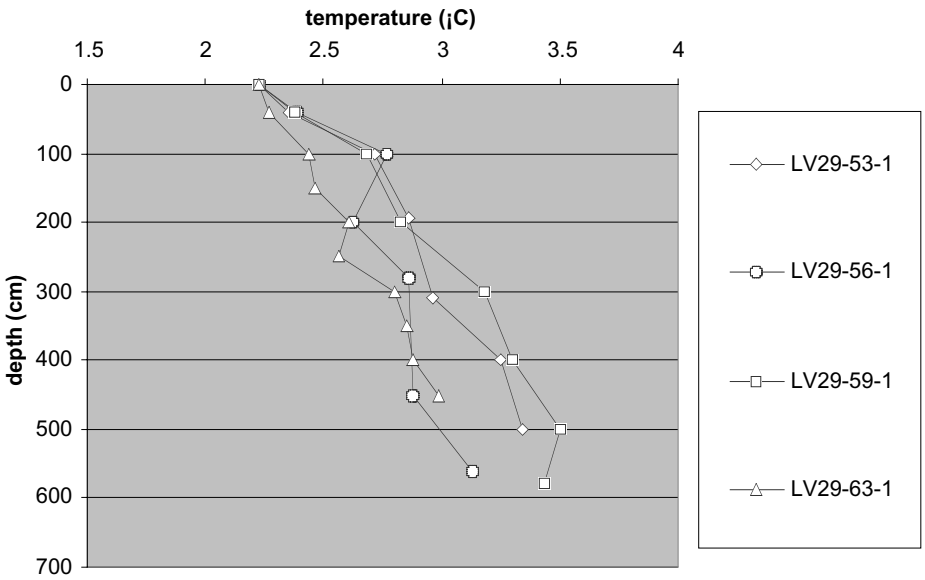

Fig. 11.2: *Temperatures measured on sediment cores from the Derugin Basin.*

11.3 Thermal conductivity

11.3.1 Method

Thermal conductivity data was collected on all cores at intervals of 0.5 to 1 m. The measurement was performed 20-40 min after core arrival on deck by inserting a needle probe in the half cores. Thermal conductivity was measured with the LITOS needle probe applying the continuous heating method. Errors are typically between 5-10%; corrections for temperature and pressure conditions were not made.

11.3.2 Preliminary results and discussion

The measured thermal conductivities are plotted in *Figure 11.3*. The range of measured thermal conductivities amounts to 0.54-1.07 W/m/K and the average is 0.76 W/m/K. Most cores yielded thermal conductivity values of about 0.70 W/m/K at 1 m depth with an increase or decrease of 0.1 W/m/K up to 4 m subbottom depth. These values are normal for diatomaceous silty clays.

Three cores show a different picture.

1) In core LV29-59-1, the thermal conductivities are much higher over the whole length of the core, ranging between 0.86 and 1.07 W/m/K. These high values probably reflect the

high sand content in the core. Also, the water content in this core was much lower than in the other cores.

2) Cores LV29-56-1 ("Barite Mounds") and LV29-50-1 ("Obzhirov flare") display a pattern that can best be explained by the presence of gas hydrates that were already dissociated during core recovery. In core LV29-56-1 the lowest thermal conductivity was measured: 0.54 W/m/K at 2 m subbottom depth. The low value is believed to result from the very high water content in this interval. 1 m upcore, a thermal conductivity of 0.88 W/m/K was obtained, corresponding to a low water content. This observation supports the suggestion that gas hydrates were present in this interval: the high water content resulted from the dissociation of hydrates during core retrieval, while the low water content and high thermal conductivity of the overlying layer resulted from water segregation during the hydrate formation process in situ. A similar pattern, but less profound was observed in core LV29-50-1. In this core from "Obzhirov flare" gas hydrates were visually observed at the core base.

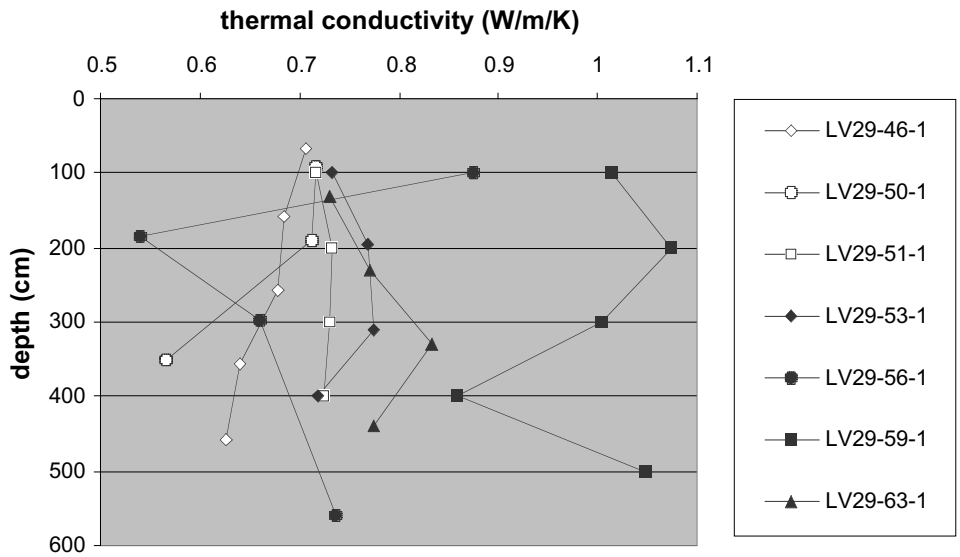

Fig.11.3: *Thermal conductivities measured on sediment cores from the Sakhalin slope (open marks) and the Derugin Basin (filled marks).*

11.4 Magnetic susceptibility

11.4.1 Method

Low-field magnetic susceptibility was measured on each half core. We measured with a Bartington MS2 susceptibility meter, which was calibrated each time with a sample of 1% Fe_3O_4. Measurements were performed in 5 cm intervals. It should be noted that the measurements were sometimes conducted not immediately and continuously on the whole core length, but in two or three sessions depending on core availability. In general, in these cases an important shift to higher values was observed at the start of a new session. These artifacts were not corrected.

11.4.2 Preliminary results

The results of the magnetic susceptibility measurements are plotted in *Figure 11.4*. The measured susceptibility varies in general between -20.10^{-6} and 40.10^{-6} CGS, with the exception of core LV29-63-1 and local high peaks in the other Derugin cores corresponding

to dropstones. For the three cores taken on the Sakhalin slope (LV29-46-1, LV29-50-1 and LV29-51-1), a general trend of maximum values near the surface (0 to 20.10^{-6}) was observed decreasing towards values of -20.10^{-6} at the core base. The larger values near the surface are probably the result of small amounts of authigenic magnetite. In three of the four cores from the Derugin Basin (LV29-53-1, LV29-56-1 and LV29-59-1) a similar decreasing trend was observed in the upper 2-3 m of the core, but with slightly higher values (from 20.10^{-6} - 40.10^{-6} to -20.10^{-6} - 0). Below 2-3 m subbottom depth, susceptibilities start to increase again. For

a. Sakhalin Slope

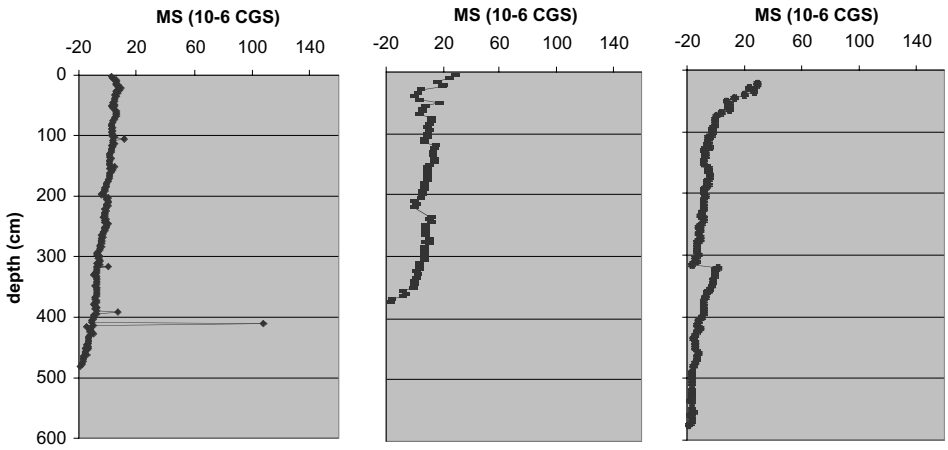

core LV29-46-1 core LV29-50-1 core LV29-51-1

b. Derugin Basin

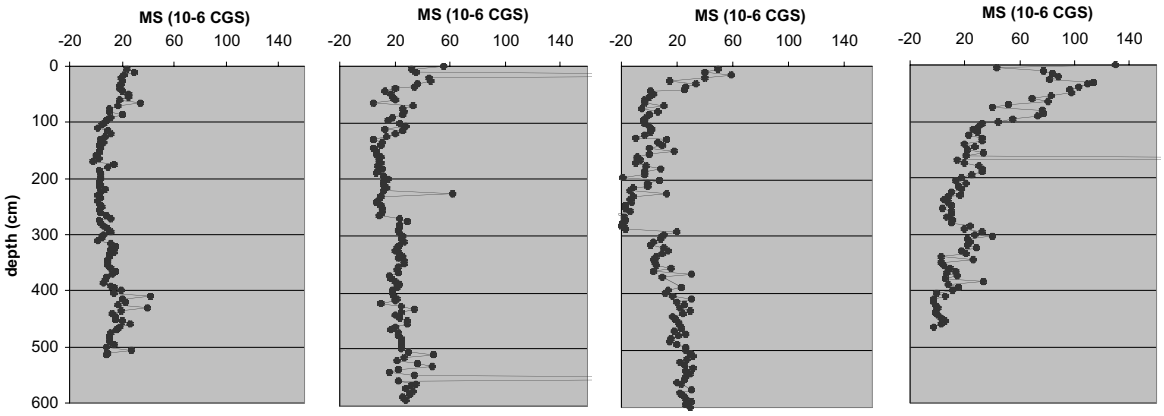

core LV29-53-1 core LV29-56-1 core LV29-59-1 core LV29-59-1

Fig. 11.4: *Magnetic susceptibility determined on half cores from the a) Sakhalin slope and b) Derugin Basin.*

interpretation we need information on pore water element and mineralogical composition. Only core LV29-63-1 revealed higher values than the other cores: the susceptibility first increases in the upper 35 cm from 43.10^{-6} to 114.10^{-6}, and then also decreases to the base of the core.

11.5 Summary

Core temperature measurements and determinations of thermal conductivity and magnetic susceptibility were performed on three sediment cores from the Sakhalin slope (in “Obzhirov flare” and flare 72) and on four cores from the Derugin Basin (“Barite Mounds” and “Clam Hill”). Temperatures were measured immediately after core arrival on deck and physical properties were measured within one hour. The thermal measurements revealed the following features:

1) The flares on the Sakhalin slope show non-elevated temperatures and very low to negative heat flow values in the upper 4-5 m of the sediment column (-13 to 36 mW/m^2). This could indicate a mixing process with sea water.

2) All sampled sites in the Derugin Basin are characterized by high overall heat flow values (100-243 mW/m^2). In general, heat flow decreased from a value of 450-550 mW/m^2 in the upper meters to 65-155 mW/m^2 at 4-5 m subbottom depth. This concave upward curving of temperature profiles is typical for areas with relatively strong upward fluid flow.

3) In two cores the presence of gas hydrates, dissociated during core recovery, was indicated at a specific interval by both temperature and thermal conductivity data. One core corresponds to “Obzhirov flare”, where hydrates were also visually observed. The other core was recovered from the “Barite Mounds” in the Derugin Basin. Gas hydrates have never been visually observed in the Derugin Basin. We suggest that the chlorinity data should be used to confirm the gas hydrate interpretation based on thermal indications.

12. BARITE-CARBONATE MINERALIZATION, METHANE ANOMALIES AND GEOPHYSICAL FIELDS IN THE DERUGIN BASIN

Ruslan Kulinich and Anatoly Obzhirov

12.1 Introduction

Barite-carbonate mineral associations discovered in the eastern part of the Derugin Basin more than twenty years ago were first described as a product of hydrothermal activity by Astakhova et al. (1987) and Astakhova et al. (1990). Detailed studies on the origin and geochemical composition of these mineral associations have already begun during the joint Russian-German cruises LV28 (August-September, 1998) and GE99 (July-September, 1999) within the KOMEX I project.
The results of these expeditions indicate that the earlier found barite samples are only single fragments of massive barite-carbonate chimney-like build-ups up to 5-10 m in height and several meters in diameter. Barite build-ups and barite crusts are widely distributed in the so-called “Barite Mounds” area. Anomalous high methane concentrations were measured in the near-bottom waters of this area, as well (Biebow & Hütten, 1999). Mineralogical and geochemical investigations already carried out within KOMEX I indicate that deep fluid venting plays an active role in barite-carbonate diagenesis and in the occurrence of high methane concentrations. There are also signs for a recent continuation of this process. The structural control on barite mineralization could also be identified (Biebow et al., 2000).

Nevertheless, the following questions have remained unclear:
1. What are the sources and mechanisms of the fluid ascent - cold seeping or deep hydrothermal processes connected with magmatic activity?
2. How large is the area affected by these processes?
3. Why is the strong methane emission on the shelf and slope of Sakhalin not accompanied by barite-carbonate mineralization as observed in the Derugin Basin? Obviously, this is due to different methane sources in these two areas.

12.2 Preliminary results and discussion

The investigations of these questions were continued during the 29th cruise of RV *Akademik Lavrentyev*. Additionally, the spatial and causal relationship of barites and gas anomalies with the structural pattern of the acoustic basement and the overlapping sediments was investigated and a correlation with gravity and magnetic anomalies was performed. The correlation of the aforementioned geophysical fields with the distribution of the barite-carbonate mineral associations was made to better understand the structural patterns of the investigated area and to estimate the degree of magmatic activity, which took place here in the past, and thus to make a contribution to the understanding of the initial (deep) sources of the strong gas emanations and barite mineralizations. For this purpose, maps of gravity and magnetic anomalies obtained during the 16th cruise of RV *Professor Gagarinsky* were used. *Figure 12.1* shows the map of gravity and free-air anomalies.
To determine the nature of the gravity anomalies, they were correlated with the acoustic basement relief mapped during the same expedition. This correlation shows that the acoustic basement structure and the bathymetry are the main sources of the gravity anomalies. Thereby, positive anomalies reflect basement uplifts and negative ones areas of depressions. According to this, a vast area of negative anomalies was observed in the Derugin Basin, whereas the Central Okhotsk Rise, a morphostructure with a very thin sediment cover, is characterized by the highest amplitudes of gravity anomalies. The studied area is part of the

Kashevarov Rift Zone (Gnibidenko, 1990), which is located between them. In accordance with the obtained seismic data, the gravity map illustrates a mosaic of near-latitudinal horsts and grabens forming the Kashevarov zone.

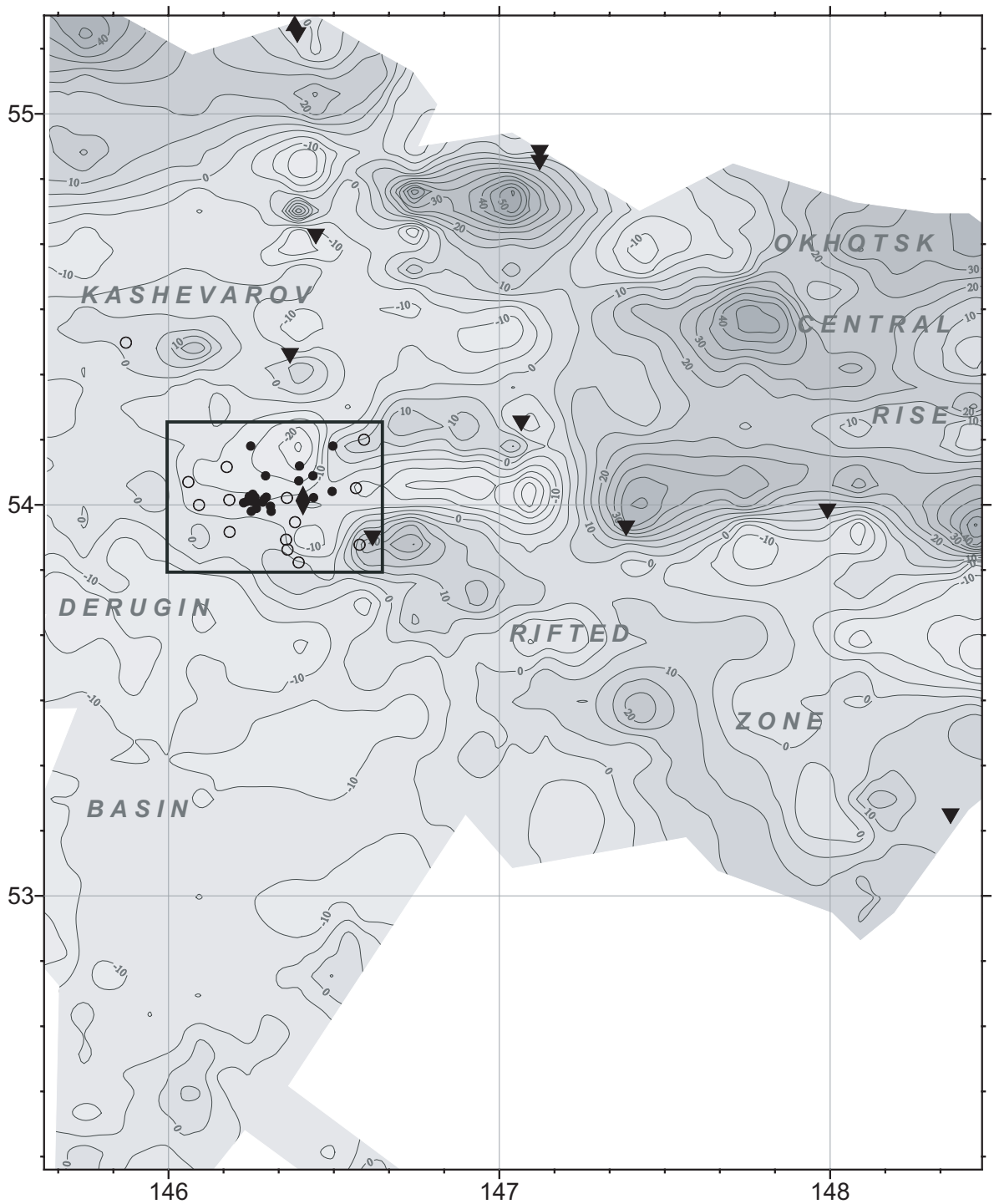

Fig. 12.1: *Gravity free-air anomaly map. Gravity data was obtained during the 16th cruise of RV Professor Gagarinsky. Filled circles indicate position of stations with methane anomalies in the bottom water. Open circles indicate stations without methane anomalies. Diamond marks the position of high heat flow values. Triangles indicate dredging sites carried out before KOMEX cruises. The investigated area is limited by a rectangular.*

The formation mode and basement composition are important indicators to understand the present conditions of this zone. The results of dredging carried out along the western part of the Central Okhotsk Rise and in the Kashevarov Rift Zone are the only data source on the

basement's composition. Dredging was carried out in the investigation area already in previous years (Catalog of dredging sites in the Okhotsk Sea, 1982). The location of the dredge sites is shown on the gravity anomaly map (*Fig. 12.1*). Apparently, almost all these sites are located within the gradient zones of gravity maximums that correspond to the flanks of basement uplifts. The samples recovered during dredging include mainly volcanic and plutonic rocks of intermediate and basic composition. Volcanic rocks are mainly represented by andesites, andesite-basalts, basalts, diabases, quartz porphyrites, dacites and tuffs. Plutonic rocks consist of diorites, granodiorites, and less often of granites. These rocks have a high average density (2.67 - 2.90 g/cm^3) and may be a source of the positive gravity anomalies.

The spatial consistence of the recovered rocks with the observed gravity maximums indicates that they are autochthonous, dominate the basement composition and are the source of these gravity disturbances. Assemblages of similar rocks were also recovered by dredging in other areas of the Kashevarov Rift Zone. The sites dredged during the 13th cruise of RV *Dmitry Mendeleev* are located nearest to the investigated area. Petrological analysis of samples recovered during this expedition (Korenbaum et al., 1981) showed that volcanic and plutonic rocks of intermediate and basic composition prevail in the investigated area. Volcanic rocks are mainly represented by andesite-basalts and andesite-dacites; plutonic rocks include most of all granodiorite and diorite. Acid types of magmatic rocks were found here less often. Pre-Cenozoic sedimentary rocks are formed mainly due to erosion of the basic and intermediate volcanic and plutonic complexes. All types of rocks show signs of methamorphic and hydrothermal alterations. The studied magmatic rocks are mainly of Upper Mesozoic to Paleogene age. The age of the youngest basalts is 11.9 Ma.
Thus, the area of barite mineralization and methane anomalies is located in a zone in which tectono-magmatic activity probably started in Mesozoic times. Transtensional tectonics which took place in the Oligocene to Miocene (Kharakhinov, 1998; Worrall et al., 1996) destroyed the existing lithosphere and resulted in riftogenic conditions with intensive heat and mass transfers towards the upper crust. In this context, the Cenozoic rebuilding of the basement is not only expressed by the development of horst and graben patterns, but also by a new activation of deep magmatic processes initiating a new stage of volcanic and hydrothermal activity. This stage ended in the Pliocene in connection with a switch from extensional to compressional tectonics (Biebow et al., 2000). The dominance of magmatic components in the basements is perfectly reflected by its high magnetic anomalies (*Fig. 12.2*).

The structural position of the "Barite Mounds" earlier determined by seismic data (Biebow et al., 2000) can be specified using anomalous gravity and magnetic fields. According to the map of gravity anomalies (*Fig. 12.1*), the area of barite mineralization is located on the northern flank of a sublatitudinal basement uplift (horst), to the north of which an almost isometric depression is situated. According to our calculation, the depth of the basement descending in relation to the surrounding uplifts is here about 3,000 m. The depression formed at a crossing point of several faults trending in EW, NW and NE directions. With regard to this, the basement of the depression is considered to be very permeable for fluids. Actively disturbed and high magnetic anomalies observed above this depression indicate the presence of volcanic formations in the sediments and basement. Taking this into account, the specified structure is most likely of volcanogenic-sedimentary origin.
Thus, the barite mineralization and anomalous emanations of methane are closely correlated to this magmatic structure. Barite mineral associations are concentrated on the margin of this structure, whereas the distribution of methane anomalies covers a much larger area. According to the results of the present expedition, high methane concentrations occur in the whole area of this depression, but do practically not exceed its borders. Thus, it is likely that the methane emanations and barite mineralization are related to the earlier formed volcanogenic structure.

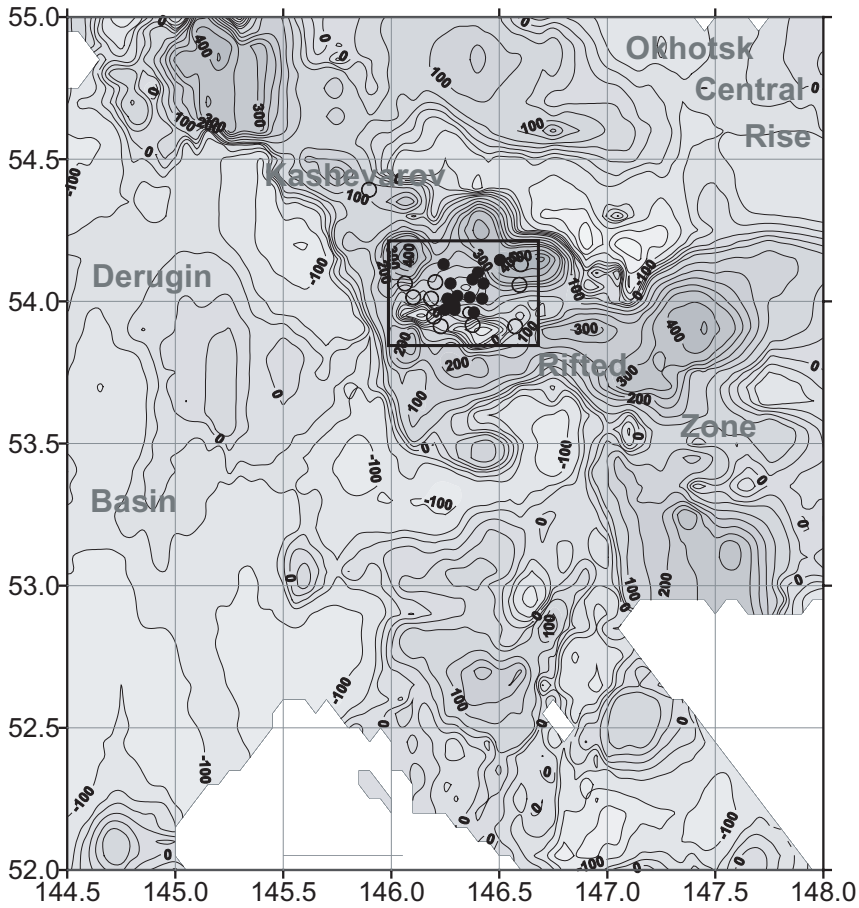

Fig. 12.2: *Magnetic anomaly map. Magnetic data was obtained during the 16th cruise of RV Professor Gagarinsky. Rectangular indicates investigated area of barite mineralization and methane anomalies. Filled circles indicate location of methane anomalies. Open circles indicate sites without methane anomalies.*

At present, it is difficult to determine the time of the last magmatic activation in this region. As mentioned above, the main magmatic processes ended possibly in Miocene or Pliocene times. However, the distinct localization and the high magnitude of the magnetic anomalies in the study area indirectly indicate a younger age of the formation of the magmatic rocks. The observed signs of fluid venting, the high heat flow near the investigation area (109.3; 155.5; 90.3 mWt/m^2), and the active emission of methane can be an indicator of remnant postmagmatic low-temperature processes. The barite-carbonate mineralogenesis is likely to be a secondary effect of the aforementioned processes.

12.3 Conclusions

The following conclusions can be drawn:

1. The barite-carbonate mineralization and anomalous concentration of methane in the bottom water of the investigated area are located within a volcanogenic-sedimentary depression formed at the crossing point of several faults. The main tectono-magmatic activity, which formed this structure, took place during the Oligocene to Miocene, but there is evidence that this activity ended much later.
2. The recently observed fluid venting, active emission of methane and high heat flow recorded near the study area can be indicative of remnant postmagmatic lowthermal processes within the borders of this volcanogenic structure. Barite-carbonate mineralogenesis can be a secondary effect of the above-mentioned processes.

13. REFERENCES

Aloisi, G., Pierre, C., Rouchy, J.-M. et al., 2000. Methane-related authigenic carbonates of eastern Mediterranean Sea mud volcanoes and their possible relation to gas hydrate destabilization. Earth and Plan. Scie. Lett., 184, 321-338.

Astakhova, N.V., Lipkina, M.I. & Mel'nichenko Yu.I., 1987. Hydrothermal barite mineralization in the Derugin Basin of the Sea of Okhotsk. Doklady Akademii Nauk SSSR (Talks of the Academy of Science of the USSR), 295, 1, 212-215 (in Russian).

Astakhova, N.V., Narnov, G.A., & Yakusheva, I.N., 1990. Carbonate-barite mineralization in the Derugin depression (Sea of Okhotsk). Tikhookeanskaya geologiya (Pacific geology), 3, 37-42 (in Russian).

Baranov, B., Werner, R., Hoernle, K., Tsoy, I., Bogaard, P.v.d. & Tararin, I., 2002a. Volcanological, geochemical, paleo-oceanological and geophysical evidence for compressionally-induced high subsidence rates in the Kurile Basin (Okhotsk Sea). Tectonophysics, 350, 63-97.

Baranov, B.V., Wong, H.K., Dozorova, K.A., Karp, B.Ya., Lüdmann, T. & Karnaukh, V., 2002b. Opening geometry of the Kurile Basin (Okhotsk Sea) as inferred from structural data. The Island Arc, August, 2002.

Biebow, N. & Hütten, E. (eds.), 1999. Cruise Reports: KOMEX I and II: RV Professor Gagarinsky cruise 22, RV Akademik M.A. Lavrentyev cruise 28. GEOMAR Report, 82, 188 pp.

Biebow, N., Lüdmann, T., Karp, B. & Kulinich, R., 2000. Cruise Reports: KOMEX V and VI: RV Professor Gagarinsky cruise 26, MV Marshal Gelovany cruise 1. GEOMAR Report, 88, 296 pp.

Boudreau, B.P., 1996. Diagenetic Models and their Implementation. Berlin: Springer Verlag.

Bruyevich, S.V., 1944. Determination alkalinity of small volumes of sea water by direct titration. In: Instruction of chemical investigation of sea water. Moscow-Leningrad: Glavsevmorput, 83 pp.

Buczynski, C. & Chafetz, H.S., 1991. Habit of bacterially induced precipitates of calcium carbonate and the influence of medium vicosity on mineralogy. J. Sedim. Petrol., 61 (2), 226-233.

Carpenter, J.H., 1965. The Chesapeake Bay Institute technique for the Winkler dissolved oxygen method. Limnol. Oceanogr., 10, 141-143.

Catalog of dredging sites in the Okhotsk Sea, 1982. Yuzhno-Sakhalinsk: Far Eastern Center of Academy of Sciences of the USSR Press, 101 pp. (in Russian).

Derkachev, A.N., Bohrmann, G., Greinert, J. & Mozherovsky, A.V., 2000. Authigenic carbonate and barite mineralization in sediments from Derugin Basin (the Sea of Okhotsk). Lithology and Mineral Res., 6, 568-585 (in Russian).

Derkachev, A.N., Obzhirov, A.I., Bohrmann, G., Greinert, J. & Suess, E., 2002. Authigenic mineral formation on the sites of a cold gas-fluid emanations at the bottom of the Sea of Okhotsk. In: Conditions of the generation of bottom sediments and related mineral deposits within marginal seas. Vladivostok: Dalnauka, 49-63 (in Russian).

Ginsburg, G.D. & Soloviev, V.A., 1994. Submarine gas hydrates. St. Petersburg: VNIIOkeangeologiya, 200 pp. (in Russian).

Ginsburg, G.D., Soloviev V.A., Cranston R.E., Lorenson, T.D. & Kvenvolden, K.A., 1993. Gas hydrates from the continental slope, offshore Sakhalin Island, Okhotsk Sea. Geo-Marine Letters, 13, 41-48.

Gnibidenko, G.S., 1990. The rift System of the Okhotsk Sea. - Proceeding of the First International Conference on Asian Marine Geology, Bejing: China Ocean Press, 73-81.

Gnibidenko, G.S., 1979. Tectonics of the seafloor from the far east marginal seas. Moscow: Nauka, 163 pp. (in Russian).

Gnibidenko, G.S., Hilde, T.W.C., Gretskaya, E.V. & Andreev, A.A., 1995. Kurile (South Okhotsk) Backarc Basin. In: Taylor, B. (ed.). Backarc Basins: Tectonics and Magmatism, New York: Plenum Press, 1995, 421-448.

Gonzalez-Mucoz, M.T., Ben-Chekroun, K., Ben-about, A., Arias, J.M. & Rodriguez-Gallego, M., 2000. Bacterially induced Mg-calcite formation: role of Mg 2+ in development of crystal morphology. J. Sedim. Res. Sec. A., 70 (3), 559-565.

Greinert, J., Bohrmann, G. & Suess, E., 2001. Gas hydrate-associated carbonates and methane-venting at Hydrate Ridge: Classification, distribution and origin of authigenic lithologies. Natural Gas Hydrates: Occurence, Distribution and Detection. AGU. Geophysical Monograph, 99-113.

Greinert, J., Bollwerk, S.M., Derkachev, A., Bohrmann, G. & Suess, E., 2002. Massive barite deposits and carbonate mineralization in the Derugin Basin, Sea of Okhotsk: precipitation processes at cold seep sites. Earth and Planetary Science Letters, 203, 165-180.

Guggenheim, E.A., 1930. Studies of cells with liquid-liquid junctions. Part II. Thermodynamic significance and relationship to activity coefficients. J. Phys. Chem., 34, 1758-1766.

Hayashi, T., 1997. The study of thermal structure and tectonic history of the Derugin Basin, Sea of Okhotsk. Master's thesis. Tokyo: Tokyo University, 39 pp.

Ivanenkov, V.N. & Bordovsky, O.K., 1978. The methods of hydrochemical investigation of the ocean. Moscow: Nauka, 271 pp. (in Russian).

Jorgensen, N.O., 1992. Methane-derived carbonate cementation of marine sediments from the Kattegat, Denmark: geochemical and geological evidence. Mar. Geol., 103, 1-13.

Kharakhinov, V.V., 1998. Tectonics of the Oil and Gas potential province of the Okhotsk Sea. Okha, 77 pp.

Korenbaum, S.A., Mishkin, M.A., Valuy, G.A., Gnibidenko, G.S. & Kurentsova, N.A., 1981. Petrology of bedrocks of the Sea of Okhotsk. In: The structure of the Okhotsk Sea bottom. Moscow: Nauka, 176 pp. (in Russian).

Kulm, L.D. & Suess, E., 1990. Relationship between carbonate deposits and fluid venting: Oregon accretionary prism. J. Geoph. Res., 95, 8899-8915.

Lueker, T.J., Dickson, A.G. & Keeling, C.D., 2000. Ocean pCO_2 calculated from dissolved inorganic carbon, alkalinity, and equations for K_1 and K_2: validation based on laboratory measurements of CO_2 in gas and sea water at equilibrium. Mar. Chem., 70, 105-119.

Luff, R. & Wallmann, K., submitted. Fluid flow, methane fluxes, carbonate precipitation and biogeochemical turnover in gas hydrate-bearing sediments at Hydrate Ridge, Cascadia Margin: Numerical modeling and mass balances. Geochim. Cosmochim. Acta.

Luff, R., Wallmann, K., Grandel, S. & Schlüter, M., 2000. Numerical modeling of benthic processes in the deep Arabian Sea. Deep-Sea Research II, 47, 3039-3072.

Millero, F., 1995. Thermodynamics of the carbon dioxide system in the oceans. Geochim. Cosmochim. Acta, 59, 661-677.

Nürnberg, D., Baranov, B.V. & Karp, B.Ya. (eds.), 1997. RV Akademik M. A. Lavrentyev cruise 27 - Cruise Report GREGORY. GEOMAR Report, 60, 69 pp.

Obzhirov, A.I., 1993. Gas and geochemical fields of the benthic layer of seas and oceans. Moscow: Nauka, 131 pp. (in Russian).

Obzhirov, A.I., 1992. Gas-geochemical manifestations of gas-hydrates in the Okhotsk Sea. Alaska Geology, 21 (7), 1-7.

Pitzer, K.S., 1991. Ionic interaction approach: Theory and data correlation. In: Pitzer, K.S. (ed.). 2nd Edition, Activity Coefficients in Electrolyte Solutions. Roca Raton, Ann Arbor, Boston, London: CRC Press, 75-153.

Sahling, H., Galkin, S.V., Foerstel, H., Greinert, J., Salyuk, A., Sosnin, V., Winckler, G. & Suess, E., submitted. Cold seep communities on the Sakhalin continental shelf and slope,

and in the Derugin Basin (Sea of Okhotsk); site description and depth related distribution patterns. Deep Sea Research.

Sakai, H., Gamo, T., Ogawa, Y. & Boulegue, J., 1992. Stable isotopic ratios and origins of the carbonates associated with cold seepage at the eastern Nankai Trough. Earth and Planet. Sci. Lett., 109 (3-4), 391-404.

Stakes, D.S., Orange, D. et al., 1999. Cold-seeps and authigenic carbonate formation in Monterey Bay, California. Marine Geology, 159, 93-109.

Suess, E., Bohrmann, G., Greinert, J., Derkachev, A.N., Kulinich, R.G. et al., 1999. Giant cold vents and barite mineralization in the Derugin Basin. 2nd Workshop on Russian-German Cooperation in the Sea of Okhotsk - Kurile Island Arc System. Kiel, January 26-29, p. 20.

Tishchenko, P.Ya., Chichkin, R.V., Il'ina, E.M. & Wong, C.S., 2002. pH Measurements in estuary by means of cell without Liquid Junction. Okeanologiya (Oceanology), 41 (1), 32-41 (in Russian).

Tishchenko, P.Ya., Pavlova, G.Yu., Salyuk, A.N. & Bychkov, A.S., 1998. Carbonate system and dissolved oxygen in the Japan Sea. Estimation of biological and thermal terms. Okeanologiya (Oceanology), 38 (5), 678-684 (in Russian).

Tishchenko, P.Ya., Wong, C.S., Pavlova, G.Yu., Johnson, W.K., Kang, D.-J. & Kim, K.-R., 2001. pH measurements of sea water by means of cell without liquid junction. Okeanologiya (Oceanology), 41 (6), 849-859 (in Russian).

Tsunogai, S., Niskimura, M. & Nakaya, S., 1968. Complexometric titration of calcium in the presence of larger amounts of magnesium. Talanta, 15, 385-390.

Wakatsuchi, M. & Martin, S., 1991. Water circulation of the Kurile Basin of the Okhotsk Sea and its relation to eddy formation, J. Oceanogr. Soc. Japan, 47, 152-168.

Werner, R., Tararin, I.A., Hoernle, K. & Lelikov, E.P., submitted. Petrology and geochemistry of submarine volcanism from the northeastern part of the Kurile Basin: Evidence for interaction of basic magma with continental crust. Gondwana Research (Special Issue).

Wong, H.K., 1999. TP7: Sedimentationsprozesse und strukturgeologische Entwicklung des Okhotskischen Meeres. In: Suess, E. (ed.). KOMEX-Zwischenbericht, Kiel, 114-143.

Worrall, D.M., Kruglyak, V., Kunst F. & Kuznetsov, V., 1996. Tertiary tectonics of the Sea of Okhotsk, Russia: Far-field effects of the India-Eurasia collision. Tectonics, 15 (4), 813-826.

Valentine, D.L., Blanton, D.C., Reebugh, W.S. & Kastner, M., 2001. Water column methane oxidation adjacent to an area of active hydrate dissociation, Eel River Basin, 65 (16), 2633-2640.

Zhuravlev, A.V., 1982. Geological structure and development of the South Okhotsk (Kurile) Basin. In: Tuezov, I.K. (ed.). Structure and Composition of the Sedimentary Cover of the Northwestern Pacific. Vladivostok: Far East Scientific Center, 23-33 (in Russian).

APPENDIX 1

Station list

Station list of LV29: 29th expedition of RV Akademik Lavrentyev, Leg 1

Date	Stat. Nr.	Equip-ment	Start	at sf	off sf	End	Dura-tion	Latitude N	Longitude E	Water depth	Recovery	Remarks
	Terpenia Bay											
03.06.	1-1	CTD	06:33		06:37	06:47	00:14	47°59.98	143°58.57	75	8 bottles	1=74, 2=61, 3=51, 4=41, 5=31, 6=21, 7=11, 8=3 (depth m)
03.06.	1-2	LOLA II	09:22			10:45	01:23	48°00.14/ 47°59.52	144°00.45/ 144°59.54	75/78		
	Derugin Basin											
05.06.	2-1	CTD	05:03		05:30	06:00	00:57	54°00.44	146°16.95	1485	12 bottles	1=1495, 2=1484, 3=1439, 4=1390, 5=1098, 6=800, 7=500, 8=299, 9=148, 10=99, 11=49, 12=3 (depth m)
05.06.	3-1	LOLA II	13:48			21:10	07:22	53°58.45/ 53°15.30	146°28.36/ 146°10.02	1460/ 1550		
05.06.	4-1	CTD	23:07		23:38	00:04	00:57	54°01.126	146°25.028	1576	12 bottles	1=1581, 2=1571, 3=1530, 4=1483, 5=1239, 6=991, 7=745, 8=498, 9=299, 10=100, 11=50, 12=3 (depth m)
06.06.	5-1	CTD	02:03		02:29	02:54	00:51	54°09.693	146°35.344	1565	12 bottles	1=1558, 2=1547, 3=1506, 4=1457, 5=1284, 6=1088, 7=789, 8=494, 9=297, 10=149, 11=50, 12=11 (depth m)
06.06.	6-1	CTD	04:52		05:18	05:45	00:53	53°54.194	146°35.264	1533	12 bottles	1=1528, 2=1519, 3=1479, 4=1429, 5=1236, 6=990, 7=743, 8=494, 9=296, 10=147, 11=62, 12=4 (depth m)
06.06.	7-1	CTD	07:24		07:53	08:17	00:53	53°51.628	146°22.409	1593	12 bottles	1=1588, 2=1576, 3=1538, 4=1498, 5=1235, 6=990, 7=744, 8=494, 9=299, 10=149, 11=80, 12=3 (depth m)
06.06.	8-1	LOLA II	09:30			23:00	13:30	53°49.50/ 53°56.51	146°14.44/ 146°13.43	1600/ 1530		
06.06.	9-1	CTD	23:42		00:08	00:32	00:50	53°56.191	146°23.211	1538	12 bottles	1=1524, 2=1516, 3=1486, 4=1428, 5=1237, 6=989, 7=743, 8=497, 9=299, 10=149, 11=64, 12=3 (depth m)
07.06.	10-1	CTD	03:28		03:58	04:21	00:53	53°59.488	146°18.005	1468	12 bottles	1=1442, 2=1432, 3=1391, 4=1237, 5=990, 6=793, 7=597, 8=397, 9=200, 10=76, 11=21, 12=3 (depth m)
07.06.	11-1	CTD	05:36		06:00	06:24	00:48	54°02.923	146°06.573	1620	12 bottles	1=1610, 2=1601, 3=1562, 4=1511, 5=1382, 6=1088, 7=792, 8=495, 9=297, 10=149, 11=74, 12=3 (depth m)
07.06.	12-1	CTD	07:11		07:36	07:59	00:48	54°04.275	146°05.336	1506	12 bottles	1=1508, 2=1498, 3=1459, 4=1409, 5=1237, 6=990, 7=743, 8=495, 9=299, 10=149, 11=77, 12=3 (depth m)
07.06.	13-1	LOLA II	09:33			21:15	11:42	53°54.24/ 53°53.33	146°19.12/ 146°20.02	1500/1580		Problems with GPS: although GPS is on the computer, multibeam software does not get any GPS data.
07.06.	14-1	CTD	23:50		00:14	00:41	00:51	54°04.131	146°25.921	1630	12 bottles	1=1632, 2=1622, 3=1583, 4=1533, 5=1383, 6=1089, 7=792, 8=455, 9=297, 10=149, 11=63, 12=3 (depth m)
07.06.	15-1	CTD	01:45		02:13	02:40	00:55	54°04.099	146°17.777	1686	12 bottles	1=1676, 2=1666, 3=1626, 4=1568, 5=1434, 6=1384, 7=990, 8=494, 9=297, 10=149, 11=70, 12=3 (depth m)
08.06.	16-1	CTD	04:14		04:41	05:11	00:57	54°01.239	146°21.101	1662	12 bottles	1=1651, 2=1641, 3=1601, 4=1551, 5=1502, 6=1432, 7=988, 8=495, 9=298, 10=148, 11=65, 12=3 (depth m)
08.06.	17-1	CTD	06:40		07:07	07:30	00:50	53°58.367	146°15.222	1531	12 bottles	1=1515, 2=1505, 3=1466, 4=1416, 5=1364, 6=1283, 7=792, 8=493, 9=296, 10=148, 11=82, 12=3 (depth m)
08.06.	18-1	LOLA II	09:17			21:33	12:16	53°52.45/ 52°57.48	146°33.02/ 146°34.34	1500/ 1480		
08.06.	19-1	CTD	23:10		23:37	00:06	00:56	54°06.091	146°23.628	1680	12 bottles	1=1676, 2=1668, 3=1628, 4=1580, 5=1432, 6=1187, 7=792, 8=494, 9=298, 10=150, 11=76, 12=3 (depth m)
09.06.	20-1	CTD	01:20		01:53	02:22	01:02	54°08.078	146°14.809	1680	12 bottles	1=1650, 2=1638, 3=1599, 4=1548, 5=1480, 6=1434, 7=987, 8=499, 9=302, 10=155, 11=74, 12=4 (depth m)
09.06.	21-1	HYC	05:13			05:57	00:44	54°00.636	146°16.766	1480	nothing	Test cancelled midway due to problems with the winch despite of repair.

Date	Stat. Nr.	Equip-ment	Start	at sf	off sf	End	Dura-tion	Latitude N	Longitude E	Water depth	Recovery	Remarks
09.06.	22-1	CTD	06:40		07:10	07:37	00:57	54°04.116	146°11.692	1680	12 bottles	1=1650, 2=1638, 3=1599, 4=1548, 5=1480, 6=1433, 7=987, 8=499, 9=303, 10=155, 11=74, 12=4 (depth m)
09.06.	23-1	CTD	11:11		11:40	12:05	00:54	54°02.150	146°29.940	1538	12 bottles	1=1536, 2=1526, 3=1587, 4=1432, 5=1384, 6=1335, 7=1283, 8=990, 9=496, 10=150, 11=68, 12=3 (depth m)
09.06.	24-1	CTD	22:35		22:57	23:22	00:47	53°56.92	146°12.03	1590	12 bottles	1=1574, 2=1565, 3=1523, 4=1473, 5=1423, 6=1332, 7=991, 8=493, 9=299, 10=151, 11=3, 12=3 (depth m)
10.06.	25-1	CTD	03:06		03:43	04:06	01:00	54°03.32	146°35.31	1500	12 bottles	1=1485, 2=1475, 3=1433, 4=1381, 5=1335, 6=1286, 7=791, 8=494, 9=297, 10=149, 11=68, 12=3 (depth m)
10.06.	26-1	HYC	05:54			06:27	00:33	54°00.440	146°16.820	1496	nothing	Cancelled midway due to problems with the winch despite of repair (did not gain enough speed).
10.06.	27-1	CTD	07:24		07:57	08:20	00:56	54°04.06	146°22.92	1685	12 bottles	1=1676, 2=1668, 3=1625, 4=1580, 5=1483, 6=1384, 7=988, 8=468, 9=297, 10=149, 11=59, 12=4 (depth m)
10.06.	28-1	CTD	09:46		10:12	10:38	00:52	54°09.22	146°30.04	1610	12 bottles	1=1611, 2=1600, 3=1561, 4=1513, 5=1463, 6=1382, 7=989, 8=495, 9=298, 10=150, 11=64, 12=3 (depth m)
Sakhalin shelf and slope												
10.06.	29-1	CTD	22:34		22:44	23:00	00:16	54°26.79	144°04.84	695	12 bottles	1=683, 2=674, 3=633, 4=583, 5=533, 6=484, 7=432, 8=386, 9=298, 10=149, 11=73, 12=3,6 (depth m)
11.06.	30-1	Winch test	02:20			02:47	00:27	54°26.50	144°04.80	695	nothing	Test midway cancelled due to problems with the winch despite repair.
11.06.	31-1	CTD	06:08		06:26	06:45	00:37	54°33.45	144°16.66	962	12 bottles	1=946, 2=890, 3=841, 4=790, 5=694, 6=595, 7=493, 8=393, 9=298, 10=149, 11=67, 12=3,5 (depth m)
11.06.	32-1	CTD	11:03		11:07	11:15	00:12	54°19.26	143°54.30	180	12 bottles	1=172, 2=164, 3=148, 4=126, 5=109, 6=90, 7=69, 8=50, 9=31, 10=20, 11=11, 12=3 (depth m)
11.06.	33-1	LOLA II	12:35			00:20	09:45	54°19.35/ 54°19.14	143°52.29/ 143°57.42	250/ 350		NMEA protocol was changed: no GPS, but Hydrostar needs GGA. After changing back, problems to detect the serial ports (Hydrostar, Windows NT): start of record at 54°19.04/ 143°55.29 at 14:30.
12.06.	34-1	HYC	02:37	02:40		02:44	00:07	54°19.202	143°54.576	182	1 m	
12.06.	34-2	OFOS	04:07	04:22	05:06	05:13	01:06	54°19.610/ 54°18.488	143°55.161/ 143°54.176	190/ 194	40 min of video + ca. 50 photos	Speed much too high - about 2 kn plus drift.
12.06.	34-3	OFOS	05:47	06:14	07:29	07:38	01:52	54°20.463/ 54°18.791	143°55.546/ 143°53.885		60-70 photos	Drifting only (190°, about 1 kn): o.k.
12.06.	34-4	OFOS	08:33	08:40	10:00	10:09	01:36	54°20.636/ 54°19.608	143°56.008/ 143°54.365		60-70 photos	Drifting o.k.
12.06.	35-1	CTD	11:52		12:07	12:19	00:27	54°22.024	143°58.832	381	12 bottles	1=372, 2=363, 3=339, 4=320, 5=290, 6=260, 7=220, 8=181, 9=131, 10=81, 11=37, 12=4 (depth m)
12.06.	36-1	LOLA II	13:16			21:18	08:02	54°19.18/ 54°22.01	143°58.30/ 144°01.46	350/ 550		Stop of track 4 at 54°22.01/ 144°01.46.
12.06.	37-1	TVG	23:41			23:46	00:05	54°19.099/ 54°19.180	143°54.254/ 143°54.203	180/ 180	nothing	Cancelled after 5 min., because TVG did not have power. Winch then did not have enough power for lifting TVG: it took 2,5 h to lift TVG with aid of crane.
13.06.	38-1	CTD	04:07		04:14	04:22	00:15	54°21.972	143°58.828	381	12 bottles	1=372, 2=360, 3=347, 4=316, 5=288, 6=257, 7=217, 8=177, 9=129, 10=79, 11=41, 12=3 (depth m)
13.06.	39-1	CTD	06:34		06:38	06:44	00:10	54°13.844	143°45.288	131	8 bottles	1=123, 2=110, 3=90, 4=70, 5=50, 6=29, 7=10, 8=3 (depth m)
13.06.	40-1	DR1	07:55	08:03	08:47	09:02	01:07	54°19.249/ 54°19.785	143°54.070/ 143°55.034	180/ 180	half full	Sand and plenty well rounded cobbles (dropstones); plenty benhic fauna: crab, sponges (?, attached to cobbles), worms, bivalve fragments
13.06.	41-1	LOLA II	09:43			22:08	12:25	54°20.24/ 54°27.48	143°55.37/ 144°05.42	200/ 720		

Date	Stat. Nr.	Equip-ment	Start	at sf	off sf	End	Dura-tion	Latitude N	Longitude E	Water depth	Recovery	Remarks
13.06.	42-1	OFOS	23:41	23:50	23:58	00:07	00:26	54°20.663/ 54°20.762	143°56.795/ 143°56.879	296/ 299	5 photos	Drifting. Aim to go over "Erwin flare" where echosounder showed flare. Image lost after few minutes: station cancelled.
14.06.	42-2	OFOS	01:57	02:03	02:48	02:54	00:57	54°19.338/ 54°19.449	143°55.262/ 143°56.140	195/ 248	30 photos	Drift of about N25 changed at beginning of drive to about N90. For some reason the protocols from 02:06 to 02:53 did not save in the files.
14.06.	42-3	OFOS	03:51	04:01	06:15	06:26	02:35	54°19.136/ 54°20.008	143°57.775/ 143°55.985	352/ 243		With engine slowly against about N100 current in order to cross "Erwin flare" seen on echosounder.
14.06.	42-4	DR1	07:08	07:08	07:52	08:12	01:04	54°20.257/ 54°19.764	143°55.643/ 143°56.031	209/ 241	half full	Trying to get carbonate ? build-ups. Sand and well rounded cobbles (dropstones); benthic fauna: crab, bivalve fragments, worms and corals (2 fragments)
14.06.	42-5	HYC	08:30		08:40	08:51	00:21	54°20.044	143°55.201	191	50 cm	Start of station not recorded. Sediment consists of sand and gravel.
14.06.	42-6	DR1	09:26	09:34	14:06	14:17	04:51	54°19.904/ 54°20.104	143°55.480/ 143°56.162	200/ 253	half full	Sand and well rounded cobbles (dropstones); bledy crabs, 1 bivalve shell, starfish, sponges ? fixed on cobbles. End of station not recorded.
14.06.	43-1	CTD	11:17		11:24	11:35	00:48	54°20.500	143°56.691	302	12 bottles	1=294, 2=281, 3=258, 4=229, 5=199, 6=173, 7=139, 8=109, 9=79, 10=39, 11=19, 12=4
14.06.	44-1	LOLA II	13:39			19:10	05:31	54°25.56/ 54°27.22	143°54.18/ 143°56.59	205/ 350		
14.06.	45-1	CTD	20:05		20:14	20:29	00:24	54°23.936	144°01.625	521	12 bottles	1=504, 2=495, 3=445, 4=397, 5=346, 6=298, 7=248, 8=198, 9=148, 10=99, 11=49, 12=3,6
14.06.	46-1	HYC	22:02		22:33	23:03	01:01	54°26.492	144°04.600	684	6 m	Winch had to be stopped during lowering of HYC (HYC already near seafloor), because cable ran out of wheels of spooling device. "Carl`s core".
15.06.	46-2	OFOS	01:14			01:19	00:05	54°25.589/ 54°25.541	144°04.204/ 144°04.168	650/ 655	nothing	Coordinates of start and end: OFOS did not reach the seafloor, because image was lost during deploying: station cancelled.
15.06.	47-1	CTD	03:15		03:30	03:44	00:29	54°29.935	144°12.213	870	12 bottles	1=863, 2=856, 3=810, 4=742, 5=692, 7=594, 8=495, 9=297, 10=197, 11=88, 12=3,5 (depth m)
15.06.	48-1	SL-R	04:58		05:33	06:00	01:02	54°26.398	144°05.837	711	nothing	Core was empty, obviously did not hit the seafloor vertically.
15.06.	48-2	OFOS	06:41	07:09	08:29			54°27.009/ 54°26.313	144°04.624/ 144°03.920	684/ 660	ca. 100 photos	Drifting ca. N190. Done in two separate drifts: dragging OFOS at 2.5 knts between one drift and the next. Hauling up OFOS 50 m to start of next line.
15.06.	48-3	OFOS		9:47	11:42	12:02	5:21	54°27.192/54°26.607	144°5.219/144°04.569	700/680	ca. 50 photos	OFOS already in water from st. 48-2.
15.06.	49-1	LOLA II	13:00			21:11	08:11	54°27.02/ 54°29.41	143°56.30/ 144°02.49	360/ 660		
15.06.	50-1	SL-R	22:30		22:58	23:27	00:57	54°26.811	144°04.870	695	4 m	Contains gas hydrates at core base.
16.06.	50-2	OFOS	01:03	01:27	03:45	04:15	03:12	54°26.111/ 54°26.676	144°02.883/ 144°04.668	624/ 688	30 photos	Going with drift. Drift changed so we haded in 50 m and started drifting from: 54°26.845/ 144°04.59. Image disappeared at 03:43. Cancelled.
16.06.	50-3	OFOS	05:51	06:08	07:34	08:07	02:16	54°26.788/ 54°25.840	144°04.490/ 144°05.680	688/ 709	ca. 100 photos	At starting position bubbling seen on sea surface. Drifting.
16.06.	51-1	SL-R	09:40		10:23	10:59	01:19	54°28.812	144°11.561	825	6 m	SL-R brought out at 09:24 (54°28.955/ 144°11.725; 839 m) prior to vessel positioning. Winch stopped several times during lowering of SL-R, because axis of spooling device did not work correctly. SL-R nevertheless got into sediment directly in center of holmy flare
16.06.	52-1	LOLA II	11:40			15:26	03:46	54°29.11/ 53°31.14	144°02.38/ 144°05.49	350/ 680		
	Derugin Basin											
17.06.	53-1	HYC	00:03		00:49	01:31	01:28	54°00.495	146°16.909	1493	5,20 m	
17.06.	53-2	OFOS	03:22	03:51	09:30	10:20	06:58	54°00.176/ 54°01.656	146°16.193/ 146°14.936	ca. 1520/ 1629	ca. 300 photos	Drifting all track at ca. N330; OFOS program crashed half way through: created 2 -prot and -nmea files.
17.06.	54-1	LOLA II	11:55			19:11	07:16	54°02.53/ 54°03.36	146°05.95/ 146°14.01	1630/ 1680		
17.06.	55-1	OFOS	21:14	23:00				53°58.888	146°21.534	1472	ca. 150 photos	Drift at 21:15 W. Before going to seafloor, moved to new position: 53°58.893/ 146°21.983. At 00:13 drift changed to SW. OFOS dragged in water to 53°59.921/ 146°20.782 (see track of station 55-2).

Date	Stat. Nr.	Equip-ment	Start	at sf	off sf	End	Dura-tion	Latitude N	Longitude E	Water depth	Recovery	Remarks
18.06.	55-2	OFOS	03:37	03:48	05:47			53°59.748/ 53°58.623	146°20.583/ 146°19.449	1485/ 1505	ca. 150 photos	Continuation of station 55-1: OFOS dragged in water to station 55-2. Drifting appr. S, then SW. Very good correlation between barites on OFOS and echosounder "barite reflector".
18.06.	55-3	OFOS	07:12	07:26	10:16	11:03	13:49	54°00.583/ 53°59.514	146°18.685/ 146°18.969	1479/ 1428	ca. 150 photos	Continuation of station 55-2: starting with OFOS in water from previous track. Drift N170.
18.06.		ECH	12:07			20:43	08:16	54°02.009/ 53°59.030	146°12.007/ 146°28.003	1610/ 1580		Hydroacoustic mapping of barite mineralization. 17 tracks of 2-3 miles length each.
18.06.	56-1	SL-R	21:38		22:19	22:52	01:14	54°00.746	146°15.947	1470	ca. 5 m	Strong degassing (plastic film bursted).
19.06.	57-1	OFOS	00:39	02:55	03:34			54°00.642/ 54°00.231	146°26.546/ 146°26.202	1588/ 1400	see st. 57-4	Drift: N190. Hauled up 300 m to move to station 57-2.
19.06.	57-2	OFOS	04:13	04:24	05:52			54°01.852/ 53°59.973	146°26.363/ 146°25.581	1440/ 1492	see st. 57-4	OFOS moved in water from station 57-1 to 57-2. Drift: N170, at the end of the line N220. Hauled up to move to station 57-3.
19.06.	57-3	OFOS	07:10	07:22	07:55			54°01.229/ 54°00.888	146°25.873/ 146°25.522	1591/ 1586	see st. 57-4	Starting with OFOS in water from previous station. Drift: ca. SW. Missed the mountain! Dragging OFOS in water to next station.
19.06.	57-4	OFOS		08:52	10:17	11:05	10:26	54°01.175/ 54°00.788	146°26.033/ 146°24.536	1477/ 1583	ca. 450 photos on station 57	Starting with OFOS in water from previous line.
19.06.	58-1	LOLA II	12:15			20:55	08:40	53°58.13/ 53°57.39	146°29.29/ 146°31.09	1480/ 1470		Problems to detect Boddon (18:30 - 19:15)
19:06	59-1	SL-R	21:43		22:10	22:39	00:56	54°00.765	146°26.054	1425	6 m	
20.06.	60-1	OFOS	00:46	01:47	06:09			54°02.695/ 54°00.144	146°15.849/ 146°13.200	1669/ 1555		Drift: SW, <1.4 knts. Dragging OFOS in water to station 61-1.
20.06.	61-1	OFOS		01:44	10:01	10:37	09:51	54°00.413/ 53°59.483	146°15.648/ 146°15.325	1519/ 1540		Drift: SW. Dragging OFOS inwater from previous station.
20.06.	62-1	LOLA II	12:05			18:19	06:14	53°58.28/ 54°04.25	146°05.26/ 146°06.16	1600/ 1546		
20.06.	63-1	HYC	21:48		22:22	22:58	01:10	54°00.698	146°26.499	1431	4,70 m	
21.06.	64-1	OFOS	00:23	01:43	02:13	05:17	04:54	54°04.403/ 54°03.994	146°05.585/ 146°05.592	1515/ 1551	ca. 150 photos	LOLA high. Top of mound 1515 m.
21.06.	65-1	OFOS	07:09	08:06	09:30	10:28	03:19	54°08.918/ 54°09.957	146°33.511/ 146°32.601	1440/ 1599	ca. 80 photos	
22.06.	66-1	CTD	23:51		00:40	00:51	01:00	47°24.004	143°43.598	735	12 bottles	1=719, 2=705, 3=667, 4=619, 5=571, 6=518, 7=467, 8=395, 9=295, 10=137, 11=50, 12=6 (depth m)

Legend

	Sampling equipment	Latitude/ Longitude
CTD	Multisonde and hydrocasts	Start
DR1	Russian dredge	At and off seafloor
ECH	Russian hydracoustic echosounder	Start and end
HYC	Hydrocorer (6 m length)	At/ off seafloor
LOLA II	Swath bathymetry multibeam echosounder	Start and end
OFOS	TV-sled, Ocean Floor Observation System	At and off seafloor
SL-R	Russian gravity corer (8 m length)	At/ off seafloor
TVG	TV-grab	At/ off seafloor

Date	dd.mm. 2002
Duration	hh:mm
Start, at sf, off sf, end	UTC
Water depth	m by ECH

APPENDIX 2

Hydroacoustic anomalies

Hydroacoustic anomalies (flares)

No	ID	Latitude	Longitude	Time (Vladivostok)	Time (UTC)
1	1	47 23.992'N	143 43.664'E	03.06.2002 11:41:40	03.06.2002 00:41:40
2	2	54 26.810'N	144 03.700'E	11.06.2002 08:18:00	10.06.2002 21:18:00
3	3	54 26.850'N	144 04.930'E	11.06.2002 08:24:00	10.06.2002 21:24:00
4	4	54 26.850'N	144 04.870'E	11.06.2002 08:45:00	10.06.2002 21:45:00
5	5	54 26.610'N	144 04.790'E	11.06.2002 08:47:00	10.06.2002 21:47:00
6	5A	54 26.260'N	144 04.730'E	11.06.2002 08:47:00	10.06.2002 21:47:00
7	6	54 26.260'N	144 04.730'E	11.06.2002 09:17:00	10.06.2002 22:17:00
8	7	54 26.740'N	144 04.790'E	11.06.2002 09:30:00	10.06.2002 22:30:00
9	8	54 26.590'N	144 04.200'E	11.06.2002 10:08:00	10.06.2002 23:08:00
10	9	54 25.350'N	144 02.630'E	11.06.2002 10:19:00	10.06.2002 23:19:00
11	10	54 20.170'N	143 55.600'E	11.06.2002 11:16:00	11.06.2002 00:16:00
12	11	54 19.260'N	143 54.470'E	11.06.2002	11.06.2002
13	12	54 17.560'N	143 52.450'E	11.06.2002 15:50:00	11.06.2002 04:50:00
14	13	54 26.410'N	144 04.430'E	11.06.2002 13:08:00	11.06.2002 02:08:00
15	14	54 28.160'N	144 09.640'E	11.06.2002 15:49:00	11.06.2002 04:49:00
16	15	54 29.110'N	144 11.260'E	11.06.2002 16:05:00	11.06.2002 05:05:00
17	16	54 29.680'N	144 12.160'E	11.06.2002 16:13:00	11.06.2002 05:13:00
18	17	54 28.210'N	144 09.520'E	11.06.2002 18:48:00	11.06.2002 07:48:00
19	18	54 26.760'N	144 04.830'E	11.06.2002	11.06.2002
20	19	54 26.680'N	144 03.620'E	11.06.2002 19:28:00	11.06.2002 08:28:00
21	20	54 26.650'N	144 04.830'E	11.06.2002 19:30:00	11.06.2002 08:30:00
22	21	54 19.040'N	143 55.080'E	11.06.2002 21:04:00	11.06.2002 10:04:00
23	22	54 19.240'N	143 54.160'E	11.06.2002 21:10:00	11.06.2002 10:10:00
24	Ervin	54 19.715'N	143 53.512'E	12.06.2002 00:48:38	11.06.2002 13:48:38
25	?			12.06.2002 11:45:00	12.06.2002 00:45:00
26	23	54 21.990'N	143 58.840'E	12.06.2002 12:45:00	12.06.2002 01:45:00
27	24	54 19.830'N	143 55.300'E	12.06.2002 13:09:00	12.06.2002 02:09:00
28	25	54 19.208'N	143 54.356'E	12.06.2002 13:16:00	12.06.2002 02:16:00
29	26	54 19.856'N	143 55.390'E	12.06.2002 15:15:00	12.06.2002 04:15:00
30	27	54 19.320'N	143 54.710'E	12.06.2002 15:51:00	12.06.2002 04:51:00
31	28	54 18.594'N	143 54.236'E	12.06.2002 16:00:00	12.06.2002 05:00:00
32	29	54 26.779'N	144 04.830'E	12.06.2002 16:23:00	12.06.2002 05:23:00
33	30	54 19.170'N	143 55.110'E	12.06.2002 16:45:00	12.06.2002 05:45:00
34	31	54 19.915'N	143 55.367'E	12.06.2002 16:50:00	12.06.2002 05:50:00
35	32	54 20.156'N	143 55.362'E	12.06.2002 17:27:00	12.06.2002 06:27:00
36	33	54 19.300'N	143 54.421'E	12.06.2002 18:05:00	12.06.2002 07:05:00
37	34	54 19.216'N	143 54.389'E	12.06.2002 19:00:00	12.06.2002 08:00:00
38	35	54 20.151'N	143 55.443'E	12.06.2002 20:10:00	12.06.2002 09:10:00
39	36	54 19.470'N	143 54.080'E	12.06.2002 21:16:00	12.06.2002 10:16:00
40	37	54 19.992'N	143 55.125'E	12.06.2002 21:36:00	12.06.2002 10:36:00
41	38A	54 21.946'N	143 58.948'E	12.06.2002 22:05:11	12.06.2002 11:05:11
42	38B	54 21.995'N	143 59.043'E	12.06.2002 22:06:15	12.06.2002 11:06:15
43	39	54 22.121'N	143 58.850'E	12.06.2002 22:12:00	12.06.2002 11:12:00
44	40	54 22.000'N	143 58.866'E	12.06.2002 22:48:00	12.06.2002 11:48:00
45	41	54 22.037'N	143 58.969'E	13.06.2002 09:29:53	12.06.2002 22:29:53
46	42	54 19.275'N	143 54.513'E	13.06.2002 09:53:00	12.06.2002 22:53:00
47	43	54 21.980'N	143 58.857'E	13.06.2002 15:15:00	13.06.2002 04:15:00
48	44	54 19.074'N	143 55.130'E	13.06.2002 16:48:45	13.06.2002 05:48:45
49	45	54 18.163'N	143 53.356'E	13.06.2002 16:55:08	13.06.2002 05:55:08
50	46	54 17.621'N	143 52.302'E	13.06.2002 16:58:56	13.06.2002 05:58:56

No	ID	Latitude	Longitude	Time (Vladivostok)	Time (UTC)
51	47	54 16.475'N	143 49.893'E	13.06.2002 17:06:45	13.06.2002 06:06:45
52	48	54 16.550'N	143 50.080'E	13.06.2002 18:20:00	13.06.2002 07:20:00
53	49	54 20.162'N	143 55.534'E	13.06.2002 20:40:16	13.06.2002 09:40:16
54	50	54 18.801'N	143 55.457'E	13.06.2002 20:59:30	13.06.2002 09:59:30
55	51	54 18.224'N	143 55.029'E	13.06.2002 21:29:31	13.06.2002 10:29:31
56	52	54 19.990'N	143 55.033'E	13.06.2002 21:44:39	13.06.2002 10:44:39
57	52A	54 19.793'N	143 55.005'E	13.06.2002 21:54:48	13.06.2002 10:54:48
58	52B	54 21.093'N	143 55.047'E	13.06.2002 22:14:22	13.06.2002 11:14:22
59	52C	54 20.938'N	143 54.483'E	13.06.2002 22:33:47	13.06.2002 11:33:47
60	52D	54 19.975'N	143 54.440'E	13.06.2002 22:49:07	13.06.2002 11:49:07
61	52E	54 19.273'N	143 54.500'E	13.06.2002 22:59:55	13.06.2002 11:59:55
62	52F	54 18.187'N	143 54.517'E	13.06.2002 23:16:27	13.06.2002 12:16:27
63	52G	54 19.517'N	143 54.038'E	13.06.2002 23:50:05	13.06.2002 12:50:05
64	52H	54 21.180'N	143 55.133'E	14.06.2002 00:30:00	13.06.2002 13:30:00
65	53	54 19.273'N	143 54.500'E	14.06.2002 01:59:53	13.06.2002 14:59:53
66	54	54 20.784'N	144 05.660'E	14.06.2002 07:26:52	13.06.2002 20:26:52
67	55	54 25.320'N	143 58.878'E	14.06.2002 09:36:24	13.06.2002 22:36:24
68	56	54 26.861'N	144 02.930'E	14.06.2002 04:25:51	13.06.2002 17:25:51
69	57	54 26.633'N	144 04.210'E	14.06.2002 05:03:23	13.06.2002 18:03:23
70	58	54 20.100'N	143 55.600'E	14.06.2002 10:11:33	13.06.2002 23:11:33
71	59	54 20.140'N	143 55.608'E	14.06.2002 16:50:00	14.06.2002 05:50:00
72	60	54 20.085'N	143 55.575'E	14.06.2002 19:27:00	14.06.2002 08:27:00
73	61	54 25.727'N	143 54.490'E	14.06.2002 23:21:23	14.06.2002 12:21:23
74	61A	54 25.790'N	143 54.222'E	14.06.2002 23:24:47	14.06.2002 12:24:47
75	61B	54 25.720'N	143 53.783'E	14.06.2002 23:37:25	14.06.2002 12:37:25
76	61C	54 26.155'N	143 53.533'E	14.06.2002 23:49:23	14.06.2002 12:49:23
77	61D	54 25.748'N	143 54.436'E	15.06.2002 00:29:31	14.06.2002 13:29:31
78	62	54 27.093'N	143 54.332'E	15.06.2002 00:52:07	14.06.2002 13:52:07
79	63	54 27.373'N	143 54.353'E	15.06.2002 00:55:52	14.06.2002 13:55:52
80	64	54 27.566'N	143 54.401'E	15.06.2002 00:58:30	14.06.2002 13:58:30
81	65	54 26.609'N	144 04.539'E	15.06.2002 07:55:00	14.06.2002 20:55:00
82	66	54 27.996'N	144 05.720'E	15.06.2002 08:01:55	14.06.2002 21:01:55
83	67	54 27.933'N	144 05.783'E	15.06.2002 08:24:00	14.06.2002 21:24:00
84	68	54 27.916'N	144 05.642'E	15.06.2002 08:40:00	14.06.2002 21:40:00
85	69	54 26.547'N	144 04.569'E	15.06.2002	15.06.2002
86	?	54 27.903'N	144 05.536'E	15.06.2002 11:27:00	15.06.2002 00:27:00
87	70	54 26.774'N	144 04.846'E	15.06.2002 11:48:00	15.06.2002 00:48:00
88	71	54 26.570'N	144 04.735'E	15.06.2002 11:51:00	15.06.2002 00:51:00
89	72	54 28.812'N	144 11.560'E	15.06.2002 13:19:31	15.06.2002 02:19:31
90	73	54 29.968'N	144 12.239'E	15.06.2002 13:41:29	15.06.2002 02:41:29
91	74	54 29.925'N	144 12.222'E	15.06.2002 13:57:00	15.06.2002 02:57:00
92	75	54 29.173'N	144 10.077'E	15.06.2002	15.06.2002
93	76	54 28.005'N	144 09.816'E	15.06.2002 15:15:00	15.06.2002 04:15:00
94	77	54 26.823'N	144 04.929'E	15.06.2002 15:44:00	15.06.2002 04:44:00
95	78	54 26.648'N	144 04.503'E	15.06.2002 15:55:00	15.06.2002 04:55:00
96	79	54 26.632'N	144 04.890'E	15.06.2002 17:13:00	15.06.2002 06:13:00
97	80	54 26.483'N	144 04.391'E	15.06.2002 20:05:00	15.06.2002 09:05:00
98	81	54 26.560'N	144 04.545'E	15.06.2002 20:30:00	15.06.2002 09:30:00
99	82	54 27.546'N	144 04.396'E	16.06.2002 08:32:48	15.06.2002 21:32:48
100	83	54 26.789'N	144 04.866'E	16.06.2002 08:36:15	15.06.2002 21:36:15
101	84	54 26.742'N	144 04.880'E	16.06.2002	16.06.2002
102	85	54 26.644'N	144 04.143'E	16.06.2002 11:48:00	16.06.2002 00:48:00
103	86	54 26.594'N	144 04.750'E	16.06.2002	16.06.2002

No	ID	Latitude	Longitude	Time (Vladivostok)	Time (UTC)
104	?	54 26.644'N	144 04.143'E	16.06.2002 17:30:00	16.06.2002 06:30:00
105	87	54 27.839'N	144 10.501'E	16.06.2002 20:05:00	16.06.2002 09:05:00
106	88	54 27.740'N	144 10.485'E	16.06.2002	16.06.2002
107	89	54 28.791'N	144 11.518'E	16.06.2002 20:12:00	16.06.2002 09:12:00
108	90	54 28.797'N	144 11.676'E	16.06.2002 20:31:34	16.06.2002 09:31:34
109	91	54 30.134'N	144 04.209'E	17.06.2002 00:30:32	16.06.2002 13:30:32
110	92	54 27.621'N	144 04.422'E	17.06.2002 01:15:16	16.06.2002 14:15:16
111	93	54 27.932'N	144 05.670'E	17.06.2002 01:36:55	16.06.2002 14:36:55
112	94	54 24.319'N	144 37.809'E	17.06.2002 04:24:49	16.06.2002 17:24:49
113	95	54 30.422'N	144 10.512'E	17.06.2002 02:53:04	16.06.2002 15:53:04
114	96	47 24.046'N	143 43.681'E	23.06.2002 10:25:37	22.06.2002 23:25:37
115	?	47 31.136'N	143 45.490'E	23.06.2002 09:15:00	22.06.2002 22:15:00
116	A	47 31.136'N	143 45.590'E	03.06.2002 12:18:23	03.06.2002 01:18:23
117	B	47 31.744'N	143 45.914'E	03.06.2002 12:21:36	03.06.2002 01:21:36
118	C	47 32.519'N	143 46.332'E	03.06.2002 12:25:45	03.06.2002 01:25:45
119	D	47 32.460'N	143 53.907'E	23.06.2002 09:24:02	22.06.2002 22:24:02
120	?	45 49.315'N	141 37.900'E	24.06.2002 02:01:40	23.06.2002 15:01:40

APPENDIX 3

Water column data

LV29 CTD: Water column analysis

St. No	Bot. No	Depth m	S	q, °C	s_0, kg/m^3	O_2 CTD mmol/kg	Tr, %	O_2 mmol/kg	TA mmol/kg	pH_t 15 °C	pH_t in situ	DIC, mmol/kg	CO_3, mmol/kg	pCO_2, matm	Lc	La	TNO µmol/l	PO_4 µmol/l	SiO_2 µmol/l	CH_4 nl/l
1-1	8	3	31.931	8.554	24.784	301.2	89.0	318.1	2.190	8.203	8.304	1.922	0.186	170	4.51	2.85	0.1	0.06	1	99
	7	11	32.588	1.254	26.091	460.3	91.4	514.0	2.236	8.154	8.355	1.986	0.172	193	4.15	2.60	0.4	0.13	1	635
	6	21	32.735	-0.856	26.313	382.7	91.4	432.0	2.248	7.924	8.171	2.099	0.109	275	2.62	1.64	2.6	0.52	1	820
	5	31	32.840	-1.201	26.410	312.2	85.3													
	4	41	32.935	-1.615	26.498	300.9	56.5	309.1	2.250	7.658	7.901	2.192	0.061	539	1.45	0.91	19.6	1.91	17	1107
	3	51	33.046	-1.665	26.589	300.4	83.9	299.1	2.253	7.657	7.899	2.195	0.061	539	1.45	0.91	19.7	1.85	36	1331
	2	61	33.085	-1.691	26.621	294.8	82.0	315.1	2.259	7.638	7.879	2.207	0.059	568	1.38	0.87	19.7	1.92	42	1557
	1	74	33.085	-1.691	26.621	302.1	81.1	311.1	2.259	7.635	7.872	2.208	0.058	577	1.37	0.86	19.2	1.84	45	1605
2-1	12	3	32.569	4.411	25.811	307.9	88.8	340.5	2.214	7.895	8.055	2.078	0.103	374	2.48	1.56	11.0	0.65	20	63
	11	49	32.700	-1.512	26.304	333.9	93.1	363.4	2.224	7.828	8.077	2.112	0.088	343	2.08	1.31	13.7	0.84	24	73
	10	98	33.023	-0.773	26.543	270.2	94.4	290.6	2.245	7.698	7.925	2.174	0.067	502	1.55	0.98	22.3	1.40	41	63
	9	147	33.290	0.574	26.696	192.8	94.5	205.1	2.256	7.547	7.739	2.231	0.048	792	1.09	0.69	30.8	2.14	63	19
	8	296	33.520	1.118	26.848	133.9	94.4	142.0	2.279	7.453	7.617	2.282	0.039	1041	0.83	0.54	33.5	2.52	83	27
	7	495	33.862	1.924	27.066	82.5	94.6	88.0	2.318	7.436	7.570	2.325	0.038	1139	0.75	0.50	36.4	2.61	117	50
	6	792	34.207	2.344	27.309	35.8	94.7	38.4	2.364	7.425	7.526	2.375	0.038	1209	0.65	0.45	40.8	2.87	158	40
	5	1086	34.386	2.298	27.456	26.0	94.7	28.6	2.376	7.443	7.520	2.381	0.039	1152	0.60	0.43	44.2	2.88	183	12
	4	1374	34.428	2.247	27.493	25.5	94.6	27.9	2.399	7.452	7.505	2.401	0.040	1129	0.54	0.40	42.7	2.87	199	30
	3	1422	34.430	2.245	27.496	25.4	94.4	27.5	2.400	7.452	7.501	2.402	0.039	1129	0.53	0.40	43.2	2.78	196	61
	2	1467	34.436	2.238	27.501	26.1	94.1	29.1	2.402	7.452	7.497	2.404	0.039	1129	0.52	0.39	44.1	2.83	199	831
	1	1478	34.436	2.237	27.501	26.2	94.0	28.9	2.404	7.452	7.497	2.406	0.039	1130	0.52	0.39	44.7	2.72	206	1213
4-1	12	3	32.504	4.599	25.740	307.9	89.9	337.7	2.236	7.892	8.049	2.101	0.103	384	2.49	1.56	10.7	0.68	23	71
	11	50	32.721	-1.543	26.322	335.0	93.1	363.7	2.224	7.821	8.070	2.114	0.086	348	2.05	1.29	14.6	0.98	27	81
	10	100	33.143	-0.198	26.616	236.3	94.6	254.6	2.248	7.622	7.835	2.201	0.057	629	1.31	0.83	26.9	2.20	56	60
	9	299	33.486	0.894	26.835	143.5	94.4	152.4	2.274	7.455	7.622	2.276	0.039	1023	0.83	0.54	34.4	2.85	86	17
	8	498	33.826	1.811	27.045	92.0	94.6	97.8	2.312	7.442	7.577	2.318	0.038	1113	0.75	0.50	38.6	2.85	124	45
	7	745	34.162	2.319	27.275	40.6	94.7	43.4	2.356	7.418	7.523	2.369	0.037	1227	0.65	0.45	42.1	3.15	167	9
	6	991	34.338	2.341	27.414	27.6	94.8	29.7	2.381	7.428	7.512	2.391	0.038	1204	0.60	0.43	43.3	3.30	191	23
	5	1239	34.412	2.267	27.479	26.3	94.8	28.4	2.393	7.447	7.512	2.396	0.039	1144	0.57	0.41	44.2	3.19	212	13
	4	1483	34.431	2.243	27.497	25.7	94.4	27.6	2.401	7.448	7.492	2.404	0.039	1140	0.51	0.38	43.5	3.20	219	155
	3	1530	34.434	2.240	27.499	26.1	94.3	27.6	2.401	7.454	7.494	2.402	0.039	1122	0.51	0.38	43.5	3.32	219	279
	2	1571	34.436	2.237	27.500	26.2	94.1	28.0	2.401	7.453	7.489	2.402	0.039	1124	0.50	0.38	44.9	3.20	219	302
	1	1581	34.435	2.238	27.500	26.2	94.2	27.8	2.401	7.451	7.486	2.403	0.039	1130	0.49	0.37	44.0	3.07	216	304
5-1	12	11	32.593	4.615	25.809	313.0	88.5	342.2	2.221	7.909	8.066	2.080	0.106	365	2.56	1.61	8.9	0.30	16	61
	11	50	32.664	-0.918	26.258	346.8	92.5	374.6	2.227	7.850	8.091	2.107	0.092	333	2.19	1.37	12.1	0.45	22	86
	10	149	33.327	0.588	26.725	182.5	94.5	193.8	2.266	7.518	7.707	2.249	0.045	858	1.02	0.65	33.0	2.35	64	

St. No	Bot. No	Depth m	S	q, °C	s_0, kg/m^3	O_2 CTD mmol/kg	Tr, %	O_2 mmol/kg	TA mmol/kg	pH_t 15 °C	pH_t in situ	DIC, mmol/kg	CO_3, mmol/kg	pCO_2, matm	Lc	La	TNO µmol/l	PO_4 µmol/l	SiO_2 µmol/l	CH_4 nl/l
	9	297	33.506	0.953	26.847	141.2	94.4	149.6	2.280	7.455	7.621	2.282	0.039	1029	0.83	0.54	36.3	2.53	80	42
	8	494	33.851	1.848	27.063	88.4	94.7	94.7	2.319	7.442	7.577	2.325	0.039	1118	0.76	0.50	40.1	2.58	116	
	7	789	34.175	2.330	27.284	37.9	94.8	42.4	2.362	7.422	7.523	2.374	0.037	1217	0.65	0.45	42.2	2.84	160	26
	6	1088	34.368	2.318	27.440	25.8	94.8	29.7	2.386	7.445	7.522	2.390	0.039	1152	0.60	0.43	44.5	2.86	183	16
	5	1284	34.418	2.259	27.485	25.8	94.7	29.2	2.396	7.457	7.519	2.396	0.040	1115	0.57	0.42	43.0	2.90	202	
	4	1457	34.436	2.237	27.501	25.8	94.1	29.4	2.401	7.461	7.508	2.400	0.040	1102	0.53	0.40	41.9	2.80	206	101
	3	1506	34.436	2.236	27.501	26.3	94.0	29.6	2.400	7.462	7.505	2.399	0.040	1098	0.52	0.39	44.0	2.97	202	80
	2	1547	34.436	2.236	27.501	26.7	94.0	30.2	2.400	7.463	7.503	2.398	0.040	1095	0.51	0.39	41.7	2.77	195	50
	1	1558	34.436	2.236	27.501	26.8	94.0	29.8	2.400	7.458	7.496	2.400	0.040	1109	0.50	0.38	40.7	2.69	199	44
6-1	12	4	32.519	4.808	25.730	306.7	88.1	339.9	2.218	7.897	8.051	2.082	0.103	379	2.50	1.57	11.0	0.90	17	4
	11	62	32.769	-1.539	26.361	323.5	93.7	345.5	2.233	7.796	8.043	2.131	0.082	373	1.94	1.22	15.5	1.20	26	62
	10	147	33.310	0.556	26.713	185.5	94.6	196.6	2.263	7.529	7.720	2.243	0.046	832	1.05	0.67	33.4	2.41	63	147
	9	296	33.517	1.128	26.845	134.1	94.5	142.1	2.281	7.455	7.619	2.283	0.039	1037	0.83	0.54	35.4	2.68	82	
	8	494	33.855	1.815	27.068	88.7	94.7	94.5	2.318	7.442	7.578	2.324	0.039	1116	0.76	0.50	38.6	2.98	115	494
	7	743	34.162	2.320	27.275	39.4	94.8	42.9	2.359	7.421	7.526	2.371	0.037	1219	0.66	0.45	43.7	3.13	154	743
	6	990	34.329	2.356	27.405	27.6	94.8	30.8	2.382	7.436	7.520	2.389	0.039	1181	0.62	0.44	41.9	3.18	185	990
	5	1236	34.416	2.262	27.483	25.0	94.9	28.5	2.396	7.451	7.516	2.398	0.040	1134	0.57	0.42	41.8	3.00	198	1236
	4	1429	34.433	2.242	27.498	23.0	94.5	26.8	2.402	7.452	7.501	2.404	0.039	1130	0.53	0.39	43.4	3.22	210	1429
	3	1479	34.437	2.236	27.502	24.5	94.3	28.1	2.401	7.454	7.499	2.402	0.040	1122	0.52	0.39	43.1	3.21	206	1479
	2	1519	34.438	2.235	27.502	24.7	94.1	28.0	2.402	7.454	7.495	2.403	0.039	1122	0.51	0.38	38.7	2.68	206	1519
	1	1528	34.438	2.235	27.503	24.7	94.1	29.2	2.402	7.454	7.494	2.403	0.039	1122	0.51	0.38	42.7	2.47	204	1528
7-1	12	3	32.509	4.565	25.748	309.1	89.4	340.5	2.213	7.899	8.057	2.076	0.104	372	2.50	1.57	12.2	0.65	20	57
	11	80	32.828	-1.715	26.413	325.9	94.0	353.4	2.231	7.800	8.049	2.128	0.083	366	1.94	1.22	17.2	1.02	24	78
	10	149	33.277	0.404	26.695	194.6	94.6	206.6	2.259	7.536	7.729	2.237	0.047	810	1.06	0.68	30.1	2.15	60	14
	9	299	33.512	0.926	26.853	136.8	94.5	145.4	2.278	7.446	7.612	2.283	0.038	1051	0.81	0.53	34.8	2.49	81	29
	8	494	33.874	1.929	27.075	81.3	94.7	87.4	2.321	7.437	7.571	2.328	0.038	1137	0.75	0.50	40.4	2.67	115	
	7	744	34.178	2.330	27.287	37.9	94.8	41.9	2.361	7.426	7.531	2.371	0.038	1205	0.67	0.46	41.8	2.84	153	19
	6	990	34.332	2.344	27.409	26.4	94.8	29.9	2.383	7.436	7.520	2.390	0.039	1181	0.62	0.44	43.4	2.89	172	12
	5	1235	34.408	2.270	27.476	25.0	94.9	28.7	2.394	7.453	7.518	2.395	0.040	1127	0.58	0.42	43.4	3.06	188	28
	4	1488	34.434	2.242	27.499	21.0	94.6	24.6	2.404	7.451	7.495	2.406	0.039	1133	0.51	0.39	41.7	2.73	210	14
	3	1538	34.438	2.234	27.503	26.4	94.2	29.4	2.401	7.461	7.501	2.400	0.040	1101	0.51	0.39	41.9	2.64	203	14
	2	1576	34.439	2.232	27.504	26.9	94.0	30.0	2.400	7.457	7.493	2.400	0.040	1111	0.50	0.38	43.9	2.82	193	11
	1	1588	34.439	2.232	27.504	27.0	94.0	30.1	2.400	7.458	7.494	2.400	0.040	1108	0.50	0.38	41.3	2.68	182	22
9-1	12	3	32.540	4.756	25.752	308.9	87.0	340.3	2.210	7.902	8.057	2.072	0.104	372	2.52	1.58	8.0	0.40	20	88
	11	64	32.816	-1.384	26.395	313.4	94.1	338.1	2.228	7.787	8.031	2.129	0.080	384	1.90	1.20	14.8	0.95	31	85
	10	149	33.313	0.500	26.718	184.9	94.4	196.7	2.260	7.527	7.718	2.241	0.046	833	1.04	0.66	29.6	2.17	74	48
	9	299	33.487	0.875	26.836	145.9	94.4	154.2	2.274	7.459	7.627	2.275	0.039	1012	0.83	0.54	30.6	2.49	89	14

St. No	Bot. No	Depth m	S	q, °C	s_0, kg/m^3	O_2 CTD mmol/kg	Tr, %	O_2 mmol/kg	TA mmol/kg	pH_t 15 °C	pH_t in situ	DIC, mmol/kg	CO_3, mmol/kg	pCO_2, matm	Lc	La	TNO µmol/l	PO_4 µmol/l	SiO_2 µmol/l	CH_4 nl/l
	8	497	33.834	1.845	27.049	92.3	94.6	98.1	2.313	7.448	7.583	2.317	0.039	1098	0.76	0.51	35.8	2.68	128	39
	7	743	34.162	2.318	27.275	40.0	94.7	43.2	2.357	7.424	7.529	2.368	0.037	1208	0.66	0.46	38.8	3.18	177	7
	6	989	34.334	2.344	27.411	27.1	94.8	29.9	2.388	7.443	7.528	2.393	0.039	1162	0.63	0.45	39.6	3.11	212	25
	5	1237	34.410	2.269	27.477	26.1	94.8	41.3	2.395	7.449	7.514	2.398	0.039	1139	0.57	0.42	39.3	3.16	218	18
	4	1428	34.432	2.240	27.498	27.9	94.3	30.9	2.399	7.458	7.507	2.399	0.040	1110	0.54	0.40	38.5	3.01	225	9
	3	1486	34.436	2.236	27.501	27.8	94.1	30.2	2.400	7.458	7.502	2.400	0.040	1110	0.52	0.39	37.5	2.95	227	9
	2	1516	34.437	2.235	27.502	28.0	94.1	30.3	2.400	7.458	7.500	2.400	0.040	1109	0.51	0.39	38.3	3.01	233	10
	1	1524	34.437	2.234	27.502	28.1	94.0	30.7	2.400	7.458	7.499	2.400	0.040	1109	0.51	0.39	37.8	2.85	229	11
10-1	12	3	32.543	4.994	25.728	311.4	89.5	340.1	2.209	7.898	8.049	2.073	0.103	380	2.50	1.57	9.2	0.54	21	67
	11	21	32.576	2.711	25.975	334.6	89.6	366.7	2.217	7.889	8.075	2.083	0.101	353	2.42	1.52	9.6	0.65	22	66
	10	76	32.766	-1.596	26.360	327.2	93.9	353.2	2.225	7.804	8.051	2.121	0.083	363	1.95	1.23	13.3	1.04	28	71
	9	200	33.383	0.672	26.765	166.5	94.2	176.7	2.266	7.490	7.672	2.258	0.042	925	0.94	0.60	29.2	2.37	72	10
	8	397	33.682	1.332	26.964	120.5	94.4	127.4	2.298	7.456	7.608	2.299	0.039	1048	0.81	0.53	31.9	2.57	96	55
	7	597	34.003	2.169	27.160	60.3	94.7	65.1	2.334	7.430	7.551	2.343	0.038	1174	0.71	0.48	34.6	2.86	130	38
	6	793	34.202	2.346	27.305	35.3	94.8	39.0	2.362	7.422	7.522	2.374	0.037	1217	0.65	0.45	36.7	2.81	156	27
	5	990	34.334	2.343	27.410	26.4	94.8	29.8	2.380	7.433	7.517	2.388	0.038	1188	0.61	0.43	35.8	2.63	171	12
	4	1237	34.413	2.265	27.480	25.3	94.8	28.6	2.394	7.442	7.506	2.399	0.039	1160	0.56	0.41	33.6	2.64	185	54
	3	1391	34.433	2.241	27.498	24.8	94.4	27.7	2.399	7.454	7.506	2.400	0.040	1123	0.54	0.40	36.3	2.65	200	844
	2	1432	34.434	2.240	27.499	25.0	94.4	27.5	2.398	7.451	7.499	2.400	0.039	1131	0.53	0.39	35.4	2.72	195	1625
	1	1442	34.435	2.239	27.500	25.0	94.3	28.1	2.398	7.454	7.502	2.399	0.040	1121	0.53	0.39	38.5	2.81	193	1961
11-1	12	3	32.550	4.966	25.737	307.9	88.1	342.6	2.210	7.909	8.061	2.069	0.106	369	2.55	1.61	10.4	0.59	9	83
	11	74	32.822	-1.670	26.407	316.8	94.0	348.6	2.228	7.790	8.038	2.128	0.081	376	1.90	1.20	17.3	1.17	23	89
	10	149	33.312	0.633	26.710	183.8	94.6	196.4	2.258	7.525	7.714	2.239	0.046	841	1.04	0.66	30.9	2.38	62	23
	9	297	33.501	1.020	26.839	138.9	94.6	147.5	2.275	7.459	7.625	2.276	0.039	1019	0.84	0.54	35.3	2.64	77	
	8	495	33.831	1.853	27.046	87.4	94.7	92.5	2.315	7.434	7.568	2.323	0.038	1140	0.74	0.49	37.7	2.86	109	
	7	792	34.219	2.343	27.319	33.5	94.8	37.2	2.364	7.422	7.523	2.376	0.037	1218	0.65	0.45	43.1	3.16	155	51
	6	1088	34.378	2.308	27.449	25.5	94.8	29.0	2.387	7.444	7.521	2.391	0.039	1155	0.60	0.43	44.2	3.14	177	
	5	1382	34.427	2.249	27.492	24.0	94.8	28.2	2.398	7.449	7.501	2.401	0.039	1138	0.53	0.40	42.5	3.20	191	13
	4	1511	34.435	2.238	27.500	24.6	94.3	28.6	2.400	7.453	7.495	2.401	0.039	1124	0.51	0.38	44.3	3.10	194	13
	3	1562	34.436	2.237	27.501	24.8	94.2	28.5	2.399	7.451	7.488	2.401	0.039	1129	0.50	0.38	43.6	3.10	190	15
	2	1601	34.436	2.237	27.501	25.0	94.2	28.4	2.399	7.451	7.485	2.401	0.039	1129	0.49	0.37	43.3	3.16	194	18
	1	1610	34.436	2.237	27.501	25.1	94.2	28.2	2.399	7.452	7.485	2.401	0.039	1125	0.49	0.37	40.9	3.12	195	17
12-1	12	3	32.553	4.963	25.740	304.0	87.9	344.7	2.227	7.910	8.062	2.085	0.107	370	2.58	1.62	10.7	0.58	10	66
	11	77	32.789	-1.632	26.379	320.7	93.8	354.6	2.227	7.796	8.044	2.125	0.082	371	1.92	1.21	16.4	1.00	21	77
	10	149	33.277	0.503	26.689	195.6	94.7	210.1	2.250	7.550	7.743	2.224	0.048	781	1.09	0.70	30.1	2.23	55	20
	9	299	33.506	1.029	26.843	136.6	94.6	144.6	2.290	7.449	7.614	2.294	0.039	1053	0.82	0.53	35.4	2.56	73	22
	8	495	33.818	1.807	27.039	90.3	94.8	95.9	2.316	7.440	7.576	2.322	0.038	1121	0.75	0.50	37.3	2.57	102	49

St. No	Bot. No	Depth m	S	q, °C	s_0, kg/m^3	O_2 CTD mmol/kg	Tr, %	O_2 mmol/kg	TA mmol/kg	pH_t 15 °C	pH_t in situ	DIC, mmol/kg	CO_3, mmol/kg	pCO_2, matm	Lc	La	TNO µmol/l	PO_4 µmol/l	SiO_2 µmol/l	CH_4 nl/l
	7	743	34.169	2.331	27.279	37.8	94.9	41.6	2.367	7.420	7.525	2.379	0.037	1227	0.66	0.45	42.7	2.89	140	19
	6	990	34.349	2.335	27.423	25.6	94.9	29.2	2.382	7.436	7.521	2.389	0.039	1180	0.62	0.44	42.8	3.08	162	70
	5	1237	34.413	2.266	27.480	24.9	94.9	28.9	2.393	7.449	7.514	2.396	0.039	1138	0.57	0.42	42.7	3.15	183	8
	4	1409	34.428	2.247	27.494	24.3	94.7	27.8	2.398	7.452	7.502	2.400	0.039	1128	0.53	0.40	42.1	3.18	192	8
	3	1459	34.431	2.243	27.497	24.3	94.6	28.3	2.399	7.453	7.499	2.400	0.039	1125	0.52	0.39	42.0	3.21	190	7
	2	1498	34.436	2.238	27.501	24.4	94.3	27.7	2.401	7.451	7.494	2.403	0.039	1131	0.51	0.38	43.0	3.13	192	26
	1	1508	34.436	2.238	27.501	24.3	94.2	27.7	2.399	7.452	7.494	2.401	0.039	1127	0.51	0.38	40.2	2.93	197	62
14-1	12	3	32.534	5.090	25.711	*311.2*	88.9	339.5	2.204	7.916	8.064	2.061	0.107	365	2.59	1.63	11.8	0.85	24	69
	11	63	32.834	-1.620	26.415	324.1	93.9	348.5	2.226	7.798	8.046	2.124	0.082	369	1.93	1.22	19.5	1.35	32	81
	10	149	33.327	0.623	26.722	186.2	94.6	197.3	2.257	7.538	7.730	2.235	0.047	808	1.07	0.68	34.0	2.50	67	11
	9	297	33.493	0.906	26.839	142.6	94.4	150.5	2.272	7.460	7.627	2.272	0.039	1012	0.84	0.54	35.9	2.86	81	14
	8	455	33.766	1.736	27.003	103.3	94.7	107.8	2.304	7.453	7.588	2.306	0.039	1082	0.77	0.51	38.3	2.95	106	45
	7	792	34.198	2.334	27.303	36.5	94.9	107.7	2.305	7.446		2.308	0.038				37.8	2.91	105	67
	6	1089	34.376	2.308	27.447	26.0	94.9	28.6	2.385	7.443	7.495	2.390	0.038	1150	0.52	0.39	41.9	3.16	180	12
	5	1383	34.426	2.250	27.492	25.3	94.8	27.5	2.397	7.452	7.500	2.399	0.039	1127	0.53	0.39	40.4	3.03	195	7
	4	1533	34.436	2.238	27.500	25.4	94.4	27.4	2.398	7.454	7.491	2.399	0.039	1120	0.50	0.38	39.8	2.54	201	78
	3	1583	34.437	2.237	27.501	25.6	94.2	27.4	2.399	7.456	7.488	2.399	0.039	1113	0.49	0.37	42.4	3.13	200	236
	2	1623	34.437	2.236	27.502	26.4	94.2	28.1	2.399	7.457	7.486	2.399	0.039	1110	0.48	0.37	41.1	2.98	201	447
	1	1633	34.438	2.235	27.503	27.1	94.1	29.5	2.398	7.459	7.487	2.397	0.040	1103	0.48	0.37	40.9	2.71	199	536
15-1	12	3	32.530	5.226	25.693	304.1	89.4	338.2	2.209	7.906	8.054	2.070	0.105	376	2.54	1.60	13.0	1.05	20	77
	11	71	32.742	-1.595	26.341	327.3	93.8	351.6	2.226	7.803	8.051	2.122	0.083	364	1.95	1.23	17.7	1.43	26	84
	10	149	33.269	0.474	26.685	198.2	94.8	209.0	2.256	7.551	7.744	2.230	0.048	781	1.10	0.70	31.2	2.63	62	55
	9	298	33.504	0.951	26.846	138.2	94.7	145.0	2.276	7.451	7.617	2.279	0.039	1037	0.82	0.53	34.7	2.92	80	
	8	495	33.852	1.899	27.060	84.6	94.9	88.8	2.317	7.439	7.573	2.323	0.038	1128	0.75	0.50	38.1	3.05	115	17
	7	990	34.326	2.346	27.404	26.3	95.0	29.6	2.379	7.430	7.514	2.388	0.038	1197	0.61	0.43	41.1	3.35	173	
	6	1384	34.424	2.252	27.490	24.2	95.0	27.9	2.396	7.451	7.503	2.398	0.039	1131	0.54	0.40	40.8	3.42	200	
	5	1434	34.429	2.246	27.494	23.4	94.9	27.0	2.399	7.450	7.498	2.401	0.039	1134	0.52	0.39	40.5	3.39	202	9
	4	1568	34.436	2.238	27.500	24.2	94.5	27.6	2.400	7.453	7.490	2.401	0.039	1124	0.50	0.38	40.0	3.36	205	
	3	1626	34.437	2.235	27.502	25.8	94.3	28.9	2.401	7.452	7.484	2.403	0.039	1126	0.48	0.37	40.8	3.39	200	128
	2	1666	34.438	2.234	27.503	26.4	94.2	29.3	2.401	7.462	7.491	2.400	0.040	1096	0.49	0.37	41.5	3.39	199	200
	1	1676	34.438	2.234	27.503	26.4	94.2	29.4	2.400	7.459	7.487	2.400	0.040	1104	0.48	0.37	41.3	3.43	196	196
16-1	12	3	32.548	5.148	25.715	306.8	89.3	337.7	2.206	7.907	8.056	2.066	0.105	373	2.54	1.60	11.0	0.69	19	72
	11	65	32.797	-1.578	26.385	321.5	93.9	340.3	2.225	7.783	8.030	2.128	0.080	384	1.87	1.18	17.5	1.18	29	80
	10	148	33.309	0.500	26.716	185.3	94.7	194.8	2.258	7.519	7.710	2.241	0.045	850	1.02	0.65	32.5	2.45	66	9
	9	298	33.528	1.004	26.861	139.5	94.6	147.4	2.278	7.458	7.624	2.279	0.039	1022	0.84	0.54	35.9	2.70	82	19
	8	495	33.854	1.877	27.063	85.7	94.9	91.6	2.316	7.440	7.575	2.322	0.038	1124	0.75	0.50	40.1	2.83	116	40
	7	988	34.330	2.345	27.407	25.9	95.0	29.5	2.380	7.436	7.521	2.387	0.039	1179	0.62	0.44	44.8	3.16	172	15

St. No	Bot. No	Depth m	S	q, °C	s_0, kg/m^3	O_2 CTD mmol/kg	Tr, %	O_2 mmol/kg	TA mmol/kg	pH_t 15 °C	pH_t in situ	DIC, mmol/kg	CO_3, mmol/kg	pCO_2, matm	Lc	La	TNO µmol/l	PO_4 µmol/l	SiO_2 µmol/l	CH_4 nl/l
	6	1432	34.429	2.246	27.495	23.4	94.9	26.9	2.399	7.447	7.495	2.402	0.039	1143	0.52	0.39	44.9	3.30	204	7
	5	1502	34.433	2.241	27.499	23.5	94.7	27.5	2.399	7.447	7.489	2.402	0.039	1142	0.50	0.38	42.4	3.21	206	10
	4	1551	34.436	2.238	27.500	23.8	94.5	27.4	2.399	7.453	7.491	2.400	0.039	1123	0.50	0.38	42.8	3.28	203	14
	3	1601	34.437	2.237	27.501	24.3	94.3	27.9	2.399	7.455	7.489	2.400	0.039	1117	0.49	0.37	42.5	3.35	203	17
	2	1641	34.437	2.236	27.502	24.8	94.3	28.0	2.400	7.454	7.484	2.401	0.039	1120	0.48	0.37	41.6	3.14	195	30
	1	1652	34.437	2.236	27.502	24.9	94.3	28.3	2.402	7.453	7.482	2.403	0.039	1123	0.48	0.37	41.5	3.01	200	35
17-1	12	3	32.548	5.086	25.722	307.0	89.0	346.2	2.210	7.910	8.060	2.069	0.106	369	2.56	1.61				70
	11	82	32.819	-1.647	26.404	315.8	94.2	335.0	2.230	7.767	8.013	2.138	0.077	400	1.80	1.14				79
	10	148	33.292	0.504	26.701	189.6	94.8	201.4	2.256	7.528	7.719	2.236	0.046	830	1.04	0.66				10
	9	296	33.515	0.949	26.854	136.4	94.5	144.5	2.275	7.445	7.611	2.280	0.038	1053	0.81	0.53				
	8	493	33.872	1.868	27.078	84.7	94.9	90.5	2.316	7.442	7.577	2.321	0.039	1117	0.76	0.50				33
	7	792	34.214	2.347	27.314	33.7	95.0	38.5	2.363	7.426	7.527	2.373	0.038	1205	0.65	0.45				
	6	1284	34.418	2.259	27.485	24.5	95.1	28.6	2.394	7.453	7.514	2.395	0.040	1126	0.56	0.41				13
	5	1365	34.428	2.247	27.494	23.9	94.9	27.5	2.398	7.450	7.504	2.400	0.039	1135	0.54	0.40				
	4	1417	34.431	2.244	27.497	23.8	94.7	27.7	2.399	7.451	7.501	2.401	0.039	1131	0.53	0.39				955
	3	1467	34.436	2.237	27.501	25.0	94.5	28.6	2.398	7.454	7.500	2.399	0.040	1121	0.52	0.39				349
	2	1506	34.438	2.233	27.503	26.6	94.2	30.2	2.398	7.456	7.498	2.398	0.040	1114	0.51	0.39				15
	1	1516	34.438	2.233	27.503	26.7	94.2	30.6	2.397	7.455	7.497	2.398	0.039	1117	0.51	0.38				10
19-1	12	3	32.534	4.983	25.722	308.4	88.3	338.2	2.210	7.905	8.057	2.071	0.105	373	2.53	1.59				65
	11	76	32.846	-1.666	26.427	326.0	94.3	350.9	2.230	7.793	8.041	2.129	0.082	373	1.91	1.21				74
	10	150	33.306	0.463	26.715	185.6	94.7	198.1	2.256	7.521	7.712	2.239	0.045	843	1.02	0.65				7
	9	298	33.491	0.906	26.838	143.3	94.6	152.4	2.275	7.453	7.620	2.278	0.039	1030	0.82	0.54				12
	8	494	33.816	1.764	27.041	94.7	94.9	101.3	2.316	7.441	7.577	2.322	0.038	1116	0.75	0.50				41
	7	792	34.202	2.348	27.305	35.3	95.0	38.9	2.363	7.418	7.518	2.376	0.037	1231	0.64	0.44				30
	6	1187	34.400	2.281	27.468	25.7	95.0	28.6	2.394	7.445	7.514	2.398	0.039	1152	0.58	0.42				9
	5	1432	34.428	2.247	27.494	24.4	94.9	27.4	2.398	7.448	7.496	2.401	0.039	1140	0.52	0.39				8
	4	1579	34.436	2.238	27.501	24.9	94.5	27.5	2.399	7.450	7.485	2.401	0.039	1132	0.49	0.37				24
	3	1628	34.437	2.236	27.501	25.7	93.8	28.6	2.398	7.451	7.482	2.400	0.039	1128	0.48	0.37				215
	2	1668	34.437	2.235	27.502	26.4	94.2	28.8	2.398	7.452	7.480	2.400	0.039	1124	0.47	0.36				242
	1	1676	34.386	2.235	27.461	26.5	1.0	29.0	2.397	7.452	7.479	2.399	0.039	1124	0.47	0.36				225
20-1	12	4	32.562	4.967	25.747	315.1	84.3	349.9	2.218	7.958	8.111	2.050	0.117	324	2.82	1.78				60
	11	74	32.736	-1.635	26.336	329.3	93.9	356.3		7.807	8.055	2.125	0.084	361	1.97	1.24				74
	10	155	33.324	0.641	26.719	182.9	94.8	195.8		7.520	7.708	2.239	0.045	852	1.02	0.65				13
	9	303	33.522	1.155	26.847	135.6	94.8	143.5		7.456	7.619	2.277	0.039	1032	0.83	0.54				19
	8	499	33.867	1.927	27.070	83.1	94.9	89.4		7.437	7.570	2.323	0.038	1135	0.75	0.50				41
	7	987	34.334	2.343	27.410	25.9	95.0	29.3	2.372	7.425	7.509	2.373	0.037	1205	0.60	0.42				10
	6	1434	34.431	2.244	27.497	22.8	94.9	25.9		7.458	7.507	2.394	0.040	1108	0.53	0.40				8

St. No	Bot. No	Depth m	S	q, °C	s_0, kg/m^3	O_2 CTD mmol/kg	Tr, %	O_2 mmol/kg	TA mmol/kg	pH_t 15 °C	pH_t in situ	DIC, mmol/kg	CO_3, mmol/kg	pCO_2, matm	Lc	La	TNO µmol/l	PO_4 µmol/l	SiO_2 µmol/l	CH_4 nl/l
	5	1480	34.434	2.240	27.499	23.5	94.6	26.7		7.454	7.498	2.399	0.039	1121	0.52	0.39				121
	4	1548	34.435	2.239	27.500	23.4	94.6	27.0		7.456	7.495	2.399	0.040	1115	0.50	0.38				148
	3	1599	34.436	2.238	27.501	23.4	94.5	26.4	2.398	7.452	7.486	2.400	0.039	1125	0.49	0.37				72
	2	1638	34.437	2.236	27.502	24.7	94.3	28.1	2.398	7.454	7.485	2.399	0.039	1119	0.48	0.37				91
	1	1650	34.437	2.236	27.502	24.4	94.3	27.8	2.398	7.455	7.485	2.398	0.039	1115	0.48	0.37				100
22-1	12	4	32.549	4.849	25.749	311.3	88.3	339.7		7.927	8.081	2.062	0.110	350	2.65	1.67				65
	11	62	32.741	-1.570	26.339	336.8	93.7	361.3		7.828	8.077	2.117	0.088	342	2.07	1.31				79
	10	151	33.294	0.579	26.699	193.7	94.7	206.4		7.553	7.745	2.229	0.049	780	1.10	0.70				17
	9	298	33.511	1.138	26.839	136.7	94.5	143.9		7.456	7.620	2.277	0.039	1032	0.83	0.54				22
	8	496	33.851	1.882	27.060	84.0	94.7	87.4		7.437	7.571	2.323	0.038	1133	0.75	0.50				40
	7	989	34.330	2.346	27.407	26.4	94.9	28.9		7.433	7.517	2.371	0.038	1180	0.61	0.43				9
	6	1429	34.429	2.246	27.495	23.7	94.7	26.1		7.448	7.496	2.397	0.039	1138	0.52	0.39				6
	5	1482	34.432	2.243	27.498	23.2	94.6	26.0		7.452	7.496	2.400	0.039	1127	0.51	0.39				6
	4	1549	34.435	2.239	27.500	23.2	94.5	26.5		7.458	7.497	2.399	0.040	1109	0.51	0.38				8
	3	1597	34.436	2.238	27.501	24.2	94.3	26.5		7.454	7.488	2.399	0.039	1119	0.49	0.37				13
	2	1639	34.437	2.237	27.502	24.9	94.1	26.9		7.454	7.485	2.399	0.039	1119	0.48	0.37				29
	1	1651	34.437	2.237	27.502	24.9	94.1	27.7		7.454	7.484	2.398	0.039	1118	0.48	0.37				30
23-1	12	4	32.548	4.654	25.769	309.8	88.8													
	11	68	32.831	-1.621	26.414	324.9	93.9													
	10	150	33.296	0.637	26.697	194.7	94.6													
	9	496	33.829	1.836	27.046	92.9	94.6													
	8	990	34.330	2.344	27.407	27.0	94.7													
	7	1283	34.416	2.263	27.483	27.1	94.5													
	6	1335	34.422	2.255	27.488	26.9	94.5													
	5	1384	34.427	2.248	27.493	26.6	94.5													3
	4	1433	34.431	2.242	27.497	26.4	94.4													4
	3	1487	34.434	2.239	27.499	26.2	94.2													49
	2	1526	34.436	2.238	27.500	25.8	94.1													184
	1	1536	34.436	2.238	27.501	25.9	94.1													170
24-1	12	4	32.521	4.247	25.790	320.3	83.2													5
	11	3	32.514	4.236	25.785	320.0	83.3													4
	10	151	33.278	0.384	26.697	195.8	94.3													3
	9	299	33.486	0.862	26.836	142.5	94.2													3
	8	493	33.837	1.821	27.053	88.9	94.4													14
	7	991	34.340	2.341	27.415	27.0	94.6													14
	6	1332	34.425	2.250	27.491	25.5	94.6													7
	5	1423	34.432	2.244	27.497	25.1	94.3													9

St. No	Bot. No	Depth m	S	q, °C	s_0, kg/m^3	O_2 CTD mmol/kg	Tr, %	O_2 mmol/kg	TA mmol/kg	pH_t 15 °C	pH_t in situ	DIC, mmol/kg	CO_3, mmol/kg	pCO_2, matm	Lc	La	TNO µmol/l	PO_4 µmol/l	SiO_2 µmol/l	CH_4 nl/l
	4	1473	34.434	2.241	27.499	24.8	94.2													13
	3	1523	34.437	2.236	27.502	27.1	93.8													18
	2	1565	34.438	2.234	27.503	27.4	93.8													16
	1	1574	34.438	2.235	27.503	27.4	93.7													15
25-1	12	3	32.516	4.592	25.750	312.3	88.4													
	11	68	32.832	-1.584	26.413	328.2	93.8													
	10	149	33.311	0.701	26.706	189.3	94.6													
	9	297	33.529	1.226	26.848	134.5	94.3													
	8	494	33.825	1.811	27.045	94.1	94.6													
	7	791	34.202	2.338	27.305	36.3	94.7													
	6	1286	34.419	2.259	27.485	27.0	94.5													5
	5	1335	34.423	2.253	27.489	26.6	94.6													4
	4	1382	34.427	2.248	27.493	26.8	94.5													3
	3	1433	34.431	2.242	27.497	27.0	94.2													3
	2	1475	34.435	2.238	27.500	27.0	94.0													14
	1	1485	34.435	2.238	27.500	27.1	94.0													14
27-1	12	4	32.529	4.276	25.793	312.6	88.7	340.4	2.208	7.899	8.062	2.071	0.103	367	2.49	1.56				66
	11	60	32.760	-1.583	26.355	331.1	93.5	355.2	2.222	7.805	8.054	2.118	0.083	362	1.97	1.24				75
	10	149	33.303	0.509	26.709	191.4	94.3	201.1	2.255	7.529	7.720	2.235	0.046	827	1.04	0.67				10
	9	297	33.521	1.105	26.850	139.4	94.4	146.0	2.276	7.454	7.618	2.278	0.039	1036	0.83	0.54				16
	8	468	33.785	1.712	27.020	98.7	94.5	104.5	2.308	7.446	7.586	2.312	0.039	1096	0.77	0.51				44
	7	988	34.334	2.343	27.410	26.6	94.7	28.7	2.380	7.430	7.514	2.389	0.038	1198	0.61	0.43				7
	6	1384	34.424	2.252	27.490	24.9	94.7	27.1	2.396	7.444	7.496	2.400	0.039	1152	0.53	0.39				5
	5	1483	34.432	2.243	27.497	24.4	94.5	26.4	2.399	7.445	7.488	2.403	0.039	1148	0.51	0.38				4
	4	1580	34.437	2.237	27.501	25.5	94.2	27.6	2.399	7.449	7.484	2.402	0.039	1135	0.49	0.37				15
	3	1625	34.437	2.235	27.502	26.4	94.0	28.1	2.400	7.448	7.479	2.403	0.039	1138	0.48	0.37				28
	2	1668	34.438	2.234	27.503	26.7	93.9	28.5	2.400	7.451	7.479	2.402	0.039	1128	0.47	0.36				161
	1	1676	34.438	2.234	27.503	26.9	93.9	28.6	2.398	7.447	7.474	2.401	0.038	1139	0.47	0.36				151
28-1	12	4	32.514	4.390	25.770	309.6	88.1													67
	11	64	32.789	-1.543	26.377	322.3	93.5													78
	10	150	33.309	0.586	26.711	186.9	94.5													15
	9	298	33.505	0.943	26.847	142.6	94.4													14
	8	495	33.835	1.756	27.057	92.5	94.6													37
	7	989	34.326	2.344	27.404	27.2	94.7													12
	6	1382	34.425	2.251	27.491	24.8	94.7													
	5	1463	34.431	2.245	27.496	24.5	94.5													28
	4	1513	34.435	2.239	27.500	25.2	94.3													100

St. No	Bot. No	Depth m	S	q, °C	s_0, kg/m^3	O_2 CTD mmol/kg	Tr, %	O_2 mmol/kg	TA mmol/kg	pH_t 15 °C	pH_t in situ	DIC, mmol/kg	CO_3, mmol/kg	pCO_2, matm	Lc	La	TNO µmol/l	PO_4 µmol/l	SiO_2 µmol/l	CH_4 nl/l
	3	1561	34.437	2.237	27.501	25.5	94.1													237
	2	1600	34.437	2.236	27.502	25.6	94.0													250
	1	1611	34.437	2.236	27.502	25.7	94.0													190
29-1	12	4	32.331	2.126	25.825	350.2	77.2	388.1	2.208	7.976	8.175	2.042	0.120	272	2.89	1.81	7.1	0.37	13	69
	11	73	32.954	-0.282	26.468	290.0	93.5	309.6	2.233	7.720	7.942	2.156	0.070	482	1.64	1.04	22.6	1.55	41	68
	10	149	33.215	0.296	26.650	217.7	94.1	232.0	2.252	7.589	7.788	2.214	0.053	700	1.19	0.76	29.1	2.04	61	55
	9	298	33.470	1.136	26.807	142.8	93.7	148.0	2.274	7.459	7.623	2.275	0.039	1023	0.84	0.54	34.1	2.50	81	45
	8	386	33.586	1.486	26.877	128.2	93.9	133.7	2.285	7.459	7.61	2.286	0.040	1041	0.81	0.53	34.9	2.54	87	146
	7	432	33.707	1.703	26.958	108.8	93.9	113.0	2.299	7.442	7.584	2.305	0.038	1103	0.77	0.51	37.0	2.64	105	35
	6	484	33.862	1.927	27.065	85.6	93.6	87.6	2.319	7.442	7.577	2.325	0.039	1122	0.76	0.51	39.4	2.78	114	144
	5	533	33.902	1.945	27.096	83.3	92.3	84.6	2.324	7.442	7.572	2.329	0.039	1124	0.74	0.50	40.6	2.79	116	95
	4	583	33.921	1.983	27.108	79.8	92.5	81.3	2.325	7.441	7.566	2.331	0.039	1128	0.73	0.49	41.0	2.78	114	1313
	3	633	33.972	2.058	27.143	73.3	92.7	73.6	2.333	7.439	7.558	2.339	0.038	1141	0.71	0.48	41.9	2.81	126	711
	2	674	34.030	2.121	27.185	66.9	92.0	66.1	2.340	7.441	7.556	2.346	0.039	1140	0.70	0.48	41.6	2.56	126	3726
	1	683	34.046	2.137	27.197	65.6	88.1	76.1	2.331	7.440	7.554	2.337	0.038	1139	0.70	0.47	39.9	2.51	129	468
31-1	12	4	32.598	3.513	25.922	323.6	85.5	355.4	2.212	7.908	8.083	2.071	0.105	347	2.54	1.59	10.9	0.27	17	71
	11	67	32.830	-0.986	26.394	318.0	93.6	338.9	2.226	7.772	8.009	2.132	0.078	407	1.83	1.16	19.0	1.00	39	72
	10	149	33.144	-0.179	26.617	243.2	94.2	255.6	2.246	7.625	7.833	2.198	0.057	623	1.29	0.82	27.3	1.71	59	60
	9	298	33.457	1.207	26.791	155.9	94.1	162.3	2.270	7.489	7.654	2.262	0.042	948	0.90	0.58	34.2	2.24	82	39
	8	393	33.622	1.561	26.900	122.1	94.0	126.6	2.287	7.456	7.605	2.288	0.039	1054	0.80	0.53	36.0	2.48	97	44
	7	493	33.859	1.926	27.063	86.1	93.9	89.3	2.316	7.440	7.574	2.322	0.038	1126	0.75	0.50	38.0	2.65	124	31
	6	595	34.024	2.110	27.181	65.4	94.0	67.0	2.340	7.433	7.554	2.348	0.038	1165	0.72	0.48	39.6	2.73	143	78
	5	694	34.108	2.184	27.242	55.7	93.7	56.8	2.349	7.430	7.541	2.358	0.038	1180	0.68	0.47	39.7	2.73	153	72
	4	790	34.162	2.224	27.283	49.6	93.4	50.5	2.358	7.431	7.533	2.367	0.038	1181	0.66	0.45	40.3	2.71	159	36
	3	841	34.191	2.245	27.304	46.4	93.5	46.8	2.363	7.429	7.526	2.372	0.038	1190	0.64	0.45	40.6	2.74	162	89
	2	890	34.217	2.258	27.324	43.8	93.1	44.2	2.366	7.433	7.526	2.374	0.038	1179	0.63	0.44	40.8	2.59	161	103
	1	946	34.252	2.280	27.350	40.3	91.5	40.2	2.369	7.430	7.518	2.378	0.038	1190	0.61	0.43	41.3	2.30	168	192
32-1	12	3	32.264	2.033	25.778	337.1	76.2	403.3	2.196	7.999	8.2	2.021	0.124	253	3.01	1.88	6.5	0.39	28	80
	11	11	32.263	2.042	25.777	331.2	75.9	395.7	2.200	7.976	8.176	2.035	0.119	270	2.87	1.80	7.7	0.48	30	80
	10	20	32.334	1.909	25.843	302.3	79.6	359.9	2.210	7.848	8.045	2.093	0.091	378	2.20	1.38	14.9	0.98	37	82
	9	31	32.571	0.070	26.142	296.3	91.9	339.7	2.219	7.776	7.999	2.125	0.078	422	1.87	1.18	19.0	1.27	44	80
	8	51	32.778	-0.489	26.334	279.1	93.1	319.1	2.228	7.730	7.958	2.148	0.071	465	1.69	1.06	21.2	1.43	48	81
	7	69	33.069	-0.351	26.564	249.1	93.9	272.1	2.245	7.643	7.862	2.191	0.059	591	1.39	0.88	25.5	1.84	57	128
	6	90	33.203	-0.083	26.660	235.6	93.2	247.4	2.255	7.597	7.807	2.215	0.054	677	1.25	0.79	26.8	2.08	63	768
	5	109	33.233	-0.243	26.691	238.9	91.5	250.4	2.259	7.596	7.807	2.219	0.054	674	1.24	0.79	25.8	2.13	62	3295
	4	126	33.253	-0.365	26.712	242.2	89.6	252.2	2.262	7.599	7.81	2.221	0.054	666	1.24	0.79	25.7	2.07	61	4969
	3	148	33.255	-0.360	26.714	243.2	89.6	251.8	2.261	7.596	7.805	2.221	0.054	671	1.21	0.77	26.3	2.19	63	5358

St. No	Bot. No	Depth m	S	q, °C	s_0, kg/m^3	O_2 CTD mmol/kg	Tr, %	O_2 mmol/kg	TA mmol/kg	pH_t 15 °C	pH_t in situ	DIC, mmol/kg	CO_3, mmol/kg	pCO_2, matm	Lc	La	TNO µmol/l	PO_4 µmol/l	SiO_2 µmol/l	CH_4 nl/l
	2	164	33.255	-0.361	26.714	244.8	89.6	251.9	2.261	7.599	7.807	2.220	0.054	665	1.21	0.78	25.7	2.08	60	6416
	1	172	33.254	-0.370	26.713	247.8	89.2	252.8	2.264	7.597	7.804	2.224	0.054	669	1.20	0.77	25.6	2.08	62	7197
35-1	12	4	32.594	2.635	25.995	331.0	80.1	380.0	2.213	7.954	8.144	2.054	0.115	295	2.79	1.75			21	83
	11	37	32.806	0.020	26.334	302.9	91.9	335.6	2.225	7.799	8.023	2.122	0.083	397	1.98	1.24			39	89
	10	80	33.004	-0.413	26.514	267.2	94.1	290.2	2.238	7.704	7.927	2.166	0.068	501	1.58	1.00			52	733
	9	129	33.170	-0.164	26.637	244.3	93.2	259.4	2.250	7.643	7.854	2.196	0.059	596	1.36	0.86			57	1804
	8	179	33.253	-0.443	26.716	242.6	91.1	257.0	2.260	7.629	7.839	2.210	0.058	612	1.29	0.83			60	2096
	7	218	33.295	-0.495	26.752	236.6	89.9	249.8	2.264	7.616	7.823	2.218	0.056	632	1.23	0.79			62	2510
	6	258	33.351	-0.283	26.788	225.1	90.8	234.6	2.269	7.590	7.788	2.231	0.053	684	1.14	0.74			67	5780
	5	288	33.380	-0.334	26.814	225.3	89.4	233.5	2.271	7.589	7.785	2.233	0.053	684	1.12	0.73			64	9338
	4	317	33.390	-0.287	26.820	225.5	88.7	233.4	2.272	7.592	7.785	2.233	0.053	680	1.12	0.73			66	7184
	3	336	33.390	-0.378	26.824	230.0	87.4	237.3	2.273	7.597	7.79	2.232	0.054	668	1.12	0.73			66	5814
	2	359	33.401	-0.396	26.834	230.8	86.3	238.2	2.274	7.598	7.79	2.233	0.054	666	1.11	0.73			68	3876
	1	372	33.405	-0.404	26.837	231.3	85.8	238.2	2.274	7.600	7.791	2.232	0.054	662	1.11	0.73			69	5494
38-1	12	4	32.618	2.877	25.994	334.8	80.3	389.5	2.216	7.963	8.149	2.053	0.118	292	2.85	1.78	10.6	0.51	16	83
	11	41	32.741	0.419	26.262	309.6	89.9	348.3	2.227	7.824	8.043	2.116	0.088	379	2.09	1.31	19.1	1.20	31	76
	10	79	32.820	-0.058	26.349	292.5	92.1	334.3	2.231	7.784	8.005	2.133	0.080	412	1.88	1.19	22.1	1.45	36	78
	9	129	33.067	-0.304	26.560	251.9	93.3	277.4	2.248	7.672	7.887	2.185	0.063	549	1.45	0.92	27.6	1.98	50	861
	8	177	33.243	-0.098	26.693	226.5	92.4	236.5	2.262	7.599	7.802	2.221	0.054	673	1.21	0.77	30.6	2.26	61	1426
	7	217	33.343	0.365	26.750	196.8	92.7	195.9	2.267	7.532	7.72	2.246	0.046	819	1.02	0.66	33.7	2.50	72	588
	6	257	33.373	0.465	26.768	200.2	92.3	198.3	2.271	7.533	7.716	2.250	0.047	821	1.01	0.65	31.3	2.37	71	1421
	5	288	33.391	0.141	26.800	210.1	89.9	207.4	2.278	7.549	7.735	2.252	0.048	778	1.03	0.67	30.4	2.33	69	2784
	4	316	33.418	0.200	26.819	223.9	89.0	215.3	2.279	7.563	7.747	2.249	0.050	752	1.05	0.69	29.9	2.28	68	711
	3	347	33.429	-0.458	26.859	238.9	84.2	241.5	2.280	7.596	7.79	2.239	0.054	669	1.11	0.73	26.9	2.17	62	777
	2	360	33.435	-0.383	26.861	236.7	83.9	233.3	2.278	7.589	7.78	2.240	0.053	683	1.09	0.71	27.3	2.24	62	395
	1	372	33.437	-0.328	26.860	238.5	83.7	232.8	2.285	7.584	7.773	2.248	0.052	696	1.07	0.70	26.9	2.15	66	359
39-1	8	3	30.894	2.210	24.669	357.9	72.7	415.0	2.116	7.988	8.185	1.957	0.114	256	2.77	1.73	7.1	0.28	30	247
	7	10	31.455	0.207	25.236	327.4	87.7	366.0	2.120	7.867	8.093	2.003	0.089	322	2.16	1.35	13.8	1.09	33	285
	6	29	33.110	-1.284	26.631	291.1	89.7	296.0	2.256	7.677	7.916	2.192	0.064	522	1.54	0.96	21.8	1.97	33	2867
	5	50	33.253	-1.337	26.749	288.2	87.7	293.0	2.265	7.666	7.904	2.203	0.063	537	1.49	0.94	21.7	1.77	44	4194
	4	70	33.256	-1.337	26.750	290.3	87.8	292.5	2.263	7.667	7.903	2.201	0.063	535	1.48	0.93	21.6	1.83	46	4217
	3	90	33.256	-1.335	26.750	294.4	87.3	292.6	2.266	7.669	7.904	2.203	0.063	532	1.47	0.93	20.9	1.80	45	4128
	2	110	33.255	-1.333	26.750	300.5	86.4	292.6	2.265	7.664	7.897	2.204	0.063	539	1.44	0.92	21.6	1.79	45	3795
	1	123	33.255	-1.332	26.750	304.7	86.6	292.2	2.264	7.664	7.895	2.203	0.063	538	1.43	0.91	20.7	1.63	47	3942
43-1	12	4	32.015	1.593	25.609	368.5	71.5	424.3	2.183	8.044	8.253	1.991	0.134	219	3.26	2.04			17	155
	11	19	32.452	1.456	25.968	338.2	79.7	389.3	2.210	7.950	8.158	2.054	0.113	283	2.72	1.71			19	132

St. No	Bot. No	Depth m	S	q, °C	s_0, kg/m^3	O_2 CTD mmol/kg	Tr, %	O_2 mmol/kg	TA mmol/kg	pH_t 15 °C	pH_t in situ	DIC, mmol/kg	CO_3, mmol/kg	pCO_2, matm	Lc	La	TNO µmol/l	PO_4 µmol/l	SiO_2 µmol/l	CH_4 nl/l
	10	39	32.834	0.040	26.356	291.3	89.9	319.2	2.230	7.767	7.989	2.138	0.078	433	1.85	1.16			40	679
	9	78	33.104	-0.452	26.596	258.7	91.3	273.4	2.251	7.661	7.882	2.192	0.062	563	1.45	0.92			52	1115
	8	109	33.158	-0.503	26.641	250.5	91.9	262.9	2.257	7.634	7.851	2.206	0.058	603	1.35	0.85			54	894
	7	139	33.195	-0.465	26.670	242.3	91.8	253.6	2.260	7.617	7.83	2.214	0.056	632	1.28	0.81			56	823
	6	173	33.281	-0.082	26.722	227.6	89.2	232.0	2.265	7.587	7.789	2.228	0.053	696	1.18	0.75			62	1272
	5	199	33.294	-0.124	26.735	229.8	87.5	232.2	2.268	7.585	7.785	2.231	0.052	699	1.16	0.75			63	2284
	4	229	33.301	-0.157	26.743	232.0	87.2	232.7	2.270	7.586	7.784	2.233	0.052	696	1.15	0.74			63	2350
	3	258	33.302	-0.186	26.744	235.5	86.9	233.2	2.270	7.586	7.782	2.233	0.052	694	1.13	0.73			64	2557
	2	281	33.304	-0.180	26.745	238.2	87.0	233.2	2.269	7.589	7.784	2.231	0.053	688	1.13	0.73			63	2744
	1	294	33.299	-0.243	26.745	242.7	86.3	236.4	2.270	7.593	7.788	2.231	0.053	679	1.13	0.73			65	3031
45-1	12	4	32.200	1.858	25.739	354.8	73.9	408.3	2.203	8.022	8.226	2.019	0.130	237	3.16	1.98			17	129
	11	49	32.945	-0.368	26.464	280.6	93.6	305.4	2.239	7.722	7.948	2.161	0.071	480	1.67	1.05			45	85
	10	99	33.041	-0.177	26.533	259.6	93.6	280.7	2.249	7.678	7.894	2.185	0.064	544	1.49	0.94			49	71
	9	148	33.203	0.126	26.650	221.0	93.9	232.9	2.258	7.596	7.798	2.218	0.054	685	1.22	0.78			62	66
	8	198	33.292	0.415	26.706	200.2	93.7	209.4	2.265	7.555	7.745	2.237	0.049	773	1.09	0.70			66	88
	7	248	33.387	0.766	26.763	168.3	93.6	174.5	2.273	7.501	7.678	2.261	0.043	904	0.94	0.61			77	62
	6	298	33.448	1.009	26.797	156.0	93.5	158.1	2.277	7.481	7.648	2.271	0.041	963	0.88	0.57			83	63
	5	347	33.487	0.932	26.833	159.5	92.0	158.1	2.283	7.486	7.65	2.276	0.042	949	0.87	0.57			85	107
	4	397	33.506	0.257	26.887	182.5	86.9	189.0	2.289	7.537	7.711	2.266	0.047	808	0.96	0.63			80	219
	3	445	33.709	1.079	27.003	137.6	84.4	138.2	2.305	7.493	7.647	2.295	0.043	944	0.86	0.57			101	172
	2	495	33.840	1.665	27.067	105.9	77.1	101.6	2.320	7.458	7.597	2.321	0.040	1065	0.78	0.52			117	307
	1	504	33.854	1.720	27.074	104.5	69.8	99.2	2.320	7.455	7.592	2.322	0.040	1076	0.77	0.52			120	269
47-1	12	4	32.187	2.780	25.658	376.5	64.4	435.6	2.178	8.115	8.306	1.985	0.158	193	3.81	2.39			11	93
	11	88	32.922	-1.011	26.469	285.1	93.6	305.4	2.220	7.709	7.941	2.153	0.068	479	1.58	1.00			47	76
	10	197	33.304	0.505	26.711	186.6	93.7	193.0	2.252	7.526	7.713	2.227	0.045	829	1.01	0.65			77	58
	9	297	33.463	1.152	26.800	142.6	93.8	145.4	2.267	7.458	7.621	2.271	0.039	1025	0.83	0.54			68	50
	8	495	33.910	1.980	27.100	82.0	93.9	82.0	2.317	7.444	7.577	2.291	0.038	1103	0.75	0.50			127	101
	7	594	34.048	2.128	27.199	65.2	92.9	64.2	2.337	7.438	7.56	2.322	0.038	1139	0.72	0.48			142	118
	6	644	34.061	2.138	27.209	64.0	92.7	62.7	2.340	7.436	7.553	2.347	0.038	1156	0.70	0.48			137	351
	5	692	34.094	2.174	27.232	60.5	93.6	58.7	2.344	7.434	7.546	2.357	0.038	1167	0.69	0.47			149	72
	4	742	34.122	2.199	27.253	57.2	92.5	56.0	2.348	7.436	7.543	2.365	0.038	1166	0.68	0.47			154	139
	3	810	34.147	2.215	27.271	54.8	93.3	52.6	2.353	7.433	7.534	2.371	0.038	1177	0.65	0.45			157	99
	2	850	34.160	2.222	27.281	54.3	92.5	50.5	2.353	7.435	7.532	2.374	0.038	1172	0.65	0.45			159	792
	1	863	34.159	2.221	27.280	54.6	91.9	50.4	2.354	7.445	7.542	2.373	0.039	1143	0.66	0.46			162	1013
66-1	12	6	32.268	7.238	25.236	279.1	86.1	324.2	2.187	8.0945	8.213	1.971	0.152	246	3.67	2.31				105
	11	50	32.854	-0.508	26.396	292.4	92.9	328.7	2.211	7.8126	8.045	2.104	0.085	371	2.01	1.27				963
	10	137	33.122	-1.572	26.649	274.7	91.0	300.0	2.231	7.7123	7.949	2.156	0.068	463	1.56	0.99				2791

St. No	Bot. No	Depth m	S	q, °C	s_0, kg/m^3	O_2 CTD mmol/kg	Tr, %	O_2 mmol/kg	TA mmol/kg	pH_t 15 °C	pH_t in situ	DIC, mmol/kg	CO_3, mmol/kg	pCO_2, matm	Lc	La	TNO µmol/l	PO_4 µmol/l	SiO_2 µmol/l	CH_4 nl/l
	9	295	33.252	-0.527	26.718	224.7	92.6	244.3	2.238	7.6442	7.847	2.184	0.059	579	1.25	0.81				246
	8	395	33.472	0.773	26.830	165.3	93.1	172.6	2.254	7.5708	7.74	2.221	0.050	745	1.03	0.67				157
	7	467	33.587	1.201	26.897	145.3	93.6	150.9	2.264	7.5519	7.707	2.236	0.048	799	0.96	0.64				148
	6	518	33.638	1.328	26.929	136.5	93.1	141.0	2.271	7.5443	7.692	2.246	0.048	822	0.92	0.62				202
	5	571	33.720	1.534	26.981	121.7	93.1	124.1	2.282	7.5328	7.672	2.260	0.047	857	0.88	0.59				247
	4	619	33.794	1.696	27.028	104.6	92.7	107.0	2.293	7.5188	7.651	2.275	0.045	898	0.84	0.57				231
	3	667	33.842	1.799	27.059	95.2	92.7	98.4	2.298	7.5113	7.637	2.282	0.045	922	0.81	0.55				263
	2	705	33.930	1.965	27.117	74.4	90.6	75.6	2.315	7.4989	7.618	2.303	0.044	964	0.78	0.54				318
	1	719	34.031	2.126	27.185	65.4	91.5	66.2	2.319	7.4924	7.607	2.309	0.043	989	0.77	0.53				337

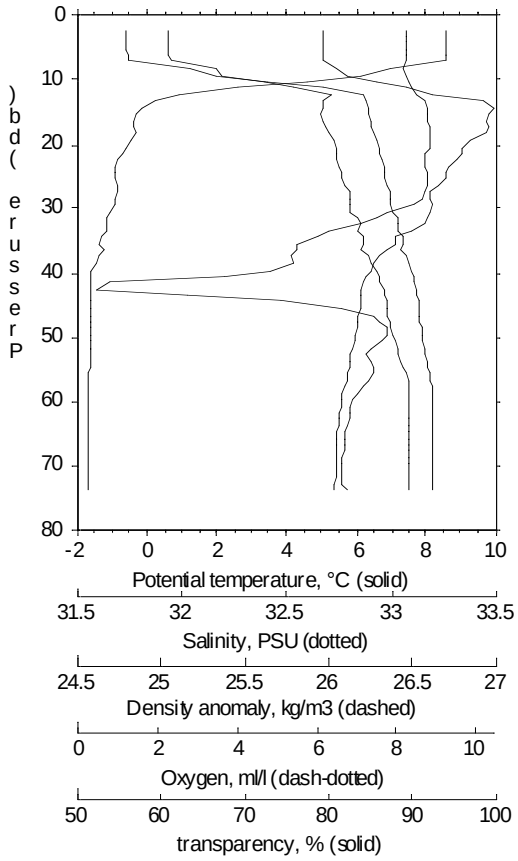

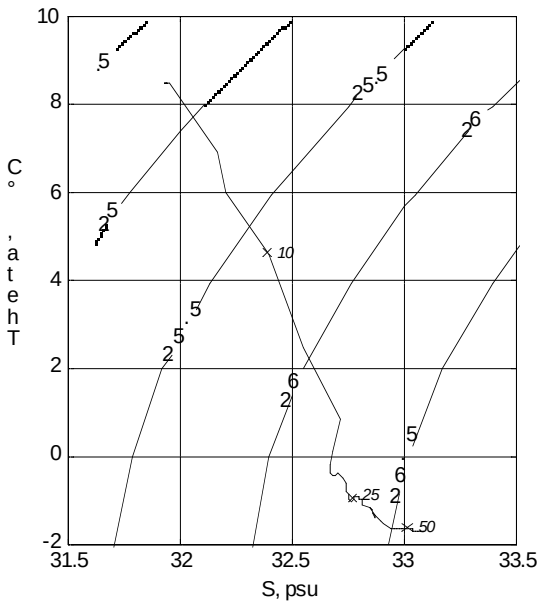

** Station: LV29-1/1
Time = Jun 03 2 06:37:54
** Latitude: 47 :59.980
** Longitude: 143:58.659
File : LV29-1D.CNV

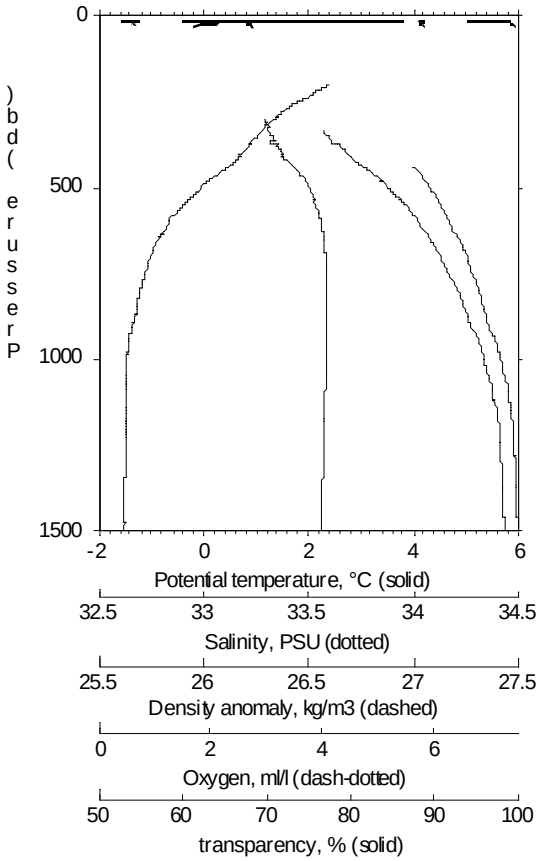

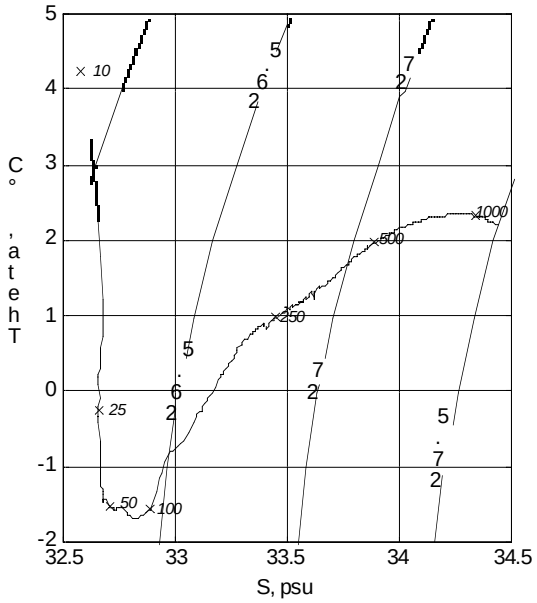

** Station: LV29-2/1
Time = Jun 05 2002 05:30:52
** Latitude: 54 :00.410
** Longitude: 146:16.988
File : LV29-2D.CNV

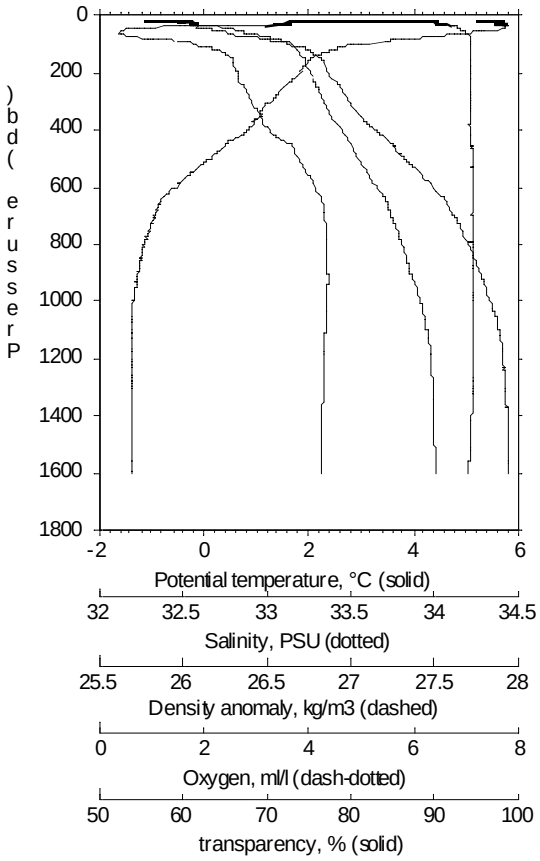

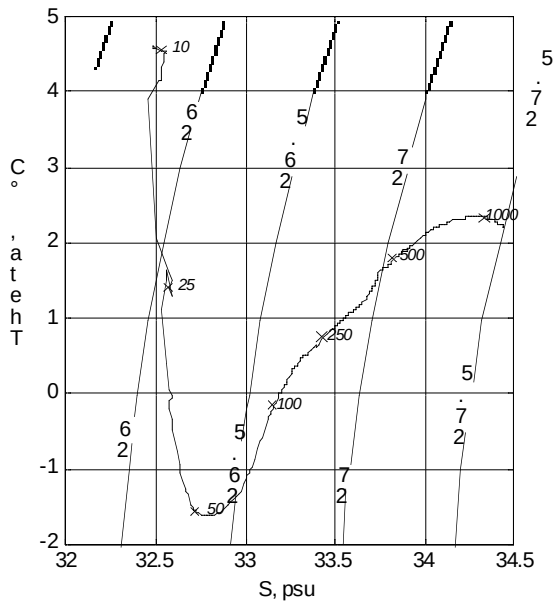

** Station: LV29-4/1
Time = Jun 05 2002 23:38:00
** Latitude: 54 :01.263
** Longitude: 146:24.086
File : LV29-4u.CNV

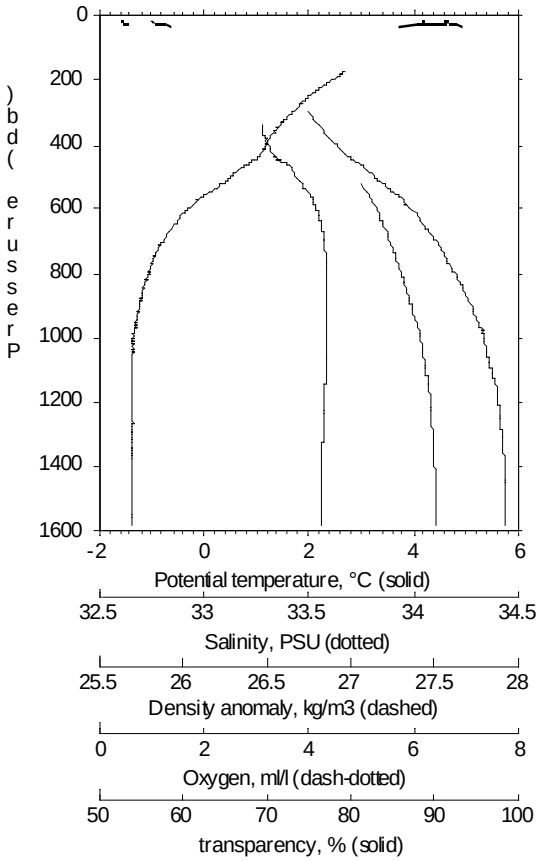

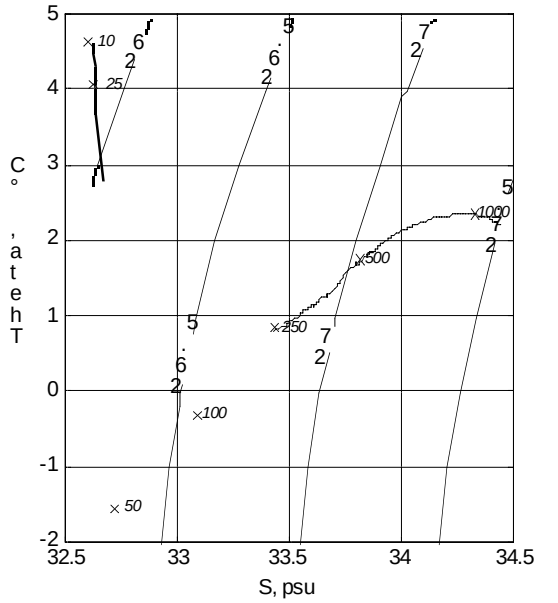

** Station: LV29-5/1
Time = Jun 06 2002 02:29:09
** Latitude: 54 :09.773
** Longitude: 146:34.738
File : LV29-5D.CNV

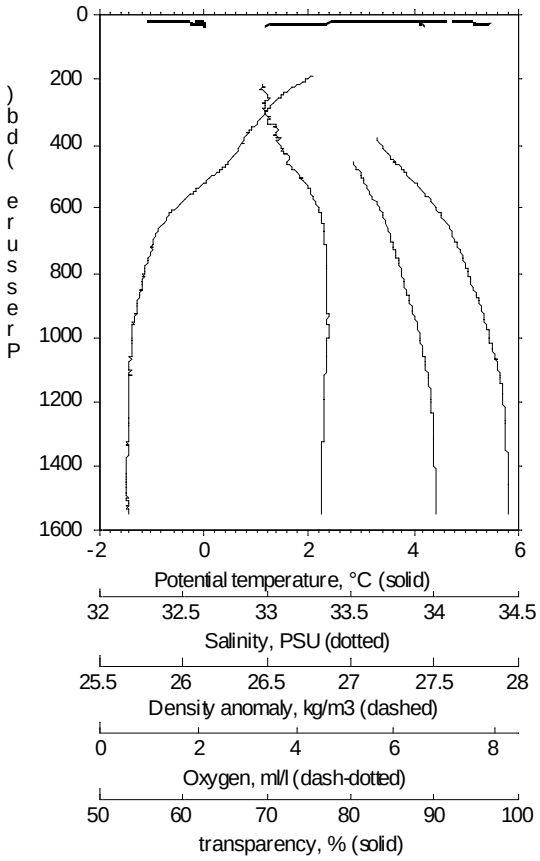

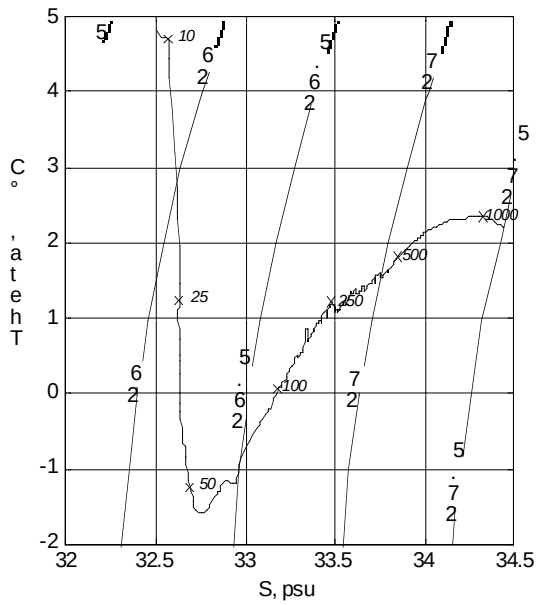

** Station: LV29-6/1
Time = Jun 06 2002 05:17:58
** Latitude: 53 :54.078
** Longitude: 146:35.277
File : LV29-6D.CNV

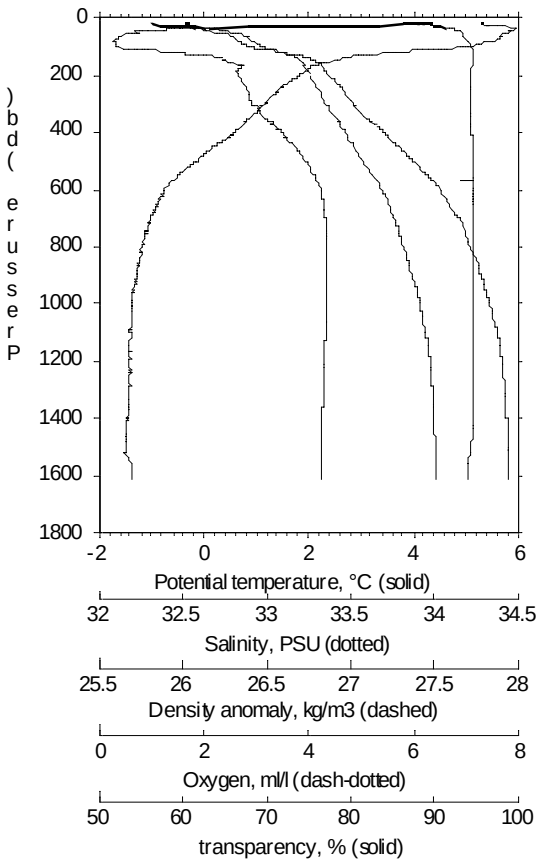

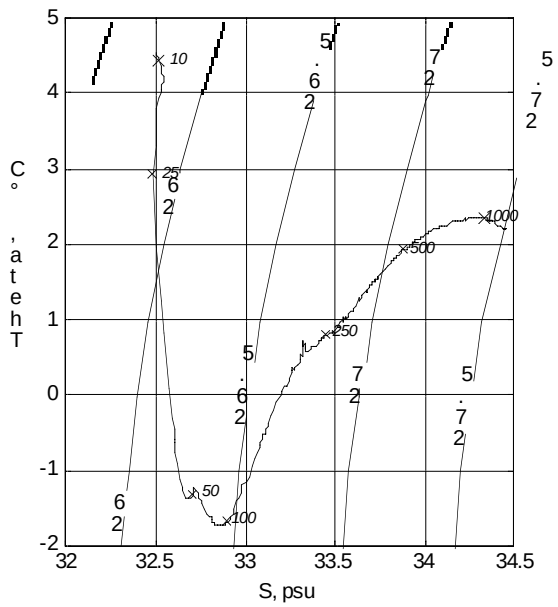

** Station: LV29-7/1
Time = Jun 06 2002 07:53:21
** Latitude: 53 :51.741
** Longitude: 146:22.839
File : LV29-7u.CNV

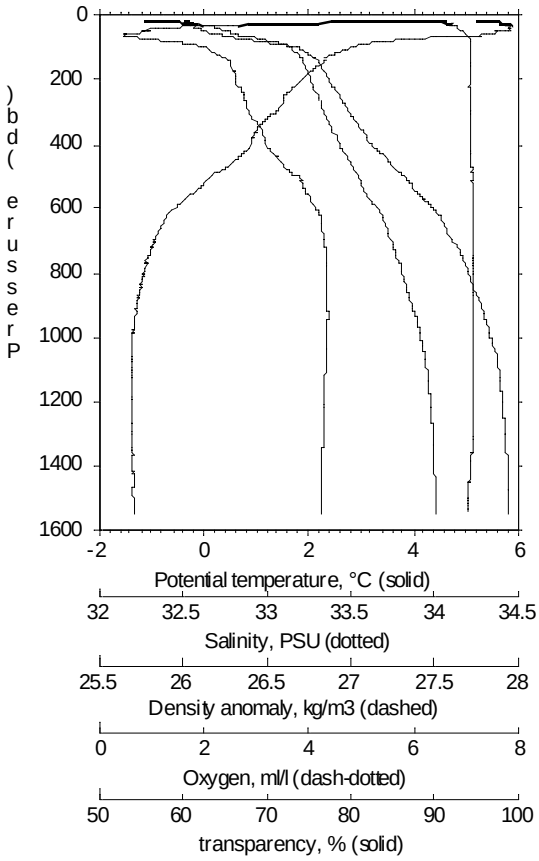

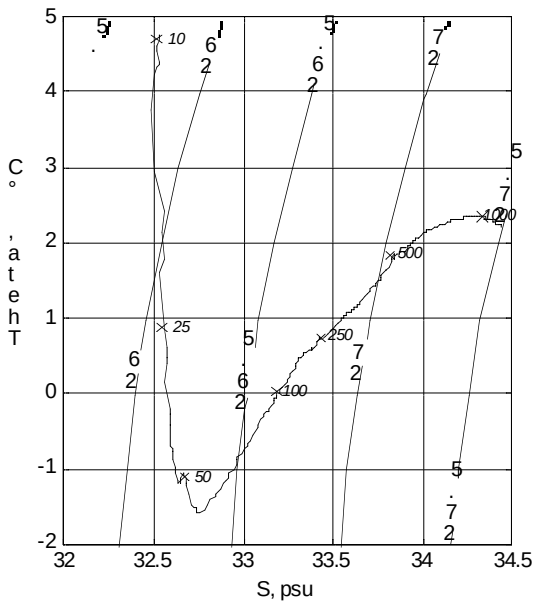

** Station: LV29-9/1
Time = Jun 07 2002 00:08:25
** Latitude: 53 :56.141
** Longitude: 146:23.752
File : LV29-9u.CNV

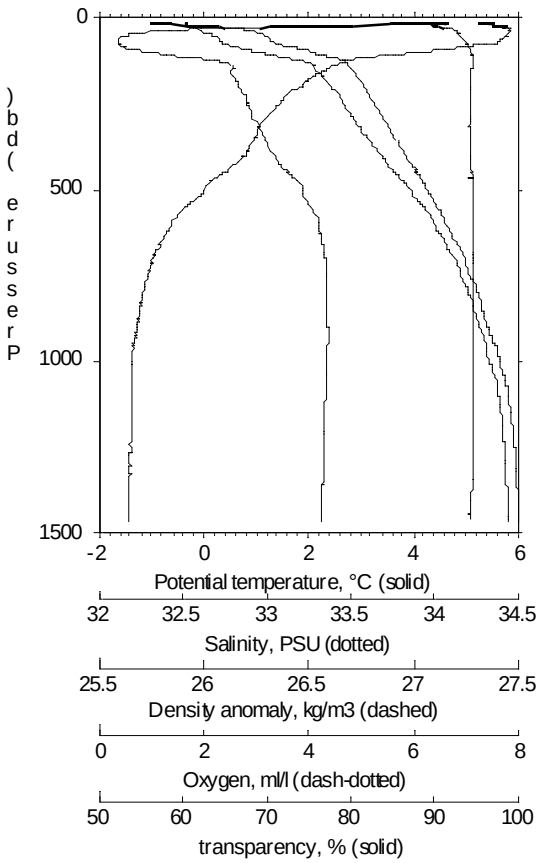

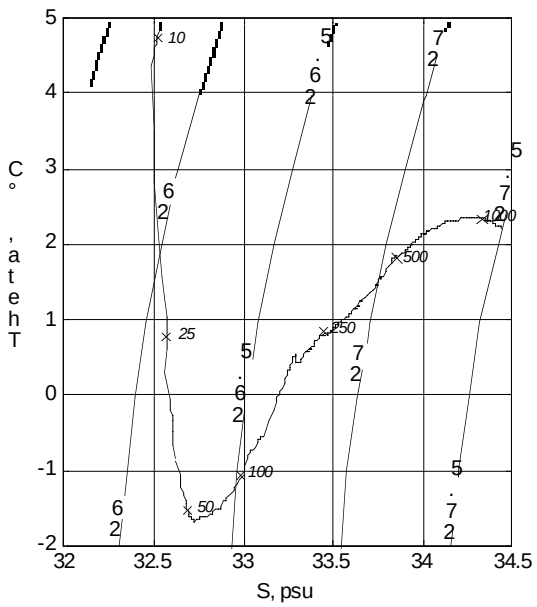

** Station: LV-10/1
Time = Jun 07 2002 03:58:45
** Latitude: 53 :59.279
** Longitude: 146:18.994
File : LV29-10u.CNV

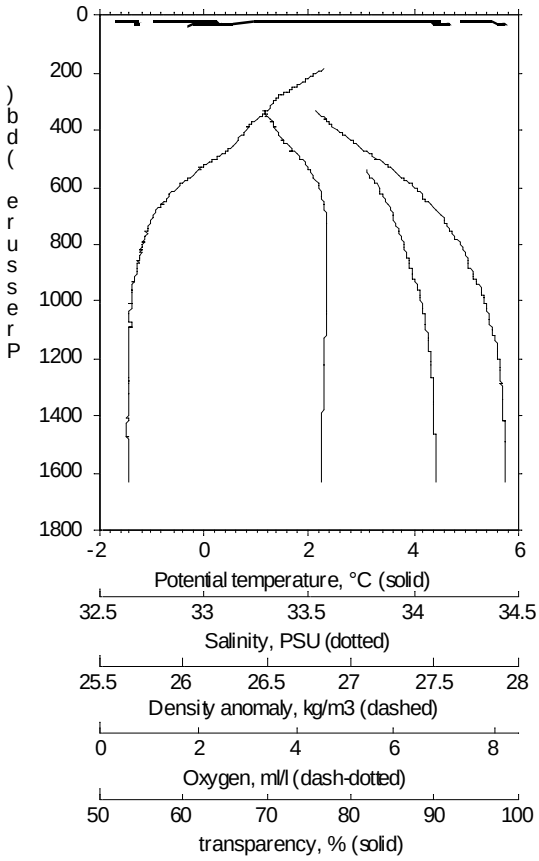

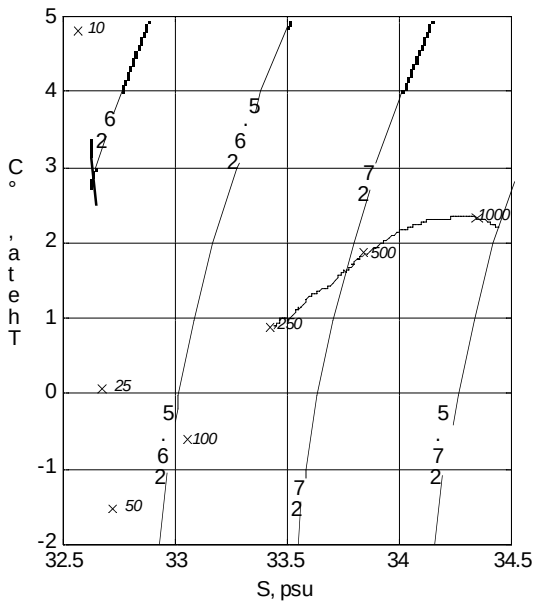

** Station: LV29-11/1
Time = Jun 07 2002 06:00:09
** Latitude: 54 :02.831
** Longitude: 146:06.857
File : LV29-11D.CNV

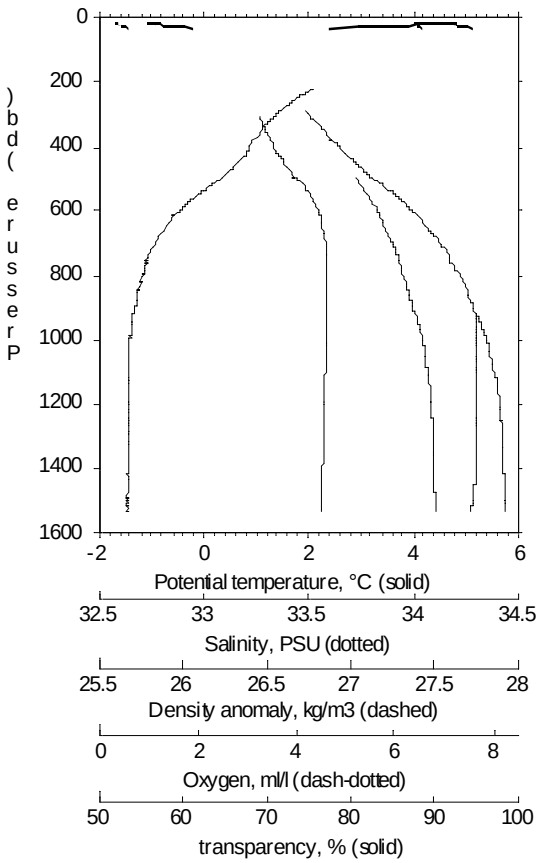

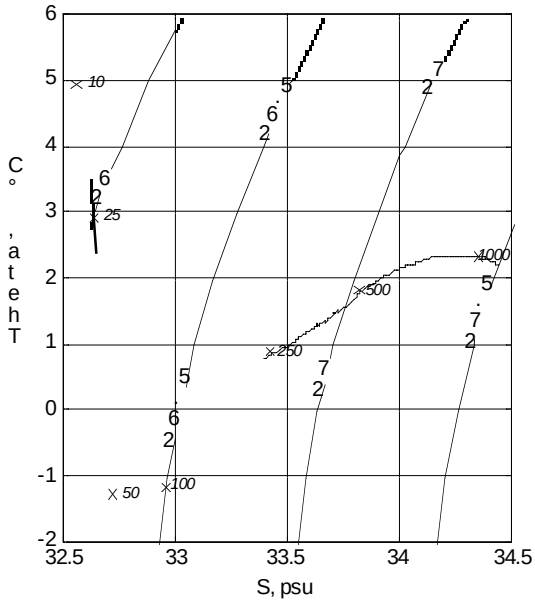

** Station: LV29-12/1
Time = Jun 07 2002 07:36:57
** Latitude: 54 :04.156
** Longitude: 146:05.792
File : LV29-12D.CNV

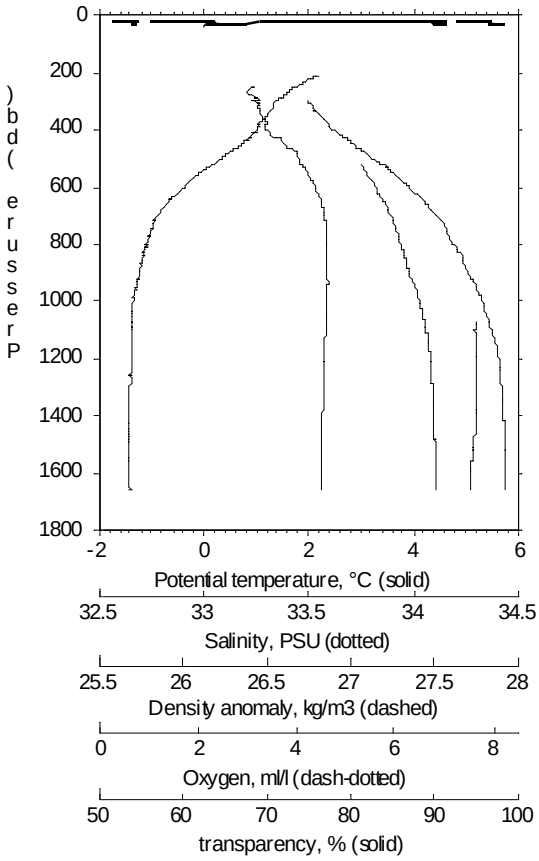

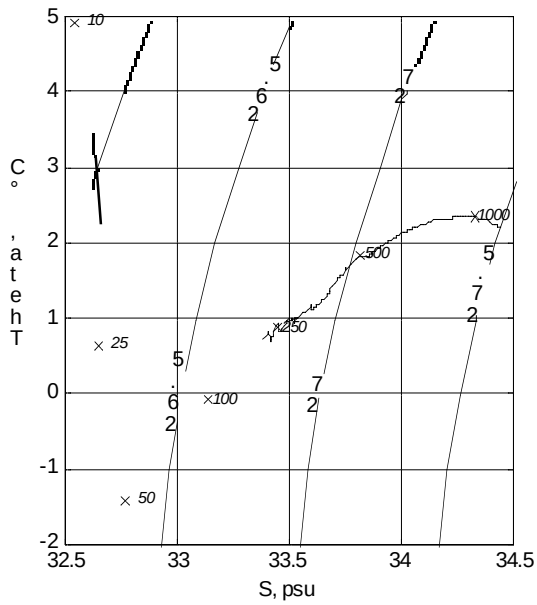

** Station: LV29-14/1
Time = Jun 08 2002 00:15:08
** Latitude: 54 :04.156
** Longitude: 146:25.568
File : LV29-14D.CNV

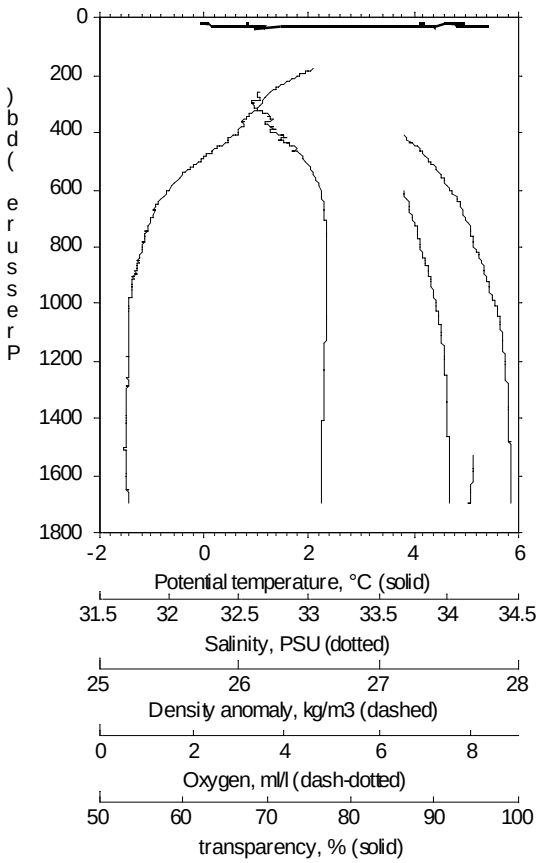

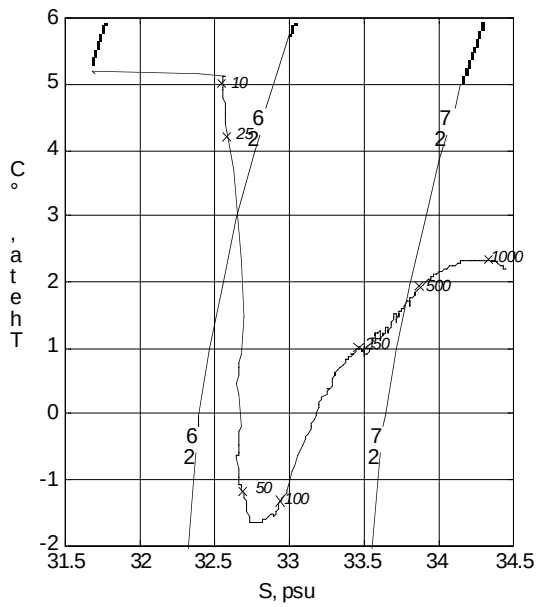

** Station: LV29-15/1
Time = Jun 08 2002 02:12:42
** Latitude: 54 :04.114
** Longitude: 146:17.594
File : LV29-15D.CNV

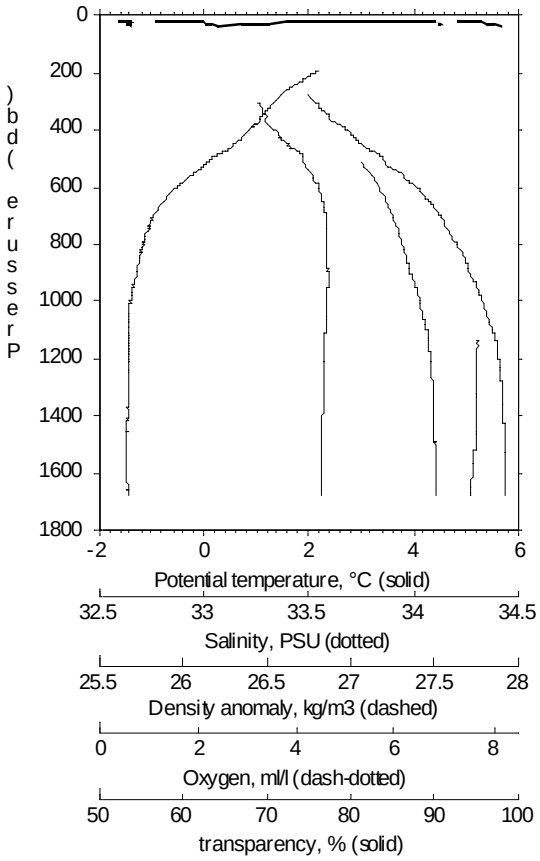

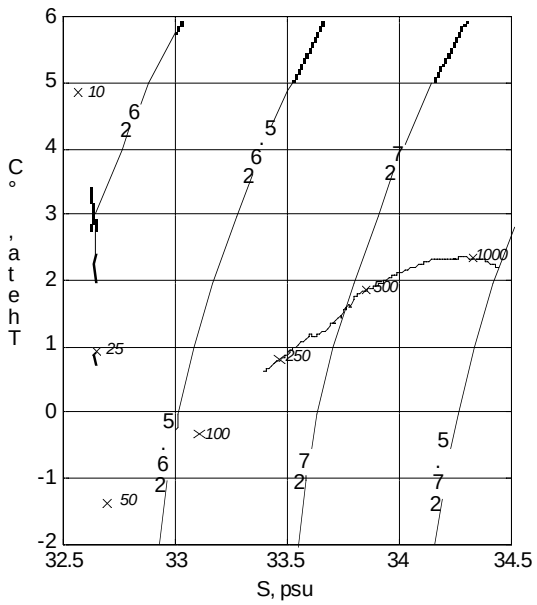

** Station: LV29-16/1
Time = Jun 08 2002 04:42:15
** Latitude: 54 :01.239
** Longitude: 146:21.101
File : LV29-16D.CNV

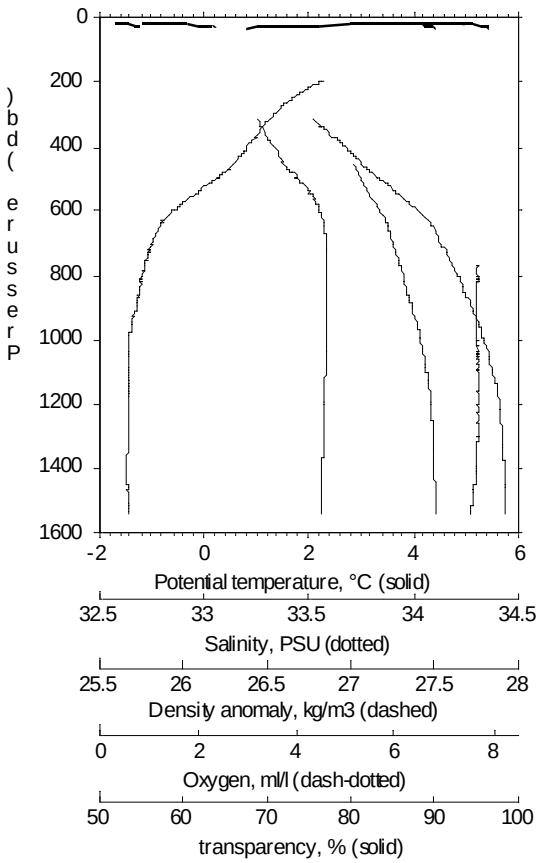

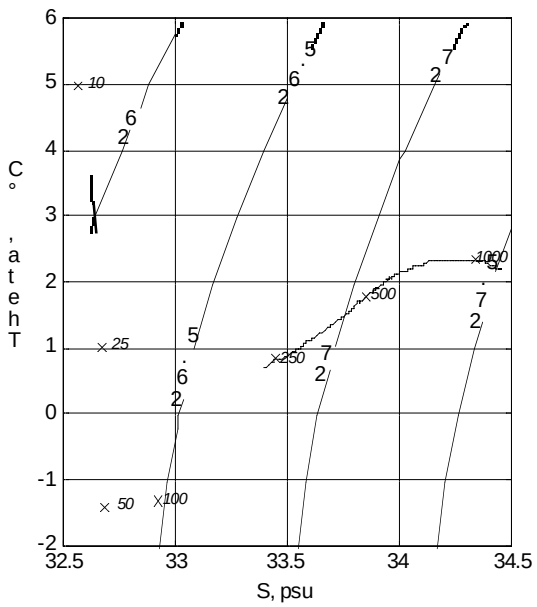

** Station: LV29-17/1
Time = Jun 08 2002 07:07:49
** Latitude: 53 :58.367
** Longitude: 146:15.222
File : LV29-17D.CNV

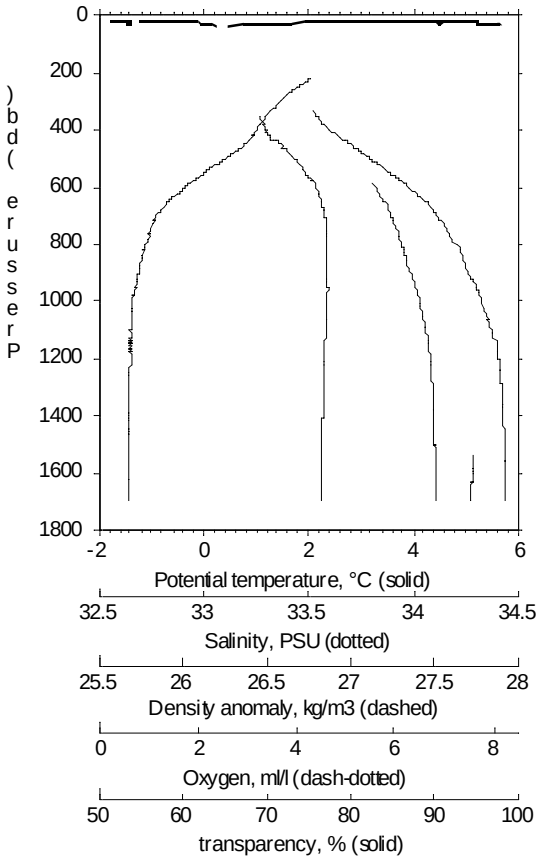

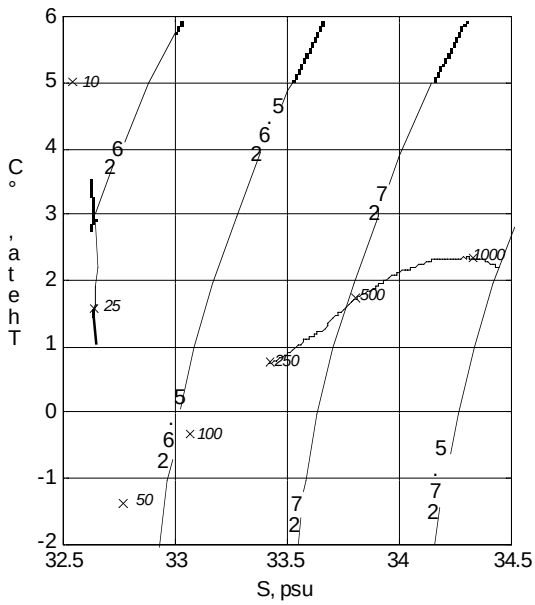

** Station: LV29-19/1
Time = Jun 08 2002 23:38:07
** Latitude: 54 :06.091
** Longitude: 146:23.628
File : LV29-19D.CNV

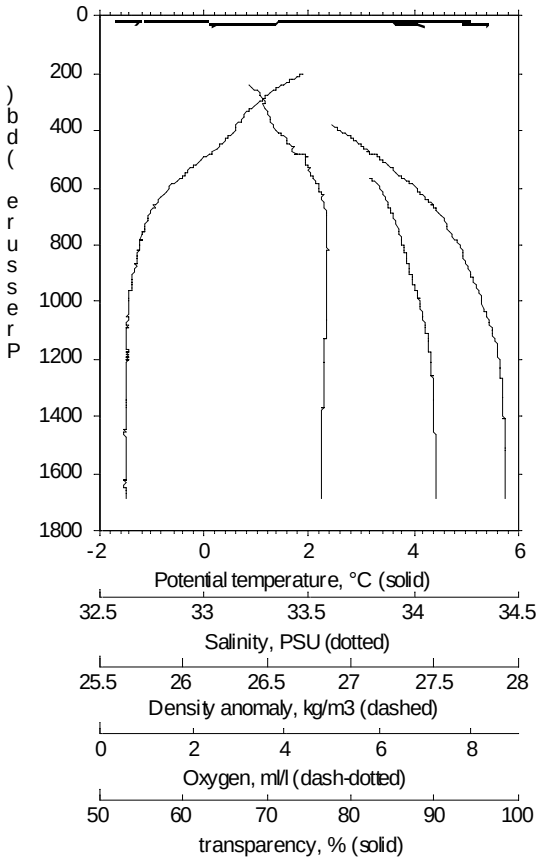

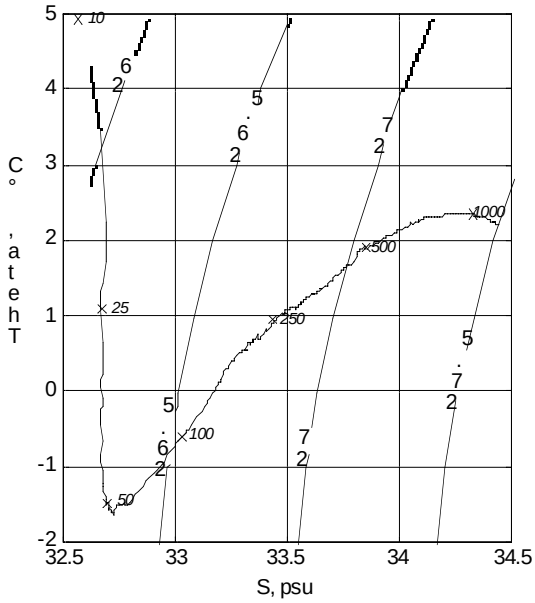

** Station: LV29-20/1
Time = Jun 09 2002 01:54:02
** Latitude: 54 :08.078
** Longitude: 146:14.809
File : LV29-20D.CNV

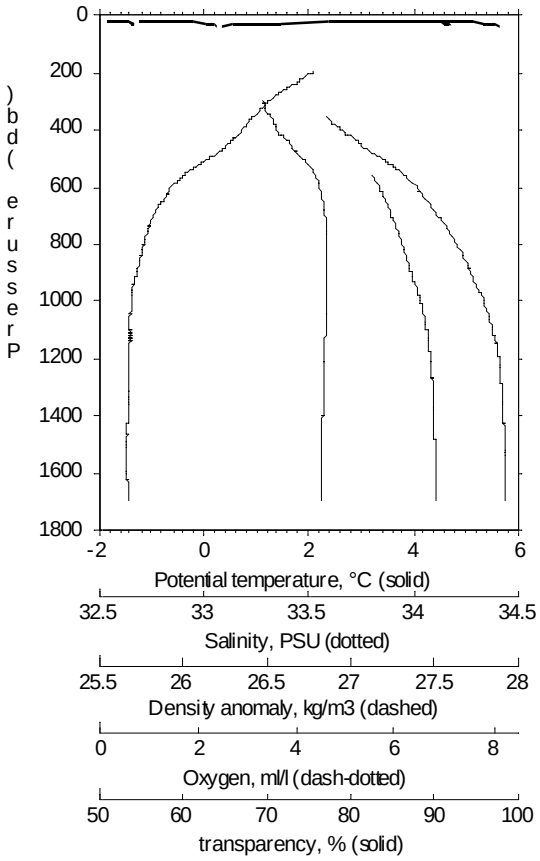

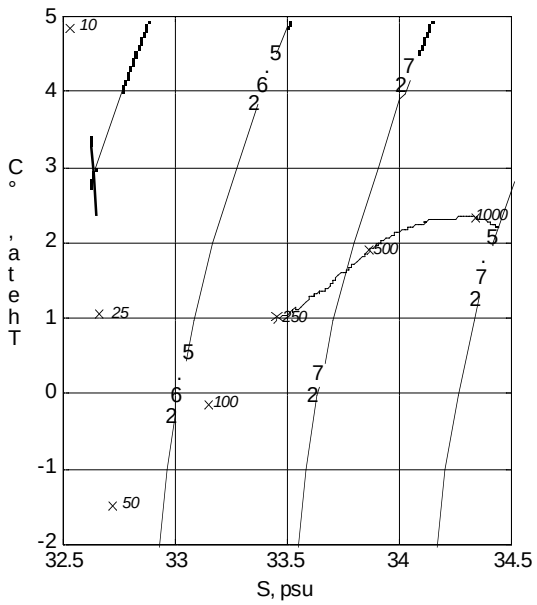

** Station: LV29-22/1
Time = Jun 09 2002 07:11:00
** Latitude: 54 :04.991
** Longitude: 146:10.607
File : LV29-22D.CNV

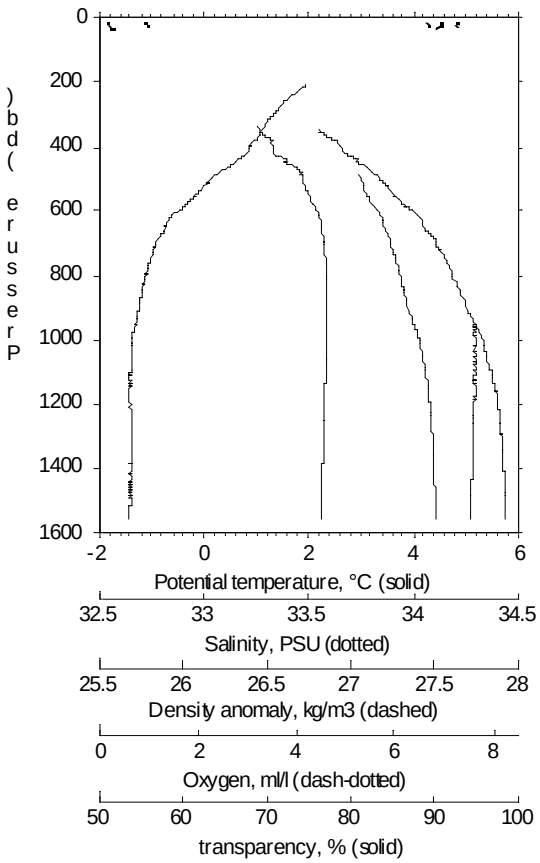

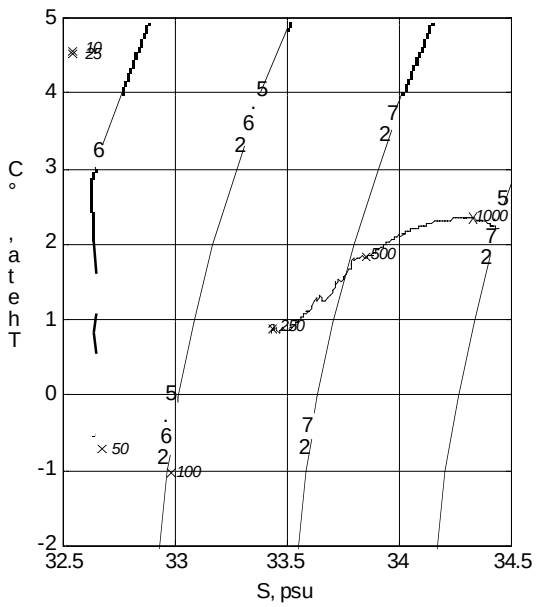

** Station: LV29-23/1
Time = Jun 09 2002 11:41:33
** Latitude: 54 :02.620
** Longitude: 146:29.580
File : LV29-23D.CNV

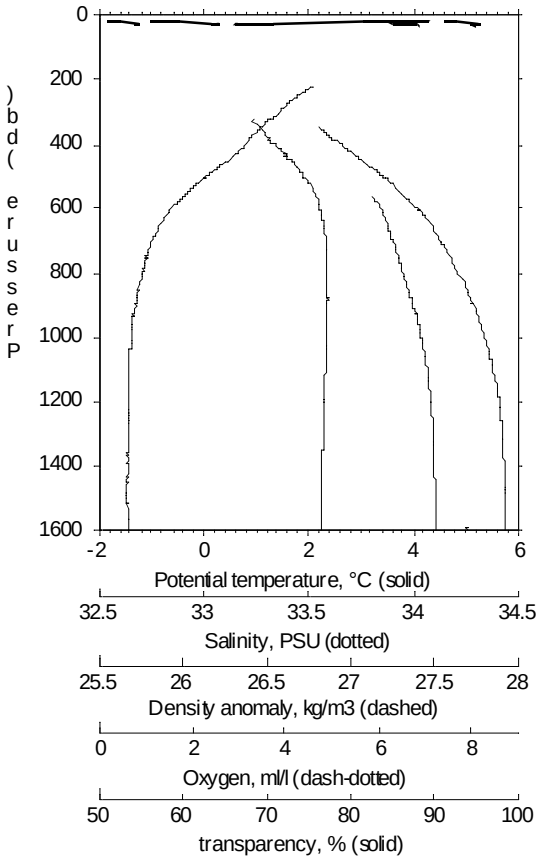

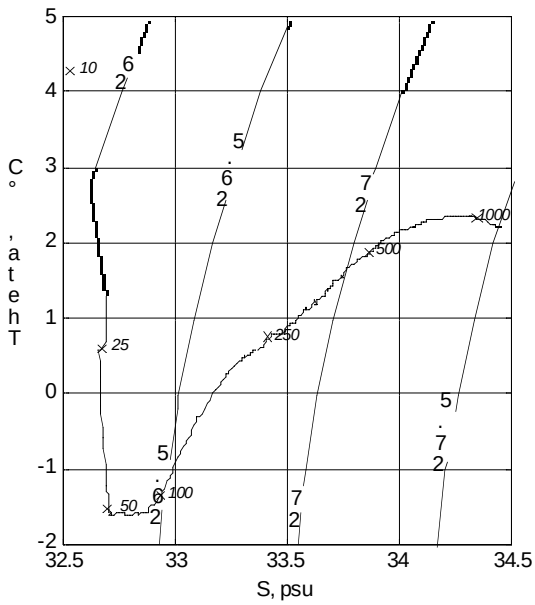

** Station: LV29-24/1
Time = Jun 09 2002 22:57:57
** Latitude: 53 :56.140
** Longitude: 146:11.800
File : LV29-24D.CNV

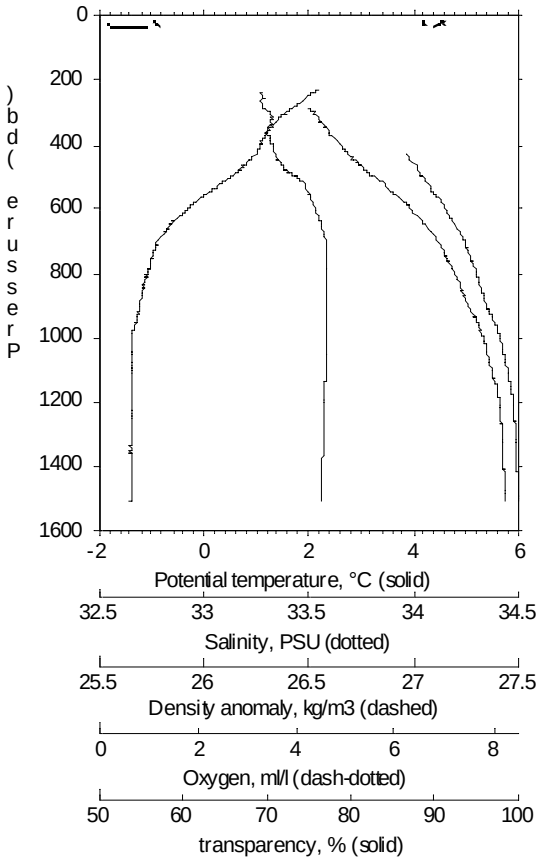

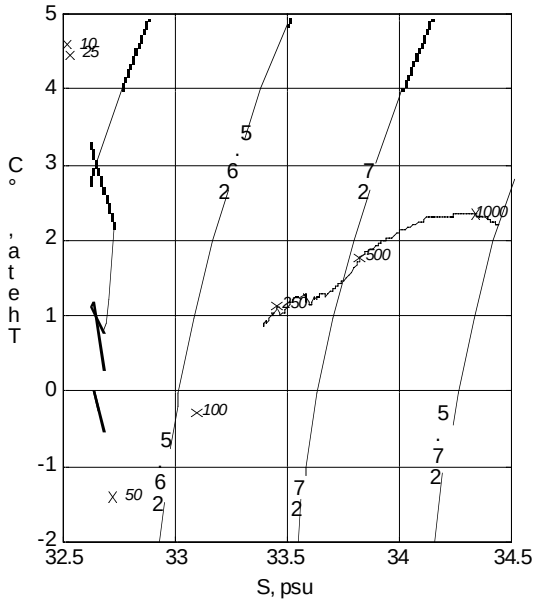

** Station: LV29-25/1
Time = Jun 10 2002 03:43:14
** Latitude: 54 :03.360
** Longitude: 146:35.340
File : LV29-25D.CNV

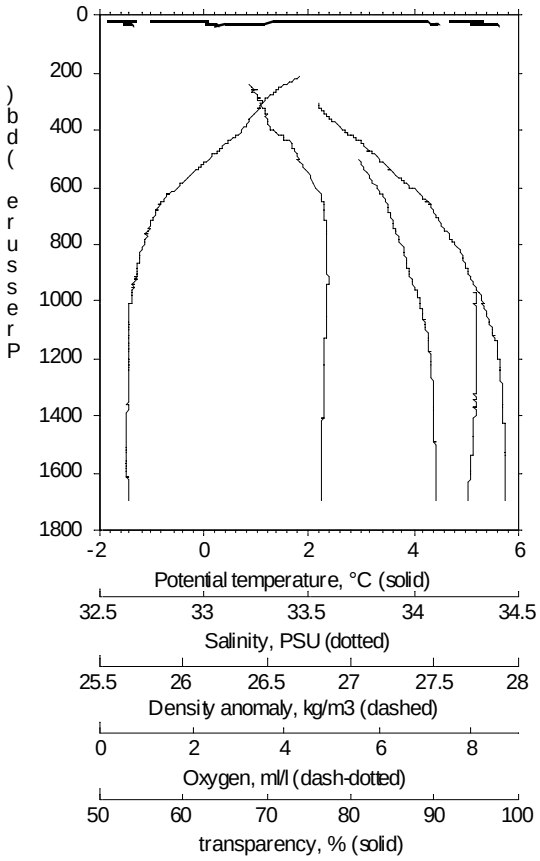

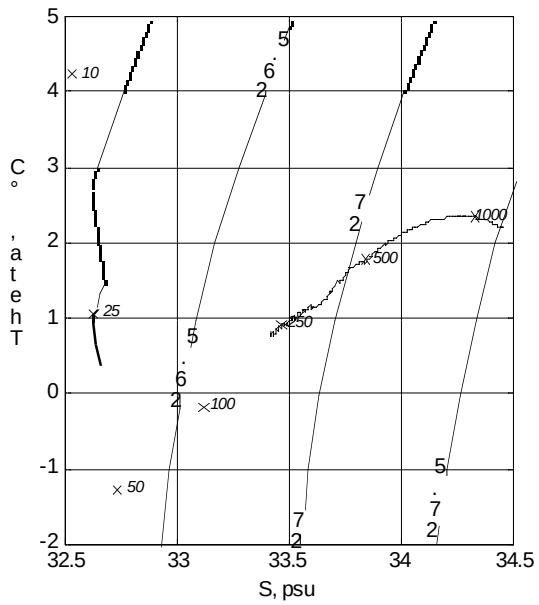

** Station: LV29-27/1
Time = Jun 10 2002 07:57:15
** Latitude: 54 :04.060
** Longitude: 146:22.920
File : LV29-27D.CNV

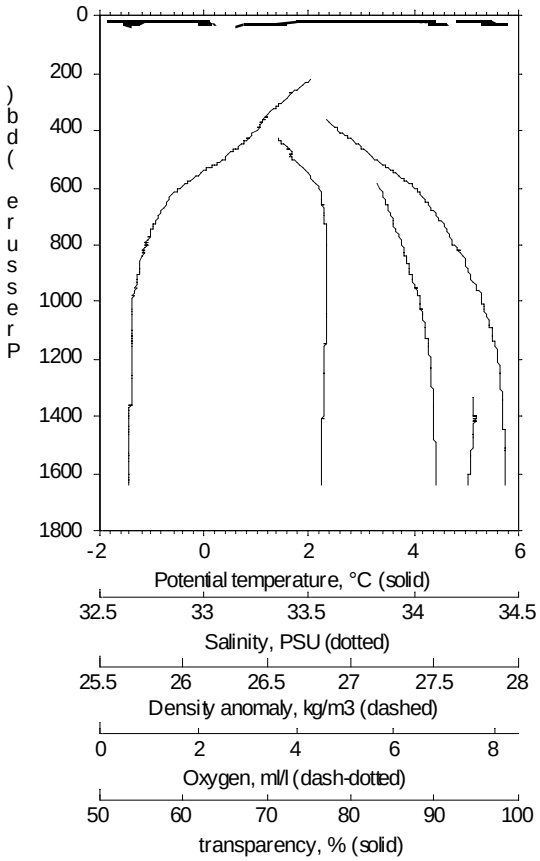

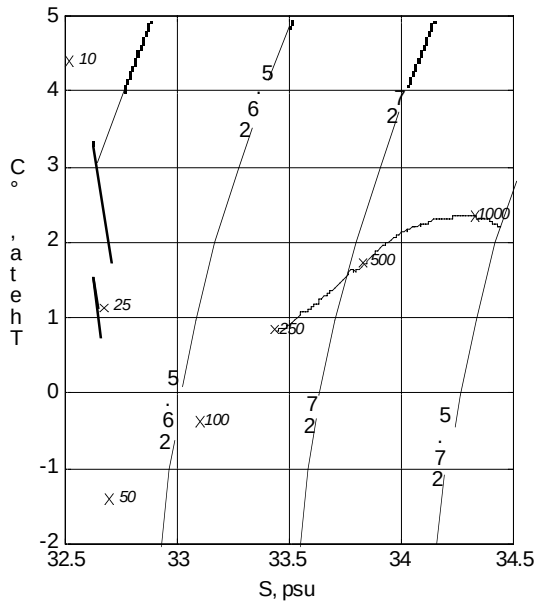

** Station: LV29-28/1
Time = Jun 10 2002 10:12:50
** Latitude: 54 :09.640
** Longitude: 146:29.880
File : LV29-28D.CNV

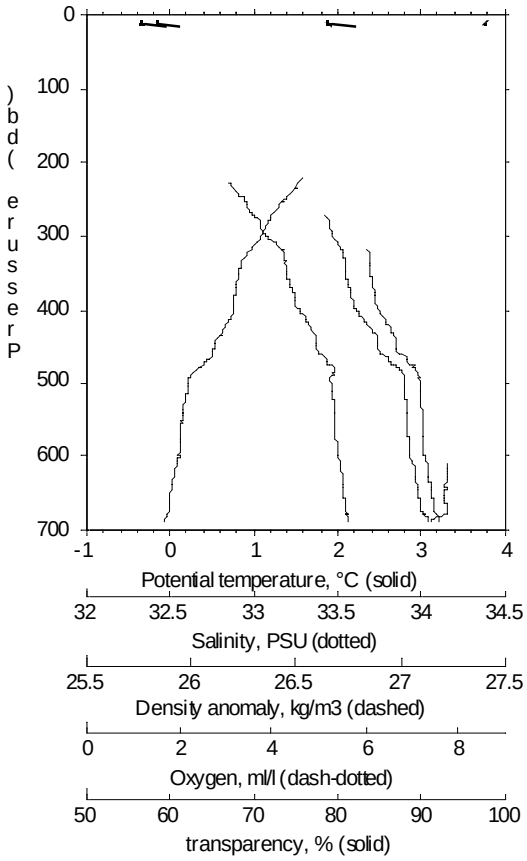

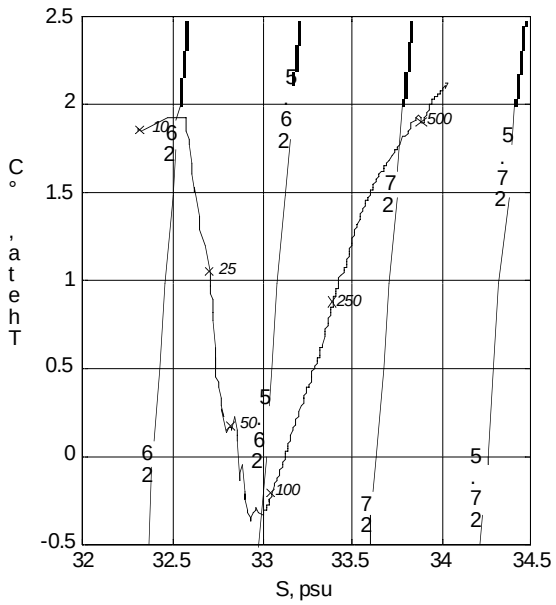

** Station: LV29-29/1
Time = Jun 10 2002 22:44:46
** Latitude: 54 :26.790
** Longitude: 144:04.790
File : LV29-29D.CNV

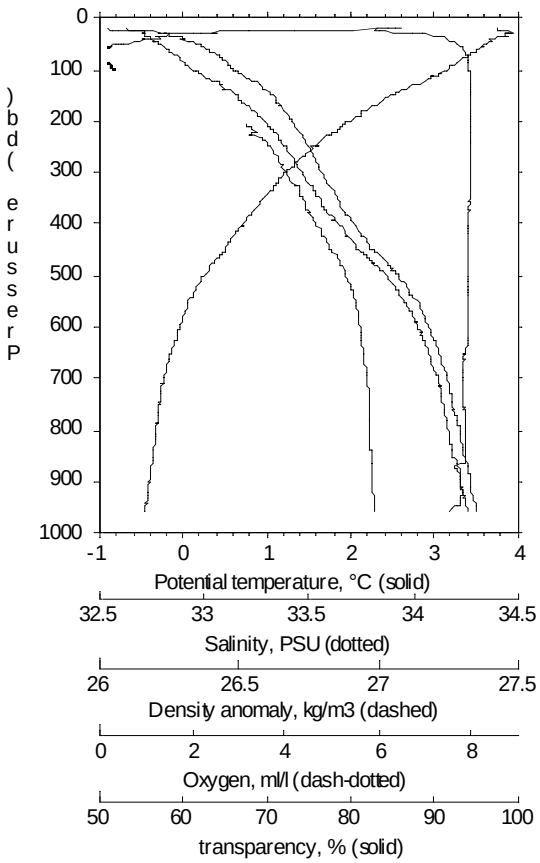

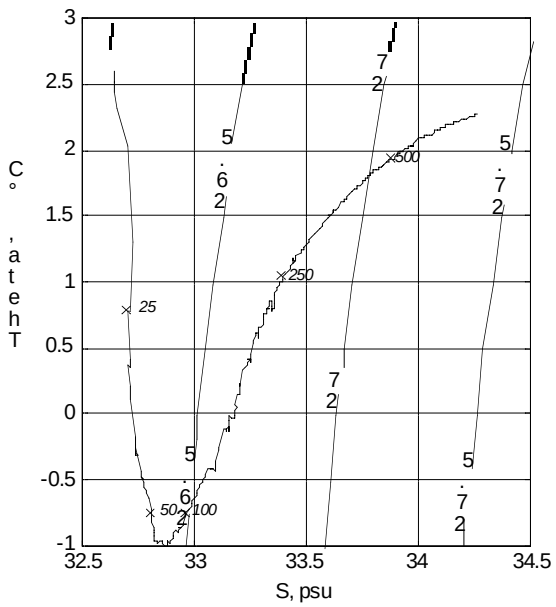

** Station: LV29-31/1
Time = Jun 11 2002 06:26:13
** Latitude: 54 :33.340
** Longitude: 144:16.340
File : LV29-31D.CNV

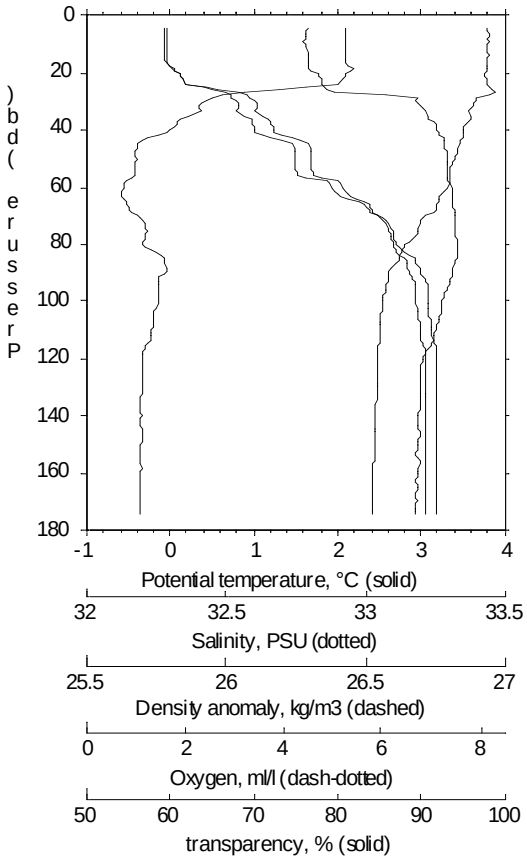

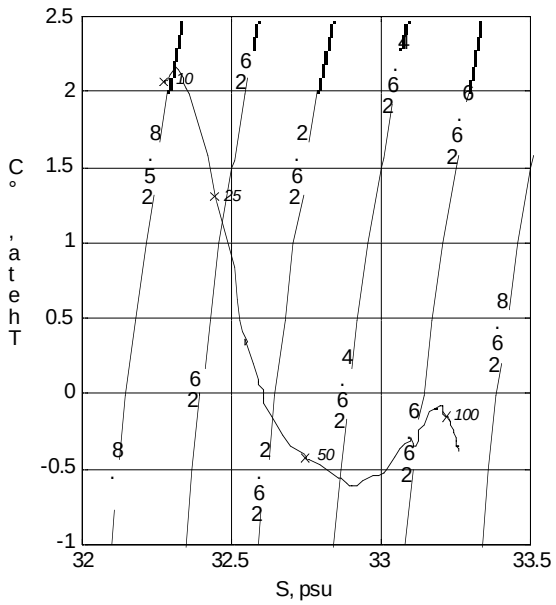

** Station: LV29-32/1
Time = Jun 11 2002 11:07:40
** Latitude: 54 :19.260
** Longitude: 143:54.32
File : Lv29-32d.cnv

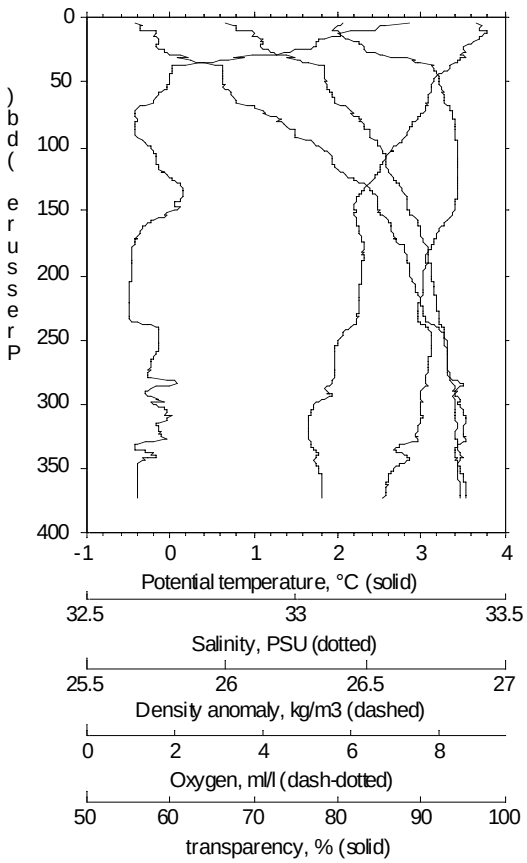

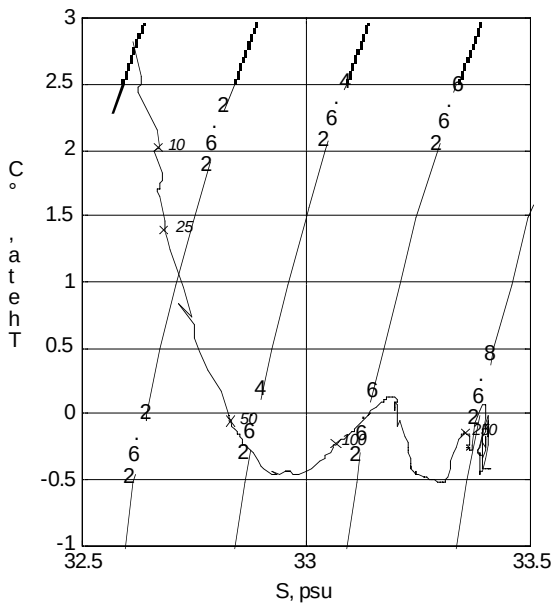

** Station: LV29-35/1
Time = Jun 12 2002 12:07:49
** Latitude: 54 :21.927
** Longitude: 143:58.740
File : LV29-35D.CNV

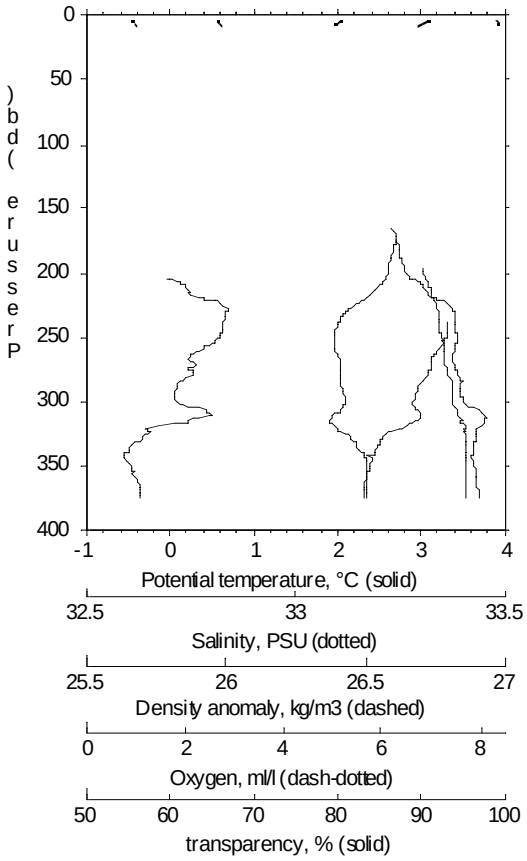

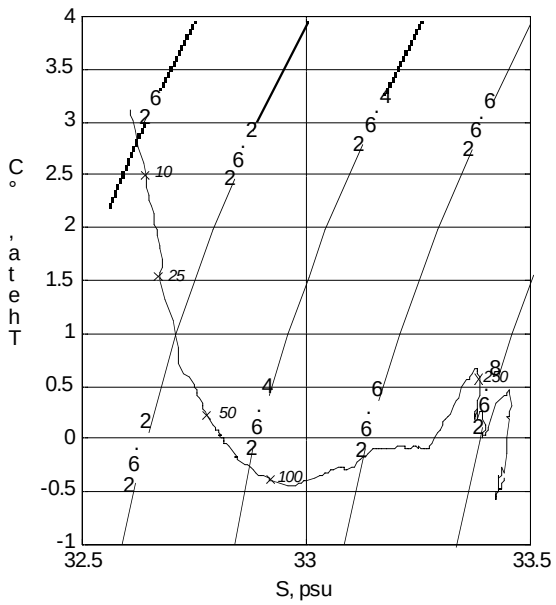

** Station: LV29-38/1
Time = Jun 12 2002 04:14:35
** Latitude: 54 :21.982
** Longitude: 143:58.857
File : LV29-38D.CNV

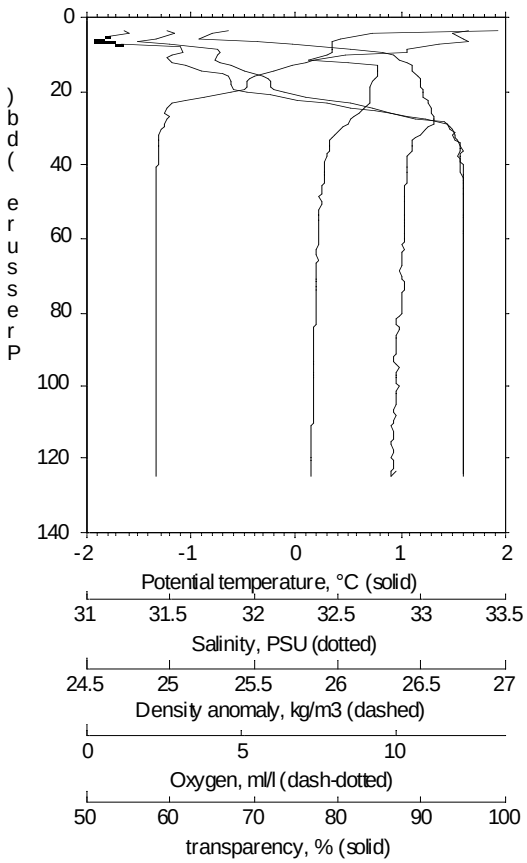

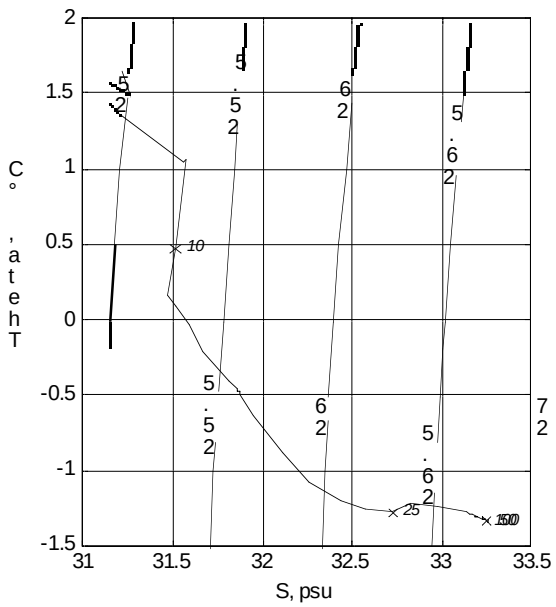

** Station: LV29-39/1
Time = Jun 13 2002 06:38:11
** Latitude: 54 :13.844
** Longitude: 143:45.288
File : LV29-39D.CNV

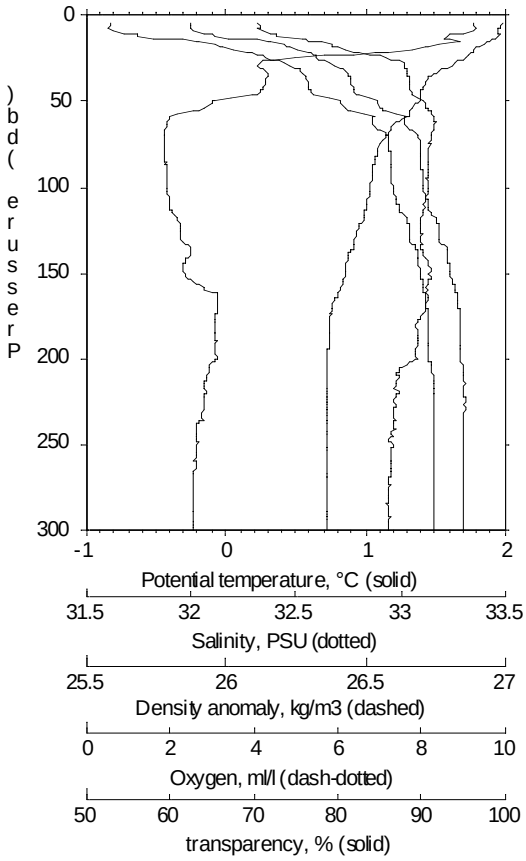

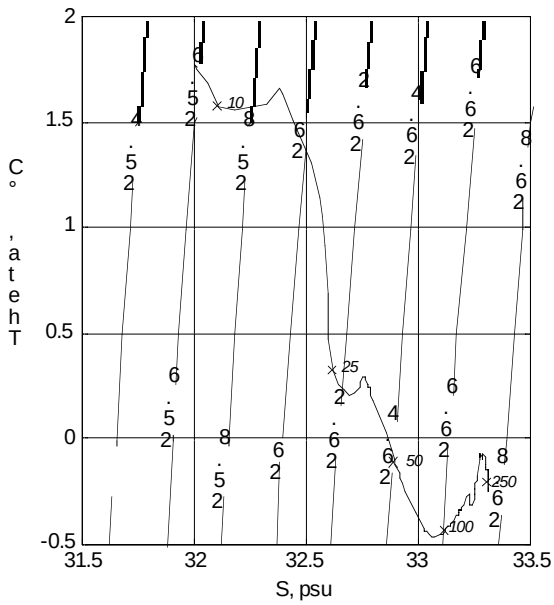

** Station: LV29-43/1
Time = Jun 14 2002 11:24:45
** Latitude: 54 :20.562
** Longitude: 143:56.902
File : LV29-43D.CNV

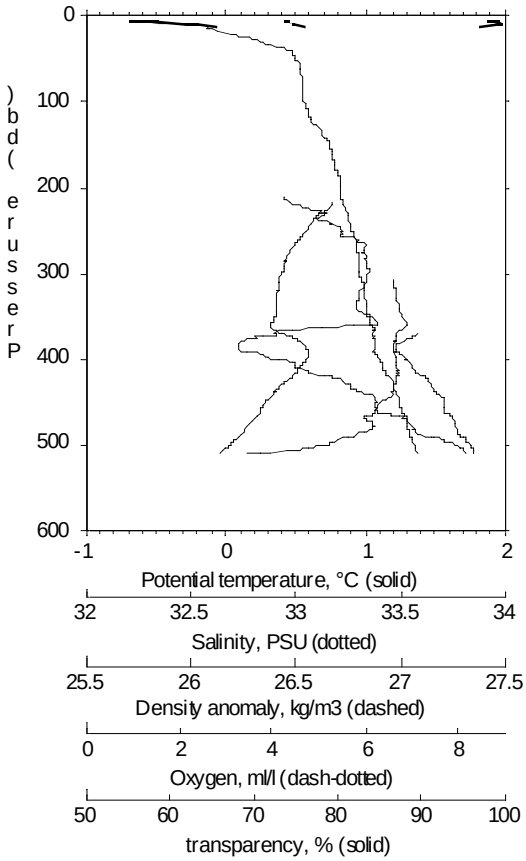

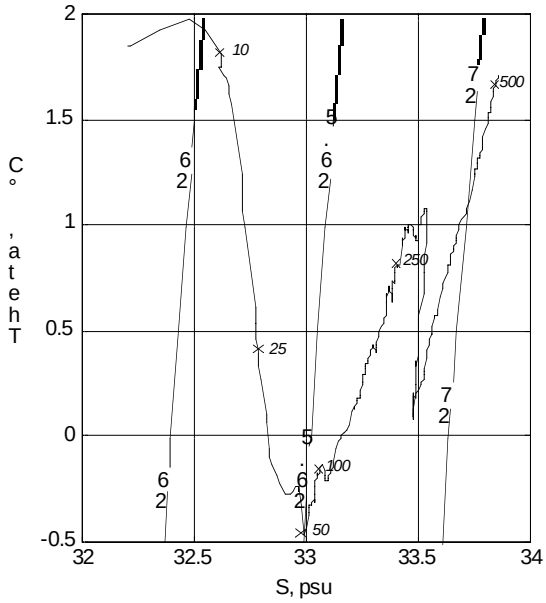

** Station: LV29-45/1
Time = Jun 14 2002 20:16:18
** Latitude: 54 :23.935
** Longitude: 144:01.751
File : LV29-45D.CNV

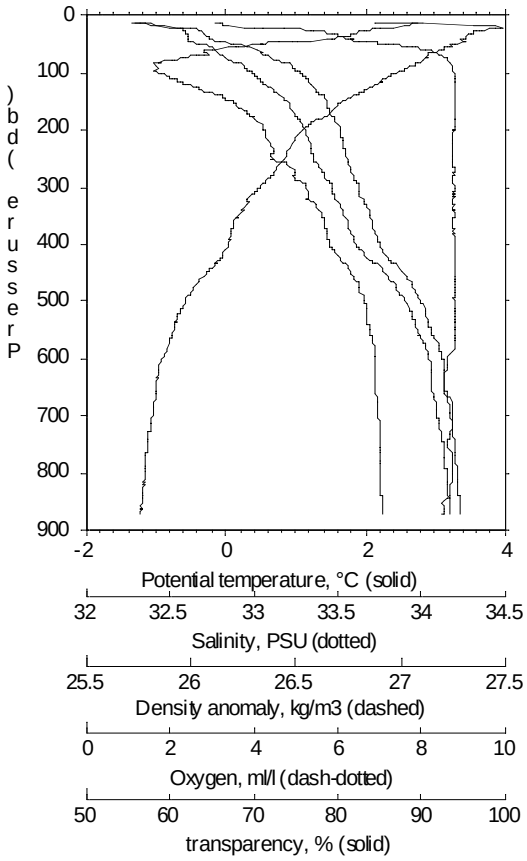

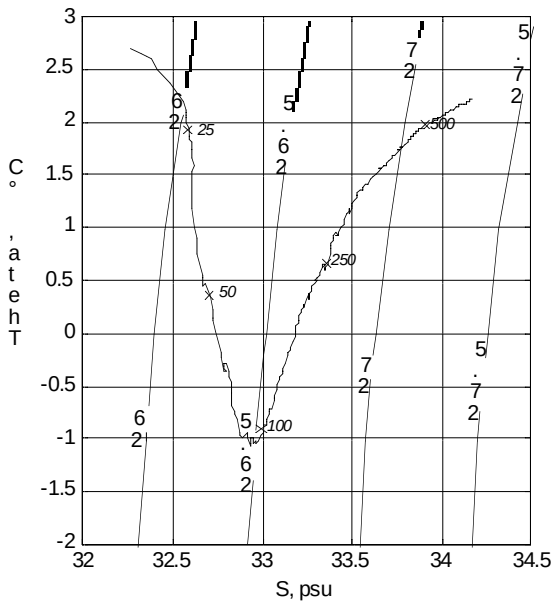

** Station: LV29-47/1
Time = Jun 15 2002 03:30:30
** Latitude: 54 :29.916
** Longitude: 144:12.272
File : LV29-47D.CNV

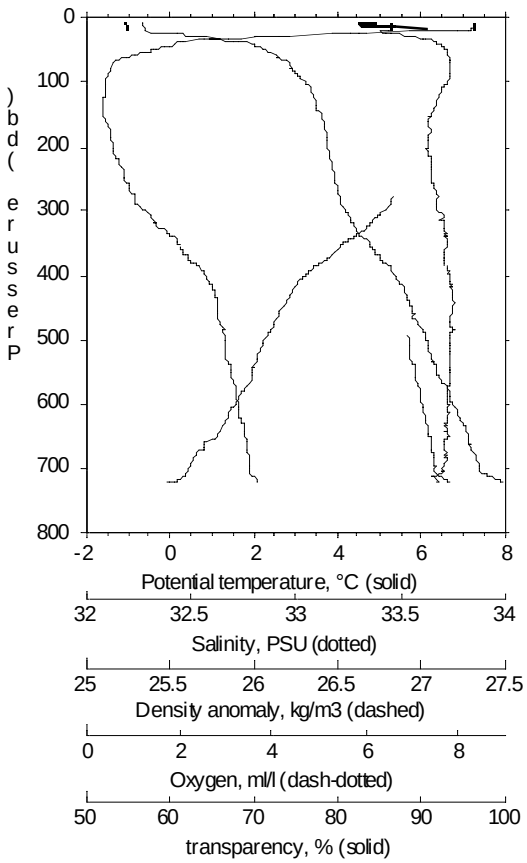

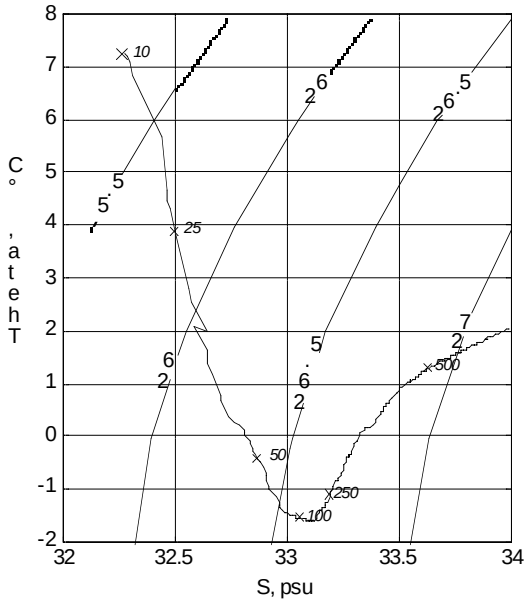

** Station: LV29-66/1
Time = Jun 23 2002 00:40:08
** Latitude: 47 23.993
** Longitude: 143 43.608
File : LV29-66D.CNV

APPENDIX 4

Methane data

Methane distribution in the water column

Station	CH_4, nl/l	depth, m
LV29-1	99	3
	635	11
	820	21
	1107	41
	1331	51
	1557	61
	1605	74
LV29-2	63	3
	73	49
	63	98
	19	147
	27	296
	50	495
	40	792
	12	1086
	30	1374
	61	1422
	831	1467
	1213	1478
LV29-4	71	3
	81	50
	60	100
	17	299
	45	498
	9	745
	23	991
	13	1239
	155	1483
	279	1530
	302	1571
	304	1581
LV29-5	61	11
	86	50
	42	297
	26	789
	16	1088
	101	1457
	80	1506
	50	1546
	44	1558
LV29-6	72	4
	81	62
	13	147
	34	494
	6	743
	82	990
	13	1236
	10	1429
	14	1479
	11	1519
	18	1528
LV29-7	57	3
	78	80
	14	149
	29	299
	19	744
	12	990
	28	1235
	14	1488
	14	1538
	11	1576
	22	1588
LV29-9	88	3
	85	64
	48	149
	14	299
	39	497
	7	743
	25	989
	18	1237
	9	1428
	9	1486
	10	1516
	11	1524
LV29-10	67	3
	66	21
	71	76
	10	200
	55	397
	38	597
	27	793
	12	990
	54	1237
	844	1391
	1625	1432
	1961	1442
LV29-11	83	3
	89	74
	23	149
	51	495
	13	1382
	13	1511
	15	1562
	18	1601
	17	1610
LV29-12	66	3
	77	77
	20	149
	22	299
	49	495
	19	743
	70	990
	8	1237
	8	1409
	7	1459
	26	1498
	62	1508
LV29-14	69	3
	81	63
	11	149
	14	297
	45	455
	67	792
	12	1089
	7	1383
	78	1533
	236	1583
	447	1623
	536	1633
LV29-15	77	3
	84	71
	55	149
	17	495
	9	1434
	128	1625
	200	1666
	196	1676
LV29-16	72	3
	80	65
	9	148
	19	298
	40	495
	15	988
	7	1432
	10	1502
	14	1551
	17	1601
	30	1641
	35	1652

Station	CH_4, nl/l	depth, m
LV29-17	70	3
	79	82
	10	148
	33	493
	13	1284
	955	1417
	349	1467
	15	1506
	10	1516
LV29-19	65	3
	74	76
	7	150
	12	298
	41	494
	30	792
	9	1187
	8	1432
	24	1579
	215	1628
	242	1668
	225	1676
LV29-20	60	4
	74	74
	13	155
	19	303
	41	499
	10	987
	8	1434
	121	1480
	148	1548
	72	1599
	91	1638
	100	1650
LV29-22	65	4
	79	62
	17	151
	22	298
	40	496
	9	989
	6	1429
	6	1482
	8	1549
	13	1597
	29	1639
	30	1651
LV29-23	170	1536
	184	1526
	49	1487
	4	1433
	3	1384
LV29-24	15	1574
	16	1565
	18	1523
	13	1473
	9	1423
	7	1332
LV29-25	14	1485
	14	1475
	3	1433
	3	1382
	4	1335
	5	1286
LV29-27	66	4
	75	60
	10	149
	16	297
	44	468
	7	988
	5	1384
	4	1483
	15	1580
	28	1625
	161	1668
	151	1676
LV29-28	67	3
	78	64
	15	150
	14	298
	37	495
	12	989
	28	1463
	100	1513
	237	1561
	250	1600
	190	1611
LV29-29	69	4
	68	73
	55	149
	45	298
	146	386
	35	432
	144	484
	95	533
	1313	583
	711	633
	3726	674
	468	683
LV29-31	71	4
	72	67
	60	149
	39	298
	44	393
	31	493
	78	595
	72	694
	36	790
	89	841
	103	890
	192	946
LV29-32	80	3
	80	11
	82	20
	80	31
	81	51
	128	69
	768	90
	3295	109
	4969	126
	5358	148
	6416	164
	7197	172
LV29-35	83	4
	89	37
	733	80
	1804	129
	2096	179
	2510	218
	5780	258
	9338	288
	7184	317
	5814	336
	3876	359
	5494	372
LV29-38	83	4
	76	41
	78	79
	861	129
	1426	177
	588	217
	1421	257
	2784	288
	711	316
	777	347
	395	360
	359	372

Station	CH_4, nl/l	depth, m	Station	CH_4, nl/l	depth, m	Station	CH_4, nl/l	depth, m
LV29-39	247	3	LV29-45	129	3.6	LV29-66	105	6
	285	10		85	49		963	50
	2867	29		71	99		2791	137
	4194	50		66	148		246	295
	4217	70		88	198		157	395
	4128	90		62	248		148	467
	3795	110		63	298		202	518
	3942	123		107	347		247	571
				219	397		231	619
LV29-43	155	4		172	445		263	667
	132	19		307	495		318	705
	679	39		269	504		337	719
	1115	78						
	894	109	LV29-47	93	3.5			
	823	139		76	88			
	1272	173		58	197			
	2284	199		50	297			
	2350	229		101	495			
	2557	258		118	594			
	2744	281		351	644			
	3031	294		72	692			
				139	742			
				99	810			
				792	850			
				1013	863			

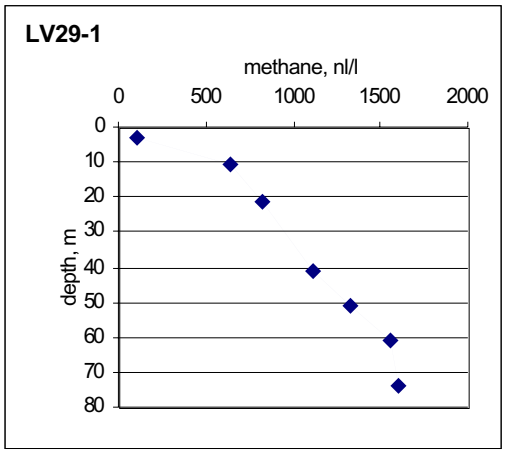
LV29-1
methane, nl/l
0
500
1000
1500
2000
depth, m
0
10
20
30
40
50
60
70
80

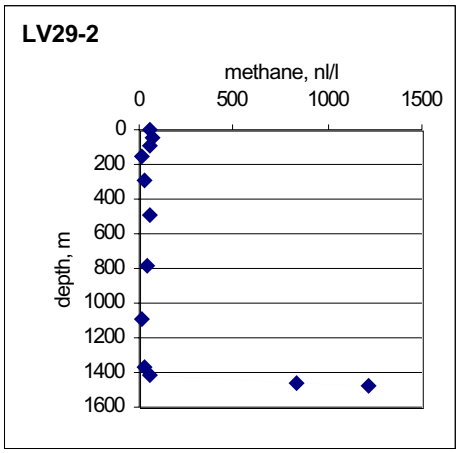
LV29-2
methane, nl/l
0
500
1000
1500
depth, m
0
200
400
600
800
1000
1200
1400
1600

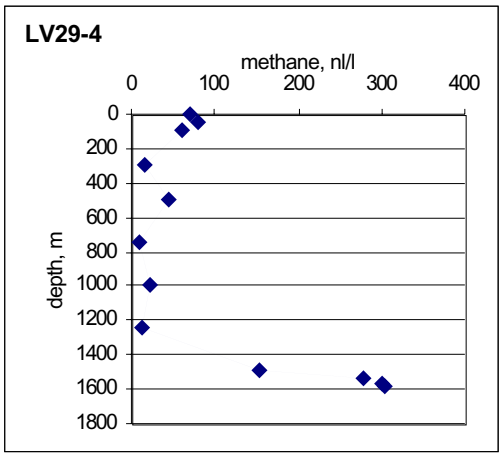
LV29-4
methane, nl/l
0
100
200
300
400
depth, m
0
200
400
600
800
1000
1200
1400
1600
1800

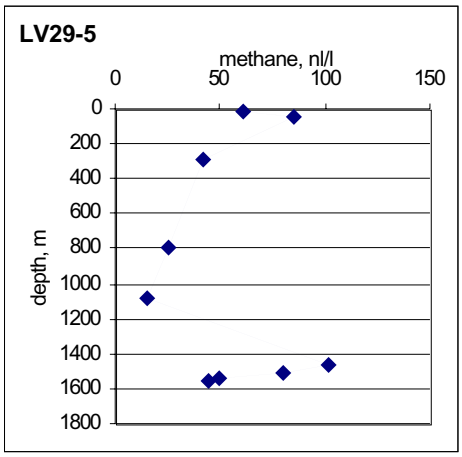
LV29-5
methane, nl/l
0
50
100
150
depth, m
0
200
400
600
800
1000
1200
1400
1600
1800

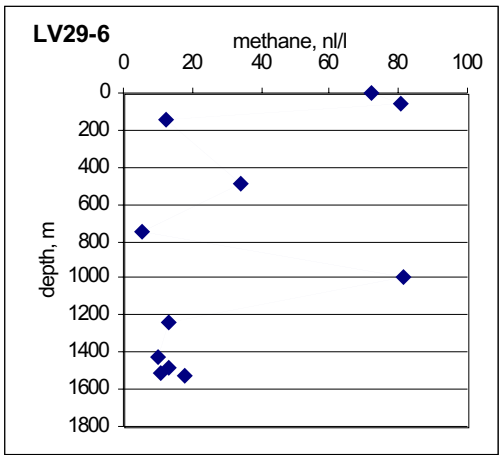
LV29-6
methane, nl/l
0
20
40
60
80
100
depth, m
0
200
400
600
800
1000
1200
1400
1600
1800

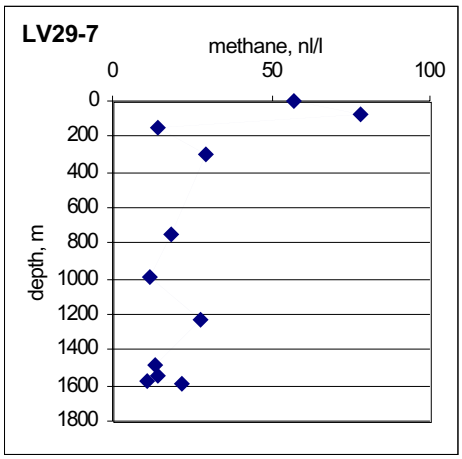
LV29-7
methane, nl/l
0
50
100
depth, m
0
200
400
600
800
1000
1200
1400
1600
1800

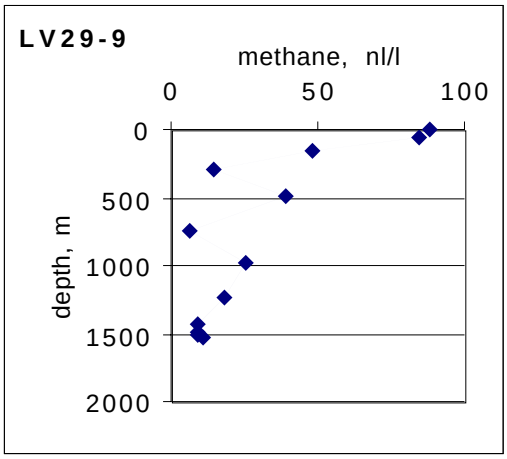
LV29-9
methane, nl/l
0
50
100
depth, m
0
500
1000
1500
2000

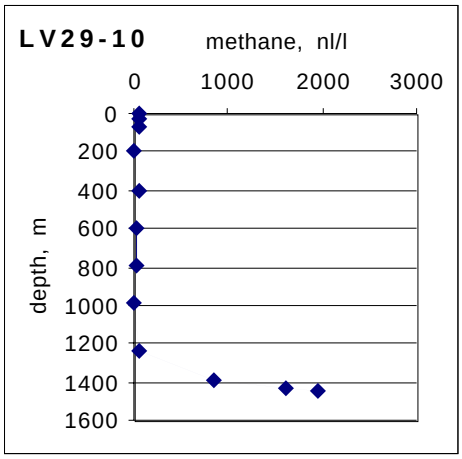
LV29-10
methane, nl/l
0
1000
2000
3000
depth, m
0
200
400
600
800
1000
1200
1400
1600

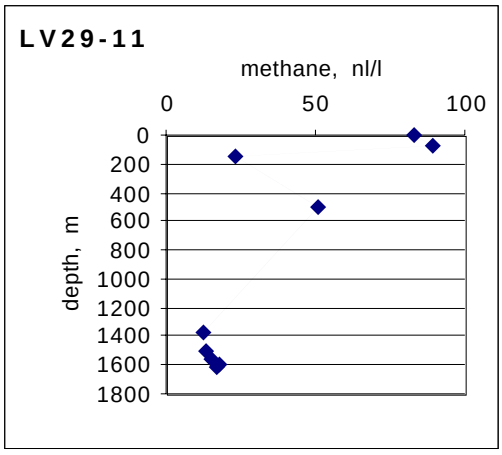
LV29-11
methane, nl/l
0
50
100
depth, m
0
200
400
600
800
1000
1200
1400
1600
1800

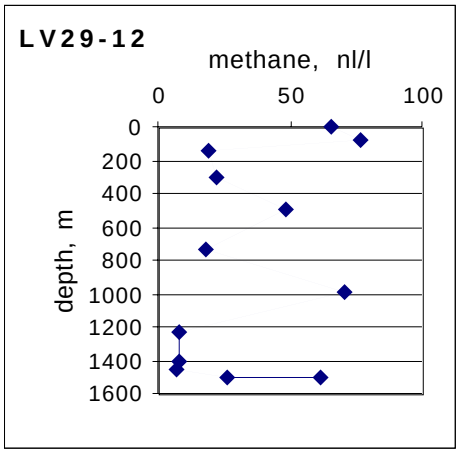
LV29-12
methane, nl/l
0
50
100
depth, m
0
200
400
600
800
1000
1200
1400
1600

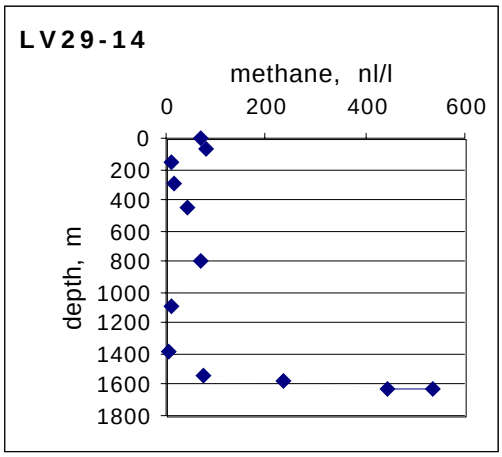
LV29-14
methane, nl/l
0
200
400
600
depth, m
0
200
400
600
800
1000
1200
1400
1600
1800

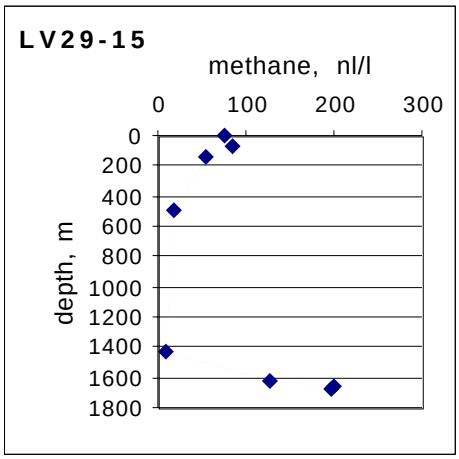
LV29-15
methane, nl/l
0
100
200
300
depth, m
0
200
400
600
800
1000
1200
1400
1600
1800

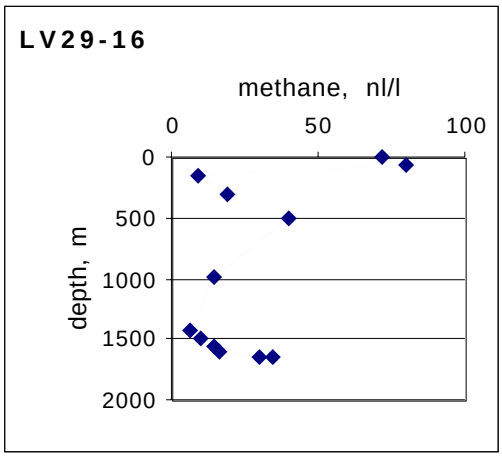
LV29-16
methane, nl/l
0
50
100
depth, m
0
500
1000
1500
2000

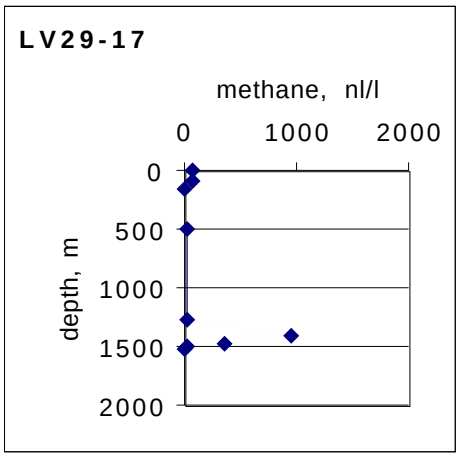
LV29-17
methane, nl/l
0
1000
2000
depth, m
0
500
1000
1500
2000

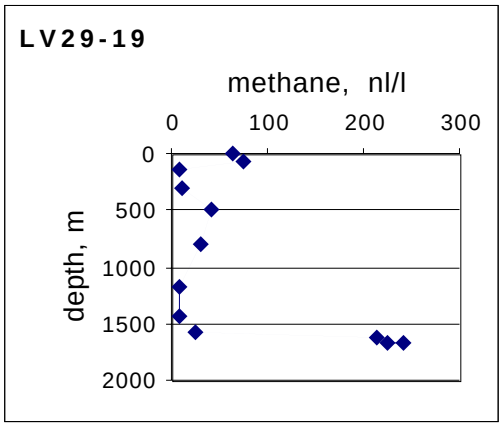
LV29-19
methane, nl/l
0
100
200
300
depth, m
0
500
1000
1500
2000

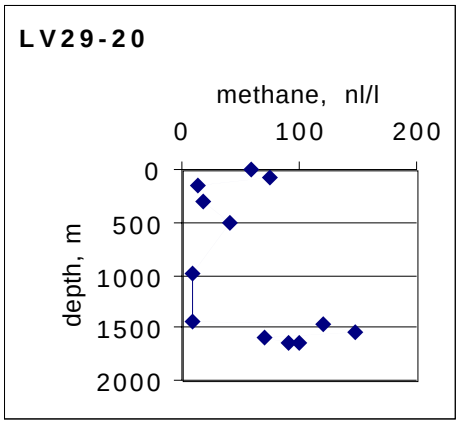
LV29-20
methane, nl/l
0
100
200
depth, m
0
500
1000
1500
2000

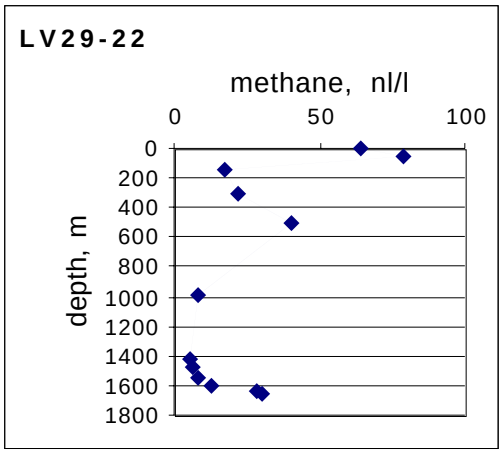
LV29-22
methane, nl/l
0
50
100
depth, m
0
200
400
600
800
1000
1200
1400
1600
1800

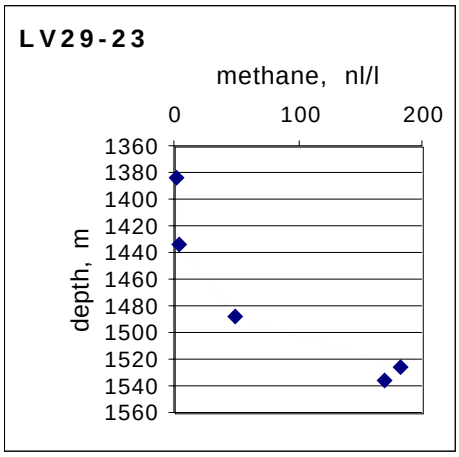
LV29-23
methane, nl/l
0
100
200
depth, m
1360
1380
1400
1420
1440
1460
1480
1500
1520
1540
1560

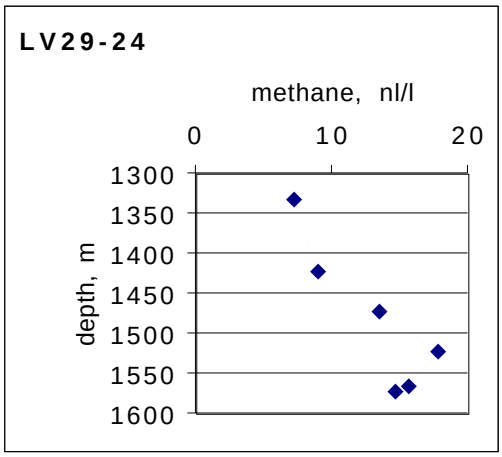
LV29-24
methane, nl/l
0
10
20
depth, m
1300
1350
1400
1450
1500
1550
1600

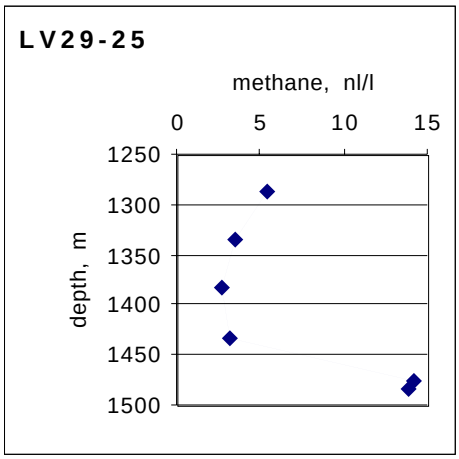
LV29-25
methane, nl/l
0
5
10
15
depth, m
1250
1300
1350
1400
1450
1500

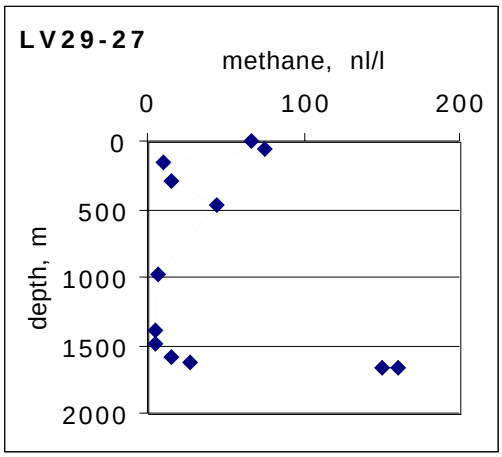
LV29-27
methane, nl/l
0
100
200
depth, m
0
500
1000
1500
2000

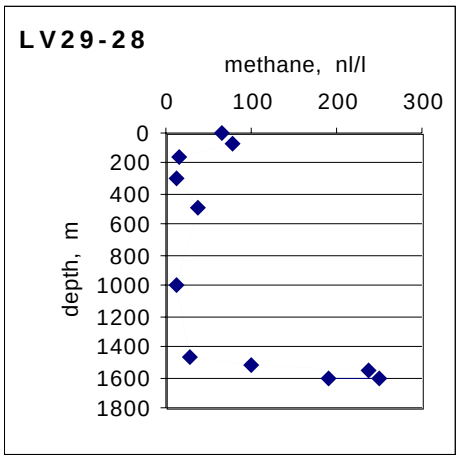
LV29-28
methane, nl/l
0
100
200
300
depth, m
0
200
400
600
800
1000
1200
1400
1600
1800

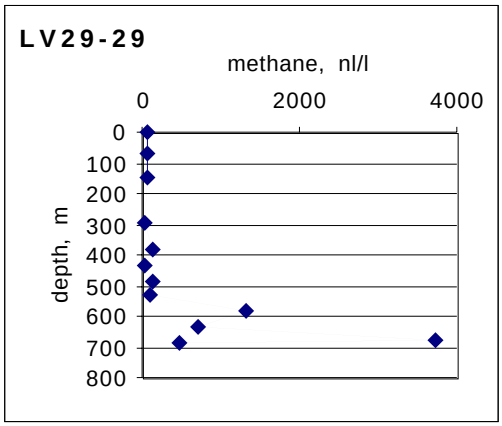
LV29-29
methane, nl/l
0
2000
4000
depth, m
0
100
200
300
400
500
600
700
800

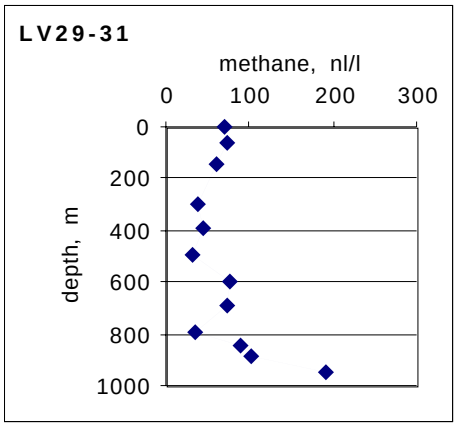
LV29-31
methane, nl/l
0
100
200
300
depth, m
0
200
400
600
800
1000

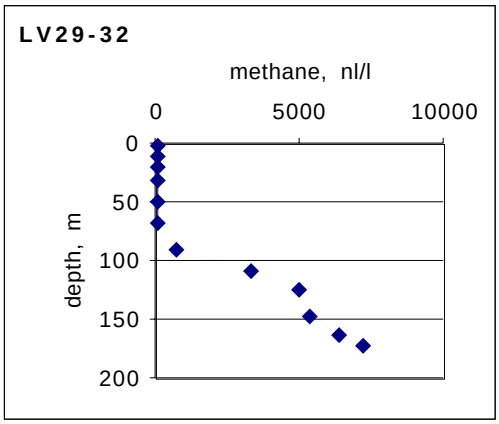
LV29-32
methane, nl/l
0
5000
10000
depth, m
0
50
100
150
200

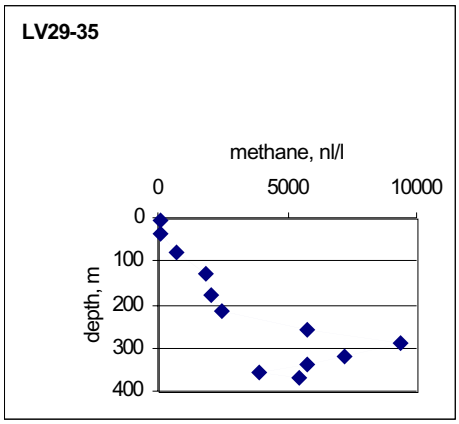
LV29-35
methane, nl/l
0
5000
10000
depth, m
0
100
200
300
400

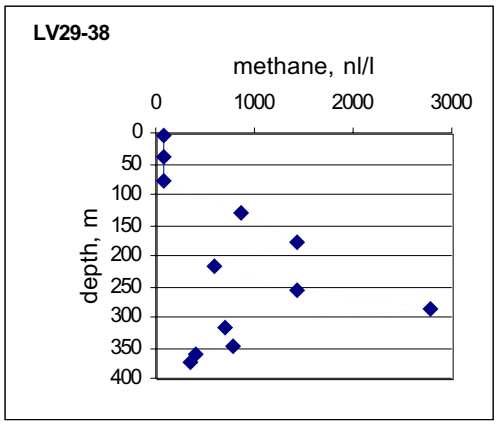
LV29-38
methane, nl/l
0
1000
2000
3000
depth, m
0
50
100
150
200
250
300
350
400

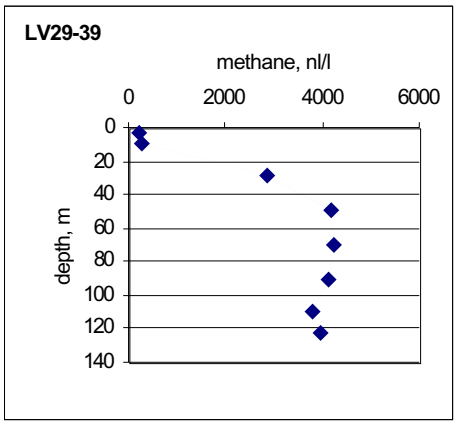
LV29-39
methane, nl/l
0
2000
4000
6000
depth, m
0
20
40
60
80
100
120
140

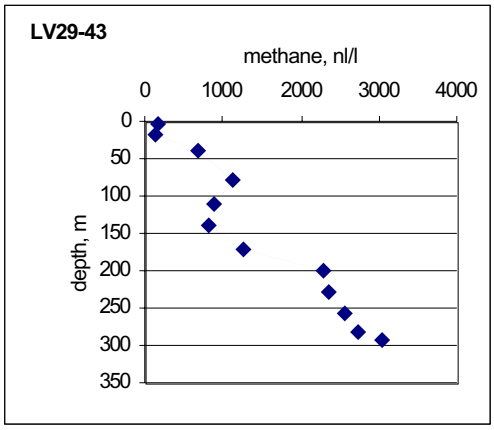
LV29-43
methane, nl/l
0
1000
2000
3000
4000
depth, m
0
50
100
150
200
250
300
350

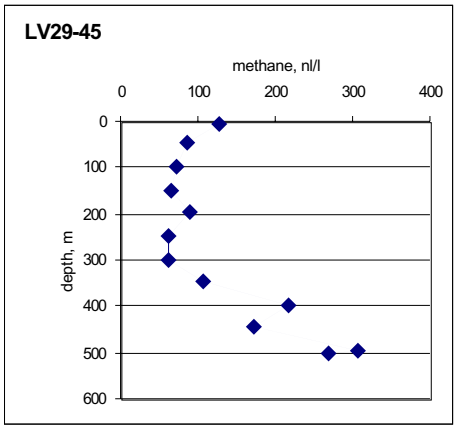
LV29-45
methane, nl/l
0
100
200
300
400
depth, m
0
100
200
300
400
500
600

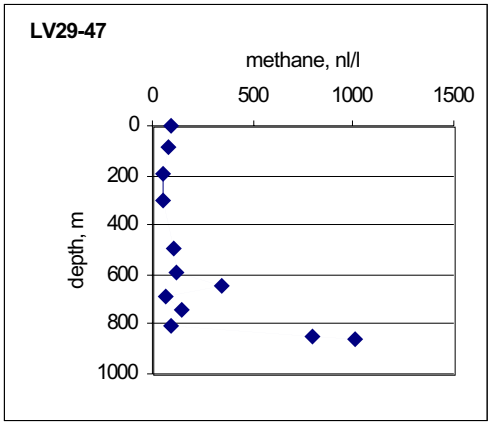
LV29-47
methane, nl/l
0
500
1000
1500
depth, m
0
200
400
600
800
1000

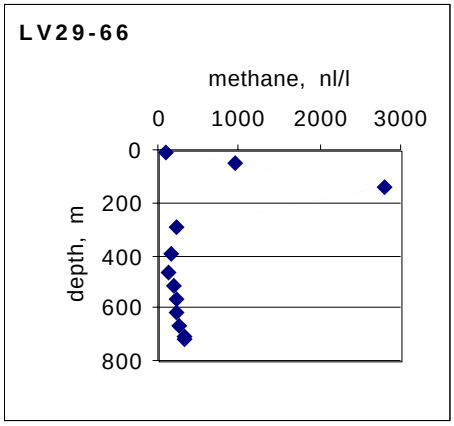
LV29-66
methane, nl/l
0
1000
2000
3000
depth, m
0
200
400
600
800

Methane distribution in sediment cores

LV29-46	
CH_4, ppm	level, cm
60	160
60	221
492	300
823	325
31348	407
45597	465
30052	505
66323	526

LV29-50	
CH_4, ppm	level, cm
22	10
22	65
118	105
230	150
35152	210
36121	250
7273	310
20121	350
18667	370
4242	420

LV29-51	
CH_4, ppm	level, cm
5	0
6	50
11	100
47	300
331	400
2207	450
5345	500
10690	550
4897	570

LV29-53	
CH_4, ppm	level, cm
13	5
6	45
9	105
18	140
23	168
53	225
61	265
88	320
41103	375
42069	425
18759	475
24414	514

LV29-56	
CH_4, ppm	level, cm
131	0
162	55
158	130
48992	155
42263	233
50742	310
11844	370
6999	430
42263	495
8008	540
8008	595

LV29-56	(Head Space)
mM/kg	level, cm
0.0042	50
0.007	100
2.8265	150
3.5533	200
2.7457	250
1.6421	300
2.564	350
1.4267	400
1.5882	450
0.6461	500
0.7201	550
1.6151	600

LV29-59	(Head Space)
nM/kg	level, cm
0.0001	50
0.0003	100
0.0005	150
0.0005	200
0.0005	250
0.0006	300
0.0006	350
0.0007	400
0.0007	450
0.0006	500
0.0005	550
0.0004	600

LV29-63	(Head Space)
nM/kg	level, cm
0.0007	14
0.0006	50
0.0014	100
0.0021	150
0.0034	200
0.0026	250
0.0037	300
0.0047	350
0.0049	400
0.006	450

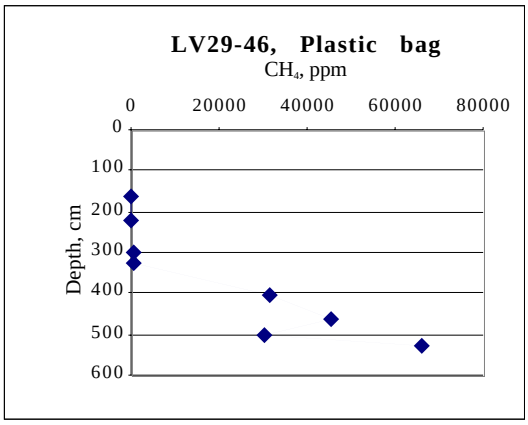
LV29-46, Plastic bag
CH4, ppm
0
20000
40000
60000
80000
Depth, cm
0
100
200
300
400
500
600

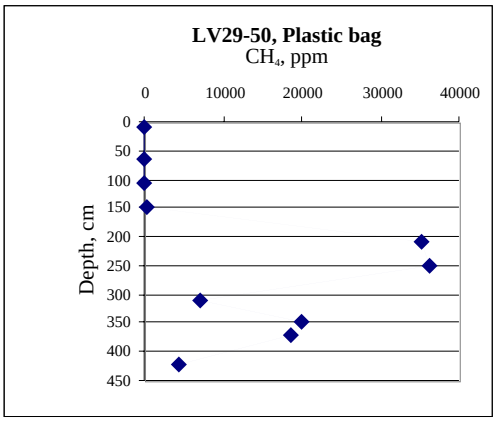
LV29-50, Plastic bag
CH4, ppm
0
10000
20000
30000
40000
Depth, cm
0
50
100
150
200
250
300
350
400
450

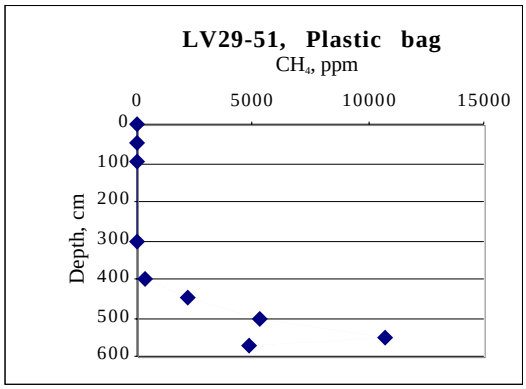
LV29-51, Plastic bag
CH4, ppm
0
5000
10000
15000
Depth, cm
0
100
200
300
400
500
600

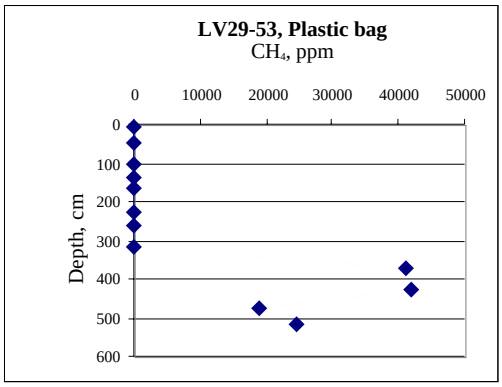
LV29-53, Plastic bag
CH4, ppm
0
10000
20000
30000
40000
50000
Depth, cm
0
100
200
300
400
500
600

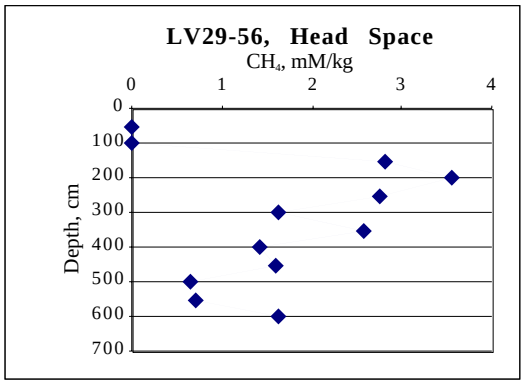
LV29-56, Head Space
CH4, mM/kg
0
1
2
3
4
Depth, cm
0
100
200
300
400
500
600
700

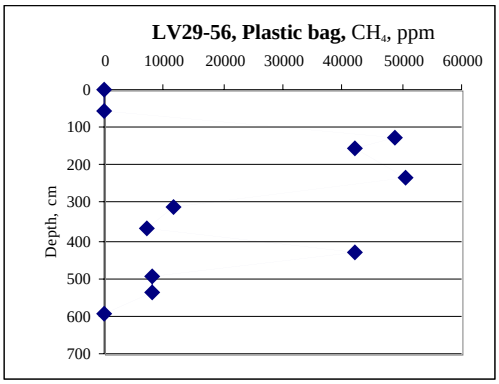
LV29-56, Plastic bag, CH4, ppm
0
10000
20000
30000
40000
50000
60000
Depth, cm
0
100
200
300
400
500
600
700

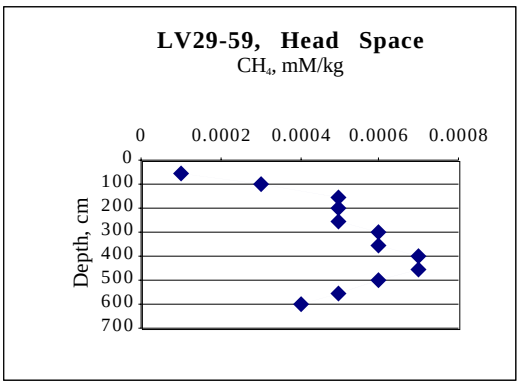
LV29-59, Head Space
CH4, mM/kg
0
0.0002
0.0004
0.0006
0.0008
Depth, cm
0
100
200
300
400
500
600
700

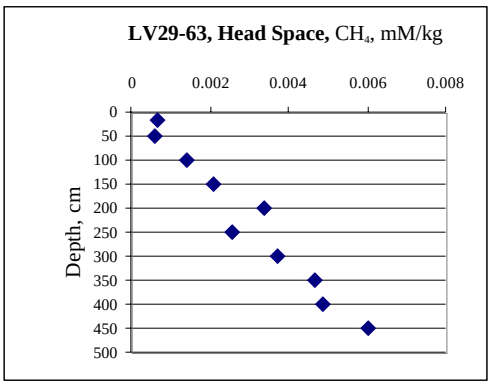
LV29-63, Head Space, CH4, mM/kg
0
0.002
0.004
0.006
0.008
Depth, cm
0
50
100
150
200
250
300
350
400
450
500

APPENDIX 5

Pore water data

Pore water analysis

Depth (cm)	NH_4 (mM)	PO_4 (μM)	SiO_2 (μM)	H_2S (mM)	Cl, (mM)	pH(5)	TALK (mM/kg)	Ca+Sr, (mM/kg)	pH in situ	DIC	pCO_2	La	Lc	Mg+Ca+Sr mmol/L
HYC 34-1														
12.5	0.036	9.6	301	0	530	7.39	1.958	9.93	7.44	2	1344.81	0.52	0.33	
82	0.217	5.7	148	0	529	7.45	2.631	9.75	7.5	2.678	1574.66	0.79	0.5	
92	0.201	6.1	189	0.053	531	7.44	3.946	9.72	7.494	3.989	2376.4	1.16	0.73	64.80
99	0.292	6.8	203	0.083	532	7.35	4.134	9.81	7.405	4.212	3056.56	0.99	0.63	64.75
SL 46-1														
2.5	0.0399	20.1	499	0	542	7.46	2.291	10.10	7.454	2.309	1475.52	0.65	0.42	62.01
17.5	0.0212	20.5	453	0	544	7.56	2.331	10.11	7.555	2.318	1178.22	0.82	0.54	62.53
30	0.0239	23.6	473	0.0017	545	7.54	2.351	10.16	7.535	2.339	1243.91	0.79	0.52	62.32
38	0.0319	23.6	487	0.047	538	7.58	2.530	10.14	7.576	2.471	1199.09	0.93	0.61	62.36
48	0.0559	26.9	492	0.104	537	7.48	2.906	10.15	7.477	2.841	1725.46	0.85	0.56	62.26
55	0.0797	31.9	523	0.193	538	7.57	3.489	10.13	7.57	3.316	1631.7	1.23	0.81	62.37
60	0.0904	34.8	528	0.348	545	7.69	3.508	10.13	7.696	3.143	1156.84	1.54	1.01	62.63
77	0.122	46.3	535	0.559	544	7.64	4.033	10.13	7.651	3.506	1433.21	1.55	1.02	62.37
97	0.173	59.9	540	0.861	540	7.69	6.070	10.11	7.699	5.242	1915.31	2.61	1.71	62.47
118	0.241	69.2	544	1.73	550	7.63	6.426	10.04	7.662	4.908	1955.47	2.18	1.43	62.99
138	0.277	72.5	583	2.02	539	7.72	7.636	9.87	7.744	5.772	1902.71	3.12	2.04	62.39
158	0.398	70	521	3.51	540	7.68	10.030	9.89	7.721	6.95	2418.06	3.56	2.33	62.18
178	0.483	83.9	578	4.07	543	7.70	12.838	9.78	7.735	9.226	3104.59	4.8	3.15	62.29
198	0.564	94	569	5.32	545	7.67	16.319	9.48	7.71	11.701	4173.8	5.53	3.62	61.68
218	0.59	97.9	578	7.07	540	7.68	18.966	9.13	7.726	12.835	4409.91	6.15	4.03	61.27
238	0.697	108	597	9.04	537	7.69	22.324	9.00	7.741	14.472	4802.55	7.12	4.66	61.26
258	0.766	115	624	10.7	550	7.70	27.978	8.36	7.751	18.642	6045.67	8.45	5.54	60.50
278	0.883	123	629	13.3	552	7.72	33.129	8.18	7.774	21.441	6582.36	9.98	6.54	60.47
298	0.962	134	586	15.4	551	7.84	37.322	7.81	7.885	23.105	5471.63	13.23	8.68	60.54
318	1.04	138	621	15.7	552	7.77	41.340	7.51	7.816	27.221	7581.56	12.8	8.4	59.71
338	1.12	146	610	16.9	550	7.78	44.588	7.23	7.824	29.33	8014.39	13.6	8.91	60.17
358	1.22	134	634	16	552	7.82	46.093	7.07	7.857	31.335	7931.12	15.23	9.99	59.39
378	1.31	148	627	15.7	554	7.88	46.809	6.78	7.912	31.89	7082.93	16.76	10.99	59.30
398	1.32	173	598	13.5	553	7.74	46.478	6.63	7.774	34.373	10563.1	12.93	8.48	59.91
418	1.51	219	586	12.9	552	7.79	47.924	6.38	7.818	35.944	9967.67	14.43	9.47	59.24
438	1.5	190	601	13.2	554	7.84	48.236	6.26	7.867	35.688	8817.82	15.64	10.26	
458	1.54	228	611	13.5	558	7.78	47.910	6.30	7.813	35.456	9938.86	13.69	8.98	
478	1.38	226	588	11.4	552	7.85	47.232	6.34	7.872	36.174	8827.78	16.3	10.69	59.68
498	1.59	235	601	12.9	541	7.85	47.626	6.30	7.871	35.266	8650.29	16.13	10.56	59.61
518	1.62	240	593	15	556	7.90	46.572	6.29	7.931	32.046	6811.12	16.21	10.63	59.20
538	--	--	--	13.3	555	8.01	45.447	6.39	8.032	31.777	5304.83	20.5	13.45	59.79
544	1.57	212	616	14.9	550	8.12	43.324	6.60	8.138	27.729	3587.29	23.59	15.47	60.01
SL 50-1		--	--			**pH (10)**								
2.5	0.07	37.2	679	0.002	515	7.60	2.610	10.15	7.664	2.548	1011.38	1.24	0.81	62.80
17.5	0.047	32.2	659	1.00E-03	497	7.68	2.672	10.00	7.739	2.592	867.8	1.54	1.01	62.90
22	0.015	27.9	540	0.002	495	7.69	2.534	10.06	7.748	2.457	806.67	1.51	0.98	62.64
38	0.014	23.6	518	0.002	489	7.75	2.476	10.23	7.806	2.385	685.1	1.73	1.12	62.87
58	0.028	20	509	0.081	474	7.73	2.755	10.17	7.786	2.606	786.01	1.86	1.21	62.38
78	0.078	25	553	0.373	513	7.65	3.899	10.10	7.743	3.509	1162.67	2.05	1.34	62.68
98	0.209	40.8	579	1.55	490	7.82	7.568	9.65	7.925	5.97	1294.48	5.33	3.47	62.40
118	0.351	47.3	602	4.49	504	7.63	12.395	9.42	7.855	8.449	2156.9	6.07	3.96	62.36
138	0.471	60.1	606	6.48	512	8.01	18.053	8.83	8.139	11.401	1475.59	14.16	9.24	61.56
158	0.68	64.4	615	9.8	518	7.65	25.313	8.14	7.894	16.676	3875.12	10.94	7.15	62.46
178	0.842	78	607	13.2	518	7.77	35.202	7.37	7.97	22.953	4460.38	16.13	10.54	61.25
198	1.075	95.8	603	15.8	521	7.78	46.059	5.87	7.963	31.269	6165.6	17.12	11.19	60.11
218	1.349	139	621	15.9	532	7.73	48.312	5.24	7.925	33.666	7265.65	14.74	9.65	60.06
238	1.499	181	624	14.2	517	7.80	49.948	5.07	7.952	36.286	7356.95	16.93	11.06	61.08
258	1.806	238	643	13.9	500	7.84	52.368	5.03	7.969	38.638	7534.91	19.35	12.61	62.18
278	1.939	293	675	9.53	472	7.89	53.725	5.00	7.97	43.52	8516.88	23.3	15.1	63.17
298	2.06	342	702	9.75	517	7.70	56.661	5.10	7.823	47.325	12998.48	16.59	10.84	64.56
318	2.242	382	673	9.53	483	7.79	59.694	5.18	7.883	49.924	11983.57	22.11	14.36	65.90
338	2.464	422	688	10	495	7.81	62.298	5.24	7.907	51.839	11719.79	23.8	15.5	66.76
358	2.586	451	697	8.64	500	7.80	63.436	5.26	7.893	54.184	12664.8	23.93	15.59	67.35
368	2.808	468	679	7.92	411	7.89	64.473	5.31	7.924	55.481	12364.79	33.46	21.37	67.74
382	2.889	485	699	8.81	496	7.81	67.025	5.38	7.899	57.457	13253.01	26.55	17.29	68.64
392	2.889	505	710	6.62	516	7.74	67.288	5.39	7.833	60.102	16129.19	22.81	14.9	68.98
398	2.889	494	696	5.77	520	7.74	64.380	5.29	7.832	57.972	15588.49	21.35	13.96	66.99
SL 51-1			--											
2.5	0.049	21.5	573	0	535	7.65	2.652	10.27	7.702	2.595	932.59	1.43	0.94	62.80
32	0.042	22.2	525	0	532	7.68	2.631	10.27	7.731	2.564	861.97	1.52	1	62.90
62	0.068	22.2	538	1.00E-03	530	7.58	2.652	10.28	7.629	2.618	1114.14	1.24	0.81	62.64
92	0.253	45	591	0.22	522	7.61	6.968	10.19	7.665	6.725	2638.91	3.48	2.28	62.87
122	0.55	88	606	0.66	525	7.60	7.205	10.01	7.681	6.549	2479.34	3.43	2.25	62.38
152	0.51	62.2	543	2.43	524	7.60	6.216	10.06	7.833	4.067	1080.47	3.03	1.99	62.68
182	1.242	173	601	2.92	523	7.66	14.929	9.49	7.78	12.155	3658.08	7.6	4.98	62.40
212	1.697	240	596	4.13	519	7.58	20.519	8.96	7.711	16.848	5950.21	8.59	5.62	62.36
242	2.121	296	609	4.79	512	7.74	25.045	8.51	7.844	20.251	5259.94	13.47	8.81	61.56
272	2.091	330	606	6.44	507	7.99	29.068	8.18	8.067	21.833	3339.56	23.24	15.18	62.46

Depth	NH_4	PO_4	SiO_2	H_2S	Cl,	pH(5)	TALK	Ca+Sr,	pH	DIC	pCO_2	La	Lc	Mg+Ca+Sr
(cm)	(mM)	(μM)	(μM)	(mM)	(mM)		(mM/kg)	(mM/kg)	in situ					mmol/L
302	2.788	367	616	7.01	498	7.75	33.336	7.76	7.854	26.418	6725.97	16.94	11.05	61.25
332	3.099	409	619	8.05	499	7.69	37.042	7.22	7.807	29.419	8360.27	15.75	10.28	60.11
362	3.474	447	639	8.3	500	7.82	41.834	6.84	7.91	33.238	7410.85	21.22	13.84	60.06
392	3.713	485	593	8.77	495	7.70	45.617	6.35	7.803	37.199	10682.64	17.52	11.42	61.08
422	4.161	515	621	9.4	493	7.85	49.557	5.79	7.929	39.613	8447.07	22.77	14.83	62.18
452	4.525	534	639	10	506	7.85	51.393	5.60	7.938	40.82	8508.17	22.38	14.62	63.17
482	4.808	622	657	9.28	499	7.66	52.759	5.35	7.763	43.976	13825.91	15.79	10.3	64.56
512	5.131	651	649	8.56	502	7.85	53.804	5.41	7.926	44.341	9516.52	23.12	15.09	65.90
542	5.252	708	649	9.04	501	7.71	55.333	5.58	7.803	46.31	13268.3	18.9	12.34	66.76
572	5.575	766	644	10.5	469	7.80	56.678	5.43	7.876	45.766	11153.75	23.15	15.01	67.35
582	5.454	751	649	8.9	465	8.03	53.000	5.50	8.071	42.078	6448.29	33.68	21.81	67.74
HYC 53-1	--	--	--	--										
2.5	0.021	36.2	336	5.00E-04	554	7.95	2.600	10.15	8.001	2.406	395.89	2.08	1.43	63.15
18	0.013	23.2	399	5.00E-04	555	7.91	2.668	10.22	7.96	2.5	453.33	1.98	1.36	63.78
38	0.013	23.2	364	5.00E-04	555	7.90	2.609	10.26	7.949	2.448	455.23	1.9	1.31	63.38
58	0.014	26.1	364	5.00E-04	555	7.88	2.511	10.21	7.928	2.359	460.9	1.74	1.2	63.25
79	0.016	24.6	361	1.00E-03	552	7.79	2.472	10.13	7.834	2.356	574.89	1.41	0.97	63.74
98	0.014	24.6	359	1.00E-03	551	7.81	2.581	10.12	7.855	2.456	571.54	1.54	1.06	63.15
118	0.019	21.6	374	1.00E-03	552	7.88	2.591	10.17	7.927	2.44	478.29	1.8	1.24	63.39
138	0.024	24.6	371	0.004	545	7.66	2.563	10.16	7.697	2.49	837.1	1.11	0.76	63.42
158	0.037	28.9	384	0.003	549	7.83	2.602	10.16	7.875	2.462	545.55	1.63	1.12	63.22
178	0.038	24.6	391	0.006	549	8.00	2.662	10.24	8.05	2.449	357.97	2.41	1.66	63.14
198	0.045	30.3	391	0.037	551	7.86	2.741	10.15	7.909	2.554	522.66	1.81	1.25	63.52
218	0.067	24.6	356	0.024	551	8.29	2.889	10.09	8.346	2.475	174.38	4.5	3.1	62.84
238	0.059	24.6	381	0.122	550	8.30	2.998	10.12	8.357	2.481	169.99	4.64	3.19	63.05
258	0.08	26.1	376	0.183	549	8.23	3.226	10.06	8.287	2.686	219.47	4.32	2.98	62.88
278	0.096	27.5	401	0.16	546	8.34	3.643	9.89	8.397	2.997	185.48	5.99	4.12	61.66
300	0.115	20	404	0.374	544	8.44	5.010	9.64	8.498	3.933	187.57	9.45	6.5	60.98
318	0.08	29.9	412	1.77	548	8.38	7.791	9.08	8.446	5.285	288.72	10.67	7.35	58.86
338	0.119	39	427	2.39	533	8.32	12.177	8.13	8.377	8.816	574.73	14.36	9.87	55.30
358	0.199	42	434	4.24	528	8.03	15.213	7.69	8.107	10.638	1357.78	9.35	6.41	54.35
379.5	0.345	146	502	6.98	512	8.12	23.853	5.89	8.183	16.076	1706.37	13.26	9.08	39.04
398	0.752	204	515	6.53	516	8.15	23.690	5.94	8.214	16.144	1589.25	14.16	9.71	36.74
418	1.005	226	515	5.15	518	8.23	22.815	5.77	8.287	16.228	1331	16.08	11.02	35.90
438	1.04	175	518	5.68	517	8.44	22.849	5.96	8.492	15.026	730.94	23.48	16.09	35.57
455	1.05	192	505	5.37	517		21.171	5.66						36.01
472	1.131	200	525	5.37	507		22.580	5.78						34.79
482	1.111	236	518	4.56	490	8.12	21.982	5.80	8.163	16.382	1835.65	13.41	9.15	35.18
492	1.091	246	492	5.86	492	8.22	22.874	5.96	8.263	15.73	1374.71	16.33	11.15	35.30
502	1.081	206	523	5.82	509	8.31	22.707	6.08	8.361	15.288	1043.03	19.02	13.02	35.28
512	1.04	246	520	5.86	515	8.27	23.065	6.06	8.326	15.679	1167.5	17.84	12.23	34.93
522	1.091	220	510	5.23	517	8.02	21.679	5.86	8.09	15.778	2099.8	10.44	7.16	35.38
SL 56-1		--												
2.5	0.051	24.7	470	0	424	7.63	2.347	10.27	7.629	2.308	934.63	1.2	0.8	63.29
9.5	0.032	14.1	434	0	326	7.73	2.387	10.34	7.687	2.351	869.37	1.9	1.24	63.45
22	0.051	14.1	417	0	340	7.91	2.655	10.14	7.858	2.558	630.44	2.86	1.87	62.90
42	0.056	14.1	404	0	373	8.04	2.841	10.20	8	2.68	464.55	3.72	2.46	62.94
62	0.096	21.2	374	0	399	7.86	2.919	10.16	7.84	2.811	703.11	2.51	1.68	62.83
82	0.119	17.7	354	0.006	396	7.99	2.890	10.06	7.965	2.731	509.03	3.23	2.15	62.78
102	0.157	14.1	343	0.015	400	8.14	3.189	10.03	8.114	2.939	381.95	4.75	3.17	62.77
122	0.243	14.1	331	0.277	402	8.05	4.085	9.95	8.032	3.61	571.88	4.8	3.21	63.08
136	--	--	--	0.897	409	8.11	5.978	9.58	8.099	4.82	648.05	7	4.68	60.29
142	0.56	38.9	508	2.774	346	8.08	22.338	5.95	8.021	18.906	3156.71	17.48	11.46	31.59
162	0.691	64.6	528	3.255	329	8.28	23.765	6.20	8.194	19.225	2127.14	28.59	18.63	30.94
182	0.787	96.5	513	2.774	380	8.07	23.458	6.58	8.034	19.88	3160.59	18.78	12.45	30.77
202	0.915	78.8	515	2.707	400	8.02	22.899	6.35	8.001	19.525	3331.05	15.6	10.4	30.80
222	1.017	68.2	520	3.188	393	8.05	23.069	6.28	8.028	19.195	3084.92	16.4	10.92	30.74
242	1.189	92.9	548	2.148	376	8.43	22.681	6.56	8.375	18.429	1265.09	36.36	24.08	30.11
262	1.348	68.2	505	1.264	351	8.17	21.949	6.43	8.103	19.565	2669.95	23.02	15.12	30.28
282	1.466	75.2	558	2.472	359	8.08	22.747	6.43	8.031	19.488	3156.4	19.04	12.54	30.13
302	1.614	89.4	561	1.801	349	8.09	22.151	6.51	8.031	19.488	3171.97	19.9	13.06	30.15
322	1.747	96.5	626	2.013	373	8.18	22.262	6.56	8.133	19.073	2398.73	22.78	15.07	29.82
342	1.99	122	571	0.268	353	8.33	21.457	6.64	8.259	19.365	1802.3	32.64	21.45	29.21
362	2	82.3	606	0.649	352	8.41	21.785	6.78	8.337	19.054	1456.4	38.74	25.45	29.25
382	2.071	122	609	0.973	370	7.98	21.379	6.65	7.939	19.7	3956	15.71	10.38	29.55
402	2.212	143	500	0.783	376	8.33	21.144	6.65	8.278	18.532	1623.54	30.35	20.1	29.79
425	2.303	122	624	1.711	300	8.24	22.255	6.59	8.137	19.277	2493.81	29.89	19.26	29.37
442	2.495	85.8	550	0.268	348	8.76	20.796	6.54	8.685	16.727	511.05	65.8	43.17	28.92
462	2.505	107	651	1.756	341	8.18	21.743	7.04	8.112	18.853	2535.54	25.6	16.75	29.17
482	2.626	136	679	2.673	330	8.10	22.194	7.05	8.035	18.691	3040.36	22.28	14.52	29.16
502	2.828	168	626	1.275	334	8.09	21.939	7.16	8.022	19.683	3300.01	22.83	14.9	28.58
522	2.929	118	664	0.66	339	8.44	21.255	7.06	8.36	18.402	1336.02	42.74	27.95	28.44
542	2.99	118	692	1.823	342	8.25	21.833	7.19	8.181	18.625	2113.12	29.87	19.55	28.48
562	2.99	107	712	2.192	347	8.20	21.589	7.38	8.139	18.228	2288.38	26.96	17.68	28.54
582	3.151	92.9	679	0.626	345	8.38	21.413	7.53	8.306	18.822	1560.6	40.86	26.78	28.47
598	3.05	92.9	684	0.067	343		19.826	6.92						28.64
SL 59-1		--		--										

Depth	NH_4	PO_4	SiO_2	H_2S	Cl,	pH(5)	TALK	Ca+Sr,	pH	DIC	pCO_2	La	Lc	Mg+Ca+Sr
(cm)	(mM)	(μM)	(μM)	(mM)	(mM)		(mM/kg)	(mM/kg)	in situ					mmol/L
2.5	0.016	20.2	490	0	548	7.42	2.236	10.12	7.451	2.243	1333.39	0.56	0.38	63.38
12.5	0.019	14.3	478	0	557	7.43	2.284	10.14	7.463	2.293	1325.15	0.58	0.4	63.14
22	0.01	18.8	483	0	550	7.48	2.384	10.11	7.514	2.376	1223.54	0.68	0.47	62.96
42	0.022	18.8	443	0	551	7.50	2.474	10.10	7.535	2.46	1207.58	0.74	0.51	63.07
62	0.014	17.2	443	0	551	7.43	2.346	10.13	7.462	2.355	1365.18	0.6	0.41	62.96
82	0.021	20.2	438	0	552	7.60	2.346	10.12	7.641	2.298	886.18	0.88	0.6	63.11
102	0.043	20.2	445	0	551	7.64	2.426	10.18	7.683	2.365	827.84	1.01	0.69	62.99
122	0.034	18.8	435	0	552	7.70	2.277		7.745	2.199	665.86	1.07	0.74	
142	0.034	18.8	458	0	546	7.74	2.268	10.14	7.785	2.178	601.38	1.18	0.81	62.75
162	0.031	17.2	463	0	542	7.54	2.358	10.10	7.575	2.333	1046.67	0.78	0.54	63.56
182	0.063	20.2	473	0	551	7.56	2.347		7.599	2.311	981.21	0.8	0.55	
202	0.039	20.2	478	0	547	7.48	2.219	9.93	7.514	2.207	1138.01	0.63	0.43	63.00
225	0.04	21.6	478	0	550	7.79	2.328		7.839	2.216	539.11	1.32	0.91	
242	0.036	21.6	483	0	550	7.75	2.305	10.05	7.797	2.207	592.36	1.21	0.83	62.48
266	0.01	21.6	488	0.003	550	7.63	2.315		7.672	2.253	808.28	0.99	0.68	
282	0.034	20.2	490	0	551	7.53	2.296	10.08	7.567	2.269	1035.54	0.73	0.5	62.29
302	0.04	21.6	503	0	557	7.45	2.276		7.485	2.271	1250.48	0.6	0.41	
322	0.04	21.6	490	0	556	7.45	2.276	9.99	7.484	2.272	1251.68	0.59	0.41	62.09
342	0.044	21.6	510	0	551	7.33	2.139		7.358	2.17	1588.78	0.44	0.3	
362	0.038	20.2	503	0	547	7.36	2.278	10.06	7.388	2.305	1577.39	0.49	0.34	62.05
382	0.043	23	498	0	547	7.43	2.248		7.461	2.249	1305.64	0.57	0.39	
412	0.036	20.2	505	0.001	547	7.37	2.248	10.12	7.399	2.27	1517.42	0.5	0.34	62.40
422	0.038	20.2	505	0.001	544	7.99	2.169		8.042	1.989	298.52	1.92	1.32	
442	0.034	18.8	505	0.007	542	7.52	2.209	10.13	7.555	2.181	1023.43	0.7	0.48	62.61
462	0.036	20.2	493	0	554	7.60	2.296		7.642	2.247	864.28	0.86	0.59	
482	0.034	20.2	508	0.004	544	8.03	2.209	10.04	8.083	2.007	273.02	2.1	1.44	62.85
502	0.033	18.8	533	0.007	550	7.54	2.109		7.578	2.073	921.83	0.69	0.47	
522	0.037	18.8	498	0.004	551	7.48	2.129	10.08	7.515	2.113	1085.82	0.61	0.42	62.54
542	0.035	20.2	523	0	551	7.37	2.218		7.399	2.24	1494.03	0.49	0.33	
562	0.039	18.8	528	5.59E-04	551	7.71	2.099		7.756	2.018	595.6	1.01	0.69	
582	0.036	20.2	513	0	552	7.78	2.287	10.08	7.829	2.18	542.37	1.28	0.88	62.69
602	0.043	18.8	523	0.002	553	7.61	2.079	10.17	7.652	2.026	760.91	0.8	0.55	62.74
622	0.041	18.8	498	0	555	7.60	2.307	10.19	7.642	2.259	868.35	0.87	0.6	62.95
632	0.05	14.3	490	0.004	557	7.62	2.159		7.664	2.106	769.46	0.85	0.58	
HYC 63-1				--										
2.5	0.051	10.3	336	0	554	7.61	2.412	10.26	7.651	2.371	892.49	0.94	0.64	64.44
22	0.06	20.6	365	5.59E-04	545	7.86	3.016	9.91	7.909	2.863	590.58	2.01	1.38	62.75
42	0.145	28.1	313	5.59E-04	547	8.08	3.862	9.79	8.137	3.542	422.57	4.04	2.77	60.77
62	0.198	45.7	328	5.59E-04	549	8.05	4.145	9.70	8.108	3.812	487.44	4.04	2.77	60.05
82	0.256	57.4	311	5.59E-04	550	8.14	4.672	9.50	8.201	4.224	430.55	5.35	3.67	58.49
102	0.332	69.3	303	0.068	550	8.13	5.295	9.27	8.193	4.744	493.17	5.76	3.95	56.96
122	0.351	78.2	295	0.104	548	8.15	5.890	9.05	8.214	5.238	516.63	6.48	4.45	55.45
142	0.399	81	292	0.213	547	8.19	6.630	8.76	8.255	5.782	515.83	7.59	5.21	53.95
162	0.478	89.9	295	0.229	547	8.21	7.147	8.62	8.275	6.21	526.65	8.39	5.76	52.56
182	0.568	98.8	308	0.452	547	8.21	7.624	8.36	8.277	6.445	543.72	8.49	5.82	51.68
202	0.56	95.7	293	0.362	548	8.39	8.228	8.19	8.458	6.774	361.25	12.68	8.7	50.55
222	0.594	102	298	0.734	549	8.42	8.783	8.02	8.49	6.884	337.77	13.43	9.22	49.72
242	0.614	106	321	1.105	547	8.25	9.153	7.97	8.322	7.21	543.73	9.9	6.79	49.09
262	0.71	106	338	0.89	547	8.13	9.613	7.78	8.2	8.023	819.87	8.34	5.72	47.95
282	0.766	105	359	1.034	547	8.13	10.051	7.65	8.201	8.306	846.97	8.51	5.84	47.36
312	0.818	106	389	1.119	548	8.11	10.178	7.46	8.182	8.38	894.69	8.04	5.51	46.23
322	--	--	--	0.497	555	8.03	10.314	7.35	8.097	9.184	1207.52	7.2	4.94	45.72
342	0.914	98.8	381	0.66	555	8.29	10.297	7.36	8.364	8.553	579.51	11.68	8.02	45.73
362	0.909	100	427	1.801	555	7.80	10.775	7.37	7.893	8.815	1884.47	4.35	2.98	46.08
382	0.979	98.8	452	2.013	551	8.03	11.275	7.27	8.116	8.758	1098.83	6.97	4.79	45.07
412	0.957	97.2	457	3.993	550	7.80	11.321	7.24	7.947	7.432	1399.63	4.1	2.81	44.98
422	1.007	95.7	455	4.06	550	7.98	11.730	7.24	8.095	7.475	985.97	5.73	3.93	44.63
442	1.005	94.3	455	4.452	550	7.88	11.750	7.12	8.02	7.316	1157.37	4.67	3.21	44.41
462	1.03	98.8	449	4.575	552	7.80	11.925	7.10	7.959	7.511	1375.55	4.17	2.86	44.13

APPENDIX 6

Authigenic mineralization – Core descritptions

Core description: legend

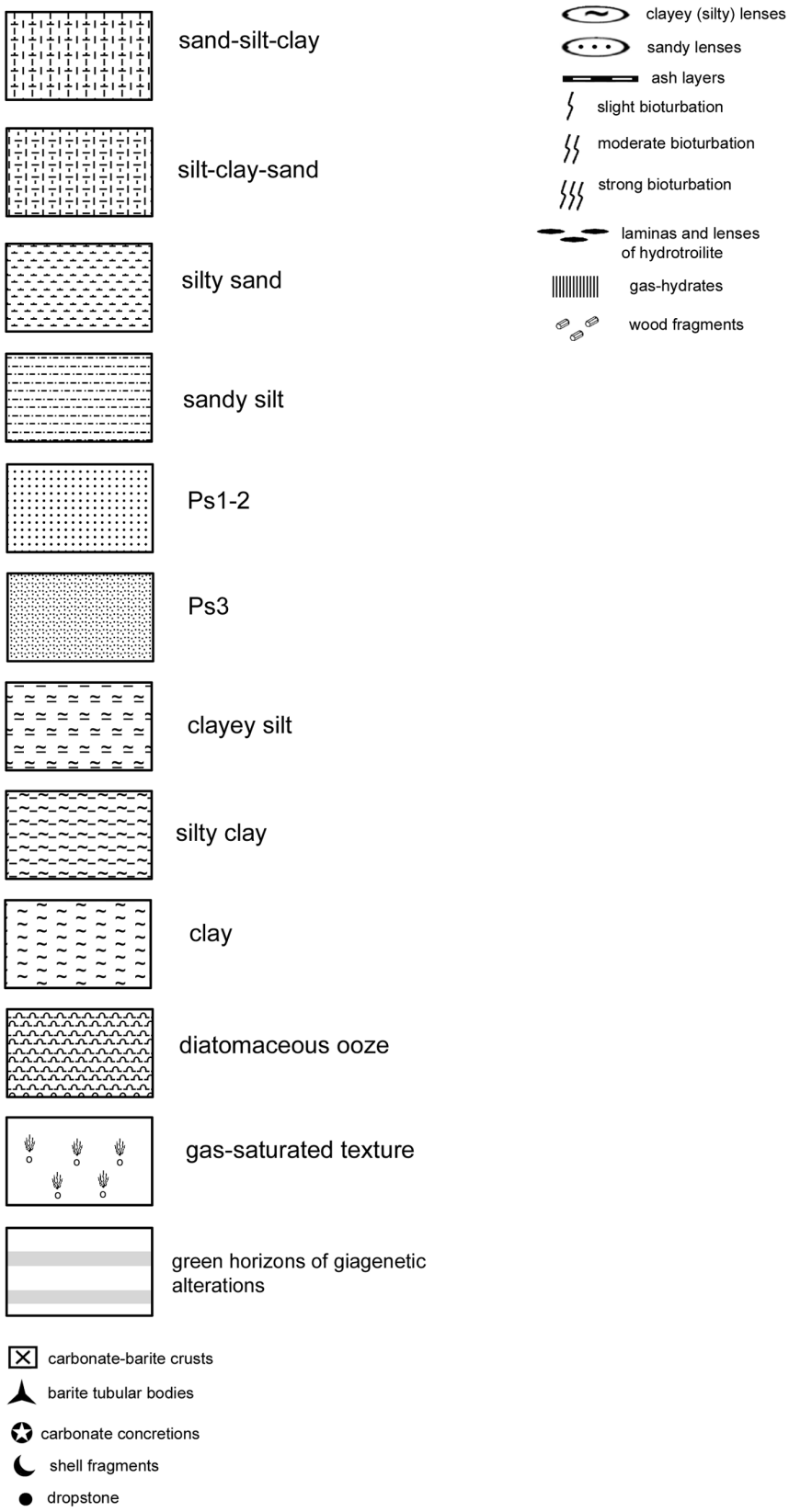

Core description : **LV29-34-1**
Cruise/Leg: **LV29, Leg 1**

Lat: **54°19.202**
Long: **143°54.576**
Water depth: **182 m**
Recovery: **100 cm**

(cm)	LITHOLOGY	TEXTURE	COLOUR	DESCRIPTION	SS
0–100	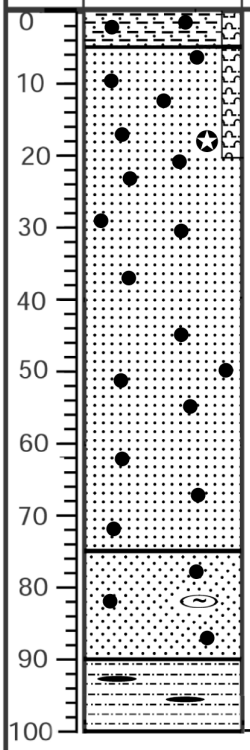			**0–5 cm: Heterogenous sand with admixtures of clayey silt, weakly diatomaceous, yellowish-green, soft, with rounded pebbles and gravel. Tubular worms occur.** **5–40 cm: Heterogenous sand, weakly diatomaceous, yellowish-green, moderately dense, with the admixtures of rounded pebbles and gravel. At 20 cm: carbonaceous** **40–60 cm: Heterogenous sand, yellowish gray, dense, well sorted, terrigenous, with laminas of hydrotroilite. Increased content of dropstones.** **60–75 cm: The same, but the color of the sediment is grayer, the content of dropstones decreases.** **75–90 cm: Medium-fine-grained sand, steel-gray, dense, well sorted, terrigenous; downwards the sand becomes fine grained. At 85 cm: lenses of clayey silt, yellowish-green, soft. Weak H2S odor.** **90–100 cm: Sandy clayey silt, steel-gray, soft, terrigenous, H2S odor. The sediment has a sharp top contact.**	

Core description : **LV29-42-5**
Cruise/Leg: **LV29, Leg 1**

Lat: **54°20.044**
Long: **143°55.201**
Water depth: **191 m**
Recovery: **55 cm**

(cm)	LITHOLOGY	TEXTURE	COLOUR	DESCRIPTION	SS
0 10 20 30 40 50	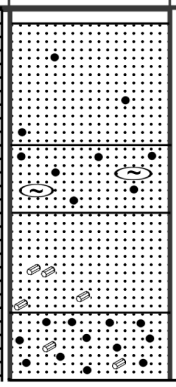			**0-2 cm: Horizon is washed out.** **2-20 cm: Heterogeneous sand, yellowish-gray, sorted, with small admixture of clayey silt, moderately dense. Dispersed fine gravel is common.** **20-30 cm: Sand layer enriched in pebble and gravel, yellowish-gray, with numerous lenses of yellowish-** **30-45 cm: Heterogeneous sand, yellowish-gray, with few admixtures of clayey silt, changing densities: denser layers alternate with soft ones. Many plant fragments (dark brown wood pieces) up to 2.5 cm in size occur.** **45-55 cm: Pebble-gravel-sand mixture, yellowish-gray, with small admixtures of silt. Rare plant fragments occur.**	

Core description : **LV29-46-1**
Cruise/Leg: **LV29, Leg 1**

Lat: **54°26.492**
Long: **144°04.600**
Water depth: **684 m**
Recovery: **550 cm**

(m)	LITHOLOGY	TEXTURE	COLOUR	DESCRIPTION	SS
0 1 2 3 4 5	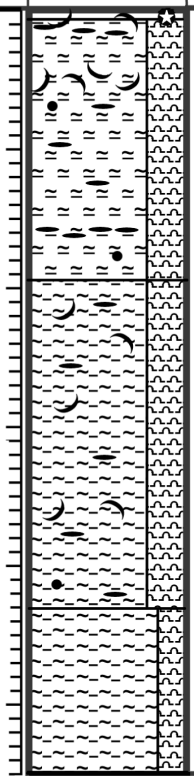			**0-5 cm: Horizon was deformed due to injection of HYC, its structural features are not clear. Shells and fragments of Calyptogena, Macoma (?) and also small (up to 1.5-2.0 cm in size) carbonate concretions (branchy in shape, with rough surface)** **5-195 cm: Silty clay, weakly diatomaceous, grayish-green, homogeneous, up to 70 cm - soft, below - moderately dense, viscous; spots and streaks of hydrotroilite are common (more intensive at 5-7, 160-162 cm); weakly bioturbated, with slight degassing texture.** **At 58 cm: congestion of small decomposed shell fragments.** **At 65 cm: large shell fragment.** **195-550 cm: Clayey silt, weakly diatomaceous, grayish-green, homogeneous, dense, viscous, spots and streaks of hydrotroilite and degassing texture are common. Interval 430-550 cm is more gas-saturated and water-saturated, moderately soft; with numerous gas outlets, strong H_2S odor.**	

Core description : **LV29-50-1**
Cruise/Leg: **LV29, Leg 1**

Lat: **54° 26.811**
Long: **144° 04.870**
Water depth: **695 m**
Recovery: **405 cm**

(m)	LITHOLOGY	TEXTURE	COLOUR	DESCRIPTION	SS
0 1 2 3 4	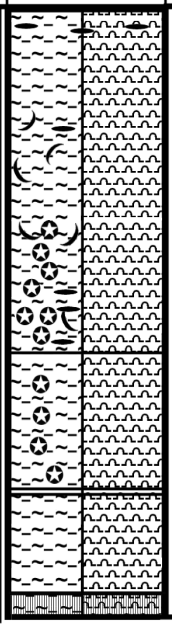			0-7 cm: Clayey silt, diatomaceous, with sand and sponge spicules, olive- 7-142 cm: Clayey silt, diatomaceous with, sponge spicules, olive-green, homogeneous, soft, mottled (dark gray mottles and lenses at 7-15 cm, more intensive at 7-10 cm), weakly bioturbated. At 85, 100, 113 cm: large fragments (up to 6 cm) of thick-valved mollusk 142-193 cm: The same, but frequent Macoma fragments. Small (~0.3-1.5 cm in size), gray, very soft, carbonate concretions occur at 157, 158, 160-162, 165, 170, 175, 177, 178, 185, 188 cm. At 185 cm: small lenses of hydrotroilite orientated in different directions. 193-230 cm: The same, but size and quantity of concretions is increased. At 202, 203, 206, 207, 210, 213 cm: flatted, rugged concretions up to 3.5 cm in size, soft on the outside, very dense inside. Some concretions have a tubular shape, their central part is filled by hydrotroilite. At 202-210 cm: layer of concretions up to 5 cm in size. 230-322 cm: The same, gas-saturated sediment with brecciated degassing texture. Many carbonaceous concretions - at 235, 238 cm (up to 5 cm in size), 263-268 (3x5, 8x5x2 cm in diameter), 278, 282-283 cm (up to 5 cm in diameter), 287,290 cm (flatted concretions 9x5x1.5 cm in size), 295, 304, 322-326 cm: Clayey silt, diatomaceous, gray-green, dense, with brecciated degassing texture. 326-345 cm: Silty clay, diatomaceous; color, density and texture are analogous to overlying horizon. 345-395 cm: The same, but sediment color is grayer with a slight 395-405 cm: In the lower part of the core (including tip), thin layers of white gas-hydrates occur; their thickness amounts to only 1-5 mm.	

Core description : **LV29-51-1**
Cruise/Leg: **LV29, Leg 1**

Lat: **54° 28.812**
Long: **144° 11.561**
Water depth: **825 m**
Recovery: **580 cm**

(m)	LITHOLOGY	TEXTURE	COLOUR	DESCRIPTION	SS
0	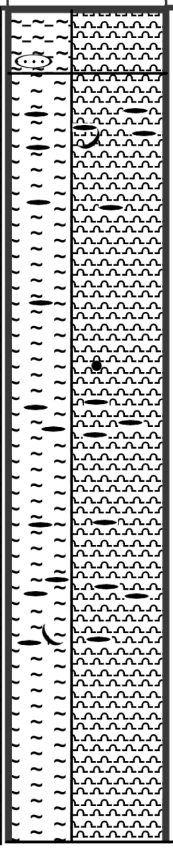			**0-45 cm: Silty clay, diatomaceous, on the top - yellowish-green, below - grayish-green, 0-15 cm: nearly fluid, 15-45 cm: soft, homogeneous.** **45-580 cm: Diatomaceous clay, grayish-green, homogeneous, moderately dense, from 160 cm - dense, viscous, ductile, with pseudo-bedded structures, mottled, weakly bioturbated (especially from 315 cm). Many lenses and layers of hydrotroilite occur in the entire core, more frequent at 75-78, 94-95, 130-135, 148-150, 213, 270-290, 365-370, 410-430 cm.** **At 98, 453, 466 cm: thin-valved shell fragments.**	
1					
2					
3					
4					
5					

Core description : **LV29-53-1**
Cruise/Leg: **LV29, Leg 1**

Lat: **54°00.495**
Long: **146°16.909**
Water depth: **1493 m**
Recovery: **530 cm**

(m)	LITHOLOGY	TEXTURE	COLOUR	DESCRIPTION	SS
0 1 2 3 4 5	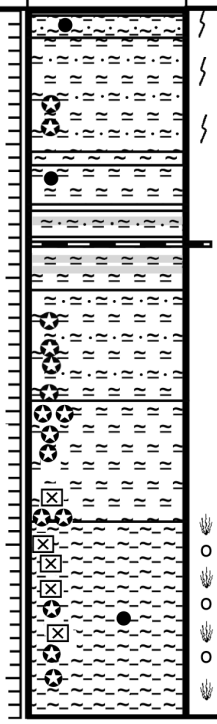			0-2 cm: Clayey silt with sand, olive greenish-gray, very dense, lumpy, terrigenous. 2-20 cm: Silty clay with sand, dark gray, dense, terrigenous, weakly bioturbated. 20-63 cm: Clayey silt with admixtures of sand, dark gray, homogeneous, dense, terrigenous, weakly bioturbated. 63-108 cm: Clayey silt with sand, from gray to dark gray, dense, terrigenous, weakly bioturbated. At 73, 84, 90 cm: soft 108-114 cm: Clay, dark gray with weak brown tone 114-145 cm: Clayey silt, dark gray, homogeneous, 145-150 cm: Clay, dark gray, homogeneous, massive, 150-170 cm: Clayey silt with sand, dark gray, terrigenous. At 155-160 cm: greenish diagenetic horizon. 170-173 cm: Clay, dark gray with weak brown tone, 173-173.5 cm: Layer of silty sand, black, sorted. 173.5-176 cm: Silt, gray, massive, terrigenous. 176-178 cm: Ash layer K2 represented by silty sand, gray with reddish tone. In lower part - transition to a greenish 178-210 cm: Clayey silt, gray, homogeneous, massive, terrigenous. 210-293 cm: Clayey silt with sand, gray, homogeneous, massive, terrigenous. At 243, 255, 264, 273, 278, 284, 288 cm: 293-310 cm: Clayey silt, gray, terrigenous, enriched in concretions (especially at 293-305 cm). 310-382 cm: Clayey silt, gray, homogeneous, massive, terrigenous. At 311, 315, 318-324, 328, 333-336: carbonate concretions, their content increases from 366 cm (more frequent at 373- 382-530 cm: Silty clay, steel-gray, terrigenous, gas-saturated, diluted, with typical pseudo-brecciated texture. H2S odor. At 393, 400, 443, 499 cm: carbonate concretions. Horizons 400-425, 450-480 cm are enriched in small and	

Core description : **LV29-56-1**
Cruise/Leg: **LV29, Leg 1**

Lat: **54°00.746**
Long: **146°15.947**
Water depth: **1470 m**
Recovery: **615 cm**

(m)	LITHOLOGY	TEXTURE	COLOUR	DESCRIPTION	SS
0 1 2 3 4 5 6	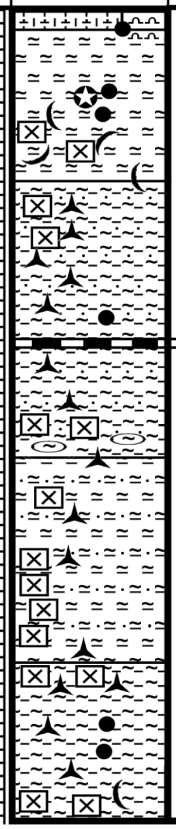			**0–3 cm: Silty clayey sand, weakly diatomaceous, brown, nearly fluid.** **7–15 cm: The same, greenish-gray, soft, admixture of small (1–3 mm in size) yellowish-white chimney fragments.** **15–90 cm: Clayey silt, gray (from steel-gray to dark gray), moderately dense, homogeneous, at 15–20 cm: weakly diatomaceous, below: terrigenous.** **At 76 cm: oval carbonate concretion (2x4 cm in size).** **At 86 cm: large (9 cm in diameter) fragment of Calyptogena** **90–130 cm: Clayey silt, gray (from steel-gray to dark gray), terrigenous, from 115 cm – diluted, enriched in shell fragments (up to 5–10 cm in diameter) cemented by barite and carbonate (at 95, 105, 115, 125, 130 cm).** **130–265 cm: Silty clay with sand, gray, diluted, gas-saturated, porous, with numerous degassing structures, enriched in carbonate-barite tubular bodies of different size at 130–160 cm, their content decreases downwards.** **265–310 cm: Silty clay with sand, gray, terrigenous, gas-saturated, porous, lumpy, with inclusions of both small barite tubular bodies and angular, fragile, dark gray barite debris.** **310–340 cm: The same, with lumpy clayey lenses.** **At 310, 317 cm: large angular, fragile barite fragments.** **340–495 cm: Clayey silt with sand, terrigenous, enriched in barite-carbonate tubular bodies, lumpy; dense lumps have a size of up to 8 cm, are of gray color, at 365–380 cm: greenish-gray.** **At 345 cm: large fragment of tubular body (up to 4 cm in diameter).** **495–508 cm: Silty clay, steel-gray, diluted, terrigenous, enriched in barite tubular bodies and barite-calcite dense** **508–597 cm: Silty clay, dark gray with greenish tone, dense, terrigenous, with brecciated texture. At 583–585 cm: layer of** **597–615 cm: Analogous to horizon 495–508 cm, with abundant inclusions of Ba-Ca crusts, a fragment of Calyptogena occurs.**	

Core description : **LV29-59-1**
Cruise/Leg: **LV29, Leg 1**

Lat: **54° 00.765**
Long: **146° 26.054**
Water depth: **1425 m**
Recovery: **630 cm**

(m)	LITHOLOGY	TEXTURE	COLOUR	DESCRIPTION	SS
0	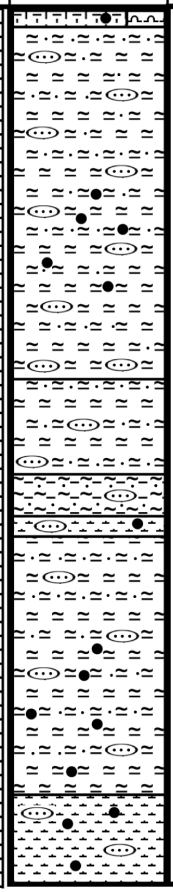			**0-3 cm: Silty clayey sand, weakly diatomaceous, brown, fluid.** **3-12 cm: Silty clayey sand, weakly diatomaceous, greenish-yellow, soft, with dropstones.** **12-120 cm: Clayey silt enriched in lenses of very dark clayey sand, gray, terrigenous, at 55-67 cm: greenish, dense. Density increases** **120-264 cm: Clayey silt enriched in sandy lenses, gray, very dense, terrigenous.** **264-266 cm: Lens of sorted fine-grained sand.** **266-335 cm: Clayey silt enriched in sand, gray, dense, with greenish tone at 280-290 cm, terrigenous.** **335-366 cm: Silty clay with sand admixture, greenish-gray, homogeneous, massive, terrigenous.** **At 337, 355 cm: sand lenses.** **366-380 cm: Silty sand, terrigenous, with pebble admixture.** **380-427 cm: Clayey silt enriched in sand, gray, with greenish tone downwards, terrigenous.** **427-497 cm: Clayey silt with sand, gray, terrigenous, with pebble admixture.** **497-562 cm: Clayey silt enriched in sand, dark greenish-gray, terrigenous.** **562-630 cm: Clayey silty sand, gray, massive, terrigenous, with admixture of pebble.** **Weak H_2S odor in lower part of core.**	
1					
2					
3					
4					
5					
6					

Core description : **LV29-63-1**
Cruise/Leg: **LV29, Leg 1**

Lat: **54 00.698**
Long: **146 26.499**
Water depth: **1431 m**
Recovery: **470 cm**

(m)	LITHOLOGY	TEXTURE	COLOUR	DESCRIPTION	SS
0 1 2 3 4	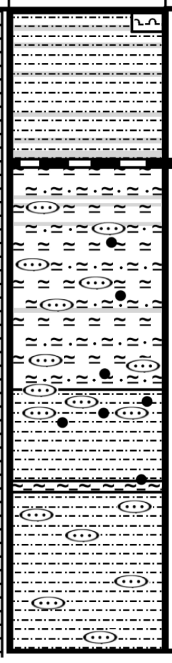			0-2 cm: Sandy silt weakly diatomaceous, grayish- 2-8 cm: Sandy silt, weakly diatomaceous, greenish- 8-115 cm: Sandy silt, greenish-gray, soft, more dense downwards, homogeneous, terrigenous. Many dark green, dense diagenetic horizons occur (at 12-13, 22, 43, 76, 78, 94-96, 103, 105, 107, 109 cm). 114-115 cm: Ash layer (K2). 115-220 cm: Clayey silt enriched in sand, greenish-gray, from 165 cm: gray, moderately dense, from 185 cm: dense, terrigenous. Sandy lenses are common in entire interval. At 137, 141, 158, 220 cm: dark green diagenetic horizons. 220-280 cm: Clayey silt with sand, gray-green, from 260 cm: greenish-gray, homogeneous, terrigenous. The sand content 280-360 cm: Sandy silt, greenish-gray, from 315 cm: gray, dense, terrigenous, with admixture of dropstones. Admixtures of dispersed At 346-353 cm: layer of gray, homogeneous silty clay. Sandy lenses are common in entire interval. 360-470 cm: Sandy silt, gray, terrigenous, with sandy lenses and dropstone.	

APPENDIX 7

Physical properties of sediment

Conductivity

LV29-63-1		LV29-59-1		LV29-56-1		LV29-53-1		LV29-51-1		LV29-50-1		LV29-46-1	
epth (cm)	Cond (W/m/K)	Depth (cm)	Cond (W/m/K)	Depth (cm)	Cond (W/m/K)	Depth (cm)	Cond (W/m/K)	Depth (cm)	Cond (W/m/K)	Depth (cm)	Cond (W/m/K)	Depth (cm)	Cond (W/m/K)
130	0.730	100	1.013	100	0.875	100	0.732	100	0.716	90	0.717	67	0.707
230	0.771	200	1.074	185	0.540	195	0.768	200	0.733	190	0.712	157	0.685
330	0.833	300	1.004	297	0.661	310	0.775	300	0.73	350	0.567	257	0.679
440	0.774	400	0.860	560	0.737	400	0.718	400	0.724			357	0.640
		500	1.048									457	0.627

Temperature

LV29-63-1		LV29-59-1		LV29-56-1		LV29-53-1		LV29-51-1		LV29-50-1		LV29-46-1	
epth (cm)	T (°C)	Depth (cm)	T (°C)	Depth (cm)	T (°C)	Depth (cm)	T (°C)	Depth (cm)	T (°C)	Depth (cm)	T (°C)	Depth (cm)	T (°C)
0	2.23	0	2.23	0	2.23	0	2.23	0	2.28	0	2.14	0	2.14
40	2.27	40	2.38	40	2.39	40	2.35	20	2.32	20	2.12	10	2.05
100	2.44	100	2.68	100	2.77	100	2.72	40	2.28	40	2.1	15	1.69
150	2.46	200	2.83	200	2.62	195	2.86	60	2.29	60	2.1	62	2.01
200	2.61	300	3.18	280	2.86	310	2.96	80	2.27	80	2.07	72	1.89
250	2.56	400	3.3	450	2.88	400	3.25	100	2.28	120	2.04	77	1.88
300	2.8	500	3.5	560	3.13	500	3.34	120	2.29	140	2.06	107	1.87
350	2.85	578	3.43	560	2.98			140	2.34	160	2.06	132	2.12
400	2.88							160	2.39	180	2.07	157	2.11
450	2.99							180	2.34	200	2.05	207	2.05
								200	2.39	220	2.07	257	2.09
								220	2.43	240	2.09	307	2.09
								240	2.45	260	2.05	357	2.14
								260	2.43	320	2.03	407	2.12
								280	2.44	340	1.99	457	2.15
								300	2.46	360	1.96	507	2.12
								320	2.44	380	2.06	537	2.14
								340	2.4	390	2.05		
								360	2.42				
								380	2.44				
								400	2.49				
								420	2.5				
								440	2.45				
								460	2.48				
								480	2.5				
								500	2.76				
								520	2.69				
								540	2.8				
								560	3				
								580	2.9				

Magnetic Susceptibility

LV29-63-1		LV29-59-1		LV29-56-1		LV29-53-1		LV29-51-1		LV29-50-1		LV29-46-1		LV29-34-1	
depth (cm)	MS	depth (cm)	MS	depth (cm)	MS	depth (cm)	MS	depth (cm)	MS	depth (cm)	MS	depth (cm)	MS	depth (cm)	MS
0	130	5	49	0	56	5	24	20	29	5	29	2.5	3	2.5	0
5	43	10	40	5	32	10	29	25	29	10	24	5	4	5	-7
10	78	15	59	10	35	15	22	30	24	15	16	7.5	6	7.5	-10
15	84	20	40	15	347	20	19	35	27	20	20	10	6	10	-14
20	88	25	15	20	45	25	20	40	20	25	19	12.5	6	12.5	-19
25	82	30	34	25	46	30	19	45	13	30	4	15	6	15	-21
30	114	35	26	30	36	35	18	50	8	35	2	17.5	7	17.5	-21
35	110	40	25	35	34	40	18	55	10	40	0	20	7	20	-27
40	103	45	1	40	21	45	20	60	9	45	3	22.5	9	22.5	-27
45	97	50	3	45	13	50	25	65	10	50	17	25	8	25	-24
50	98	55	0	50	17	55	25	70	4	55	8	27.5	6	27.5	-30
55	83	60	-3	55	18	60	18	75	1	60	5	30	7	30	-32
60	69	65	-3	60	20	65	34	80	0	65	5	32.5	5	32.5	-32
65	81	70	10	65	5	70	17	85	0	70	3	35	6	35	-32
70	52	75	-5	70	33	75	10	90	-1	75	11	37.5	5	37.5	-34
75	40	80	6	75	26	80	10	95	-3	80	11	40	5	40	-38
80	76	85	0	80	27	85	21	100	-2	85	10	42.5	5	42.5	-37
85	77	90	-2	85	26	90	12	105	-3	90	9	45	4	45	-39
90	73	95	-4	90	18	95	9	110	-5	95	10	47.5	5	47.5	-34
95	55	100	-3	95	15	100	7	115	-5	100	9	50	3	50	-38
100	44	105	0	100	24	105	5	120	-6	105	9	52.5	5	52.5	-37
105	32	110	2	105	28	110	1	125	-4	110	7	55	4	55	-43
110	30	115	1	110	13	115	9	130	-8	115	7	57.5	5	57.5	-43
115	26	120	-3	115	26	120	11	135	-7	120	15	60	6		
120	29	125	-9	120	20	125	7	140	-7	125	14	62.5	6		
125	23	130	13	125	14	130	4	145	-8	130	12	65	6		
130	32	135	6	130	4	135	6	150	-9	135	12	67.5	6		
135	33	140	9	135	11	140	3	160	-5	140	13	70	5		
140	20	145	0	140	10	145	4	165	-5	145	14	72.5	5		
145	27	150	18	145	4	150	2	170	-4	150	10	75	4		
150	22	155	0	150	7	155	2	175	-4	155	9	77.5	4		
155	34	160	-8	155	7	160	0	180	-6	160	9	80	3		
160	21	165	-6	160	10	165	2	185	-5	165	9	82.5	3		
165	333	170	-10	165	9	170	-2	190	-7	170	9	85	3		
170	14	175	-2	170	10	175	14	195	-8	175	9	87.5	4		
175	20	180	8	175	8	180	9	200	-8	180	6	90	3		
180	30	185	-3	180	11	185	2	205	-7	185	7	92.5	4		
185	33	190	-3	185	8	190	4	210	-8	190	6	95	3		
190	32	195	-19	190	7	195	4	215	-8	195	5	97.5	4		
195	25	200	7	195	12	200	4	220	-9	200	5	100	3		
200	18	205	-1	200	15	205	2	225	-8	205	4	102.5	5		
205	13	210	-1	205	12	210	4	230	-10	210	0	105	12		
210	21	215	-12	210	12	215	3	235	-11	215	1	107.5	4		
215	15	220	-14	215	14	220	7	240	-9	220	0	110	4		
220	17	225	13	220	12	225	4	245	-9	235	11	112.5	5		
225	10	230	-12	225	62	230	1	250	-10	240	10	115	4		
230	16	235	-14	230	10	235	4	255	-12	245	11	117.5	3		
235	8	240	-13	235	9	240	1	260	-11	250	8	120	4		
240	5	245	-17	240	7	245	2	265	-12	255	8	122.5	3		
245	8	250	-17	245	10	250	5	270	-11	260	8	125	3		

LV29-63-1		LV29-59-1		LV29-56-1		LV29-53-1		LV29-51-1		LV29-50-1		LV29-46-1		LV29-34-1	
depth (cm)	MS	depth (cm)	MS	depth (cm)	MS	depth (cm)	MS	depth (cm)	MS	depth (cm)	MS	depth (cm)	MS	depth (cm)	MS
250	10	255	-14	250	11	255	2	275	-11	265	8	127.5	3		
255	4	260	-23	255	11	260	4	280	-13	270	10	130	2		
260	10	265	-18	260	10	265	8	285	-13	275	8	132.5	2		
265	10	270	-17	265	9	270	12	290	-13	280	10	135	2		
270	7	275	-19	270	24	275	2	295	-13	285	7	137.5	3		
275	11	280	-20	275	29	280	4	300	-12	290	6	140	2		
280	10	285	-17	280	24	285	6	305	-14	295	6	142.5	2		
285	24	290	20	285	24	290	9	310	-13	300	6	145	1		
290	20	295	10	290	23	295	12	315	-16	305	6	147.5	2		
295	33	300	9	295	24	300	6	320	2	310	3	150	5		
300	27	305	8	300	26	305	5	325	0	315	3	152.5	3		
305	40	310	3	305	25	310	1	330	-1	320	3	155	2		
310	22	315	1	310	27	315	11	335	-1	325	1	157.5	4		
315	24	320	10	315	24	320	15	340	-2	330	2	160	3		
320	22	325	14	320	22	325	11	345	-2	335	1	162.5	1		
325	28	330	9	325	20	330	14	350	-3	340	0	165	2		
330	18	335	5	330	24	335	10	355	-4	345	0	167.5	2		
335	21	340	3	335	26	340	10	360	-6	350	-2	170	1		
340	2	345	4	340	23	345	9	370	-7	355	-9	172.5	0		
345	26	350	5	345	27	350	9	375	-8	360	-6	175	0		
350	3	355	16	350	27	355	9	380	-9	365	-8	177.5	-1		
355	5	360	3	355	23	360	11	385	-9	370	-17	180	-1		
360	9	365	30	360	22	365	15	390	-9	375	-18	182.5	-1		
365	13	370	9	365	23	370	13	395	-9			185	-1		
370	7	390	23	370	16	375	8	400	-10			187.5	-2		
375	14	395	14	375	17	380	7	405	-12			190	-2		
380	6	400	12	380	20	385	6	410	-12			192.5	-2		
385	34	405	17	385	24	390	12	415	-13			195	-3		
390	8	410	31	390	22	395	14	420	-11			197.5	-4		
395	15	415	20	395	18	400	19	425	-13			200	-2		
400	11	420	25	400	18	405	14	430	-14			202.5	0		
405	-1	425	22	405	19	410	42	435	-15			205	-1		
410	6	430	29	410	22	415	20	440	-14			207.5	0		
415	-3	435	24	415	21	420	23	445	-14			210	0		
420	-3	440	17	420	10	425	17	450	-14			212.5	-1		
425	-2	445	19	425	25	430	40	460	-12			215	0		
430	0	450	21	430	34	435	19	465	-13			217.5	-1		
435	-1	455	22	435	25	440	13	470	-13			220	-1		
440	-2	460	23	440	20	445	15	475	-14			222.5	-2		
445	0	465	18	445	24	450	15	480	-15			225	-1		
450	2	470	26	450	29	455	21	490	-16			227.5	-2		
455	6	475	21	455	29	460	26	495	-17			230	-2		
460	3	480	16	460	21	465	18	500	-17			232.5	-2		
465	-3	485	15	465	17	470	16	505	-17			235	-3		
		490	20	470	23	475	12	510	-16			237.5	-1		
		495	26	475	23	480	10	520	-17			240	-2		
		500	26	480	25	485	10	525	-16			242.5	-2		
		505	29	485	25	490	10	530	-16			245	0		
		510	32	490	25	495	14	535	-18			247.5	-1		
		515	27	495	25	500	8	540	-17			250	-2		
		520	22	500	25	505	27	550	-17			252.5	-1		
		525	25	505	30	510	9	555	-15			255	-2		
		530	32	510	48	515	8	560	-18			257.5	-2		

LV29-63-1		LV29-59-1		LV29-56-1		LV29-53-1		LV29-51-1		LV29-50-1		LV29-46-1		LV29-34-1	
depth (cm)	MS	depth (cm)	MS	depth (cm)	MS	depth (cm)	MS	depth (cm)	MS	depth (cm)	MS	depth (cm)	MS	depth (cm)	MS
		535	26	515	27			565	-17			260	-3		
		540	29	520	22			570	-16			262.5	-3		
		545	26	525	36			575	-19			265	-4		
		550	25	530	47							267.5	-3		
		555	20	535	23							270	-4		
		560	23	540	16							272.5	-4		
		570	30	545	34							275	-4		
		575	22	550	380							277.5	-4		
		580	24	555	23							280	-5		
		585	26	560	35							282.5	-4		
		590	30	565	32							285	-5		
		595	26	570	28							287.5	-5		
		600	29	575	33							290	-5		
				580	31							292.5	-6		
				585	26							295	-7		
				590	28							297.5	-7		
												300	-5		
												302.5	-6		
												305	-5		
												307.5	-5		
												310	-7		
												312.5	-5		
												315	-7		
												317.5	0		
												320	-7		
												322.5	-7		
												325	-7		
												327.5	-8		
												330	-10		
												332.5	-8		
												335	-7		
												337.5	-8		
												340	-7		
												342.5	-8		
												345	-7		
												347.5	-9		
												350	-8		
												352.5	-8		
												355	-8		
												357.5	-8		
												360	-8		
												362.5	-7		
												365	-8		
												367.5	-9		
												370	-9		
												372.5	-8		
												375	-8		
												377.5	-10		
												380	-9		
												382.5	-8		
												385	-8		
												387.5	-9		
												390	-8		

LV29-63-1		LV29-59-1		LV29-56-1		LV29-53-1		LV29-51-1		LV29-50-1		LV29-46-1		LV29-34-1	
depth (cm)	MS	depth (cm)	MS	depth (cm)	MS	depth (cm)	MS	depth (cm)	MS	depth (cm)	MS	depth (cm)	MS	depth (cm)	MS
												392.5	7		
												395	-7		
												397.5	-10		
												400	-10		
												402.5	-10		
												405	-11		
												407.5	-11		
												410	108		
												412.5	-10		
												415	-14		
												417.5	-11		
												420	-12		
												422.5	-12		
												425	-12		
												427.5	-10		
												430	-12		
												432.5	-13		
												435	-13		
												437.5	-13		
												440	-13		
												442.5	-13		
												445	-14		
												447.5	-13		
												450	-13		
												452.5	-15		
												455	-14		
												457.5	-15		
												460	-16		
												462.5	-14		
												465	-17		
												467.5	-17		
												470	-17		
												472.5	-17		
												475	-18		
												477.5	-18		
												480	-19		

APPENDIX 8

Participant list

Participant list

Scientists

1. Kulinich, Ruslan	chief scientist
2. Obzhirov, Anatoly	co-chief scientist
3. Botsul, Anatoly	co-chief scientist
4. Nikolayeva, Natalya	scientist
5. Derkachev, Alexander	scientist
6. Salomatin, Alexander	scientist
7. Salyuk, Anatoly	scientist
8. Tishchenko, Pavel	scientist
9. Bosin, Alexander	student scientist
10. Vereshchagina, Olga	scientist
11. Koptev, Andrey	scientist
12. Kraynikov, Gennady	scientific worker
13. Nepomiluyev, Gennady	scientific worker
14. Pavlova, Galina	scientist
15. Sagalayev, Sergey	scientist
16. Sosnin, Valery	scientist
17. Khodorenko, Natalya	scientist
18. Baranov, Boris	scientist
19. Matveyeva, Tatyana	scientist
20. Radyukin, Alexey	student scientist
21. Biebow, Nicole	co-chief scientist
22. Georgeleit, Katharina	foreign language assistant
23. Wallmann, Klaus	scientist
24. Aloisi, Giovanni	scientist
25. Bohlmann, Harald	technician
26. Repschläger, Janne	student scientist
27. Domeyer, Bettina	scientist
28. Hein, Hartmut	scientist
29. Nöske, Carl-Ulrich	technician
30. Poort, Jeffrey	scientist

Ship`s crew

1.	Nikiforov, Valery	master
2.	Feshchenko, Oleg	chief mate
3.	Soleny, Konstantin	2nd mate
4.	Vashchenko, Vladimir	3rd mate
5.	Oblakov, Sergey	radio navigator
6.	Golublev, Vladimir	mate
7.	Khrapko, Yevgeny	chief engineer
8.	Khlynin, Vitaly	2nd engineer
9.	Tsimbalov, Igor	3rd engineer
10.	Vedernikov, Igor	3rd engineer
11.	Nagornov, Alexander	chief electric engineer
12.	Naydenov, Roman	2nd electric engineer
13.	Kucherov, Yevgeny	doctor
14.	Sychev, Andrey	boatswain
15.	Yurevich, Oleg	sailor
16.	Zeky, Yury	sailor
17.	Logachev, Igor	sailor
18.	Sobolev, Mikhail	sailor
19.	Yushkevich, Viktor	sailor
20.	Derkach, Vasily	sailor
21.	Kuchumov, Dmitry	motorman
22.	Alfeyev, Nikolay	motorman
23.	Barsukov, Gennady	motorman
24.	Goncharuk, Valery	motorman
25.	Timoshenko, Vasily	motorman
26.	Gubarev, Viktor	motorman
27.	Derkach, Alexander	electrician
28.	Konovalov, Alexander	cook
29.	Sheremetyeva, Yelena	cook
30.	Ovechkina, Marina	stewardess
31.	Golubkina, Lyudmila	stewardess
32.	Varfolomeyeva, Vera	stewardess
33.	Tsymbalova, Anzhelika	stewardess
34.	Timoshenko, Natalya	stewardess
35.	Kushch, Lyudmila	cook-mate

PART II:

RV AKADEMIK LAVRENTYEV CRUISE 29

LEG 2

PUSAN - SEA OF OKHOTSK - PUSAN - VLADIVOSTOK

JUNE 27 - AUGUST 7, 2002

Table of contents

PART II: CRUISE REPORT LV29: SECOND LEG OF THE 29TH CRUISE OF RV *AKADEMIK LAVRENTYEV*, JUNE-AUGUST 2002

1. CRUISE NARRATIVE

Nicole Biebow and Ruslan Kulinich

After having completed the first leg RV *Akademik Lavrentyev* entered Pusan harbor again in the morning of June 27th. There, the video equipment and the multibeam echosounder were offloaded, and the German coring equipment, the sediment echosounder, the multinet and spares for the winch were onloaded. In addition, 5 German and 9 Russian colleagues left the ship, being replaced by new working groups.

We left Pusan harbor again at noon of June 28th in direction of the Okhotsk Sea. Those of us who had taken part in Leg 1 used the transit for finishing their cruise reports, while the new colleagues aboard equipped the labs and installed the new equipment. The scientific focus of the second leg was mainly paleoceanographic: we wanted to find out how the environment changed during the last several thousands of years and where these changes arose from. Therefore, we mainly wanted to take long cores in the key areas of the Okhotsk Sea, e.g. the estuary of the Amur River and along the straits into the Pacific Ocean. Furthermore, we planned to take many plankton samples, to dredge submarine volcanoes and to carry out seismic investigations in the Kurile Basin. The complete cruise track is shown in *Figure 1.1*; the working areas and stations are given in *Figure 1.2*.

During transit through the Japan See we stopped at 39.03.561´ N/ 133.00.650´ E for a sea bath at 21°C water and air temperature. The water depth was there 2,500 m. A bath in the ocean is a tradition on Russian research vessels, and all participants enjoyed it very much.

On July 1st, RV *Akademik Lavrentyev* passed La Perusa Strait and thereby reached the Okhotsk Sea. In the night from July 1st to 2nd, we began to work west of La Perusa Strait. At our first station we deployed the sediment echosounder SES-2000DS from Rostock University with which we were for the first time able to survey and sample sediments which continuously deposited without disturbance. In the beginning, there were problems with deploying the echosounder, because the mounting at the ship's side did not keep the echosounder in a stable position. As a result, the echosounder started strongly vibrating. Thanks to active help of the Russian crew and some improvisation we could solve the problem, and since then the echosounder worked well.
After having received spares for the deep-sea winch in Pusan and having made some modifications on it, the winch worked more or less fine, too.

The usual daily work on the paleoceanographic stations now was performed as follows: Firstly, we mapped the seafloor with the sediment echosounder. The Russian scientists ran their seismics at the same time. Secondly, we deployed the multicorer, the Russian and German gravity corers, CTD and a multinet for plankton sampling. From July 2nd to 4th we successfully carried out these works at three stations on the northwestern continental slope of the Kurile Basin at water depths from 2,500 to 1,000 m. All gravity core deployments were successful, and we recovered three 12 m long sediment cores with the German gravity corer which cover, according to first analyses, a period of 60,000 years. Subsequent to core deploying, the Russian and German colleagues together described and sampled the cores and determined their physical properties.

In the period of July 4th to 8th RV *Akademik Lavrentyev* slowly went north along the continental slope off Sakhalin. We successfully carried out two coring transects north of 52°N and 53°N at the continental slope off northeastern Sakhalin. Mainly the perfectly working sediment echosounder made it easy for us to choose favorable stations so that every

deployment of the 12 m long core was a success. Additionally, water and plankton samples were taken.

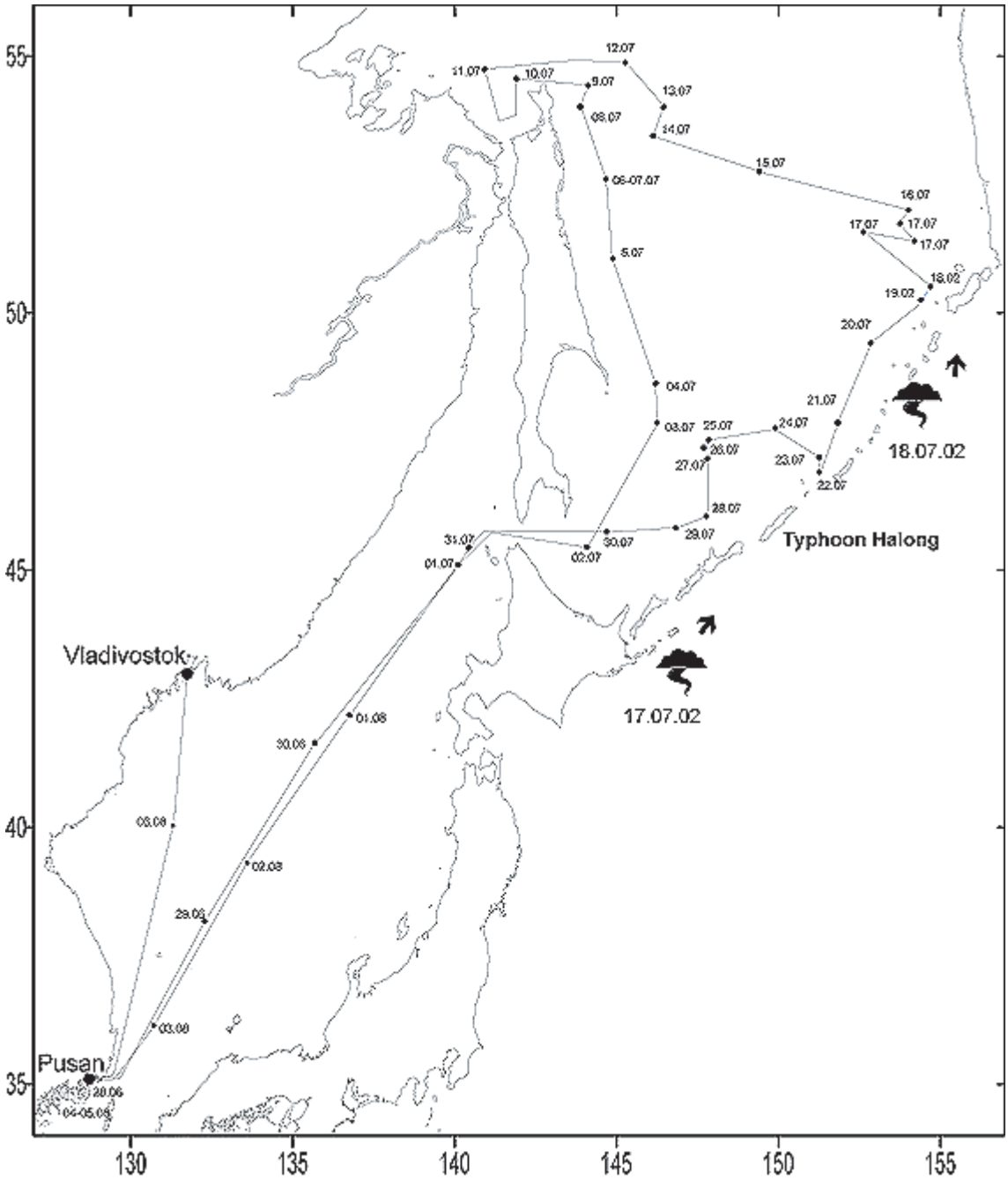

Fig. 1.1: *Ship's track of RV Akademik Lavrentyev 29th cruise, Leg 2, June - August 2002.*

After having finished the sediment core transects, we went around the northern tip of Sakhalin into the Sakhalin Gulf (Amur River estuary) on July 9th in order to take water and sediment samples there. Amur River is the largest source for fresh water and sediment of the Okhotsk Sea and the 4th largest Siberian river. Apart from that, Amur River is the only of the large Siberian rivers which does not flow into the Arctic Ocean. We were mainly interested in the effect the Amur waters have on sea-ice formation and productivity of the Okhotsk Sea. We mapped the area of the Amur River estuary two days and carried out extensive water sampling. The fact that Amur River transports large amounts of sediment into the Okhotsk Sea is visible even from the vessel, because the water here is of brownish color.

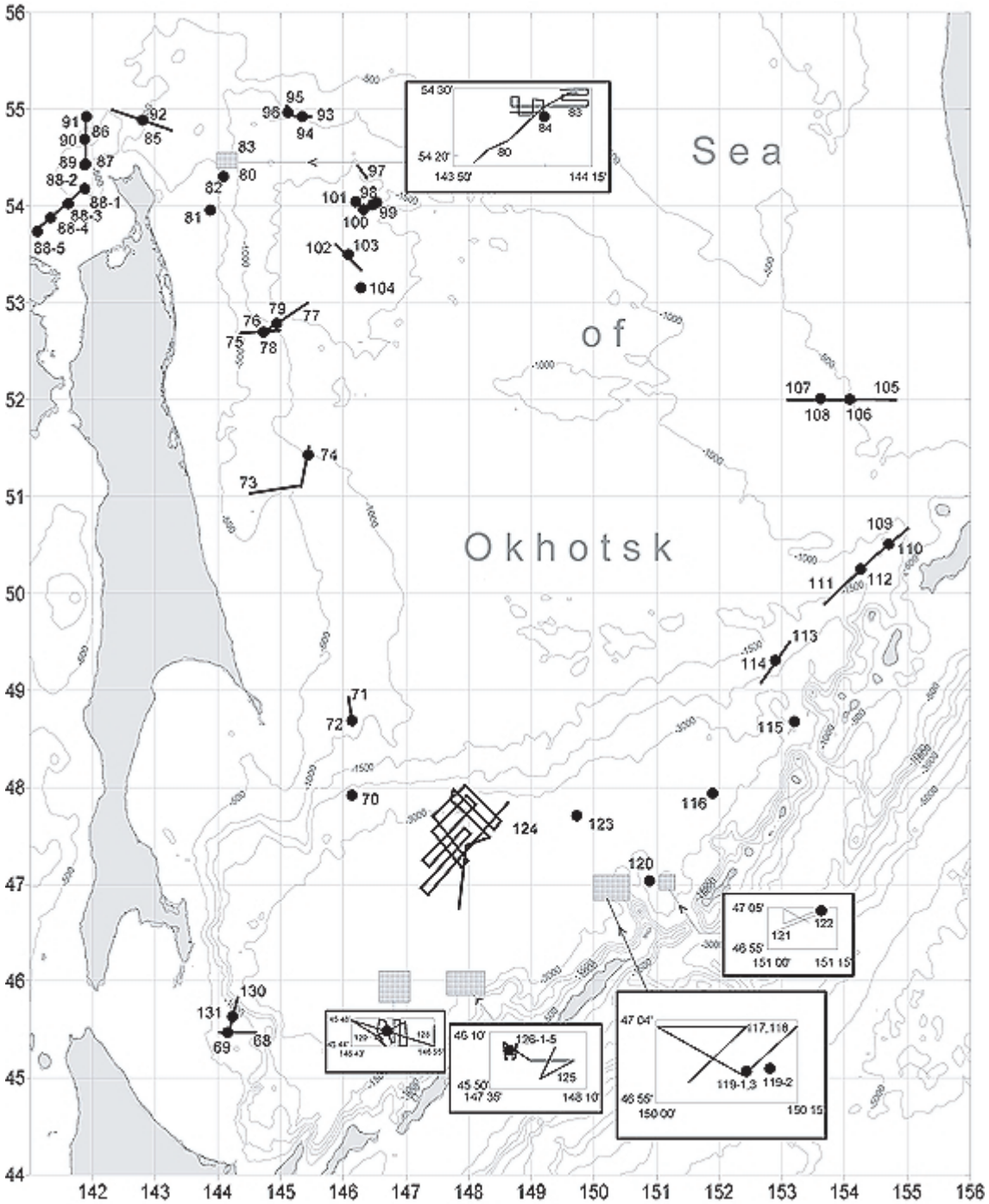

Fig. 1.2: *Locations of stations (filled circles), echosounding and seismic profiles (bold lines) and areas of detailed investigations (shaded rectangles) carried out during the 29th cruise of RV Akademik Lavrentyev, June - August 2002.*

Unfortunately, it quickly became clear that exclusively sand up to coarse gravel is deposited in the Sakhalin Gulf. Our attempts to directly sample the Amur sediments at three stations thus were unsuccessful as the cores could not penetrate the sand layers. We recovered only fist-sized pebbles. Fortunately, the coring equipment was not damaged.

From July 11th to 14th we worked again in the Derugin Basin at 54°00 N/ 146°26 E and sampled with sediment cores and dredges that barite area which we had mapped during the first leg by the video-sled OFOS. On July 13th a dredge recovered barite crusts and living vent clams which were directly conserved in alcohol. On July 14th we finished our work in the northwestern Okhotsk Sea with two stations in the deepest part of the Derugin Basin which is

characterized by a very low oxygen content in the bottom water. For the first time on this cruise, a 15 m long gravity core was successfully deployed. The multicorer, which did not work well up to that time, also worked fine after some modifications. In the evening of July 14th we left for Kamchatka, our next investigation area. We used the 36 hours transit to Kamchatka for an early "half time party" with our Russian colleagues and the crew. In traditional Russian style we celebrated with vodka, sausages and mandolin music until early morning.

On July 16th we reached the coast of Kamchatka and successfully completed the E-W transect begun during LV28 cruise with two coring stations at 500 and 600 m water depth at the continental slope off Kamchatka. Our attempts to core at shallower water depths, however, had to be cancelled, because according to echosounding records the sediment there consists mainly of sands. In the morning of July 17th we were forced to interrupt our program in order to seek shelter from the typhoon Halong coming with 35 knots per hour into our direction. Our attempt to seek shelter from it north of the Kurile island Paramushir had to be cancelled, too, because of a sudden change of direction of the typhoon. We therefore went west into the central Okhotsk Sea. There, we waited for one night at more or less calm sea and could then, in the morning of July 18th, continue our station work west of Paramushir Island. We successfully carried out there sediment, water and plankton sampling at three stations at water depths of 1,000-2,000 m.

After having completed the paleoceanographic work in the eastern part of the Kurile Basin we started dredging at the submarine Browton Ridge. During transit to this area we had a great view on the partly snow-covered volcanoes of the 5 Kurile islands Chirinkotan, Kharinkotan, Shiashikotan, Ekarta and Matua. From the 21st to 22nd of July we carried out volcanologic-petrological works in the Kurile Basin. The main investigation objective was the submarine Browton Ridge spreading from the central part of the Kurile Island Arc about 80 km northwest into the Kurile Basin. The highest rise of the ridge is represented by the small volcanic island Browton, and the submarine part of the ridge is at least partly formed of volcanoes, as well. The origin and the development of this ridge are up to now fairly unknown and probably cannot be explained only by the island arc volcanism of the Kurile Islands. Subsequent to extensive seismic and hydroacoustic mapping, 4 dredging tracks were carried out near Browton Island at the northwestern end of the ridge. This part of the ridge had not been successfully sampled before. During 3 dredging tracks rock material was recovered containing apart from up to 80 cm large dropstones (ice-rafted debris) a large variety of different, mainly old and already consolidated sediments. Additionally, manganese and fossil sponges were often dredged. It therefore can be assumed that the volcanic activity in this region had extincted a long time ago. The sediments will nevertheless allow to determine the minimum age of this structure.
Additionally to the ridge, a neighboring volcano was dredged, too. Due to the fact that also here only old sediment was recovered the dredging was cancelled in order to be continued subsequent to the planned seismic mapping at submarine volcanoes in the southwestern Kurile Basin.

On the way to the central Kurile Basin we sampled the deepest station of this cruise with 3,500 m water depth with the CTD, the plankton net and the multicorer. The oxygen anomaly in the bottom waters which had already been discovered on the MV *Marshal Gelovany* cruise in 1999 and which probably yields the influence of Pacific water masses could thereby be confirmed.

From July 24th to 27th we mapped the northern connection and transition of the spreading ridge discovered on the SAKURA cruise in 1999 to the continental slope in the central Kurile

Basin with seismic profiles. To our great delight the discovery of 1999 could be confirmed by the new profiles. Of special interest was the transition from the ridge to the northern slope of the Kurile Basin, because we found there an extensive zone of submarine volcanism. The discovery and confirmation of a spreading ridge in the Kurile Basin means that the basin did not, as formerly assumed, open in NW-SE direction as a consequence of the sinking of the Pacific plate under the Kurile Island Arc, but in E-W direction as a kind of "pull-apart" basin.

From July 28th to 29th we continued volcanologic-petrological investigations at Hydrographer Ridge and Loskutov seamount northwest off the Kurile island Iturup. These both submarine, up to 1,600 m high mountains are partly of volcanological origin and had so far not been investigated in detail. In total, 9 dredge tracks were carried out subsequent to hydroacoustic and seismic mapping. Apart from different kinds of sediment and dropstones (ice-rafted debris), fragments of submarine lava flows (pillow lava) were thereby recovered at Hydrographer Ridge. The little alteration of these basalts and basaltic andesites and their high content of different minerals allow extensive lab analyses by which we hope to gain interesting information about the origin of these volcanoes as well as about the structure of the Kurile Basin.

The last station of this cruise was carried out on July 30th in La Perusa Strait. There, the water and the sediment were once more sampled. We successfully deployed an 18 m long gravity core for the first time on this research vessel and thus broke our own record set in 1998.

On the evening of June 30th, RV *Akademik Lavrentyev* started its way back to Pusan. We used the transit for taking last samples, packing the equipment and writing cruise reports. In the night from August 1st to 2nd the ship stopped for several hours for fishing squid.
The very last station was then carried out on August 2nd at 4 p.m. local time in the Japan Sea at 39.19.9 N/ 133.28.03 E. To our great delight we were allowed to go once more offboard and take a bath in the ocean at 1,286 m water depth and a water temperature of 24°C. In the evening of the same day we were invited by our Russian colleagues to a farewell party with vodka, snacks and dancing until early morning.

Altogether, 131 stations were successfully carried out during the whole cruise LV29. Thereby, no equipment was lost and no banana recovered. The second part of the cruise was especially a great success for our colleagues from Rostock University who got to know during one of the last deployments of the sediment echosounder in the deep Kurile Basin that their echograms record a seafloor penetration of about 10 m at 3,200 m water depth. At the beginning of the cruise they had expected that the sediment echosounder can be deployed only up to 2,000 m water depth.

RV *Akademik Lavrentyev* arrived in Pusan in the evening of August 3rd. The next morning, a pilot was taken aboard and we proceeded into the port of Pusan and tied up at pier at 7:00 am local time. During daytime the German equipment was unloaded and the German scientists left the ship in the same evening. On August 5th RV *Akademik Lavrentyev* left Pusan again and made is way to Vladivostok harbor, where it tied up on August 7th.

2. HIGH-RESOLUTION ECHOSOUNDER PROFILING ON LV29 – TECHNICAL ASPECTS

Jens Wunderlich

2.1 Echosounders for high-resolution subbottom profiling

Echosounders for acoustic subbottom profiling use sound pulses generated by electrical transducers and send them to the seafloor. The seafloor and sediment layers reflect the sound waves. These reflections are received by the echosounder device, and an echo print is calculated. To get echo prints with high vertical and horizontal resolution the echosounding equipment should fulfill the following requirements:

- A narrow sound beam is needed to hit only a small part of the seafloor.
- If only one frequency is used, the sounded bottom area should be equal in size independent from the transmitted frequency.
- The transmitted sound pulses should be as short as possible without ringing.
- The use of stacking algorithms for enhancing the signal to noise ratio (SNR) requires high repetition rates.
- Beam stabilizing and steering as well as heave compensation is useful especially at greater water depths.

2.2 Linear and non-linear acoustics

Sediment echosounders use two different ways to generate the sound pulse, linear or non-linear (parametric) acoustics.
Linear echosounders generate the sound pulse of the desired frequency directly. The directivity depends on the ratio of the transducer dimension and the signal frequency. Therefore, a narrow beam at low frequencies requires large transducers. But such transducers are heavy and expensive.
Parametric echosounders transmit two signals of slightly different high frequencies at high sound pressures (primary frequencies f_1 and f_2). Because of non-linearity's in the sound propagation in the water column at high pressures, both signals interact and new frequencies arise. The difference frequency ($\Delta f = f_2 - f_1$) is low and penetrates the seafloor. The primary frequencies may be used for exact determination of water depths even in difficult situations, e.g. soft sediments.

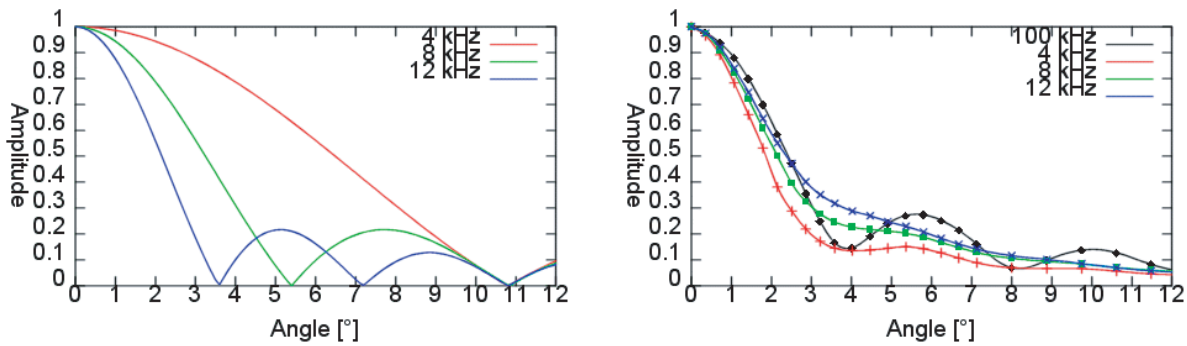

Fig. 2.1: *Beam pattern for linear (left) and parametric transducer at different frequencies.*

Parametric systems have a small beam width in spite of small transducer dimensions independent of the difference frequency. The beam width only depends on the primary frequency related to the transducer aperture, even for the secondary frequency. There are no significant sidelobes and you will get a constant directivity for different secondary frequencies. Therefore, the size of the sounded area is independent of the frequency used for bottom penetration.

Figure 2.1 shows in the right subfigure experimental data from a parametric transducer array with an active sound area of about 0.2 m x 0.2 m. All difference frequencies between 4 and 12 kHz (ratio 1:3) have nearly the same half power beam width as the primary frequency of about 100 kHz. The left subfigure shows the computed directivity of a linear transducer that is 10 times larger (2 m x 2 m). In this case, different radiated frequencies have different half power beam widths. Therefore, the sounded area will not be the same at different frequencies, and the echo prints cannot be compared.
The high bandwidth of parametric systems allows to generate very short sound pulses without ringing for a high vertical resolution.

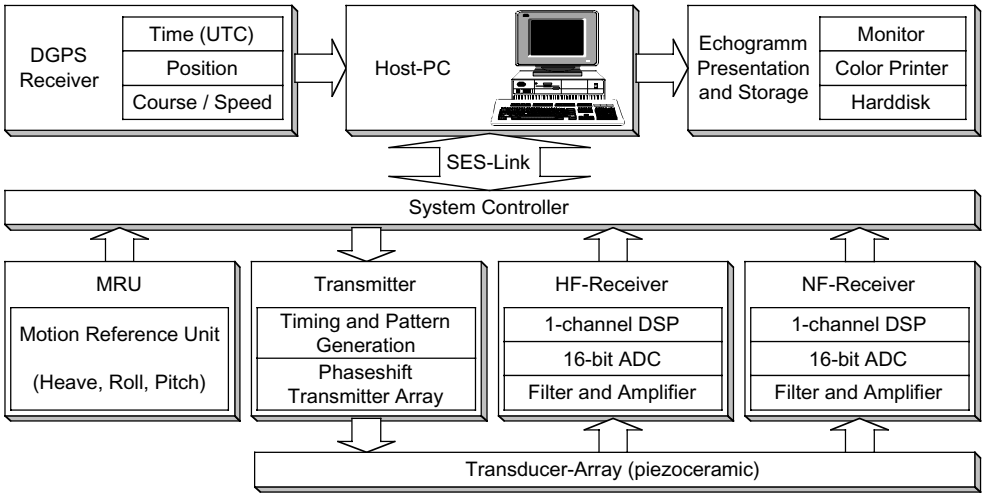

Fig. 2.2: *SES-2000 system architecture.*

2.3 Parametric Sediment Echosounder System SES-2000DS

During cruise LV29 the sediment echosounder system SES-2000DS, developed by the research group of underwater acoustics of the Rostock University, was used. The echosounder system SES-2000 was originally designed for shallow water to detect small buried objects and sediment structures at high three-dimensional resolution. The system was optimized to improve the power for greater water depths (SES-2000DS).
The echosounder system SES-2000DS consists of a main device, a host PC and a transducer array (*Fig. 2.2*). The main device comprises integrated transmitters, receivers and modules for analog and digital real-time signal processing. Analog to digital converters (ADC) are used for digitizing the receiver signal with 16-bit resolution at sampling rates of up to 200 kHz depending on the signal bandwidth.
A special link module connects the echosounder main device to the PC which is used for system controlling and data display. All received data are stored digitally on harddisk including GPS data and other important system parameters. The echosounder file format is device-specific, but may be converted into the standard SEG-Y format for postprocessing using conventional equipment. Analog data storage on a DAT-recorder is also possible, but was not used on cruise LV29.

Sound pulses are generated by a small piezoceramic phase shifted transducer array with 32 separately controlled elements (32 x 1 matrix). Electronic beam stabilizing and steering is possible in roll direction. Thus, all the ship movements are detected by a motion reference unit (MRU). This sensor, made by SEATEX (Norway), outputs the absolute roll, pitch and yaw, and dynamic heave. Roll and pitch values are used for electronic beam stabilizing. Echo prints are heave-compensated using the MRU heave value.

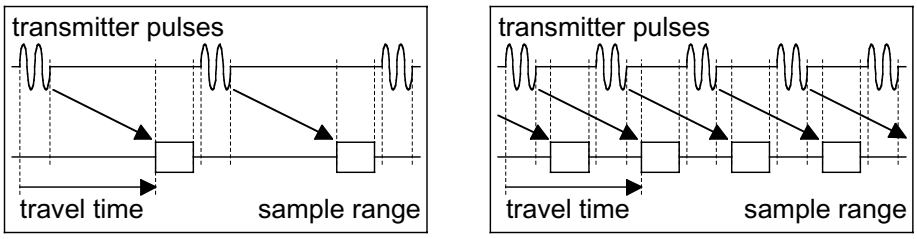

Fig. 2.3: *Transmitter regime at shallow water (left) and deep sea.*

High repetition rates are used to improve the signal to noise ratio and to raise the degree of probability to find small single objects and small bottom structures. At greater water depths a special regime is used to get higher repetition rates (*Fig. 2.3*).
A color echo print is generated immediately using 12 colors at a logarithmic scale. The echo print includes all important parameters, e.g. GPS position, time (UTC), pulse frequency, pulse length and echo stacking rate. All transmitter and recording parameters are controlled by software, designed for this purpose.

Table 2.1: *SES-2000DS main parameters.*

Water depth range	0.5 ... 3,000 m
Vertical resolution	up to 6 cm
Penetration depth (near the bottom surface)	up to 50 m
Transmitter power (electrical pulse power)	> 32 kW
Primary transmitter frequency	about 100 kHz
Secondary transmitter frequencies	4, 5, 6, 8, 10, 12 kHz
Transmitter pulse length	0.08 ... 1 ms
Repetition rate	1 ... 100 s^{-1}
Beam width	±1 x 2 deg @ 4...12 kHz
Beam steering range	± 16 deg roll
Transducer principle	piezoceramic
Separately controlled transducer elements	32
Transducer dimensions	ca. 20 x 40 cm^2
Transducer weight (in air, incl. 40 m cable)	ca. 70 kg

2.4 Installing the echosounder equipment

The echosounder equipment was installed on transit from Pusan to the working area. There is no hydroacoustic shaft available on RV *Akademik Lavrentyev*. Therefore, the transducer had to be mounted at the ship's hull using a long pipe (*Fig. 2.4*). Because of the high freeboard, there was no possibility to fix the mounting pipe near the water surface. This caused a lot of vibrations and noise. After the first profile, the mounting construction was slightly modified, and less noise was produced by the transducer itself. Good echo prints were produced up to a ship's speed of about 5 knots at calm sea.

Mounting the transducer inside an acoustic shaft would give a lot of advantages like less noise and the ability to use the echosounder all day, even during transit and at higher speed.

Fig. 2.4: *Pipe.*

2.5 Results

Profile data with a total length of about 480 nm (890 km) was produced. Echo print examples are shown in *Figures 2.5-2.7*. Depth values were computed from travel times assuming a constant sound velocity of 1,500 m/s. Variations of sound velocity due to water temperature, pressure or salinity were not taken into account. The data was plotted time-sequentially from the left to the right. Heave components were removed from the echo prints by an enhanced algorithm using the heave data delivered by the MRU.

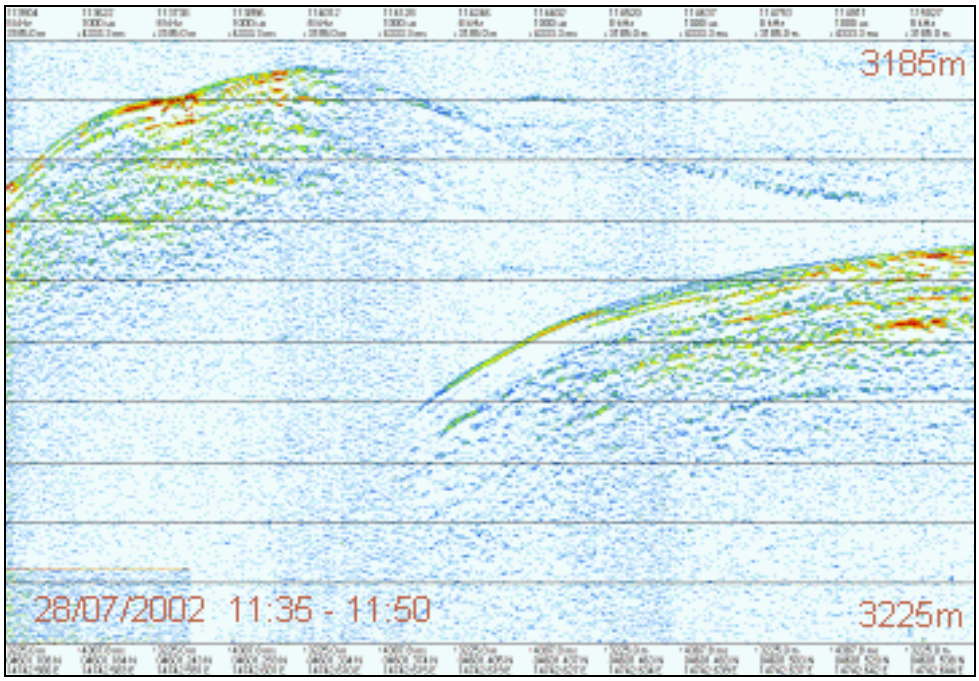

Fig. 2.5: *Echoprint example (Range 2,185 m … 3,225 m; Frequency 8kHz / 1ms).*

All received signals were stored digitally on a harddisk together with the GPS data and system parameters. The total volume of digitally stored echosounding information is about 8.8 GB.

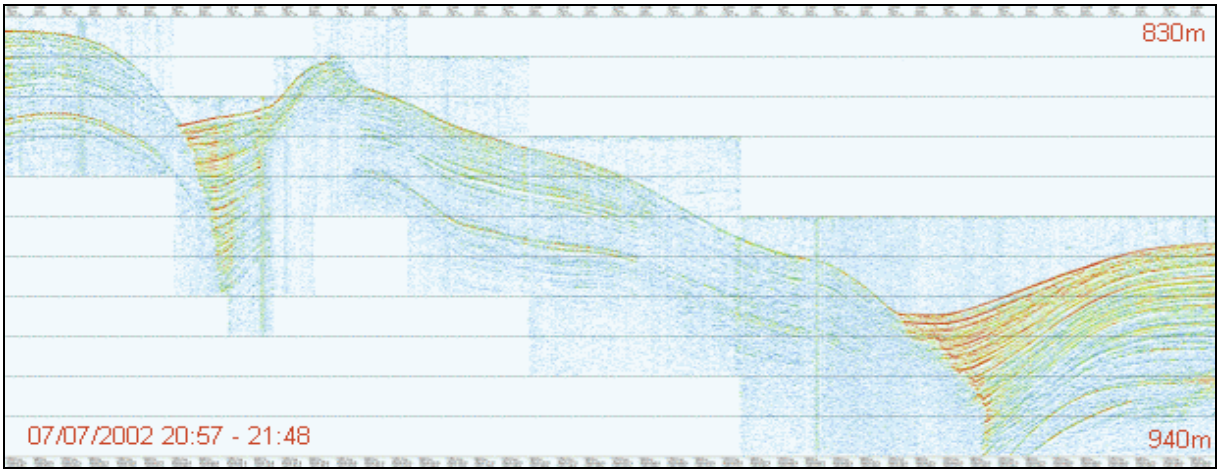

Fig. 2.6: *Echoprint example (Part of profile 7; Range 830 m … 940 m; Frequency 8kHz / 0.75ms).*

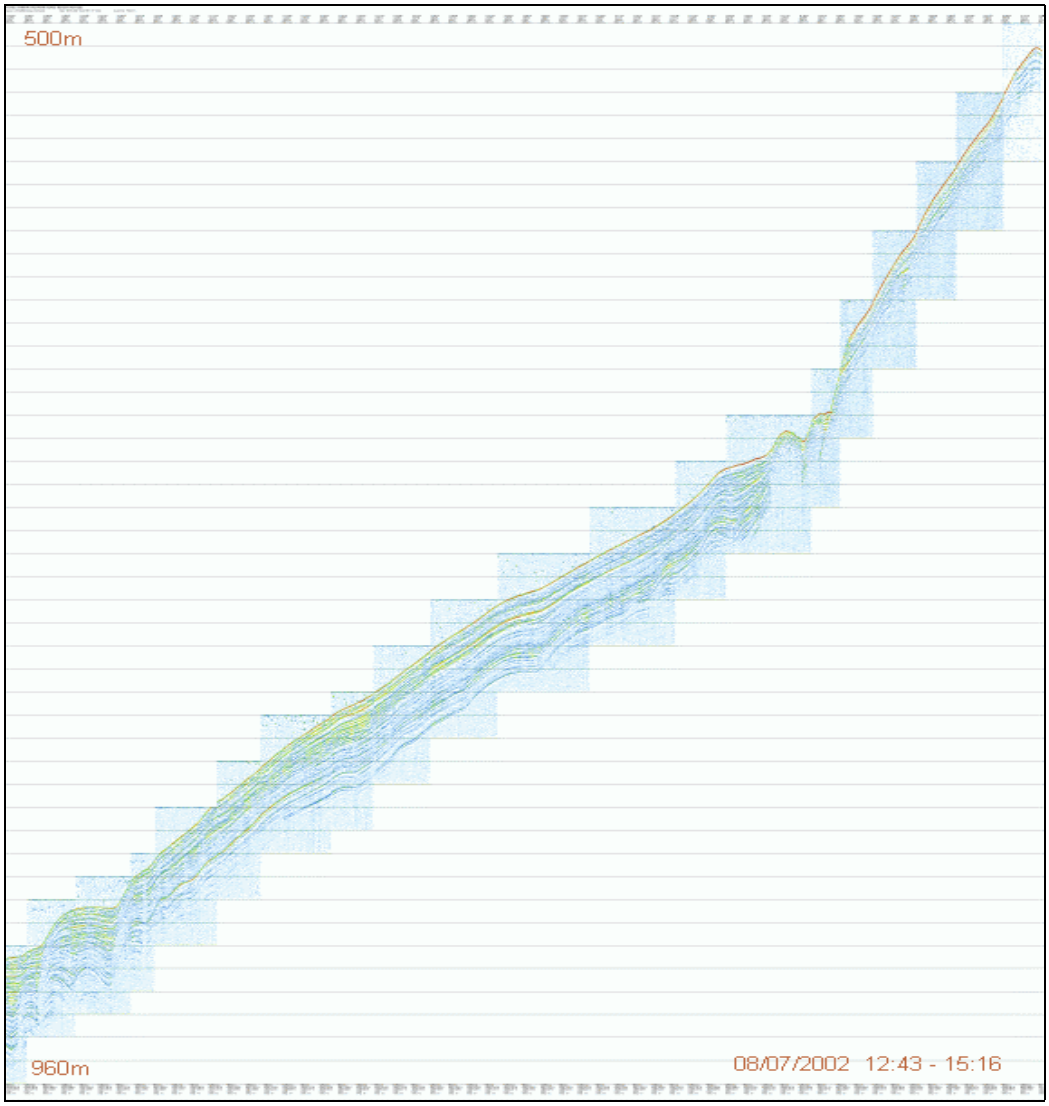

Fig. 2.7: *Echoprint example (Profile 14; Range 500 m … 960 m; Frequency 8kHz / 1ms).*

The investigated area included different regions with water depths between 50 m and 3,200 m. This means that there were very different conditions for applying the echosounder system. Different frequencies were used under varying conditions. Best results were received using 8 kHz especially at greater water depths. This frequency gave good penetration and good resolution and caused no additional noise at the ship's echosounder (ELAC) which operates at 12 kHz.

Tests showed that good echo prints are produced up to water depths of about 3,200 m assuming nearly flat bottom (*Fig. 2.5*). At water depths of about 700-1,500 m the SES-2000DS achieved a penetration up to 40 m. Even at steeper slopes a penetration of about 10-20 m was possible (*Fig. 2.6*).

The results at the slopes could be improved if beam steering was possible not only sideways but also in forward and backward direction. For this purpose, greater transducers are necessary which cannot be mounted at a pipe like on LV29, but they could be placed easily inside a hydroacoustic shaft. This would also lead to greater acoustical power available, and therefore the water depth range could be increased. The SES-2000DS echosounder system can be adopted in this way.

3. RESULTS OF HIGH-RESOLUTION SUBBOTTOM PROFILING

Thomas Lüdmann

For the detection of the uppermost strata of the sedimentary column a high-resolution subbottom profiler (SES-2000DS) from the University of Rostock was used. The main purpose of its deployment was to support the sediment sampling program by finding appropriate coring stations. In general, the device achieved a penetration of 30-25 m with an average resolution of ca. 25 cm depending on the selected frequency and pulse length of the source signal. During the cruise, 36 profiles with a total length of ca. 860 km were obtained (*Fig. 3.1*).

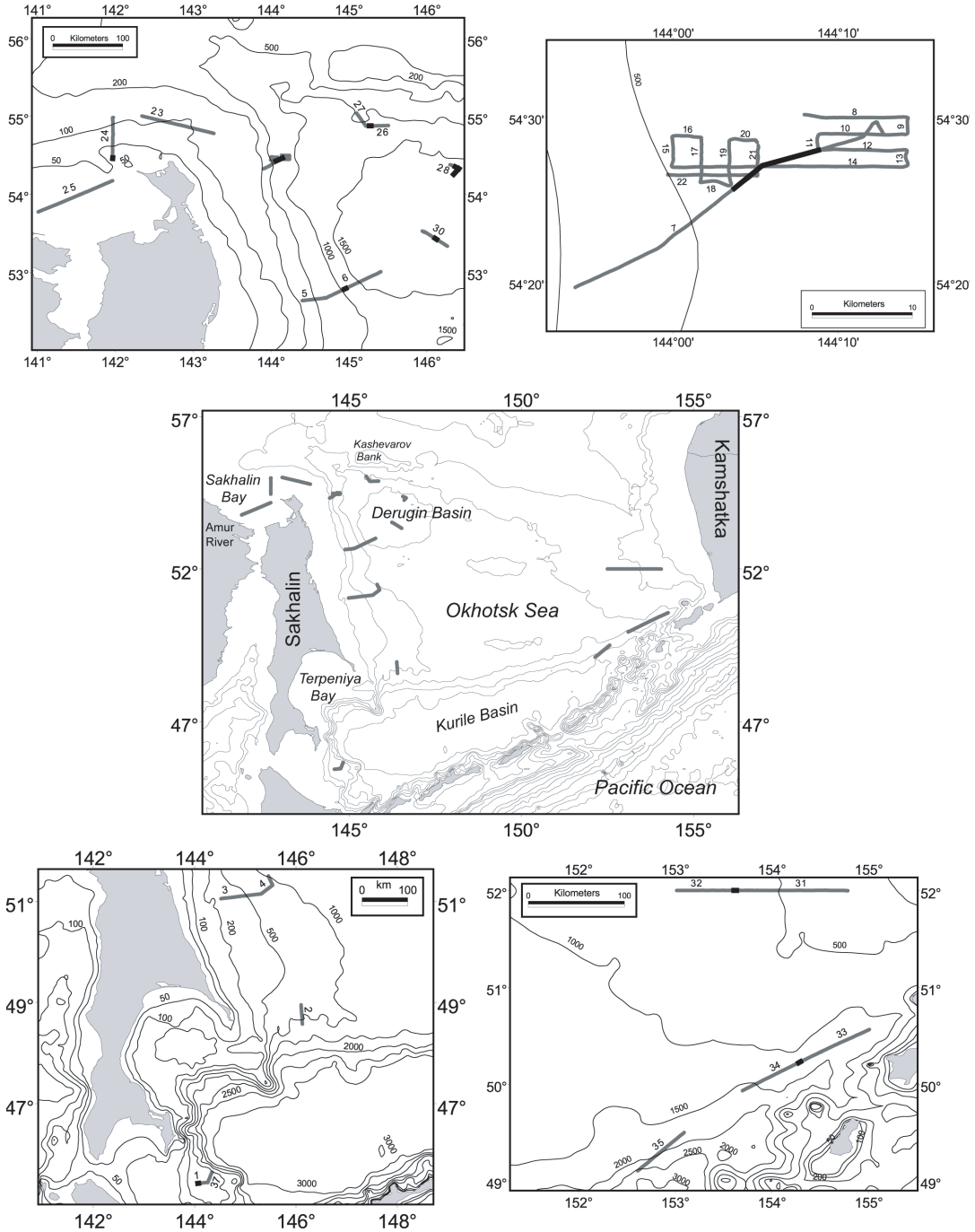

Fig. 3.1: *Maps exhibit the location of track lines (gray lines) of the sediment echosounder SES-2000DS. Black lines mark examples of profiles.*

A seismic facies analysis of the high-resolution reflection data allows to characterize the depo-environment and lithofacies of the sediments. Seismic reflection termination and configuration can be interpreted as stratification pattern of the depositional sequences. Hence, the attempt was made to use the amplitude, continuity and frequency information of the reflections in order to correlate the echograms with the lithology of the sediment cores (Payton, 1977; Emery & Myers, 1996). Therefore, we chose 6 locations which represent different types of depositional environments: La Perusa Strait, the central East Sakhalin continental slope, Sakhalin Gulf in the vicinity of the Amur River mouth, the North Okhotsk continental margin, the central Derugin Basin, the continental slope of southwestern Kamchatka and the slope of the Kurile back-arc basin.

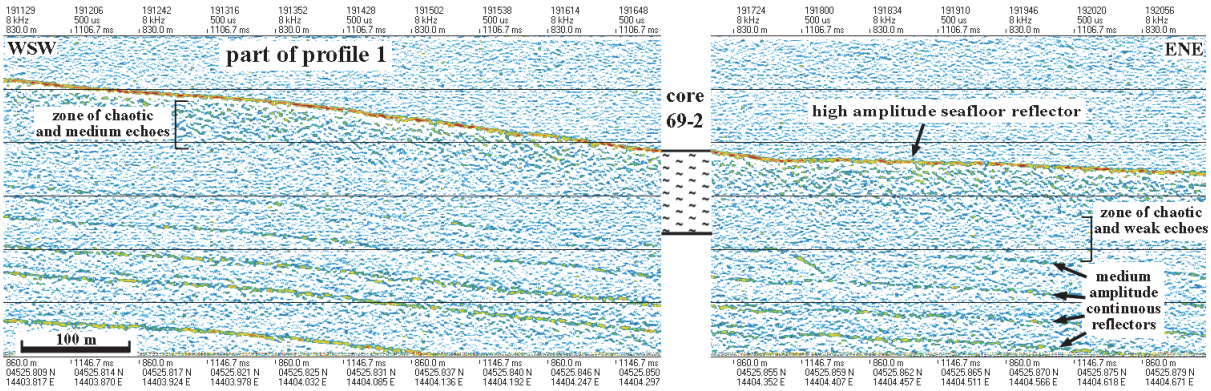

Fig. 3.2: *Part of subbottom profiler profile 1 (see Fig. 3.1 for location) near La Perusa Strait. Indicated is sediment core station LV29-69-2 (see Appendix 6 for detailed description) which is mainly composed of clay (see text for discussion).*

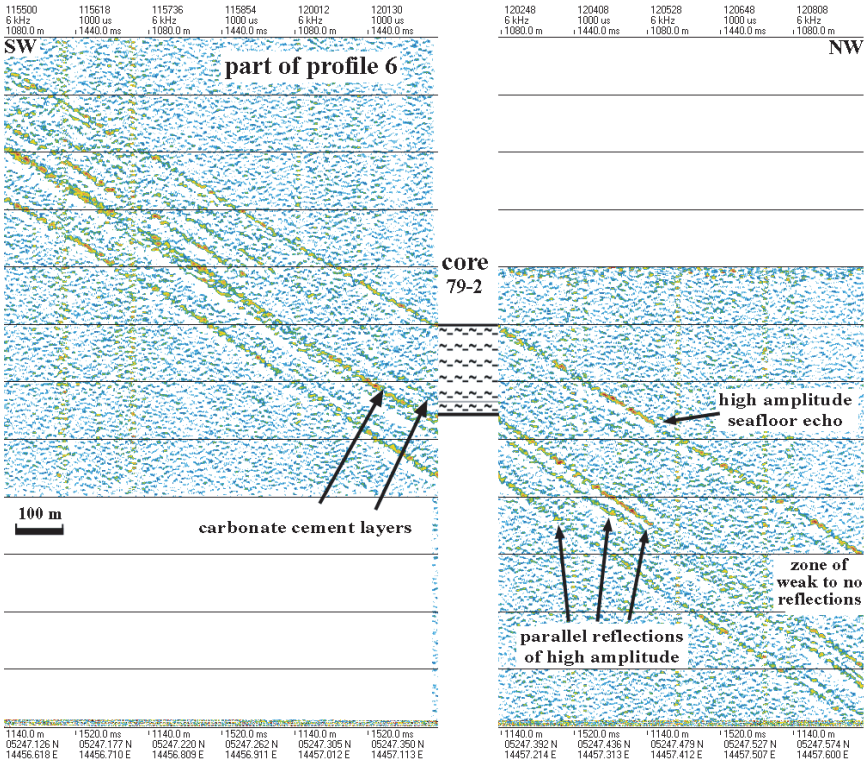

Fig. 3.3: *Part of sediment echosounder profile 6 (see Fig. 3.1 for location) at the central East Sakhalin slope. Sediment core station LV29-79-2 (see Appendix 6 for detailed description) is shown. The core is composed of silty clay, incorporated are layers of carbonate cement (see text for discussion).*

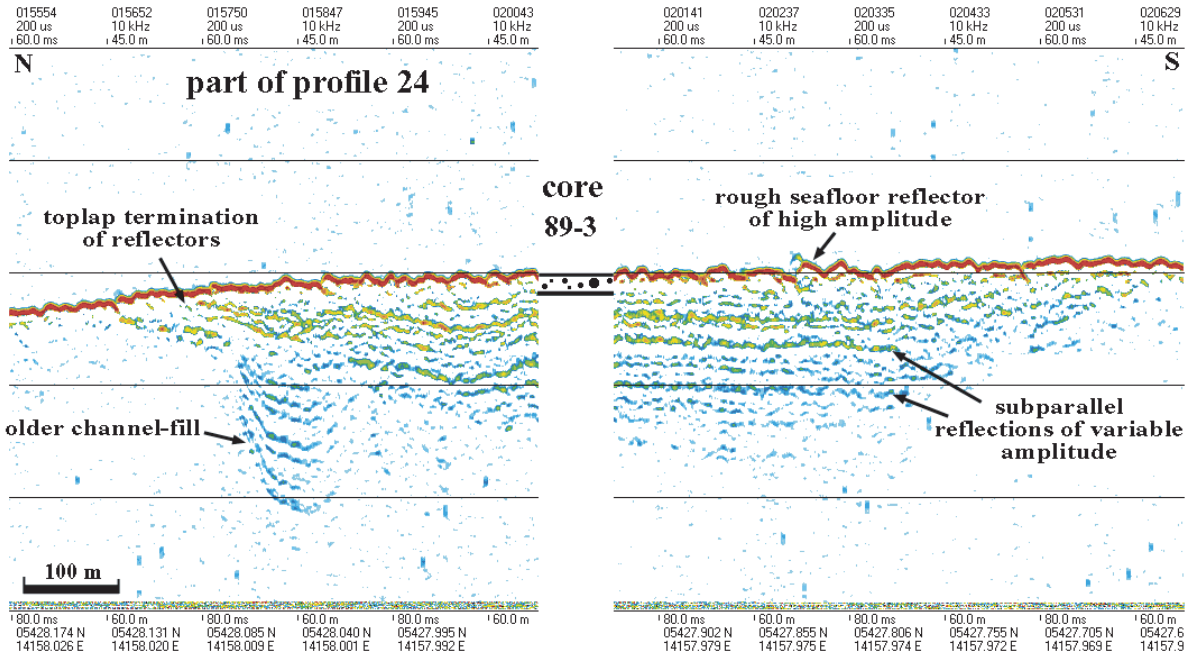

Fig. 3.4: *Part of subbottom profiler profile 24 (see Fig. 3.1 for location) in the Sakhalin Gulf near the Amur River mouth. Sediment core station LV29-89-3 (see Appendix 6 for detailed description) is indicated. The core is mainly composed of clay (see text for discussion).*

Gravity core LV29-69-2 (see Appendix 6 for detailed core description) was taken approximately 156 km eastward of La Perusa Strait at a water depth of ca. 868 m. The echogram at the coring station (*Fig. 3.2*) exhibits a strong seafloor reflector followed by a succession of subparallel reflectors of medium amplitude and high continuity. Intercalated are sections of apparent chaotic reflections of low amplitude and low continuity. Since this pattern is comparable to that of the background noise (see seismic signal above the seafloor, *Fig. 3.2*), it is only an effect of high signal amplification and therefore these zones should be correctly described as more or less reflection-free or transparent. The upper zone of structureless and weak reflectors directly beneath the seafloor has a thickness of 8-9 m, whereas the lower ones range between 2-5 m. Their internal reflection configuration points to layers which might be too thin to be seismically resolved or layers of the same lithology accumulated under uniform energy. The lithology of core LV29-69-2 supports the second interpretation, because the entire core is mainly composed of clay with increasing density downcore. The thin subparallel reflectors inserted below ca. 9 m are possibly attributed to beds of relatively coarse material. The carbonate concretions which are located in a core depth of ca. 650 cm are seismically not resolved. There is not a significant reflection at this depth. The high amplitude of the surface reflection is possibly due to the dispersed gravel in the surface layer. The subparallel reflections of medium amplitude below ca. 8.5 m might be due to thin sand-rich layers intercalated into the fine mud-rich hemipelagic sediments (see core LV29-69-3, Appendix 6).

The lower slope of central East Sakhalin in a water depth of ca. 1,100 m is characterized by parallel reflectors of high amplitude and high to medium continuity (*Fig. 3.3*). They are separated by segments of 1-3 m in thickness with weak to no reflections. A correlation of the seismogram with the lithology of sediment core LV29-79-3 demonstrates that the zones of weak echoes are related to the silty clay deposits and the high amplitude reflections are generated by dense carbonate cement beds (gray line in *Fig. 3.3* at ca. 686 cm and at the bottom of the core section at 780 cm).

In general, a high-amplitude bottom reflection with weak or no subbottom signals is characteristic for the shallow water (ca. 50 m) area of the Sakhalin Gulf (*Fig. 3.4*). Here, close

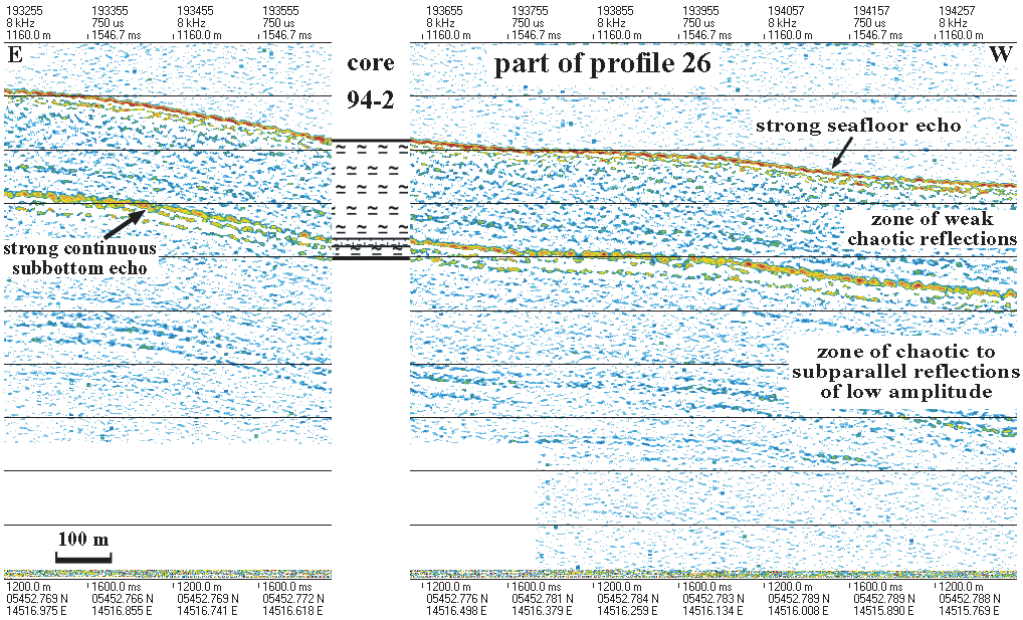

Fig. 3.5: *Part of subbottom profiler profile 26 (see Fig. 3.1 for location) at the North Okhotsk continental margin. Sediment core station LV29-94-2 (see Appendix 6 for detailed description) is shown. The core is mainly composed of clayey silt (see text for discussion). Strong parallel reflections might be generated by a prominent lithological change (see text for discussion).*

to the depo-center of Amur River, the uppermost strata consists mainly of coarse material. Samples of the surface sediments reveal unsorted clasts from fine sand to coarse gravel (core LV29-89-3). *Figure 3.4* shows one of the few places where pockets of well stratified sediments occur. The subparallel reflection of variable amplitude and medium continuity have a spacing of 50-30 cm. At the rim of the pocket the reflectors terminate with toplap against the surface layer indicating their former erosion. The channel-fill-like structure has a width of 1 km and a depth of 5 m. At the northern rim of the pocket a smaller channel filled with ca. 3 m of sediments is unconformably overlaid.

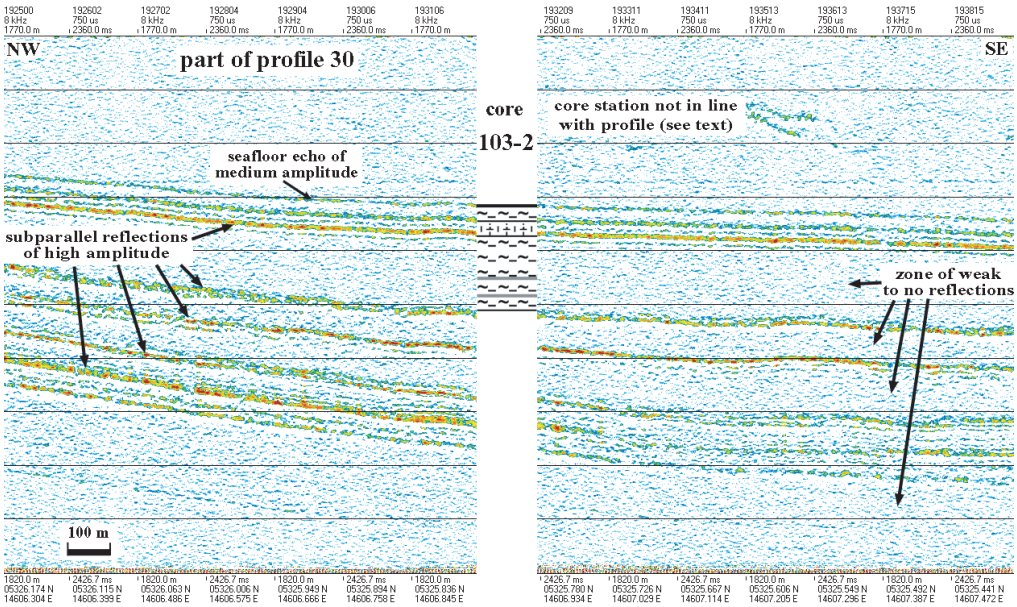

Fig. 3.6: *Part of sediment echosounder profile 30 (see Fig. 3.1 for location) in the central Derugin Basin. Sediment core station LV29-103-2 (see Appendix 6 for detailed description) is indicated. The core is mainly composed of silty clay with two turbiditic layers (gray lines) near the base (see text for discussion).*

It may represent an older channel which was later truncated by the upper broader channel. The internal reflection pattern of the sediment pocket is typical for a fluvial environment of variable energy.

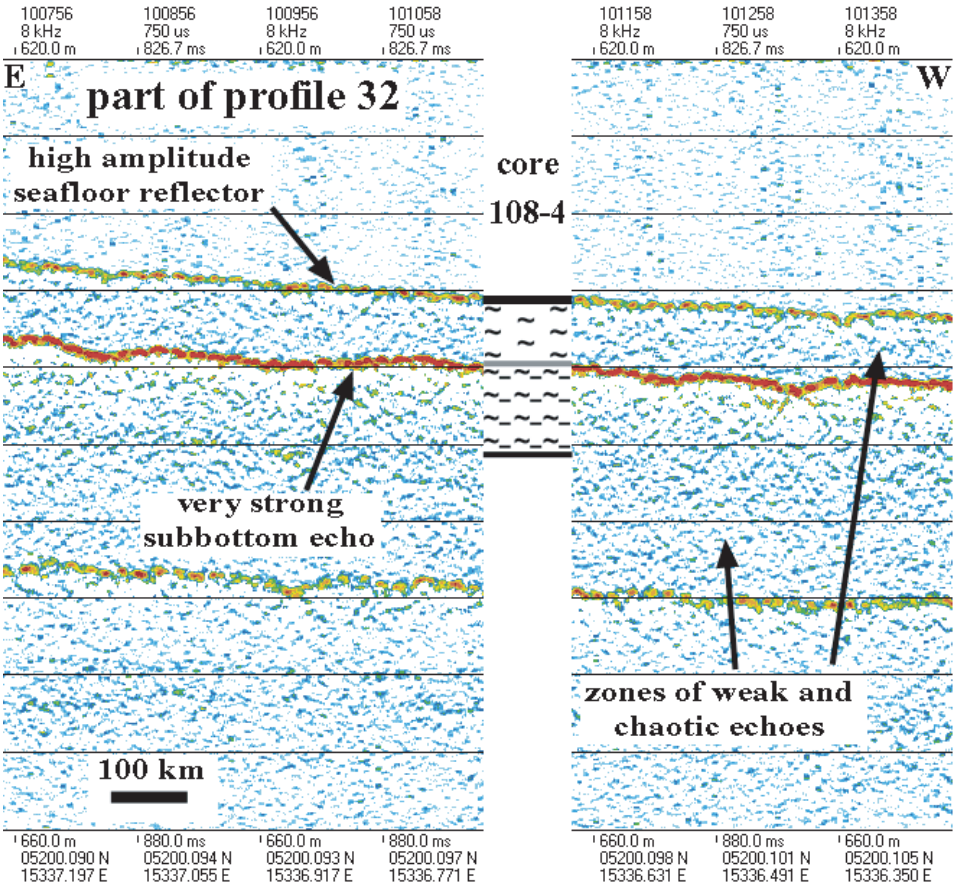

Fig. 3.7: *Part of subbottom profiler profile 32 (see Fig. 3.1 for location) at the lower slope off southwestern Kamchatka. Sediment core station LV29-108-4 (see Appendix 6 for detailed description) is shown. The core is mainly composed of silty clay and an ash layer at about ca. 315 cm (gray line) which is seismically expressed by a subparallel very high amplitude reflection (see text for discussion).*

The seismic image from the lower slope of the North Okhotsk continental margin south of the Kashevarov Bank (ca. 1,170 m, *Fig. 3.5*) illustrates a section of about 25 m with parallel reflections interbedded by broad zones (ca. 8 m) of weak echoes. The surface reflector exhibits a strong amplitude which assigns to coarse bottom sediments of a sandy silt composition with dispersed pebbles and sand lenses (core LV29-92-2 in *Fig. 3.5*, see also Appendix 6). Chaotic reflections of low amplitude characterize the subjacent zone with several discontinuous subparallel reflectors at its base. Subsequently a 2 m thick band of medium amplitude reflectors occur, followed by a zone of weak chaotic to subparallel echoes. The chaotic reflections correspond to clayey silt layers intercalated by a 10 cm thick layer of clay-silt-sand material with lenses of pebbles and sand. This lithological change produced a strong subbottom echo at ca. 740 cm (*Fig. 3.5*).

Profile LV29-30 located in the central Derugin Basin (*Fig. 3.6*) shows a pattern of several continuous parallel surface reflectors of medium amplitude comprising the topmost 3 m of the deep-basin deposits. Below these layers, a more or less transparent zone with a thickness of ca. 7-8 m occurs. It is replaced downwards by an alternation of parallel reflectors of medium amplitude and zones with weak or no echoes of 2-3 m thickness. The weak seafloor reflection may be due to the soft silty clay which thereafter pass into sandy silty clay with dense green diagenetic interlayers at ca. 150 cm, producing parallel high-amplitude reflections. The

subsequent silty clay deposits (from 286 cm to the bottom of the core) are seismically not expressed, whereas the two turbiditic sequences (at ca. 685 and 850 cm) are marked by prominent reflections. Unfortunately, the core station is located more to the west, beside the seismic track, therefore the correlation especially of the turbiditic layers with the observed strong subbottom reflectors seems to be questionable. However, the seismic profile shows (*Fig. 3.6*) that the sediment section above these reflectors markedly thins to the northwest and that they become shallower.

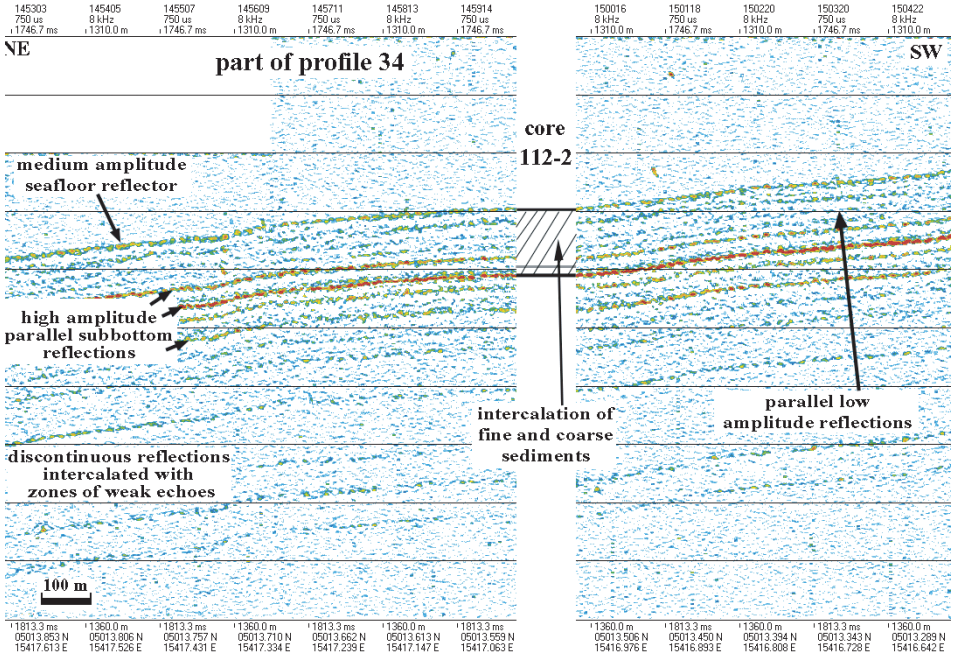

Fig. 3.8: *Part of sediment echosounder profile 34 (see Fig. 3.1 for location) west of Paramushir Island near Fourth Strait. Sediment core station LV29-112-2 (see Appendix 6 for detailed description) is indicated. The core consists of an intercalation of fine and coarse sediments (parallel low-amplitude reflectors) and ash layers (gray line, strong parallel echoes) (see text for discussion).*

At the lower slope off southwestern Kamchatka (ca. 630 m, *Fig. 3.7*) undulating continuous isolated reflectors with medium to high amplitude appear. They are separated by thicker zones of weak chaotic echoes. 3-4 m below the seafloor a subbottom reflector with a remarkable high amplitude occurs. This reflector represents a volcanic ash layer (core LV29-108-4, see Appendix 6 for detailed description) which is characterized by a marked density contrast of the volcanic minerals to the neighboring silty to clayey sediments. The zone of weak and chaotic echoes reflect the more or less homogeneous clayey sediments.

The echogram west of Paramushir Island near Fourth Strait (*Fig. 3.8*) reveals a series of subparallel wavy reflections with a wave length of ca. 500 m and an interval of about 1 m. They comprise the uppermost 15 m of the sedimentary column. Below it, reflectors of medium amplitude occur intercalated with zones of very weak echoes. The parallel low-amplitude reflections (*Fig. 3.8*) correspond to an alternating lithology of fine and coarse sediments (core LV29-112-2, see Appendix 6 for detailed description). High amplitude subbottom echoes are probably generated by volcanic ash layers.

In summary, the seismic facies analyses demonstrate that the zone of weak to no echoes correspond to more or less homogeneous fine sediments. In the Okhotsk Sea, this sediment type is represented mainly by silty to clayey hemipelagic deposits at the continental slopes and in the deep basin. Reflectors of high amplitude and continuity correspond to volcanic ash layers or to carbonate-cemented sediments. Near the Kurile Islands, the seismogram is dominated by parallel reflectors which indicate a more variable depo-environment with an alternating input of fine to coarser material and volcanic ashes.

4. WATER COLUMN STUDIES

Anatoly Salyuk, Valery Sosnin, Anatoly Obzhirov, Galina Pavlova, and Nicole Biebow

4.1 Introduction

Water column sampling was carried out using a rosette water sampling system consisting of a Sea-Bird-32 twelve position system with Niskin Bottles (10 l) and CTD probe Sea-Bird-911 with standard temperature, pressure, conductivity sensors and also sensors for oxygen light transmission, altimeter and bottom contact. The CTD was lowered to 3 m above the seafloor at stations shallower than 100 m and to 8 m at deeper ones. Water sampling was started at maximum depths and the samples were taken during upcasts. The interval of water sampling depended on the purpose of investigation, and the water depths varied during observations from 5 to 500 m.

A total of 29 stations were carried out during Leg 2 of LV29. Water samples were collected for pH, alkalinity, methane, δO^{18} and δC^{13} isotopes, calcium, and deuterium. All data is tabulated in Appendix 3.

The second leg started under conditions of unusually active tropical cyclones. They came one by one from the tropics to East Asia and the Japan Islands. Such an unusual early beginning of the typhoon activity in Asia is in good agreement with an anomaly in the atmospheric circulation of the Northern Hemisphere this year. But only one of the typhoons (“Halong”, July 17th-18th, 2002) passed just through the Kurile Islands and disturbed routine observations. So, in spite of the cyclonic activity far south, a high atmospheric pressure field predominated over the Okhotsk Sea and in general weather conditions were convenient for all kinds of observations.
Ice conditions in the sea have changed and the sea-ice fields in the Tugur area disappeared after July 5th. Sometimes ice conditions in the Tugur region remain until August.
During this stage of the expedition oceanographic observations were carried in the NW Sakhalin area (Sakhalin Gulf), in the deepest part of the Derugin Basin, West Kamchatka and the Kurile Basin.

4.2 Amur River and NW Sakhalin area

The region is characterized by shallow water depths. The minimum depth of observations was 22 m in the mouth of the Sakhalin Gulf. The salinity field in the gulf is strongly influenced by the Amur River outflow (16.91 at the sea surface of station LV29-88-1). Amur River plays an important role in delivering dissolved and suspended organic matter into the western part of the Okhotsk Sea. Due to this, the water color was dark green and even black. There were a lot of ground-grown grasses at the sea surface. The light transmission of the water column was the lowest for all observed areas. Besides the suspended material, we suppose the Amur outflow to be responsible for the appearance of the methanotrophic but pathogenic bacteria *Listeria monocytogena* in the western part of the sea and around Northeast Sakhalin.
The vertical structure of the water column consists of two layers. An upper warm layer with a temperature up to 12.89°C is located in the uppermost 10 m and is divided from the lower one by a very sharp thermocline and strong halocline. The properties of the bottom layer (temperature: -1.69°C, salinity: 33.27 and a very high density up to 26.83) reflect winter conditions (*Fig. 4.1*, station LV29-88-1). The whole water column is oxygen-rich (~7-8 ml/l) up to the seafloor (more than 100 m).

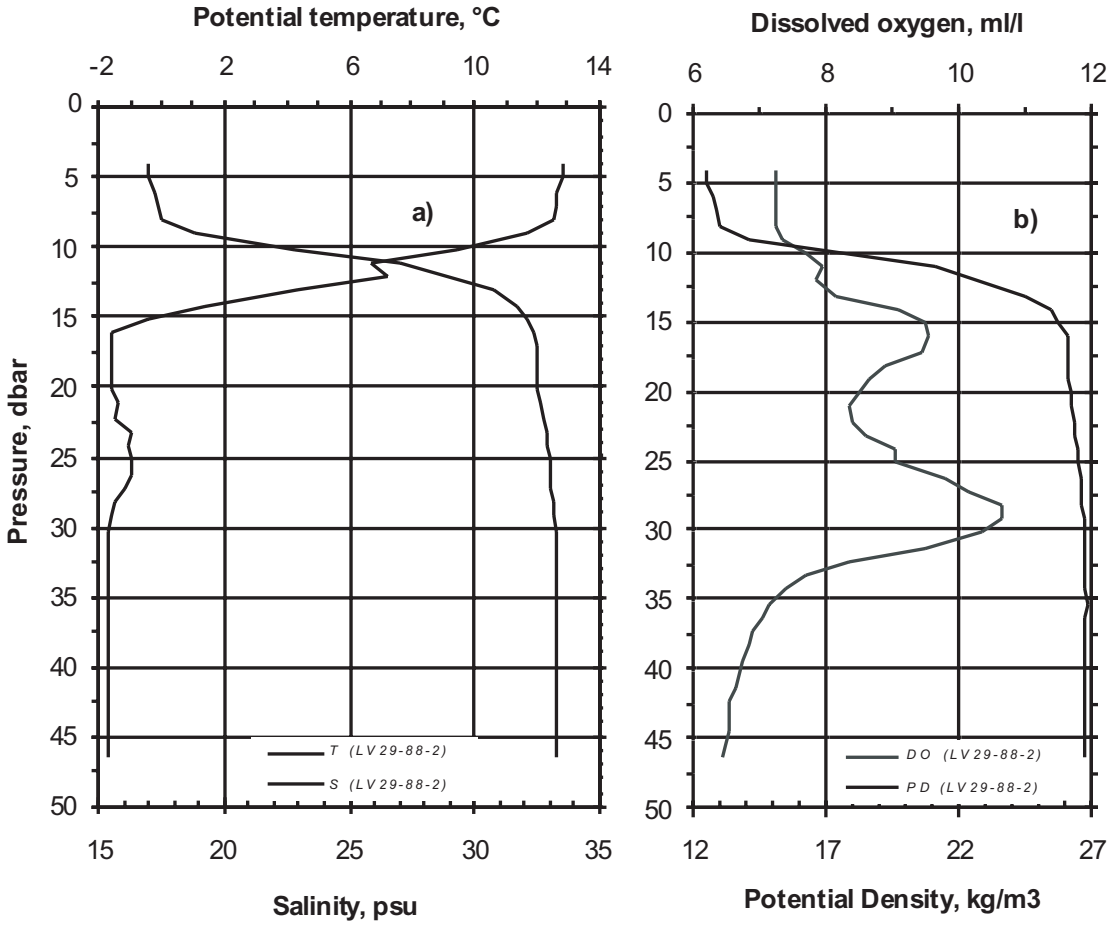

Fig. 4.1: *Potential Temperature and Salinity (a) and Dissolved Oxygen and Potential Density (b) at station LV29-88-2.*

The water column of this area shows no signs of vertical mixing and, moreover, seems to keep the winter properties in a stable way in comparison with the water column of the East Sakhalin shelf area. This is not surprising, as the ice conditions in the region disappeared only from July 5th on. Additional stability of the water column is derived from the Amur fresh-water input and the melting of sea ice.

The East Sakhalin shelf and slope area is characterized by relatively high temperatures in the cold subsurface layer (-0.4 - 0.7°C) and frequent intrusions with negative temperature values at intermediate depths and near the bottom (station LV29-76, -81). In our opinion, these cold intrusions originate from dense water northwest and west off Sakhalin. They occur as a result of sinking and diapycnal entrainment of shallow shelf waters with winter properties along the continental slope in the vicinity of Cape Elizabeth and a mixing with the surrounding waters with a subsequent lateral transport southward along the slope. During summer, the volume of dense shelf waters is much less than in winter and, as a consequence, the vertical scale of intrusions is less in summer time than in winter.

4.3 Derugin Basin

Two CTD stations were carried out in the deepest part of the Derugin Basin (stations LV29-103 and -104) (*Fig. 4.2*, station LV29-104). Both stations showed the lowest values of dissolved oxygen in near-bottom layers amounting to ~0.30 ml/l. In comparison with the observations during the first leg in the “Barite Mounds” area (0.5-0.6 ml/l), this is twice less.

Such low oxygen values in the deepest part of the basin indicate stagnant conditions which are also reflected in the representative sediment cores (see Appendix 6). Besides, in contrast to the barite mineralization area, the oxygen minimum layer was missing in both stations.

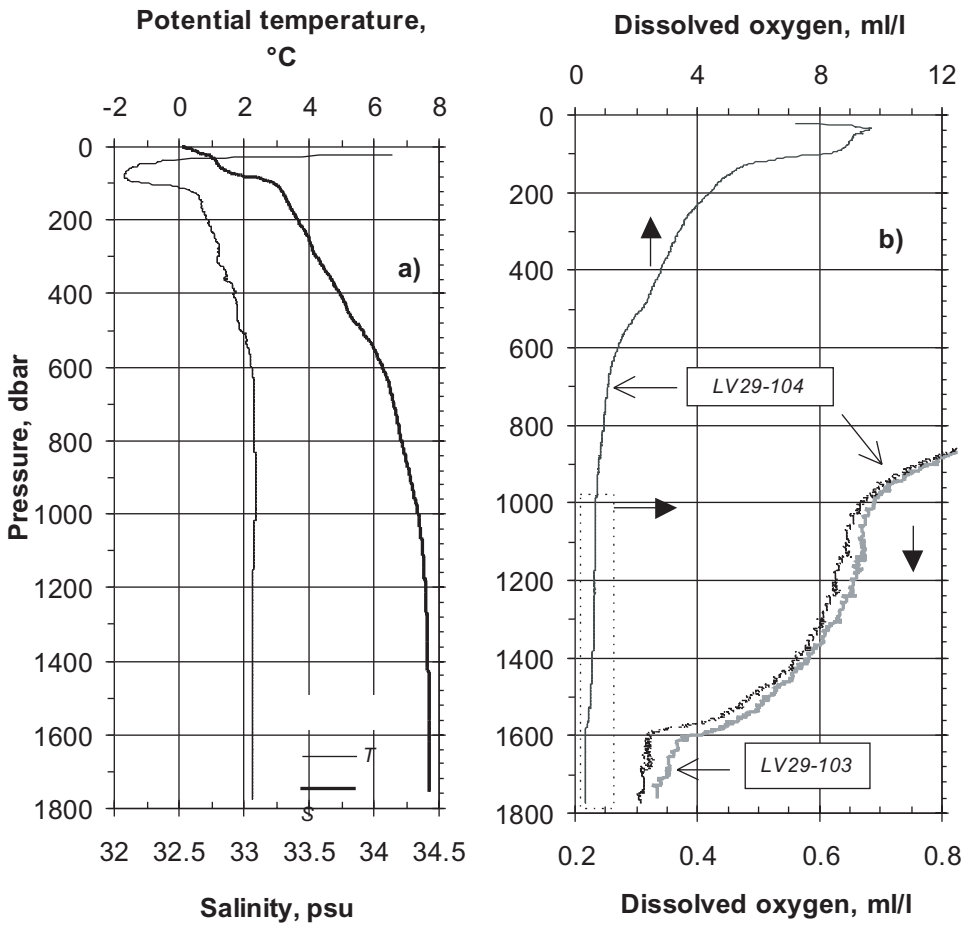

Fig. 4.2: *Potential Temperature and Salinity (a) at station LV29-104 and Dissolved Oxygen (b) at stations LV29-103 and LV29-104.*

4.4 Kurile Basin

The eastern part of the Okhotsk Sea in the vicinity of the Kurile Straits was covered by 7 CTD stations. Observations were made in the deepest part of the basin - up to 3,334 m depth (stations LV29-116, -120, -123) - as well as on the northern slope of the basin with lower depths. This area is under strong influence of tidal currents of diurnal period coming from the North Pacific through the deep and also shallow Kurile Straits. It is well known that the Okhotsk Sea is a region with strong tidal currents. This is due to the wide and shallow shelf in the northern part and also due to the near-resonant trapping nature at diurnal frequency. The tide amplitude is maximal in Penzginskaya Bay (13.9 m) and in the Tugur area (9.7 m). Tidal currents, especially diurnal, are dominant also in and around the Kurile Straits, and their speed is up to a few knots. For example, a maximum tidal current of 11 knots was observed in Nadezhda Strait. In Srednego, Severgina, Kreniczina, and Diany straits the tidal speed reaches 10.4, 9.4, 9.0 and 8.8 knots, correspondingly. In all other straits, the minimum current speed amounts to 6 knots. Due to astronomic reasons, the maximum tides and tidal currents take place in June-July and in December-January.

Tidal currents in and around the Kurile Straits are expected to play a major role in water exchange processes between the Okhotsk Sea and the North Pacific and also in internal water mixing. The diurnal cycle of CTD observations made by one of the authors in Friza Strait in the summer of 1989 revealed a mixing of the whole water column resulting in a homogeneity up to the seafloor in the middle part of the strait in one phase of the tidal cycle. There is no doubt that this leads to a cyclic mixing of the water masses in this area.
In the southern part of the sea (Kurile Basin) an anticyclonic circulation of several eddies with diameters of 100-150 km was observed which are often recorded by hydrographic data and by satellite imaging. The eddies appear each year, developing in summer and decaying in winter. Although eddy-like motions are dominant in the Kurile Basin, the mean eastward flow with a speed of 0.1 m/s still exists.

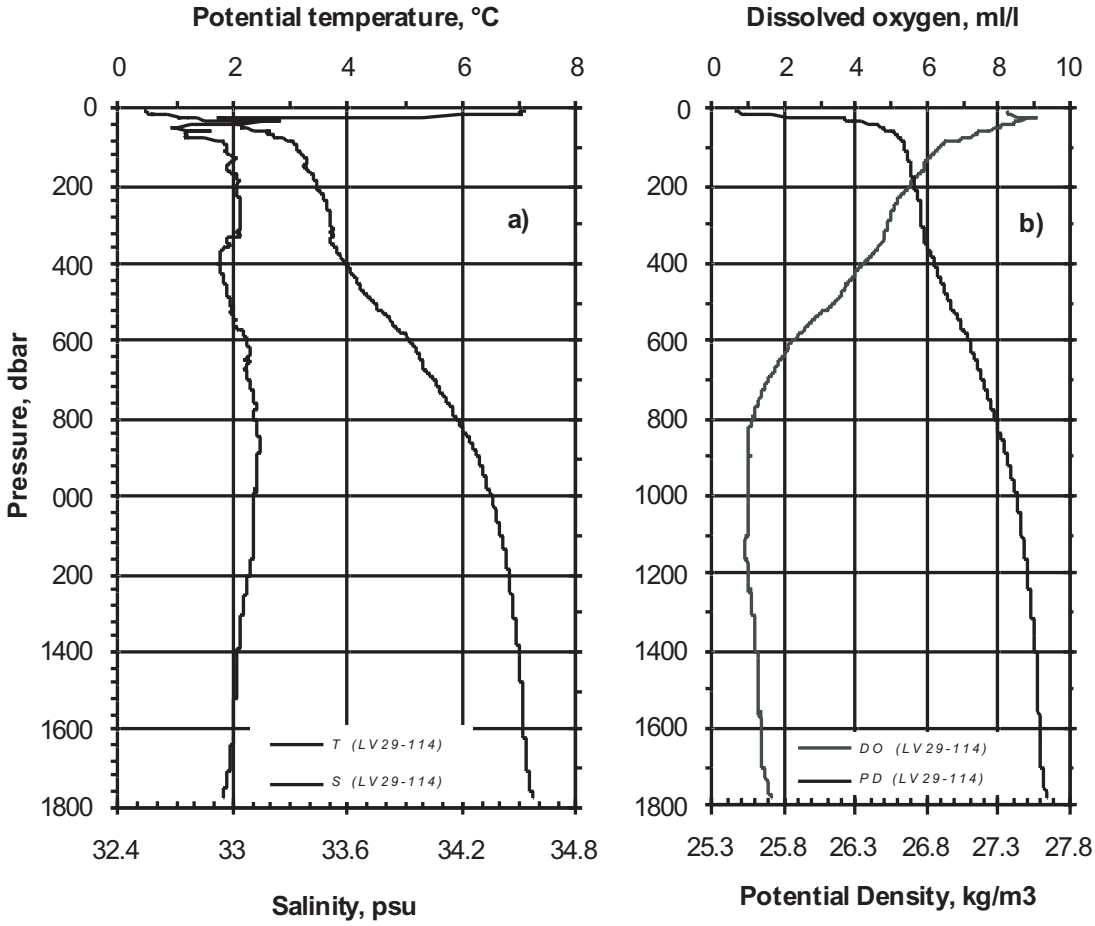

Fig. 4.3: *Potential Temperature and Salinity (a) and Dissolved Oxygen and Potential Density (b) at station LV29-114.*

All CTD stations in this area have the following characteristic features: relatively high (up to 1.8°C) temperatures in the cold subsurface layer, a smooth lower boundary and a huge amount of small intrusions up to 1,600 meters depth. For example, at station LV29-114 (*Fig. 4.3*, station LV29-114) a well pronounced but very small dichothermal layer was observed caused by intrusions of warm water on its lower boundary. Besides, a lot of intrusions of different vertical scales can be observed at intermediate depths up to 1,000 m. Even in the oxygen minimum zone which coincides with the intermediate temperature maximum, there is a local increase of the oxygen value connected with intrusions of colder waters.
An increase of the oxygen concentration value was also observed corresponding to a relatively sharp temperature decrease in the near-bottom layer at 70 m depth.

CTD station LV29-115 is, on the contrary, characterized by a massive cold subsurface layer (up to 600 m) with high values of temperature (1.8°C) but with a lot of small intrusions. Of course, such a vertical distribution indicates a very intensive mixing at these depths.
The next deep station (station LV29-116) (*Fig. 4.4*, station LV29-116) is also characterized by numerous intrusions, and signs of internal mixing can be seen up to 1,600 m. Additionally, there is an intrusion of cold and oxygen-rich waters at the depths of the intermediate temperature maximum.
A very strong interleaving of the water column was observed at the station in the central part of the basin which is located farest from the straits but which contains a lot of very sharp intrusions beneath the cold subsurface layer. As a rule, sharp intrusions indicate the very beginning and the first phase of internal mixing processes.

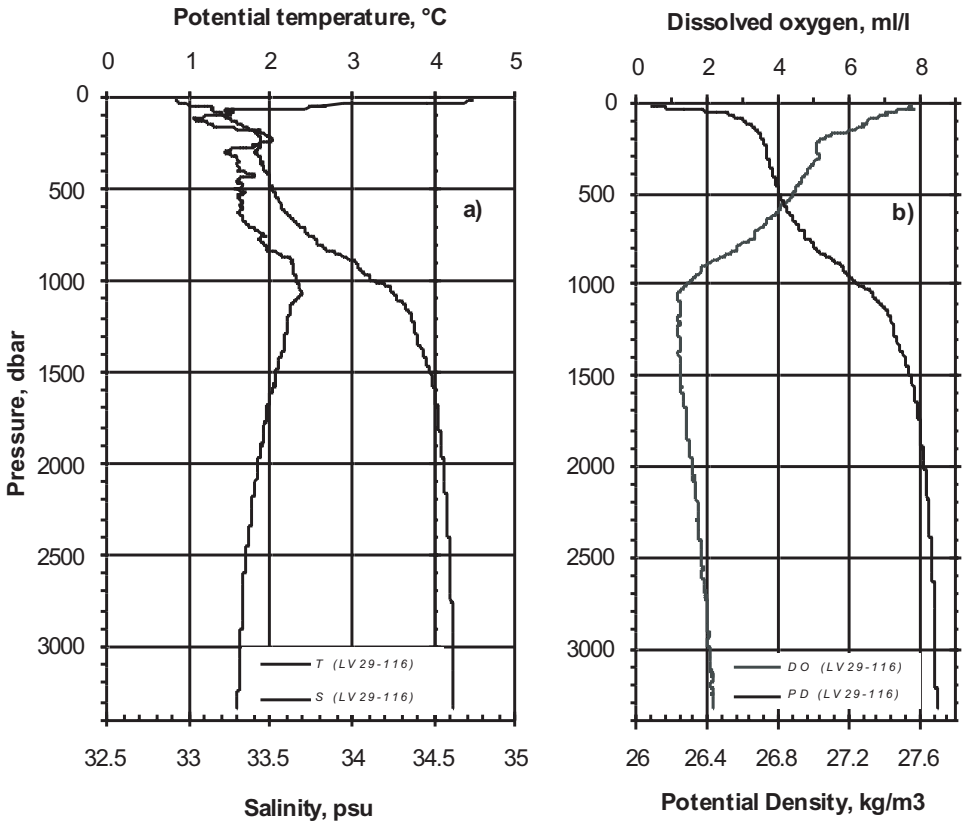

Fig. 4.4: *Potential Temperature and Salinity (a) and Dissolved Oxygen and Potential Density (b) at station LV29-116.*

It is suggested that the Okhotsk Sea surface waters migrate from the Kurile Basin into the North Pacific Ocean through the deepest of the straits, Bussol Strait (sill depth 2,300 m), and several shallower straits in the southern part of the Kurile Island Arc. A two-way flow is supposed to exist in Bussol Strait: the outflow from the Okhotsk Sea was found in the upper layers of the western side of the strait, while the Pacific inflow entered the Okhotsk Sea in the eastern part of the strait down to depths of 1,700 m. Strong tidal mixing occurs in the straits. In some phases of the tide, the whole water column up to the bottom could be homogeneous (Friza Strait). Thus, Pacific waters flowing into the Okhotsk Sea at different levels and in various stages of transformation strongly influence the vertical thermohaline structure in the eastern part of the sea.
Obviously, our observations in the deep Kurile Basin demonstrate that the waters originating from the Pacific are enriched with respect to oxygen (station LV29-120, -114). This data supports the role the North Pacific plays in the ventilation of the deep Okhotsk Sea. The same results were obtained during the MV *Marshal Gelovany* cruise in 1999.

5. THE CARBON DIOXIDE SYSTEM IN THE OKHOTSK SEA

Galina Pavlova, Anatoly Salyuk, Valery Sosnin, Nicole Biebow, and Lester Lembke

5.1 Sea water sampling and analysis

On this cruise, we studied the carbonate system (pH, Total Alkalinity, dissolved calcium) in the water column (CTD stations) and in the bottom waters (MUC stations). *pH* measurements were carried out by means of a cell without liquid junction (Tishchenko et al., 2001). *Total Alkalinity (TA)* was analyzed by Bruyevich`s method (Bruyevich, 1944). Samples for *dissolved calcium* (*Ca*) were preserved with hydrochloric acid and will be analyzed by Tsunogai's method (Tsunogai, 1968) in the shore-based laboratory at POI. Various carbonate parameters were in situ computed by a combination of the measured parameters according to a generally accepted scheme. A detailed description of the methods and designations used in the text are given in Chapter 7, Part I of this Report. *Biological productivity* was estimated using the "biological" term of apparent oxygen utilization (AOU_b), which was calculated using the data for dissolved oxygen and measured parameters of the carbonate system (Tishchenko et al., 1998). A negative value of AOU_b implies that the oxygen production by photosynthesis surpasses the oxygen consumption by respiration and oxidation of organic matter. A correction factor for *dissolved oxygen* (O_2) CTD data was applied to draw near the Winkler method data.

5.2 Results and Discussion

The carbonate chemistry data was obtained at 29 CTD and 17 MUC stations for three main areas of the Okhotsk Sea: the Sakhalin slope (stations LV29-69, -72, -76, -79, -81, -82, -84, -94, -103, -104), Sakhalin Gulf (stations LV29-87, -88-2, -88-3, -88-4, -88-5, -90, -91) and Kurile Basin (stations LV29-70, -110, -112, -114, -115, -116, -120, -123). Stations LV29-92, -106, -108 and -131 were located separately. The complete list of the measured and calculated carbonate parameters for CTD stations is given in the Appendix 3 and for MUC stations in *Table 5.1* in this chapter.

5.2.1 Slope of Sakhalin Island (depth 370-1,800 m)

The CTD stations investigated at the slope of Sakhalin Island were divided into two groups using the common features of the carbonate parameters distribution:
1. South-north transect along Sakhalin (stations LV29-69, -72 , -76 , -79 , -81, -82 , -84 , -94, depth 370-1,100 m)
2. Derugin Basin (stations LV29-103, -104, depth 1,800 m)

5.2.1.1 South-north transect

Figure 5.1 displays vertical profiles of selected carbonate parameters and shows a clear separation of some water properties for the stations along the transect.
A minimum normalized Total Alkalinity (NTA) value (2.372 mmol/kg) was found at about 220 m with little variation along the transect. It is related to the biogenic $CaCO_3$ formation in water layer 0-220 m. The greatest decrease in NTA for this layer by 53 µmol/kg was observed at the northern end of the transect (station LV29-82) compared to 10 µmol/kg at station LV29-72. Therefore, the intensity of biogenic $CaCO_3$ formation increases towards the north of the Sakhalin slope. Below 220 m, NTA increases steadily with depth due to dissolution of

biogenic carbonate. This implies that $CaCO_3$ is accumulated in the sediments of the Sakhalin slope up to a water depth of 1,100 m.

***Tab. 5.1**: Carbonate parameters for bottom water samples (MUC, CTD).*

Station	Depth m	Temp °C	Salinity	pHt in situ	*TA* mmol/kg	DIC, mmol/kg	CO_3, mmol/kg	pCO_2, µatm	Lc	La
MUC69	845			7.6	2.36	2.348	0.044	997	0.75	0.52
CTD69	837	2.313	34.165	7.532	2.359	2.367	0.038	1177	0.66	0.46
MUC70	1988			8.017	2.211	2.033	0.115	250	1.21	0.97
CTD70	1984	1.945	34.566	7.599	2.406	2.367	0.052	786	0.56	0.45
MUC72	1121			7.551	2.385	2.38	0.042	1066	0.64	0.46
CTD72	1113	2.375	34.373	7.531	2.382	2.383	0.04	1119	0.61	0.44
MUC76	627			7.89	2.23	2.139	0.075	483	1.39	0.94
CTD76	618	2.147	34.037	7.556	2.338	2.345	0.038	1154	0.71	0.48
MUC84	753			7.666	2.255	2.227	0.048	830	0.85	0.58
CTD84	747	2.205	34.1063	7.544	2.349	2.356	0.038	1160	0.68	0.47
MUC89	46			8.011	2.069	1.981	0.071	375	1.69	1.06
CTD87	45	-1.696	33.351	7.829	2.284	2.246	0.053	650	1.27	0.8
MUC92	99			7.887	2.274	2.218	0.061	556	1.41	0.89
CTD92	87	-1.671	33.33	7.894	2.283	2.224	0.062	548	1.44	0.91
MUC94	1123			7.556	2.39	2.384	0.043	1058	0.65	0.46
CTD94	1113	2.379	34.371	7.505	2.388	2.397	0.038	1195	0.58	0.41
MUC103	1748			7.443	2.409	2.42	0.036	1215	0.43	0.33
CTD103	1739	2.368	34.436	7.431	2.409	2.423	0.035	1251	0.42	0.32
MUC104	1762			7.5	2.41	2.404	0.041	1057	0.49	0.38
CTD104	1751	2.368	34.436	7.436	2.408	2.421	0.036	1230	0.42	0.33
MUC108	617			7.572	2.324	2.327	0.039	1107	0.74	0.5
CTD108	608	2.19	33.868	7.559	2.322	2.328	0.038	1141	0.72	0.48
MUC110	1215			7.584	2.393	2.376	0.046	968	0.67	0.49
CTD110	1205	2.298	34.449	7.531	2.393	2.391	0.041	1098	0.6	0.43
MUC112	1373			7.533	2.395	2.389	0.042	1057	0.57	0.42
CTD112	1367	2.253	34.474	7.519	2.393	2.391	0.041	1090	0.56	0.41
MUC114	1764			7.599	2.412	2.378	0.051	828	0.59	0.46
CTD114	1755	1.938	34.567	7.556	2.417	2.396	0.046	920	0.54	0.42
MUC116	3292			7.504	2.416	2.372	0.05	741	0.32	0.3
CTD116	3277	1.835	34.623	7.503	2.417	2.374	0.05	743	0.32	0.3
MUC123	3329			7.508	2.418	2.372	0.051	729	0.32	0.3
CTD123	3322	1.898	34.611	7.494	2.418	2.376	0.05	755	0.31	0.29
MUC131	762			7.572	2.358	2.357	0.041	1089	0.72	0.5
CTD131	749	2.286	34.134	7.52	2.353	2.367	0.037	1231	0.65	0.44

pCO_2 is much lower in the surface water than in the atmosphere at all stations. Extremely low values (190-220 µatm) were observed in the northern part of the transect (station LV29-76 – LV29-84). They are associated with increased photosynthesis processes (and organic-debris formation) in the north of Sakhalin Island. Below the photic zone, organic debris is oxidized to carbon dioxide. The pCO_2 value increases with depth to maximums of more than 1,000 µatm, which is comparable to pCO_2 values in intermediate and deep water layers in the North Pacific (Broecker et al., 1982).

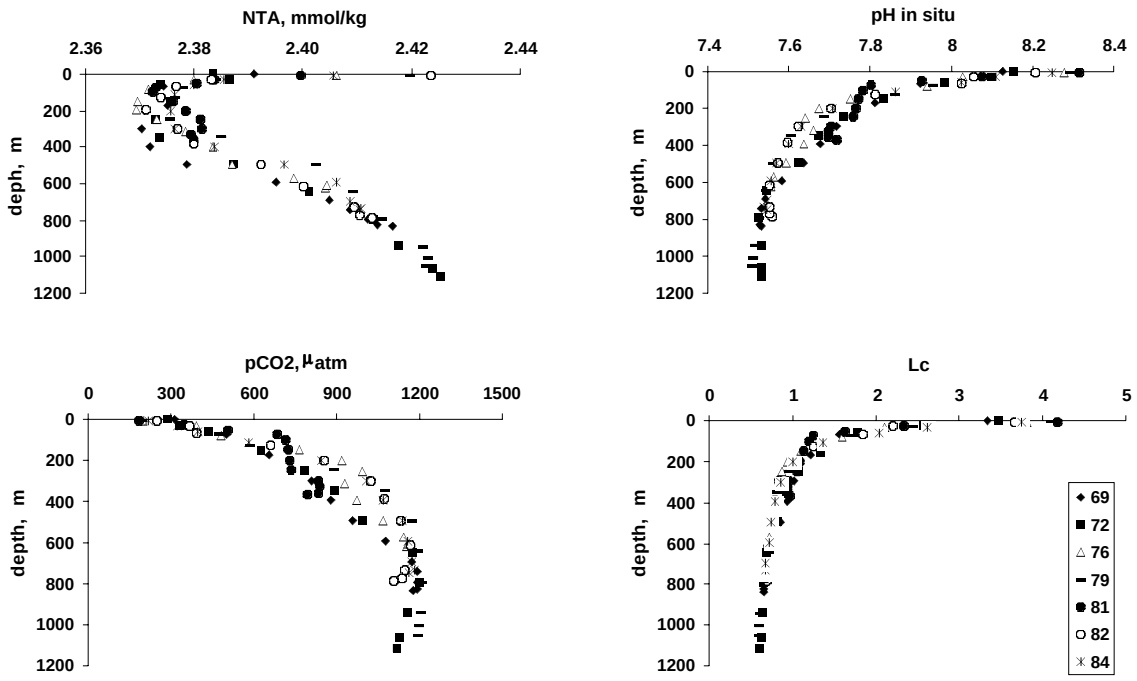

Fig. 5. 1. *Vertical profiles of normalized total alkalinity (NTA), pH in situ, partial pressure of CO_2 (pCO_2) and saturation degree of calcite (Lc) at a slope of Sakhalin Island.*

The investigation of the carbon dioxide system along the Sakhalin slope showed that the northern part of the slope is more productive in biogenic material than the southern one. These results coincide with the distribution of dissolved organic matter in the waters (Agatova et al., 1996) and in the sediments (Bruyevich, 1956) of the Okhotsk Sea.

5.2.1.2 Derugin Basin

Numerous observations of the water column in the Derugin Basin, including our own investigations of several years, showed that the water structure here is very homogeneous below 1,000 m. Hydrochemical data obtained in Leg 2 provided new informations with regard to the Derugin Basin.

Stations LV29-103 and -104 are located in the Derugin Basin at a depth of approximately 1,760 m. The vertical profiles of selected carbonate parameters for these stations and for station LV29-19, sampled at a shallower depth (1,684 m) in Leg 1, are shown in *Figure 5.2*. As it is clear from the figure, the vertical profiles of the water properties are found to be nearly identical from the surface to approximately 1,600 m. The carbonate parameter distribution in the water column for this group of stations is not described here, because detailed investigations of the carbonate system for 17 stations of the Derugin Basin were carried out during Leg 1.

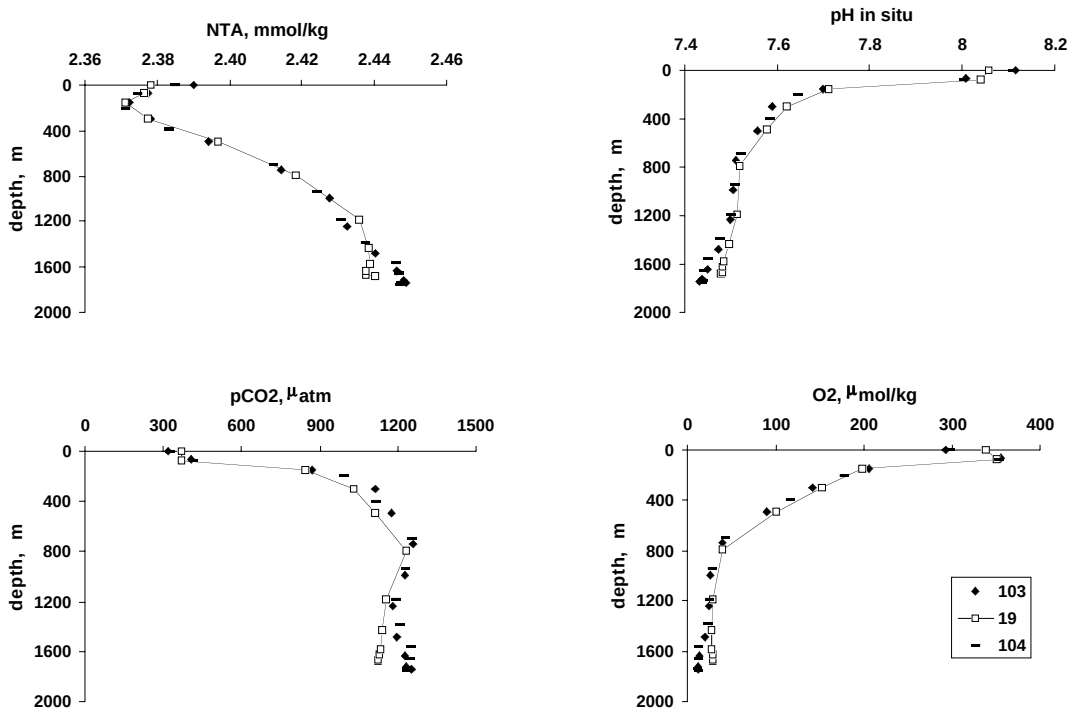

Fig. 5.2: *Vertical profiles of normalized total alkalinity (NTA), pH in situ, partial pressure of CO_2 (pCO_2) and dissolved oxygen content (O_2) in Derugin Basin.*

As a striking feature of the new locations (stations LV29-103 and -104), the existence of a water column layer with very low oxygen contents located 200 m above the seafloor was observed. Such a low oxygen content had never been measured before in the Okhotsk Sea. Oxygen concentrations of 14 μmol/kg and of 13 μmol/kg were found in the bottom water of station LV29-103 and -104, respectively. They were accompanied by an increase in alkalinity (by 10 μmol/kg) and a decrease in pH (*Fig. 5.2*).

We believe that carbonate dissolution in the bottom water is responsible for the alkalinity increase. The question arises what processes affect an enhanced carbonate dissolution within a zone with low oxygen concentration. The dissolution of carbonate can be favored by conditions that create high levels of CO_2 and low pH values, and these processes seem to be sufficient to lead to carbonate dissolution. The remineralization of organic matter by oxygen and nitrate leads to very high CO_2 partial pressures (and therefore low pH) in the oxygen minimum zone. The question arises whether the denitrification starts before the oxygen is fully depleted. We believe that the substantial lack of oxygen in this zone may initiate the consumption of nitrate for the oxidation of organic carbon. Most probably a combined effect of oxygen utilization and denitrification led to the carbonate dissolution in the study region.

We also believe that the bottom water at stations LV29-103 and -104 might be influenced by the underlying sediments. Both cores contained anoxic sediments with a strong H_2S odor. The change in the pH value in the bottom water depends on the extent of removal of generated hydrogen sulfide in the underlying sediments (Ben-Yaakov, 1973). Probably, the hydrogen sulfide remaining in sea water decreased the pH value at these stations.

Obviously, additional investigations, including H_2S and nutrient measurements in the sea water and in the pore water, are required to understand this interesting region in the Derugin Basin.

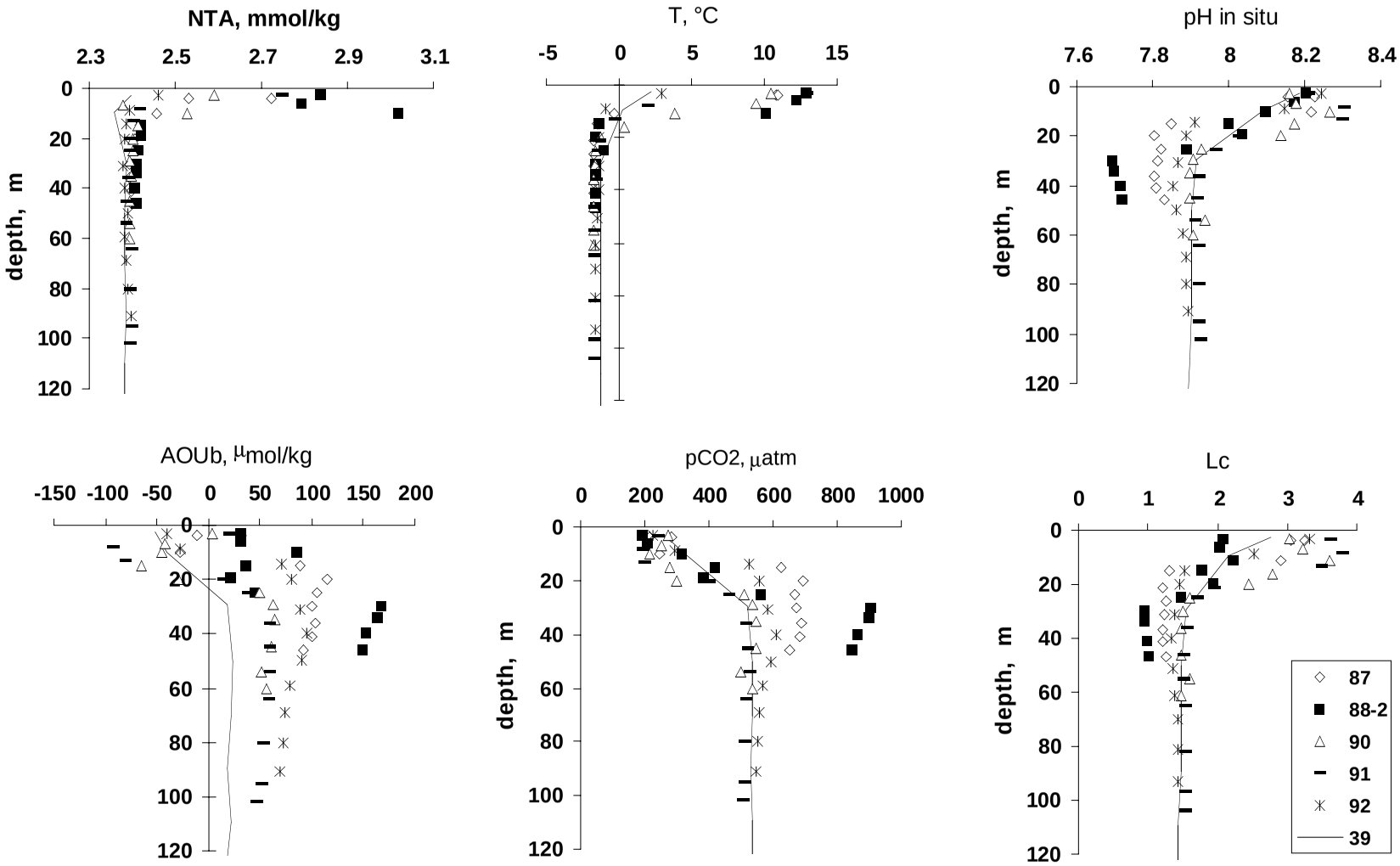

Fig. 5.3: *Vertical profiles of normalized total alkalinity (NTA), temperature (T), pH in situ, "biological" term of apparent oxygen utilization (AOUb), partial pressure of CO_2 (pCO_2) and saturation degree of calcite (Lc) at a South-North transect across the Sakhalin Gulf.*

5.2.2 Sakhalin Gulf

The spatial distribution of carbon dioxide equilibrium species is presented for 7 locations in the Sakhalin Gulf. A south-north transect (transect 1) comprising 4 sites (stations LV29-88-2, -87, -90, -91) along 142°E in combination with an east-west transect (transect 2) also consisting of 4 sites (stations LV29-88-2, -88-3, -88-4, -88-5) along 54°N were carried out to study the carbonate system of the Sakhalin Gulf and to investigate the influence of Amur River on the major components of the Okhotsk Sea waters. In this section, they are compared with stations LV29-39 and -92 on the northern Sakhalin shelf. The surface water properties for station LV29-92 varied more than those for station LV29-39 due to the inflow of fresh waters from Amur River.

Figures 5.3 and *5.4* display vertical profiles of measured and calculated hydrochemical parameters in the sea water for transect 1 and transect 2, respectively.

The high input of alkalinity from Amur River contributes to the observed spatial gradients in carbonate chemistry at the surface and at all depths for both study areas of the Sakhalin Gulf. In contrast to this, the fresh-water influence was observed at station LV29-92 only in the upper 10 m. The surface NTA values are highly variable. They are higher in the east (3.016 mmol/kg, station LV29-88-2) and in the north (2.749 mmol/kg, station LV29-91) than in the west (2.537 mmol/kg, station LV29-88-5). It seems likely that the area along the eastern shore was influenced by the Amur River input to a higher degree than the area along the western shore.

The behavior of selected carbonate parameters showed a significance of photosynthetic activity on the carbon dioxide equilibrium in the Sakhalin Gulf. pCO_2 is one of the most sensitive parameters for small variations in the sea-water properties caused by photosynthetic activity. Therefore, in order to obtain a detailed pCO_2 profile in the water column, we measured TA and pH every 5 m from the surface to the bottom and computed pCO_2 values using these measured properties.
Photosynthetic carbon dioxide consumption at the surface results in reduced levels of carbonic acid (pCO_2 decreasing to only 200 μatm), an increase in pH to 8.2-8.3, and increased concentrations of carbonate ions, leading to a higher degree of calcium carbonate saturation (Lc = 3.4-3.8). The pCO_2 profiles show (*Figs. 5.3* and *5.4*) that pCO_2 decreases with depth and reaches its minimum value in the subsurface layer at 10-23 m, which coincides with a negative maximum of AOU_b. Most probably, this observed pCO_2 minimum reflects both the consumption of CO_2 by photosynthesis and the observed sharp temperature gradient, which decreases the sea-water temperature from 10°C at the surface to -0.3°C in subsurface waters. At station LV29-88-4, where the temperature gradient was not that sharp (within 5°C), a pCO_2 minimum was not observed in the subsurface water. The distribution of the properties pH, AOU_b, and Lc at station LV29-88-2 did not indicate an active photosynthetic process. This corresponds to the observations made in the mixing areas of the Okhotsk Sea (Bruyevich et al., 1960), where the surface water is not oxygen-supersaturated despite the abundance of phytoplanktic biomass.
If we assume that the atmospheric CO_2 concentration was close to 350 µatm at the time of the cruise, the difference of pCO_2 between the atmosphere and the sea surface of the Sakhalin Gulf was more than 100 μatm, thus indicating that the basin represented a sink for atmospheric CO_2 in July 2002. We may conclude that the high input of alkalinity from Amur River contributes to the observed spatial gradients in carbonate chemistry and thus directly influences the equilibrium conditions. The direct chemical influence on the carbon dioxide equilibrium was compared with the indirect impact of nutrient-stimulated photosynthetic uptake of carbon dioxide. Thereby, the carbonate

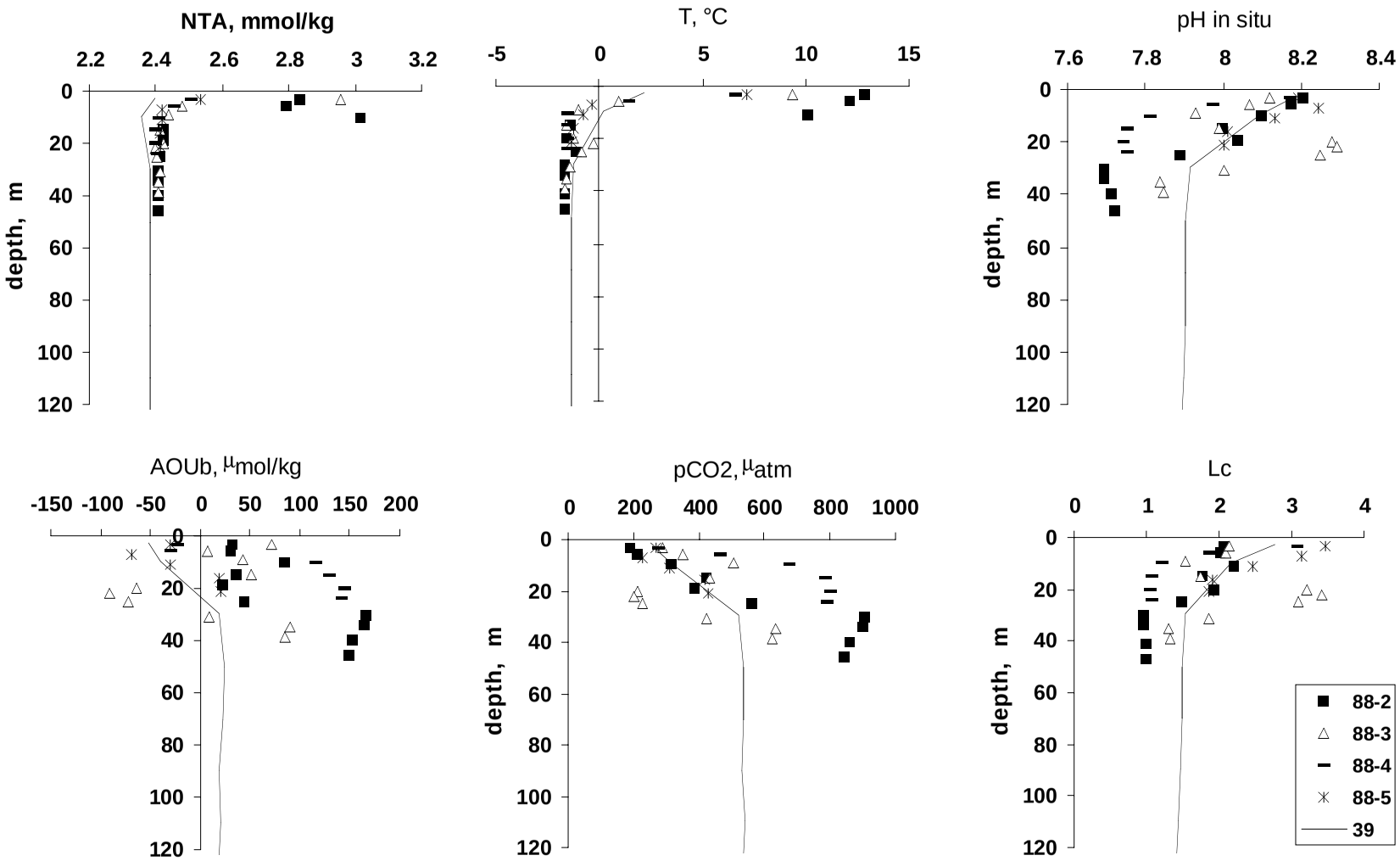

Fig. 5.4: *Vertical profiles of normalized total alkalinity (NTA), temperature (T), pH in situ, "biological" term of apparent oxygen utilization (AOUb), partial pressure of CO_2 (pCO_2) and saturation degree of calcite (Lc) at a East-West transect through the Sakhalin Gulf.*

chemistry investigations in the Sakhalin Gulf yielded a great sensitivity of the carbonate system with respect to biological as well as physical-chemical influences.

Future sample analyses for dissolved calcium will reveal the Amur River influence on the major components of the Okhotsk Sea.

5.2.3 Kurile Basin

The distribution of inorganic carbon equilibrium species is given for 8 stations representing the deepest part of the Okhotsk Sea, the Kurile Basin. Carbonate parameters (pH, Total Alkalinity and dissolved calcium) measurements covered the eastern (stations LV29-110 and -112) and the western (station LV29-70) slopes of the basin, the Kurile Straits areas via which the Okhotsk and Pacific waters exchange (stations LV29-114, -115, -120) and the deep Kurile Basin (stations LV29-116, -120, -123).

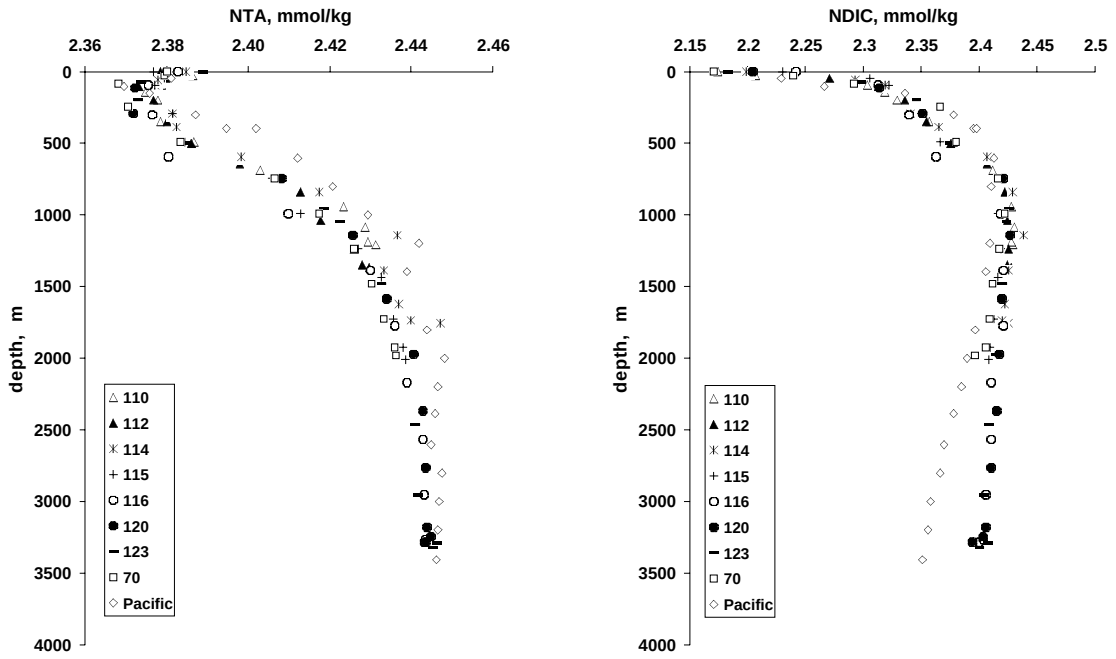

Fig. 5.5: *Depth scatter plots of normalized total alkalinity (NTA) and dissolved inorganic carbon (NDIC) in the Kurile Basin and the northwestern Pacific.*

The distribution of carbonate parameters in the surface layer reflects the spatial variability of the entire study area. Despite the summer photosynthetic activity, the highest values of pCO_2 (about 400 µatm) were observed at stations LV29-115 and -116 located in the Kruzenshtern`s Strait area. This can be explained by intensive vertical mixing and rising of deep, CO_2-rich water to the surface. In the surrounding waters, pCO_2 was less; and extremely low values were observed at the slopes of the Kurile Basin (300 µatm).
The distribution of carbonate parameters in the water column is almost homogeneous in the entire study area and may be summarized as follows. The consumption rate of dissolved $CaCO_3$ from sea water exceeds the rate of carbonate dissolution at water depths of 100 m due to biogenic $CaCO_3$ formation. Below 100 m biogenic calcium carbonate is dissolved, but accumulated in the sediments of the Kurile Basin up to a water depth of 1,200 m. The surface waters are highly supersaturated with respect to calcium carbonate. The saturation horizons

for calcite and aragonite are at 350 m and 100 m, respectively. Thus, the Kurile Basin waters are undersaturated with respect to calcium carbonate below 350 m and highly undersaturated (Lc <0.5) beneath a depth of about 2,000 m.

One of the most intensively discussed question during the investigation of the Kurile Basin, the process of the bottom water renewal, is not clear in detail. We compared two regions, the Kurile Basin and the open Pacific. Station 3 (44°59.90 N; 152°48.43 E) located in the northwestern Pacific Ocean was used to characterize the waters of the open Pacific. This station was performed for summer season in 1993; Total Alkalinity and dissolved inorganic carbon in the water column were measured using Bruyevich`s method (Bruyevich, 1944) and the coulometric method (Johnson et al., 1985), respectively. Since precipitation and evaporation affect the distribution of alkalinity and dissolved inorganic carbon, we chose to present and compare the data at the same salinity (NTA, NDIC).

Scatter plots of NTA and dissolved inorganic carbon (NDIC) for the entire study area in the Kurile Basin and for station 3 in the open Pacific are shown in *Figure 5.5*.
As it can be seen from the figure, the NTA profiles of the Kurile Basin and the open Pacific are substantially similar suggesting a possible water exchange between these two regions.
Scatter plots of NDIC show that the sea-water properties in the open Pacific and in the Kurile Basin are identical up to a depth of about 2,000 m. Below this depth, NDIC decreases with depth in the open Pacific by 40 µmol/kg, whereas in the Kurile Basin by 10 µmol/kg. The observed offset perhaps resulted from the difference between measured (open Pacific) and calculated (Kurile Basin) NDIC data. But the same distinct difference in the dissolved inorganic carbon content between the Kurile Basin and the open Pacific was also reported by Bychkov et al., 1996 for both measured profiles.
For station LV29-116, -120, and -123 (depth >3,000 m) an additional decrease in NDIC by 10 µmol/kg, resulting in a NDIC value of 2.394 mmol/kg, was found in a thin (about 30 m thick) near-bottom layer. Pacific waters with the same NDIC value (2.395 mmol/kg) were observed at approximately 2,200 m depth (the sill depth of Bussol Strait). This supports the idea of new Pacific waters intruding into the Kurile Basin through Bussol Strait (Salyuk et al., 2001). Thus, the process of bottom water renewal continues.

5.2.4 Bottom water study

The study of the carbonate system in the bottom water is very important for the understanding of geochemical processes in the underlying sediments. As parameters like the concentration of carbonate ions and the saturation degree of calcium carbonate indicate $CaCO_3$ preservation in the sediments, the carbonate parameters of the bottom water layer are also very useful for different diagenetic model calculations.

Bottom water samples were taken by 17 multicorer (MUC) deployments and were analyzed for pH and TA. Various carbonate parameters were in situ computed by the combination of the measured parameters according to a generally accepted scheme. A complete list of measured and calculated concentrations is given in *Table 5.1*. For comparison, the properties of the bottom water from CTD measurements, carried out at the same stations, are also listed in *Table 5.1*. The differences in depth between the MUC samples and the samples from the deepest horizons of CTD amounted to no more than 1-12 m.

Alkalinity is a good indicator for the bottom water as far as this parameter is very stable there. Striking differences in the TA values of the two sample groups were observed at stations LV29-70, -76, -84, -89. Obviously, the low alkalinity values of the MUC samples do not reflect the bottom water properties, but are artifacts produced by multicorer sampling.

Probably, sea water from shallow depths was trapped in the tubes overlying the sediment/water interface. Therefore, MUC stations LV29-70, -76, -84 and -89 were excluded from the further description.
Figure 5.6 shows the coincidence (within experimental uncertainty) between MUC and CTD Total Alkalinity values for the other 13 MUC stations.

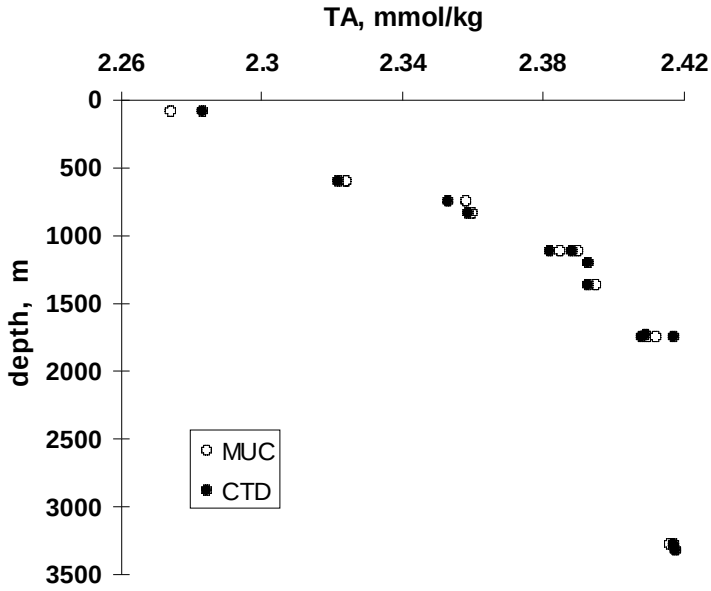

Fig. 5.6: *Comparison between total alkalinity (TA) values in bottom water for MUC and CTD stations.*

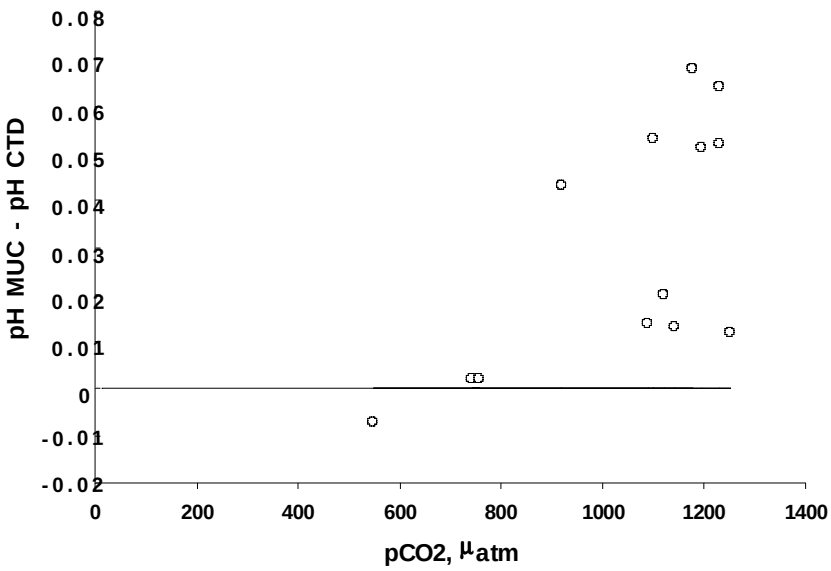

Fig. 5.7: *Difference between in situ pH values in bottom water for MUC and CTD samples versus partial pressure of carbon dioxide.*

The comparison of the pH values for this group of samples showed that pH of bottom water is higher in the MUC than in the CTD (*Fig. 5.7*). As it is clear from the figure, pH_{MUC} - pH_{CTD} values depend on the partial pressure of CO_2 in the bottom water. They do not exceed 0.01 pH

unit (the error of pH measurements is ±0.003 pH unit) when the pCO_2 values in the bottom water are less than 800 µatm, but they considerably increase (up to 0.07 pH unit) when pCO_2 is >1,000 µatm. Obviously, the increased pH value in MUC samples is a result of a loss of CO_2 from the bottom water to the atmosphere during the opening of the multicorer tubes and sampling of the bottom water. The loss is more intensive in samples with a very high CO_2 content.

We believe that the CTD carbonate parameters data reflects the in situ bottom water properties more correctly.

6. METHANE INVESTIGATIONS

Anatoly Obzhirov

6.1 Introduction

The first leg of cruise LV29 was devoted to gas-geochemical investigations and the second leg mainly to paleoceanological objectives. Gas investigations were an important task on both legs, because they provide informations about the methane distribution in the water column of different areas of the Okhotsk Sea. This is necessary to better distinguish between background and anomalous methane values and to use methane as a tracer for the sources of methane and for the direction of moving water layers. This is important for both gas-geochemical parameters of the water layers and for paleoceanological reconstructions. Apart from that, methane was measured in the sediment cores of 3 stations to compare the methane distribution in the sediment in different areas inside and outside of the fields of methane anomalies in the water column.
The main goal of methane investigations was to use methane like a tracer to distinguish water masses and to study the Sakhalin Gulf area and the Kurile Basin in more detail.

6.2 Method

Water samples were taken from the Niskin Bottles of the CTD-rosette. Gas was extracted from water by a vacuum line and analyzed by a chromatograph. Methane and heavy hydrocarbon values were measured. Standard gas produced in the USA was used for calibration. Gas in the sediments was studied by the Head Space method.

6.3 Results

6.3.1 Methane distribution in the water column

Methane measurements in the water column were carried out at 29 CTD stations. 2 stations were located at the western slope of the Kurile Basin, 7 at the Sakhalin slope, 4 at the northern Derugin slope, 5 in the Sakhalin Gulf, 2 in the northern Derugin Basin, 2 at the Kamchatka slope and 8 in the Kurile Basin. The methane distribution is given in Appendix 4.

6.3.1.1 Western slope of the Kurile Basin

Stations LV29-69 and LV29-131 were carried out at the western slope of the Kurile Basin located near station GE99-1 (Biebow et al., 2000) and in the open part of La Perusa Strait. The methane distribution in the water column of stations LV29-69 and GE99-1 is very similar – background concentrations at the surface (60-70 nl/l) and maximum concentrations in the subsurface layer (about 200-250 nl/l, depth 70-80 m). High methane concentrations (100-150 nl/l) were observed at 400 m and 700 m depth as well as in the bottom waters. The methane concentration at station LV29-131 increases in the near-bottom layer (225-433 nl/l, depth 749-692 m). This is possibly an indication for a mixture of different water layers with the upper layer containing a subsurface methane maximum originating from the Kurile Basin and the bottom layer with maximum methane concentrations from Aniva Bay. The methane anomaly in the bottom waters (more than 400 nl/l) of station LV29-131 may be caused by methane migrating from oil-gas-bearing sediments via a fault zone into the water column or by transport with water masses from the northern shelf and slope of South Sakhalin where methane flares and anomalous high methane concentration were found in the bottom waters.

6.3.1.2 Sakhalin slope

7 CTD stations were carried out along the Sakhalin slope (Appendix 4). Stations LV29-70 and LV29-72 are located in the northwestern Kurile Basin and on the Sakhalin slope at depths of more than 1,000 m. Methane is nearly equally distributed in the water column of both stations with a background concentration (45-50 nl/l) at the surface, a subsurface maximum (90-200 nl/l) and background values in deeper water layers (20-40 nl/l).
Stations LV29-76, -79, -81, -82, and -84 are located on the northeastern Sakhalin slope. As usual for this area (Biebow & Hütten, 1999; Biebow et al., 2000; Chapter 6, Part I of this Report) methane anomalies were found here especially in bottom waters (500-3,000 nl/l), whereas the content at the surface does not exceed background concentrations (50-80 nl/l). The concentration decreases (200-300 nl/l, station LV29-79) at depths greater 1,000 m. A large methane anomaly (15,000 nl/l) was measured at station LV29-81 in the intermediate water layer (depth 200 m). Perhaps, there is a flare near this station, and methane-containing waters migrate from the flare to station LV29-81. Methane sources in this area are oil-gas-bearing sediments and decomposing gas hydrates (see Biebow & Hütten, 1999; Biebow et al., 2000; Chapter 6, Part I of this Report).

6.3.1.3 Sakhalin Gulf

Stations LV29-88-2, -88-3, -88-4, and -88-5 are located in the Sakhalin Gulf. The methane distribution in the bottom water of this area was already studied in 1985 (Obzhirov, 1993). A comparison of the methane concentrations in the bottom waters obtained in 1985 and on this cruise shows similar values: there is a methane anomaly (200-300 nl/l) in the bottom water of the eastern part of the Sakhalin Gulf and a concentration at background level (60-70 nl/l) in the western part. A great methane anomaly (930 nl/l, depth 6 m) was measured in the surface layer of station LV29-88-3. The surface layers at all stations in this area contain high methane concentrations (115-650 nl/l), as well. The sources of methane and the reason for higher methane concentrations in the surface layers in comparison to the bottom water are still unclear. Oil-gas deposits are frequent on the Sakhalin coast and in the eastern part of the gulf. Methane can get into the bottom water from oil-gas-bearing sediments and into the water column from coastal oil-gas deposits. The high methane concentration at the surface possibly formed as a result of a mixture of water masses of Amur River and the Sakhalin Gulf. The methane distribution in the eastern part of the Sakhalin Gulf is similar to that on the shallow northeastern Sakhalin shelf.

6.3.1.4 Northern part of the Okhotsk Sea

Stations LV29-87, -90, -91, -92, -94 are located in the northern part of the Okhotsk Sea. Station LV29-87 is located between the Sakhalin Gulf and the open Okhotsk Sea. The methane distribution in the water column is here similar to that of station LV29-88-2, but the concentration is twice less. There is a methane anomaly (280 nl/l, depth 10 m) in the subsurface layer and a background concentration in the bottom layer. In northern direction (stations LV29-90, -91 and -94), background methane concentrations were observed in the water column with the exception for station LV29-92 where a high methane value (450-550 nl/l) was detected extending from the bottom (91 m) up to 60 m depth. Here, methane possibly emanates from oil-gas-bearing sediment and migrates via fault zones into the water.

6.3.1.5 Derugin Basin

Stations LV29-103 and LV29-104 are located in the deeper part of the Derugin Basin. The methane content is at background level over the whole water column from the surface to a depth of 1,400 m. A slightly increased methane content (100-150 nl/l) was found in the bottom water of station LV29-103, whereas the concentration in the bottom water of station LV29-104 is 10 times less (background concentration). But the water layer at 1,400-1,600 m depth of LV29-104 contains an about 3 times higher methane concentration (30 nl/l) than the bottom layer. Maybe this water layer with a thickness of about 200 m at station LV29-104 is stagnant.

6.3.1.6 Western slope of Kamchatka

Stations LV29-106 and LV29-108 are located on the western slope of Kamchatka. These stations were conducted to continue the station profile of cruise LV28 (Biebow & Hütten, 1999, stations LV28-40 – LV28-43) from the Sakhalin slope to the Kamchatka slope. The methane values in the water column of these stations do not exceed the background concentration and equal those obtained on cruise LV28 (stations LV28-42, -43).

6.3.1.7 Kurile Basin

Stations LV29-110, -112, -114, -115, -116, -120, -123 are located in the Kurile Basin. A regularity in the methane distribution of all these stations are decreasing methane concentrations from the sea surface (50-150 nl/l) to a depth of 1,000 m (7-15 nl/l) with this value being constant down to the bottom (depth 3,300 m). An exception from this was observed at station LV29-110 where the intermediate water layer (depth 700-900 m) contains a small methane anomaly (90 nl/l). An explanation could be that the water layer intruded into the area of station LV29-110 from the Paramushir slope where a high methane value was measured in a gas hydrate-bearing area. Methane measurements in the water column of stations GE99-6, -7, -8 carried out in 1999 (Biebow et al., 2000) yielded similar values with the exception of station GE99-7 containing a higher methane concentration (70 nl/l) in the bottom water. Here, methane possibly emanates from a fault zone connected with the acoustic basement rise (see Chapter 12). Another observed regularity is a subsurface methane maximum (150-250 nl/l, depth 100-150 m) in the water column of almost all areas of the Kurile Basin, especially in its western part.

6.3.1.8 Discussion

High methane concentrations of 1,600 nl/l at the seafloor depth of 367 m to 14,600 nl/l at 199 m depth were measured at station LV29-81. The methane distribution is here similar to that of “Giselle flare” where gas hydrates were found. This could mean that the sediments in the area of station LV29-81 (Sakhalin slope) possibly contain gas hydrates.
Another new area (station LV29-92) with an increased methane concentration of 528 nl/l at the seafloor depth of 91 m to 438 nl/l at 59 m depth was discovered on the northern shelf of the Derugin Basin. Methane emanates here probably from oil-gas deposits in the sediment via a fault zone.
Water layers intruding from the oil-gas-bearing area at the Sakhalin coast or from Amur River are supposed to be the source of the unusually high methane concentrations (600-900 nl/l) in the 10 m thick surface water layer in the eastern part of the Sakhalin Gulf. The methane flux goes here directly into the atmosphere and thereby may influence the primary productivity of this area and change biological tracers used for paleoceanographic purposes.

The low methane concentrations at the seafloor of the Derugin Basin (station LV29-104) of 7-8 nl/l from a depth of 1,754 m up to 1,650 m indicate that a methane flux caused by microbiological processes is almost missing. Methane was also measured in the core recovered at this station (Appendix 4): the concentrations vary from 0.003 mM/kg at 200 cm to 0.4-0.5 mM/kg at the depth interval 600-870 cm.
At the Sakhalin slope high methane concentrations in the water column were measured in an area where the concentrations in the core are less than at station LV29-104. This means that here, the methane anomalies in the water column are created when methane emanates from destabilizing gas hydrates, oil-gas deposits and is transported there by water layers from other areas (intruded water).
The bottom waters of the Kurile Basin contain very low (5-10 nl/l) methane concentrations. Deep Pacific Ocean water masses usually have the same concentration. It is supposed that the water layer of the deep part of the Kurile Basin consists of Pacific water masses from the seafloor depth of 3,300 m to a depth of about 700-500 m, while the upper water layer from 700-500 m to the surface consists of Okhotsk water. The methane anomaly (70 nl/l at 3,300-2,800 m depth) in the bottom water of station GE99-7 shows that there is also a source of methane in this area. Methane is here supposed to come from the interior of the basement rise via a fault zone.
The methane anomaly measured at station LV29-131 possibly intruded into this area with the current from the Sakhalin shelf and slope. Methane was measured here in a sediment core (see Appendix 4) yielding a similar concentration as in the core of station LV29-104. A background value (0.0001 mM/kg at 15 cm) was found in the core surface and a high methane concentration at the base of the core (0.4-0.7 mM/kg at interval 750-830 cm). In contrast to station LV29-104 where the bottom water contained very low methane concentrations (7-8 nl/l), a methane anomaly (about 400 nl/l) was measured in the bottom water of station LV29-131. This means that methane migrated into the area of station LV29-131 from the sediment via a fault zone or was transported into this area by water layers from the north, but that it is not of microbiological origin.

6.3.1.9 Conclusions

The results of methane measurement are the following:

1. There is a high methane anomaly in the water column of the Sakhalin slope (station LV29-81) providing evidence of the existence of gas hydrates in this area.
2. The high methane anomaly in the bottom water of the northern shelf of the Derugin Basin indicates that this area possibly is oil-gas-bearing.
3. The high methane anomaly in the surface layer (10 m thick) of the eastern part of the Sakhalin Gulf shows that the methane flux now emanates into the atmosphere.
4. The low methane concentration in the water column of the deep Kurile Basin (about 3,300-1,000 m water depth) serves as tracer for the presence of Pacific water masses.
5. The anomaly of methane in the bottom water of the western slope of the Kurile Basin marks the migration of water layers from the southern Sakhalin shelf and slope into this area.

6.3.2 Methane distribution in sediment cores

Methane was measured in the cores of stations LV29-78, -104, -112, -131 in order to compare the methane concentration in the cores from areas with and without methane anomalies in the bottom water and in core intervals in which gas is visible.
The results are presented in Appendix 4. The methane concentrations of different areas are almost the same. At the sediment surface (15 cm) the concentration is low (about 0.0001mM/kg). It slowly increases to a depth of about 200 cm up to 0.001 nM/kg, but then

increases very sharply below interval 200 cm reaching 0.4-0.7 mM/kg at interval 600-800 cm. This regularity in the methane distribution changes in the gas hydrate-containing sediment core where a methane anomaly (3-4 mM/kg, Appendix 4) was observed in the gas hydrate layer.

In the sediment of the core from station LV29-104 a black-colored layer was found at a depth of about 700-800 cm. This layer contains high methane concentrations (0.4-0.5 mM/kg) which are, however, not different from that in layers of another color (gray) in other cores (for example at station LV29-131).

6.3.2.1 Conclusions

1. There is a regularity of the methane distribution in sediment cores: a low (background) methane concentration (about 0.0001mM/kg) in the surface layer and a high concentration (0.4-0.5 mM/kg) at the base of the core (600-800 cm).
2. The concentration of methane in the bottom water does almost not depend on the methane concentration in sediment cores, because microbiologically produced methane concentrates in the lower layers of the sediment and, due to the influence of the biological filter, does not rise to upper sediment intervals.

7. PLANKTON SAMPLING

Andrea Abelmann and Tanja Pollak

Based on comprehensive plankton and surface sediment studies accomplished during KOMEX I, we were able to define radiolarian “key species and assemblages” to reconstruct Pleistocene changes in the water mass structure and biological productivity system of the Okhotsk Sea. For further paleoceanographic studies, which will focus on cores from the Sakhalin shelf, the Kamchatka slope and the western Kurile Basin, our plankton and sediment data sets were enlarged in Leg 2 of cruise LV29.

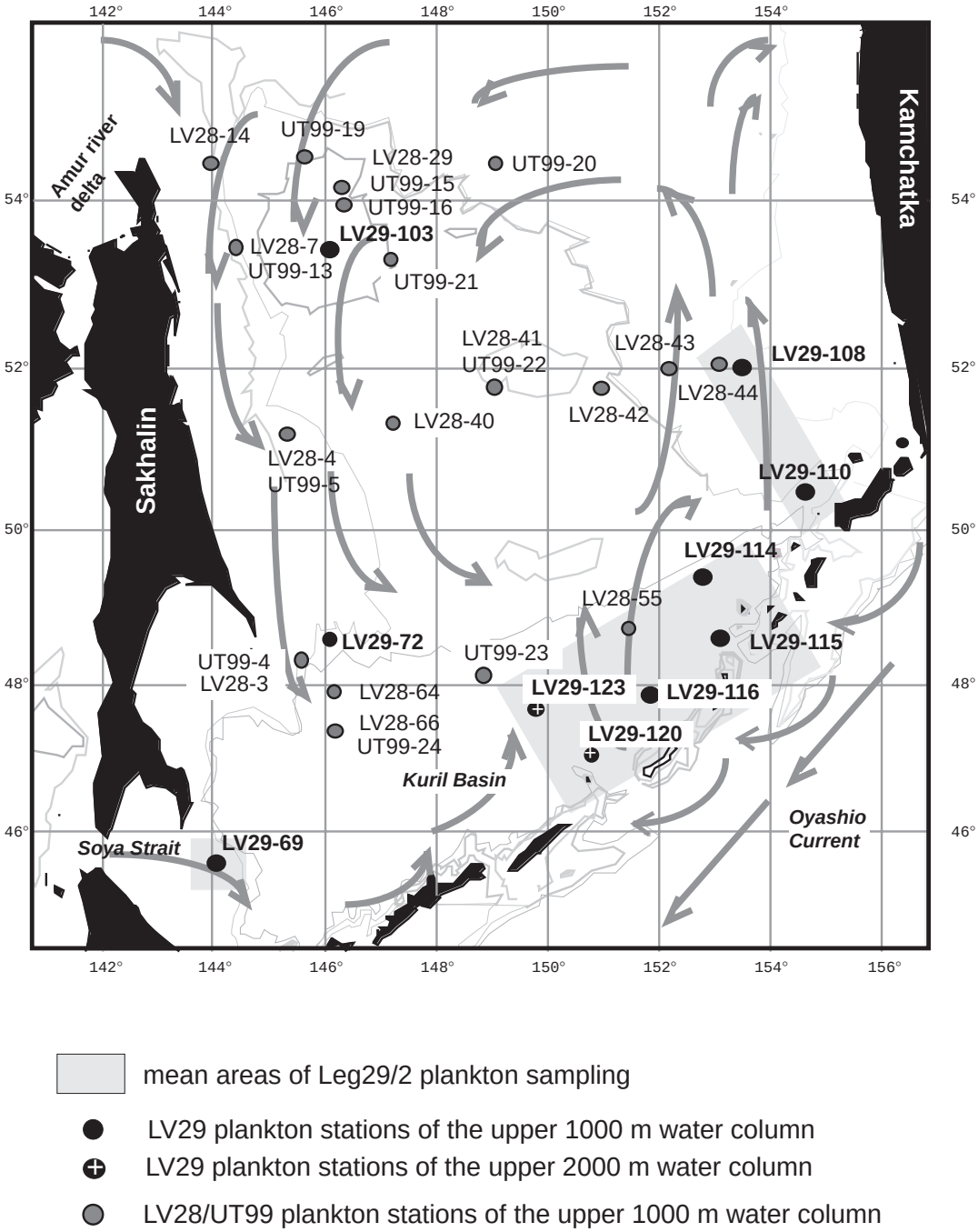

Fig. 7.1: *Locations of plankton stations sampled during Leg LV29/2 and previous cruises within KOMEX.*

7.1 Water column studies

Baseline for reconstructing the paleobiological system is the exact knowledge of the autecology of living radiolarians. On LV29 cruise we focussed our plankton sampling on the Kamchatka slope area, transects from the inner Kurile Basin towards the North Pacific and the Soya inflow area (*Fig. 7.1*). The goal of these investigations is to define
1) the boundary conditions of the biological system between the Okhotsk Sea and the North Pacific and
2) the import of taxa via the Kamchatka current (from the North Pacific) and the Soya Current (from the Japan Sea) into the Okhotsk Sea.

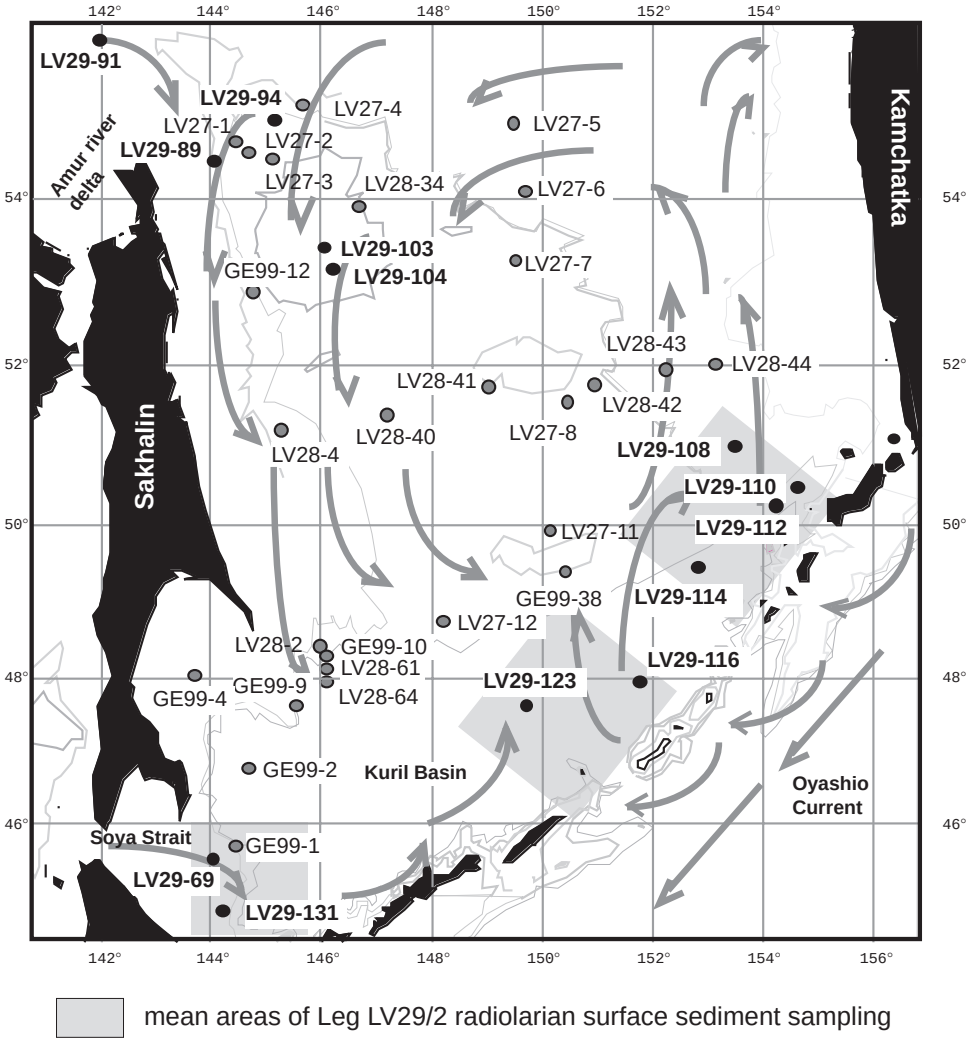

Fig. 7.2: *Locations of radiolarian surface sediment samples collected during Leg LV29/2 and previous cruises within KOMEX.*

We used an opening/closing net (Type MPS 92 B, "Hydrobios" Kiel, Germany), which consists of five nets, each 2.5 m long, with a mesh size of 55 µm fixed to a steel frame. This frame has a 50 x 50 cm large opening and is equipped with a motor and an electronic system for opening and closing the nets as well as a depth-measuring device. Both are connected with the board instrument, which displays the actual depth and which allows to open and to close the nets in specific water depths during heaving of the net. Each net ends with a sample beaker, equipped with a net window of 41 µm mesh size. Generally, we sampled five depth intervals in the upper 1,000 m of the water column according to the water mass distribution in combination with a CTD survey at each station. At two stations the water column was

sampled twice down to 2,000 m, including 9 different depth intervals. Depth intervals of each station are given in Appendix 5. Samples were preserved with a 2% dilution of formaldehyde.

The nets were towed vertically at low speed of 0.5 m s^{-1} (slacking) / 0.3 m s^{-1} (heaving) at all stations to avoid net clogging. The volume of water filtered was measured with calibrated flowmeters, which were installed at the inside of the mouth of each net. Thus, we could record the water passing through each net and for each depth interval. The application of flowmeters situated within the nets allows the quantification of the biological record, but also to recognize if the net has been clogged in areas of high productivity.

The differences between the flow meter values (the flow meter rotation values are proportional to the water volume flown through the net) after (F = final value) and before (S = start value) deployment multiplied by the opening diameter of the net frame (0.25 m^2) (A) and the impeller gradient (0.3 m) (P) defines the water volume (V) in m^3 flown through each net (Appendix A5).

$$\begin{aligned} V\,[m^3] &= (F-S) \times P \times A \\ &= (F-S) \times 0.3 \times 0.25 \\ &= (F-S) \times 0.75 \end{aligned}$$

7.2 Surface sediment studies

In contrast to plankton studies, which provide a spot-like information on the vertical distribution of taxa, surface sediment records provide a latitudinal signal integrated over a longer time period. To enlarge our radiolarian surface sediment dataset, needed as a reference for our paleoceanographic investigations, surface sediments were taken from various sites within the Okhotsk Sea, with emphasis on the Kamchatka area, the Kurile Basin and the Soya inflow area (*Fig. 7.2*). The sampling was done with a multicorer (MUC), which provides undisturbed sediment surfaces. For the radiolarian investigations the upper 0-1 cm were taken and preserved in formaldehyde. At most stations, we sampled one core in 1 cm slices to document the youngest sediment record, which may lack in the downcore record of the gravity cores.

8. PALEOCEANOLOGY AND SEDIMENTATION

Sergey Gorbarenko, Anatoly Botsul, Nicole Biebow, Lester Lembke, Anatoly Astakhov, Thomas Lüdmann, Alexander Derkachev, Natasha Nikolayeva, and Anatoly Salyuk

8.1 Introduction

Based on previous results of the RV *Akademik Lavrentyev* and MV *Marshal Gelovany* expeditions LV27, LV28 and GE99, we planned to clarify several important paleoceanographic problems in the Okhotsk Sea during the late Quaternary on cruise LV29:

8.1.1 Interaction of Amur River with oceanography and sedimentation in the Okhotsk Sea

We will further investigate the variability in Amur River runoff and influx of suspended material (development of Amur sediment drift). The prime area of investigation is set along a transect from the northern Sakhalin slope via the Derugin Basin to the Sakhalin Gulf.
Remarkably high sedimentation rates on the Sakhalin slope allow us to obtain high-resolution records to reconstruct rapid past changes of surface water conditions, supply of terrigenous matter and primary productivity during the Late Pleistocene – Holocene. The determination of these factors will help us to understand climate variability in the late Quaternary. Furthermore, we intend to clarify the varying production of North Shelf Density Water (NSDW) and the interconnected formation of Okhotsk Sea Intermediate Water (OSIW).
Our ongoing studies aim at the connection of marine productivity and terrigenous matter proxy records on the one hand with datasets from terrestrial climatic changes in the Amur drainage basin area and the surrounding Siberian hinterland. We try to evaluate the significance and impact of highly variable factors as precipitation, temperature, sea-ice cover in the Okhotsk Sea, their possible feedback mechanisms with the atmosphere and inherent ocean-continent interactions

8.1.2 High-resolution time scale study of the Pacific water inflow variability and the influence on paleoceanography

The sources of water masses in the Okhotsk Sea are from intermediate water layers of the NW Pacific (NPIW) and thence, also the newly formed OSIW is the product of mixing of the NSDW and inflowing Pacific water (Freeland, 1998). Today sea water masses below 800-1,000 m show parameters comparable to the Pacific via the deep Kurile Straits. Thus, oceanographic changes in the subarctic Pacific during Quaternary climate changes entail strong impacts on the Okhotsk Sea paleoceanography and -productivity. The areas of investigation are a southwest Kamchatka continental slope transect and a deeper profile on the eastern section of the Kurile Basin's slope. Our studies should provide a preliminary assessment of the Pacific water inflow changes into the Okhotsk Sea during the Quaternary and a connection with global climate and North Pacific paleoceanography. The changes derived from NPIW in the dichothermal layer; intermediate water production and the history of deep water ventilation will be studied in their response to climate change.

8.1.3 History of water exchange with the Japan Sea – La Perusa Strait's influence on the Okhotsk Sea paleoenvironment during the Quaternary and Holocene

The shallow depth of the La Perusa Strait sill (water depth 53 m) is a crucial key in regulating the warm subtropical water of the warm and saline Soya Current inflow from the Japan Sea into the Okhotsk Sea during glacioeustatical sea level changes.

Critical places for carrying out this part of our investigation are the southwestern part of the Okhotsk Sea close to La Perusa Strait and the deep profile from the northwestern Kurile Basin to the south Sakhalin slope. The influence of the relatively saline, dense Soya water on the OSIW formation will be studied during this part of work, as well.

8.2 Material and methods

During cruise LV29 the following steps of sediment sampling and processing were performed:

8.2.1 POI approach

8.2.1.1 Sampling

1. Sediment recovery was conducted with the POI Gravity Corer (SL-R): max. length 11 m, weight 850 kg, with an inner tube diameter of 145 mm. Polyethylene tubular film was inserted into the core before deployment. The attained sediment was removed from the corer in the PE foil. The Hydrostatic Corer (hydrocorer, HYC) with 126 mm in diameter and 6 m in length was used at vent areas with authigenic minerals and for gas hydrate sampling. The hydrocorer was also used for coring of harder sandy sediments. During Leg 2 of LV29 the total core recovery with the Gravity Corer and the Hydrostatic Corer added up to ca. 127 m. Aboard, a total of 114 m core was opened, described, measured and sampled in the matter described below.
2. Sediment cores were splitted. One half was used for sediment description, measurements and sampling, the other half was stored for archive.
3. Measurements of humidity and magnetic susceptibility were carried out every 2 cm by a microwave meter (MWM-8) and magnetic susceptibility meter (IMV-2) in direct contact with the sediment which is covered by cling wrap. Sampling every 20-50 cm for measuring sediment humidity and density according to the weight method as described below.
4. Sampling for micropaleontological (diatoms, radiolarians, foraminifers), granulometric (every 10 cm) and geochemical (every 5-10 cm) investigations.
5. Visual core description, sampling, preparation and the preliminary study of smear slides with microscope POLAM L-211.
6. Preliminary mineralogical investigations of volcanic ashes.
7. Separation and microscopic study of authigenic minerals, calcite, nodules and calcite-baritic crusts.

8.2.1.2 Mechanical properties of sediments

The analysis of sedimentary mechanical properties was mainly performed to establish a lithostratigraphy of the Quaternary sediments. In addition, the mechanical properties are necessary to calculate sediment accumulation rates. Since it is difficult to preserve the sediments natural humidity, humidity measurements were directly carried out aboard the ship immediately after core cutting.
Two methods were used: the standard weight method and humidity measurements with the MWM-meter. The first method includes sampling of 50 cm^3 of non-disturbed sediment, subsequent drying at 105°C temperature, and weighing before and after drying. On the basis of these data, the density of the natural sediment (D), the density of the mineral base (Dp), the volume humidity (Wv), and the weight humidity (Ww) were calculated applying the following equations:
D = Po / V;

DP = P / V;
Wv = (Po - P) / V x g x 100%;
Ww = (Po - P) / Po x 100%,
where Po and P are the sediment sample weight before and after drying; V - sample volume (cm^3); g - slime water density (g/cm^3) (1.00).

8.2.1.3 Magnetic susceptibility of sediments

Records of magnetic susceptibility mainly reflect the content of ferromagnetic minerals in the sediments. During the cruise measurements of magnetic susceptibility were obtained with the following method:
Cores retrieved with the POI gravity corer were measured with a sensor directly at the sediment surface. Magnetic susceptibility and humidity values were obtained every 2 cm alongcore. Magnetic susceptibility was measured in CGS-units using the microwave moisture meters MWM-8.

8.2.2 GEOMAR Approach

The KIEL Gravity Corer System was used for sediment sampling. The system consists of hot-dip galvanized steel tubes (575 cm length each, 125 mm diameter) connected by simple nail sockets and is equipped with a coretop penetration weight of 2 tons. The system is used with rigid PVC-liner tubes for sediment recovery allowing the permanent assessment of original sediment in the liner. During Leg 2 of LV29 the total core recovery with the KIEL Gravity Corer added up to 144 m.

Aboard, a total of 115 m core was opened, described, measured and sampled in the matter described below:

1. Cores were cut into segments of 1m length, and labeled following recommendations of Holler (1995)
2. Measurement of magnetic susceptibility: We used a Bartington loop sensor (MS2C) with a control unit (MS2) directly connected to a PC-laptop for data storage. The ring-shaped sensor generates a low-intensity magnetic field (f = 565 Hz), which is altered in its frequency by the sediment put into the loop depending on the amount of ferromagnetic minerals in the core section measured. Sampling interval was 1 cm.
3. Cores were split vertically and divided into work (W) and archive (A) halves. Sediment in the liner segments was leveled and covered with cling film.
4. The archive half was color-scanned with a handheld Minolta CM 2002 Spectrophotometer in 1 cm sample spacing according to the method outlined in Biebow & Hütten (1999).
5. X-radiographs were continuously taken from the work half of the cores (modified after Holler, 1995; Rehder, pers. comm.).
6. 5cc (10cc) syringe samples were taken at 5 cm (10 cm) intervals for subsequent land-based analysis of physical properties (pp-samples). Syringes were closed with caps and sealed with TEMFLEX tape. Sealed syringes were welded airtight in evacuated PE foil bags to minimize loss of pore water content. During the cruise, samples were stored refrigerated at 4-6°C.
7. Visual core descriptions were carried out on the archive halves of core segments. Classification of sedimentary texture and lithology generally follows modified recommendations of the ODP program (Sachs et al., 2000). Classification of randomly occurring dropstones is described by Powers (1982), grain sizes of the terrigenous fraction are classified as recommended by Shepard (1954).

8. A total of 337 smear slides was taken from the cores in order to corroborate the on-board visual core descriptions. Initial analysis (estimates of grain size distribution and components) was carried out at GEOMAR, Kiel using a Leitz Laborlux 12 POL S polarization microscope with a 100 x - 500 x magnification according to grain size composition.

8.2.3 Sediment stratigraphy and age model

In order to get an initial sediment stratigraphy and preliminary age models of the cores, we used the following proxies: visual sediment description, semi-quantitative analysis of smear slides, color spectra, magnetic susceptibility, water content, dry bulk density and tephrachronology. For stratigraphic interpretation of these datasets we follow the multi-proxy stratigraphy developed for Okhotsk Sea sediments based on oxygen isotope stratigraphy, AMS radiocarbon datings, sediment color and magnetic susceptibility records, calcium carbonate/opal content and tephrachronology (Gorbarenko et al., 1998; Biebow & Hütten, 1999; Biebow et al., 2000; Gorbarenko et al., 2002).

8.3 Results

8.3.1 Northwestern Kurile Basin - south Sakhalin slope profile

Stations LV29-70 and LV 29-72 are located at intermediate water depths of 2,325 and 1,380 m, respectively.

8.3.1.1 SL-R (LV29-70-2, LV29-72-2)

Records for these cores (*Fig. 8.1* and Appendix 6) show that both have sedimentation patterns typical for this part of the Okhotsk Sea and a rather clear stratigraphy and age model after correlation to existing records (Gorbarenko et al., 2002). Diatomaceous sediment with a base age of 6-8 kyr covers the upper 60 and 170 cm in cores LV29-70-2 and LV29-72-2, respectively. According to MS records, biogenic opal and carbonate content (smears slides description), the MIS 1/2 boundary is placed in LV29-70-2 and LV29-72-2 at a depth of 120 cm and 340 cm, respectively. With regard to ash layer K2 with an age of 26 kyr (Gorbarenko et al., 2002), MS records and the main component composition the boundary of MIS 2/3 can be determined at a depth of 370 cm and 545 cm in both cores. A gray ash layer at a depth 727 cm in core LV29-70-2 was preliminary identified by mineralogy as Spfa-1. Thus, the lower parts of both cores likely belong to MIS 3.

8.3.1.2 SL-G (LV29-70-3, LV29-72-3)

Records of magnetic susceptibility (MS) and color spectra allow us to set up a preliminary age model for the two cores LV29-70-3 and LV29-72-3, though our results remain preliminary and need further proof by independent proxy data.

LV29-70-3

Diatomaceous ooze extends down to 237 cm, thereby decreasing in total diatom abundance downcore. This upper section is interrupted by a brief setback at 166-180 cm with decreased diatom content and slightly elevated MS values that might represent a climatic rebound and the establishment of high biogenic productivity hereafter (i.e. visibly high diatom content in sediments). Later works for refined stratigraphic control will show if this offset correlates with global climatic signals like the commonly known early Holocene Northern Hemisphere climatic collapse at around 8,200 yrs BP. According to that, the sub-

sequent excursions in the MS signal (*Fig. 8.1*) might mark the terminations Ic, Ib and Ia at ca. 238 cm, 256 cm and 295 cm, respectively, with the Bølling-Allerød period between

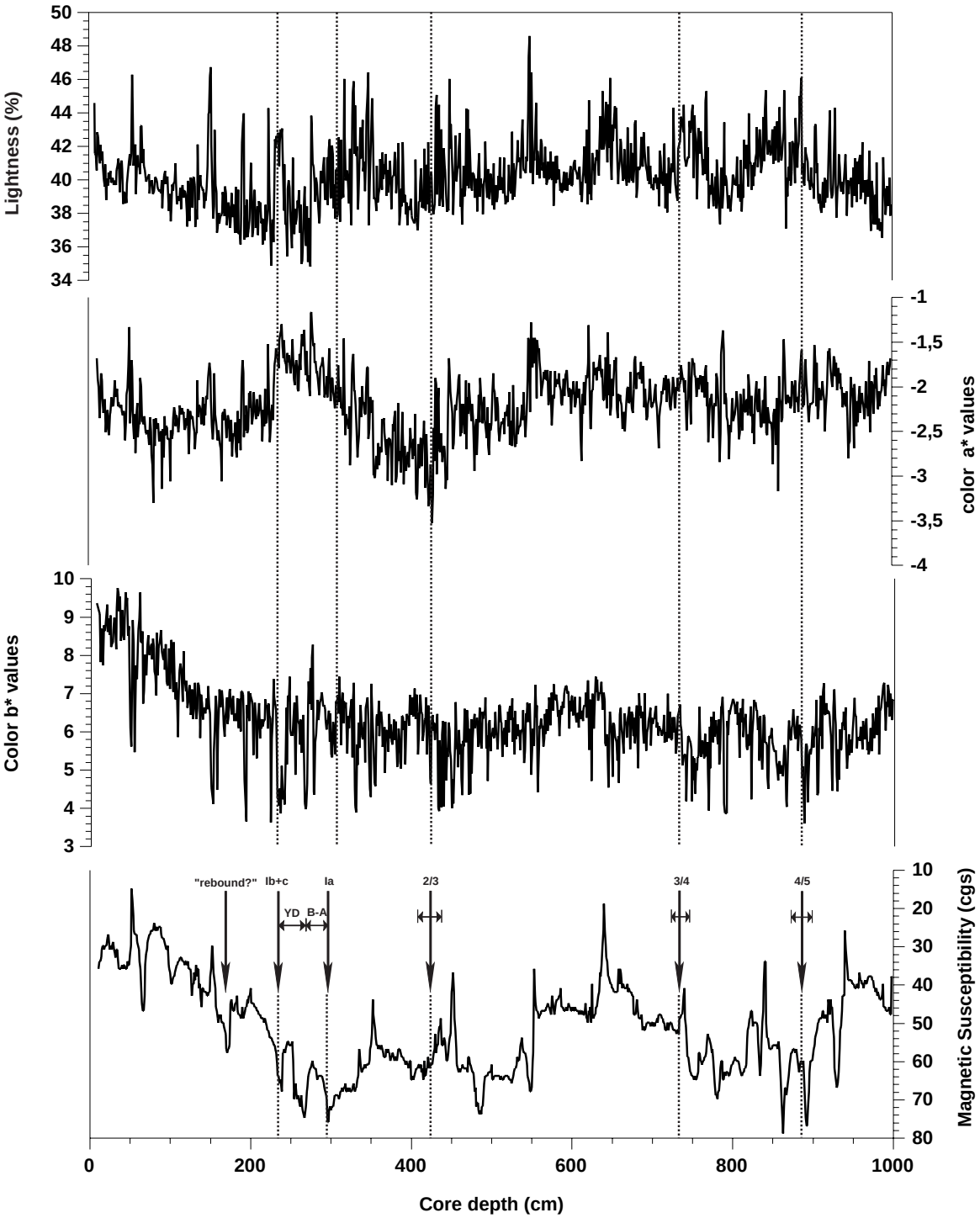

Fig. 8.1: *LV29-70-3, from top to bottom, Lightness of color reflectance spectra, Color spectrum of red-green chroma, Color Spectrum of yellow-blue chroma and magnetic susceptibility.*

the latter depth and ca. 270 cm. The MIS 2/3 transition occurs around 439 cm core depth with a slight decrease in MS values, accompanied by a notable increase in diatom content between 366-439 cm. Our findings are endorsed by the occurrence of cm-large lenses of volcanic ash (identified as K2 ≈ 26 ka) in core LV29-70-4 at a core depth of 483.5 cm and eventually ash layer Spfa-1 (≈40 ka), forming a 3-4 mm thick sandy layer at a depth of 706.5 cm. The MIS 3/4 boundary we prefer to leave rather unascertained, we believe it to

occur around 732-745 cm as we see there a decrease in diatom abundance and increased MS values. From 880 cm downcore, slightly higher contents of biogenic silica (diatom fragments mostly) and lower MS values might point to a change towards ameliorating climatic conditions. Further high-resolution studies of biogenic opal content, terrigenous supply and extended stratigraphic framework will elucidate if LV29-70-3 really reaches MIS 5 at its basal part.

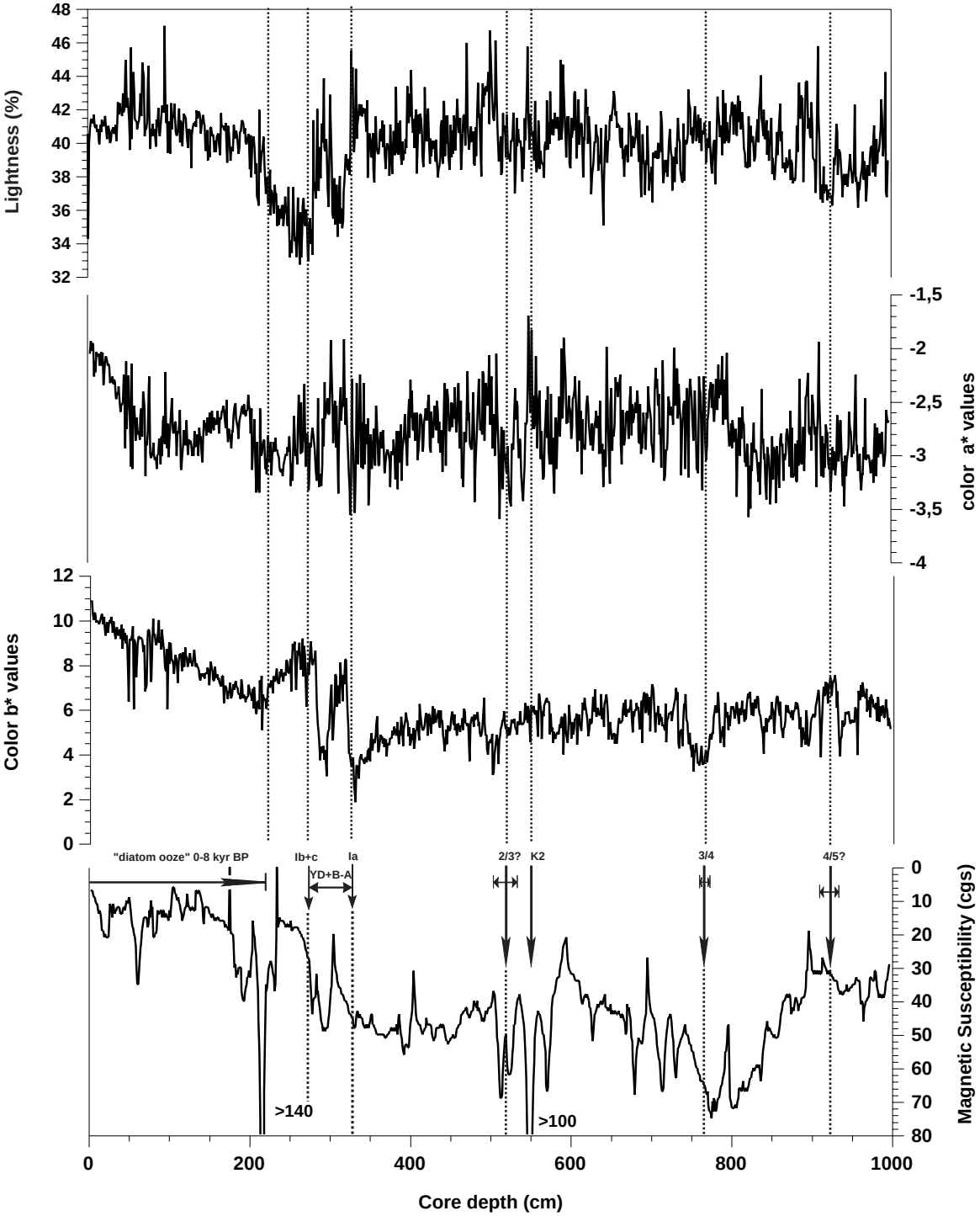

Fig. 8.2: *LV29-72-3, from top to bottom, Lightness of color reflectance spectra, Color spectrum of red-green chroma, Color Spectrum of yellow-blue chroma and magnetic susceptibility.*

LV29-72-3

In this core, typical late Holocene diatomaceous ooze (deposited during the last 6-8 kyr, according to Gorbarenko et al., 2002) extends down to 229 cm as indicated by decreasing lightness and – more pronounced – color b* values as well as smear slide analysis (*Fig. 8.2*). We place the last deglaciation/Termination Ib around 275-283 cm, preceded by the Younger Dryas (YD)/ Bølling-Allerød (B-A) interval at 283-322 cm. This interval is characterized by coarser grain sizes and weaker sorting, respectively, in the terrigenous fraction and reduced diatom content as well. We suppose the B-A warmer period might be separated from the YD event by notably elevated color b* and a* values pointing towards increased abundance of biogenic particles, though this criterion is not as clearly seen in the lithological description yet. Larger dropstones occur at depths of 510 cm and 526 cm, biasing the color and MS signals. Accordingly, we assume that the MIS 2/3 boundary in this core lies within this interval (ca. 505-530 cm), since we identified ash layer K2 (26 kyr BP) at a depth of 550-555 cm.

Slight changes in lithology and the increase in MS values point to the MIS 3/4 transition to be located around 788-91 cm as we observe frequent dropstones and higher sand/silt content between 788 cm and 930 cm, indicating colder climatic conditions. Finally, we dare to place the MIS 4/5 transition at 925-935 cm core depth due to a remarkable decrease in MS values and coincident appearance of diatoms (mostly fragments), though quite rare.

8.3.2 North Sakhalin slope

8.3.2.1 Setting

The study area is located on the northeastern Sakhalin continental slope proximate to the Derugin Basin. The goals of this investigation are the influence of Amur River on the paleoceanography and sedimentation in the Okhotsk Sea within the last 10,000 to 15,000 years. Extremely high sedimentation rates on the Sakhalin slope allow us to get high-resolution records of the climate, surface water conditions, sea-ice cover and varying productivity. Two echosounding profiles and four stations (LV29-78, LV29-79, LV29-81, LV29-82) were conducted in this area.

8.3.2.2 SL-R (LV29-78-2, LV29-79-2, LV29-82-1)

Cores LV29-78-2 and LV29-79-2 were taken on the southern profile from depths of 655 m and 1,102 m respectively. The echosounding data shows parallel reflections of high amplitude at depths of more than 7-8 m (see Chapter 3). Station LV29-82 was set at a depth of 795 m on the northern profile. The echosounding data shows here exposed ancient sediments, but core LV29-82-1 penetrated only sediment of MIS 1 and did not reach older strata.

All these cores showed similar sediment sequences. Diatom ooze or diatomaceous silty clays compose the upper part. Weakly diatomaceous silty clays and clayey silt follow below. The core descriptions (see Appendix 6) and records of the component composition, physical properties (see Appendix 6) allow us to determine the sediment age to be not older than MIS 1. An additional age record may be established by the biogenic opal content. The base of intensive diatom accumulation in the Okhotsk Sea usually corresponds to the 6-8 ka period (Gorbarenko et al., 2002).

8.3.2.3 SL-G (LV29-78-3, LV29-79-3)

Onboard work concentrated on cores LV29-78-3 and LV29-79-3 (*Figs. 8.3* and *8.4*). Both cores show sedimentation patterns very similar to the Russian gravity cores (SL-R). MS are very low in both cores, it is generally assumed that below values of 30 cgs units, pre-

cise analysis is hampered by a low signal/noise ratio. However, neither do we see an increase in MS values nor complete changes in lithology in the lower parts of both cores, thus we strongly believe that they consist entirely of Holocene sediments without covering the last deglaciation. This in turn points to an extremely high sedimentation rate of more than 100 cm/kyr averaged over the complete core length. In LV29-78-3, we may put the basal boundary of the diatom-rich facies at ca. 600-640 cm, based on slight changes in color a*, b* values and a decrease in diatom content.

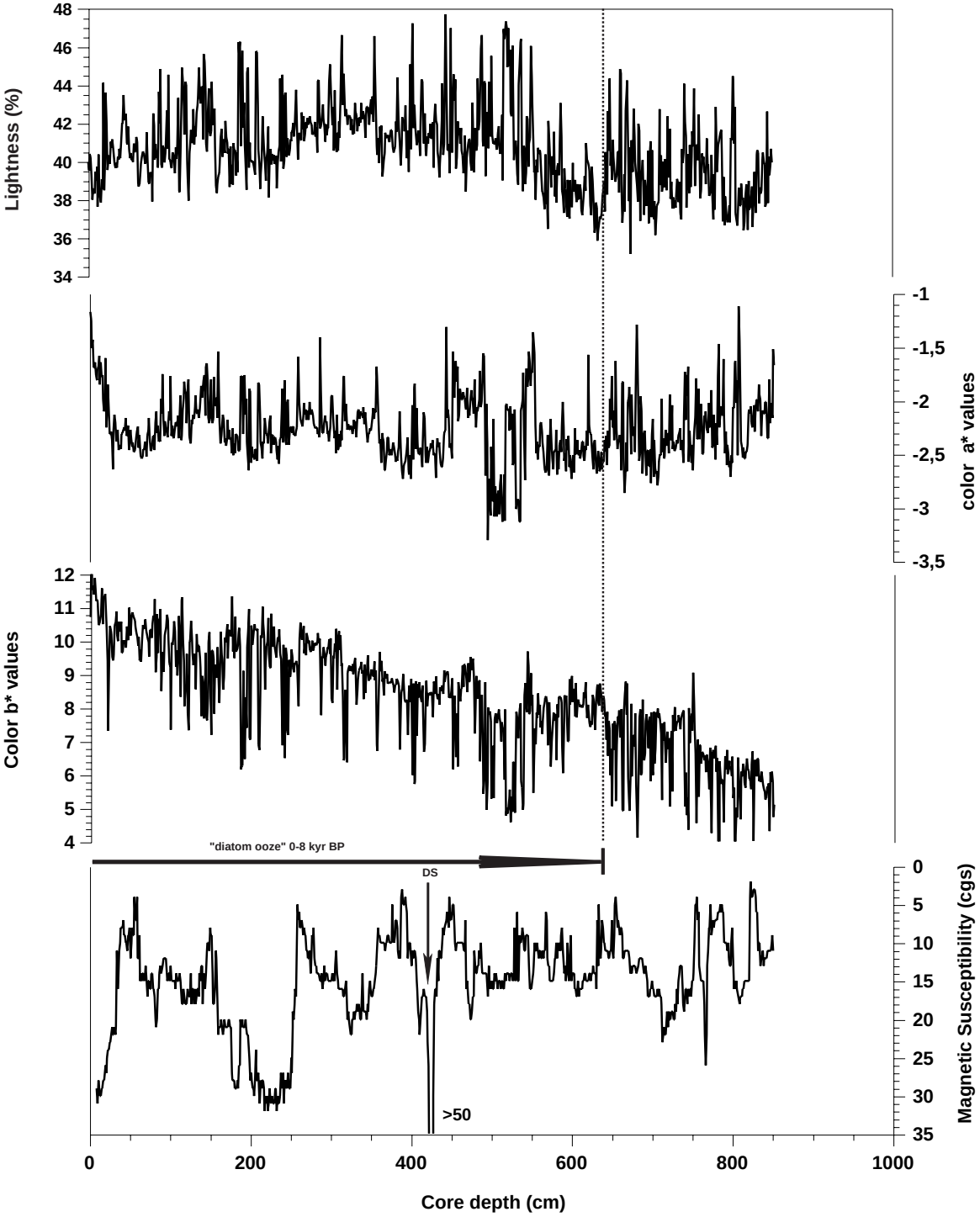

Fig. 8.3: *LV29-78-3, from top to bottom, Lightness of color reflectance spectra, Color spectrum of red-green chroma, Color Spectrum of yellow-blue chroma and magnetic susceptibility.*

At core LV29-79-3 we observe a distinct decrease in diatom abundance around 650 cm, though several intervals with lower diatom abundance occur in the upper part, e.g. around 540 and 570 cm, together with a slight coarsening of the siliciclastic fraction downcore. So far, we did not succeed in reliably correlating MS or color records of the two new cores to our well dated core LV28-4-4 from a more southern position at the Sakhalin continental margin.

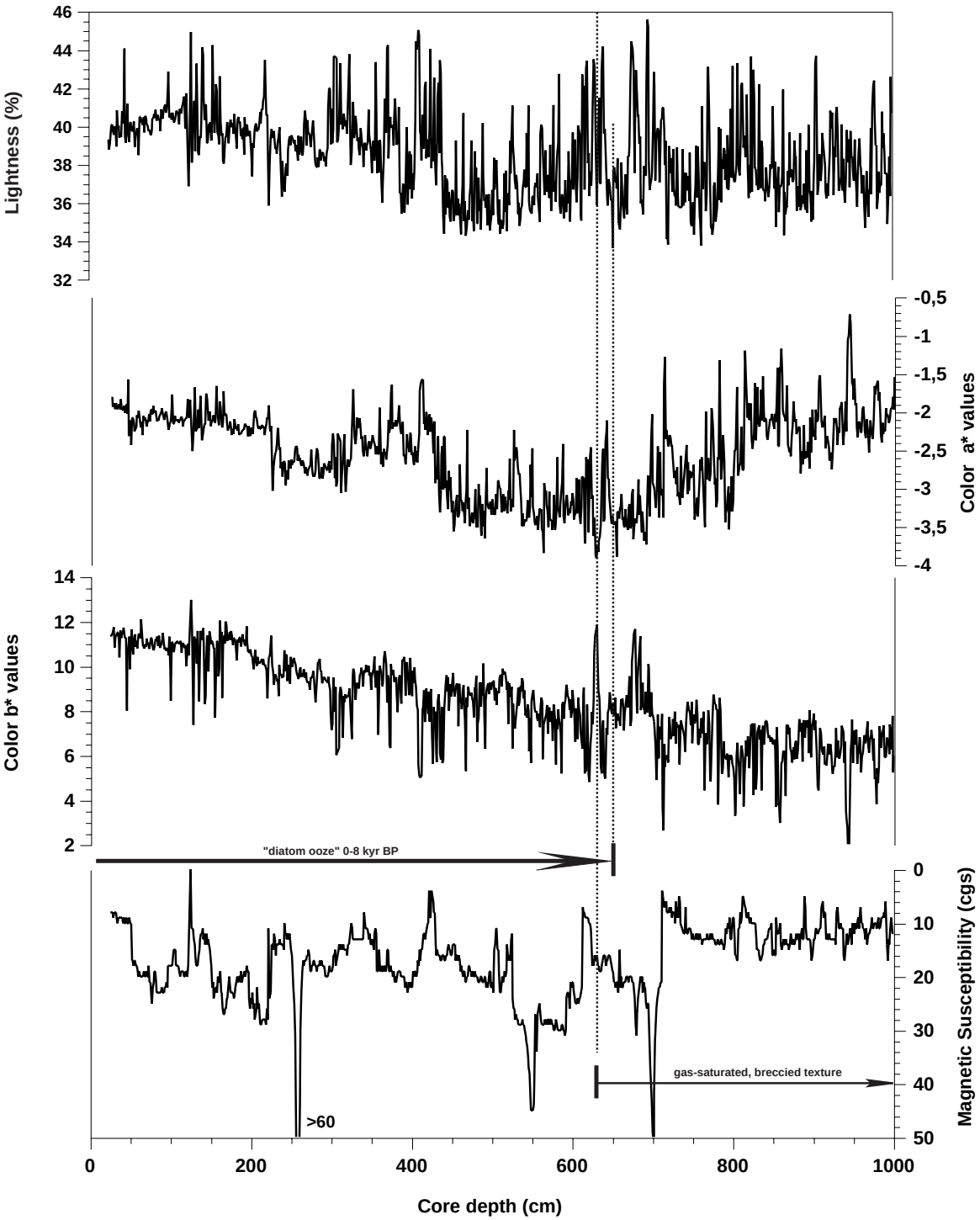

Fig. 8.4: *LV29-79-3, from top to bottom, Lightness of color reflectance spectra, Color spectrum of red-green chroma, Color Spectrum of yellow-blue chroma and magnetic susceptibility.*

However, we put forth the proposition that the occurrence of early diagenetic alterations (see Chapter 8.3.2.3) has appeared rather synchronously at the Sakhalin margin due to a

regional event (degassing, as indicated from seismic profiles and the correlation of the new cores diagenetic alterations and primary lithology). At core LV29-78-3, diagenesis starts at a core depth of 491 cm, at core LV29-79-3 at 631-635 cm and at reference core LV28-4-4 at 427 cm core depth currently resembling an age of ca. 3,700 cal. yrs BP.
Further stratigraphic work will have to be carried out to achieve a precise age model of our new cores and in turn solve the question if diagenetic alterations really represent a regional feature possibly recorded in other sites (Tiedemann et al., 2001).

8.3.2.4 Early diagenetic alterations

Typical textures of gas migration and an H_2S odor were revealed in all cores at depths of more than 400-500 cm. At or below this border an intensive diagenetic mineralization occurs in the form of globule pyrite and microcrystalline carbonate (see *Figs. 8.3 and 8.4*). Lenses and interlayers of dense diagenetic sediment with carbonate cement compose the bases of cores LV29-78-2 and LV29-79-2. Diagenetic layers of low water content and low porosity with globule pyrite cementation were revealed in cores LV29-79-2 and LV29-82-1. Reflector boundaries on the 8 kHz profiles of the studied cores are well correlated with diagenetic changes in the sediment like diagenetic carbonate cement, diagenetic sulfide layer, the top boundary of brecciated sediment.

8.3.3 Kashevarov Bank (LV29-94-2)
8.3.3.1 Setting

The cores at station LV29-94 were recovered from the southern slope of the Kashevarov Bank from a depth of 1,142 m (LV29-94-2, SL-R) and 1,134 m (LV29-94-3, SL-G), respectively. Previous studies indicate that the sedimentation pattern at this location is completely governed by material input from the northern shelf of the Okhotsk Sea while being separated from the Amur River influence by Staretsky Trough. The Kashevarov Bank with a shallow top is exposed to strong tidal currents having large influence on the sedimentary regime in this area.

8.3.3.2 SL-R (LV29-94-2)

The MIS 1 sediment in core LV29-94-2 has a very small thickness (16 cm) and consists of sandy silt with diatoms, likely being reworked (see Appendix 6). The sediment of this core bears a significant proportion of sand through the entire core. Especially large amounts of sand with gravel were observed in horizon 625-750 cm, which may be very preliminary correlated with MIS 4. The strongly reflected boundary in the 8 kHz records at a depth of nearly 9 m is apparently connected with this horizon. In line with the MS records, water content and an ash layer hypothetically identified as K2 (see Appendix 6), the MIS 2/3 transition was set at 360 cm.

8.3.3.3 SL-G (LV29-94-3)

In this core the abundance of diatomaceous sediments drastically decreases in the upper 80 cm pointing towards either a reworking of sediment or a missing upper section of softer sediment. Though at this location, a non-continuous sedimentation regime is very likely, MS records point out the possibility of a rather undisturbed record in the upper part of the core. We presume the YD and the preceding B-Al period to occur at depths of 241-260 cm and 260-286 cm, respectively, the latter mainly based on MS record (*Fig. 8.5*). As well, we put the MIS 2/3 transition at ca. 400-410 cm, due to a significant decrease in MS values. MIS 3/4 boundary is assumed to appear at 638-640 cm, based on remarkable increases in

small dropstones, sand lenses and layers and a general coarsening of the siliciclastic fraction. MIS 4/5 might be set at a depth of ca. 840 cm as MS values decrease to minimum MIS 3 values, though not reaching Holocene minima.

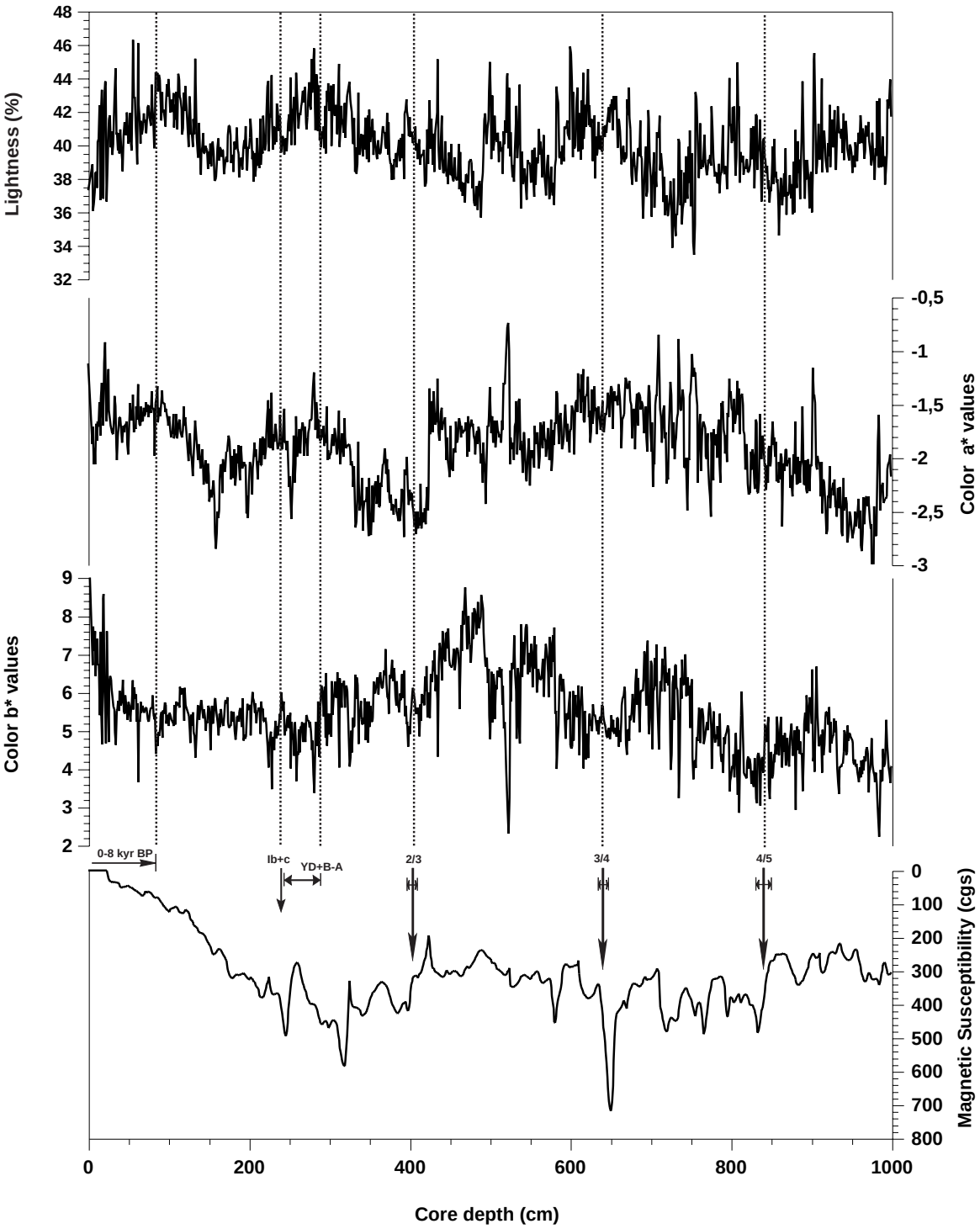

Fig. 8.5: *LV29-94-3, from top to bottom, Lightness of color reflectance spectra, Color spectrum of red-green chroma, Color Spectrum of yellow-blue chroma and magnetic susceptibility.*

8.3.4 Sakhalin Gulf (LV29-89, LV29-91)

8.3.4.1 Setting

Sampling points were chosen subsequent to a preliminary analysis of the 3.5 kHz echosounder data. Practically the entire seafloor of the gulf is covered by sediments of sandy

grain size (Astakhov, 1986; Dudarev et al., 2000). Within the upper part of the sedimentary section (0-15 cm), well sorted medium-fine-grained sands of grayish-green color usually occur. They are related to palimpsest deposits according to the classification of McManus (McManus, 1975).

In the area of station LV29-91, the upper part of the sedimentary layer is composed of marine sediments with a thickness of about 27 cm, consisting of well sorted sands amongst which mixed sandy-gravel-pebble sediments occur. Below 35 cm this lithology is replaced by gravel-pebble deposits, which probably belong to a beach facies.

8.3.4.2 SL-R/ SL-G

Core LV29-89 recovered a typical section of relict inshore-marine and lagoon-estuarine deposits of hypothetically late Pleistocene age. The upper part of the core (5-22 cm) is described as inshore-marine and beach deposits consisting of silty sand, sand with admixture of gravel and pebble; rare shell fragments occur. Below, these deposits are gradually replaced by lenticular-bedded compact sediments of dark gray color with an interchange of thin laminae of silt, clayey silt, sandy silt, and they have a lagoon-estuarine origin. Besides, fragments of wood branches and a large quantity of mica occur in this facies.

8.3.5 Derugin Basin (LV29-103, LV29-104)
8.3.5.1 Recent environments and coring position

The investigation of the southern depression of the Derugin Basin was made for discovering and studying anoxic sediments and environments in different glacial-interglacial periods based on the existence of closed depressions and recent hydrochemistry of bottom waters. They are located within the oxygen minimum layer (OML), and the oxygen content in the water column decreases towards the bottom. The oxygen content of the Okhotsk Sea bottom waters is very low (Bezrukov, 1957; Bruyevich et al., 1960; Freeland et al., 1998). These bottom waters of the deeper part of the Derugin Basin can be interpreted as suboxic due to the absence of oxygen. An anoxic environment can arise from small changes in hydrochemical conditions. The deeper part of the Derugin Basin is one of the possible places for the development of anoxic conditions.
Besides, the investigation goal was to study the Amur River deep paleo-fan during glaciation when the river delta was located on the recent shelf to the north of Schmidt Peninsula. The possible deep-sea fan enriched in fine organic matter sediment and turbidities was recovered earlier in the northern part of the Derugin Basin (stations LV27-3, GE99-30, GE99-31) (Astakhov et al., 2000). In this region, turbid seismic facies were mapped (Lüdmann et al., 2002). Their location indicates the nearest part of the deep fan to the river mouth during glaciation (Astakhov, 1986). Such specific seismic facies were also revealed on the shelf (prograding clinoforms) and slope (lenticular, stratified to wavy) (Lüdmann et al., 2002).
On the outer part of the deep fan outside the turbid facies two coring stations (LV29-103 and LV29-104) were chosen on the basis of preceding echosounding. According to the echosounding data, the bottom of the southern Derugin Basin is rough with many smooth elevations. On the top of one of these elevations ancient sediments are exposed. On the sides of the elevations, older sediments are covered by stratified sediments with several reflectors. The first one can be traced areawide at a depth of 2-4 m. The next reflectors submerge to the central part of the depression from 5-8 to 15-20 m. The deeper part of the depression has a smooth relief and is covered by stratified sediment with horizontal reflectors. It is noteworthy that, according to our data, the depth of the deeper part of the Derugin Basin does not prevail 1,760-1,770 m, although many bathymetric maps show

depths of more than 1,800 m. The 12 kHz echosounder (ELAC) was calibrated by the CTD sound and pressure sensor for water depth. The coring position for station LV29-103 was selected on the slope of a small elevation not far from its top. The reflectors are here close to one another with the first 10 m including 3-4 reflectors. Station LV29-104 is located in the central part of the depression. Here, all reflectors are situated in deeper layers (15-20 m).

8.3.5.2 Sediment peculiarities

All four cores from the Derugin Basin recovered similar sediments about 10 m thick. In the following, core LV29-104-2 from the central deeper part of the southern depression is discussed as an example for the general sedimentary sequence (see Appendix 6). The sedimentary sequence basically consists of two units. The upper one part can be grouped together as sequences of MIS 1 and 2 (Gorbarenko et al., 2002), including a Holocene diatom layer (0-37 cm), a terrigenous, weakly diatomaceous and foraminifera layer of 1 MIS (37-95 cm) with carbonate peaks IA, IB, IC, and Younger Dryas sediments (67-78 cm). These layers are well visible as color changes, which were recorded in the visual description as well as in colormetric data (see Appendix 6). A black and brownish-black layer of oxic sediments is also indicated well in interval 0-13 cm of the color data.
The sediment unit of interval 5-242 cm correlates with the MIS 2 sediments of previously dated cores (Gorbarenko et al., 2002) with regard to component composition and physical sediment properties. These sediments contain a significant amount of IRD and include green diagenetic dense lenses typical for glacial sediments of the northern Okhotsk Sea. In interval 170-200 cm a more intense diagenetic alteration with microcrystalline carbonate cement and an enrichment in pyrite globules occur.
The core part below 242 cm consists of homogeneous silty clay without IRD and a significant portion of marine biogenic matter (rare diatoms). However, it is also enriched with respect to terrestrial plant debris. This layer was possibly formed during short-time periods in the distal part of Amur River at times of intensive suspension input. The homogenous composition is confirmed by the main component distribution and physical properties values (see Appendix 6). According to color spectra this layer is divided into two horizons. The upper olive-green layer (242-710 cm) formed in oxic or suboxic conditions, whereas the black layer (>710 cm) was deposited under anoxic conditions. These layers are mainly distinguished by the composition of diagenetic minerals.
The first unit of the olive-green sediment contains a large amount of globular pyrite (see Appendix 6) and coarse-grained broken carbonate aggregates. The latter consist of large yellow grains and microcrystalline aggregates of white carbonate. Possibly, these represent remains of large crystals of hydrocarbonate (Ikaite) as revealed in similar sediments of core LV27-3 (Nürnberg et al., 1997). The black sediments do not contain any coarse authigenic minerals. The smear slides show large amounts of black amorphous matter (hydrotroilite?). Its color quickly disappears after air contact of the sediment or smear slides. Beside the black color and absence of diagenetic alteration, this sediment is distinguished from the olive-green sediment by shell fragments and less water content.
Core LV29-103-2 displays a similar sequence including MIS 1 sediment (0-149 cm), top sediments of MIS 2 (149-256 cm) and homogeneous olive-gray and black organic-rich silty clay (see Appendix 6) of the Amour's deep-sea fan. It differs from core LV29-104-2 by the appearance of turbidity layers (683-703, 846-857 cm) and interlayers of normal accumulation (936-983 cm). The turbiditic layers were determined from MS records and clastic grains content (see Appendix 6). Diagenetic processes intensively change sediment layers under turbidites. They are enriched in large pyrite aggregates as "globules", "grains" and "sticks" and partly cemented by microcrystalline carbonate.

8.3.5.3 Stratigraphy and origin of black sediments

The age of the top boundary of the deep-sea fan deposits is lithostratigraphically established as MIS 2. The age of the bottom part of the sequence is not determined. Based on the absence of ash layer K2, which was discovered in cores to the north (GE99-36 (Biebow et al., 2000)) and south (GE99-37 (Gorbarenko, pers. com.), it can be supposed that the age of the investigated core is less than 24 ka. Still, other suppositions may be considered, especially for core LV29-103-2 which seems to have penetrated older parts of the fan sequence.
The black sediments are discovered in the Okhotsk Sea for the first time. Today, a number of opinions exists about the depositional environment leading to the formation of anoxic sediments and its ancient analogy – black shales. Apart from anoxic water (Kristensen & Blackburn, 1987; Canfield, 1989; Wortmann et al., 1999), another necessary condition is a massive input of organic matter of possibly terrestrial origin (Habib, 1982) by different ways, specifically by turbidity currents (Dean et al., 1978; Jansa et al., 1979; Dean & Gadner, 1982), or high primary production (Pedersen & Calvert, 1990; Calvert & Pedersen, 1993).
Possible sources of organic matter (OM) leading to the formation of black sediments in the Derugin Basin might be massive input of terrestrial OM by debris flow from the paleo-river mouth. The cause for the appearance of anoxia waters has yet not been found out. One of the possible causes is the extraction of oxygen from bottom waters for oxidation of OM at times of low vertical convection. Another cause may be a special geodynamic and fluid activity of the Derugin Basin.

8.3.6 West Kamchatka profile (LV29-106, LV29-108)
8.3.6.1 Setting

The goals of this sediment profile were extended investigations of the influx of northwestern Pacific waters into the Okhotsk Sea and their influence on the regional paleoceanography. Station LV29-106 was set on the continental slope of Kamchatka Peninsula at a water depth of 510-511 m. The cores at station LV29-108 were recovered from depths of 625-627 m close to the older core LV28-44. The sediments of the shallow cores (LV29-106-2 and LV29-106-6) are characterized by coarser grain sizes than those of the deeper ones.
The sediments of this region reveal a significant influx of volcanogenic material from the eastern Kurile Islands and Kamchatka and, consequently, show high MS values.

8.3.6.2 SL-R (LV29-106-2, LV29-108-4)

The description of cores LV29-106-2 and LV29-108-4 and records of the component composition and physical properties (see Appendix 6) allow us to establish the stratigraphy in terms of marine oxygen isotope stages. Ash layer K0 (see Chapter 8.3.9) with an age of 8 ka (Gorbarenko et al., 2002) is clearly expressed in both cores, confirming the position of the MIS 1/2 boundary. The sediment of the cold MIS 2 is characterized by high MS values, dry bulk density and a clastic component content. Regularities of these records allow us to determine the MIS 2/3 boundary in both cores (see Appendix 6).
Sediment with high diatom abundance starts to accumulate in both cores just above ash K0 after 8 kyr. Sediments enriched in diatoms were observed in core LV29-108-4 below ash K0 down to the boundary MIS 1/2. In core LV29-106-2, there diatom contents increase during stage 3 (see Appendix 6). Apparently, the variability in biogenic opal accumulation is a special feature of this region related with the strong influence of Pacific waters (Haug et al., 1995; Gorbarenko, 1996).

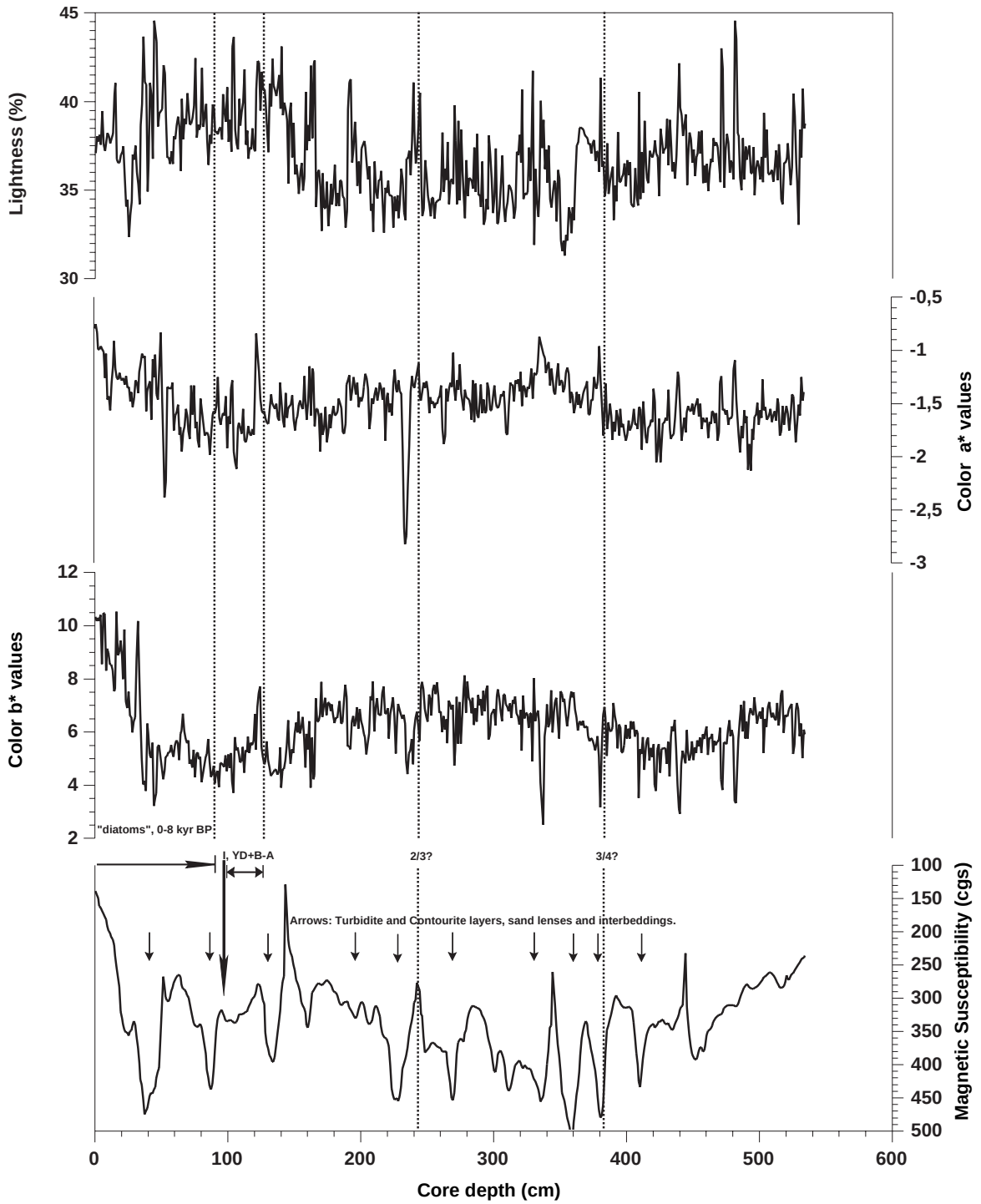

Fig. 8.6: *LV29-106-6, from top to bottom, Lightness of color reflectance spectra, Color spectrum of red-green chroma, Color Spectrum of yellow-blue chroma and magnetic susceptibility.*

8.3.6.3 SL-G (LV29-106-6, LV29-108-5)

At one of the locations, we were able to establish a preliminary age model primarily based upon the records of MS and the lithological changes.
At core LV29-106-6 we obtained a record rather disturbed by frequent intercalation's of sand lenses and layers presently inhibiting us to put forward a precise age model. Prominent layers and lenses enriched in sand and silt, sometimes with graded bedding and signs of eroded paleo-surfaces, occur at core depths 33-43, 90-95, 130-136, 199-208, 225-228, 267-273 cm, etc., a feature also depicted in the records of MS (*Fig. 8.6*). At present, we are

only able to assume that the Holocene diatom-rich layer ends somewhere around 60 and 90 cm (based upon color values) and that the Younger Dryas/Bølling-Allerød might appear close to 100-130 cm, but this assumption is very preliminary. Due to the numerous events of rapid clastic sedimentation in this core indicating frequent turbidites, contourites with sediment erosion and reworking, considerable work has to be undertaken for developing a precise age model.

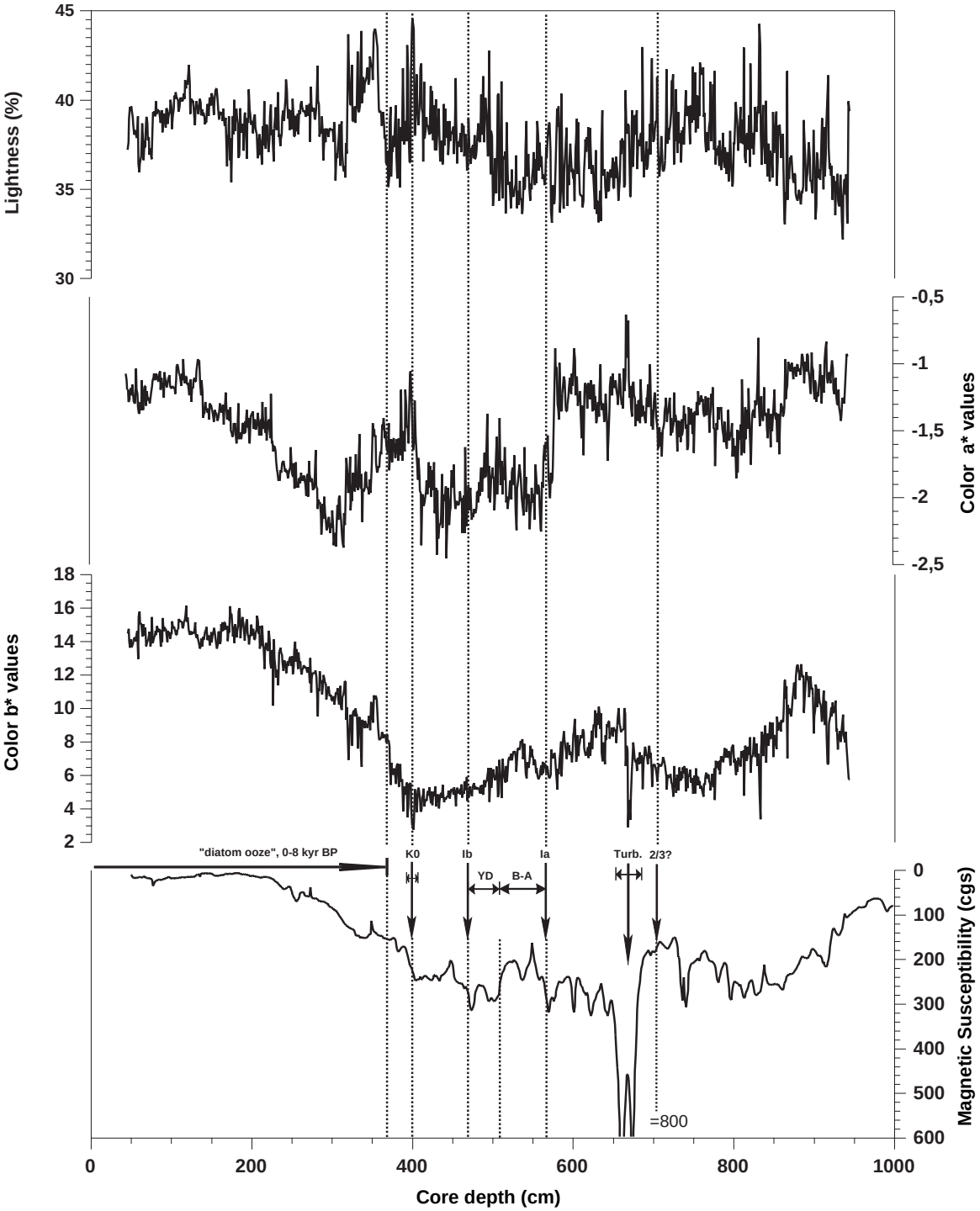

Fig. 8.7: *LV29-108-5, from top to bottom, Lightness of color reflectance spectra, Color spectrum of red-green chroma, Color Spectrum of yellow-blue chroma and magnetic susceptibility.*

Core LV29-108-5 gives a somewhat different picture: according to the MS records and changes in lithology, at LV29-108-5 we attribute the upper ca. 373 cm of the core to late

Holocene diatomaceous ooze with rather abundant foraminifera, representing the last 6,000-8,000 yrs BP (*Fig. 8.7*). We have to admit, though that we already see a slight decrease in diatom content and compaction of sediment from 301-305 cm downcore.
However, in good agreement with our first assumption, ash layer K0 (8,000 cal. yrs BP; Gorbarenko et al., 2002) was deposited in this core shortly below the basal boundary of the diatom-rich facies at 397-405 cm.
A short interval enriched in tiny dropstones and detrital terrigenous grains corresponds to Termination Ib at 470-479 cm, preceded by the YD down till approximately 510 cm. Between 510 and 561 cm, we note a characteristic double peak in the MS record, which we attribute to the warmer Bølling-Allerød interval. The basal boundary of this section consists of an interval with enhanced black streaks and mottles (661-668 cm) and an underlying coarser-grained 2 cm thick layer with sand particles which then would represent Termination Ia. At present, we are unable to present a clear indication for the MIS 2/3 boundary. A lithological change at ca. 610 cm towards sandier material (coarsening downward) to us seems to indicate LGM conditions (~18-24 kyr BP). Unfortunately, both MS values and lithology show the deposition of a ca. 28-30 cm thick incomplete turbidite sequence at 657-686 cm core depth. Preliminary we set the MIS 2/3 transition shortly below the turbidite sequence at ca. 700-705 cm as we already note an increased abundance of diatoms in the sediment. This assumption would also correlate quite well with the age model of the Russian core LV29-108-4 (SL-R), seemingly offset by 70-90 cm towards the top as can be seen from the position of K2, the aforementioned turbidite sequence and another contourite at 734-746 cm (German core, SL-G) and ca. 660-690 cm (Russian core, SL-R).
However, we are aware of the fact that one could also determine a gradual lithological change between 900 and 935 cm as MIS 2/3 boundary. Here, we observe an increased content of diatoms and finer-grained detrital components as well as a clear decrease in MS values pointing towards slightly warmer transitional climatic conditions. Yet, the latter age model would mean the average sedimentation rate to decrease not more than by a factor of two compared to Holocene values, a feature that seems unlikely by comparison with older nearby cores featuring well established age models (e.g. LV28-44 shows a fivefold decrease in Holocene to LGM sedimentation rates).
Further investigation of geochemical parameters (opal content, XRF-scanning) will hopefully help to resolve this question.
There are several turbiditic layers and layers with large content of black sand throughout all cores (*Figs. 8.6 and 8.7*). An influx of coarse material is clearly observed in the MS records and induced peculiarities of the Kamchatka slope accumulation.

8.3.7 Eastern Kurile Basin slope profile (LV29-110, LV29-112, LV29-114)

8.3.7.1 Setting

Coring stations LV29-110, LV29-112 and LV29-114 are located on the northeastern slope of the Kurile Basin in a depth range from 1,218, 1,309 to 1,764 m. These sites are strongly influenced by the proximate North Pacific water inflow into the Okhotsk Sea and should therefore permit to reconstruct the temporal evolution of the deeper Pacific water in comparison to the east Kamchatka profile.

8.3.7.2 SL-R (LV29-110-2, LV29-112-2, LV29-114-2)

The sediment of core LV29-110-2 belongs to MIS 1 according to available records (see Appendix 6). The upper 180 cm contain weakly diatomaceous sandy silt with a basal age close to 6 kyr. Carbonate peaks occur at 140 cm, 280 cm and 340 cm core depth, apparently correlated with carbonate spikes of terminations IC, IB and IA with ages of 5, 9.5 and

12.5 C^{14} kyr (Gorbarenko et al., 2002). An unidentified volcanic ash is located at the core base (345-350 cm). MS record and core description indicate the appearance of two turbidite layers at 231-232 cm and 301-302 cm.
According to physical property records and color spectra, core LV29-112-2 has principally to be filed as of MIS 1-3's age. In agreement with the location of the bottom boundary of terrigenous-diatomaceous sediment at 140 cm, the MIS 1/2 boundary is set at 240 cm depth. A pronounced, so far unidentified volcanic material layer with complex composition was found at a depth of 494-510 cm. In line with our available data, the boundary of MIS 2/3 may be preliminary placed at a depth of 520 cm, just below the volcanic ash. The core description and MS record indicate several sandy layers through the entire core length likely induced by turbidites.
The strong reflector boundary at nearly 5.5 m depth in the 8 kHz echosounder records in profile 34 (*Fig. 3.8,* Chapter 3) definitely correlates with the aforementioned ash layer located at 494-510 cm core depth in LV29-112-2. A less strong boundary at nearly 4 m depth may be correlated with the accumulation of sandy sediment with high MS values in interval 430-460 cm. The weak reflector boundary in the seismic records at nearly 1 m depth likely correlates with the base of diatomaceous sediment (0-140 cm).
Core LV29-114-2 supposably encompasses MIS 1-4. The beginning accumulation of diatomaceous sediment in the upper 175 cm and changes of other parameters allow us to set the MIS 1/2 boundary at a depth of 190 cm. The high MS values, low color b values and absence of diatoms in depth interval 250-300 cm place the MIS 2 base at 330 cm. The boundary MIS 3/4 may be very preliminary put at core depth 560 cm in consistence with color spectra variability. Volcanic ash preliminary identified by mineralogy as K3 was found at the core base (766-767 cm) and accumulated within MIS 4 (Gorbarenko et al., 2002). The high values of MS and presence of several sandy layers in this core, similar to cores LV29-110-2 and LV29-112-2, indicate a strong influence of volcanic activity from the northern Kurile Islands and southern part of Kamchatka, transported into the sea likely by sea ice.

8.3.8 La Perusa Strait (LV29-69, LV29-131)

8.3.8.1 Setting

At this location, the goal was to reconstruct the Soya Current inflow into the Okhotsk Sea and its influence on paleoceanography.
Stations LV29-69 and LV29-131 were set in a rather flat area with a depth range of 800-1,000 m between La Perusa Strait and the western part of the Kurile Basin.

8.3.8.2 SL-R/ SL-G

Cores LV29-131-2 and LV29-131-3 were taken from the top of a smooth hill with a depth of 760-761 m and cores LV29-69-3 (841 m) and LV29-69-5 (652 m) roughly at the same location.
The onboard results of MS, color spectra, dry bulk density, water content and main component composition according to smear slide analysis are plotted in Appendix 6. Generally, the MIS 1 sediments show a high water content and low bulk density and a considerable amount of diatoms according to the smear slides analysis. The sediment of MIS 2 is represented by an increased terrigenous material with high density and slightly increased MS values. The transition from MIS 2 to 1 is clearly indicated by changes in the color spectra. The MIS 2 and 3 sediments have low b values that show a prevalence of blue chroma in the sediment of the cold MIS 2 and intermediate MIS 3. The boundary of MIS 2/3 in core

LV29-131 was determined based on a significant sand admixture in the sediments of the cold stage 2 and a relative decrease in the MS values in stage 3.
The sedimentation rate in core LV29-69 is higher than in core LV29-131, which coincides with the bottom topography and sedimentation regularities. Cores LV29-131 were recovered from an elevated relief comparable with core LV29-69.
The sediments of the early part of MIS 1 have low MS values, which are typical for the Okhotsk Sea sediments (Gorbarenko et al., 2002). The considerable increase in MS values in the late part of MIS 1, which was registered in both cores, was likely induced by the opening of La Perusa Strait and an additional influx of magnetic terrigenous material with the Soya Current. According to the curve of the sea level change during last 18 kyr (Fairbanks, 1989), La Perusa Strait opened approximately 8 kyr ago (the modern depth of the La Perusa Strait equals 53 m). Therefore, considerably warm and saline Soya Current water masses began to flow into the Okhotsk Sea 8-7 kyr ago. The rise in the MS values presumably caused by transport of additional terrigenous material by the Soya Current allows us to interpret the higher MS values during MIS 3 as a possible earlier opening of La Perusa Strait.

8.3.9 Mineralogy of volcanic ash layers

In sediments of cores studied aboard, we discovered frequent pyroclastic material. Tracing tephra as pure layers or lenses is of considerable interest for investigation. Their identification with already known Okhotsk Sea ash layers conduces to carry out a stratigraphic intercore correlation.
Tephra layers in Holocene-Pleistocene sediments of the Okhotsk Sea have already been studied in the past (Gorbarenko et al., 2000; Biebow et al., 2000). On the basis of mineralogical features, chemical composition, stratigraphic position and radiocarbon dating of these layers, their connections with eruptions of Kamchatka or Kurile volcanoes and also areas of distribution were distinguished (Gorbarenko et al., 2000, 2002).
Samples for mineralogical analysis were selected from the most pristine parts of ash layers. However, it was not always possible to completely avoid contamination's by terrigenous particles of the surrounding sediment (due to bioturbation and the small thickness of some ash lenses). From thicker layers, some samples were selected with regard to particle size, color or texture. The results of mineralogical analysis were processed with multivariate statistics (cluster and R-mode factor analyses) (*Figs. 8.8* and *8.9*).
Pyroclastic material was discovered in 12 cores taken within near-Sakhalin and Kurile-Kamchatka areas (*Tab. 8.1*). As can be seen from *Figure 8.8*, stations can be grouped according to our mineralogical study. The analysis of these data, and also their comparison with known Okhotsk Sea ash layers permitted to identify them as tephra marker layers K0, K2 and K3. Some fluctuations in the composition of the main components (even within one ash layer) are related with the differentiation of volcanic particles in density and size during transport and settling on the bottom (Kir'yanov & Solovyeva, 1990; Felitsin & Kir'yanov, 1987) which can be especially seen in thick layers (station LV29-108, horizon 313-316 cm; station LV29-112, horizon 494-510 cm). This regularity was already observed in Okhotsk Sea cores recovered on previous cruises (Gorbarenko et al., 2000; Biebow et al., 2000). On the other hand, samples selected from thin layers or lenses contain admixtures of terrigenous particles. This is well expressed in the r-mode factor analysis (*Fig. 8.9)*. Minerals of terrigenous origin (hornblendes, epidote, garnet, zircon etc.) form associations with stable positive correlative connections. One can see that the main components of volcanoclastics - clinopyroxene and orthopyroxene - are sharply isolated from terrigenous components sharing negative correlation's.

Table 8.1. *Mineralogical composition of ash layers from sediments of the Sea of Okhotsk*

N st.	Horizon, cm		Cpx	Opx	bgHb	bHb	gHb	OHb	Ep	Gar	Zr	Ap	Sph	Chl	Mt	Ol	Act	Bi	Ilm	Mgt	Rf
LV29-53*	174	K_2	18.86	23.14	18.28	0.28	1.14	0.29	10.00	2.00	0.28	0.86	1.14	0.28	0.00	0.00	1.14	4.86	1.71	4.57	11.17
LV29-53*	175-176	K_2	26.97	34.24	5.76	0.00	0.61	0.00	4.85	0.30	0.30	1.21	0.30	0.61	0.00	0.00	0.61	1.82	1.52	9.70	11.21
LV29-53	178-179	K_2	27.13	48.58	2.52	0.32	0.00	0.00	1.89	0.00	0.00	0.63	0.32	0.00	0.31	0.00	0.00	0.95	0.31	5.99	11.04
LV29-56	251-252	K_2	19.94	42.68	7.16	0.93	0.93	0.00	2.49	0.00	0.00	1.87	0.00	0.93	0.00	0.00	0.00	2.49	0.00	8.10	12.46
LV29-63	114-115	K_2	24.76	41.27	0.32	0.00	0.95	0.32	0.95	0.00	0.32	0.63	0.00	0.00	0.00	0.32	0.00	0.63	0.32	17.46	11.75
LV29-70*	381	K_2	11.66	46.36	4.37	0.29	2.62	0.00	3.50	0.00	0.00	0.29	0.00	0.58	0.29	0.58	0.29	3.68	2.92	11.66	10.91
LV29-70*	727-727.6	Spfa-1	14.39	14.11	19.66	0.00	3.00	0.00	9.66	1.61	2.44	3.83	0.78	1.33	0.00	1.89	1.05	4.66	3.83	4.39	13.37
LV29-72*	569	K_2	13.40	36.92	2.81	0.00	0.00	0.00	1.34	0.00	0.00	0.00	0.00	0.00	0.00	0.00	0.75	1.92	2.51	34.28	6.07
LV29-94*	468	K_2	19.66	16.02	18.34	0.37	1.24	0.37	9.36	0.95	0.00	0.95	0.37	0.37	0.00	0.37	0.66	4.72	3.85	5.00	17.40
LV29-100	195	K_2	25.30	36.61	5.65	0.00	0.89	0.30	1.49	0.30	0.30	1.19	0.60	0.00	0.00	0.00	0.00	0.30	0.89	14.58	11.61
LV29-106	54-56	Ko	17.47	29.62	9.87	0.00	0.00	0.00	0.25	0.00	0.00	0.76	0.00	0.00	0.25	0.00	0.25	0.25	5.32	23.80	12.15
LV29-108	313-315	Ko	17.58	30.84	4.32	0.00	0.00	0.29	1.44	0.00	0.00	0.86	0.00	0.00	0.00	0.29	0.00	0.29	6.34	27.67	11.53
LV29-108	315-316	Ko	14.77	23.01	4.83	0.00	0.00	0.28	0.28	0.00	0.00	1.14	0.00	0.00	0.28	0.57	0.00	0.56	6.53	36.93	11.08
LV29-110	350	?	24.36	22.56	3.08	0.26	0.26	1.54	3.59	0.00	0.00	0.51	0.00	0.00	0.00	0.26	0.26	0.26	2.31	31.28	9.49
LV29-112	496.5-499	?	31.31	22.47	8.59	0.25	0.00	2.53	2.27	0.00	0.00	0.76	0.00	0.00	1.01	1.52	0.25	0.76	5.05	14.37	8.84
LV29-112	500.5-505	?	26.36	25.27	8.15	0.00	0.27	0.27	3.53	0.27	0.00	0.00	0.00	0.00	0.27	0.00	0.00	0.82	6.79	14.40	13.59
LV29-112	505-507.5	?	23.91	23.37	10.05	0.00	0.00	0.00	2.99	0.00	0.00	2.17	0.00	0.27	0.27	0.00	0.00	0.54	4.08	16.30	16.03
LV29-112	507.5-510	?	16.80	22.46	8.98	0.20	0.00	0.39	1.56	0.00	0.00	0.78	0.00	0.00	0.00	0.20	0.39	0.40	16.41	25.98	5.47
LV29-114	766	K_3?	18.99	24.33	0.89	0.00	0.00	0.30	0.30	0.00	0.00	2.08	0.00	0.30	0.00	0.00	0.00	0.00	3.26	35.61	13.95

Minerals: Cpx - clinopyroxene, Opx - orthopyroxene, bgHb - brown-green hornblende, bHb - brown hornblende, gHb - green hornblende, OHb - basaltic hornblende, Ep - epidote, Gar - garnet, Zr - zircon, Ap - apatite, Sph - sphene, Chl - chlorite, Mt - metamorphic minerals (andalusite, staurolite, sillimanite etc.), Ol - olivine, Act - actinolite, Bi - biotite, Ilm - ilmenite, Mgt - magnetite, Rf - rock fragments.

Note: * - Asterisk marks samples selected from thin interlayers and lenses; they contain admixture of terrigenous particles.
Ko, K_2, K_3, Spfa-1 - indexes of ash layers.

8.3.9.1 Tephra marker layer A

This layer was discovered at stations LV29-106 (54-56 cm) and LV29-108 (313-316 cm). At the first station, the tephra is traced as bioturbated lenses with small thickness. At the second, it gains in thickness and complex composition. The light gray (to white) tephra of silty sand in size (~1 cm in thickness) lies within the lower part of the ash layer. Volcanic glass shows a fluid-vesicular variety, and a large quantity of white pumiceous fragments causes the layer's whitish tone. This tephra is overlapped by a gray interlayer of sandy silt in size and variable thickness (0.6-2.5 cm). The volcanic glass has an analogous variety, but pumiceous fragments occur in smaller quantities. Overlying terrigenous sediments are enriched in very fine ash particles; thus, these sediments have a whitish tone. Volcanic ash consists of fragmentary-vesicular and lamellar glass.

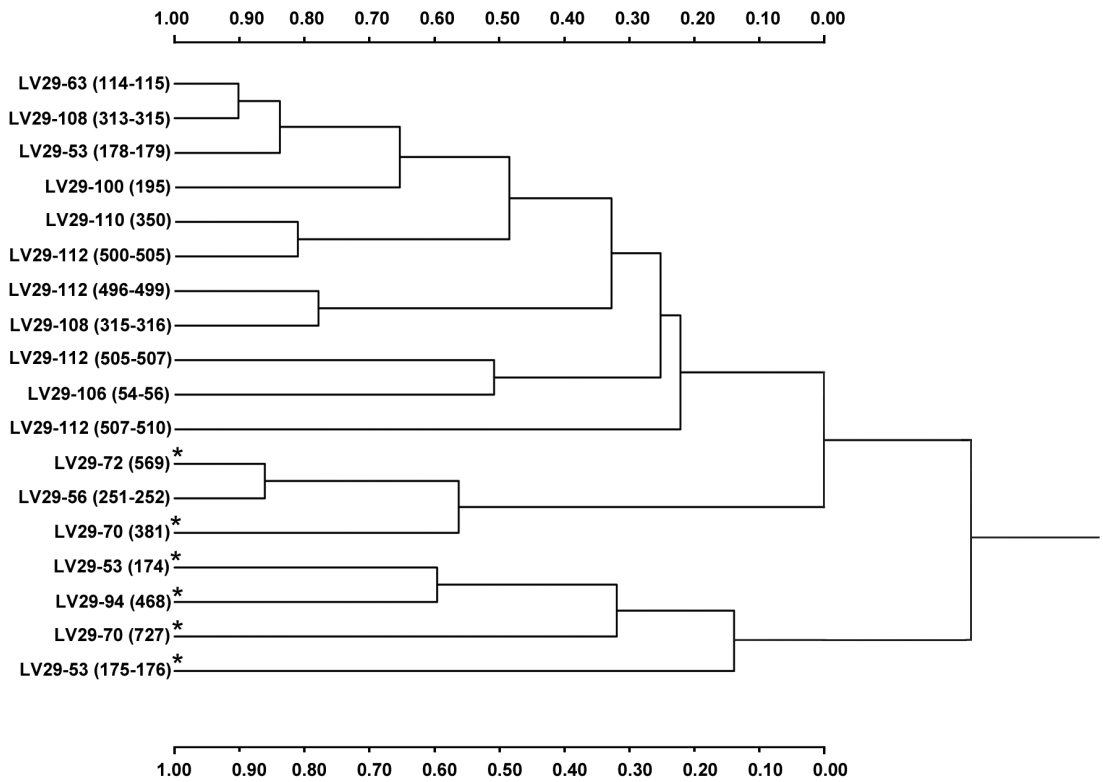

Fig. 8.8: *Cluster graph of the mineralogical composition of different ash layers from sediments of the Okhotsk Sea.*

8.3.9.2 K0 ash layer

The mineral complex of ash layer K0 is characterized by a prevalence of orthopyroxene (23.0-30.8% or 50.6-55.2% after recalculation on transparent minerals) and clinopyroxene (14.8-17.6% or 29.9-31.4%, accordingly). Besides, the high content of dark ore minerals is typical (29.1-43.5%). The distinctive feature of this ash layer is the increased content of brown-green hornblende, often with grains encased in volcanic glass, and also the presence of brown and basaltic hornblendes.
The source of pyroclastics for ash layer K0 is the explosive eruption of Kurile Lake volcano (southern Kamchatka) which happened, according to new radiocarbon data on wood remains, 7618 ±14 years ago (Zaretskaia et al., 2001).

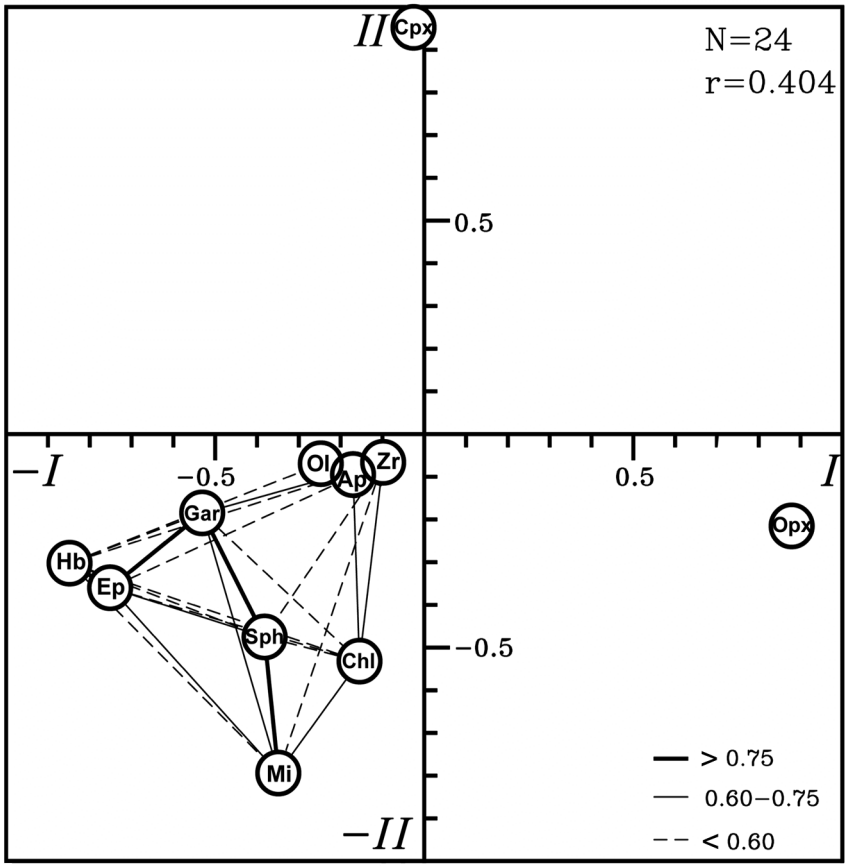

N - quantity of mineralogical analyses (6 analyses from other cruises with identified ash layers as standard are added to the initial data);
r - significant correlation's between minerals; which are shown by lines of different thickness: bold line - strong positive correlation, regular line - moderate correlation, dotted line - weak correlation. Indexes of minerals are given in *Table 8.1*.

Fig. 8.9: *Plot of R-mode factor analysis for heavy minerals from ash layers in sediments of the Okhotsk Sea.*

8.3.9.3 Tephra marker layer K2

This layer is distributed over a wide area in the central part of the Okhotsk Sea (Gorbarenko et al., 2000; Biebow et al., 2000). So far, it has been found in cores LV29-53, LV29-56, LV29-63, LV29-70, LV29-72, LV29-94 and LV29-100. This tephra is a gray ash with pink tone of sandy silt in size, which is one of the main characteristic features of this layer. It occurs as interlayers of 1-2 cm in thickness (stations LV29-53, LV29-56, LV29-63, LV29-100) or as small lenses of 0.5-0.6 cm in diameter (stations LV29-70, LV29-72, LV29-94). The volcanic glass has mainly a fragmentary-vesicular and fluid-fibroid and rarely a fluid-cellular shape. There is a small quantity of light gray (to white) pumiceous fragments. Characteristic for this layer is the prevalence of orthopyroxene in comparison with clinopyroxene (36.6-48.6% and 11.7-27.1%, accordingly). The content of dark ore minerals varies widely (*Tab. 8.1*). *Figure 8.8* shows the scattering of stations containing ash layer K2 in the form of small lenses. It is related with the admixture of terrigenous particles of surrounding sediments (*Tab. 8.1*).
The absence of ash layer K2 within near-Kamchatka areas (stations LV29-106, LV29-108, LV28-44) allows the suggestion that most probably its source is a large explosive eruption of one volcano situated in the northern part of Kurile Island Arc. The stratigraphic position

of this layer in sediment cores (~26,000 years) (Gorbarenko et al., 2002), and also the data of radiocarbon dating on land within sections with similar tephra characteristics (Braitseva et al., 1995; Melekestsev et al., 1997) allow us to consider the most real source of this ash layer to be the largest caldera-forming explosive eruption of volcano Nemo-III situated in northern part of Onekotan Island that happened about 25,000 years ago.

8.3.9.4 Unknown tephra layer – Paramushir Island

Among the other ash layers discovered in the cores, the tephra of station LV29-112 taken near Paramushir Island is of highest interest. A thick ash layer was recovered here at 494-510 cm core depth. Its consists of light gray ash of fine sandy silt in size. Within the layer, thin lenses and interlayers of darker color occur. The quantity of sandy particles decreases from bottom to top, whereas the amount of fine silty particles increases. At 494-505 cm, a high content of light gray pumice of gravel in size was observed.
The investigation of the ash mineral composition shows a differentiation of tephra in both particle density and size. Within the coarse lower part of the layer, the ore minerals content (42.4 %) increases in comparison with the fine-grained upper part. The content of clinopyroxene and orthopyroxene is approximately equal to the small prevalence of orthopyroxene in the lower part of the layer (*Tab. 8.1*). Among coarser ash particles, light gray pumiceous fluid and white volcanic glass prevails, while fluid-vesicular glass occurs in small quantity. On the contrary, the prevalence of colorless fluid-vesicular and lamellar glass is characteristic for fine ash particles; pumiceous glass occurs rarely.
In spite of the close stratigraphic position of the studied layer to ash layer K2, at present it seems impossible to identify it as K2 because of some distinctions. First of all, there is no characteristic pink tone as typical for K2 ash. Besides, the ratio clinopyroxene/orthopyroxene is lower (*Tab. 8.1*), and the content of pumiceous glass is higher than for layer K2. These distinctions in the mineral composition are reflected well in our results from cluster and factor analyses (*Figs. 8.8* and *8.9*).

8.3.9.5 Tephra marker layer K3

This layer may be preliminary distinguished at station LV29-114 at 766-767 cm. It consists of sandy silt with admixture of coarse sand and pumice. Coarse ash particles are represented by gray and dark gray pumiceous fluid fragments, and also by dark brown (almost black) fine-porous fragments. Fine ash particles consist of mainly colorless fragmentary-vesicular and fluid glass.
In the same core and also in core LV29-110 (at 350 cm), small lenses of volcanic ash and large quantities of dispersed pumice were discovered, but it is currently not possible to determine their significant features for a stratigraphic correlation.

8.3.9.6 Unknown tephra layer #2 – Spfa-1?

One more tephra layer differing in composition and morphology from other layers was discovered in the western part of the Okhotsk Sea in core LV29-70 (at 727-727.6 cm). It has a light gray color with glassy lustre. The ash of this layer consists of only colorless volcanic glass of sandy silt in size with a very small admixture of crystalloclastics. This glass is mainly made up of fragmentary lamellar and fragmentary vesicular particles. A low content of heavy minerals is characteristic for this layer. It is similar to the ash layer of station LV28-62 (at 1,108-1,113 cm) (Biebow & Hütten, 1999) and may be compared with ash layer *Spfa-1* of the eruption of volcano Sikotsu (Hokkaido Island) that happened about 40,000 years ago (Machida, 1999).

9. INVESTIGATION OF FORAMINIFERA IN SURFACE SEDIMENTS OF THE OKHOTSK SEA

Natalya Bubenshchikova, Lester Lembke, and Nicole Biebow

9.1 Introduction

Quite a few previous investigations have dealt with the distribution and ecology of benthic foraminifera of the Okhotsk Sea (e.g. Asano, 1958; Saidova, 1961, 1997; Fursenko et al., 1979) covering a wide range of environments from the Amur River estuary to the deep basins extending temporally from modern conditions to glaciated shelves in the past. It has been shown that late Quaternary glacial-interglacial changes in oceanography and productivity of this region are closely coupled to strong variations of benthic foraminiferal assemblages in sediment samples (Saidova, 1961; Fursenko et al., 1979; Belyaeva & Burmistrova, 1997; Gorbarenko, 1991; Barash et al., 2001).
However, the vast majority of studies are hampered by the fact that almost no regional data of living benthic foraminfera is available in connection with their environmental characteristics (Basov & Khusid, 1983). This in turn considerably aggravates any attempt to calibrate existing datasets against oceanographic and ecological boundary conditions like nutrient supply, water depth, ventilation of water masses, current strength, surface sediment composition, etc. As well, little is still known about microhabitat preferences of the majority of benthic foraminiferal taxa in the Okhotsk Sea.
Hence to date, few attempts have succeeded in quantifying physical and chemical changes in bottom water characteristics by using benthic foraminiferal assemblages as proxy datasets.
Modern planktic foraminifera assemblages of the Okhotsk Sea are strongly dominated by the polar species *N. pachyderma sin.* and subpolar species *G. bulloides* both in sediments traps and in Late Quaternary sediments (Shchedrina, 1958; Saidova, 1961; Lipps & Warme, 1966; Alderman, 1996). The rare subpolar species *N. pachyderma dex., G. glutinata, T. quinqueloba, G. uvula, G. scitula* and tropical specimens *N. dutertrei, G. ruber, G. conglobatus, G. quadrilobatus* were found only as minor faunal components.
The aim of the study is to investigate the ecological preferences of living benthic foraminiferal assemblages and to extend their options to serve as paleoceanographic proxies. Concomitant counts of planktic foraminifera shall further elucidate possible interconnections with overlying surface water mass properties.

Within this main objective the tasks are considered as following:

Russian Group:
1. to determine abundance, diversity, taxonomic composition of living and dead benthic foraminifera from a set of sediment surface samples (0-1 cm) from different sites (shallow, intermediate, deep-water environments);
2. to determine the microhabitat preferences of the dominant benthic species from living assemblages in the upper surface sediments (0-8 cm);
3. to assess the preservation potential of benthics for Quaternary paleoceanographic reconstruction's from comparing living and related dead assemblages;
4. to investigate planktic foraminiferal distribution in surface sediments (0-1 cm) and to determine factors controlling the changes in faunal distributions;

German Group:
5. to distinguish responses of different selected species to oceanographic changes by comparison to stable isotope analyses and sediment geochemistry (TC/TOC, opal, chlorine's, etc.);

6. to calibrate the imposed dataset from benthic communities against stable isotope data from bottom water samples taken simultaneously;
7. to evaluate response of benthic communities to subtle oceanographic changes during the last 15,000 years caused by variations in the riverine discharge of Amur River;
8. to calculate SST-proxydata from planktic foraminifera (MAT, Mg-Ca);
9. numerical approximation of T/S characteristics from combined foraminiferal geochemical data for OSIW (σ_θ =26.7-26.9) on a transect along the Sakhalin continental margin.

Finally, we plan to jointly relate the observed living benthic assemblages to present and past environmental conditions (nutrient supply, water depth and chemistry, oxygen content, current strength, surface sediment composition).

9.2 Materials and methods

We collected undisturbed surface sediments from multicorer tubes. The upper 8-10 cm of the sediment were cut in slices of 1cm thickness and stored in dyed Ethanol (min. 70%, with added Rose Bengal: 2g/l) solution immediately after MUC retrieval according to modified methods described e.g. in Lutze & Altenbach (1991). To obtain a sufficient amount of material for the array of investigations, we took three parallel sample series from each station, whenever possible. A total of 457 single samples was collected during the cruise, out of which we chose a set of 11 samples from intermediate water depths for preliminary analysis (see *Tab. 9.1*, and *Figs. 9.1-9.3* for locations of samples).

Tab. 9.1: *Samples for preliminary analysis.*

Station No.	Sample depth (cm)	Water depth (m)
LV29-69-1	0-1	881
LV29-78-1	0-1	640
LV29-84-1	0-1	720
LV29-108-3	0-1	625
LV29-110-1	0-1	1218
LV29-110-1	1-2	1218
LV29-110-1	2-3	1218
LV29-110-1	3-4	1218
LV29-110-1	4-5	1218
LV29-110-1	5-6	1218
LV29-110-1	7-8	1218

Samples were wet sieved over 63 μm mesh size and dried at about 70°C. Foraminifera were counted in the fraction >100μm in splits estimated to contain at least 300 specimens of planktic, 300 living (Rose Bengal-stained) and 300 dead benthic foraminifera (Appendix 7). Samples containing little foraminifera were analyzed without splitting. Planktic foraminifera were identified following the taxonomy of Hemleben et al. (1989). Benthic foraminifera were classified according to the taxonomic works of Loeblich & Tappan (1953), Saidova (1961, 1975), Feyling-Hanssen et al., (1971), Fursenko et al. (1979), Scott et al., 2000 etc., see Appendix 7 for species references and full names. For abundance analyses counts of foraminifera were calculated to 1 cm^3 surface.
We restricted our study aboard to calcareous benthic foraminifera assemblages, as we noticed that agglutinated foraminifera disintegrated easily after death which typically resulted in very low downcore abundance's of tests. In our samples, the ratio of calcareous to agglutinated foraminifera increases sharply from 77% in 0-1 cm to 91% in 1-2 cm and to 96-99% in deeper

samples of MUC LV29-110-1 (*Fig. 9.6*). A rather good preservation of foraminiferal carbonate tests is expected in the chosen samples due to the low carbonate ion concentration (CO_3) of 0.038-0.044 mmol/kg and the high saturation degree of calcite of 0.66-0.72 (Chapter 5). Thus, variations in foraminiferal assemblage compositions can be mainly attributed to ecological environmental parameters and not to preferential dissolution of specific taxa. At our sites, the present sedimentation rates are estimated to range from 30 cm/kyr at "Obzhirov flare" via 50 cm/kyr on the Kamchatka margin to more than 100 cm/kyr at the Sakhalin margin (Chapter 8). Thus, the uppermost centimeter of the sediment approximately represents an approximate time frame of the past 0-500 years, considering the maximal bioturbation depth to range around 15 cm (own observations at MUC tubes).

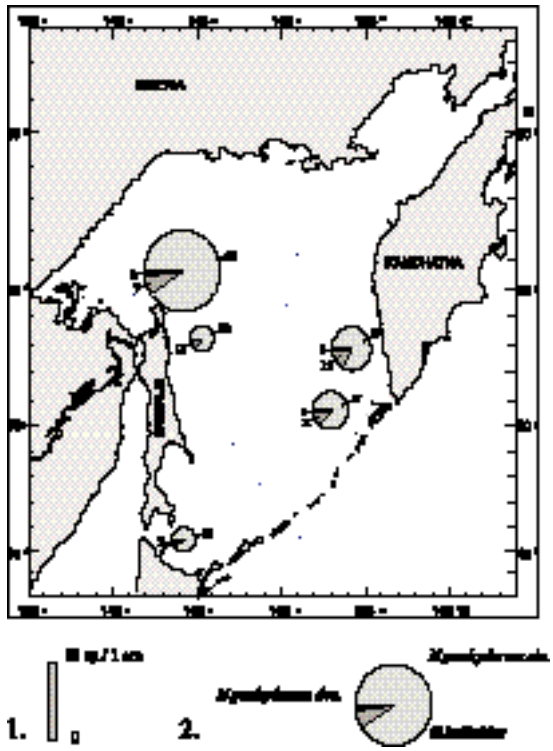

Fig. 9.1: *Distribution of planktonic foraminifera in the surface sediments (0-1cm) of the Okhotsk Sea: 1 - abundance (specimen per 1cm^3); 2 - species composition.*

9.3 Results and Discussion

9.3.1 Planktic foraminifera

The planktic assemblages are characterized by the predominance of two species, *N. pachyderma sin.* and *G. bulloides* (*Figs. 9.1* and *9.7*, Appendix 7). The total maximal abundance of 18 spec./cm^3 occurs in the surface sediments (0-1cm) at site LV29-84-1 ("Obzhirov flare") (*Fig. 9.1*). A species-specific maximum of *G. bulloides* (15%) was found in LV29-108-3 at the southwestern Kamchatka slope (*Fig. 9.1*), suggesting an influence of a relatively warmer surface water inflow of Northwest Pacific origin through Kruzenshtern Strait.

On the downcore profile of LV29-110-1 (eastern slope of the Kurile Basin), the maximum of planktic foraminiferal abundance of 21-28 spec./cm^3 occurs between 3-6 cm (*Fig. 9.7*, Appendix 7). It coincides with an increase of *G. bulloides* up to 20 % and, thus, can be interpreted as an increase of planktic foraminifera productivity and surface water temperature in response to the influence of Northwest Pacific waters.

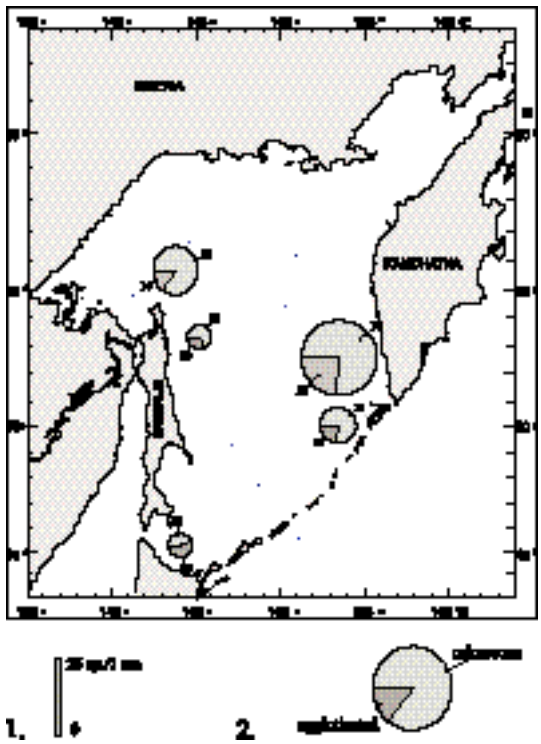

Fig. 9.2: *Distribution of living benthic foraminifera in the surface sediments (0-1 cm) of the Okhotsk Sea. 1 - calcareous and agglutinated abundance (specimen per 1 cm^3), 2 - ratio of calcareous and agglutinated foraminifera.*

9.3.2 Benthic foraminifera in surface sediments (0-1 cm)

Totally 66 species and groups of related species are identified in the samples, 33 species in total were counted as living (Appendix 7). *Figures 9.2* and *9.3* summarize living and dead assemblage abundance's and compositions.

The total abundance of living (calcareous and agglutinated) benthic foraminifera increases from 1.7-1.8 to 5.8 spec./cm^3 along a Sakhalin S–N transect (*Fig. 9.2*). In addition, the percentage of agglutinated foraminifera diminishes, which can be regarded both as higher benthic productivity and better carbonate preservation (*Fig. 9.2*). We observed a maximal abundance of living benthic foraminifera of 25 spec./cm^3 at LV29-108-3 (*Fig. 9.2*) on the southwestern Kamchatka slope. This maximum can be related to the absence of seasonal sea-ice cover in this area of the sea and high primary surface productivity of the western Kamchatka shelf and slope areas (Arzhanova & Zubarevich, 1997). Strong upwelling of cold, nutrient-rich water induced by inflow of North Pacific waters has been reported by Sapozhnikov et al. (1999) for the western Kamchatka shelf and continental slope. Similarly to the Kamchatka region, the Sakhalin epicontinental areas exhibit high primary surface productivity as well (Arzhanova & Zubarevich, 1997; Sapozhnikov, 1999) and, thus, high benthic foraminifera productivity should be expected. However, the preliminary results presented in this report do not show high living benthic abundance's at the Sakhalin slope.

The absolute values of living benthics of 1.7-25 spec./cm^3 in the surface sediments (0-1 cm) are rather low. Maxima of living benthics are very likely to occur at deeper sediment levels corresponding to mostly infaunal living species (*Fig. 9.3*). This assumption is justified by our analysis of profile LV28-110-1, where the maximum of living benthics is found at 2-5 cm (*Figs. 9.5* and *9.6*).

The absolute abundance's of the counted living benthic foraminifera are rather low, but the assemblage compositions are typical for high-productivity areas (*Fig. 9.3*). The living species *Uvigerina akitaensis* is one of the major components in almost all of the analyzed samples

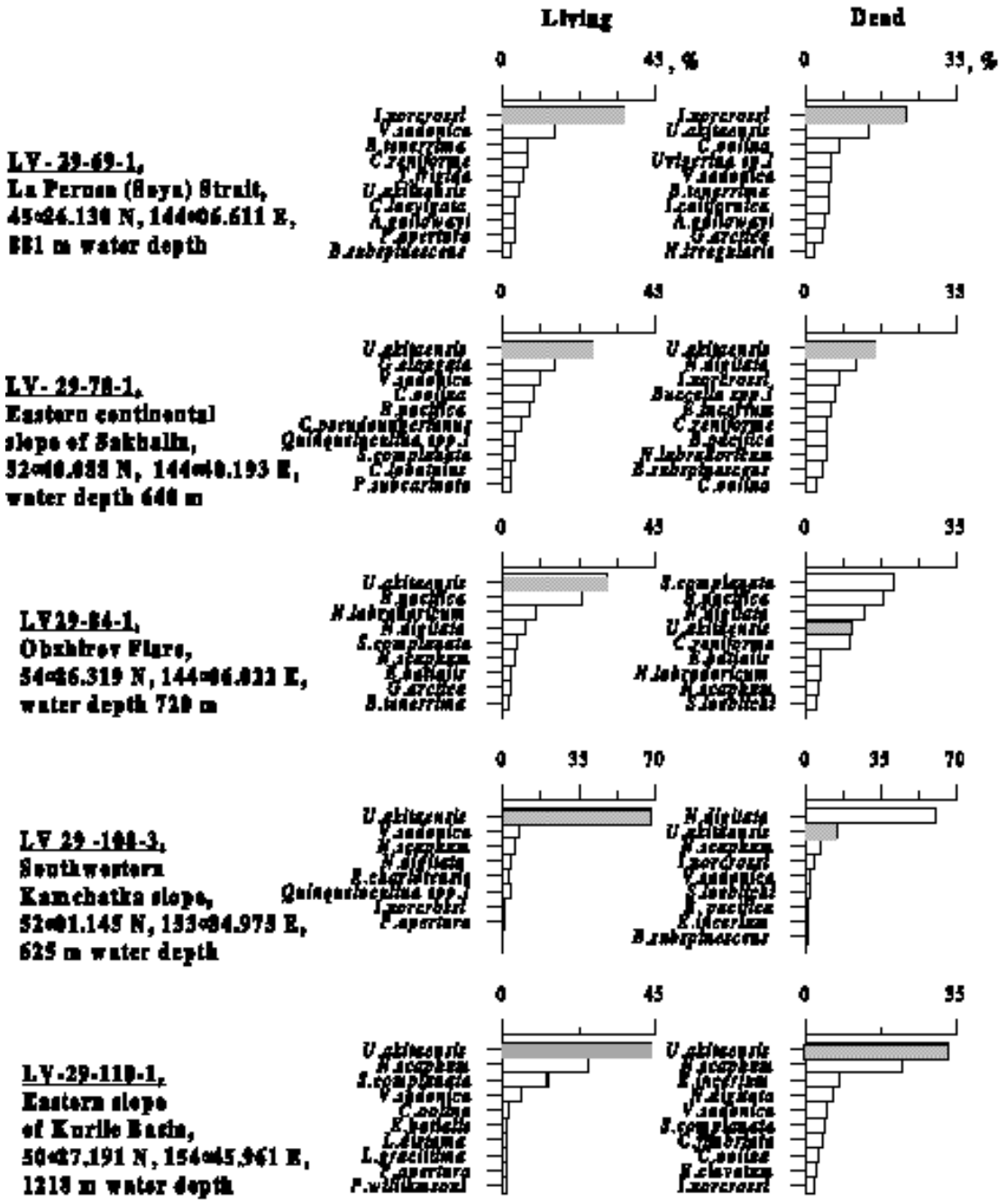

Fig. 9.3: *Rank diagrams (%) for benthic foraminiferal samples from surface sediments (0-1 cm), showing the ten most abundant species in a sample. Grey bars correspond to the dominant living species.*

(*Fig. 9.3*). We suppose the species *U. akitaensis* Asano to be distinct but morphologically close to the species *U. peregrina* Cushman according to original descriptions (Cushman, 1923; Asano, 1950) and investigation of Jung (1988). However, recent taxonomical work (Scott et al., 2000) determined *U. akitaensis* as synonym to *U. peregrina*. The species *Uvigerina genera* is globally abundant in regions of high surface productivity and, hence, of increased flux of organic matter (Loubere, et al., 1995; Mackensen et al., 1995). Thus, *U. akitaensis* is used as a principal proxy indicator of surface productivity in the Sea of Okhotsk. Other dominant living species of surface assemblages (*Fig. 9.3*, Appendix 7) belong to taxa *Nonion, Nonionella, Chilostomellina, Chilostomella, Bolivina, Globobulimina* and *Pullenia* – infaunal genera inhabiting continental slope areas with increased flux of organic matter (Sen Gupta & Machain-Castillo, 1993; Bernhard et al.,1997; Jannink et al., 1998).

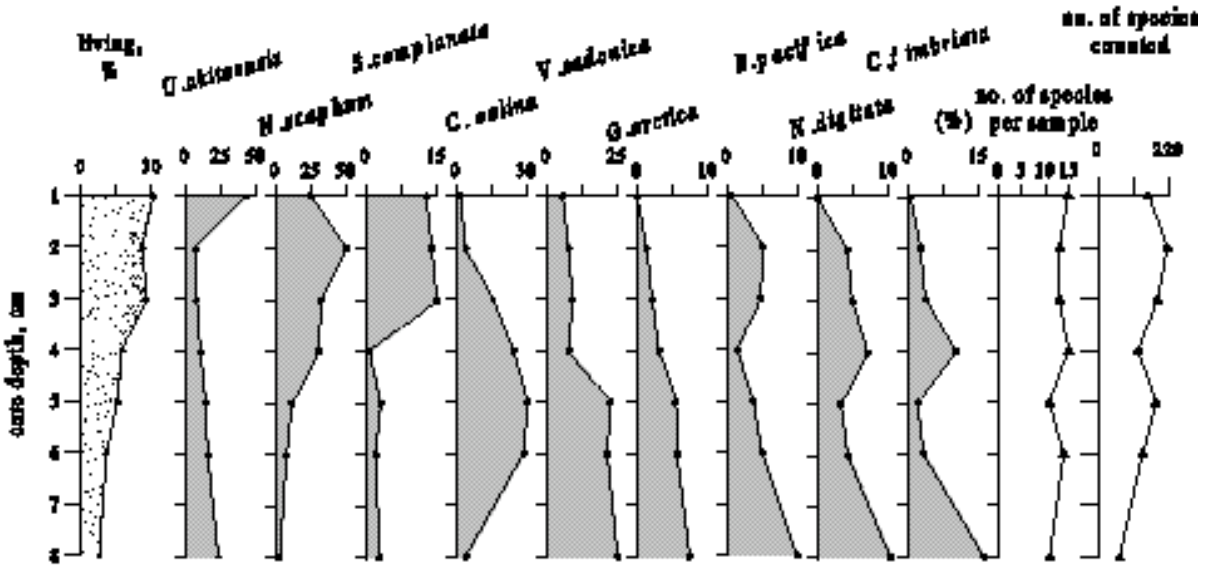

Fig. 9.4: *Percentages of major taxa of living benthic foraminifera in core LV-29-110-1.*

Living benthic foraminiferal assemblages characterizing relatively high, moderate and low primary productivity of the overlying surface waters are discriminated based on the percentage of the dominant species and on the presence of common taxa. The relatively low productivity assemblage is characterized by the dominance of *I. norcrossi* (up to 40 %) and the presence of *V. sadonica, B. tenerrima, C. reniforme, B. frigida* and *U. akitaensis* (Appendix 7, *Fig. 9.3*; revealed in LV29-69-1, La Perusa Strait). The lowest portion of calcareous foraminifera (*Fig. 9.2*) and low total abundance of living foraminifera point towards a relatively low surface productivity in this part of the Okhotsk Sea.

The main feature of the moderate-productivity assemblage is a high content of *U. akitaensis* (25-40%). Other dominant species of this assemblage are *V. sadonica, N. scaphum, B. pacifica, S. complanata, G. elongata* (*Fig. 9.3*). On the southwestern Kamchatka slope, the high productivity group is strongly dominated by *U. akitaensis* with up to 70% of living fauna (*Fig. 9.3*). Thus, both the species composition and the abundance of living benthics (*Figs. 9.2* and *9.3*) from the Kamchatka slope sample show the highest benthic foraminiferal productivity as compared to analyzed data from other parts of the Okhotsk Sea.

The observed maxima of foraminiferal abundance correlate with Okhotsk Sea Intermediate Water (OSIW) properties (app. 600-1,200 m water depth, σ_θ 26.8–27.4; Aramaki et al., 2001, Wong et al., 1998), as well. While bottom water temperature and salinity variations are insignificant for all the samples under study, oxygen concentrations show pronounced differences (2.07ml/l at LV29-108-3 and 1.16 ml/l at LV29-69-1; Chapter 4). Different values of oxygenation correlate quite well with the observed minimal and maximal living benthic foraminifera productivity at stations LV29-108-3 and LV29-69-1. Thus, our preliminary analysis shows that both surface productivity and hydrological conditions are likely vital for ongoing studies of living benthic foraminifera in the Okhotsk Sea.

The species composition of living and dead benthic foraminiferal assemblages differs little at stations LV29-69-1, -78-1, -108-1 (*Fig. 9.3*) reflecting low carbonate dissolution and bioturbation effect on the fauna. However, we found pronounced differences between living and dead assemblages at stations LV-29-84 and LV-29-110 at "Obzhirov flare" and the southwestern Kamchatka slope. These results cannot be explained by poor carbonate preservation, because high occurrences of translucent and easily degraded foraminiferal shells of *N. digitata, S. complanata* and *B. pacifica* were found in the dead assemblages (*Fig. 9.3*). The high percentage of living *U. akitaensis* is probably attributed to a recent seasonal increase in benthic productivity.

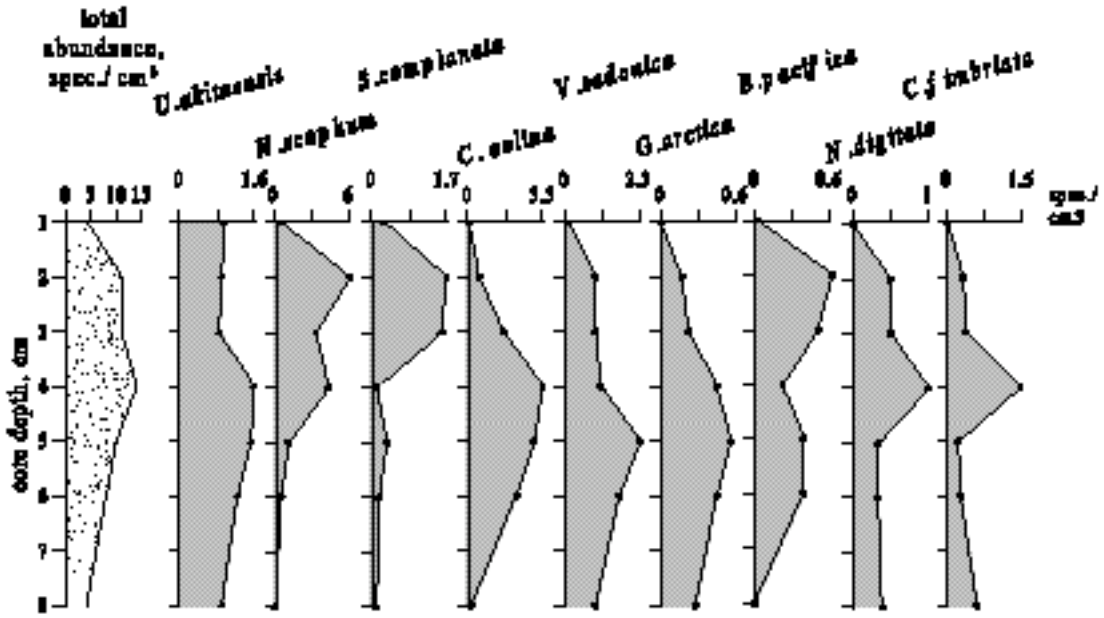

Fig. 9.5: *Abundance's (spec./cm³) of major taxa of living benthic foraminifera in core LV-29-110-1.*

9.3.3 Vertical distribution of benthic foraminifera in subsurface sediments (0-8 cm)

The species *N. scaphum, C. oolina, S. complanata, V. sadonica* and *U. akitaensis* are the major components of living benthic foraminifera assemblages of MUC LV29-110-1 as it is seen from relative concentrations (%) and abundance's (spec./cm³) (*Figs. 9.4* and *9.5*). Rare *P. apertura, C. lobatulus, C. pseudoungerianus*, some species of *Elphidium* and *Lagena* genera are also found as living (Appendix 7). The species diversity of living benthic foraminifera amounts to 11–15 species/cm-interval. The abundance of living foraminifera reaches 10–14 spec./cm³ at 2–5 cm (*Fig. 9.4*, Appendix 7) and decreases down to 4 spec./cm³ at 8 cm.

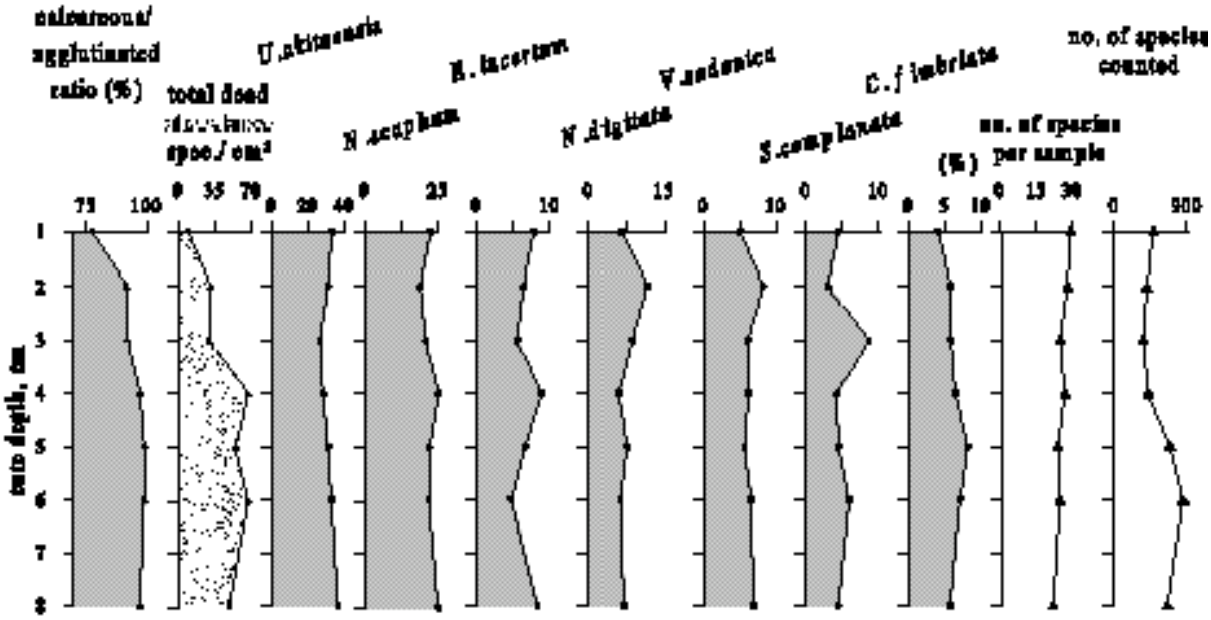

Fig. 9.6: *Percentages of major taxa of dead benthic foraminifera in core LV-29-110-1.*

The downcore variation in relative concentrations (%) and abundance's (spec./cm³) of living benthic foraminifera (species representing >5 % of the assemblage in at least one interval) allows a preliminary subdivision of the species into the following microhabitat categories:

shallow infauna 0-3 cm (*U. akitaensis, N. scaphum, S. complanata*), intermediate infauna 3-6 cm (*C. oolina, B. pacifica*) and deep infauna >6 cm (*V. sadonica, G. auriculata, N. digitata, C. fimbriata*). The dominating species *U. peregrina* has a maximum of 50% in the upper 0-2 cm decreasing down to 25% at 7-8 cm core depth. It remains dominant in all intervals and thus cannot be ascribed to a single microhabitat category.

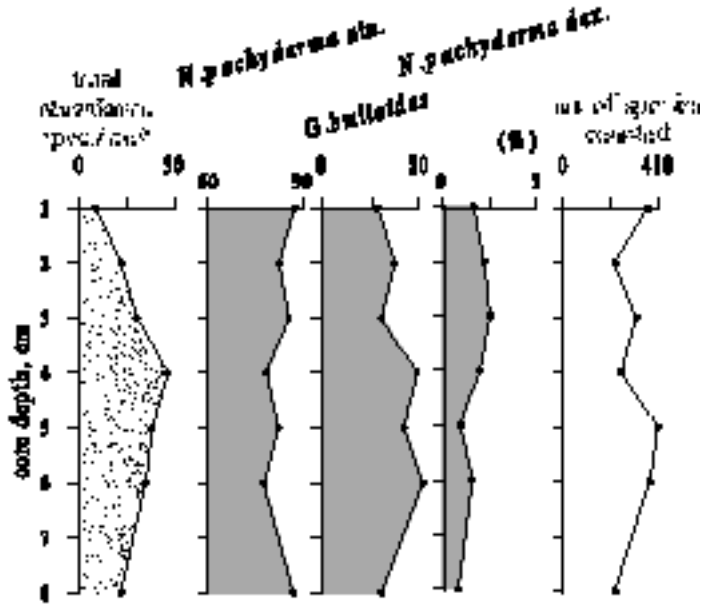

Fig. 9.7: *Percentages of planktonic foraminifera in core LV-29-110-1.*

Dead and living benthics assemblages of LV29-110-1 show a very similar species composition (*Figs. 9.4 - 9.6*). Relatively weak differences of these assemblages can be likely related to processes of bioturbation and dissolution of some calcareous foraminifera. The effect of dissolution is seen from the increase of concentrations of the dissolution-resistant species *U. akitaensis* and *E. incertum* and the decrease of the more fragile *C. oolina* and *G. auriculata* in dead benthic assemblages (*Figs. 9.4 - 9.6*). Little downcore variations in relative concentrations of the dead species through the section (*Fig. 9.6*) are likely resulted from bioturbation. The poor preservation of agglutinated foraminifera in this section is likely caused by taphonomical processes.

9.4 Conclusions

1. The preliminary analysis shows that both surface productivity and bottom water features are important for further studies of benthic foraminifera in the Okhotsk Sea;
2. The total abundance of living benthic foraminifera, the percentage of calcareous benthics and dominance of the species *U. akitaensis* show the highest benthic foraminifera productivity on the western Kamchatka slope as compared to analyzed data from other parts of the Okhotsk Sea;
3. Pronounced differences between living and dead assemblages from ”Obzhirov flare” and the southwestern Kamchatka slope probably reflect a recent increase in benthic foraminiferal productivity;
4. Relatively high (*U. akitaensis* up to 70% of total living fauna), moderate (*U. akitaensis* 25-40%) and low productivity groups (*I. norcrossi* up to 40%) of living benthic foraminiferal assemblages are distinguished;
5. Dominant benthic foraminifera occurring in the LV29-110-1 profile are subdivided into three microhabitat categories: shallow infauna (*U. akitaensis, N. scaphum, S.*

complanata), intermediate infauna (*C. oolina, B. pacifica*) and deep infauna *(V. sadonica, G. auriculata, C. fimbriata, N. digitata*).

10. MAIN MORPHOLOGICAL FEATURES OF THE SUBMARINE KURILE BACK-ARC VOLCANOES

Boris Baranov, Andrey Koptev, and Anatoly Salyuk

10.1 Introduction

Bathymetric investigations conducted during Leg 2 of LV29 concentrated on the mapping of the submarine volcanoes chosen for dredging. The shipboard single-beam echosounder ELAC was used for this purpose. This echosounder operated also on all tracks run during the second leg.

3 volcanoes, namely volcanoes 6.4, 6.5, and 7.12 (according to Avdeiko et al., 1992), and Loskutov seamount were mapped in the rear arc zone of the Kurile Island Arc. The first three volcanoes are located inside the Browton and Iturup transverse zones; Loskutov seamount is an isolated volcano located in a distance of ca. 55 nm from the Kurile Island Arc.
Due to lack of time, we did not have the possibility to regularly survey each volcano except for Loskutov seamount where tracks were run in NS and WE direction with a space between them of 0.5-1 nm. But in any case, the obtained data provides information which will be useful for the understanding and classification the volcanoes` main morphological features. Taking into account that the survey of the volcanoes was carried out for dredging purpose, the description of the studied volcanoes and the maps are presented in the Chapter 11 and only summarized preliminary conclusions are given below.

10.2 Methods

During LV29 digital records were made by the ELAC 12 kHz echosounder parallel to the investigation of hydroacoustic anomalies and flare imaging. Depending on the depth range, the period of registration was 1-6 s. A sound velocity of 1,500 m/s was applied. A total of about 500,000 seafloor records were made in the first leg. Using the GPS coordinates and real time of depth measurements, a depth file was generated including date, coordinates and depth. The total size of this ASCII file amounts to about 27 MB. The depth records can be calibrated by a comparison with the bottom depth at corresponding CTD stations, where the seafloor can be determined very accurately for regions with steep relief by calculating the depth from CTD pressure measurements at the moment of bottom contact. The length of the wire between the bottom sensor and the sea floor was 8 m. Furthermore, these calibrated profiles will be used to calibrate data previously obtained mainly from manually digitized analog records of standard shipboard echosounder and multibeam echosounder surveys of cruise GE99 and Leg 1 of LV29.

The central echosounding beam of 12° by 12° was recorded on the LAZ72 Echograph and the depth was digitally displayed on the STG721 Surveying Digitizer.

The ELAC deep-sea echosounding system consists of the following operating elements:
- Echograph LAZ72
- Display selector DSG 4
- Surveying Digitizer STG 721
- Transducer selector SCK 80
- Listening Adapter HV 14

10.3 Preliminary conclusions

1. Different kinds of volcanoes occur in the rear arc zone of the Kurile Island Arc. Some of them have a classic shape like volcano 6.4, others represent volcanic ridges consisting of many volcanic cones accreted to each other (Browton and Hydrographer Ridges, Loskutov seamount). Certainly, the latest are connected with weak zones represented by continuous faults. As the strike of these ridges consistently changes from the NW (Browton Ridge) via WNW (Hydrographer Ridge) to the WE (Loskutov seamount), we can suggest the same change in the ridge-controlling faults.
2. A field of parasitic cones was observed west of volcano 6.4 (Browton transverse zone). The thick sediment layers indicate young eruption processes.
3. One of the submarine volcano (Loskutov seamount) shows an evident imprint of the Kurile Basin tectonics. It consists of three dextral en-echelon chains of volcanic cones striking in WE direction. In contrast, the Kurile back-arc volcanic chains are mainly orientated in NW-SE, SW-NE and NS directions (Avdeiko et al., 1992). The strike and alignment of Loskutov seamount differ from that of the volcanic chains located on the slope and near the Kurile Island Arc and therefore could be connected with the tectonic of the Kurile Basin itself.

11. PETROLOGY AND VOLCANOLOGY

Reinhard Werner, Igor Tararin, Yevgeny Lelikov, and Boris Baranov

11.1 Introduction

Petrological sampling on cruises within the scope of KOMEX I (LV27, LV28, GE99; Nürnberg et al., 1997; Biebow & Hütten, 1999; Biebow et al., 2000) aimed mainly to extend our northern, central (Bussol Strait) and southern transects across the Kurile Island Arc as far as possible into the Kurile Basin in order to study interaction and dependencies between crustal and mantle sources, petrogenetic processes as well as the type and amount of volatiles in the eruptive products in different plate tectonic environments (e.g., rear arc/back-arc vs. volcanic front). These studies are continued and extended within KOMEX II by focussing on profiles across and along the active continental margin of Kamchatka and on detailed investigations of selected island volcanoes of the Kurile Island Arc. Extensive sampling of Geophysicist seamount in the northeastern part of the Kurile Basin on the above mentioned KOMEX I cruises and subsequent lab analyses of the dredged rocks also provided new informations on the structure and geodynamic evolution of the Kurile Basin (e.g., Baranov et al., 2002; Werner et al., subm.). Therefore, the major goal of the volcanological, petrological, and geochemical studies of seamounts in the Okhotsk Sea within KOMEX II is to make further contributions - in cooperation with other KOMEX II working groups - to a model for the geodynamic evolution of marginal basins by reconstruction of volcanic, magmatic and tectonic processes in the Kurile Basin. These objectives should be achieved by:

(1) reconstruction of the paleo-environment of the volcanoes at the time of their activity (e.g., subaerial vs. shallow water vs. deep water) with volcanological methods,
(2) age dating of the volcanoes, and
(3) characterization of tectonic setting of the volcanoes (situated on continental or oceanic crust; mid-ocean-ridge vs. back-arc vs. arc signatures; etc.) with petrological and geochemical methods.

Accordingly, the planned dredge sites on RV *Akademik Lavrentyev* cruise LV29 did not primarily focus on submarine arc volcanoes but on volcanic structures in the Kurile Basin being probably not directly related to the Kurile Island Arc as, for example, the western foothills of Browton Ridge in the central Kurile Basin, Hydrographer Ridge west of Iturup Island, and Loskutov seamount in the southern Kurile Basin. These structures had been discovered on former Russian cruises but had not been mapped in detail, and the sampling of basement rocks failed since the volcanoes seem to be largely covered by marine sediment, ice-rafted debris (dropstones) and/or encrustation's. Despite these difficulties we decided to focus on these volcanoes on cruise LV29 since we expected very interesting new results in case of successful sampling. To achieve the best possible results, approximately half of the time designated for petrological sampling was spent for detailed bathymetric and, at some places, additional seismic surveys. The hydroacoustic and seismic data gained on these surveys did not only enable us to select the most promising sites for dredge hauls, but also provided additional new informations on these volcanoes (see below).

Apart from the Kurile Basin volcanoes, the dredging schedule on cruise LV29 included several structures in the Derugin Basin. The objectives of these dredging operations were:

- Sampling of basement rocks at the northern slope of the Derugin Basin (southern part of the Kashevarov Bank) in order to get information on the basement structure of this area. According to seismic reflection data and echosounding surveys, basement outcrops occur there on a steep slope of a prominent tilted block. Gnibidenko (1985) proposed that this tectonic block is composed of deformed geosynclinal rocks intruded by granodiorites being Upper Cretaceous to Lower Paleogene in age.

- Sampling of tabular calcite and barite-calcite precipitates at the "Barite Mounds" in the northeastern part of the Derugin Basin (see also Chapter 10, Part I of this Report). OFOS (Ocean Floor Observation System) records showed big clamfields consisting of thousands of shells in this area. These shells are considered to be a reliable indicator for active gas seepage.
- Sampling of (sedimentary?) rocks at a small hill (so-called "Lola Hills") close to the "Barite Mounds" in order to gain information on the composition and origin of this structure.

11.2 Methods

Sampling of volcanic, sedimentary and plutonic rocks in the Kurile and Derugin Basins was carried out using rectangular chain bag dredges and a cylindrical ton dredge. Chain bag dredges are similar to large buckets with a chain bag attached to their bottom and steel teeth at their openings, which are dragged along the ocean floor by the ship or the ship's winch.
General station areas were chosen on the basis of bathymetric data, seismic reflection profiles or OFOS data gained on former cruises. The final selection of dredge sites was critically dependent on detailed echosounding surveys carried out at most station areas prior to dredging (e.g., *Fig. 11.1 – 11.4*). The final positioning of the ship over the dredge sites was done using GPS and the bathymetric data gained on the surveys, and allowing for weather and drift conditions. Dredge tracks at the seamounts were usually located - depending on the morphology of the structures - on steep slopes or at small cones on the flanks or tops of the seamounts. This was done (1) to avoid areas of thick sediment cover and (2) to receive rocks as young and accordingly as fresh as possible.
Taking into account the widespread ice-rafted debris in the Okhotsk Sea, detailed analysis of the obtained rocks was carried out to identify bedrock fragments. The criteria used for distinction include but are not restricted to (1) shape of the fragments (angular vs. well-rounded), (2) existence of fresh surfaces formed by tearing away from the bedrock outcrops, and (3) homogeneity of the dredged material.

11.3 Results

Altogether 18 dredge hauls at 4 sites in the Derugin Basin and 4 seamounts in the Kurile Basin on cruise LV29 recovered a wide variety of volcanic, plutonic and sedimentary rocks.

11.3.1 Derugin Basin

The first dredge haul in the Derugin Basin was carried out on its northern slope where – according to seismic reflection surveys – prominent tectonic blocks of the acoustic basement were revealed. The dredge track at the northwestern slope of a tectonic block rose up to 600-700 m above the seafloor of the Derugin Basin and yielded 80-100 kg of rocks comprising some boulders (up to 50 cm) of granodiorites, fragments of rhyodacite and quartz with sulfide mineralization, dropstones (pebbles and fragments of plutonic, volcanic, sedimentary and metamorphic rocks) and Fe-Mn-oxide crusts up to 1 cm thick. Many pebbles are encrusted with ferromanganese minerals.

Granodiorites: Medium-grained light gray rocks composed of plagioclase, quartz, K-feldspar, biotite and hornblende containing sub-rounded fine-grained diorite enclaves up to 3-5 cm in diameter. In terms of mineral assemblages, these rocks are very similar to Upper Cretaceous granodiorites of diorite-granite units being widespread on the Kashevarov Bank, on the Okhotsk Rise and on the Institute of Oceanology and Academy of Sciences Rises.

Rhyodacite: Dark gray sparsely porphyritic or rare aphyric rock with predominant plagioclase phenocrysts. Analogical rhyodacite with K-Ar age of 93.4 Ma associated with dacite, andesite and dolerite were sampled near this dredge site (Emel'yanova, 2001). These volcanic rocks have geochemical peculiarities of high-Al calc-alkaline series that allow to compare them with the Upper Cretaceous volcanic rocks from the Okhotsky-Tchukotsky volcanic belt (Bely, 1978).

The second target in the Derugin Basin was a rise in its northern part – the so-called "Barite Mounds" (Biebow et al., 2000). Detail studies of this rise yielded a wide distribution of various types of carbonate and barite mineralization (Astakhova, 1987; Derkachev et al., 1999, 2002; Biebow et al., 2000). For example, calcite-barite tabular bodies, calcite and barite concretions, barite spherulites and crusts were revealed in Holocene-Pleistocene sediments. At the upper part of the "Barite Mounds" outcrops of pure travertine-like barite chimneys up to 3-10 m high were also discovered (Biebow & Hütten, 1999). On cruise LV29 additional investigations of the eastern part of the "Barite Mounds" were conducted by OFOS surveys, dredging and core sampling. Two dredge hauls at the "Barite Mounds" (stations LV29-98 and -99) recovered various sedimentary rocks, dropstones, barite crusts and specific benthic fauna associated with seeping processes. The barite mineralization is described in Chapter 10, Part I of this Report.
A dredge haul on the slope of a hill ("Lola Hills") of unclear origin (possible diapir) located west of the "Barite Mounds" (station LV29-101) yielded only a small amount of unlithified sediments in the sediment traps of the dredge suggesting that this structure is covered by marine sediments. Therefore, dredging was ceased at this site.

11.3.2 Browton Ridge (Kurile Basin/ rear arc zone of the Kurile Island Arc)

The submarine Browton Ridge is located on the traverse of the Bussol Strait in the central part of the Kurile Island Arc and belongs to the Browton transverse zone (Avdeiko et al., 1992) which comprises the ridge and four discrete conical volcanoes located northeast of the ridge. Browton Ridge extends about 80 km from the arc northwest into the Kurile Basin and consists of several large volcanoes (like Vavilov Massif) and many smaller volcanic edifices. Its base is located at 3,000-3,200 m below sea level (b.s.l.). The conical volcanic edifices on the volcanic (?) basement of Browton Ridge have a sharp top, steep upper slopes (20°-30°) and rise up to ca. 2,500 m over the ocean floor of the Kurile Basin. The highest rise of the ridge is represented by the small volcanic island Browton.
Recent geological and geophysical surveys of this region provide the geologic, tectonic and petrologic framework for the investigations on cruise LV29. The origin and evolution of Browton Ridge, however, are up to now fairly unknown and probably cannot be explained only by the island arc volcanism of the Kurile Islands. Dredging on former cruises at the submarine volcanoes of Browton Ridge yielded a wide range of rocks (basalt, basaltic andesite, dacite, tuff, tuffaceous sandstone and siltstone, granite, granodiorites, diorite, gialospongia, manganese crust etc.), but many of them are believed to be ice-rafted dropstones (Avdeiko et al., 1992). In particular, the structure and composition of the northwestern part of the ridge is still unclear. Therefore, bathymetric survey and subsequent dredging operations on cruise LV29 focussed on the area of volcano 6.5 (according to the catalog of Avdeiko et al., 1992) at the northwestern Browton Ridge. Notwithstanding that the survey tracks were not closely spaced, it is evident that this part of the ridge consists of many volcanic cones and edifices accreted to each other. Four separated edifices including volcano 6.5 can be distinguished on the profile running along this part of the ridge. Their bases are located at similar depths of 3,000-3,100 m b.s.l., but the tops submerge from ca. 1,900 m b.s.l. in the southeast up to ca. 2,600 m b.s.l. to the northwest. The subsidence occurs not progressive but intermittent with the location of the tops at depths of 1,900, 2,300 and 2,600 m b.s.l., correspondingly. The most southeastern and highest cone (unlisted in the catalog of

Avdeiko et al., 1992) was selected for dredging because of its steep flanks and many small cones and, therefore, was mapped in more detail (*Fig. 11.1*).

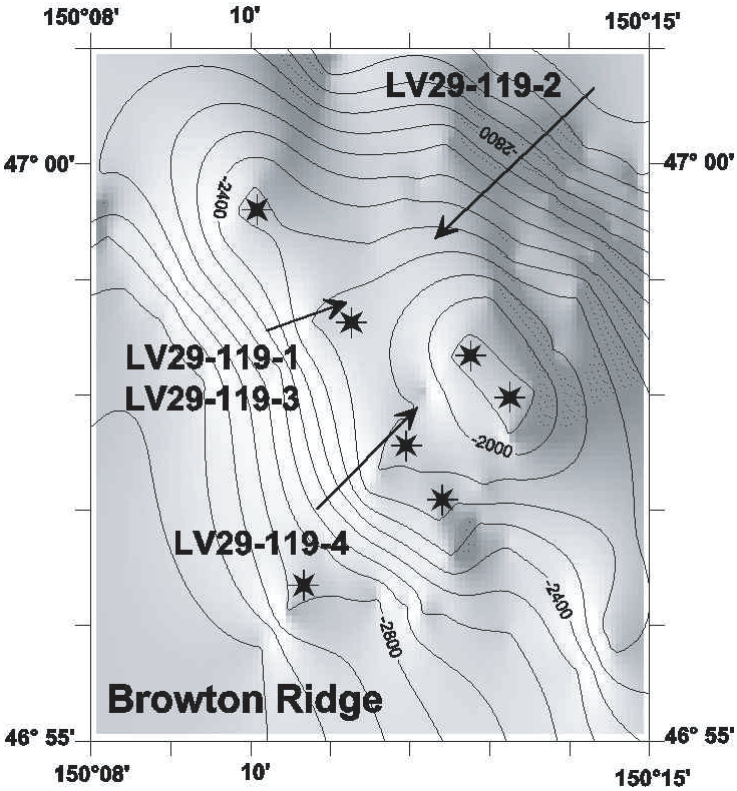

***Fig. 11.1**: Bathymetric map of the northwestern Browton Ridge volcano. This volcano as the ridge itself consists of many cones (stars) accreted to each other. Numbered solid arrows mark the dredge tracks and station number. Contour interval is 100 m.*

Four dredge hauls were carried out at this volcano: LV29-119-1, -119-3 and -119-4 from the southwestern slope and LV29-119-2 from its northeastern slope (*Fig. 11.1*). Dredge haul LV29-119-1 (2,600-2,200 m b.s.l.) did not recover rock samples, because the chain bag of the dredge opened during dredging, but a few manganese fragments (<1 cm) were found in the sediment traps of the dredge. Dredge haul LV29-119-2 (3,000-2,400 m b.s.l.) yielded about 30 kg of boulders and fragments of ice-rafted debris.

Dredge haul LV29-119-3 (2,600-2,200 m b.s.l.) recovered about 50 kg rocks comprising predominantly blocks and fragments of tuffaceous diatomite's and tuffaceous sandstone's, gialospongia and dropstones (pebbles, fragments and boulders of volcanic and plutonic rocks). Most fragments of the stratified tuffaceous sedimentary rocks contain numerous small fragments and pebbles of altered volcanic rocks and are coated and impregnated by ferromanganese material. Their shape, the fresh surfaces and homogeneity indicate an in situ origin of these sedimentary rocks at Browton Ridge.

Dredge haul LV29-119-4 (2,700-2,400 m b.s.l.) yielded about 250 kg rocks comprising dropstones, numerous blocks and fragments of yellow-greenish slightly lithified tuffaceous diatomite's and tuffaceous sandstone's, gray-greenish highly lithified tuffaceous sandstone's and diatomite's, boulders (up to 50-80 cm) of black volcanogenic conglomerato-breccia with tuffaceous matrix, blocks of gialospongia impregnated by manganese, and a fragment (up to 25 cm) of comparatively fresh, sparsely porphyric vesicular olivine-plagioclase basalt (probably dropstone?).

Additionally, one dredge haul (LV29-122) was carried out on the submarine volcano 6.4 (according to the catalog of Avdeiko et al., 1992) located ca. 47 km northeast of Browton

Island and ca. 50 km northwest of Simushir Island. This seamount has a very regular, conical volcanic edifice with a sharp top and steep upper slopes (up to 25º-30º), and rises up to ca. 1,800 m above the Kurile Basin floor. Its base is equal to 20 km in diameter; the total volume of the edifice is ca. 280 km^3 (Avdeiko et al., 1992). The volcano is characterized by a slightly negative magnetic anomaly with maximum values under the northeastern slope (-20 nT) and minimum values (-110 nT) under the southwestern slope (Avdeiko et al., 1992). Dredging on former cruises yielded fragments, blocks and boulders of plutonic, volcanic and sedimentary rocks (e.g., layered gravel, breccias, altered basalt, andesite, dacite, diorite, porphyric granite and granodiorites) being most likely ice-rafted debris (Avdeiko et al., 1992).
The bathymetric survey on cruise LV29 proved that this seamount is a classic volcanic edifice being slightly elongated in NW-SE direction (*Fig. 11.2*). Bends of the contour lines may indicate parasitic cones on the flanks of the volcano. Furthermore, a field of small volcanic cones was detected on a bathymetric profile extending westward from the base of the volcano. One dredge haul (LV29-122, 2,700-2,200 m b.s.l.) on the northeastern slope of volcano 6.4 (*Fig. 11.2*) recovered about 30 kg rocks comprising predominantly blocks and fragments of tuffaceous diatomite's and tuffaceous sandstone's impregnated by manganese, gialospongia and dropstones (pebbles, fragments and boulders of volcanic and plutonic rocks).

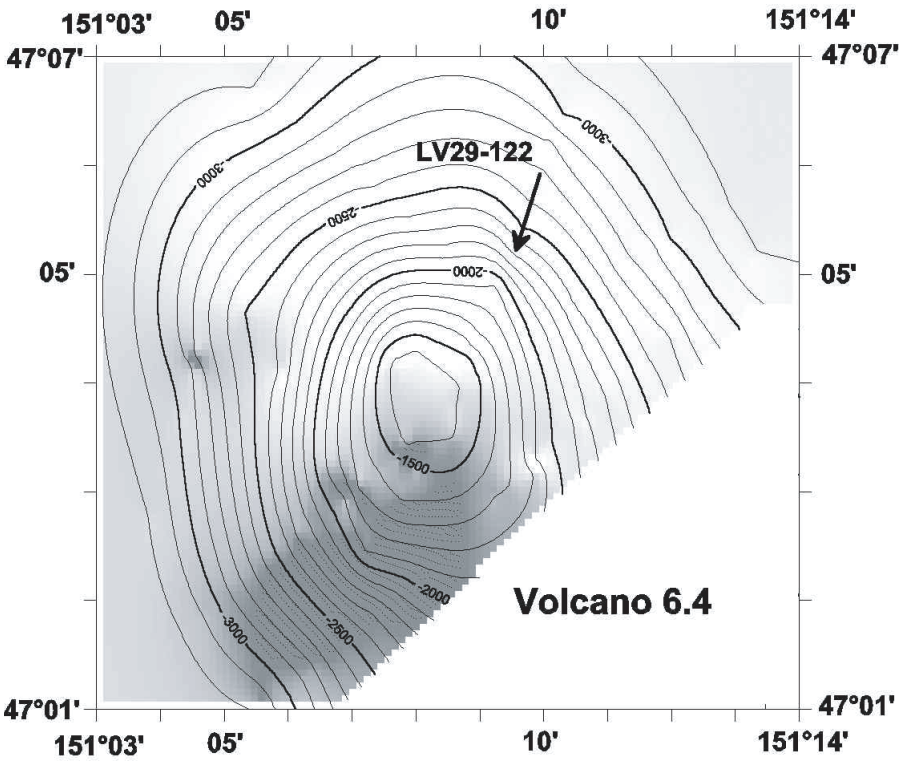

***Fig. 11.2**: Bathymetric map of volcano 6.4. This volcano has a very regular shape and uplifts above the flat Kurile Basin floor up to ca. 1,800 m. Arrow marks the dredge track. Contour interval is 100 m.*

In summary, the dredged material yielded at Browton Ridge and volcano 6.4 indicates that the slopes of these structures are most likely completely covered by slightly to highly lithified diatomaceous sedimentary rocks, manganese crusts, (fossil) colonies of gialospongia impregnated by manganese, and dropstones ranging in composition from basalt to granodiorites. The diatomaceous sedimentary rocks represent probably the sedimentary bedrock's of Browton Ridge. Land-based studies of these rocks may provide information on the (minimum) age of the ridge (Miocene-Pliocene?).

11.3.3 Submarine volcanoes of the North-Iturup transverse zone (Hydrographer Ridge)

Hydrographer Ridge, located in the North-Iturup transverse zone of the Kurile Island Arc, is a ca. 20 km long, WNW-ESE-trending ridge structure elevating up to ca. 1,600 m above the floor of the Kurile Basin. According to Avdeiko et al. (1992), the ridge represents a chain of three volcanoes (7.12, 7.13, 7.14). Dredging on former cruises yielded a wide variety of rocks, among them basalts and basaltic andesites, yet these have been considered to be most likely dropstones. The bathymetric and seismic survey conducted on cruise LV29 revealed significant differences in the morphology of the western and eastern part of the ridge. The eastern part (volcano 7.14) shows a cross section of a typical stratovolcano with a flat top probably tilting towards the Kurile Basin, whereas the western Hydrographer Ridge (volcano 7.12) has an asymmetric profile with a steeper southern slope.

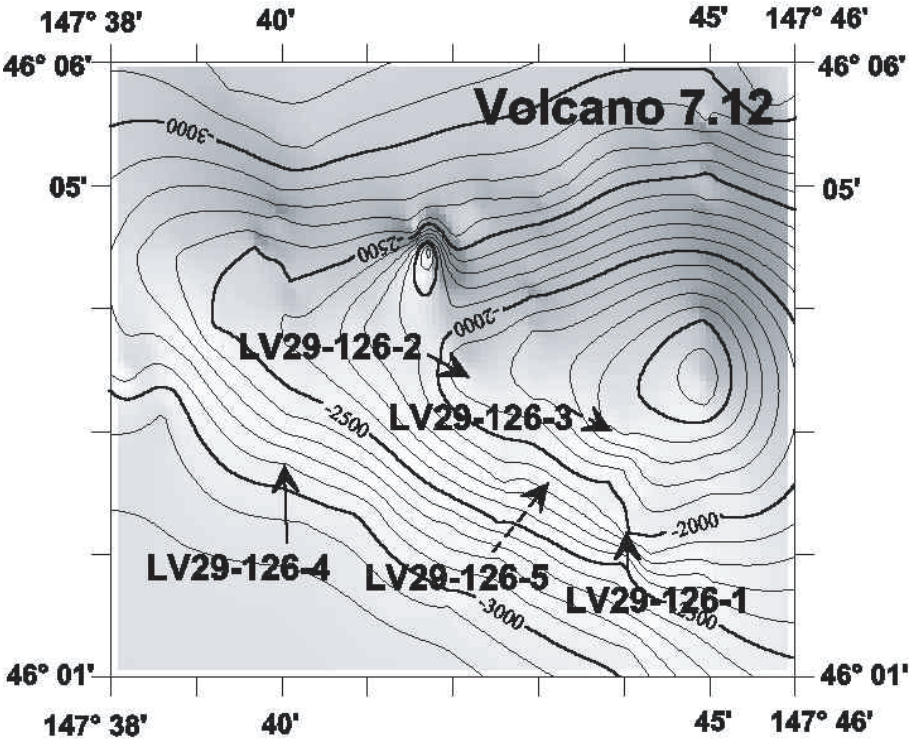

***Fig. 11.3**: Bathymetric map of the western Hydrographer Ridge (volcano 7.12). This part of the ridge has an asymmetric cross section. Numbered solid arrows mark the dredge tracks and station number, dashed where the dredge was empty or only ice-rafted material was recovered. Contour interval is 100 m.*

Five dredge hauls were carried out at volcano 7.12 subsequent to the hydroacoustic and seismic survey: LV29-126-1, -126-4 and 126-5 from the lower southern slope to the top and LV29-126-2 and -126-3 at the small cones on the crest of the ridge (*Fig. 11.3*). Dredge hauls LV29-126-3 and -126-5 yielded only numerous fragments of gialospongia and dropstones ranging in composition from granodiorites to basalt. Dredge haul LV29-126-2 recovered besides dropstones a small (ca. 5 cm in size) fragment of orthopyroxene-clinopyroxene-plagioclase basaltic andesite which possibly represents the bedrock of this site.
Dredge haul LV29-126-1 (ca. 2,500-2,000 m b.s.l.) on the southern slope of volcano 7.12, however, yielded ca. 100 kg of angular fragments of homogeneous pillow-like basaltic lava, ranging from a few centimeters to ca. 30 x 30 cm in size. The homogeneity, angular shape and rough surfaces of the dredged rocks strongly indicate that they are fragments of a (pillow)-lava flow once formed by an eruption of volcano 7.12, i.e. they represent in situ rocks. The lava fragments are highly porphyric (up to 5-10 vol.%), frequently vesicular

basalts or basaltic andesites with rounded to oval-shaped vesicles being commonly 1-3 mm in diameter. Major phenocrysts are plagioclase, clinopyroxene, olivine, amphibole, and Fe-Ti-oxides; orthopyroxene occurs minor. The groundmass is characterized by a microlitic texture and consists of glass with numerous plagioclase microlites and varying amounts of clinopyroxene, amphibole and Fe-Ti-oxides. The phenocrysts and the groundmass of these rocks are fresh or show only minor alteration.
Dredge haul LV29-126-4 recovered numerous fragments (ca. 8-10 kg) of slightly lithified diatomaceous sedimentary rocks, gialospongia, and a block (ca. 25 x 30 cm in size) of porphyric, vesicular olivine-orthopyroxene-clinopyroxene-plagioclase basalt. The material yielded by this dredge shows some evidence for an in situ origin as homogeneity (sedimentary rocks), angular form, and rough, "broken" surfaces (sedimentary rocks, basaltic block). The basaltic block is only minor affected by alteration with the exception of the olivine phenocrysts which are partially replaced by secondary minerals. The noteworthy feature of this lava is common glomerophyric clusters of gabbro (cpx+plag) and wehrlite (ol+cpx±plag), which are considered to be enclaves of cumulated rocks.

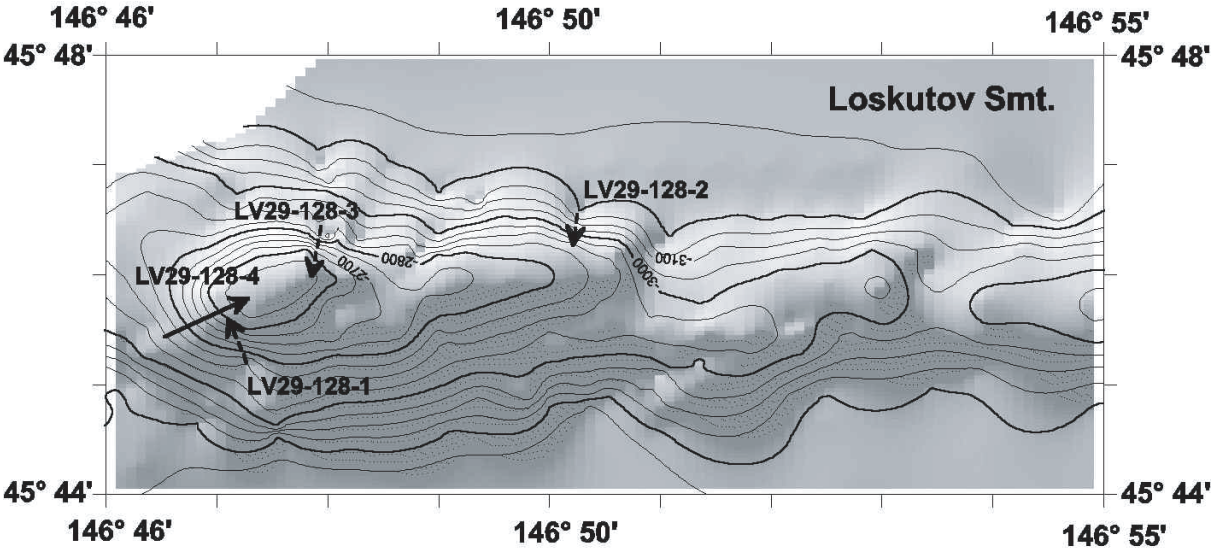

Fig. 11.4: *Bathymetric map of the deepest volcano (Loskutov seamount) dredged on cruise LV29. This volcano consists of many volcanic cones and shows a dextral en-echelon pattern. Numbered solid arrows mark the dredge tracks and station number, dashed where the dredge was empty or only ice-rafted material was recovered. Contour interval is 25 m.*

11.3.4 Loskutov submarine volcano

Loskutov seamount is located ca. 100 km northwest of the Kurile Island Arc in the Kurile Basin. The seamount does not show any visible relationship with the arc, and its origin and evolution is still unknown. It has a ridge-like structure which is outlined by the 3,500 m contour line and extends ca. 20 km in W-E direction (*Fig. 11.4*). The bathymetric survey on cruise LV29 proved that this ridge consists of several volcanic cones (similar to Browton Ridge). The highest cone is located in the western part and elevates up to 2,510 m b.s.l. The cones align in three chains that show a dextral en-echelon pattern.
Altogether 4 dredge hauls were carried out on the southern slope (LV29-128-1), the northern base (LV29-128-2), and in the top area of the western cone (LV29-128-3, -4) of Loskutov seamount (*Fig. 11.4*). None of these dredge hauls recovered in situ volcanic (or plutonic) rocks. Dredging at sites LV29-128-1, -2, and -3 yielded only a couple of dropstones and small amounts of unlithified (marine) sediments. However, paleoceanological studies of slightly

lithified sedimentary rocks recovered at site LV29-128-4 may possibly provide informations on the (minimum) age and evolution of Loskutov seamount.

12. REFLECTION SEISMICS

Boris Karp, Boris Baranov, Viktor Karnaukh, and Vladimir Prokudin

12.1 Method and instruments

The applied seismic reflection system consists of one air gun, a single-channel streamer, a digital data acquisition system and air gun trigger unit. The Pulse-6™ air gun pressurized nominally at 130 bar was towed in a distance of ca. 10 m behind the ship and triggered every 10-11 sec with pulses generated by a master clock. The streamer has an active section with a length of 25 m and two inactive sections (ahead and behind of the active section) with a length of 25 m each, leading to a total length of the streamer of 75 m. The towing depth of the streamer was 6 m, and the offset was 150 m.
The operational characteristics of the single-channel seismic reflection system are summarized in *Table 12.1*.

Table 12.1: *Operational characteristics of the single-channel reflection system.*

Source	
Type	Pulse-6™ air gun
Volume	3.5 or 2.5 liters
Pressure	130 bar nominal
Firing interval	10-11 sec
Source depth	5 m
Streamer	
Streamer depth	6 m
Active section offset	175 m
Length of active section	25 m
Total length of streamer	75 m
Recording	
Recording length	3-4 sec
Sampling frequency	1000 Hz
Bandpass analog filter	20-400 Hz

The analog seismic signals are digitized via a PC-based commercial sound card (Sound Blaster 16, Vibra) and written onto the harddisk of a Pentium-PC. A backup copy was made on CD. A single-channel digital acquisition system permits real-time data monitoring (quality control) on screen. The GPS unit is connected to the serial port of the PC. Recording and adjustment of the dynamic range of the seismic signals are controlled on the PC monitor by software developed for this purpose.

Specification of the single-channel data acquisition system:

- data format: SEG-Y files, 16 bit
- sampling rate: 1 or 2 ms
- length of trace: 4…6 sec
- software: acquisition, filtering, viewing, printing, testing

12.2 Results

Reflection seismic profiling was carried out during cruise LV29 of RV *Akademik Lavrentyev* continuing and extending the study area of the SAKURA expedition in the central part of the Kurile Basin and on Browton and Hydrographer Ridges to the north (*Fig. 12.1*). In addition,

seismic profiling was carried out parallel to the sediment echosounder SES-2000DS profiles excluding the profiles in the Sakhalin Gulf and in the enter of La Perusa Strait (see Appendix 8). This report includes the preliminary interpretation of seismic profiles in the central part of the Kurile Basin.

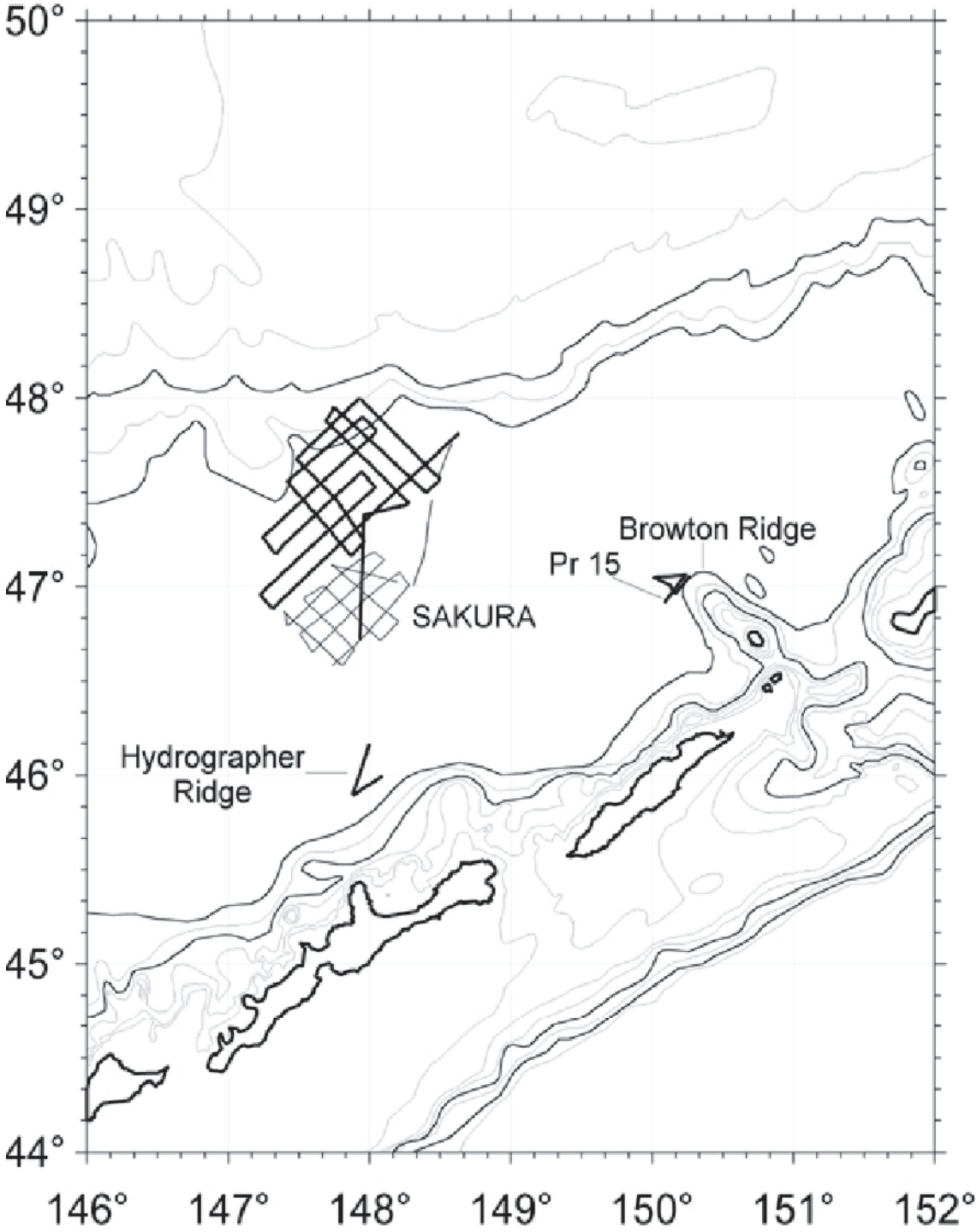

Fig. 12.1: *Seismic profiles of the present expedition and of the SAKURA cruise in the central Kurile Basin. Marked are the present expedition lines.*

The acoustic basement can be seen on most parts of the profiles. It is clearly expressed up to a depth of 6.0 s TWT below the sea surface and appears as a weak reflector at greater depth. The acoustic basement is represented by an envelope of diffraction hyperbolas. The chaotic internal reflections of the basement probably indicate a volcanic (basaltic) composition of the

basement. A map of the distribution of basement depths compiled from the SAKURA and the present expedition data is shown in *Figure 12.2*. The main structural element of the SAKURA area is Sakura Ridge (Biebow et al., 2000). It is clear from *Figure 12.2* that Sakura Ridge extends to the north. Its crest is displaced to the east at approximately 47°23'N.

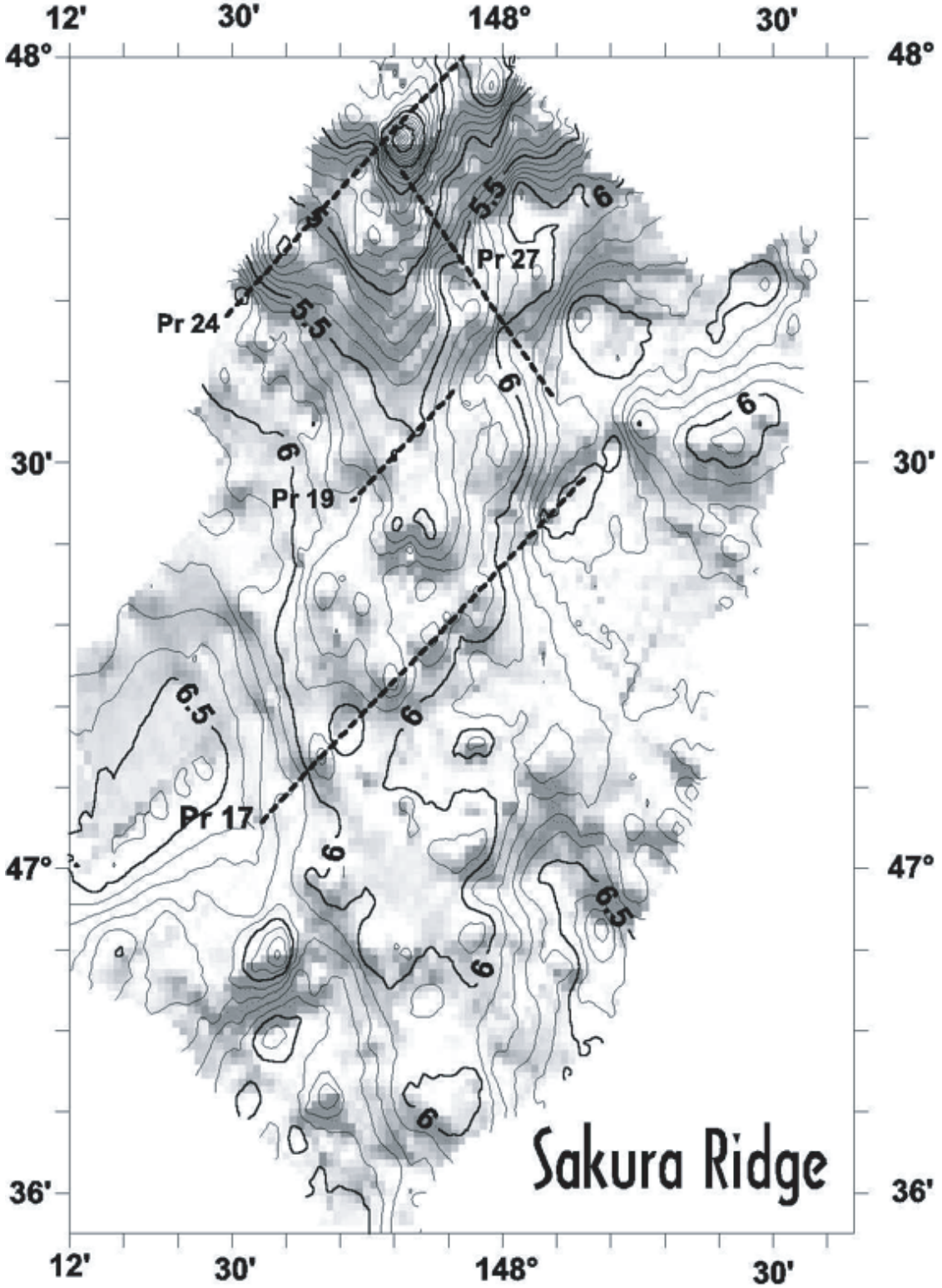

Fig. 12.2: *Basement morphology of Sakura Ridge. This ridge has very pronounced wedge-shape outlines suggesting propagated rift. Contour interval is 0.1 s. Dashed lines mark location of the seismic profiles shown in Fig. 12.4 — 12.8.*

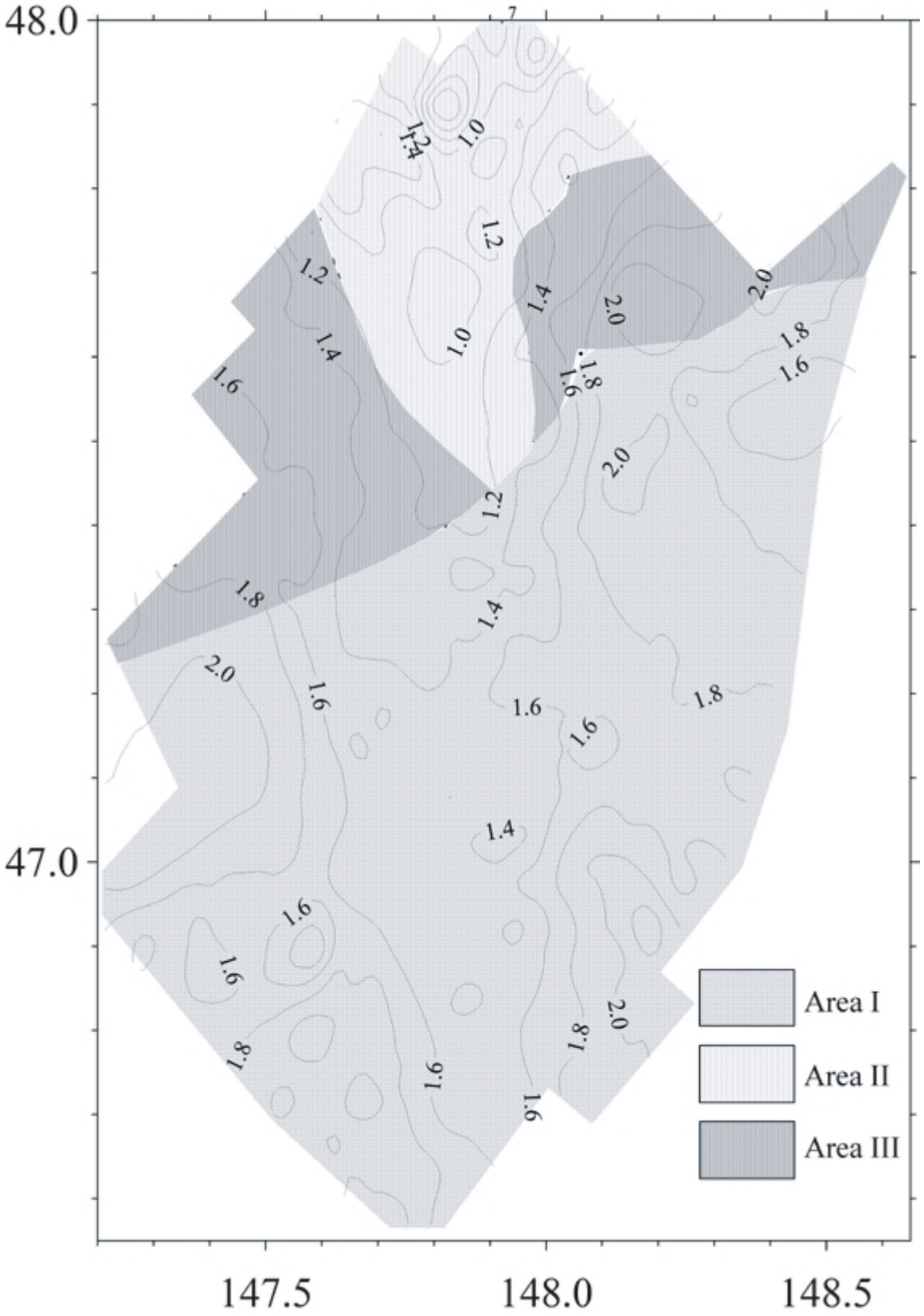

Fig. 12.3: *Map of location of areas with different seismo-stratigraphic characteristics. 1 = area I, 2 = area II, 3 = area III. Thin continuous lines mark thickness of sedimentary layer in sec. Contour interval is 0.2 s.*

The ridge is bounded by an acoustic basement high striking in SW-NE direction in the north. The sediment thickness above the ridge does not exceed 1.6 s. However, it reaches 2.0 s (*Fig.*

12.3) in the basement depressions that are located to the southwest and to the northeast of the ridge.

The investigated part of the Kurile Basin can be divided into three areas, each having its own distinct seismo-stratigraphic characteristics (*Fig. 12.3*). The first (area I) is located in the south. Its sedimentary section comprises two seismic units: an upper, well stratified unit and a lower, semi-transparent unit (*Fig. 12.4*). The thickness of the upper unit is nearly constant at 0.8 – 1.0 s. Fluctuations in the total thickness of the sedimentary layer are largely a result of variations in the thickness of the semi-transparent unit. The well stratified unit consists of a series of subparallel, subhorizontal reflectors. In contrast, the semi-transparent unit comprises only occasional, low-amplitude, continuous reflectors that drape the acoustic basement. The boundary between these two units is marked by a high-amplitude, low-frequency reflector. The well stratified unit may be subdivided into two sequences (A1 and A2, *Fig. 12.4*) that differ in the thickness of the intercalated transparent layers and layers with discontinuous reflectors of low amplitude.

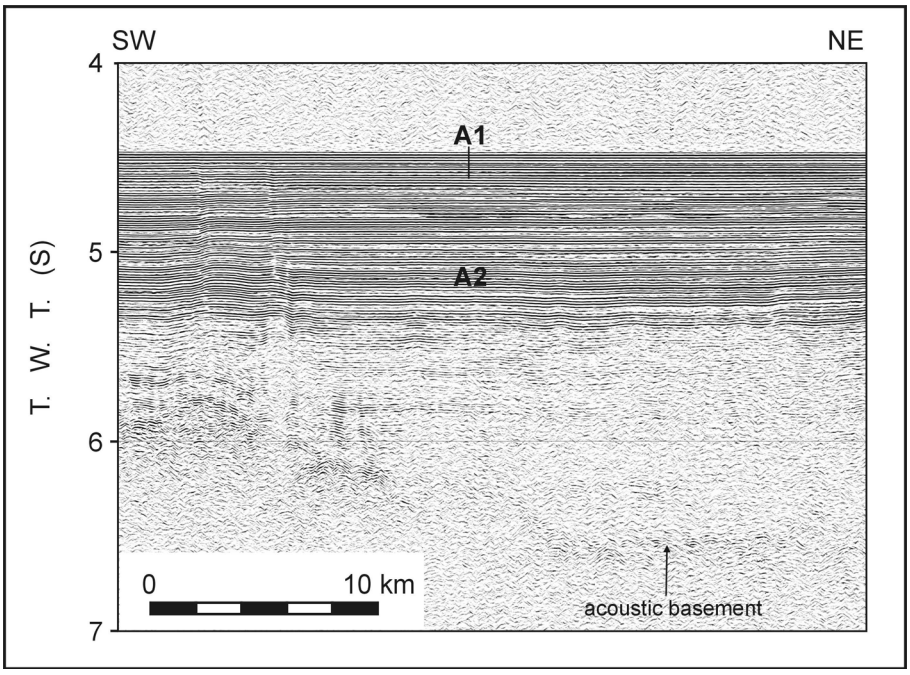

Fig. 12.4: *Part of seismic profile 17 showing the seismic section in area I. Location of profile is shown in Fig. 12.2.*

Area II occupies the ridge and its slopes. The sedimentary section of area II, where the ridge is buried by sediments and does practically not manifest in the seafloor (profiles 19 and 20), comprises seven seismic units: four well stratified sequences and three semi-transparent sequences (profile 19, *Fig. 12.5*). The upper two well stratified sequences consist of subparallel seismic reflections. The upper of them is characterized by continuous reflectors of high amplitude. The reflectors have a curve upward configuration. The lower sequence comprises subparallel continuous reflectors of medium amplitude and a curve downward configuration. These sequences are bounded by an unconformity. All semi-transparent sequences have only occasional, low-amplitude, discontinuous reflectors. The lower two well stratified sequences drape underlying semi-transparent sequences. The sedimentary section of area II where the ridge manifests in topography is characterized by the presence of four well stratified sequences on the top and upper slope of the ridge (profile 27, *Fig. 12.6*). A semi-transparent sequence is subjacent to these sequences. The well stratified sequences are separated by three unconformities that show erosion truncation in places. On the middle and lower slopes three upper well stratified sequences are truncated by the seafloor. The semi-

transparent unit separates the lower well stratified sequence and the upper well stratified sequence. The external configuration of the semi-transparent unit is mound-like (downlap of the reflectors). On the middle slope buried sediment waves occur. There are scarps and displaced masses (slides) on the ridge lower slope.

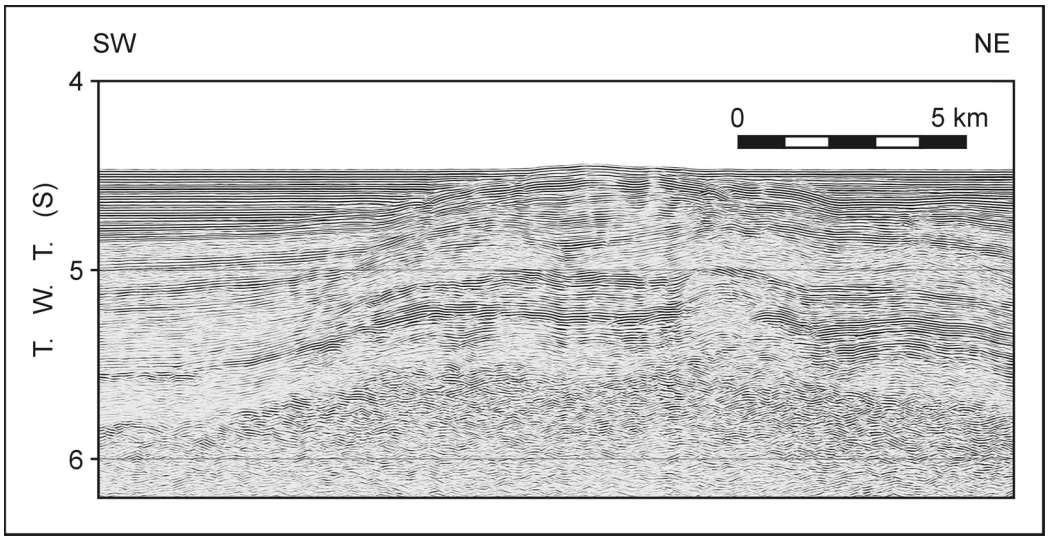

Fig. 12.5: *Part of seismic profile 19 showing the seismic section of the ridge buried by sediments (area II). Location of profile is shown in Fig. 12.2.*

Area III differs from area I by the fact that several (2-3) semi-transparent layers thicken considerably in the interior of the upper well stratified unit and that a prominent well stratified layer appears within the lower semi-transparent unit. The boundary between area II and area III coincides with the ridge's lower slope buried by sediments. In general, area I grades area III and the boundary between them is not clear.

12.3 Discussion

12.3.1 Sediment processes

The sedimentary section of the Kurile Basin consists of an upper stratified and a lower semi-transparent sequence. The boundary between them is marked by a high-amplitude reflector (Gnibidenko et al., 1995). The same sedimentary section is observed in area I. In addition, the upper sedimentary column directly above Sakura Ridge is repeatedly interrupted by vertical regions of acoustic turbidity in which diffraction hyperbolas dominate. Typical are also the accompanying apparent deformations and interruptions of the flat-lying horizons. These regions are probably fissure zones. Sediment processes change abruptly in the northern part of Sakura Ridge (area II). The lower semi-transparent sequence displays an apparent drape of the basement highs of the ridge. In contrast, the upper well stratified sequence onlaps the ridge's proper sedimentary layers. These relationships between sedimentary section and ridge basement indicate that the Kurile Basin sediments accumulated here during an inactive period of the basin's development.

The depositional history of the ridge after semi-transparent sequence accumulation includes at least three periods. Turbidites and interbedded hemipelagits overlay the semi-transparent sequence. The deposits appear as well stratified units on the seismic section. The thickness of the unit decreases from north to south amounting to 0.3 – 0.4 s in the north (profile 24) and 0.1 – 0.15 s in the south (profile 19). This unit extends to area III as the prominent well stratified layer within the lower semi-transparent unit. The reduction of the thickness of the

well stratified unit from north to south suggests that a source of turbidites was located on the northern Kurile Basin slope. The top of the unit is an erosional discontinuity. Simultaneously with erosional processes, the ridge slope became more instable. The instability resulted in mass movements causing erosion at the top and the middle of the slope as well as debris flows at the base of the slope. These debris flows extend to the basin (probably as turbidity currents) and create semi-transparent layers in area III. This process was repeated at least two times during the depositional history of the ridge. At present, the processes of mass wasting prevail in the northern part of the ridge. The topographic Sakura Ridge is a sediment ridge except for its northern termination.

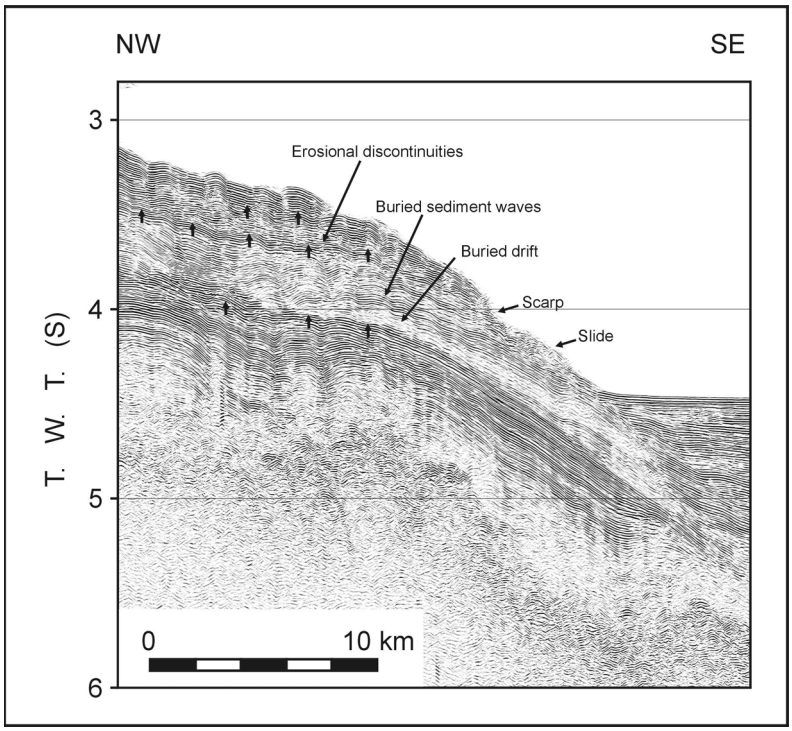

Fig. 12.6: *Part of seismic profile 27 showing the seismic section of the northern termination of the ridge (area II). Location of profile is shown in Fig. 12.2.*

12.3.2 Tectonic structure of Sakura Ridge

12.3.2.1 Previous studies

The seismic survey in the central part of the Kurile Basin was carried out to study the nature of a specific basement rise, which separates two subbasins with a depth to the basement of up to 7 km.

For the first time this basement rise in the central part of the basin was investigated during the Pacific expedition “Souzmorgeo” in 1976. The expedition showed that the rise has a complicated structure and consists of isometric basement highs. The depressions between them form fan-like, undulating systems that resemble river valleys. Over the top of the swell, the basement lies at a depth of about 5 km; in the depressions to the southwest and the northeast, it was found at depths of 8 and 7 km, respectively (Zhuravlev, 1982). The origin of the rise remained unknown. It was only much later that they were supposed to represent shear/lateral fault zones that defined an opening direction orthogonally to the general strike of the Kurile Basin (Gnibidenko et al., 1995).

For the second time, the rise was investigated during the SAKURA expedition in 1999 (Biebow et al., 2000). The data obtained showed that this rise (named Sakura Ridge) has a clear rift imprint. The morphology of its axial high suggests that it corresponds to a spreading axis. This axis (a spreading ridge) strikes N-S, i.e. in correspondence to the general strike of

the Kurile Basin. Although this data is insufficient for a reliable identification of the spreading axis, it provides clear evidence for a SW-NE spreading direction, implying that the Kurile Basin opened along its general strike as a pull-apart basin (Baranov et al., 2002). During the SAKURA expedition we mapped only one segment of it and the question how far the ridge continues to the north and south remained open. Obvious is only that it becomes wider to the north, and it was suggested that the ridge is apparently bounded near the northern slope of the Kurile Basin by a strike-slip or transform fault. On cruise LV29 the mapping of the ridge was therefore continued to the north.

12.3.2.2 Recent study

Six seismic profiles crossing the ridge axis were obtained (*Fig. 12.1*); the ridge shows symmetry on each of them. On the most southern cross-section it consists of a central dome and two adjacent blocks (*Fig. 12.7*). These outwardly tilted blocks are bounded by inward-facing fault scarps. The ridge is getting higher to the north and the central dome becomes more massive. Two symmetrical heights appearing on its top can be interpreted as small volcanic edifices.

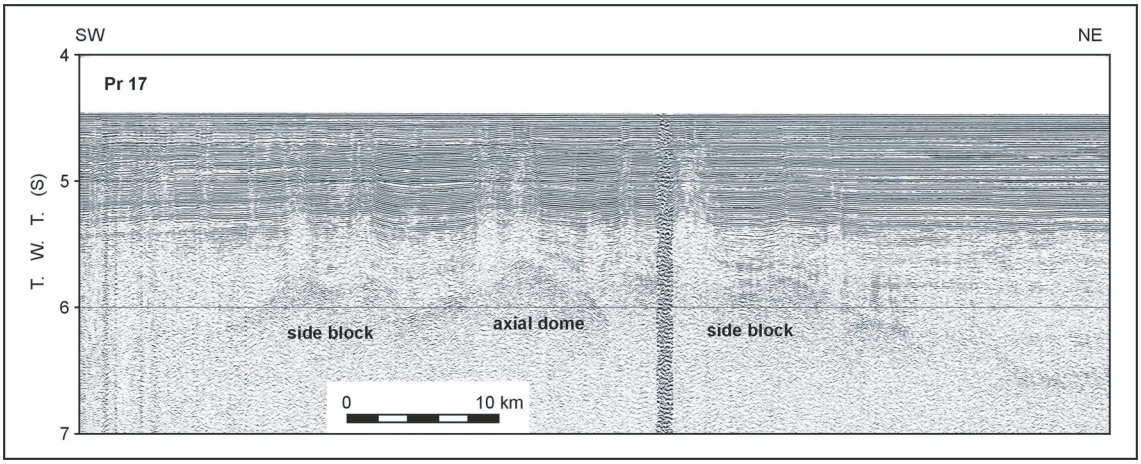

Fig. 12.7: *Part of seismic profile 17 showing the symmetry of Sakura Ridge where on both sides of central dome two blocks are located. Location of the profile is shown in Fig. 12.2.*

At the latitude of ca. 47°30’ the ridge starts to appear at the seafloor as a small gentle swell. Our investigations do not support the suggestion (Gnibidenko et al., 1995) that this swell continues to the south across the whole Kurile Basin. At an approximate latitude of 47°45’ N the ridge goes onto the northern slope of the Kurile Basin or, to be more exact, forms this part of the northern slope. The high mount occupies the central part of the ridge in the northernmost cross-section (*Fig. 12.8*). It has rounded outlines and its altitude equals ca. 1 km. This gives us the opportunity to suggest that this mount is an axial volcano. The NW-SE profile running across this structure shows that its top outcrops on the seafloor. The sedimentary layer covering the ridge on the northern slope is strongly deformed. The character of the deformations is very complex, but some of them are very similar to a wipe-out structure and maybe indicate gas emanations. As seen from *Figure 12.2*, Sakura Ridge tends to be wider and higher to the north as was found before. Therefore, the ridge has wedge-shaped outlines with an acute angle directed to the north. The ridge axis strikes in N-S direction; a very pronounced dextral shift is visible in the central part of the investigation area. This shift is connected with the strike-slip (transform) fault that appears on the axis as a steep SW-WE-striking scarp.

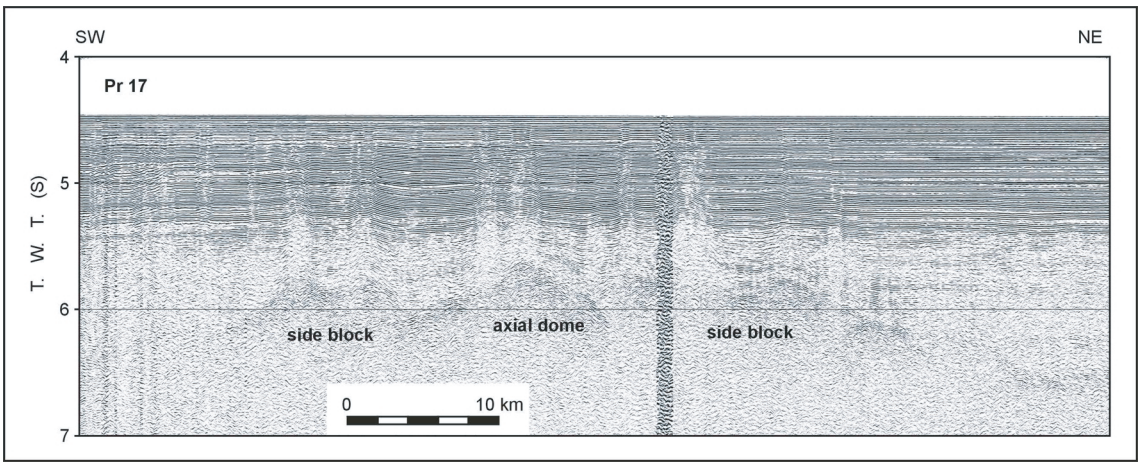

Fig. 12.8: *Large axial volcano located on the northern boundary of the study area as seen on seismic profile 24. Sakura Ridge forms here the northern slope of the Kurile Basin. Location of the profile is shown in Fig. 12.2.*

12.3.2.3 Preliminary conclusions

1. The seismic data allows us to interpret Sakura Ridge as a single structure extending at least up to the middle northern slope of the Kurile Basin (depth ca. 2,300 m). As seen on profiles, the axial zone of this structure represents a high, the dimensions of which increase to the north. Therefore, the axial zone looks like a volcanic dome on the southern cross-sections and on the northern one like a large volcanic edifice (the diameter is about 5 nm and the altitude is approximately 1 km). At least one pair of the blocks bounded by inward-facing fault scarps exists on both sides of the axial zone. This shows a symmetric pattern typical for spreading zones. The symmetry is observed for the small heights on the top of the axial zone, as well. Based on this structural data we can confirm the spreading nature of Sakura Ridge suggested after the SAKURA expedition.
2. There is a change in the morphology of the axial zone with a dimension of ca. 10 nm along the strike of the ridge that suggests the existence of some kind of discontinuities connected with transform faults, the length of magmatic cells and so on. One of such changes occurs in the central part of the ridge where its axis is dextrally shifted indicating on a transform fault.
3. Sakura Ridge has wedge-shaped outlines typical for propagated rifts. From the fact that it propagated from north to south, we can suggest by parity of reasoning with the Japan Sea (Tamaki, 1995) the existence of a large dextral strike-slip zone on the northern slope of the Kurile Basin.
4. There are lots of propagated rifts and spreading ridges, which pass through the ocean basin to the continental margin and further to the continent. Sakura Ridge probably extends from the continental margin to the basin, and in this case the structure of the northern slope of the Kurile Basin is very ambiguous.

13. REFERENCES

Agatova, A.I., Dafner, E.V., Sapozhnikov, V.V. et al., 1996. The trends of distribution of dissolved and particulate organic matter in the Okhotsk Sea. Okeanologiya (Oceanology), 36 (6), 856-864 (in Russian).

Alderman, S.E., 1996. Planktonic foraminifera in the Sea of Okhotsk: population and stable isotope analyses from a sediment trap. Unpublished MS thesis. Massachusettes Institute of Technology. Woods Hole Oceanographic Institution, 88 pp.

Aramaki, T., Watanabe, S., Kuji, T. & Wakatsuchi, M., 2001. The Okhotsk-Pacific seawater exchange in the viewpoint of vertical profiles of radiocarbon around the Bussol' Strait. Geophysical Research Letters, 28, 3971-3974.

Arzhanova, N.V. & Zubarevich, V.L., 1997. The chemical basis of the bioproductivity in the Sea of Okhotsk. Complex studies of ecosistem of the sea of Okhotsk. Moscow: VNIRO Publishing, 86-92 (in Russian).

Asano, K., 1958. The foraminifera from the adjacent seas of Japan, collected by S.S.Soyomary, 1922-1930, Part 4. Buliminidae. Tohoku University, Science Reports, 2nd series (Geology), 28, 1-26.

Asano, K., 1950. Part 2: Buliminidae. In: Stach, I.W. (ed.). Illustrated catalogue of Japanese Teritary smaller foraminifera. Tokio: Hosokawa Printing Co., 14.

Astakhov, A.S., 1986. Late Quaternary sedimentation on the Okhotsk Sea shelf. Vladivostok: Dalnauka, 140 pp. (in Russian).

Astakhov, A., Gorbarenko, S., Tiedemann, R., Wallmann, K. & Volokhin, Yu.G., 2000. Variation of the heavy metals deposition in the Derugin Basin (the Sea of Okhotsk) for the last 25 000 years: evidence of paleoceanological events or fluid venting intensity? Third Workshop on Russian-German Cooperation in the Okhotsk Sea - KOMEX. Program & Abstracts. Moscow, 8-9.

Astakhova, N.V., Lipkina, M.I. & Mel'nichenko, Yu.I., 1987. Hydrothermal barite mineralization in the Derugin Basin of the Okhotsk Sea. Doklady Akademii Nauk SSSR (Talks of the Academy of Science of the USSR), 295 (1), 212-215 (in Russian).

Avdeiko, G.P., Antonov, A.Yu., Volynetz, O.N., Rashidov, V.A., Tsvetkov, A.A., Bondarenko, V.I., Gladkov, N.G., Markov, I.A. & Palueva, A.A., 1992. Submarine volcanism and zonality of the Kurile Island Arc. Moscow: Nauka, 528 pp. (in Russian).

Baranov, B., Werner, R., Hoernle, K., Tsoy, I., Bogaard, P.v.d. & Tararin, I., 2002a. Volcanological, geochemical, paleo-oceanological and geophysical evidence for compressionally-induced high subsidence rates in the Kurile Basin (Okhotsk Sea). Tectonophysics, 350, 63-97.

Baranov, B.V., Wong, H.K., Dozorova, K.A., Karp, B.Ya., Lüdmann, T. & Karnaukh, V., 2002b. Opening geometry of the Kurile Basin (Okhotsk Sea) as inferred from structural data. The Island Arc, August, 2002.

Barash, M.S., Bubenshchikova, N.V., Kazarina, G.Kh., Khusid, T.A., 2001. Paleoceanographic studies in the central part of the Okhotsk sea during the last 200 Kyr (on the basis of micropaleontological data). Okeanologiya (Oceanology), 41 (2), 755-767 (in Russian, English translation).

Basov, I.A., Khusid, T.A., 1983. The living benthic foraminifera and their biomass in sediment of the Okhotsk Sea. Biologiya morya (Biology of the sea), 6, 31-43 (in Russian).

Bely, V.F., 1978. Formations and tectonics of the Okhotsky-Tchukotsky volcanic belt. Moscow: Nauka, 212 pp. (in Russian).

Belyaeva, N.V. & Burmistrova, I.I., 1997. Paleohydrology of Sea of Okhotsk during the last 60 ka. Okeanologiya (Oceanology), 3, 377-385 (in Russian, English translation).

Ben-Yaakov, S., 1973. PH buffering of pore water of recent anoxic marine sediments. Limnol. Oceanogr., 18, 86-94.

Bernhard, J.M., Sen Gupta, B.K. & Borne, P.F., 1997. Benthic foraminiferal proxy to estimate dysoxic bottom-water oxygen concentrations: Santa Barbara Basin, US Pacific continental margin. Journal of foraminiferal Research, 27, p. 301-310.

Bezrukov, P.L., 1957. Bottom sediments of the Okhotsk Sea. Trudy Instituta okeanologii (Proceedings of the Institute of Oceanology), 22, 3-68 (in Russian).

Biebow, N. & Hütten, E. (eds.), 1999. Cruise Reports: KOMEX I and II: RV Professor Gagarinsky cruise 22, RV Akademik M.A. Lavrentyev cruise 28. GEOMAR Report, 82, 188 pp.

Biebow, N., Lüdmann, T., Karp, B. & Kulinich R., 2000. Cruise Reports: KOMEX V and VI: RV Professor Gagarinsky cruise 26, MV Marshal Gelovany cruise 1. GEOMAR Report, 88, 296 pp.

Braitseva, O.A., Melekestsev, I.V., Ponomareva, V.V et al., 1995. Ages of calderas, large explosive craters and active volcanoes in the Kurile-Kamchatka region, Russia. Bull. volcanol., 57, 383-402.

Broecker, W.S., Spencer, D.W., & Craig, H., 1982. Hydrographic data, 1973-1974. In: GEOSECS Pacific Expedition. Natl. Sci. Found, Washington, D.C., 3, 137 pp.

Bruyevich, S.V., 1944. Determination alkalinity of small volumes of sea water by direct titration. In: Instruction of chemical investigation of sea water. Moscow-Leningrad: Glavsevmorput, 83 pp. (in Russian).

Bruyevich, S.V., 1956. Chemistry of the sediments of the Okhotsk Sea. Trudy Instituta okeanologii Akademii Nauk SSSR (Proceedings of the Institute of Oceanology of the Academy of Science of the USSR), 17, 41-132 (in Russian).

Bruyevich, S.V., Bogoyavlensky, A.N. & Mokievskaya, V.V., 1960. Hydrochemical characteristic of the Okhotsk Sea. Trudy Instituta okeanologii Akademii Nauk SSSR (Proceedings of the Institute of Oceanology of the Academy of Science of the USSR), 62, 125-198 (in Russian).

Bruyevich, S.V., Bogoyavlensky, A.N. & Mokievskaya, V.V., 1960. Hydrochemistry of Okhotsk Sea. Trudy Instituta okeanologii AN SSSR (Proceedings of the Institute of Oceanology of the Academy of Science of the USSR), 42 (in Russian).

Bychkov, A.S., Rogachev, K.A., Tishchenko, P.Ya., Pavlova, G.Yu. & Salyuk, A.N., 1996. Hydrochemistry of the Okhotsk Sea: reflection of mesoscale physical processes. Proceedings of the 11th Intern. Symp. on Okhotsk Sea, Mombetsu, Japan, 324-330.

Calvert, S.E. & Pedersen, T.F., 1993. Geochemistry of recent oxic and anoxic marine sediments: implications of the geological record. Mar. Geol, 113, 67-88.

Canfild, D.E., 1989. Sulfate reduction and oxic respiretion in marine sediments: Implication for the organic carbon preservation in euxinic environments. Deep Sea Res. Part A, 36, 121-138.

Cushman, J.A., 1923. The foraminifera of the Atlantic ocean: Part 4 - Lagenidae: U.S. Nat.Mus. Bull., Washington, D.C., U.S.A, 1923, 104, 166.

Dean, W.E. & Gardner, J.V., 1982. Origin and geochemistry of redox cycles of Jurassic to Eocene ago, Cape Verde Basin (DSDP Site 367) continental margin of northwest Africa. In: Nature and Origin of Cretaceous Carbon-rich Facies. Academic, San Diego, Calif., 55-78.

Dean, W.E., Gardner, J.V., Jansa, L.F., Cerek, P. & Seibold E., 1978. Cyclic sedimentation along the continental margin of Northwest Africa. Initial Rep. Deep Sea Drill. Proj., 41, 965-986.

Derkachev, A.N., Bohrmann, G. & Greinert, J., 1999. Mineralogical and morphological types of authigenic precipitates from Derugin Basin sediments. Second Workshop on Russian-German Cooperation in the Okhotsk Sea – Kurile Island Arc System KOMEX. Program and Abstracts, Kiel, 31-32.

Derkachev, A.N., Tararin, I.A., Lelikov, E.P., Mozherovsky, A.V., Greinert, J. & Barinov, N.N., 2002. Manifestation of low-temperature hydrothermal activity in the backarc basin,

Okhotsk Sea (Kurile deep-sea basin). Tikhookeanskaya geologiya (Pacific geology), 21 (3), 14-26 (in Russian).

Dudarev, O.V., Botsul, A.I., Anikiev, V.V. et al., 2000. Modern sedimentation within Amur River estuary. Pacific oceanology, 19 (3), 30-43 (in Russian).

Emel'yanova, T.A., Kornev, O.S., Lelikov, E.P. et al., 2001. Composition and radioisotopic age of volcanic rocks from the floor of Okhotsk Sea. Vladivostok, POI RAS, 44 pp. (in Russian).

Emery, D. & Myers, K.J., 1996. Sequence Stratigraphy. Oxford: Blackwell Science Ltd., 297 pp.

Fairbanks, R.G., 1989. A 17,000 years glacio-eustatic sea level record: influence of glacial melting rates on the Younger Dryas event and deep-ocean circulation. Nature, 342, 637-642.

Felitsin, S.B. & Kir'yanov, V.Yu., 1987. Area variation of tephra composition from some volcanic eruptions on the basis of gross silicate analysis data. Volcanology and seismology, 1, 3-14 (in Russian).

Feyling-Hanssen, R.W., Jorgensen, J.A., Knudsen, K.L. & Andersen, A-L.L., 1971. Late Quaternary foraminifera from Vendsyssel, Denmark and sandnes, Norway. Bull. Geol. Soc. Denm., 21, (2-3), Copenhagen, 317 p.

Freeland, H.J., Bychkov, A.S., Whitney, F., Taylor, C., Wong, C.S. & Yurasov, G.I., 1998. WOCE section P1W in the Sea of Okhotsk. 1. Oceanographic description. J. of Geoph. Res. 1998, 103 (C8), 15613-15623.

Fursenko, A.V., Troitskaya, T.S., Levtchuk, L.K., et al., 1979. Foraminifery dal`nevostochnykh moryey SSSR (Foraminifera of the Far East seas of the USSR). Novosibirsk: Nauka, 287 pp. + 54 pls. (in Russian).

Gnibidenko, G.S., 1985. The Okhotsk Sea - Kurile Island ridge and Kurile-Kamchatka trench. In: Nairn, A.E.M., Stehli, F.G. & Uyeda, S. The Ocean Basin and Margins, Vol. 7A, Plenum Press, 377-418.

Gnibidenko, G.S., Hilde, T.W.C., Gretskaya, E.V. & Andreev, A.A., 1995. Kurile (South Okhotsk) Backarc Basin. In: Taylor, B. (ed.). Backarc Basins: Tectonics and Magmatism, New York: Plenum Press, 1995, 421-448.

Gorbarenko, S.A., 1991. The Stratigraphy of the Upper Quaternary sediments in the central part of the Sea of Okhotsk and its paleooceanography according to data obtained by the $\delta^{18}O$ and other methods. Okeanologiya (Oceanology), 6, 761-765 (in Russian, English translation).

Gorbarenko S.A., 1996. Stable isotope and lithologic evidence of Late Glacial and Holocene oceanography of the Northwestern Pacific and its marginal seas. Quaternary Research, 46, 230-250.

Gorbarenko, S.A., Chekhovskaya, M.P. & Southon, J.R., 1998. Detailed environmental changes of the Sea of Okhotsk Central part during the last glaciation-Holocene. Oceanology, 38 (2), 277-280 (translated from Okeanologiya, 38 (2), 305-308).

Gorbarenko, S.A., Derkachev, A.N., Astakhov, A.S., Southon, J.R., Nuernberg, D. & Shapovalov-Chuprynin, V.V., 2000. Lithostratigraphy and tephrochronology of the Upper Quaternary deposits in the Sea of Okhotsk. Tikhookeanskaya geologiya (Pacific geology), 19, 58-72 (in Russian).

Gorbarenko, SA., Nürnberg, D., Derkachev, A.N., Astakhov, AS., Souton, J.R & Kaiser, A., 2002. Magnetostratigraphy and tephrochronology of the Upper Quaternary sediments in the Okhotsk Sea: implication of terrigenous, volcanogenic and biogenic matter supply. Marine Geology, 183 (1-4), 107-129.

Habib, D., 1982. Sedimentary supply origin of Cretaceous black shales. In: Schlander, S.O. & Cita, M.B. (eds.). Nature and Origin of Cretaceous Carbon-rich Facies. Academic, San Diego, Calif., 113-127.

Haug, G.H., Maslin, M.A., Sarnthein, M., Stax, R. & Tiedemann, R., 1995. Evolution of northwestern Pacific sedimentation patterns since 6 MA (site 882) In: Rea, D.K., Basov, I.A., Scholl, D.W. & Allan, J. F. (eds.). Proceeding of the Ocean Drilling Program, Scientific Results Vol. 145, 293-314.

Hemleben, C., Splinder, M. & Anderson, O.R., 1988. Modern Planktonic Foraminifera. New York: Springer-Verlag Ed., 327 pp.

Holler, P., 1995. Arbeitsmethoden der marinen Geowissenschaften, Stuttgart: Enke.

Jannink, N.T., Van der Zwaan, G.J. & Zachariasse, W.J., 1998. Living (Rose Bengal stained) foraminifera from an upwelling environment: the continental margin south of Karachi, Arabian sea. Deep-Sea Res. I ,145, 1483-1513.

Jansa, L.F., Enos, P., Tucholke, B.E., Gradstein, F.M. & Sheridan, R.E., 1979. Mesozoic-Cenozoic sedimentary formations of the North Atlantic Basin; western North Atlantic. In: Deep drilling results in the Atlantic ocean: Continental margins and Paleoenvironments. Maurice Ewing Ser., 3, AGU, Washington, D.C., 1-57.

Johnson, K.M., King, A.E. & Sieburth, J.M., 1985. Coulometric TCO_2 analysis for marine studies: an introduction. Mar. Chem., 16, 61-82.

Jung, K.K., 1988. Morphology and taxonomy of Late Cenozoic uvigerine foraminifera from Japan: Tohoku University, Science Reports, 2nd series (Geology) 59, 99-175.

Kir'yanov, V.Yu. & Solovyeva, N.A., 1990. The changes of volcanic ash matter composition as a result of gravitational eolian differentiation. Volcanology and seismology, 4, 10-19 (in Russian).

Kristensen, E. & Blackburn, T.H., 1987. The fate of organic carbon and nitrogen in experimental marine sediment system: Influence of bioturbation and anoxia. J. Mar. Res., 45, 231-257.

Lipps, J.Y. & Warme, J.E., 1966. Planktonic foraminiferal biofacies in the Okhotsk Sea. Contrib. Cush. Found. Foram. Research, XVII, Part 4, 125-134.

Loeblich, A.R., Tappan, H., 1953. Studies of Arctic Foraminifera: Smithsonian Miscellaneous Collections, 121 (7), 151 p.

Loubere, P., Meyers, P. & Gary, A., 1995. Benthic foraminiferal microhabitat selection, carbon isotope values, and association with larger animals: a test with Uvigerina peregrina. Journal of Foraminiferal Research, 25 (1), 83-95.

Lüdmann, T., Baranov, B. & Karp, B. (eds.), 2002. Cruise Reports: KOMEX VII. RV Professor Gagarinsky Cruise 32, SERENADE. Seismo-stratigraphic research of northern Sakhalin and in Derugin Basin. GEOMAR Report, 105, Kiel, 42 pp.

Lutze, G. & Altenbach, A., 1991. Technik und Signifikanz der Lebendfärbung benthischer Foraminiferen mit Bengalrot, Geol. Jb, A128, 251-265.

Machida, H., 1999. The stratigraphy, chronology and distribution of distal marker-tephras in and around Japan. Global and Planet. Change, 71-94.

Mackensen, A., Schmiedel, G., Harloff, J. & Giesse, M., 1995. Deep-sea foraminifera in the South Atlantic Ocean: Ecology and assemblages generation. Micropaleontology, 41 (4), 342-358.

McManus, D.A., 1975. Modern versus relict sediment on the continental shelf. Geol. Soc. Amer. Bull., 86 (8), 1154-1160.

Melekestsev, I.V., Volynes, O.N. & Antonov, A.Yu., 1997. Nemo III caldera, Onekotan Island, Northern Kuriles: structure, C^{14} dating, time history of the caldera-generating eruption and the evolution of juvenile products. Volcanology and seismology, 1, 32-51 (in Russian).

Moroshkin, K.V., 1966. Water masses of the Okhotsk Sea. Moscow: Nauka, 66 pp. (in Russian).

Nürnberg, D., Baranov, B.V. & Karp, B.Ya. (eds.), 1997. RV Akademik M.A. Lavrentyev cruise 27 – Cruise Report GREGORY, GEOMAR Report, 60, 69 pp.

Obzhirov, A.I., 1993. Gas and geochemical fields of the benthic layer of seas and oceans. Moscow: Nauka, 131 pp. (in Russian).

Payton, C.E., 1977. Seismic Stratigraphy – Application to Hydrocarbon Exploration. AAPG, Memoir 26, 516 pp.

Pedersen, T.F. & Calvert, S.E., 1990. Anoxia vs. Productivity: what controls the formation of organic-carbon-rich sediments and sedimentary rocks. AAPG Bull., 74, 454-466.

Powers, M.C., 1982. Comparison chart for estimating roundness and sphericity. AGI data sheet 18, American Geological Institute.

Sachs, I.S., Suyehiro, K., Acton, G.D. & Shipboard Scientific Party**,** 2., 2000. Explanatory Notes, In: Proceedings of the Ocean Drilling Programme, Initial reports, 186.

Saidova, Kh.M., 1961. Ecology of foraminifera and paleogeography of the USSR Far Eastern Seas and the northwestern Pacific. Moscow: Nauka, 221 pp. (in Russian).

Saidova, Kh.M., 1975. Benthic foraminifera of the Pacific ocean. Academy of Science of the USSR, P.P. Shirshov Instintute of Oceanology, Moscow, part I-III, 631 pp. (in Russian).

Saidova, Kh.M., 1997. Deep-sea foraminiferal communities of the Bering and Okhotsk seas. Okeanologiya (Oceanology), 1, 105-112 (in Russian, English translation).

Salyuk, A.N., Winckler, G., Sosnin, V.A., 2001. Renewal of the bottom waters in the Okhotsk Sea. In: Danchenkov, M.A. (ed.). Oceanography of the Japan Sea. Proceeding of CREAMS 2000 Intern. Symp. Vladivostok: Dalnauka, 226-229 (in Russian).

Sapozhnikov, V.V., Gruzevich, A.K., Arzhanova, N.V., Naletova, I.A., Zubarevich, V.L. & Sapozhnikov, M.,V., 1999. Principal features of the spatial distribution of organic and inorganic nutrient compounds in the Sea of Okhotsk. Okeanologiya (Oceanology), 39 (2), 198-204 (in Russian, English translation).

Sen Gupta, B.K. & Machain-Castillo, M.L., 1993. Benthic foraminifera in oxygen-poor habitats. Mar. Micropaleontology 20, 183-201.

Scott, D.B., Takayanagi, Y., Hasegawa, S., Saito, T., 2000. Illustration and reevaluation of affinities of Neogene foraminifera described from Japan: Paleontologia Electronica 3 (2), 41 pp., 1.06 MB; http://palaeo-electronica.org/2000-2/foram/issue2_00.htm.

Shchedrina, Z.G., 1958. Foraminiferal fauna off Southern Sakhalin and Kurile Islands. Issled. Dalnev. Moryey SSSR (Investigations of the Far Eastern seas of the USSR), 5 (1), 5-41 (in Russian).

Shepard, F.S., 1954. Nomenclature based on Sand-Silt-Clay ratios. Journ. Sed. Petrol., 24, 151-158.

Tamaki, K., 1995. Opening Tectonics of the Japan Sea. In: Taylor, B. (ed.). Backarc Basins: Tectonics and Magmatism. New York: Plenum Press, 1995, 407-420.

Tiedemann, R. et al., 2001. Abschlussbericht zum KOMEX-Teilprojekt 5: Stratigraphie, CO_2-Kreislauf, Paläo-Ozeanologie und Produktivität im Ochotskischen Meer. In: Suess, E. et al. (eds.). KOMEX - Abschlussbericht zum BMBF-Vorhaben 03G0535A. Kiel, Heidelberg, Bremerhaven, Hamburg, Mai 2001.

Tishchenko, P.Ya., Pavlova, G.Yu., Salyuk, A.N. & Bychkov, A.S., 1998. Carbonate system and dissolved oxygen in the Japan Sea. Estimation of biological and thermal terms. Okeanologiya (Oceanology), 38 (5), 678-684 (in Russian).

Tishchenko, P.Ya., Wong, C.S., Pavlova, G.Yu., Johnson, W.K., Kang, D.-J. & Kim, K.-R., 2001. pH measurements of sea water by means of cell without liquid junction. Okeanologiya (Oceanology), 41 (6), 849-859 (in Russian).

Tsunogai, S., Niskimura, M. & Nakaya, S., 1968. Complexometric titration of calcium in the presence of larger amounts of magnesium. Talanta, 15, 385-390.

Werner, R., Tararin, I.A., Hoernle, K. & Lelikov, E.P., submitted. Petrology and geochemistry of submarine volcanism from the northeastern part of the Kurile Basin: Evidence for interaction of basic magma with continental crust. Gondwana Research (Special Issue).

Wong, C.S., Matear, R.J., Freeland, H.J., Whitney, F.A. & Bychkov, A.S., 1998. WOCE line P1W in the Sea of Okhotsk 2. CFCs and the formation rate of intermediate water, J. Geophys. Res., 103, 15625-15642.

Wortmann, U.G., Hesse, R. & Zacher, W., 1999. Major element analysis of cyclic black shales: Paleoceanographic implications for the Early Cretaceous deep western Tethys. Paleoceanography, 14 (4), 525-541.

Zaretskaia, N.E., Ponomareva, V.V., Sulerzhitsky, L.D. et al., 2001. Radiocarbon dating of the Kurile Lake caldera eruption (South Kamchatka, Russia). Geochronometriya (Geochronometry), 20, 95-102.

Zhuravlev, A.V., 1982. Geological structure and development of the South Okhotsk (Kurile) Basin. In: Tuezov, I.K. (ed.). Structure and Composition of the Sedimentary Cover of the Northwestern Pacific. Vladivostok: Far East Scientific Center, 23-33 (in Russian).

GEOMAR REPORTS

1 GEOMAR FORSCHUNGSZENTRUM FÜR MARINE GEOWISSENSCHFTEN DER CHRISTIAN-ALBRECHTS-UNIVERSITÄT ZU KIEL. BERICHT FÜR DIE JAHRE 1987 UND 1988. 1989. 71 + 6 pp. In German

2 GEOMAR FORSCHUNGSZENTRUM FÜR MARINE GEOWISSENSCHAFTEN DER CHRISTIAN-ALBRECHTS-UNIVERSITÄT ZU KIEL. JAHRESBERICHT/ANNUAL REPORT 1989. 1990. 96 pp. In German and English

3 GEOMAR FORSCHUNGSZENTRUM FÜR MARINE GEOWISSENSCHAFTEN DER CHRISTIAN-ALBRECHTS-UNIVERSITÄT ZU KIEL. JAHRESBERICHT/ANNUAL REPORT 1990. 1991. 212 pp. In German and English

4 ROBERT F. SPIELHAGEN
DIE EISDRIFT IN DER FRAMSTRASSE WÄHREND DER LETZTEN 200.000 JAHRE. 1991. 133 pp.
In German with English summary

5 THOMAS C. W. WOLF
PALÄO-OZEANOGRAPHISCH-KLIMATISCHE ENTWICKLUNG DES NÖRDLICHEN NORDATLANTIKS SEIT DEM SPÄTEN NEOGEN (ODP LEGS 105 UND 104, DSDP LEG 81). 1991. 92 pp. In German with English summary

6 SEISMIC STUDIES OF LATERALLY HETEROGENOUS STRUCTURES – INTERPRETATION AND MODELLING OF SEISMIC DATA. Ed. by ERNST R. FLUEH
Commission on Controlled Source Seismology (CCSS), Proceedings of the 8th Workshop Meeting, held at Kiel – Fellhorst (Germany), August 27-31, 1990. 1991. 359 pp. In English

7 JENS MATTHIESSEN
DINOFLAGELLATEN-ZYSTEN IM SPÄQUARTÄR DES EUROPÄISCHEN NORDMEERES: PALÖKOLOGIE UND PALÄO-OZEANOGRAPHIE. 1991. 104 pp. In German with English summary. Out of print

8 DIRK NÜRNGERG
HAUPT- UND SPURENELEMENTE IN FORAMINIFERENGEHÄUSEN – HINWEISE AUF KLIMATISCHE UND OZEANOGRAPHISCHE ÄNDERUNGEN IM NÖRDLICHEN NORDATLANTIK WÄHREND DES SPÄTQUARTÄRS. 1991. 117 pp. In German with English summary. Out of print

9 KLAS S. LACKSCHEWITZ
SEDIMENTATIONSPROZESSE AM AKTIVEN MITTELOZEANISCHEN KOLBEINSEY RÜCKEN (NÖRDLICH VON ISLAND). 1991. 133 pp. In German with English summary. Out of print

10 UWE PAGELS
SEDIMENTOLOGISCHE UNTERSUCHUNGEN UND BESTIMMUNG DER KARBONATLÖSUNG IN SPÄTQUARTÄREN SEDIMENTEN DES ÖSTLICHEN ARKTISCHEN OZEANS. 1991. 106 pp.
In German with English summary

11 FS POSEIDON. EXPEDITION 175 (9.10.-1.11.1990)
175/1:OSTGRÖNLÄNDISCHER KONTINENTALRAND (65°N)
175/2: SEDIMENTATION AM KOLBEINSEYRÜCKEN (NÖRDLICH VON ISLAND).
Hrsg. von J. MIENERT und H.-J. WALLRABE-ADAMS. 1992. 56 pp. + app. In German with some English chapters

12 GEOMAR FORSCHUNGSZENTRUM FÜR MARINE GEOWISSENSCHAFTEN DER CHRISTIAN-ALBRECHTS-UNIVERSITÄT ZU KIEL. JAHRESBERICHT/ANNUAL REPORT 1991. 1992. 152 pp. In German and English.
Out of print

13 SABINE E. I. KÖHLER
SPÄTQUARTÄRE PALÄO-OZEANOGRAPHISCHE ENTWICKLUNG DES NORDPOLARMEERES UND EUROPÄISCHEN NORDMEERES ANHAND VON SAUERSTOFF- UND KOHLENSTOFF-ISOTOPENVERHÄLTNISSEN DER PLANKTISCHEN FORAMINIFERE *Neogloboquadrina pachyderma* (sin.).
1992. 104 pp. In German with English summary

14 FS SONNE. FAHRTBERICHT SO78 PERUVENT: BALBOA, PANAMA - BALBOA, PANAMA, 28.2.1992-16.4.1992
Hrsg. von ERWIN SUESS. 1992. 120 pp. In German with some English chapters. Out of print

15 FOURTH INTERNATIONAL CONFERENCE ON PALEOCEANOGRAPHY (ICP IV): SHORT- AND LONG-TERM GLOBAL CHANGE: RECORDS AND MODELLING. 21-25 SEPTEMBER 1992, KIEL/GERMANY.
PROGRAM & ABSTRACTS. 1992. 351 pp. In English

16 MICHAELA KUBISCH
DIE EISDRIFT IM ARKTISCHEN OZEAN WÄHREND DER LETZTEN 250.000 JAHRE. 1992. 100 pp.
In German with English summary

17 PERSISCHER GOLF: UMWELTGEFÄHRDUNG, SCHADENSERKENNUNG, SCHADENSBEWERTUNG AM BEISPIEL DES MEERRESBODENS; ERKENNEN EINER ÖKOSYSTEMVERÄNDERUNG NACH ÖLEINTRÄGEN.
Schlußbericht zu den beiden BMFT-Forschungsvorhaben 03F0055 A + B. 1993. 108 pp. In German with English summary

18 TEKTONISCHE ENTWÄSSERUNG AN KONVERGENTEN PLATTENRÄNDERN / DEWATERING AT CONTINENTAL MARGINS. Hrsg. von/ed. by ERWIN SUESS. 1993. 196 + 32 + 68 + 16 + 22 + 38 + 4 + 19 pp.
Some chapters in English, some in German

19 THOMAS DICKMANN
DAS KONZEPT DER POLARISATIONSMETHODE UND SEINE ANWENDUNGEN AUF DAS SEIMISCHE VEKTORWELLENFELD IM WEITWINKELBEREICH. 1993. 121 pp. In German with English summary

20 GEOMAR FORSCHUNGSZENTRUM FÜR MARINE GEOWISSENSCHAFTEN DER CHRISTIAN-ALBRECHTS-UNIVERSITÄT ZU KIEL. JAHRESBERICHT/ANNUAL REPORT 1992. 1993. 139 pp. In German and English

21 KAI UWE SCHMIDT
PALYNOMORPHE IM NEOGENEN NORDATLANTIK - HINWEISE ZUR PALÄO-OZEANOGRAPHIE UND PALÄOKLIMATOLOGIE. 1993. 104 + 7 + 41 pp. In German with English summary

22 UWE JÜRGEN GRÜTZMACHER
DIE VERÄNDERUNGEN DER PALÄOGEOGRAPHISCHEN VERBREITUNG VON *Bolboforma* - EIN BEITRAG ZUR REKONSTRUKTION UND DEFINITION VON WASSERMASSEN IM TERTÄR. 1993. 104 pp.
In German with English summary

23 RV PROFESSOR LOGACHEV. Research Cruise 09 (August 30 - September 17, 1993): SEDIMENT DISTRIBUTION ON THE REYKJANES RIDGE NEAR 59°N. Ed. by H.-J. WALLRABE-ADAMS & K.S. LACKSCHEWITZ. 1993. 66 + 30 pp.
In English

24 ANDREAS DETTMER
DIATOMEEN-TAPHOZÖNOSEN ALS ANZEIGER PALÄO-OZEANOGRAPHISCHER ENTWICKLUNGEN IM PLIOZÄNEN UND QUARTÄREN NORDATLANTIK. 1993. 113 + 10 + 25 pp. In German with English summary

25 GEOMAR FORSCHUNGSZENTRUM FÜR MARINE GEOWISSENSCHAFTEN DER CHRISTIAN-ALBRECHTS-UNIVERSITÄT ZU KIEL. JAHRESBERICHT/ANNUAL REPORT 1993. 1994. 69 pp. In German and English

26 JÖRG BIALAS
SEISMISCHE MESSUNGEN UND WEITERE GEOPHYSIKALISCHE UNTERSUCHUNGEN AM SÜD-SHETLAND TRENCH UND IN DER BRANSFIELD STRASSE - ANTARKTISCHE HALBINSEL. 1994. 113 pp.
In German with English summary

27 JANET MARGARET SUMNER
THE TRANSPORT AND DEPOSITIONAL MECHANISM OF HIGH GRADE MIXED-MAGMA IGNIMBRITE TL, GRAN CANARIA: THE MORPHOLOGY OF A LAVA-LIKE FLOW. 1994. 224 pp. In English with German summary. Out of print

28 GEOMAR LITHOTHEK. Ed. by JÜRGEN MIENERT. 1994. 12 pp + app. In English. Out of print

29 FS SONNE. FAHRTBERICHT SO 97 KODIAK-VENT: KODIAK - DUTCH HARBOR - TOKYO - SINGAPUR, 27.7.-19.9.1994. Hrsg. von ERWIN SUESS. 1994. Some chapters in English, some in German. Out of print

30 CRUISE REPORTS:
RV LIVONIA CRUISE 92, KIEL-KIEL, 21.8.-17.9.1992: GLORIA STUDIES OF THE EAST GREENLAND CONTINENTAL MARGIN BETWEEN 70°AND 80°N
RV POSEIDON PO200/10, LISBON-BREST-BREMERHAVEN, 7.-23.8.1993: EUROPEAN NORTH ATLANTIC MARGIN: SEDIMENT PATHWAYS, PROCESSES AND FLUXES
RV AKADEMIK ALEKSANDR KARPINSKIY, KIEL-TROMSÖ, 5.-25.7.1994: GAS HYDRATES ON THE NORTHERN EUROPEAN CONTINENTAL MARGIN
Edited by JÜRGEN MIENERT. 1994. 186 pp.
In English; report of RV AKADEMIK ALEKSANDR KARPINSKIY cruise in English and Russian

31 MARTIN WEINELT
BECKENENTWICKLUNG DES NÖRDLICHEN WIKING-GRABENS IM KÄNOZOIKUM - VERSENKUNGSGESCHICHTE, SEQUENZSTRATIGRAPHIE, SEDIMENTZUSAMMENSETZUNG. 1994. 85 pp.
In German with English summary

32 GEORG A. HEISS
CORAL REEFS IN THE RED SEA: GROWTH, PRODUCTION AND STABLE ISOTOPES. 1994. 141 pp.
In English with German summary

33 JENS A. HÖLEMANN
AKKUMULATION VON AUTOCHTHONEM UND ALLOCHTHONEM ORGANISCHEM MATERIAL IN DEN KÄNOZOISCHEN SEDIMENTEN DER NORWEGISCHEN SEE (ODP LEG 104). 1994. 78 pp.
In German with English summary

34 CHRISTIAN HASS
SEDIMENTOLOGISCHE UND MIKROPALÄONTOLOGISCHE UNTERSUCHUNGEN ZUR ENTWICKLUNG DES SKAGERRAKS (NE NORDSEE) IM SPÄTHOLOZÄN. 1994. 115 pp. In German with English summary

35 BRITTA JÜNGER
TIEFENWASSERERNEUERUNG IN DER GRÖNLANDSEE WÄHREND DER LETZTEN 340.000 JAHRE / DEEP WATER RENEWAL IN THE GREENLAND SEA DURING THE PAST 340,000 YEARS. 1994. 6 + 109 pp.
In German with English summary

36 JÖRG KUNERT
UNTERSUCHUJNGEN ZU MASSEN- UND FLUIDTRANSPORT ANHAND DER BEARBEITUNG REFLEXIONSSEISMISCHER DATEN AUS DER KODIAK-SUBDUKTIONSZONE, ALASKA. 1995. 129 pp.
In German with English summary

37 CHARLOTTE M. KRAWCZYK
DETACHMENT TECTONICS DURING CONTINENTAL RIFTING OFF THE WEST IBERIA MARGIN: SEISMIC REFLECTION AND DRILLING CONSTRAINTS.1995. 133 pp. In English with German summary

38 CHRISTINE CAROLINE NÜRNBERG
BARIUMFLUSS UND SEDIMENTATION IM SÜDLICHEN SÜDATLANTIK - HINWEISE AUF PRODUKTIVITÄTSÄNDERUNGEN IM QUARTÄR. 1995. 6 + 108 pp. In German with English summary

39 JÜRGEN FRÜHN
TEKTONIK UND ENTWÄSSERUNG DES AKTIVEN KONTINENTALRANDES SÜDÖSTLICH DER KENAI-HALBINSEL, ALASKA. 1995. 93 pp. In German with English summary

40 GEOMAR FORSCHUNGSZENTRUM FÜR MARINE GEOWISSENSCHAFTEN DER CHRISTIAN-ALBRECHTS-UNIVERSITÄT ZU KIEL. JAHRESBERICHT/ANNUAL REPORT 1994. 1995. 125 pp. In German and English.
Out of print

41 FS SONNE. FAHRTBERICHT / CRUISE REPORT SO 103 CONDOR 1 B: VALPARAISO-VALPARAISO, 2-21.7.1995. Hrsg. von ERNST R. FLUEH. 1995. 140 pp. Some chapters in German, some in English

42 RV PROFESSOR BOGOROV CRUISE 37: CRUISE REPORT "POSETIV": VLADIVOSTOK-VLADIVOSTOK, September 23 - October 22, 1994. Edited by CHRISTOPH GAEDICKE, BORIS BARANOV, and EVGENY LELIKOV. 1995. 49 + 33 pp. In English

43 CHRISTOPH GAEDICKE
DEFORMATION VON SEDIMENTEN IM NANKAI-AKKRETIONSKEIL, JAPAN. BILANZIERUNG TEKTONISCHER VORGÄNGE ANHAND VON SEISMISCHEN PROFILEN UND ERGEBNISSEN DER ODP-BOHRUNG 808. II + 89 pp. In German with English summary

44 MARTIN ANTONOW
SEDIMENTATIONSMUSTER UM DEN VESTERIS SEAMOUNT (ZENTRALE GRÖNLANDSEE) IN DEN LETZTEN 250.000 JAHREN. 1995. 121 pp. In German with English summary

45 INTERNATIONAL CONGRESS: CORING FOR GLOBAL CHANGE - ICGC '95. KIEL, 28 - 30 June, 1995. Edited by JÜRGEN MIENERT and GEROLD WEFER. 1996. 83 pp. In English

46 JENS GRÜTZNER
ZUR PHYSIKALISCHEN ENTWICKLUNG VON DIAGENETISCHEN HORIZONTEN IN DEN SEDIMENTBECKEN DES ATLANTIKS. 1995. 96 pp. In German with English summary

47 INGO A. PECHER
SEISMIC STUDIES OF BOTTOM SIMULATING REFLECTORS AT THE CONVERGENT MARGINS OFFSHORE PERU AND COSTA RICA. 1996. 159 pp. In English with German summary

48 XIN SU
DEVELOPMENT OF LATE TERTIARY AND QUATERNARY COCCOLITH ASSEMBLAGES IN THE NORTHEAST ATLANTIC. 1996. 120 pp. +7 pl. In English with German summary

49 FS SONNE - FAHRTBERICHT/CRUISE REPORT SO108 ORWELL: SAN FRANCISCO - ASTORIA, 14.4. - 23.5.1996 Edited by ERNST R. FLUEH and MICHAEL A. FISHER. 1996. 252 pp. + app. In English with German summary

50 GEOMAR FORSCHUNGSZENTRUM FÜR MARINE GEOWISSENSCHAFTEN DER CHRISTIAN-ALBRECHTS-UNIVERSITÄT ZU KIEL. JAHRESBERICHT/ANNUAL REPORT 1995. 1996. 93 pp. In German and English

51 THOMAS FUNCK
STRUCTURE OF THE VOLCANIC APRON NORTH OF GRAN CANARIA DEDUCED FOM REFLECTION SEISMIC, BATHYMETRIC AND BOREHOLE DATA. 1996.VI, 144 pp. In English with German summary

52 PETER BRUNS
GEOCHEMISCHE UND SEDIMENTOLOGISCHE UNTERSUCHUNGEN ÜBER DAS SEDIMENTATIONSVERHALTEN IM BEREICH BIOSTRATIGRAPHISCHER DISKONTINUITÄTEN IM NEOGEN DES NORDATLANTIK, ODP LEG 104, SITES 642B UND 643A. 1996. V, 73 pp. In German with Engllish summary

53 CHRISTIANE C. WAGNER
COLD SEEPS AN KONVERGENTEN PLATTENRÄNDERN VOR OREGON UND PERU: BIOGEOCHEMISCHE BESTANDSAUFNAHME. 1996. 108, XXXVI pp. In German with English summary

54 FRAUKE KLINGELHÖFER
MODEL CALCULATIONS ON THE SPREADING OF SUBMARINE LAVA FLOWS. 1996. 98 pp. In English with German summary

55 HANS-JÜRGEN HOFFMANN
OBJEKTORIENTIERTE ANALYSE UND MIGRATION DIFFRAKTIERTER WELLENFELDER UNTER VERWENDUNG DER STRAHLENMETHODE UND DER EDGE-WAVE-THEORIE. 1996. XXI, 153 pp. In German with English summary

56 DIRK KLÄSCHEN
STRAHLENSEISMISCHE MODELLIERUNG UNTER BERÜCKSICHTGUNG VON MEHRFACHDIFFRAKTIONEN MIT HILFE DER EDGE-WAVES: THEORIE UND ANWENDUNGSBEISPIELE 1996. X, 159 pp. In German with English summary

57 NICOLE BIEBOW
DINOFLAGELLATENZYSTEN ALS INIKATOREN DER SPÄT- UND POSTGLAZIALEN ENTWICKLUNG DES AUFTRIEBSGESCHEHENS VOR PERU. 1996. IV, 100, 17, 14 (7 pl.) pp. In German with English summary

58 RV SONNE. CRUISE REPORT SO109: HYDROTRACE ASTORIA-VICTORIA-ASTORIA-VICTORIA. MAY 23 - JULY 8, 1996. Ed. by PETER HERZIG, ERWIN SUESS, and PETER LINKE. 1997. 249 pp. In English

59 RV SONNE. CRUISE REPORT SO110: SO - RO (SONNE - ROPOS). VICTORIA-KODIAK-VICTORIA. JULY 9 - AUGUST 19, 1996. Ed. by ERWIN SUESS and GERHARD BOHRMANN. 1997. 181 pp. In English

60 RV AKADEMIK M. A. LAVRENTYEV CRUISE 27. CRUISE REPORT: GREGORY. VLADIVOSTOK-PUSAN-OKHOTSK SEA-PUSAN-VLADIVOSTOK. SEPTEMBER 7 - OCTOBER 12, 1996. Ed. by DIRK NÜRNBERG, BORIS BARANOV, and BORIS KARP.1997. 143 pp. In English

61 GEOMAR FORSCHUNGSZENTRUM FÜR MARINE GEOWISSENSCHAFTEN DER CHRISTIAN-ALBRECHTS-UNIVERSITÄT ZU KIEL. JAHRESBERICHT / ANNUAL REPORT 1996. 1997. 169 pp. In German and English

62 FS SONNE. FAHRTBERICHT/CRUISE REPORT SO123: MAMUT (MAKRAN MURRAY TRAVERSE - GEOPHYSIK PLATTENTEKTONISCHER EXTREMFÄLLE). Maskat - Maskat, 07.09 - 03.10.1997. Ed. by ERNST R. FLUEH, NINA KUKOWSKI, and CHRISTIAN REICHERT. 1997. 292 pp. In English with German summary

63 RAINER ZAHN
NORTH ATLANTIC THERMOHALINE CIRCULATION DURING THE LAST GLACIAL PERIOD: EVIDENCE FOR COUPLING BETWEEN MELTWATER EVENTS AND CONVECTIVE INSTABILITY. 1997. 133 pp. In English

64 FS SONNE. FAHRTBERICHT/CRUISE REPORT SO112 HIRESBAT (HIGH RESOLUTION BATHYMETRY). Victoria, B.C., Canada - Apra Harbor, Guam. 17.09 - 08.10.1996. Hrsg. von WILHELM WEINREBE. 1997. 90 pp. Some chapters in German, some in English

65 NIELS NØRGAARD-PEDERSEN
LATE QUATERNARY ARCTIC OCEAN SEDIMENT RECORDS: SURFACE OCEAN CONDITIONS AND PROVENANCE OF ICE-RAFTED DEBRIS. 1997. 115 pp. In English with German summary

66 THOMAS NÄHR
AUTHIGENER KLINOPTILOLITH IN MARINEN SEDIMENTEN - MINERALCHEMIE, GENESE UND MÖGLICHE ANWENDUNG ALS GEOTHERMOMETER. 1997. 119, 43 pp. In German with English summary

67 MATTIAS KREUTZ
STOFFTRANSPORT DURCH DIE BODENGRENZSCHICHT: REGIONALISIERUNG UND BILANZIERUNG FÜR DEN NORDATLANTIK UND DAS EUROPÄISCHE NORDMEER. 1998. IV, 166 pp. In German with English summary

68 AMIT GULATI
BENTHIC PRIMARY PRODUCTION IN TWO DIFFERENT SEDIMENT TYPES OF THE KIEL FJORD (WESTERN BALTIC SEA). 1998. 139 pp. In English with German summary

69 RÜDIGER SCHACHT
DIE SPÄT- UND POSTGLAZIALE ENTWICKLUNG DER WOOD- UND LIEFDEFJORDREGION NORDSPITZBERGENS. 1999. 123 pp. + app. In German with English summary

70 GEOMAR FORSCHUNGSZENTRUM FÜR MARINE GEOWISSENSCHAFTEN DER CHRISTIAN-ALBRECHTS-UNIVERSITÄT ZU KIEL. JAHRESBERICHT/ANNUAL REPORT 1997. 1998. 155 pp. In German and English

71 FS SONNE. FAHRTBERICHT/CRUISE REPORT SO118 BIGSET (BIOGEOCHEMICAL TRANSPORT OF MATTER AND ENERGY IN THE DEEP SEA). MUSCAT (OMAN) - MUSCAT (OMAN). 31.03.-11.05.1997. Ed. by OLAF PFANNKUCHE and CHRISTINE UTECHT. 1998. 188 pp. In English

72 FS SONNE. FAHRTBERICHT/CRUISE REPORT SO131 SINUS (SEISMIC INVESTIGATIONS AT THE NINETY EAST RIDGE OBSERVATORY USING SONNE AND JOIDES RESOLUTION DURING ODP LEG 179). KARACHI - SINGAPORE. 04.05-16.06.1998. Ed. by ERNST R. FLUEH and CHRISTIAN REICHERT. 1998. 337 pp. In English

73 THOMAS RICHTER
SEDIMENTARY FLUXES AT THE MID-ATLANTIC RIDGE: SEDIMENT SOURCES, ACCUMULATION RATES, AND GEOCHEMICAL CHARACTERISATION. 1998. IV, 173 + 29 pp. In English with German summary

74 BARBARA MARIA SPRINGER
MODIFIKATION DES BODENNAHEN STRÖMUNGSREGIMES UND DIE DEPOSITION VON SUSPENDIERTEM MATERIAL DURCH MAKROFAUNA. 1999. 112 pp. In German

75 SABINE JÄHMLICH
UNTERSUCHUNGEN ZUR PARTIKELDYNAMIK IN DER BODENGRENZSCHICHT DER MECKLENBURGER BUCHT. 1999. 139 pp. In German

76 WOLFRAM W. BRENNER
GRUNDLAGEN UND ANWENDUNGSMÖGLICHKEITEN DER MIKRO-ABSORPTIONSPHOTOMETRIE FÜR ORGANISCH-WANDIGE MIKROFOSSILIEN. 1999. 141 pp. In German with English summary

77 SUSAN KINSEY
TERTIARY BENTHIC FORAMINIFERAL BIOSTRATIGRAPHY AND PALAEOECOLOGY OF THE HALTEN TERRACE, NORWAY. 1999. VI, 145 pp. In English with German summary

78 HEIDI DOOSE
REKONSTRUKTION HYDROGRAPHISCHER VERHÄLTNISSE IM CALIFORNIENSTROM UND IM EUROPÄISCHEN MITTELMEER ZUR BILDUNGSZEIT ORGANISCH KOHLENSTOFFREICHER SEDIMENTE. 1999. IV, 111 pp. + app. In German with English summary

79 CLAUDIA WILLAMOWSKI
VERTEILUNGSMUSTER VON SPURENMETALLEN IM GLAZIALEN NORDATLANTIK: REKONSTRUKTION DER NÄHRSTOFFBILANZ ANHAND VON CADMIUMKONZENTRATIONEN IN KALKSCHALIGEN FORAMINIFEREN. 1999. 86, XXI pp. In German with English summary

80 FS SONNE. FAHRTBERICHT/CRUISE REPORT SO129. BIGSET (BIOGEOCHEMICAL TRANSPORT OF MATTER AND ENERGY IN THE DEEP SEA). PORT SULTAN QUABOOS - DUBAI. JANUARY 30 - MARCH 9, 1998. Ed. by OLAF PFANNKUCHE and CHRISTINE UTECHT. 1999. 107 pp. In English

81 FS SONNE. FAHRTBERICHT/CRUISE REPORT SO138. GINCO-2 (GEOSCIENTIFIC INVESTIGATIONS ON THE ACTIVE CONVERGENCE ZONE BETWEEN THE EAST EURASIAN AND AUSTRALIAN PLATES ALONG INDONESIA). JAKARTA - JAKARTA. 29.12.1998 - 28.01.1999. Ed. by ERNST R. FLUEH, BERND SCHRECKENBERGER, and JÖRG BIALAS. 1999. 333 pp. In English

82 CRUISE REPORTS: KOMEX I and II (KURILE OKHOTSK SEA MARINE EXPERIMENT)
RV PROFESSOR GAGARINSKY CRUISE 22
RV AKADEMIK M. A. LAVRENTYEV CRUISE 28
VLADIVOSTOK - PUSAN - OKHOTSK SEA - PUSAN - VLADIVOSTOK. 7 JULY - 12 SEPTEMBER 1998. Ed. by NICOLE BIEBOW and EDNA HÜTTEN. 1999. 188, 89 pp. In English

83 GREGOR REHDER
QUELLEN UND SENKEN MARINEN METHANS ZWISCHEN SCHELF UND OFFENEM OZEAN. REGIONALE VARIABILITÄT UND STEUERNDE PARAMETER DER METHANVERTEILUNG UND DER AUSTAUSCH MIT DER ATMOSPHÄRE. 1999. 161, 20 pp. In German with English summary

84 SVEN-OLIVER FRANZ
PLIOZÄNE ZEITREIHEN ZUR REKONSTRUKTION DER TIEFENWASSERZIRKULATION UND DER SILIZIKLASTISCHEN AMAZONASFRACHT IM ÄQUATORIALEN WESTATLANTIK (CEARA SCHWELLE, ODP LEG 154). 1999. 183 pp. In German with English summary

85 SYLKE HLAWATSCH
Mn-Fe-AKKUMULATE ALS INDIKATOR FÜR SCHAD- UND NÄHRSTOFFFLÜSSE IN DER WESTLICHEN OSTSEE. 1999. 132 pp. In German with English summary

86 BETTINA GEHRKE
ZUSAMMENSETZUNG UND VERTEILUNG DER LITHOGENEN FEINFRAKTION IN SPÄTQUARTÄREN SEDIMENTEN DES MITTELATLANTISCHEN REYKJANES RÜCKENS (59°N) - TONMINERALE ALS INDIKATOREN FÜR LIEFERGEBIETE, TRANSPORTMECHANISMEN UND ABLAGERUNGSPROZESSE. 1999. 102 pp.
In German with English summary

87 JENS GREINERT
REZENTE SUBMARINE MINERALBILDUNGEN: ABBILD GEOCHEMISCHER PROZESSE AN AKTIVEN FLUIDAUSTRITTSSTELLEN IM ALEUTEN- UND CASCADIA-AKKRETIONSKOMPLEX. 1999. 196, XX pp.
In German with English summary

88 CRUISE REPORTS: KOMEX V and VI (KURILE OKHOTSK SEA MARINE EXPERIMENT)
RV PROFESSOR GAGARINSKY CRUISE 26
MV MARSHAL GELOVANY CRUISE 1
VLADIVOSTOK - PUSAN - OKHOTSK SEA - PUSAN - VLADIVOSTOK. 30 JULY - 5 SEPTEMBER, 1999.
Ed. by NICOLE BIEBOW, THOMAS LÜDMANN, BORIS KARP, and RUSLAN KULINICH. 2000. 296 pp. In English

89 FS SONNE. FAHRTBERICHT/CRUISE REPORT SO136. TASQWA (QUATERNARY VARIABILITY OF WATER MASSES IN THE SOUTHERN TASMAN SEA AND THE SOUTHERN OCEAN, SW PACIFIC SECTOR). WELLINGTON - HOBART. OCTOBER 16 - NOVEMBER 12, 1998. Ed. by JÖRN THIEDE, STEFAN NEES et al. 1999. 78, 106 pp. In English

90 FS SONNE. FAHRTBERICHT/CRUISE REPORT SO142. HULA (INTERDISCIPLINARY INVESTIGATIONS ON THE TIMING OF THE HAWAII-EMPEROR BEND AND THE ORIGIN OF LITHOSPHERIC ANOMALIES ALONG THE MUSICIAN SEAMOUNT CHAIN. MIDWAY - HONOLULU. MAY 30 - JUNE 28, 1999. Ed. by ERNST R. FLUEH, JOHN O'CONNOR, JASON PHIPPS MORGAN, and JOCHEN WAGNER. 1999. 224 pp. In English

91 J. HAUSCHILD, T. GINDLER, D. RISTOW, A. BERHORST, C. BÖNNEMANN, K. HINZ
DFG-FORSCHUNGSPROJEKT *„KRUSTENSPLITTER“*. 3D-MAKRO-GESCHWINDIGKEITSBESTIMMUNGEN UND 3D-TIEFENMIGRATION DES SEISMISCHEN 3D-COSTA-RICA-DATENSATZES. 1999. 85 pp.
In German with English summary

92 FS AKADEMIK MSTISLAV KELDYSH. Fahrtbericht Reise Nr. 40: Norwegisch-Grönländische See, 27.6.-29.7.1998. Hrsg. von J. MIENERT, A. OMLIN, T. GÖLZ, D. LUKAS, J. POSEWANG. 1999. 65, 7 pp. In German

93 FS SONNE. FAHRTBERICHT/CRUISE REPORT SO143 TECFLUX. Ed. by GERHARD BOHRMANN, PETER LINKE, ERWIN SUESS, and OLAF PFANNKUCHE. 2000. 243 pp. In English

94 FS SONNE. FAHRTBERICHT/CRUISE REPORT SO144-1&2. PAGANINI (PANAMA BASIN AND GALAPAGOS "PLUME" - NEW INVESTIGATIONS OF INTRAPLATE MAGMATISM). SAN DIEGO - CALDERA. SEPTEMBER 7 - NOVEMBER 7, 1999. Ed. by JÖRG BIALAS, ERNST R. FLUEH, and GERHARD BOHRMANN. 1999. 437 pp. + app.
In English

95 CHRISTIAN MATTHIAS HÜLS
MILLENNIAL-SCALE SST VARIABILITY AS INFERRED FROM PLANKTONIC FORAMINIFERAL CENSUS COUNTS IN THE WESTERN SUBTROPICAL ATLANTIC. 2000. 81 pp. + app. In English with German summary

96 FS SONNE. FAHRTBERICHT/CRUISE REPORT SO146-1&2. GEOPECO (GEOPHYSICAL EXPERIMENTS AT THE PERUVIAN CONTINENTAL MARGIN - INVESTIGATIONS OF TECTONICS, MECHANICS, GASHYDRATES, AND FLUID TRANSPORT). ARICA - TALCAHUANO. MARCH 1 - MAY 4, 2000. Ed. by JÖRG BIALAS and NINA KUKOWSKI. 2000. 508 pp. In English

97 GEOMAR FORSCHUNGSZENTRUM FÜR MARINE GEOWISSENSCHAFTEN DER CHRISTIAN-ALBRECHTS-UNIVERSITÄT ZU KIEL. JAHRESBERICHT/ANNUAL REPORT 1998/1999. 2000. 261 pp. In German and English

98 RV SONNE. CRUISE REPORT SO148. TECFLUX-II-2000 (TECTONICALLY-INDUCED MATERIAL FLUXES. VICTORIA - VICTORIA - VICTORIA. 20.07.-15.08.2000. Ed. by PETER LINKE and ERWIN SUESS. 2001. 122 pp. In English

99 GEOMAR FORSCHUNGSZENTRUM FÜR MARINE GEOWISSENSCHAFTEN DER CHRISTIAN-ALBRECHTS-UNIVERSITÄT ZU KIEL. JAHRESBERICHT/ANNUAL REPORT 2000. 2001. 180 pp. In German and English

100 FS POSEIDON. FAHRTBERICHT/CRUISE REPORT POS 260 BIGSET (BIOGEOCHEMICAL TRANSPORT OF MATTER AND ENERGY IN THE DEEP SEA). LEIXOES/OPORTO (PORTUGAL) - GALWAY (IRELAND) - CORK (IRELAND). 26.04.-23.06.2000. Ed. by OLAF PFANNKUCHE and CHRISTINE UTECHT. 2001. 67 pp. In English

101 FS SONNE. FAHRTBERICHT/CRUISE REPORT SO159. SALIERI (SOUTH AMERICAN LITHOSPHERIC TRANSECTS ACROSS VOLCANIC RIDGES). GUAYAQUIL - GUAYAQUIL. AUGUST 21 - SEPTEMBER 17, 2001. Ed. by ERNST R. FLÜH, JÖRG BIALAS, and PHILIPPE CHARVIS. 2001. 256 pp. In English

102 FS SONNE. FAHRTBERICHT/CRUISE REPORT SO161-1&4. SPOC (SUBDUCTION PROCESSES OFF CHILE). ANTOFAGASTA - VALPARAISO. OCTOBER 9 - OCTOBER 15, 2001 &
VALPARAISO - VALPARAISO. NOVEMBER 30 - DECEMBER 23, 2001.
Ed. by ERNST R. FLÜH, HEIDRUN KOPP, and BERND SCHRECKENBERGER. 2002. 383 pp. In English

103 FS SONNE. FAHRTBERICHT/CRUISE REPORT SO162. INGGAS TEST (INTEGRATED GEOPHYSICAL CHARACTERISATION AND QUANTIFICATION OF GAS HYDRATES - INSTRUMENT TEST CRUISE). VALPARAISO - BALBOA. FEBRUARY 21 - MARCH 12, 2002.
Ed. by TIMOTHY JOHN RESTON and JÖRG BIALAS. 2002. In English

104 FS SONNE. FAHRTBERICHT/CRUISE REPORT SO158. MEGAPRINT (MULTIDISCIPLINARY EXAMINATION OF GALÁPAGOS PLUME RIDGE INTERACTION). ISLA DE PASCUA - GUAYAQUIL. JULY15 - AUGUST 20, 2001.
Ed. by REINHARD WERNER. 2002. 53 pp + app. In English

105 CRUISE REPORT: KOMEX (KURILE OKHOTSK SEA MARINE EXPERIMENT)
RV PROFESSOR GAGARINSKY CRUISE 32. SERENADE. SEISMO-STRATIGRAPHIC RESEARCH OFF NORTHERN SAKHALIN AND IN THE DERUGIN BASIN. VLADIVOSTOK - PUSAN - SEA OF OKHOTSK - PUSAN - VLADIVOSTOK. AUGUST 31 - SEPTEMBER 29, 2001.
Ed. by THOMAS LÜDMANN, BORIS BARANOV, and BORIS KARP. 2002. 42 pp. In English

106 FS SONNE. FAHRTBERICHT/CRUISE REPORT SO163. SUBDUCTION I. MULTI-SYSTEM ANALYSIS OF FLUID RECYCLING AND GEODYNAMICS AT THE CONTINENTAL MARGIN OFF COSTA RICA.
SO163-1. BALBOA- CALDERA. MARCH 13 - APRIL 20, 2002
SO163-2. CALDERA - BALBOA. APRIL 20 - MAY 21, 2002.
Ed. by WILLI WEINREBE and ERNST R. FLÜH. 2002. 534 pp. In English

107 GEOMAR FORSCHUNGSZENTRUM FÜR MARINE GEOWISSENSCHAFTEN DER CHRISTIAN-ALBRECHTS-UNIVERSITÄT ZU KIEL. JAHRESBERICHT/ANNUAL REPORT 2001. In prep. In German and English

108 RV METEOR. CRUISE REPORT M52/1: MARGASCH (MARINE GAS HYDRATES OF THE BLACK SEA). ISTANBUL - ISTANBUL. JANUARY 2 - FEBRUARY 1, 2002.
Ed. by GERHARD BOHRMANN and SILKE SCHENCK. 2002. 202 pp. In English

109 RV SONNE. CRUISE REPORT SO164. RASTA (Rapid Climate Changes in the Western Tropical Atlantic - Assessment of the biogenous and sedimentary record). BALBOA - BALBOA. MAY 22 - JUNE 2002. Ed. by DIRK NÜRNBERG, JOACHIM SCHÖNFELD, WOLF-CHRISTIAN DULLO, and MARCUS RÜHLEMANN. 2003. 151 pp. In English

110 CRUISE REPORT : KOMEX (KURILE OKHOTSK SEA MARINE EXPERIMENT)
RV AKADEMIK M.A. LAVRENTYEV CRUISE 29, LEG 1 and LEG 2. VLADIVOSTOK – PUSAN – OKHOTSK SEA – PUSAN – OKHOTSK SEA – PUSAN – VLADIVOSTOK. MAY 25 – AUGUST 05 2002. Ed. by NICOLE BIEBOW, RUSLAN KULINICH, and BORIS BARANOV. 2003. 190, 176 pp. In English

APPENDIX 1

Station list

Station list of LV29: 29th expedition of RV Akademik Lavrentyev, Leg 2

Date	Stat. Nr.	Equip-ment	Start	at sf	off sf	End	Dura-tion	Latitude N	Longitude E	Water depth	Recovery	Remarks
Japan Sea												
29.06.	67-1	SB	06:54			07:23	00:29	39°03.3	133°01.2	ca. 2000		Water temperature: 20° C, air temperature: 21°C. Bath enjoyed by all participants.
La Perusa Strait												
01.07.	68-1	SES	18:00	19:07	21:31	21:45	03:45	45°25.768/ 45°26.924	144°03.368/ 144°15.602	831/ 882		18:00 - 18:20 test without speed. 18:20 - 19:07 parameter optimization. Frequency: 8 kHz/ 0,5 ms.
01.07.	68-2	SEI	19:00			21:00	02:00	45°25.70/ 45°26.23	144°02.79/ 144°13.05	844/ 912		Speed ca. 3 knots.
01.07.	69-1	MUC	21:36		22:59	23:39	02:03	45°26.130	144°06.611	881	5 full tubes, 3 tubes partly full	Bottom water; BEN=23, BEN 2x 0-1, ISO=41, POI=32, POL=41, RAD=17 (samples depth in cm)
02.07.	69-2	SL-R	00:09		00:20	00:37	00:28	45°26.447	144°05.840	868	1,40 m	SL-R hit the seafloor, but obviously fell sidewards.
02.07.	69-3	SL-G	01:28		01:48	02:06	00:38	45°26.602	144°04.243	841	bit more than 10 m	
02.07.	69-4	CTD	02:38		02:57	03:15	00:37	45°26.841	144°04.574	852	12 bottles	1=837, 2=827, 3=793, 4=741, 5=692, 6=544, 7=495, 8=396, 9=298, 10=171, 11=70, 12=3 (depth m)
02.07.	69-5	SL-R	03:58		04:11	04:29	00:31	45°26.960	144°04.442	852	7,80 m	
02.07.	69-6	MUN	04:48		05:13	05:55	01:07	45°27.087/ 45°27.185	144°04.157/ 144°03.543	849/ 839	5 bottles	1=800-500, 2=500-200, 3=200-150, 4=150-50, 5=50-0 (depth m)
Eastern continental slope of Sakhalin												
02.07.	70-1	MUC	21:17		22:50	00:23	03:06	47°55.174	146°10.610	2506	nothing	GPS did not work at start. Winch did not gain speed; brought into working condition during operation. Strong drift. All bottles closed, but filled only with water.
03.07.	70-2	SL-R	00:55		01:23	02:09	01:14	47°56.117	146°10.209	2325	8,50 m	Strong drift. Recovered sediment of green-gray colour (clay).
03.07.	70-3	MUC	02:24		03:44	05:20	02:56	47°58.945	146°09.466	2165	4 tubes with little sediment	Strong drift. MUC obviously hit seafloor, but contained very little sediment. Samples: bottom water; 7x0-1 cm ISO; 2xFluff ISO
03.07.	70-4	SL-G	05:40		06:06	06:46	01:06	48°00.086	146°08.530	2062	ca. 10 m	Strong drift. Full penetration
03.07.	70-5	CTD	07:15		08:03	08:37	01:22	48°01.790	146°08.080	1978	12 bottles	Strong drift. 1=1980, 2=1926, 3=1729, 4=1484, 5=1237, 6=990, 7=743, 8=496, 9=249, 10=89, 11=31, 12=3 (depth m)
03.07.	71-1	SES	14:00	14:40	21:40	21:58	07:58	48°57.119/ 48°34.371	146°06.151/ 146°07.664	810/ 1186		Frequency: 10 kHz/ 0,5 ms. Up to position 48°52.38/ 146°06.04 homogenous seafloor, afterwards visibly stronger layering.
03.07.	71-2	SEI	15:15			21:20	06:05	48°55.37/ 48°35.388	146°06.25/ 146°07.516	825/ 1200		Seismic profile Nr. 2
03.07.	72-1	MUC	22:51		23:28	00:41	01:50	48°36.671	146°07.348	1172	2 full tubes	2 tubes sampled in 1 cm slices: 1 series BEN 0-7 cm stained, 1 series ISO 0-18 cm stained, rest as whirlpacks; 6 sediment surface samples (stained).
04.07.	72-2	SL-R	01:10		01:24	01:45	00:35	48°37.701	146°07.037	1380	8,50 m	
04.07.	72-3	SL-G	01:59		02:13	02:35	00:36	48°38.259	146°07.098	1142	nearly 10 m	Full penetration.
04.07.	72-4	CTD	02:47		03:10	03:30	00:43	48°38.596	146°07.180	1129	12 bottles	1=1113, 2=1062, 3=941, 4=794, 5=645, 6=495, 7=347, 8=249, 9=151, 10=60, 11=30, 12=3 (depth m)
04.07.	72-5	MUN	04:14		04:45	05:31	01:17	48°39.435/ 48°39.976	146°07.139/ 146°06.913	1118/ 1117	5 bottles	1=1000-5000, 2=500-200, 3=200-150, 4=150-50, 5=50-0 (depth m)
04.07.	73-1	SES	19:50	20:33	05:37	06:00	10:10	51°02.794/ 51°08.503	144°31.402/ 145°18.927	268/ 674		Frequency: 10 kHz/ 0,4 ms. Speed: 3 kn. 22:06+23:08 - transmitter switched off for test. Channel 05:27: depth 718 m (51°08.431/ 145°18.031).

Date	Stat. Nr.	Equip-ment	Start	at sf	off sf	End	Dura-tion	Latitude N	Longitude E	Water depth	Recovery	Remarks
04.07.	73-2	SEI	20:50			05:17	08:27	51°03.05/ 51°08.313	144°32.55/ 145°17.093	120/ 645		Seismic profile Nr. 3
05.07.	74-1	SES		07:44	14:40		ca. 8 hours	51°08.943/ 51°29.656	145°19.439/ 145°27.357	683/ 1332		Frequency: 8 kHz/ 0,5 ms. No online print 08:18 - 08:24 (printer error).
05.07.	74-2	SEI	08:00			14:38	06:38	51°09.6/ 51°29.439	145°20.34/ 145°27.416	690/ 1335		Seismic profile Nr. 4
05.07.	75-1	SES		22:36	02:02		ca. 4,5 hours	52°38.177/ 52°40.216	144°24.063/ 144°42.256	225/ 684		Frequency: 6 kHz/ 0,5 ms.
06.07.	76-1	MUC	03:59		04:31	04:55	00:56	52°39.962	144°39.234	624	nothing	MUC obviously hit seafloor, but tubes filled only with bottom water; no sediment. Samples: bottom water.
06.07.	76-2	SL-R	05:17			05:24	00:07	52°39.802	144°39.201	638	nothing	Cancelled due to winch defect (spooling device does not gain enough speed). Latitude/ longitude coordinates of start. Winch suddenly for unknown reasons changed direction.
06.07.	76-3	CTD	07:27		07:47	08:00	00:33	52°40.356	144°39.585	630	12 bottles	1=619, 2=609, 3=570, 4=495, 5=395, 6=316, 7=250, 8=198, 9=149, 10=79, 11=30, 12=3 (depth m)
06.07.	77-1	SES		08:33	18:46		ca. 11 hours	52°40.440/ 53°00.065	144°41.185/ 145°23.800	670/ 1755		Frequency: 6 kHz/ 0,5 ms until 10:53, then 6 kHz/ 1 ms. No record 10:49-10:53 and 11:15-11:19 (system modification).
06.07.	78-1	MUC	22:51		23:40	00:11	01:20	52°40.088	144°40.193	640	little surface sediment	MUC was made heavier by 3 additional weights (60 kg each) for improving penetration. Operation had to be stopped midway in order to fasten block. All tubes filled only with bottom water. Samples: 9x0-1 cm sediment surface; 2x bottom water.
07.07.	78-2	SL-R	00:26		00:34	00:48	00:22	52°40.244	144°41.187	655	7,80 m	Strong smell of H_2S. Degassing structures. Sediment of Holocene age.
07.07.	78-3	SL-G	01:22		01:32	01:48	00:26	52°40.388	144°42.203	673	ca. 8,50 m	
07.07.	79-1	CTD	03:07		03:31	03:51	00:44	52°47.218	144°56.603	1065	12 bottles	1=1053, 2=1005, 3=942, 4=794, 5=643, 6=496, 7=347, 8=247, 9=129, 10=73, 11=23, 12=3 (depth m)
07.07.	79-2	SL-R	04:15		04:27	04:47	00:32	52°47.477	144°57.900	1102	8 m	Sediment of Holocene age.
07.07.	79-3	SL-G	06:50		07:02	07:28	00:38	52°47.272	144°57.318	1082	more than 10 m	
Obzhirov Flare												
07.07.	80-1	SES	16:15	16:40	21:58	22:25	06:10	54°19.701/ 54°29.078	143°54.079/ 144°12.688	176/ 886		Frequency: 8 kHz/ 0,5 ms until 19:31, then 8 kHz/ 0,75 ms. Profile did not start at the given position and did not follow the given line until first turn. Given profile end was not reached, ship stopped and turned before.
08.07.	81-1	SL-G	01:37		01:45	01:52	00:15	53°59.558	143°57.759	356	ca. 2,4 m	Sediment coarse-grained.
08.07.	81-2	CTD	02:03		02:11	02:24	00:21	53°59.618	143°57.933	375	12 bottles	1=367, 2=358, 3=327, 4=298, 5=248, 6=199, 7=149, 8=100, 9=74, 10=51, 11=27, 12=4 (depth m)
08.07.	82-1	SL-R	04:30		04:47	05:05	00:35	54°18.150	144°10.795	795	8 m	
08.07.	82-2	SL-G	05:27		05:39	05:51	00:24	54°18.020	144°10.682	782	ca. 5,7 m	
08.07.	82-3	CTD	05:58		06:16	06:32	00:34	54°17.876	144°10.911	800	12 bottles	1=787, 2=771, 3=731, 4=614, 5=496, 6=386, 7=298, 8=198, 9=127, 10=64, 11=30, 12=3,5 (depth m)
08.07.	83-1	SES	08:00	08:23	20:04	20:25	12:25	54°30.155/ 54°26.515	144°07.981/ 143°59.676	766/ 490		Frequency: 8 kHz/ 1 ms.
08.07.	83-2	SEI	09:40			19:50	10:10	54°29.55/ 54°26.49	144°14.19/ 144°00.62	915/ 536		Seismic profile Nr. 8
08.07.	84-1	MUC	21:59		22:28	22:55	00:56	54°26.319	144°06.022	720	little surface sediment	1 tube filled with sediment, ca. 8 tubes filled with surface sediment samples and bottom water. Samples: 1-20 cm ISO/ living benthos; 10x0-1 cm surface sediment samples/ living benthos; bottom water.
08.07.	84-2	SL-G	23:12		23:20	23:32	00:20	54°25.692	144°07.436	752	ca. 7,6 m	
08.07.	84-3	CTD	23:49		00:05	00:21	00:32	54°25.382	144°07.952	762	12 bottles	1=745, 2=732, 3=694, 4=596, 5=495, 6=396, 7=299, 8=199, 9=110, 10=59, 11=32, 12=4 (depth m)

Date	Stat. Nr.	Equip-ment	Start	at sf	off sf	End	Dura-tion	Latitude N	Longitude E	Water depth	Recovery	Remarks
Sakhalin Gulf												
09.07.	85-1	SES	04:20	04:44	13:46	14:10	09:50	54°46.975/ 54°59.934	143°15.948/ 144°22.183	110/ 100		Frequency: 8 kHz/ 0,5 ms.
09.07.	86-1	SES	15:55	16:16	02:12	02:30	10:35	54°59.219/ 54°27.371	141°58.506/ 141°58.032	121/ 51		Frequency: 8 kHz/ 0,5 ms until 23:58, then 10 kHz/ 0,2 ms.
10.07.	87-1	CTD	02:28		02:32	02:37	00:09	54°27.015	141°58.044	51	10 bottles	1=46, 2=41, 3=36, 4=30, 5=25, 6=20, 7=15, 8=10, 9=5, 10=3 (depth m)
10.07.	88-1	SES	04:45	05:00	16:50	17:10	12:25	54°10.517/ 53°46.493	141°57.929/ 141°00.658	51/ 26		Frequency: 10 kHz/ 0,2 ms. No data record 11:41 - 12:03.
10.07.	88-2	CTD	04:42		04:47	04:53	00:11	54°10.497	141°58.049	50	10 bottles	1=46, 2=41, 3=35, 4=30, 5=25, 6=20, 7=15, 8=10, 9=6, 10=3 (depth m)
10.07.	88-3	CTD	09:07		09:10	09:19	00:12	54°01.918	141°37.975	43	10 bottles	1=39, 2=35, 3=31, 4=25, 5=20, 6=15, 7=9, 8=6, 9=2,5, 10=22,5 (depth m)
10.07.	88-4	CTD	13:33		13:37	13:41	00:08	53°53.804	141°18.538	27	6 bottles	1=23, 2=20, 3=15, 4=10, 5=6, 6=3 (depth m)
10.07.	88-5	CTD	16:54		16:57	17:01	00:07	53°46.448	141°00.645	26	5 bottles	1=21, 2=16, 3=11, 4=7, 5=3 (depth m)
10.07.	89-1	MUC	22:34		22:37	22:40	00:06	54°27.973	141°58.077	52	3 tubes with little sediment	4 tubes did not close despite of repair of closing mechanism. Samples: bottom water; POL - 0-4,5 cm in 0,5 cm slices; ISO - 0-4 cm in 0,5 cm slices, stained 0-3,5 cm; BEN - 0-5 cm in 1 cm slices, stained; RAD - 0-0,5 cm; POL II - sed. surface; ISO II - 0-0,5 cm; 2x ARC - surface?, 1 stained. Half a fish caught.
10.07.	89-2	HYC	22:50		22:55	23:00	00:10	54°27.896	141°57.988	51	0,5 m	Fish caught.
10.07.	89-3	SL-G	23:09		23:10	23:11	00:02	54°27.938	141°58.001	51	ca. 0,7 m	Sandy sediment.
11.07.	90-1	CTD	01:15		01:21	01:30	00:15	54°41.797	141°58.276	65	11 bottles	1=60, 2=55, 3=45, 4=35, 5=30, 6=25, 7=20, 8=15, 9=10, 10=7, 11=3 (depth m)
11.07.	91-1	CTD	02:58		03:03	03:13	00:15	54°53.926	141°58.190	109	12 bottles	1=102, 2=95, 3=80, 4=64, 5=54, 6=45, 7=36, 8=25, 9=20, 10=13, 11=8, 12=3 (depth m)
11.07.	91-2	MUC	03:25		03:29	03:34	00:09	54°53.984	141°58.115	108	Bottom water and sediment surface	MUC hit seafloor, but for some reason did not penetrate. Samples: bottom water; ISO/ POL - 0-? cm sed. surface + 50 ml eth. 80%, r.b.; ISO - 0-0,5 cm, stained; BEN - 2x sed. surface, stained; RAD - 0-0,5 cm; ISO II - 0-0,5 cm, stained.
11.07.	91-3	HYC	03:45		03:48	04:00	00:15	54°54.131	141°58.236	108	0,5 m	Sediment consists only of coarse gravel: station cancelled (no SL-R deployment).
11.07.	92-1	CTD	07:07		07:12	07:22	00:15	54°52.995	142°51.965	100	12 bottles	1=91, 2=90, 3=80, 4=69, 5=59, 6=50, 7=40, 8=31, 9=20, 10=14, 11=9, 12=3 (depth m)
11.07.	92-2	MUC	07:27		07:32	07:38	00:11	54°53.000	142°52.283	100	4 tubes with little sediment	Bottom water; ISO - 0-7 cm in 0,5 cm slices, stained; BEN - 0-6 cm in 1 cm slices, stained; POL - 0-5 cm in 1 cm slices; ARC - 1-4 cm in WP (unsafe, changed to Kautex bottles); macrobenthos with 100 ml (washed out) ethanol.
11.07.	92-3	HYC	07:50		07:53	08:00	00:10	54°53.271	142°52.253	100	nothing	Small quantity of coarse-grained sand with admixture of gravel and pebbles.
Derugin Basin												
11.07.	93-1	SES	17:05	17:32	22:56	23:10	06:05	54°53.037/ 55°02.590	145°30.282/ 145°05.906	1100/ 1293		Profile Nr. 26. Frequency: 8 kHz/ 0,75 ms. Turn at ca. 20:00.
11.07.	93-2	SEI	17:45			22:43	04:58	54°53.00/ 55°01.85	145°28.74/ 145°06.35	1080/ 1305		Seismic profile Nr. 9
12.07.	94-1	MUC	00:43		01:29	02:15	01:32	54°52.836	145°15.912	1147	3 tubes	Sediment coarse-grained. Samples: RAD - 0-2 cm sed. surface, 2-27 cm 1 cm slices + 1 drpstone; POI - 0-2 cm sed. surface, 2-28 cm 1 cm slices; POL - 0-2 cm sed. surface, 2-28 cm 1 cm slices.
12.07.	94-2	SL-R	02:52		03:08	03:26	00:34	54°52.816	145°16.554	1442	8,90 m	
12.07.	94-3	SL-G	03:39		03:53	04:10	00:31	54°53.095	145°16.610	1134	more than 10 m	
12.07.	95-1	SL-G	07:29		07:50	08:08	00:39	54°54.827	145°11.408	1215	less than 6 m	
12.07.	96-1	DR1	09:33	10:20	11:53	12:45	03:12	54°59.413/ 54°58.385	145°02.521/ 145°04.275	1377/ 634	70-90 kg	Boulders and pebbles of biotite-amphibole granodiorite, rhyolite-dacite and quarty vein with sulphides.

Date	Stat. Nr.	Equip-ment	Start	at sf	off sf	End	Dura-tion	Latitude N	Longitude E	Water depth	Recovery	Remarks
12.07.	97-1	SES	18:00	18:20	21:14	21:30	03:30	54°22.180/ 54°15.466	146°17.920/ 146°20.619	1608/ 1565		Frequency: 8 kHz/ 0,75 ms. 19:45 - turn to new position (WD: 1525).
12.07.	97-2	SEI	18:30			21:00	02:30	54°22.53/ 54°16.13	146°18.85/ 146°21.15	1575/ 1530		Seismic profile Nr. 10
12.07.	98-1	DR	23:30	00:23	01:29	02:00	02:30	54°00.895/ 54°00.579	146°26.269/ 146°25.290	1300/ 1435	ca. 15 kg	8-10 kg pebbles of different magmatic and sedimentaryrocks - dropstones.
13.07.	99-1	DR	02:30	03:00	03:15	04:30	02:00	54°00.040/ 54°00.298	146°25.778/ 146°26.050	1480/ 1400	ca. 40 kg	Barite crusts, specific benthic fauna associated with seeping processes, dropstones.
13.07.	100-1	SL-R	05:51		06:08	06:31	00:40	53°58.810	146°19.847	1479	5 m	
13.07.	101-1	DR2	08:03	08:32	09:30	09:55	01:52	54°04.627/ 54°04.392	146°05.598/ 146°05.800	1580/ 1480	nothing	Dredge empty (exept of sediment traps). Wire damaged.
13.07.	102-1	SES	13:45	14:00	21:15	21:30	07:45	53°31.747/ 53°20.244	145°56.446/ 146°15.634	1740/ 1803		Frequency: 8 kHz/ 0,75 ms. 14:26 - break because of problems with the ship`s machine; 17:15 - SES back into water; 17:35 - start of data storage; 17:43 - profile continued.
13.07.	103-1	MUC	22:45		00:01	01:17	02:32	53°26.627	146°05.344	1746	11 cores	RAD - 45 cm, ARC - 43 cm, POI I - 44 cm, POI II - 44,5 cm, POL - 43 cm, BEN I - 48,5 cm, BEN II - 48 cm, ISO - 43 cm, GEO - 44,5 cm, pp - 40, 5 cm, RAD II - surface.
14.07.	103-2	SL-R	01:29		01:57	02:20	00:51	53°26.151	146°06.050	1746	9,8 m	
14.07.	103-3	SL-G	02:33		03:05	03:34	01:01	53°25.488	146°06.461	1748	more than 10 m	
14.07.	103-4	CTD	03:39		04:18	04:46	01:07	53°25.411	146°06.853	1750	12 bottles	1=1740, 2=1719, 3=1639, 4=1482, 5=1236, 6=990, 7=743, 8=496, 9=297, 10=150, 11=69, 12=3 (depth m)
14.07.	103-5	MUN	05:02		05:37	06:33	01:31	53°26.170/ 53°26.893	146°06.527/ 146°05.638	1750/ 1748	5 nets	1=1000-500; 2=500-200, 3=200-150, 4=150-50, 5=50-0 (depth m)
14.07.	104-1	MUC	08:35		09:29	10:25	01:50	53°12.952	146°15.144	1752	9 tubes	Bottom water; POL - 42 cm; POI - 46 cm; RAD - 48 cm; ARC - 44 cm; BEN I - 46 cm; BEN II - 44 cm; pp - 43, 5 cm (every 1,5 cm: 5 cc); ISO I - 1-10 cm living, 10-43 cm 1 cm slices; ISO II - 1-4 cm 1 cm slices, 4-8 cm 1 sample.
14.07.	104-2	SL-R	10:36		11:00	11:25	00:49	53°12.850	146°15.642	1758	9,80 m	
14.07.	104-3	SL-G	11:48		12:03	12:27	00:39	53°12.740	146°16.152	1760	ca. 10,5 m	Long core: 15 m.
14.07.	104-4	CTD	12:37		13:19	13:51	01:14	53°12.732	146°16.460	1762	12 bottles	1=1754, 2=1734, 3=1655, 4=1557, 5=1384, 6=1187, 7=940, 8=694, 9=396, 10=148, 11=75, 12=3 (depth m)
Southwestern Kamchatka slope												
15.07.	105-1	SES	18:20	18:40	01:35	01:45	07:25	51°59.873/ 51°59.981	154°46.907/ 153°58.662	335/ 543		Frequency: 8 kHz/ 0,75 ms.
15.07.	105-2	SEI	19:00			01:23	05:23	51°59.99/ 52°00.01	154°44.93/ 154°00.20	333/ 622		Seismic profile Nr. 11
16.07	106-1	MUC	02:58		03:15	03:36	00:38	51°59.988	154°02.309	515	little surface sediment	MUC did not penetrate - only sediment surface recovered. ISO - 0-0,5 cm sed. surface; BEN - 0-0,5 cm sed. surface.
16.07.	106-2	SL-R	03:51			04:07	00:16	51°59.849	154°02.459	511		Coordinates of start. Coring cancelled and repeated at st. 106-5 because of technical problems with weights.
16.07.	106-3	CTD	04:29		04:40	04:54	00:25	51°59.767	154°02.569	514	12 bottles	1=502, 2=491, 3=445, 4=396, 5=346, 6=296, 7=248, 8=198, 9=119, 10=70, 11=29, 12=3 (depth m)
16.07.	106-4	MUN	05:10		05:26	05:52	00:42	51°59.868/ 51°59.967	154°02.637/ 154°02.804	512/ 510	5 nets	1=500-300, 2=300-200, 3=200-150, 4=150-50, 5=50-0 (depth m)
16.07.	106-5	SL-R	05:49		06:07	06:14	00:25	51°59.848	154°02.854	510	more than 4 m	
16.07.	106-6	SL-G	06:29		06:37	06:46	00:17	51°59.943	154°03.324	510	ca. 5,5 m	Short core: 6 m.
16.07.	107-1	SES	07:15	07:36	14:37	14:50	07:35	52°00.029/ 51°59.996	153°57.992/ 153°00.894	547/ 710		Frequency: 8 kHz/ 0,75 ms.
16.07.	107-1	SEI	07:50			14:29	06:39	52°00.04/ 52°00.01	153°56.43/ 153°02.12	554/ 705		Seismic profile Nr. 12.

Date	Stat. Nr.	Equip-ment	Start	at sf	off sf	End	Dura-tion	Latitude N	Longitude E	Water depth	Recovery	Remarks
16.07.	108-1	MUN	18:57		19:18	20:00	01:03	52°01.077/ 52°01.438	153°34.755/ 153°34.760	624/ 626	5 nets	1=600-400, 2=400-200, 3=200-150, 4=150-50, 5=50-0 (depth m)
16.07.	108-2	CTD	20:10		20:26	20:42	00:32	52°01.492	153°34.815	625	12 bottles	1=610, 2=584, 3=545, 4=446, 5=346, 6=299, 7=248, 8=197, 9=150, 10=70, 11=30, 12=2 (depth m)
16.07.	108-3	MUC	21:05		21:25	21:46	00:41	52°01.145	153°34.975	625	10 tubes	Bottom water; BEN I - 29 cm (1-8 cm stained, rest 1 cm slices); BEN II - 34 cm (1-8 cm stained, rest 1 cm slices); ISO - 38 cm (1-10 cm stained, rest 1 cm slices); ISO II - 19 cm (1-10 cm living (bags), rest 1 cm slices); GEO - 33 cm (1 cm slices); POI - 34 cm; ARC - 32,5 cm; POL - 39 cm; RAD - 29 cm.
16.07.	108-4	SL-R	21:59		22:08	22:19	00:20	52°01.311	153°35.059	625	ca. 8 m	
16.07.	108-5	SL-G	22:29		22:39	22:50	00:21	52°01.330	153°35.006	627	ca. 10 m	12 m core.
Eastern slope of Kurile Basin												
17.07.	109-1	SES	20:48	21:04	03:01	03:14	06:26	50°33.853/ 50°19.660	155°00.306/ 154°29.450	1118/ 1382		Frequency: 8 kHz/ 0,75 ms.
17.07.	109-2	SEI	21:23			02:47	05:24	50°33.08/ 50°20.09	154°58.73/ 154°30.4	1125/ 1387		Seismic profile Nr. 13.
18.07.	110-1	MUC	04:44		05:22	06:04	01:20	50°27.191	154°45.961	1218	5 tubes	Bottom water; ISO - 1-10 living, 10-20,5 dead; BEN I - 0-8 living, 8-19 dead; BEN II - 0-8 living, 8-19 dead; POL I - 16 cm; POL II - 0-0,5 cm sed. surface WP; POL III - 0-0,5 cm sed. surface WP; ARC - 0-0,5 cm sed. surface WP; RAD - 16 cm.
18.07.	110-2	SL-R	07:26		07:41	08:02	00:36	50°27.079	154°46.165	1218	3,4 m	
18.07.	110-3	CTD	06:38		07:04	07:23	00:45	50°27.069	154°45.967	1220	12 bottles	1=1207, 2=1188, 3=1088, 4=940, 5=692, 6=494, 7=347, 8=199, 9=140, 10=94, 11=30, 12=3 (depth m)
18.07.	110-4	SL-G	08:14		08:33	08:56	00:42	50°27.300	154°46.100	1220	ca. 3,5 m	12 m core
18.07.	110-5	MUN	09:08		09:41	10:29	01:21	50°27.288/ 50°25.736	154°46.240/ 154°48.721	1218/ 1213	5 nets	1=1000-500, 2=500-200, 3=200-150, 4=150-50, 5=50-0 (depth m)
18.07.	111-1	SES	12:08	12:25	21:03	21:15	09:07	50°19.840/ 49°55.905	154°30.460/ 153°41.610	1400/ 1595		Frequency: 8 kHz/ 0,75 ms. Profile start at 12:36. SES-profile Nr. 34.
18.07.	111-2	SEI	12:50			20:51	08:01	50°19.00/ 49°56.40	154°28.33/ 153°42.571	1372/ 1582		Seismic profile Nr. 14.
19.07.	112-1	MUC	00:25		01:00	01:51	01:26	50°13.524	154°17.422	1306	11 tubes	Bottom water; POL - 36 cm; POI - 39 cm; RAD - 36 cm; ARC - 32 cm; GEO - 37 cm; GEO II - 35 cm; BEN I - 0-8 cm living, 8-36 cm dead; BEN II - 0-8 cm living, 8-36 cm dead; ISO - 0-10 cm living, 10-36 cm dead; ISO II - 0-0,5 cm living, 0,5-26,5 cm dead in 0,5 cm slices; pp - 1,5-31,5 cm in 1,5 cm slices, sed.surface: RAD II.
19.07.	112-2	SL-R	02:00		02:15	02:42	00:42	50°13.497	154°17.369	1309	ca. 4,5 m	
19.07.	112-3	SL-G	02:51		03:10	03:35	00:44	50°13.492	154°17.206	1304	ca. 4,5 m	12 m core
19.07.	112-4	MUN	03:37		04:06	05:04	01:27	50°13.275/ 50°12.804	154°17.416/ 154°19.327	1312/ 1364	5 nets	1=1000-500, 2=500-200, 3=200-150, 4=150-50, 5=50-0 (depth m)
19.07.	112-5	CTD	05:19		05:48	06:12	00:53	50°12.761	154°19.672	1371	12 bottles	1=1365, 2=1345, 3=1237, 4=1039, 5=843, 6=645, 7=496, 8=347, 9=199, 10=100, 11=49, 12=3 (depth m)
19.07.	113-1	SES	12:10	12:30	19:18	19:33	07:23	49°29.939/ 49°06.225	153°05.473/ 152°36.678	1780/ 2275		Frequency: 8 kHz/ 0,75 ms. SES-profile Nr. 35
19.07.	113-2	SEI	12:40			19:05	06:25	49°29.4/ 49°06.82	153°04.88/ 152°37.46	1770/ 2205		Seismic profile Nr. 15
19.07.	114-1	MUC	21:30		22:22	23:37	02:07	49°21.701	152°54.086	1789	3 tubes	MUC hit seafloor, but seemed to fell to side due to strong current: only 3 tubes closed. Samples: Bottom water; POL - 37 cm; RAD - 37 cm; ISO - 37 cm (upper 10 cm living)
19.07.	114-2	SL-R	23:47		00:10	00:43	00:56	49°22.465	152°52.756	1764	ca. 7,8 m	
20.07.	114-3	SL-G	00:55		01:24	01:59	01:04	49°22.540	152°52.676	1762	ca. 9,5 m	12 m core

Date	Stat. Nr.	Equip-ment	Start	at sf	off sf	End	Dura-tion	Latitude N	Longitude E	Water depth	Recovery	Remarks
20.07.	114-4	CTD	02:00		02:35	03:04	01:04	49°22.617	152°53.232	1765	12 bottles	1=1756, 2=1733, 3=1627, 4=1384, 5=1138, 6=847, 7=595, 8=390, 9=290, 10=99, 11=52, 12=3 (depth m)
20.07.	114-5	MUN	03:22		03:48	04:38	01:16	49°22.338/ 49°21.598	152°53.375/ 152°53.328	1770/ 1780	5 nets	1=1000-500, 2=500-200, 3=200-150, 4=150-50, 5=50-0 (depth m)
20.07.	115-1	CTD	09:54		10:40	11:17	01:23	48°35.233	153°09.956	1702	12 bottles	1=2011, 2=1925, 3=1728, 4=1433, 5=1234, 6=989, 7=742, 8=495, 9=297, 10=99, 11=51, 12=3 (depth m)
20.07.	115-2	MUN	11:38		12:09	13:04	01:26	48°36.260/ 48°37.044	153°09.787/ 153°10.013	2126/ 2503	5 nets	1=1000-500, 2=500-200, 3=200-150, 4=150-50, 5=50-0 (depth m)
20.07.	116-1	MUN	19:24		19:53	20:28	01:24	47°55.025/ 47°56.285	151°54.743/ 151°53.824	3278/ 3264	5 nets	1=1000-500, 2=500-200, 3=200-150, 4=150-50, 5=50-0 (depth m)
20.07.	116-2	CTD	21:11		22:22	23:11	02:00	47°56.301	151°53.847	3265	12 bottles	1=3284, 2=3265, 3=2956, 4=2564, 5=2170, 6=1776, 7=1384, 8=987, 9=593, 10=298, 11=99, 12=3 (depth m)
20.07.	116-3	MUC	23:19		00:42	02:38	03:19	47°57.895	151°52.771	3260	9 tubes	Bottom water; POL - 34 cm; POI - 36 cm; ARC - 37 cm; RAD - 37 cm + 0-2 cm sed. surface; GEO - 31 cm; ISO - 34 cm (0-10 cm living, rest in 1 cm slices); BEN I - 0-8 cm living, 8-34 cm dead; BEN II - 0-8 cm living, 9-17 cm dead; GEO II - 0-1 cm living, pp 5 cc every 1,5 cm, rest 1 cm slices. From st.116-3 on: ca. 5% Formalin solution in deionized water with ca. 2g/l Rose Bengal instead of 80% Ethanol.
	Kurile Basin											
21.07.	117-1	SEI	10:43			15:10	04:27	47°01.76/ 46°55.28	150°14.03/ 150.05.5	3221/ 3187		Seismic profile Nr. 16
21.07.	118-1	ECH	09:57			17:15	07:18	47°03.535/ 46°56.105	150°15.856/ 150°12.112	3220/ 2600		Mapping of submarine volcano 6.5 (Bussol Strait)
21.07.	119-1	DR3	19:02	19:42	21:28	22:09	03:07	46°58.471/ 46°58.593	150°09.970/ 150°10.829	2692/ 2214	nothing	Dredge did not recover rock samples because chain bag opened during dredging. A few maganese fragments (<1 cm) in sediment traps.
21.07.	119-2	DR3	23:00	23:43	02:37	03:16	04:16	47°00.656/ 46°59.368	150°14.310/ 150°12.348	3147/ 2274	ca. 100 kg	Well rounded dropstones incl. blocks up to 60x40 cm size. Dropstones comprise, among others, granitic and various volcanic rocks. Apart from dropstones, the dredge contained sponges etc.
22.07.	119-3	DR3	04:02	04:46	06:50	07:30	03:28	46°58.565/ 46°58.936	150°10.199/ 150°09.384	2590/ 2570	30 kg	Dredging yielded some rocks, mainly lithified sediments (partly bedded) with lava clasts up to 10x10 cm (possibly volcanic clastic sediment). Dredge stuck: vessel turned and returned to the beginning point of the dredge track for freeing dredge.
22.07.	119-4	DR3	08:54	09:31	11:15	11:38	02:44	46°57.012/ 46°57.864	150°10.843/ 150°11.075	2540/ 2150	ca. half full	Various dropstones up to 50x30 cm, sediments, maganese, sponge etc., one block of dacite which may be in situ (?).
22.07.	120-1	CTD	15:06		16:14	17:14	02:08	47°02.512	150°54.126	3268	12 bottles	1=3280, 2=3249, 3=3177, 4=2760, 5=2367, 6=1975, 7=1581, 8=1138, 9=744, 10=297, 11=115, 12=3 (depth m)
22.07.	120-2	MUN	17:34		18:39	20:26	02:52	47°03.263/ 47°02.061	150°55.809/ 150°56.143	3278/ 3273	5 nets	1=2000-1500, 2=1500-1200, 3=1200-1000, 4=1000-800, 5=800-0 (depth m). Net 5 was thought to sample only from 800-600 m depth, but itwas found out that it does not close, so that it sampled up to surface. St. 120-2 and 120-3 are MUN double stations.
22.07.	120-3	MUN	20:57		21:41	22:14	01:17	47°01.765/ 47°01.141	150°55.883/ 150°55.501	3273/ 3263	5 nets	1=800-500, 2=500-200, 3=200-150, 4=150-50, 5=50-0 (depth m).
22.07.	121-1	ECH	23:38			03:15	03:37	46°59/ 47°06.466	151°02/ 151°10.307	3224/ 3000		Mapping of submarine volcano 6.4 (Bussol Strait)
23.07.	122-1	DR3	04:02	04:48	06:51	07:24	03:22	47°05.231/ 47°05.078	151°09.574/ 151°10.119	2263/ 2421	ca. 20 kg	Dropstones and sponges. Dredge stuck, vessel turned and returned towards the beginning point of dredge track for freeing dredge.
23.07.	123-1	MUN	13:49		14:50	16:43	02:54	47°41.453/ 47°41.239	149°52.929/ 149°50.728	3311/ 3312	5 nets	1=2000-1500, 2=1500-1200, 3=1200-900, 4=900-600, 5=600-0 (depth m).

Date	Stat. Nr.	Equip-ment	Start	at sf	off sf	End	Dura-tion	Latitude N	Longitude E	Water depth	Recovery	Remarks
23.07.	123-2	MUN	17:05		17:46	18:05	01:00	47°41.200/ 47°40.948	149°50.394/ 149°49.509	3312/ 3312	5 nets	1=600-400, 2=400-200, 3=200-150, 4=150-50, 5=50-0 (depth m).
23.07.	123-3	CTD	18:25		19:35	20:35	02:10	47°40.826	149°49.224	3303	12 bottles	1=3321, 2=3296, 3=2956, 4=2466, 5=1973, 6=1482, 7=1047, 8=951, 9=496, 10=198, 11=73, 12=3 (depth m)
23.07.	123-4	MUC	20:40		22:04	23:57	03:17	47°39.681	149°46.073	3307	5 tubes	Bottom water; POL - 38 cm; RAD - 37 cm + 0-2 cm sed. surface; POI - 23 cm; BEN I - 0-8 cm living benthos, 8-10 cm dead; BEN II - 0-2 cm living stained; ISO - 0-11 cm living, 11-19 cm dead.
24.07. - 27.07.	124-1	SEI	04:54			06:38		47°48.24/ 46°43.28	148°37.13/ 147°55.83	3337/ 3349		Seismic profiles Nr. 17-28
27.07.	125-1	SEI	09:48			14:00	04:12	46°09.79/ 45°59.47	147°59.79/ 148°04.86	3337/ 2923		Seismic profile Nr. 29
27.07.	126-1	DR3	22:09	22:51	23:50	00:28	02:19	46°02.007/ 46°01.941	147°44.019/ 147°44.401	2141/ 2200	ca. 100 kg	Angular or slightly rounded, homogeneous fragments of basaltic andersite, most likely fragments of a lava flow.
28.07.	126-2	DR3	01:40	02:08	03:02	03:29	01:49	46°03.728/ 46°03.047	147°41.806/ 147°42.227	2022/ 1921	ca. 15 kg	Dropstones and sponges.
28.07.	126-3	DR3	04:13	04:40	06:02	06:28	02:15	46°09.168/ 46°02.922	147°43.316/ 147°44.327	1734/ 1647	little	Dredge contained only a few dropstones and sediment.
28.07.	126-4	DR3	07:55	08:28	09:55	10:34	02:39	46°02.658/ 46°03.517	147°40.054/ 147°40.459	2815/ 2400	little	A few angular basalt fragments being most likely bedrocks, sediments (lithified) and dropstones.
28.07.	126-5	DR3	11:43	12:13	13:24	14:01	02:18	46°02.081/ 46°02.588	147°42.500/ 147°43.111	2589/ 2073	little	One small dropstone, sediment in sediment traps.
28.07.	127-1	SES	09:20	09:33	13:27	13:50	04:10	46°03.401/ 46°02.602	147°40.220/ 147°43.143	2503/ 2243		SES-profile Nr. 36. Frequency: 8 kHz/ 1 ms. Profile parallel to dredging, good results on flat bottom in water depth of about 3200 m.
28.07.	128-1	DR3	22:47	23:24	00:58	01:33	02:46	45°44.989/ 45°45.822	146°47.359/ 146°47.546	2900/ 2521	little	2 dropstones, sediment in sediment traps.
29.07.	128-2	DR3	02:04	02:51	04:02	04:50	02:46	45°46.528/ 45°45.826	146°50.270/ 146°51.362	3100/ 2930	nothing	Dredge was emtpy (sediment in sediment traps).
29.07.	128-3	DR3	05:37	06:16	07:37	08:26	02:49	45°46.352/ 45°45.523	146°47.943/ 146°48.111	2709/ 2680	little	2 dropstones, sediment in sediment traps.
29.07.	128-4	DR3	09:16	10:02	11:30	12:16	03:00	45°45.454/ 45°46.337	146°46.700/ 146°48.630	2820/ 3000	ca. 25 kg	Lithified (?) sediments and dropstones.
29.07.	129-1	ECH	12:53			17:24	04:31	45°46.904/ 4°44.245	146°46.311/ 146°45.964	2958/ 2894		Echosounder mapping of Loskutov seamount.
30.07.	130-1	SES	02:16	02:28	05:20	05:45	03:29	45°38.911/ 45°26.791	144°20.817/ 144°15.617	904/ 885		SES-profile Nr. 37. Frequency: 8 kHz/ 1ms.
30.07.	131-1	MUC	06:34		06:57	07:26	00:52	45°32.763	144°18.320	760	11 tubes	Bottom water; POL - 37 cm; RAD - 35 cm; GEO - 33 cm; POI - 34 cm; POI II - 45 cm; ARC - 41 cm; ISO - 37 cm; ISO II - 42 cm; BEN - 37,5 cm; BEN II - 36 cm; PP - 36 cm.
30.07.	131-2	SL-R	07:33		07:44	07:52	00:19	45°32.506	144°18.002	761	8,7 m	
30.07.	131-3	SL-G	08:23		08:33	08:46	00:23	45°32.590	144°18.333	760	ca. 11,2 m	18 m gravity core
30.07.	131-4	CTD	09:04		09:24	09:44	00:40	45°32.663	144°18.334	765	12 bottles	1=745, 2=731, 3=692, 4=594, 5=494, 6=397, 7=297, 8=198, 9=99, 10=67, 11=30, 12=2,3 (depth m)
02.08.	132-1	SB	04:57					39°18.900	133°28.029	1286		Air temperature: 26°C, water temperature: 24°C. Sea bath enjoyed by all participants.

Legend

	Sampling equipment	Latitude/ Longitude	Remarks
CTD	Multisonde and hydrocasts	Start	
DR1	Russian dredge	At and off seafloor	
DR2	Small German chain bag dredge	At and off seafloor	
DR3	Large German chain bag dredge	At and off seafloor	
ECH	Russian hydracoustic echosounder	Start and end	
HYC	Hydrocorer (6 m length)	At/ off seafloor	
MUC	Multicorer	At/ off seafloor	Abbreviations of samples: BEN - benthos, ISO - isotopes, POI - samples for POI, POL - pollen, RAD - radiolarien, ARC - archive, GEO - geology, PP - physical properties, WP - whirlpack
MUN	Multinet	Start and end	"At/ off seafloor" is the deepest position of net
SB	Sea bath	Start	
SEI	Seismics (airgun, streamer)	Start and end	
SES	Sonar echosounder SES 2000	Start and end of track	Start and end of track in protocol as "at seafloor" and "off seafloor".
SL-G	German gravity corer (usually 12 m length)	At/ off seafloor	
SL-R	Russian gravity corer (8 m length)	At/ off seafloor	

Date	dd.mm. 2002
Duration	hh:mm
Start, at sf, off sf, end	UTC
Water depth	m by ECH

APPENDIX 2

SES-2000DS profiles

List of SES-2000DS profiles

Longitude	Latitude	Date	Time	Depth	Profile	Length	Length
				(m)		(nm)	(km)
144.0500	45.4283	02.07.2002	19:07	831	1	7.52	13.93456
144.2600	45.4487	02.07.2002	21:31	882	1	7.52	13.93456
146.1008	48.9473	03.07.2002	14:40	810	2	19.76	36.61528
146.1263	48.5788	03.07.2002	21:40	1186	2	19.76	36.61528
144.6458	51.0592	04.07.2002	20:33	268	3	23.92	44.32376
145.3097	51.1413	05.07.2002	05:37	674	3	23.92	44.32376
145.3097	51.1413	05.07.2002	07:44	683	4	22.79	42.22987
145.5417	51.3158	05.07.2002			4	22.79	42.22987
145.4583	51.4867	05.07.2002	14:40	1332	4	22.79	42.22987
144.3975	52.6354	05.07.2002	22:36	225	5	11.14	20.64242
144.7043	52.6703	06.07.2002	02:02	684	5	11.14	20.64242
144.6864	52.6740	06.07.2002	08:33	670	6	31.64	58.62892
145.3967	53.0010	06.07.2002	18:46	1755	6	31.64	58.62892
143.9013	54.3284	07.07.2002	16:40	176	7	14.82	27.46146
143.9305	54.3412	07.07.2002			7	14.82	27.46146
143.9823	54.3665	07.07.2002			7	14.82	27.46146
144.0891	54.4499	07.07.2002			7	14.82	27.46146
144.1927	54.4802	07.07.2002			7	14.82	27.46146
144.2115	54.4846	07.07.2002	21:58	886	7	14.82	27.46146
144.1330	54.5026	08.07.2002	08:23	766	8	3.69	6.83757
144.2372	54.4992	08.07.2002	09:33	928	8	3.69	6.83757
144.2372	54.4990	08.07.2002	09:35	926	9	0.97	1.79741
144.2362	54.4832	08.07.2002	09:50	924	9	0.97	1.79741
144.2351	54.4828	08.07.2002	09:51	905	10	3.09	5.72577
144.1478	54.4828	08.07.2002	10:45	810	10	3.09	5.72577
144.1464	54.4814	08.07.2002	10:48	785	11	0.8	1.4824
144.1464	54.4683	08.07.2002	11:06	805	11	0.8	1.4824
144.1472	54.4675	08.07.2002	11:07	790	12	3.14	5.81842
144.2356	54.4668	08.07.2002	12:17	787	12	3.14	5.81842
144.2362	54.4661	08.07.2002	12:18	920	13	0.87	1.61211
144.2369	54.4519	08.07.2002	12:39	905	13	0.87	1.61211
144.2356	54.4508	08.07.2002	12:41	905	14	8.34	15.45402
144.0000	54.4496	08.07.2002	15:13	510	14	8.34	15.45402
143.9985	54.4507	08.07.2002	15:14		15	1.78	3.29834
143.9989	54.4800	08.07.2002	15:40		15	1.78	3.29834
144.0000	54.4810	08.07.2002	15:42		16	1.02	1.89006
144.0284	54.4795	08.07.2002	16:00		16	1.02	1.89006
144.0286	54.4792	08.07.2002	16:00	640	17	2.71	5.02163
144.0274	54.4346	08.07.2002	17:04	580	17	2.71	5.02163
144.0279	54.4342	08.07.2002	17:04		18	1.05	1.94565
144.0569	54.4311	08.07.2002	17:21		18	1.05	1.94565
144.0588	54.4326	08.07.2002	17:23		19	2.65	4.91045
144.0566	54.4760	08.07.2002	17:56		19	2.65	4.91045
144.0581	54.4773	08.07.2002	17:58		20	0.9	1.6677
144.0833	54.4768	08.07.2002	18:13		20	0.9	1.6677
144.0844	54.4752	08.07.2002	18:15		21	2.07	3.83571
144.0853	54.4413	08.07.2002	18:53		21	2.07	3.83571
144.0845	54.4407	08.07.2002	18:54		22	3.18	5.89254
143.9946	54.4419	08.07.2002	20:02		22	3.18	5.89254
143.2667	54.7833	09.07.2002	04:44	110	23	34.66	64.22498
142.3667	55.0000	09.07.2002	13:46	100	23	34.66	64.22498
141.9667	54.9833	09.07.2002	16:16	121	24	31.64	58.62892
141.9667	54.4667	10.07.2002	02:12	51	24	31.64	58.62892
141.9654	54.1753	10.07.2002	05:00	51	25	41.42	76.75126
141.0110	53.7749	10.07.2002	16:50	26	25	41.42	76.75126
145.5047	54.8840	11.07.2002	17:32	588	26	21.31	39.48743

145.5047	54.8840	11.07.2002	17:32	588	26	21.31	39.48743
145.2180	54.8783	11.07.2002			27	21.13	39.15389
145.0984	55.0432	11.07.2002	22:56	1245	27	21.13	39.15389
146.2987	54.3802	12.07.2002	18:20	1608	28	4.97	9.20941
146.4111	54.3200	12.07.2002	19:45	1315	28	4.97	9.20941
146.4093	54.3302	12.07.2002	19:47	1490	29	4.47	8.28291
146.3437	54.2578	12.07.2002	21:14	1565	29	4.47	8.28291
145.9408	53.5291	13.07.2002	14:00	1740	30	16.05	29.74065
146.2606	53.3374	13.07.2002	21:15	1800	30	16.05	29.74065

APPENDIX 3

Water column data

LV29, Leg 2 CTD: Water column analysis

St. No	Bot. No	Depth m	S	q, °C	s_0, kg/m³	O_2 CTD mmol/kg	Tr, %	TA mmol/kg	pH_t 15 °C	Ca, mmol/kg	pH_t in situ	DIC, mmol/kg	CO_3, mmol/kg	pCO_2, µatm	Lc	La	CH_4 nl/l
69-4	1	837	34.165	2.262	27.282	50.3	92.9	2.359	7.433	10.045	7.532	2.367	0.038	1177	0.66	0.46	103
	2	827	34.163	2.260	27.280	49.5	92.9	2.356	7.428	10.043	7.527	2.366	0.038	1191	0.65	0.45	111
	3	793	34.130	2.242	27.256	51.7	93.7	2.352	7.427	10.036	7.529	2.362	0.038	1192	0.66	0.45	78
	4	741	34.075	2.192	27.215	57.6	94.0	2.345	7.426	10.028	7.533	2.355	0.037	1190	0.67	0.46	82
	5	692	34.012	2.115	27.171	67.5	94.2	2.337	7.429	10.000	7.542	2.346	0.038	1174	0.69	0.47	143
	6	594	33.858	1.859	27.067	99.2	94.3	2.317	7.455	9.951	7.582	2.318	0.040	1079	0.75	0.51	49
	7	496	33.710	1.607	26.967	143.6	94.2	2.291	7.494	9.911	7.636	2.281	0.043	956	0.85	0.57	33
	8	396	33.571	1.359	26.873	167.3	94.0	2.275	7.521	9.873	7.678	2.257	0.045	878	0.94	0.62	82
	9	298	33.415	0.809	26.783	178.0	93.6	2.263	7.542	9.821	7.717	2.239	0.047	810	1.02	0.66	60
	10	171	33.202	-0.448	26.675	230.3	93.4	2.253	7.602	9.726	7.811	2.211	0.054	655	1.22	0.78	48
	11	70	32.974	-0.764	26.503	272.1	93.8	2.237	7.696	9.654	7.925	2.167	0.066	503	1.57	0.99	192
	12	3	32.263	8.766	25.012	264.8	87.8	2.204	8.032	9.492	8.127	2.015	0.136	313	3.34	2.11	73
70-5	1	1980	34.566	1.809	27.639	69.2	94.3	2.406	7.579	10.196	7.599	2.367	0.052	786	0.56	0.45	7
	2	1926	34.558	1.835	27.631	67.1	94.5	2.405	7.551	10.202	7.572	2.375	0.049	849	0.54	0.43	13
	3	1729	34.538	1.903	27.609	60.5	94.7	2.401	7.532	10.195	7.567	2.377	0.047	897	0.56	0.44	21
	4	1484	34.507	2.000	27.577	53.5	94.7	2.396	7.513	10.162	7.566	2.378	0.045	949	0.6	0.45	11
	5	1237	34.450	2.155	27.519	44.8	94.7	2.388	7.486	10.125	7.556	2.379	0.043	1026	0.63	0.46	12
	6	990	34.312	2.321	27.395	37.1	94.6	2.370	7.446	10.073	7.531	2.374	0.039	1143	0.63	0.45	16
	7	744	34.133	2.285	27.254	49.5	94.6	2.347	7.429	10.028	7.535	2.356	0.038	1186	0.67	0.46	16
	8	496	33.773	1.666	27.013	115.7	94.4	2.300	7.469	9.835	7.609	2.297	0.041	1027	0.8	0.53	40
	9	249	33.399	0.856	26.767	164.6	94.0	2.262	7.475	9.831	7.648	2.258	0.041	966	0.89	0.58	41
	10	89	32.987	-0.836	26.517	279.1	94.0	2.232	7.703	9.696	7.932	2.160	0.067	491	1.58	1	197
	11	31	32.462	1.540	25.971	307.4	86.1	2.207	7.883	9.537	8.086	2.077	0.098	338	2.38	1.5	96
	12	3	32.323	8.858	25.045	278.3	86.1	2.198	8.040	9.495	8.133	2.005	0.138	307	3.38	2.13	51
72-4	1	1113	34.373	2.303	27.445	37.1	94.1	2.382	7.455	10.124	7.531	2.383	0.040	1119	0.61	0.44	30
	2	1062	34.351	2.315	27.426	38.1	94.4	2.379	7.453	10.125	7.533	2.380	0.040	1125	0.62	0.44	19
	3	941	34.282	2.348	27.368	39.8	94.6	2.368	7.442	10.104	7.531	2.373	0.039	1156	0.64	0.45	23
	4	794	34.159	2.309	27.274	46.2	94.5	2.355	7.425	10.045	7.526	2.366	0.037	1203	0.65	0.45	24
	5	645	33.991	2.135	27.153	68.6	94.4	2.332	7.428	10.005	7.545	2.342	0.037	1177	0.69	0.47	25
	6	495	33.705	1.664	26.959	131.8	94.4	2.299	7.482	9.917	7.623	2.292	0.042	992	0.82	0.55	34
	7	347	33.485	1.119	26.819	170.6	94.1	2.271	7.510	9.835	7.674	2.256	0.044	894	0.92	0.6	34
	8	248	33.363	0.978	26.730	200.4	94.1	2.262	7.558	9.801	7.736	2.233	0.049	783	1.07	0.69	41
	9	151	33.210	0.739	26.621	242.4	94.1	2.254	7.639	9.744	7.834	2.201	0.059	627	1.34	0.86	45
	10	60	32.806	-0.400	26.353	300.1	93.6	2.225	7.756	9.636	7.983	2.137	0.075	435	1.78	1.12	86
	11	30	32.382	3.337	25.766	309.5	87.8	2.208	7.922	9.518	8.098	2.063	0.107	331	2.57	1.62	77
	12	3	32.219	8.902	24.956	293.9	84.2	2.194	8.061	9.460	8.154	1.993	0.144	290	3.47	2.19	46
76-3	1	619	34.037	2.112	27.191	68.7	81.1	2.338	7.436	10.003	7.556	2.345	0.038	1154	0.71	0.48	701
	2	609	34.004	2.076	27.168	71.3	87.1	2.336	7.434	9.996	7.555	2.344	0.038	1158	0.71	0.48	672
	3	570	33.945	2.011	27.125	79.6	92.6	2.326	7.437	9.975	7.563	2.333	0.038	1142	0.73	0.49	
	4	495	33.752	1.587	27.002	109.9	89.6	2.302	7.453	9.907	7.593	2.304	0.039	1067	0.77	0.51	296
	5	395	33.599	0.955	26.922	148.7	89.2	2.288	7.476	9.870	7.635	2.283	0.041	976	0.84	0.55	
	6	316	33.477	0.555	26.847	167.2	90.4	2.275	7.486	9.825	7.659	2.268	0.042	931	0.88	0.57	189
	7	250	33.420	0.928	26.780	162.1	94.2	2.266	7.481	9.836	7.654	2.260	0.041	956	0.9	0.58	
	8	198	33.357	0.784	26.737	179.5	94.1	2.258	7.494	9.787	7.674	2.248	0.042	917	0.94	0.6	99
	9	149	33.262	0.488	26.678	207.0	93.9	2.252	7.558	9.767	7.752	2.224	0.049	766	1.11	0.71	
	10	79	32.912	-0.763	26.452	287.9	92.5	2.230	7.711	9.656	7.940	2.156	0.068	483	1.6	1.01	80
	11	31	32.663	1.310	26.147	317.0	66.3	2.221	7.824	9.583	8.029	2.110	0.088	393	2.1	1.32	
	12	4	29.877	7.720	23.292	321.2	90.5	2.054	8.165	8.767	8.277	1.830	0.156	198	3.81	2.38	46
79-1	1	1053	34.370	2.310	27.442	28.2	88.8	2.379	7.430	10.128	7.509	2.388	0.038	1194	0.59	0.42	241
	2	1005	34.324	2.349	27.402	30.6	93.5	2.376	7.430	10.138	7.512	2.385	0.038	1196	0.6	0.43	149
	3	942	34.276	2.327	27.365	36.0	93.5	2.372	7.427	10.102	7.515	2.382	0.038	1203	0.61	0.43	
	4	794	34.197	2.313	27.303	43.0	94.1	2.359	7.424	10.069	7.525	2.370	0.037	1208	0.65	0.45	264
	5	643	34.127	2.218	27.255	53.9	93.5	2.349	7.427	10.038	7.543	2.359	0.038	1192	0.7	0.47	
	6	496	33.989	2.069	27.157	71.3	93.9	2.333	7.429	9.985	7.560	2.342	0.038	1173	0.74	0.49	250
	7	347	33.637	1.535	26.913	124.5	93.9	2.292	7.449	9.891	7.602	2.296	0.039	1075	0.81	0.53	
	8	247	33.360	0.839	26.737	183.4	93.5	2.264	7.507	9.800	7.683	2.251	0.044	890	0.95	0.61	42
	9	129	33.036	-0.410	26.539	266.5	93.2	2.243	7.643	9.699	7.858	2.190	0.059	588	1.35	0.86	
	10	73	32.837	-0.009	26.361	304.2	91.8	2.231	7.734	9.630	7.953	2.150	0.072	471	1.69	1.07	51
	11	29	32.609	2.443	26.023	334.5	81.7	2.221	7.893	9.580	8.083	2.086	0.102	345	2.44	1.53	
	12	4	30.046	8.617	23.298	311.0	90.2	2.077	8.195	8.878	8.293	1.836	0.168	192	4.1	2.57	61
81-1	1	367	33.399	0.154	26.806	199.9	88.2	2.271	7.539	9.816	7.718	2.248	0.047	795	0.97	0.63	1664
	2	358	33.398	0.151	26.806	198.9	88.3	2.271	7.520	9.816	7.698	2.254	0.045	836	0.93	0.61	1728
	3	328	33.391	0.113	26.802	199.6	88.5	2.270	7.517	9.829	7.698	2.254	0.045	841	0.94	0.61	
	4	298	33.349	-0.075	26.777	204.8	88.9	2.269	7.518	9.797	7.704	2.252	0.045	832	0.95	0.62	2916
	5	248	33.232	-0.570	26.705	234.2	90.5	2.261	7.557	9.764	7.758	2.233	0.049	734	1.06	0.68	
	6	199	33.227	-0.577	26.701	237.8	90.6	2.258	7.560	9.766	7.766	2.229	0.049	728	1.09	0.7	14640
	7	149	33.201	-0.419	26.673	239.3	92.0	2.254	7.565	9.759	7.773	2.224	0.050	723	1.13	0.72	
	8	100	33.208	0.302	26.645	231.2	93.8	2.251	7.581	9.758	7.783	2.216	0.052	716	1.2	0.76	175
	9	74	33.175	0.208	26.622	237.3	93.7	2.249	7.596	9.747	7.803	2.209	0.054	686	1.25	0.79	
	10	51	32.877	0.092	26.388	282.9	91.9	2.236	7.710	9.672	7.928	2.162	0.069	505	1.63	1.02	75
	11	27	32.582	1.651	26.060	319.3	79.5	2.219	7.875	9.575	8.077	2.091	0.098	349	2.34	1.47	
	12	4	31.198	6.622	24.474	342.0	89.6	2.139	8.184	9.191	8.314	1.890	0.172	184	4.18	2.62	91
82-1	1	787	34.135	2.191	27.264	55.2	91.7	2.353	7.454	10.063	7.560	2.354	0.040	1109	0.69	0.48	916
	2	771	34.135	2.191	27.264	55.1	91.9	2.351	7.445	10.045	7.551	2.355	0.039	1135	0.68	0.47	942
	3	731	34.120	2.178	27.253	57.2	94.1	2.349	7.441	10.032	7.551	2.355	0.039	1146	0.69	0.47	898
	4	614	34.035	2.174	27.185	63.0	94.5	2.334	7.432	10.001	7.551	2.342	0.038	1168	0.71	0.48	205
	5	496	33.840	1.878	27.051	91.5	94.2	2.313	7.437	9.943	7.571	2.320	0.038	1131	0.75	0.5	
	6	386	33.617	1.491	26.901	125.4	94.1	2.286	7.447	9.887	7.597	2.290	0.038	1075	0.79	0.52	47
	7	298	33.469	1.124	26.807	148.8	93.9	2.273	7.459	9.837	7.623	2.274	0.039	1022	0.84	0.54	
	8	198	33.315	0.667	26.710	193.7	94.2	2.257	7.520	9.794	7.704	2.240	0.045	852	1	0.64	19
	9	127	33.145	-0.029	26.610	243.7	94.3	2.248	7.606	9.732	7.813	2.205	0.055	660	1.25	0.79	
	10	64	32.768	-1.544	26.360	331.7	93.2	2.225	7.778	9.625	8.024	2.130	0.079	390	1.85	1.17	60
	11	30	32.618	1.166	26.120	344.6	80.6	2.221	7.847	9.594	8.055	2.102	0.092	368	2.2	1.38	
	12	4	31.107	8.379	24.164	315.2	86.9	2.154	8.107	9.240	8.208	1.941	0.150	248	3.66	2.3	49
84-1	1	745	34.106	2.161	27.243	59.9	93.3	2.349	7.436		7.544	2.356	0.038	1160	0.68	0.47	341
	2	732	34.104	2.158	27.241	60.0	93.1	2.349	7.429		7.538	2.358	0.038	1181	0.67	0.46	468
	3	694	34.073	2.130	27.219	63.5	92.7	2.345	7.431		7.544	2.354	0.038	1172	0.68	0.47	223
	4	596	34.008	2.055	27.172	71.8	94.2	2.338	7.434		7.557	2.346	0.038	1158	0.72	0.48	73

LV29, Leg 2 CTD: Water column analysis

St. No	Bot. No	Depth m	S	q, °C	s_0, kg/m³	O_2 CTD mmol/kg	Tr, %	TA mmol/kg	pH_t 15 °C	Ca, mmol/kg	pH_t in situ	DIC, mmol/kg	CO_3, mmol/kg	pCO_2, µatm	Lc	La	CH_4 nl/l
	5	495	33.854	1.872	27.063	92.0	94.1	2.318	7.435		7.569	2.326	0.038	1139	0.74	0.5	111
	6	396	33.595	1.442	26.886	131.4	94.1	2.288	7.449		7.599	2.292	0.039	1068	0.79	0.52	50
	7	299	33.461	1.159	26.798	156.5	94.0	2.272	7.465		7.629	2.271	0.040	1008	0.85	0.55	48
	8	199	33.280	0.369	26.699	202.0	93.8	2.259	7.520		7.708	2.242	0.045	842	1	0.64	31
	9	110	33.020	-0.419	26.527	275.3	93.3	2.242	7.647		7.864	2.187	0.060	582	1.37	0.87	20
	10	59	32.766	0.859	26.257	332.4	90.3	2.228	7.815		8.025	2.120	0.086	395	2.04	1.28	25
	11	31	32.587	2.989	25.960	338.8	76.5	2.221	7.927		8.109	2.073	0.110	323	2.62	1.65	90
	12	4	30.915	7.450	24.143	325.1	87.6	2.125	8.131		8.247	1.905	0.154	220	3.75	2.36	33
87-1	1	46	33.351	-1.697	26.838	313.8	88.2	2.284	7.590	9.760	7.829	2.246	0.053	650	1.27	0.8	84
	2	40	33.350	-1.698	26.837	309.4	88.2	2.284	7.570	9.759	7.808	2.252	0.051	685	1.21	0.76	
	3	36	33.349	-1.697	26.836	305.3	88.5	2.283	7.568	9.757	7.806	2.251	0.051	688	1.21	0.76	
	4	30	33.335	-1.694	26.825	305.9	89.4	2.282	7.576	9.746	7.815	2.248	0.052	674	1.23	0.78	128
	5	25	33.186	-1.697	26.703	299.8	89.6	2.282	7.581	9.740	7.821	2.247	0.052	666	1.25	0.78	
	6	20	33.160	-1.689	26.682	290.2	89.8	2.280	7.566	9.719	7.805	2.249	0.050	692	1.21	0.76	98
	7	15	32.865	-1.455	26.437	317.0	90.0	2.270	7.608	9.659	7.847	2.228	0.055	625	1.32	0.83	
	8	10	31.920	-0.339	25.635	423.2	65.1	2.241	7.977	9.519	8.216	2.075	0.120	247	2.9	1.81	276
	9	4	25.790	10.782	19.651	319.1	80.4	2.007	8.092	8.403	8.156	1.842	0.122	282	3.06	1.9	
	10	4	25.821	10.876	19.660	310.9	80.5	1.868	8.163	7.725	8.225	1.684	0.130	217	3.26	2.02	75
88-2	1	46	33.270	-1.649	26.771	270.7	83.9	2.289	7.491	9.748	7.721	2.281	0.042	846	1.01	0.63	262
	2	40	33.269	-1.656	26.770	267.8	84.2	2.288	7.484	9.747	7.714	2.282	0.042	861	0.99	0.62	275
	3	34	33.259	-1.669	26.762	256.9	84.8	2.288	7.467	9.745	7.697	2.287	0.040	900	0.95	0.6	
	4	30	33.232	-1.665	26.740	255.5	86.7	2.288	7.465	9.728	7.695	2.288	0.040	905	0.95	0.6	221
	5	25	32.957	-1.070	26.500	372.5	91.5	2.274	7.656	9.697	7.891	2.216	0.062	562	1.48	0.93	
	6	19	32.471	-1.600	26.120	367.6	90.6	2.246	7.786	9.575	8.037	2.149	0.080	386	1.94	1.21	385
	7	15	32.096	-1.424	25.811	350.6	88.9	2.221	7.752	9.455	7.999	2.137	0.073	422	1.77	1.11	
	8	10	21.187	10.120	16.175	332.4	66.3	1.826	8.027	7.460	8.099	1.717	0.087	314	2.22	1.34	440
	9	6	17.934	12.161	13.350	312.8	66.7	1.432	8.133	5.435	8.175	1.328	0.078	213	2.03	1.21	
	10	3	16.935	12.893	12.463	308.7	70.2	1.372	8.173	5.177	8.204	1.266	0.079	193	2.08	1.23	123
88-3	1	39	33.258	-1.620	26.761	322.0	86.6	2.286	7.608	9.736	7.847	2.242	0.056	623	1.33	0.83	66
	2	35	33.256	-1.608	26.758	318.6	86.7	2.290	7.601	9.747	7.840	2.248	0.055	636	1.31	0.82	
	3	31	33.090	-1.438	26.619	398.8	90.0	2.279	7.757	9.708	8.003	2.188	0.078	424	1.86	1.17	
	4	25	32.950	-0.797	26.485	493.9	90.6	2.263	8.001	9.673	8.247	2.080	0.129	227	3.1	1.94	44
	10	22	32.796	-0.274	26.339	522.1	91.0	2.248	8.052	9.582	8.290	2.044	0.142	201	3.41	2.14	135
	5	20	32.609	-1.229	26.222	484.2	88.7	2.258	8.023	9.620	8.277	2.068	0.134	210	3.22	2.02	
	6	15	32.357	-1.539	26.027	321.5	81.5	2.233	7.743	9.539	7.991	2.151	0.073	431	1.75	1.1	
	7	9	31.881	-1.039	25.627	369.1	88.6	2.222	7.691	9.476	7.928	2.158	0.064	505	1.54	0.96	846
	8	6	30.319	0.944	24.286	390.0	86.9	2.147	7.855	9.023	8.068	2.038	0.086	351	2.1	1.3	930
	9	3	20.750	9.341	15.942	344.3	55.6	1.753	8.036	7.011	8.121	1.646	0.083	286	2.14	1.29	650
88-4	1	23	33.043	-1.562	26.584	267.9	86.4	2.267	7.517	9.684	7.750	2.251	0.044	787	1.07	0.67	292
	2	20	32.978	-1.599	26.532	264.1	85.8	2.260	7.509	9.666	7.742	2.247	0.043	801	1.04	0.65	441
	3	15	32.871	-1.547	26.444	284.0	86.8	2.250	7.517	9.640	7.750	2.235	0.044	783	1.06	0.66	579
	4	10	32.665	-1.583	26.278	282.0	86.1	2.247	7.574	9.619	7.812	2.215	0.050	674	1.21	0.76	525
	5	6	31.777	1.419	25.427	470.5	88.5	2.229	7.767	9.523	7.970	2.141	0.076	464	1.85	1.16	361
	6	3	29.502	6.577	23.143	376.3	82.6	2.111	8.043	8.957	8.172	1.938	0.125	271	3.06	1.91	115
88-5	1	21	33.028	-1.290	26.564	376.3	87.9	2.279	7.757	9.684	8.002	2.188	0.078	427	1.86	1.17	69
	2	16	33.017	-1.255	26.555	377.6	88.7	2.278	7.766	9.699	8.011	2.184	0.079	418	1.9	1.19	102
	3	11	32.885	-0.762	26.431	434.2	90.4	2.270	7.887	9.673	8.130	2.134	0.102	310	2.47	1.55	81
	4	7	32.600	-0.332	26.184	491.5	89.5	2.253	8.006	9.622	8.246	2.071	0.129	228	3.13	1.96	104
	5	3	30.490	7.168	23.847	394.8	87.0	2.210	8.072	9.385	8.192	2.013	0.142	267	3.46	2.17	142
90-1	1	60	33.343	-1.697	26.831	343.2	86.1	2.282	7.663	9.776	7.906	2.221	0.063	536	1.49	0.94	47
	2	54	33.343	-1.696	26.832	341.6	86.1	2.281	7.691	9.767	7.936	2.211	0.067	498	1.59	1	
	3	45	33.342	-1.694	26.830	337.8	86.2	2.282	7.655	9.771	7.898	2.223	0.062	548	1.47	0.93	52
	4	35	33.334	-1.692	26.824	334.8	86.9	2.283	7.655	9.782	7.899	2.224	0.062	548	1.48	0.93	
	5	29	33.315	-1.676	26.808	333.8	88.7	2.280	7.662	9.770	7.907	2.219	0.063	538	1.5	0.94	42
	6	24	33.237	-1.573	26.742	349.1	91.8	2.281	7.686	9.756	7.931	2.213	0.066	508	1.59	1	
	7	20	33.109	-1.330	26.631	425.4	92.0	2.273	7.886	9.716	8.137	2.136	0.103	302	2.46	1.54	34
	8	15	32.915	0.380	26.404	484.6	91.7	2.269	7.946	9.688	8.172	2.109	0.116	279	2.8	1.75	
	9	10	30.771	3.894	24.434	451.3	89.8	2.222	8.096	9.479	8.268	2.012	0.149	217	3.62	2.26	35
	10	7	29.483	9.375	22.746	333.0	84.1	2.004	8.092	8.417	8.177	1.818	0.132	255	3.22	2.02	35
	11	3	26.671	10.415	20.394	324.7	80.9	1.975	8.091	8.241	8.160	1.807	0.122	271	3.04	1.89	62
91-1	1	102	33.304	-1.698	26.799	352.0	84.1	2.278	7.684	9.756	7.925	2.210	0.066	506	1.53	0.97	97
	2	95	33.305	-1.699	26.800	347.2	84.6	2.282	7.680	9.757	7.921	2.216	0.065	512	1.52	0.96	
	3	80	33.305	-1.700	26.800	342.1	84.7	2.278	7.679	9.759	7.921	2.212	0.065	513	1.52	0.96	90
	4	64	33.300	-1.703	26.797	337.7	86.4	2.281	7.676	9.759	7.919	2.216	0.065	518	1.53	0.96	
	5	54	33.281	-1.705	26.781	332.8	88.4	2.271	7.667	9.741	7.911	2.209	0.063	528	1.5	0.94	76
	6	45	33.253	-1.696	26.758	331.8	90.8	2.267	7.670	9.745	7.914	2.204	0.064	523	1.51	0.95	
	7	36	33.196	-1.629	26.710	331.2	90.6	2.267	7.676	9.727	7.920	2.202	0.064	517	1.54	0.97	60
	8	24	33.147	-1.512	26.667	351.7	90.0	2.266	7.719		7.965	2.188	0.071	464	1.7	1.07	
	9	20	33.109	-1.403	26.633	372.2	90.2	2.266	7.779	9.713	8.027	2.168	0.081	399	1.95	1.22	48
	10	13	33.034	-0.403	26.538	496.5	92.0	2.268	8.057	9.682	8.299	2.059	0.145	199	3.5	2.19	
	11	8	32.598	1.942	26.051	506.2	90.2	2.253	8.100	9.583	8.304	2.027	0.157	196	3.79	2.37	55
	12	3	25.378	12.921	18.967	321.5	85.2	1.993	8.180	8.303	8.211	1.797	0.144	243	3.61	2.25	46
92-1	1	91	33.330	-1.673	26.820	326.2	82.1	2.283	7.655	9.762	7.894	2.224	0.062	548	1.44	0.91	528
	2	90	33.330	-1.673	26.820	325.7	82.2										
	3	80	33.329	-1.672	26.820	319.2	82.5	2.275	7.649	9.775	7.889	2.218	0.061	555	1.42	0.9	561
	4	69	33.328	-1.670	26.818	314.4	82.5	2.271	7.647	9.765	7.887	2.215	0.061	557	1.42	0.9	
	5	59	33.268	-1.621	26.768	308.1	87.8	2.264	7.638	9.746	7.878	2.211	0.059	570	1.39	0.88	438
	6	50	33.180	-1.537	26.695	297.7	93.0	2.265	7.624	9.726	7.862	2.217	0.057	594	1.35	0.85	
	7	40	33.165	-1.390	26.678	288.9	93.5	2.256	7.616	9.730	7.852	2.210	0.056	609	1.33	0.84	81
	8	31	33.144	-1.429	26.663	295.3	93.0	2.253	7.629	9.719	7.867	2.203	0.058	587	1.37	0.86	
	9	20	33.088	-1.448	26.618	301.7	86.8	2.254	7.649	9.707	7.890	2.198	0.060	557	1.45	0.91	47
	10	14	33.048	-1.417	26.584	309.7	86.6	2.253	7.671	9.689	7.913	2.191	0.063	526	1.52	0.95	
	11	9	32.954	-0.921	26.492	406.6	77.9	2.253	7.901	9.670	8.147	2.112	0.105	294	2.53	1.58	63
	12	3	31.191	2.865	24.856	409.8	83.2	2.192	8.057	9.359	8.246	1.999	0.137	227	3.33	2.08	49
94-4	1	1115	34.371	2.307	27.443	30.6	87.8	2.388	7.431	10.146	7.505	2.397	0.038	1195	0.58	0.41	12
	2	1102	34.370	2.305	27.442	30.6	91.6	2.387	7.430	10.141	7.505	2.396	0.038	1197	0.58	0.42	14

LV29, Leg 2 CTD: Water column analysis

St. No	Bot. No	Depth m	S	q, °C	s_0, kg/m³	O_2 CTD mmol/kg	Tr, %	TA mmol/kg	pH_t 15 °C	Ca, mmol/kg	pH_t in situ	DIC, mmol/kg	CO_3, mmol/kg	pCO_2, µatm	Lc	La	CH_4 nl/l
	3	1067	34.346	2.294	27.424	32.9	93.8	2.386	7.430	10.116	7.508	2.395	0.038	1197	0.59	0.42	12
	4	991	34.209	2.267	27.316	45.3	94.3	2.365	7.420	10.080	7.504	2.377	0.037	1218	0.59	0.42	12
	5	843	34.132	2.203	27.260	55.4	94.2	2.356	7.423	10.057	7.521	2.367	0.037	1204	0.63	0.44	57
	6	696	34.080	2.165	27.221	61.7	94.2	2.348	7.425	10.039	7.537	2.359	0.037	1194	0.67	0.46	31
	7	545	33.862	1.958	27.064	90.9	94.5	2.319	7.431	9.952	7.559	2.328	0.038	1155	0.72	0.48	13
	8	396	33.581	1.301	26.885	139.6	94.4	2.285	7.451	9.875	7.603	2.288	0.039	1055	0.79	0.52	15
	9	249	33.412	1.096	26.763	177.7	94.2	2.271	7.498	9.819	7.670	2.260	0.043	923	0.94	0.61	15
	10	101	33.080	0.123	26.551	277.4	93.7	2.252	7.658	9.711	7.868	2.194	0.062	582	1.43	0.9	31
	11	46	32.745	-1.114	26.330	348.6	91.8	2.231	7.789	9.621	8.030	2.132	0.081	388	1.92	1.21	46
	12	3	32.498	8.422	25.247	312.6	89.3	2.222	8.044	9.542	8.144	2.025	0.141	301	3.41	2.15	44
103-4	1	1740	34.436	2.246	27.500	14.3	94.3	2.409	7.413	10.172	7.431	2.423	0.035	1251	0.42	0.32	91
	2	1719	34.436	2.246	27.500	14.3	94.4	2.409	7.419	10.174	7.439	2.422	0.036	1231	0.43	0.33	155
	3	1639	34.436	2.246	27.500	15.3	94.4	2.407	7.421	10.172	7.448	2.419	0.036	1225	0.45	0.34	70
	4	1482	34.432	2.238	27.498	21.6	95.0	2.401	7.430	10.165	7.472	2.410	0.037	1195	0.49	0.37	25
	5	1237	34.412	2.261	27.480	26.3	95.0	2.392	7.434	10.161	7.498	2.400	0.038	1183	0.55	0.4	16
	6	990	34.346	2.337	27.421	27.8	95.0	2.382	7.421	10.136	7.504	2.394	0.037	1227	0.6	0.42	16
	7	743	34.186	2.333	27.293	39.9	95.0	2.358	7.408	10.070	7.512	2.374	0.036	1260	0.64	0.44	25
	8	496	33.867	1.917	27.070	88.2	94.8	2.317	7.424	9.981	7.557	2.328	0.037	1173	0.72	0.48	17
	9	297	33.533	1.148	26.856	139.5	94.6	2.278	7.427	9.870	7.588	2.288	0.037	1114	0.78	0.51	34
	10	150	33.311	0.691	26.706	201.2	94.6	2.258	7.512	9.794	7.699	2.243	0.044	872	1	0.64	33
	11	69	32.824	-1.703	26.410	345.4	94.3	2.230	7.760	9.648	8.008	2.140	0.076	407	1.78	1.12	43
	12	3	32.104	10.624	24.587	284.6	90.5	2.192	8.051	9.427	8.117	1.996	0.141	321	3.42	2.16	36
104-4	1	1754	34.436	2.246	27.500	13.1	94.4	2.408	7.419	10.184	7.436	2.421	0.036	1230	0.42	0.33	7
	2	1734	34.436	2.246	27.500	13.0	94.4	2.408	7.418	10.189	7.437	2.421	0.036	1234	0.42	0.33	7
	3	1655	34.436	2.246	27.500	13.1	94.5	2.407	7.416	10.180	7.441	2.420	0.036	1241	0.44	0.34	8
	4	1557	34.436	2.245	27.500	13.8	94.8	2.406	7.415	10.172	7.449	2.420	0.036	1245	0.46	0.35	31
	5	1384	34.426	2.241	27.492	23.5	95.1	2.397	7.427	10.162	7.477	2.407	0.037	1204	0.51	0.38	23
	6	1187	34.405	2.269	27.473	25.9	95.1	2.389	7.431	10.153	7.499	2.397	0.038	1192	0.56	0.4	12
	7	940	34.320	2.352	27.399	28.2	95.0	2.377	7.420	10.121	7.507	2.389	0.037	1229	0.61	0.43	17
	8	694	34.151	2.321	27.266	43.2	94.9	2.353	7.410	10.060	7.519	2.368	0.036	1251	0.65	0.45	17
	9	396	33.710	1.719	26.959	114.6	94.7	2.295	7.438	9.918	7.583	2.302	0.038	1114	0.77	0.51	12
	10	198	33.392	0.856	26.761	172.2	94.6	2.262	7.467	9.830	7.644	2.261	0.040	988	0.89	0.57	27
	11	75	32.829	-1.696	26.413	341.8	94.2	2.227	7.754	9.646	8.001	2.139	0.075	413	1.75	1.1	56
	12	3	32.308	10.215	24.815	288.6	89.4	2.201	8.039	9.500	8.111	2.009	0.139	326	3.36	2.13	37
106-4	1	502	33.758	2.017	26.975	106.2	87.8	2.309	7.448	9.919	7.580	2.313	0.039	1104	0.76	0.51	62
	2	491	33.758	2.016	26.975	105.9	88.8	2.308	7.447	9.929	7.580	2.312	0.039	1107	0.76	0.51	69
	3	445	33.664	1.885	26.910	133.2	94.1	2.296	7.481	9.900	7.623	2.290	0.042	1004	0.84	0.56	
	4	396	33.566	1.704	26.845	156.5	94.8	2.285	7.508	9.870	7.659	2.271	0.044	926	0.91	0.6	44
	5	346	33.495	1.661	26.791	172.3	94.8	2.277	7.525	9.868	7.682	2.258	0.046	882	0.96	0.63	
	6	296	33.427	1.584	26.742	193.0	94.8	2.269	7.554	9.819	7.718	2.241	0.049	814	1.05	0.68	71
	7	248	33.374	1.536	26.702	210.3	94.7	2.266	7.578	9.816	7.749	2.231	0.052	763	1.13	0.73	
	8	198	33.307	1.405	26.658	233.4	94.8	2.257	7.611	9.793	7.790	2.212	0.056	695	1.24	0.8	73
	9	119	33.140	0.736	26.565	293.9	94.5	2.247	7.689	9.725	7.890	2.179	0.066	549	1.52	0.97	
	10	70	33.006	0.684	26.461	320.8	94.0	2.244	7.752		7.961	2.156	0.076	465	1.78	1.13	66
	11	29	32.833	6.868	25.730	324.4	86.0	2.242	8.121	9.660	8.244	2.005	0.166	229	3.95	2.5	44
	12	3	32.857	9.163	25.415	298.9	89.7	2.237	8.140	9.654	8.230	1.991	0.173	240	4.16	2.63	51
108-2	1	609	33.868	2.155	27.053	90.0	90.9	2.322	7.439	9.960	7.559	2.328	0.038	1141	0.72	0.48	84
	2	584	33.864	2.150	27.050	89.8	91.2	2.321	7.436	9.969	7.558	2.328	0.038	1149	0.72	0.48	81
	3	545	33.837	2.115	27.031	97.1	94.2	2.317	7.445	9.954	7.572	2.322	0.039	1120	0.75	0.5	
	4	446	33.642	1.836	26.896	138.4	94.6	2.292	7.480	9.889	7.622	2.286	0.042	1003	0.83	0.55	56
	5	346	33.494	1.656	26.791	171.3	94.5	2.277	7.515	9.844	7.671	2.261	0.045	905	0.94	0.61	
	6	299	33.437	1.592	26.749	190.7	94.6	2.272	7.543	9.822	7.706	2.248	0.048	839	1.02	0.66	59
	7	248	33.376	1.520	26.706	213.3	94.6	2.267	7.579	9.799	7.750	2.232	0.052	761	1.13	0.73	
	8	197	33.307	1.425	26.657	230.4	94.6	2.259	7.602	9.785	7.780	2.217	0.055	712	1.22	0.78	58
	9	150	33.210	1.067	26.602	266.1	94.5	2.252	7.647	9.743	7.838	2.197	0.060	623	1.37	0.87	
	10	70	33.028	0.771	26.474	311.6	94.0	2.245	7.736	9.729	7.943	2.162	0.073	487	1.72	1.09	66
	11	30	32.842	4.140	26.056	326.7	86.2	2.244	8.030	9.672	8.196	2.050	0.138	260	3.28	2.07	
	12	2	32.806	9.140	25.379	294.1	89.6	2.236	8.112	9.660	8.202	2.004	0.164	259	3.94	2.49	48
110-2	1	1207	34.449	2.220	27.513	46.5	90.7	2.393	7.462	10.169	7.531	2.391	0.041	1098	0.6	0.43	22
	2	1188	34.449	2.219	27.513	46.5	91.1	2.391	7.461	10.179	7.532	2.390	0.041	1101	0.6	0.44	21
	3	1088	34.415	2.292	27.480	44.6	94.1	2.388	7.452	10.157	7.530	2.390	0.040	1130	0.61	0.44	15
	4	940	34.346	2.393	27.416	40.5	93.8	2.378	7.442	10.146	7.531	2.383	0.039	1163	0.64	0.45	88
	5	692	34.009	2.303	27.154	76.1	94.3	2.335	7.434	10.013	7.545	2.343	0.038	1167	0.69	0.47	91
	6	494	33.699	1.913	26.936	136.3	94.3	2.298	7.487	9.911	7.625	2.290	0.042	990	0.83	0.55	68
	7	347	33.508	1.592	26.807	180.8	94.0	2.277	7.527	9.860	7.685	2.257	0.046	875	0.96	0.63	42
	8	199	33.370	1.615	26.694	233.8	94.1	2.267	7.614	9.799	7.790	2.221	0.057	698	1.26	0.81	46
	9	140	33.265	1.142	26.641	261.9	93.9	2.257	7.639	9.760	7.829	2.204	0.060	639	1.36	0.86	54
	10	94	33.192	1.666	26.547	283.7	93.7	2.256	7.701	9.752	7.890	2.184	0.069	557	1.6	1.01	59
	11	30	32.940	6.460	25.868	326.3	85.4	2.246	7.970	9.671	8.098	2.077	0.123	339	2.94	1.86	54
	12	3	32.875	7.452	25.683	330.5	78.0	2.236	8.032	9.642	8.147	2.042	0.139	299	3.36	2.12	58
112-5	1	1365	34.474	2.163	27.537	46.4	90.2	2.393	7.463	10.162	7.519	2.391	0.041	1090	0.56	0.41	22
	2	1345	34.469	2.175	27.533	46.5	91.6	2.391	7.465	10.165	7.523	2.388	0.041	1085	0.56	0.42	19
	3	1237	34.450	2.230	27.513	43.3	92.5	2.388	7.457	10.150	7.523	2.388	0.040	1110	0.58	0.42	21
	4	1039	34.353	2.410	27.420	41.5	94.6	2.373	7.436	10.115	7.515	2.380	0.038	1178	0.6	0.43	15
	5	843	34.204	2.451	27.298	49.7	94.7	2.358	7.430	10.066	7.525	2.367	0.038	1195	0.64	0.45	16
	6	645	33.950	2.227	27.112	85.2	94.6	2.326	7.432	9.978	7.548	2.335	0.038	1166	0.69	0.47	21
	7	496	33.709	1.934	26.942	142.1	94.6	2.298	7.494	9.911	7.632	2.288	0.043	973	0.85	0.56	36
	8	347	33.526	1.698	26.813	184.5	94.6	2.280	7.540	9.854	7.697	2.256	0.048	851	1	0.65	43
	9	199	33.399	1.602	26.718	222.8	94.5	2.268	7.593	9.808	7.768	2.229	0.054	737	1.2	0.77	50
	10	100	33.286	1.542	26.632	257.4	94.3	2.257	7.650	9.783	7.838	2.200	0.061	633	1.42	0.9	64
	11	49	33.076	3.361	26.317	302.6	92.5	2.249	7.796	9.718	7.966	2.146	0.085	468	2.01	1.27	53
	12	3	32.830	7.615	25.625	308.5	84.8	2.231	7.976	9.645	8.088	2.061	0.124	349	3	1.89	59
114-4	1	1756	34.567	1.820	27.639	71.1	93.3	2.410	7.523	10.191	7.556	2.396	0.046	920	0.54	0.42	9
	2	1733	34.557	1.860	27.628	68.5	93.9	2.408	7.520	10.181	7.554	2.389	0.046	927	0.54	0.42	10
	3	1627	34.528	1.983	27.595	59.6	94.6	2.403	7.502	10.172	7.542	2.390	0.044	977	0.54	0.42	10
	4	1384	34.494	2.104	27.558	51.9	94.9	2.397	7.480	10.153	7.537	2.391	0.042	1042	0.58	0.43	12
	5	1138	34.430	2.342	27.487	39.3	94.8	2.390	7.452	10.127	7.525	2.399	0.040	1136	0.6	0.44	11
	6	842	34.257	2.476	27.338	39.8	94.8	2.365	7.419	10.087	7.513	2.378	0.037	1235	0.63	0.44	19

LV29, Leg 2 CTD: Water column analysis

St. No	Bot. No	Depth m	S	q, °C	s_0, kg/m³	O_2 CTD mmol/kg	Tr, %	TA mmol/kg	pH_t 15 °C	Ca, mmol/kg	pH_t in situ	DIC, mmol/kg	CO_3, mmol/kg	pCO_2, µatm	Lc	La	CH_4 nl/l
	7	595	33.946	2.254	27.107	83.2	94.7	2.325	7.433	9.984	7.553	2.334	0.038	1165	0.71	0.48	23
	8	390	33.582	1.756	26.854	167.5	94.5	2.285	7.517	9.878	7.668	2.269	0.045	907	0.93	0.61	36
	9	290	33.508	2.142	26.765	199.7	94.5	2.279	7.590	9.841	7.749	2.241	0.054	763	1.15	0.75	46
	10	99	33.335	1.863	26.648	244.8	94.4	2.263	7.648	9.785	7.831	2.208	0.061	647	1.42	0.9	58
	11	52	33.030	0.990	26.462	305.7	93.7	2.243	7.727	9.708	7.931	2.164	0.072	504	1.7	1.07	64
	12	3	32.540	7.620	25.397	317.1	84.6	2.216	7.988	9.562	8.100	2.044	0.126	337	3.04	1.92	57
115-1	1	2011	34.577	1.763	27.651	76.24	94.8	2.408	7.551	10.187	7.566	2.379	0.049	846	0.51	0.41	4
	2	1925	34.570	1.794	27.643	73.71	94.7	2.407	7.545	10.184	7.566	2.380	0.048	862	0.53	0.42	4
	3	1728	34.547	1.892	27.618	66.24	94.8	2.403	7.527	10.187	7.562	2.382	0.047	909	0.55	0.43	5
	4	1433	34.517	1.997	27.585	57.60	94.9	2.398	7.506	10.173	7.563	2.383	0.045	968	0.6	0.45	5
	5	1234	34.451	2.159	27.520	47.42	94.9	2.388	7.481	10.151	7.551	2.381	0.043	1040	0.62	0.45	6
	6	989	34.308	2.326	27.391	43.47	94.9	2.364	7.444	10.152	7.529	2.369	0.039	1147	0.62	0.44	8
	7	742	34.072	2.297	27.205	56.88	94.9	2.341	7.421	10.039	7.526	2.354	0.037	1209	0.65	0.45	9
	8	495	33.687	1.997	26.920	149.62	94.6	2.294	7.521	9.917	7.660	2.277	0.046	908	0.9	0.6	28
	9	297	33.537	1.797	26.815	183.92	94.5	2.281	7.559	9.854	7.720	2.252	0.050	815	1.07	0.7	42
	10	99	33.379	2.068	26.668	226.24	94.1	2.266	7.636	9.811	7.815	2.214	0.060	674	1.39	0.88	56
	11	51	33.212	2.275	26.518	263.73	93.6	2.257	7.693	9.752	7.876	2.188	0.068	586	1.6	1.01	63
	12	3	32.824	5.526	25.890	317.92	84.5	2.228	7.895	9.640	8.038	2.092	0.105	394	2.52	1.59	58
116-2	1	3284	34.623	1.577	27.702	96.46	94.5	2.416	7.591	10.208	7.503	2.374	0.050	743	0.32	0.3	10
	2	3265	34.620	1.594	27.698	93.31	94.6	2.416	7.580	10.208	7.492	2.377	0.049	766	0.32	0.29	8
	3	2956	34.612	1.628	27.690	87.82	94.8	2.415	7.573	10.207	7.511	2.379	0.049	785	0.36	0.32	4
	4	2564	34.601	1.676	27.677	80.00	94.9	2.414	7.557	10.199	7.526	2.383	0.048	825	0.41	0.35	5
	5	2170	34.572	1.785	27.645	70.92	94.9	2.409	7.543	10.192	7.543	2.381	0.047	863	0.47	0.38	5
	6	1776	34.528	1.930	27.599	58.90	94.9	2.402	7.505	10.173	7.533	2.388	0.044	965	0.51	0.4	4
	7	1384	34.439	2.114	27.513	50.29	94.9	2.391	7.487	10.151	7.545	2.382	0.043	1021	0.58	0.43	7
	8	987	34.118	2.305	27.240	58.28	94.8	2.349	7.429	10.042	7.513	2.358	0.037	1185	0.6	0.42	11
	9	593	33.565	1.655	26.847	165.40	94.5	2.282	7.517	9.856	7.652	2.266	0.045	899	0.84	0.57	37
	10	298	33.415	1.458	26.741	210.20	94.3	2.268	7.579	9.811	7.747	2.234	0.052	759	1.11	0.72	45
	11	99	33.209	0.965	26.607	274.18	94.3	2.253	7.662	9.735	7.859	2.194	0.063	598	1.45	0.92	51
	12	3	32.830	5.149	25.938	318.12	87.0	2.234	7.881	9.635	8.030	2.103	0.102	404	2.45	1.54	65
120-1	1	3280	34.620	1.588	27.699	94.64	94.7	2.416	7.607	10.207	7.521	2.368	0.052	712	0.33	0.31	11
	2	3249	34.618	1.600	27.696	91.70	94.6	2.417	7.584	10.207	7.498	2.377	0.050	759	0.32	0.3	14
	3	3177	34.616	1.614	27.693	87.81	94.8	2.416	7.573	10.208	7.492	2.379	0.048	782	0.32	0.3	15
	4	2760	34.605	1.660	27.681	79.74	95.0	2.415	7.558	10.213	7.510	2.383	0.048	820	0.37	0.33	9
	5	2367	34.588	1.723	27.663	74.64	95.0	2.413	7.542	10.199	7.526	2.387	0.047	863	0.43	0.36	8
	6	1975	34.563	1.815	27.636	67.04	95.0	2.409	7.529	10.192	7.544	2.387	0.046	900	0.5	0.4	7
	7	1581	34.510	1.961	27.582	55.81	95.0	2.399	7.501	10.171	7.545	2.386	0.044	978	0.55	0.42	8
	8	1138	34.369	2.182	27.452	44.74	95.0	2.381	7.453	10.133	7.528	2.383	0.040	1119	0.6	0.43	10
	9	744	34.068	2.193	27.210	57.98	94.8	2.343	7.417	10.017	7.523	2.357	0.037	1218	0.65	0.44	13
	10	297	33.421	0.986	26.777	191.49	94.2	2.264	7.528	9.820	7.699	2.245	0.046	847	0.98	0.64	57
	11	115	33.182	0.647	26.604	256.72	94.1	2.249	7.647	9.745	7.847	2.194	0.060	611	1.39	0.88	93
	12	3	32.617	5.949	25.676	325.56	80.5	2.218	7.963	9.596	8.101	2.055	0.119	334	2.88	1.81	92
123-1	1	3321	34.611	1.635	27.688	82.89	94.7	2.418	7.595	10.206	7.504	2.373	0.051	737	0.32	0.3	8
	2	3296	34.611	1.637	27.688	82.61	94.8	2.419	7.578	10.212	7.487	2.380	0.049	772	0.31	0.29	5
	3	2956	34.607	1.650	27.684	80.76	95.0	2.414	7.570	10.211	7.507	2.377	0.049	791	0.35	0.32	5
	4	2466	34.599	1.682	27.675	77.39	95.0	2.413	7.559	10.211	7.537	2.380	0.048	821	0.43	0.36	4
	5	1973	34.564	1.812	27.637	66.08	95.0	2.410	7.537	10.207	7.553	2.384	0.047	881	0.51	0.4	6
	6	1482	34.500	2.021	27.569	50.20	95.0	2.398	7.497	10.182	7.548	2.385	0.044	991	0.57	0.43	9
	7	1047	34.343	2.207	27.429	43.35	94.8	2.377	7.453	10.136	7.536	2.378	0.040	1119	0.62	0.44	8
	8	951	34.270	2.303	27.362	40.18	95.0	2.368	7.435	10.097	7.523	2.375	0.038	1175	0.62	0.44	6
	9	496	33.746	1.802	26.982	130.82	94.7	2.299	7.492	9.936	7.631	2.289	0.043	973	0.84	0.56	31
	10	198	33.334	0.717	26.723	208.40	94.3	2.260	7.550	9.800	7.735	2.234	0.048	791	1.07	0.69	50
	11	73	33.002	-0.474	26.515	295.52	94.4	2.238	7.699	9.688	7.923	2.167	0.067	506	1.57	0.99	157
	12	3	32.380	9.019	25.065	294.63	85.5	2.210	8.034	9.499	8.125	2.019	0.138	315	3.33	2.1	131
131-4	1	749	34.134	2.241	27.259	51.41	93.0	2.353	7.415		7.520	2.367	0.037	1231	0.65	0.44	225
	2	731	34.093	2.213	27.229	55.79	93.3	2.349	7.415		7.522	2.363	0.036	1228	0.65	0.45	433
	3	692	34.068	2.186	27.211	59.52	94.1	2.347	7.416		7.527	2.361	0.037	1223	0.66	0.45	433
	4	594	33.922	1.991	27.109	83.50	94.4	2.328	7.423		7.546	2.339	0.037	1184	0.69	0.47	40
	5	494	33.727	1.626	26.980	126.22	94.4	2.303	7.467		7.607	2.301	0.041	1032	0.79	0.53	70
	6	397	33.591	1.325	26.892	151.98	94.3	2.285	7.480		7.634	2.279	0.041	980	0.85	0.56	83
	7	297	33.411	0.727	26.784	176.29	94.0	2.270	7.481		7.653	2.264	0.041	949	0.88	0.57	85
	8	198	33.262	-0.081	26.707	228.97	93.8	2.262	7.546		7.743	2.237	0.048	773	1.06	0.68	54
	9	99	33.067	-0.893	26.583	287.10	94.3	2.247	7.645		7.870	2.193	0.059	574	1.38	0.87	184
	10	67	32.920	-1.135	26.472	315.11	94.2	2.236	7.707		7.943	2.163	0.068	481	1.6	1.01	256
	11	30	32.594	1.306	26.092	334.11	90.4	2.223	7.842		8.048	2.106	0.091	376	2.18	1.37	200
	12	2	31.934	12.908	24.037	273.28	90.2	2.193	8.068		8.099	1.991	0.147	338	3.56	2.26	82

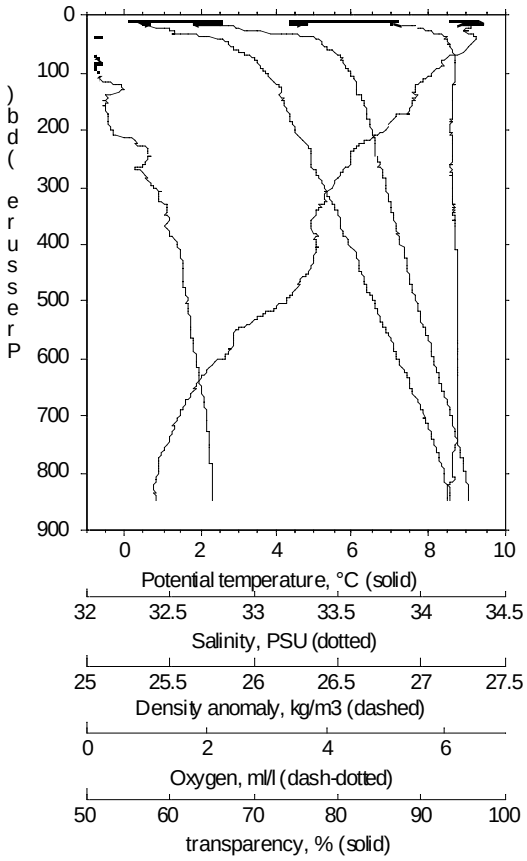

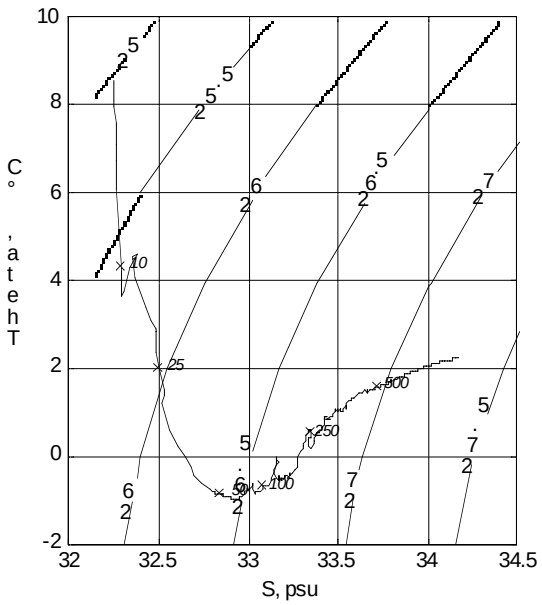

** Station: LV29-69/4
Time = Jul 02 2002 02:57:47
** Latitude: 45 26.826
** Longitude: 144 04.404
File : LV29-69U.CNV

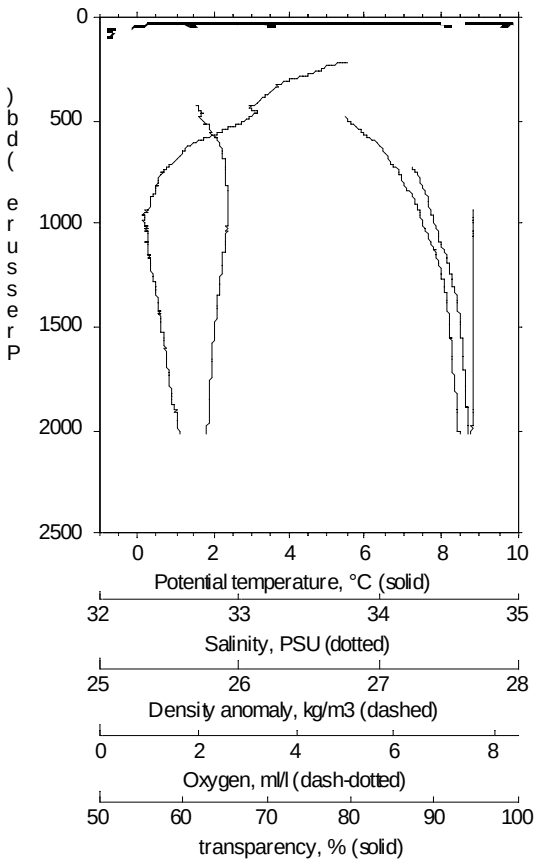

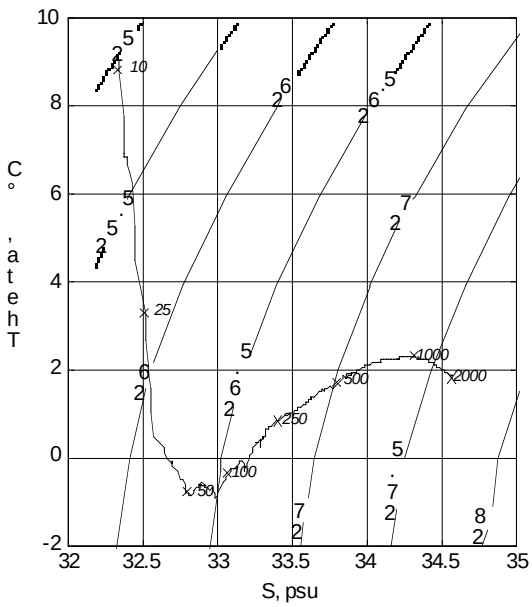

** Station: LV29-70/4
Time = Jul 03 2002 08:02:57
** Latitude: 48 01.790
** Longitude: 146 08.080
File : LV29-70D.CNV

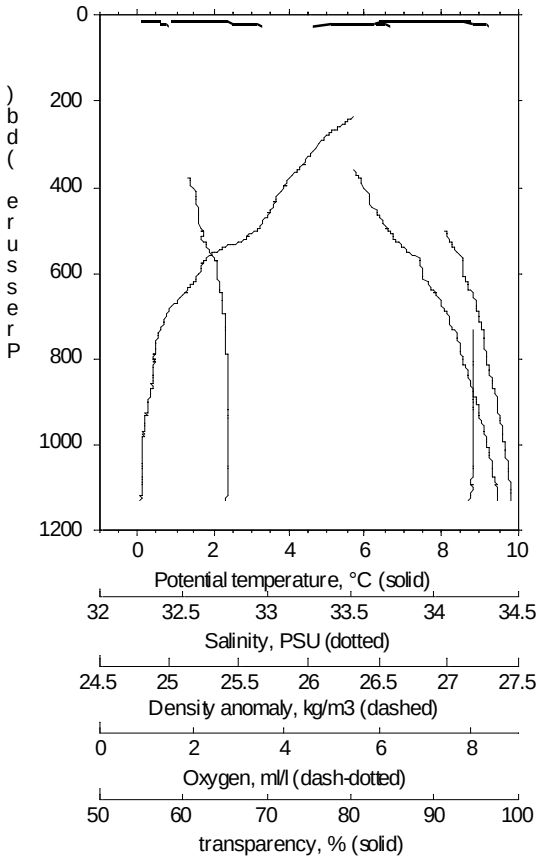

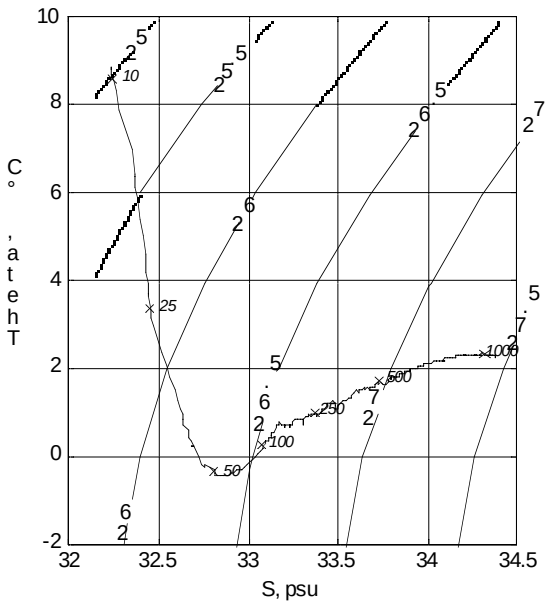

** Station: LV29-72/4
Time = Jul 04 2002 03:10:51
** Latitude: 48 38.840
** Longitude: 146 07.185
File : LV29-72D.CNV

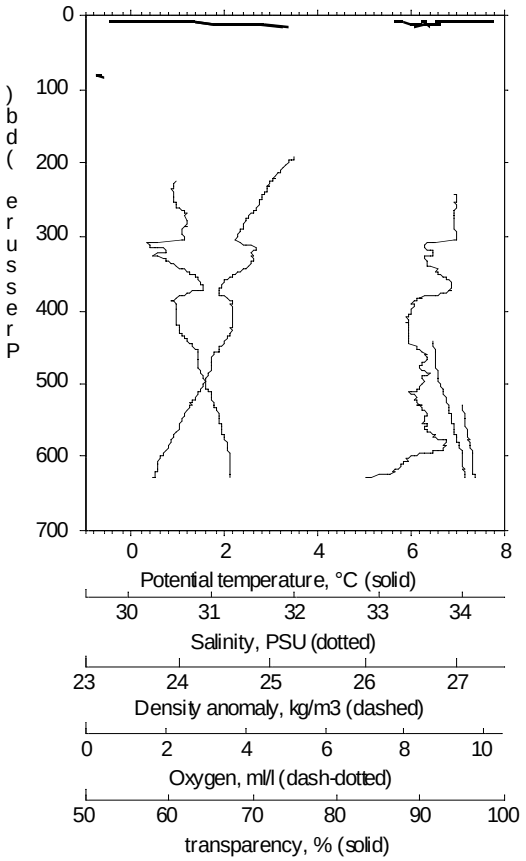

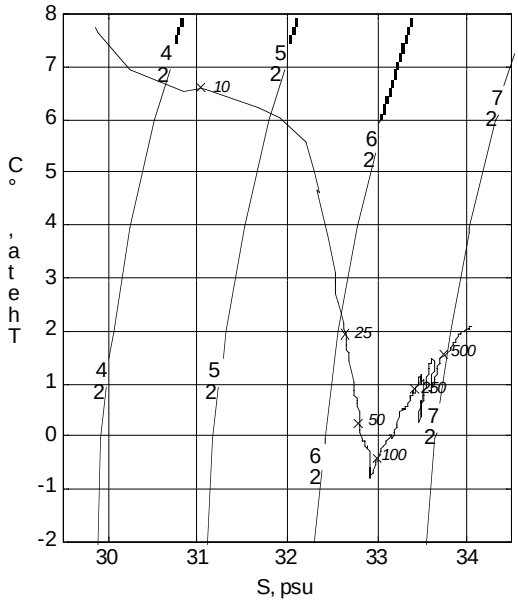

** Station: LV29-76/3
Time = Jul 06 2002 07:43:21
** Latitude: 52 40.356
** Longitude: 144 39.585
File : LV29-76D.CNV

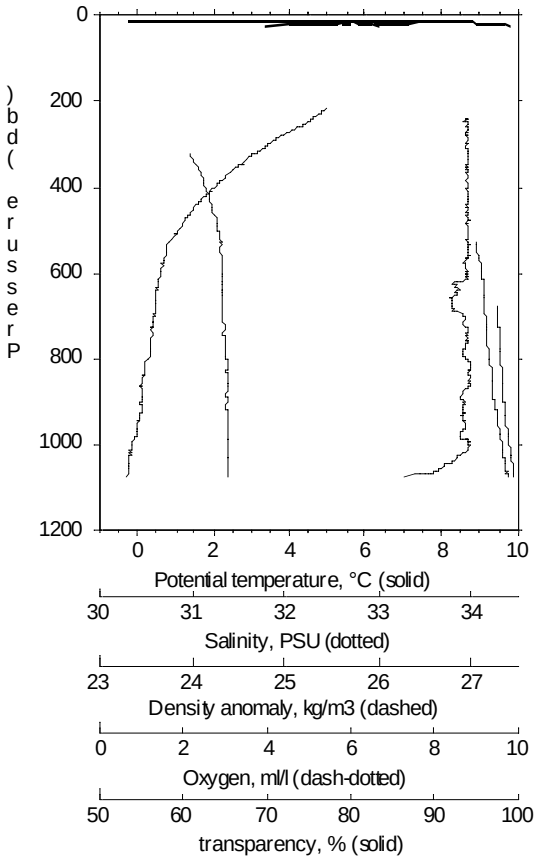

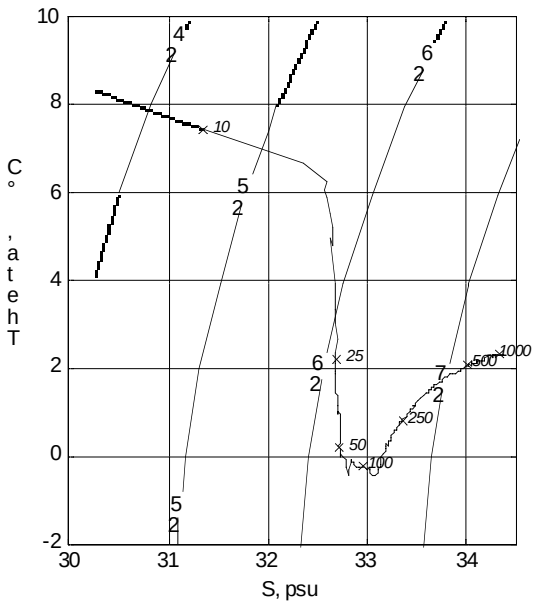

** Station: LV29-79/1
Time = Jul 07 2002 03:31:31
** Latitude: 52 47.355
** Longitude: 144 56.947
File : LV29-79D.CNV

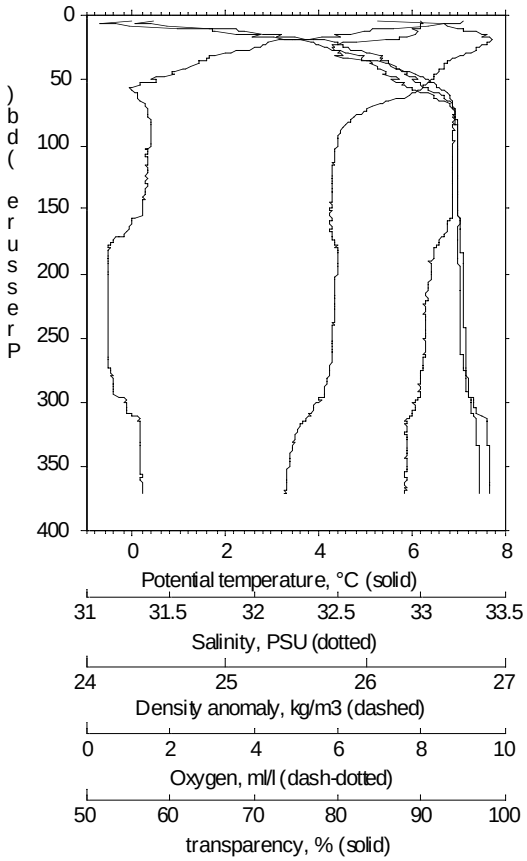

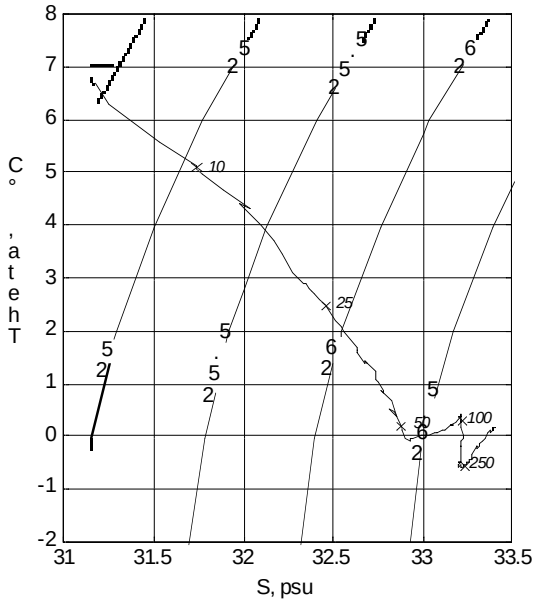

** Station: LV29-81/2
Time = Jul 08 2002 02:12:40
** Latitude: 53 59.632
** Longitude: 143 58.038
File : LV29-81D.CNV

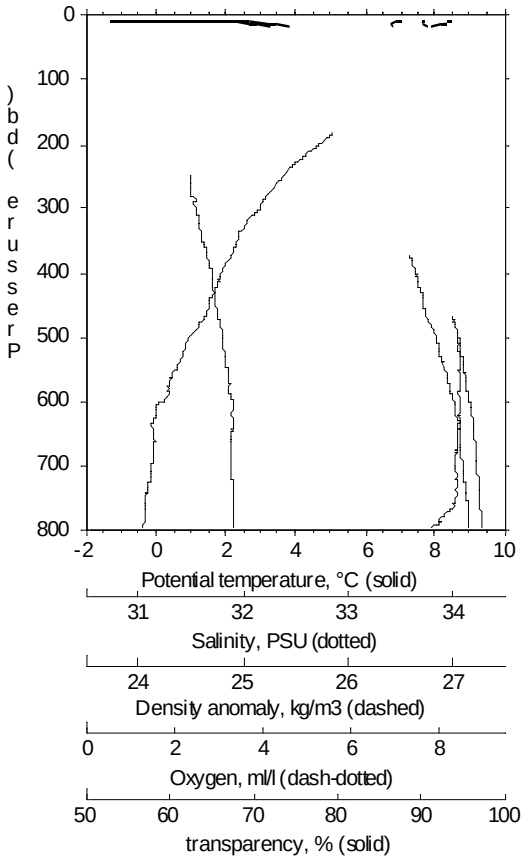

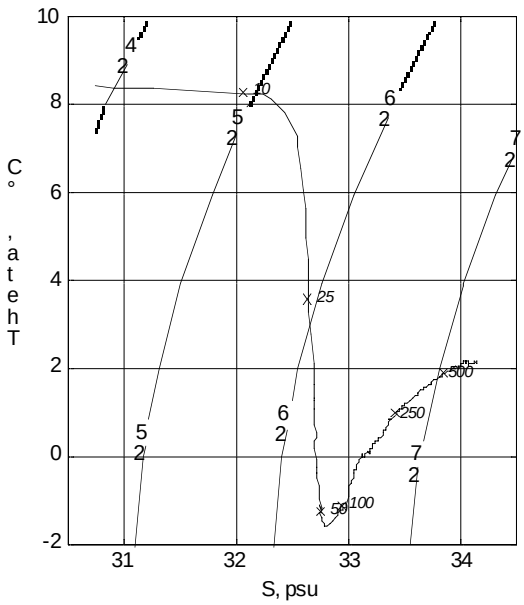

** Station: LV29-82/3
Time = Jul 08 2002 06:17:30
** Latitude: 54 17.712
** Longitude: 144 11.152
File : LV29-82D.CNV

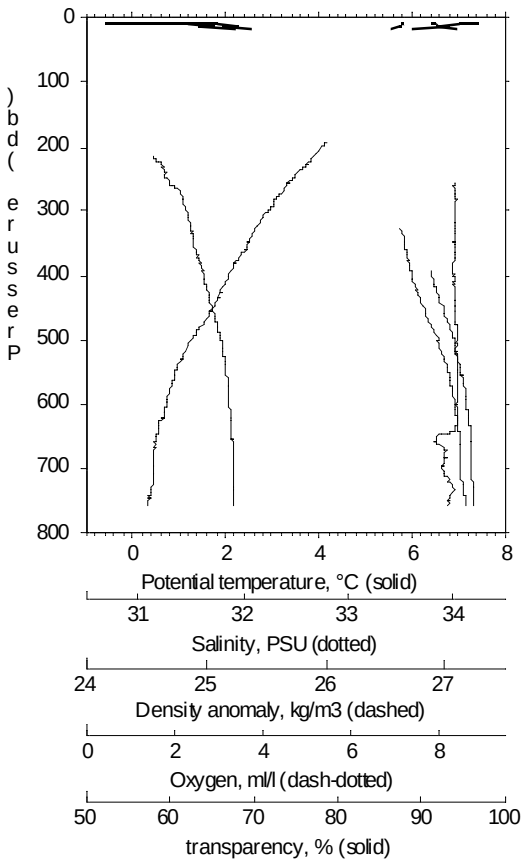

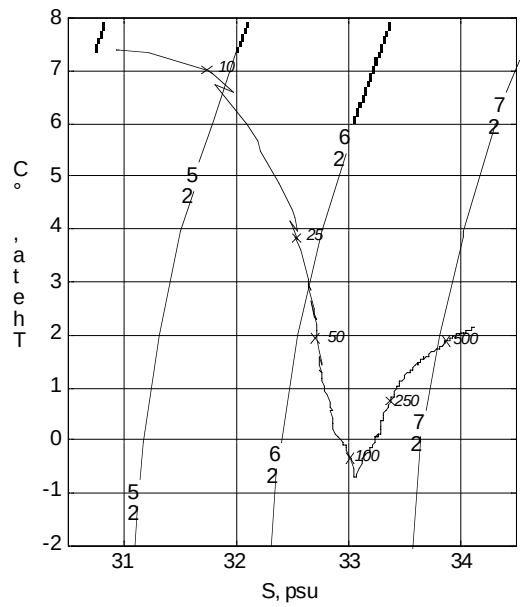

** Station: LV29-84/3
Time = Jul 09 2002 00:05:19
** Latitude: 54 25.168
** Longitude: 144 08.295
File : LV29-84D.CNV

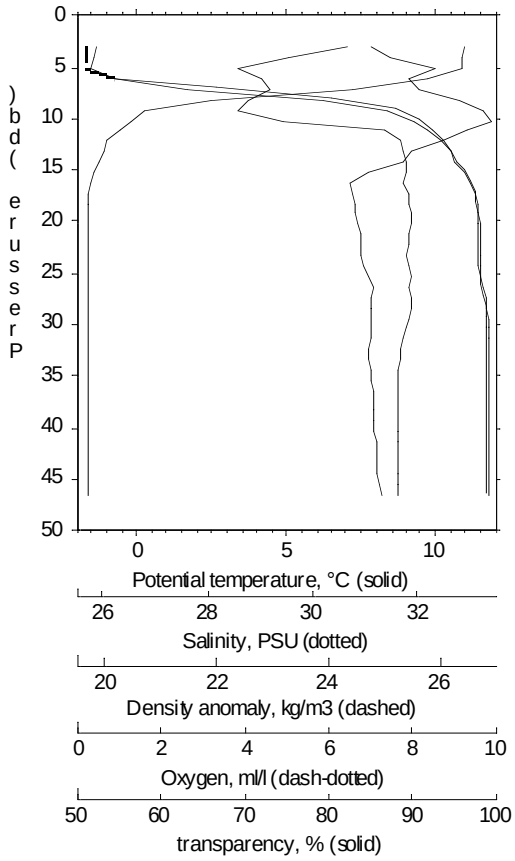

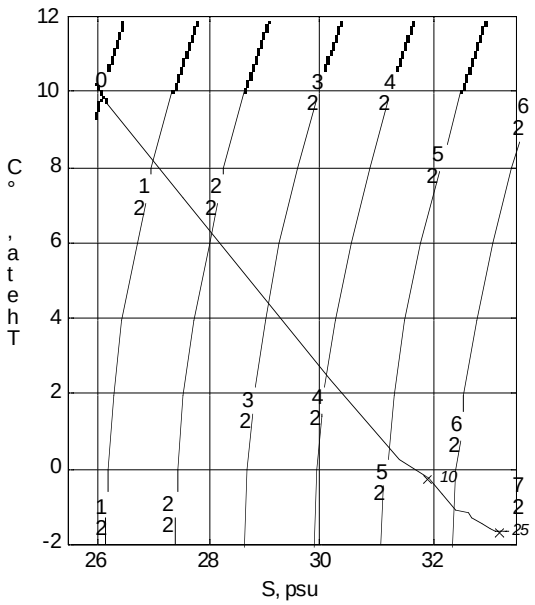

** Station: LV29-87/1
Time = Jul 10 2002 02:30:39
** Latitude: 54 27.015
** Longitude: 141 58.044
File : LV29-87U.CNV

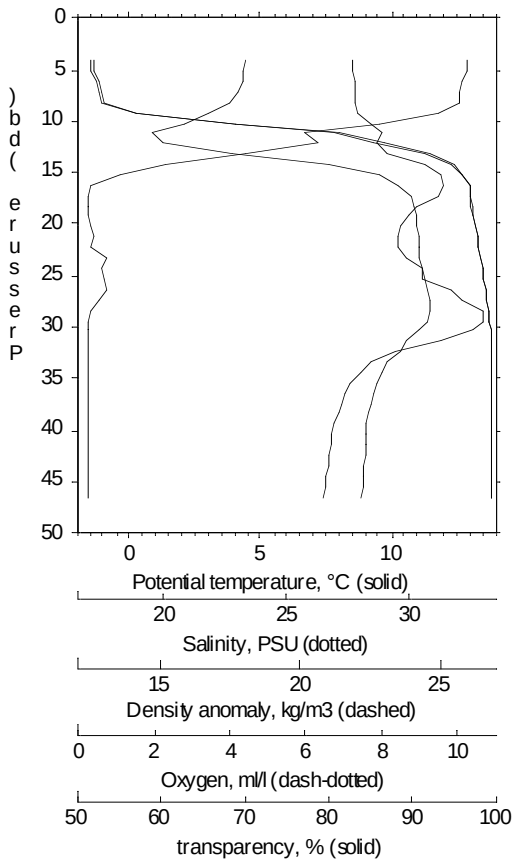

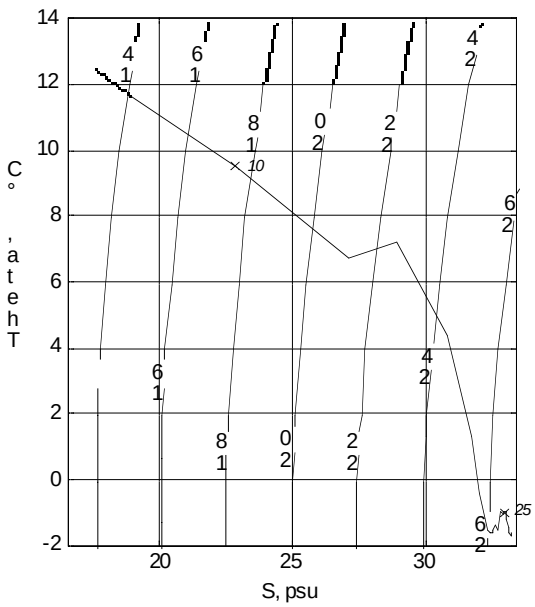

** Station: LV29-88/2
Time = Jul 10 2002 04:46:56
** Latitude: 54 10.497
** Longitude: 141 58.049
File : LV29-88d.CNV

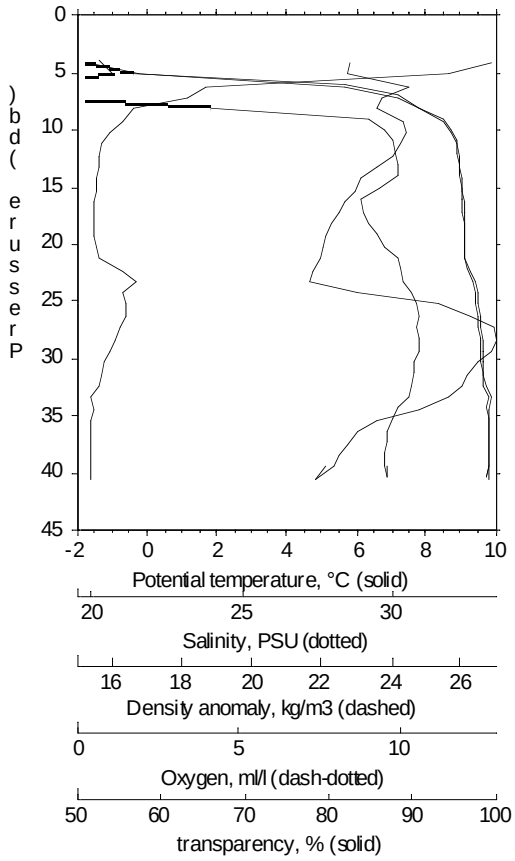

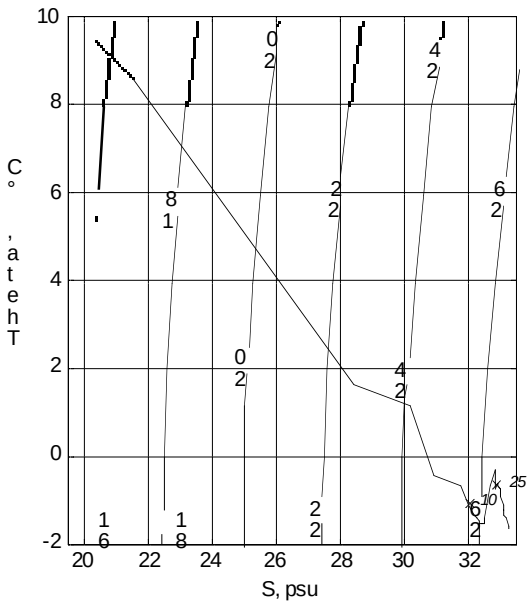

** Station: LV29-88/3
Time = Jul 10 2002 09:10:57
** Latitude: 54 01.938
** Longitude: 141 37.949
File : LV29883d.CNV

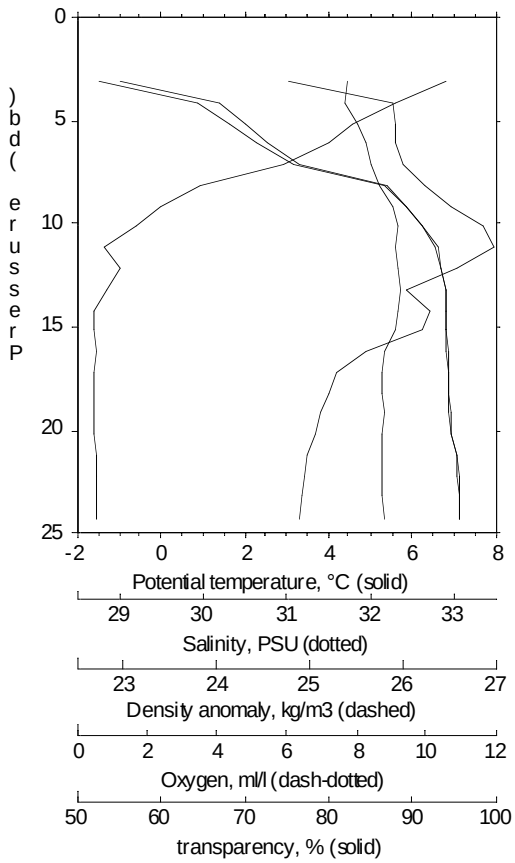

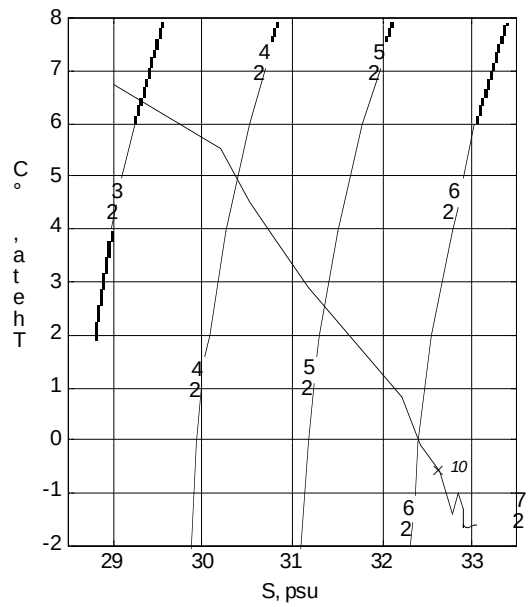

** Station: LV29-88/4
Time = Jul 10 2002 13:37:02
** Latitude: 53 53.775
** Longitude: 141 18.469
File : LV29884D.CNV

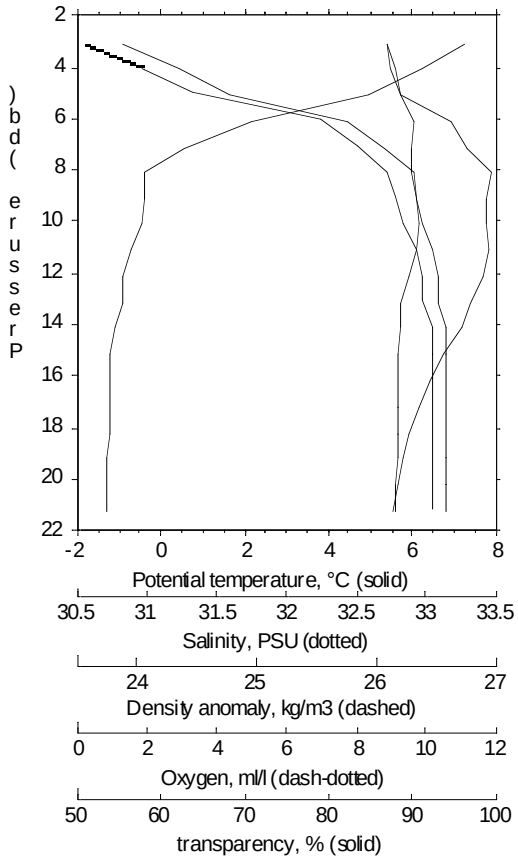

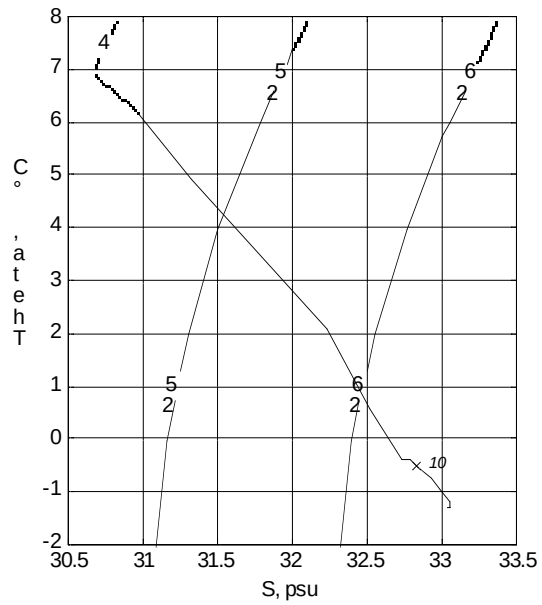

** Station: LV29-88/5
Time = Jul 10 2002 16:57:32
** Latitude: 53 46.448
** Longitude: 141 00.645
File : LV29885D.CNV

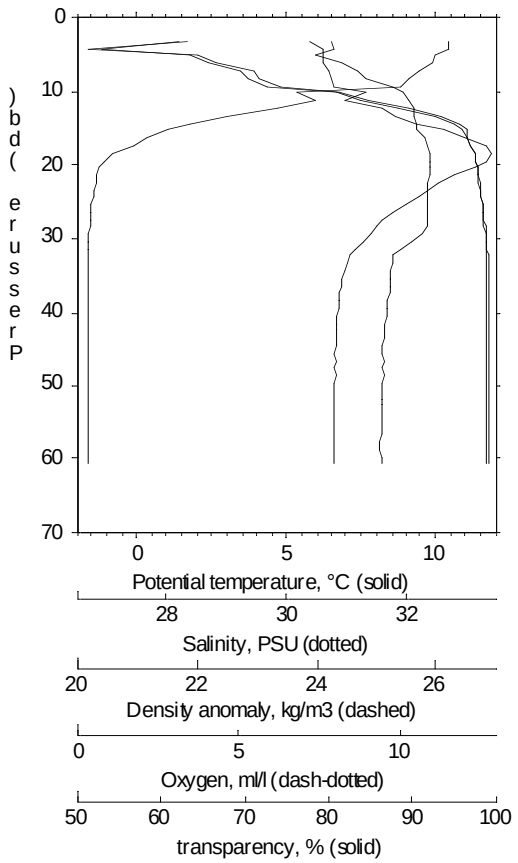

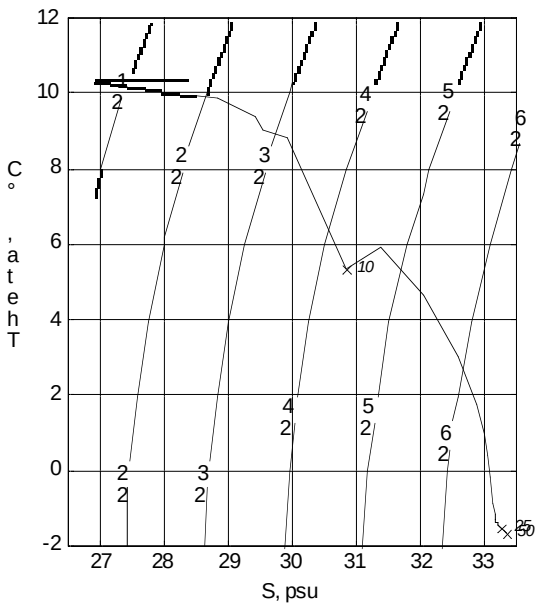

** Station: LV29-90/1
Time = Jul 11 2002 01:21:08
** Latitude: 54 41.817
** Longitude: 141 58.319
File : LV29-90D.CNV

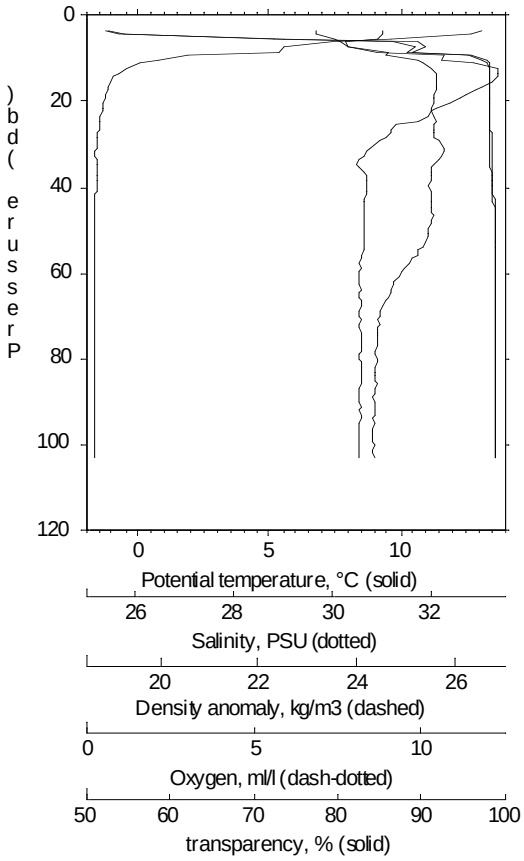

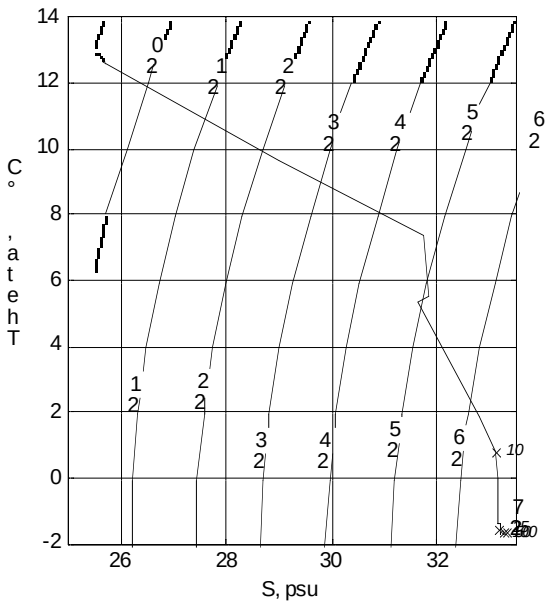

** Station: LV29-91/1
Time = Jul 11 2002 03:03:29
** Latitude: 54 53.885
** Longitude: 141 58.221
File : LV29-91D.CNV

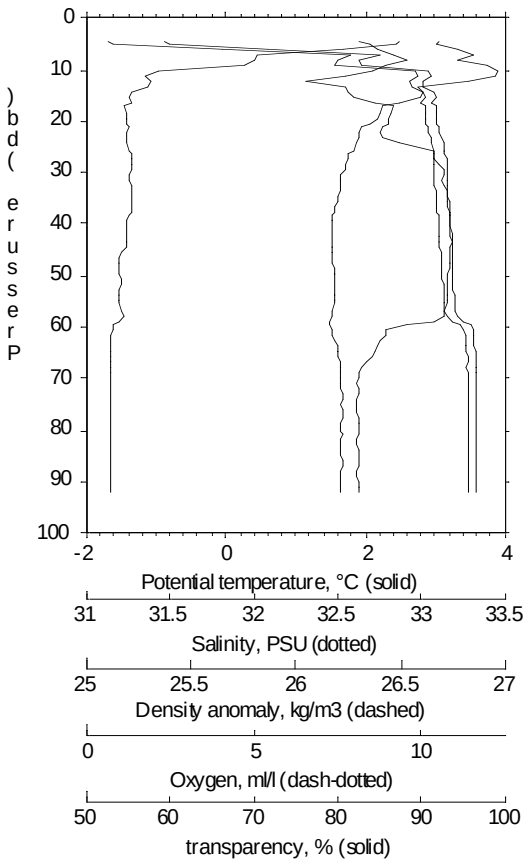

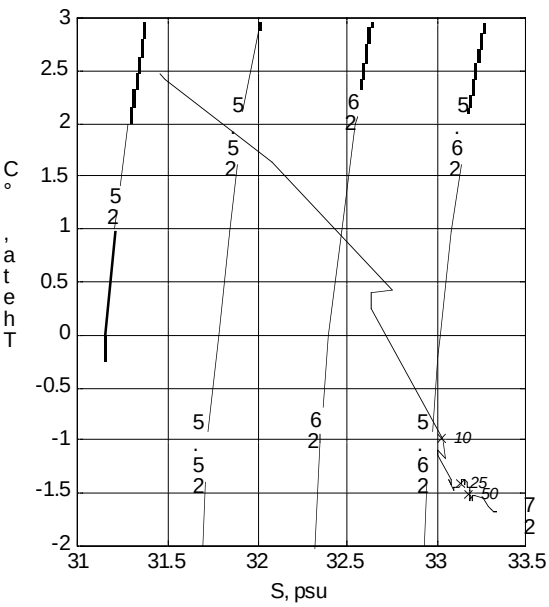

** Station: LV29-92/1
Time = Jul 11 2002 07:12:22
** Latitude: 54 52.993
** Longitude: 142 52.062
File : LV29-92D.CNV

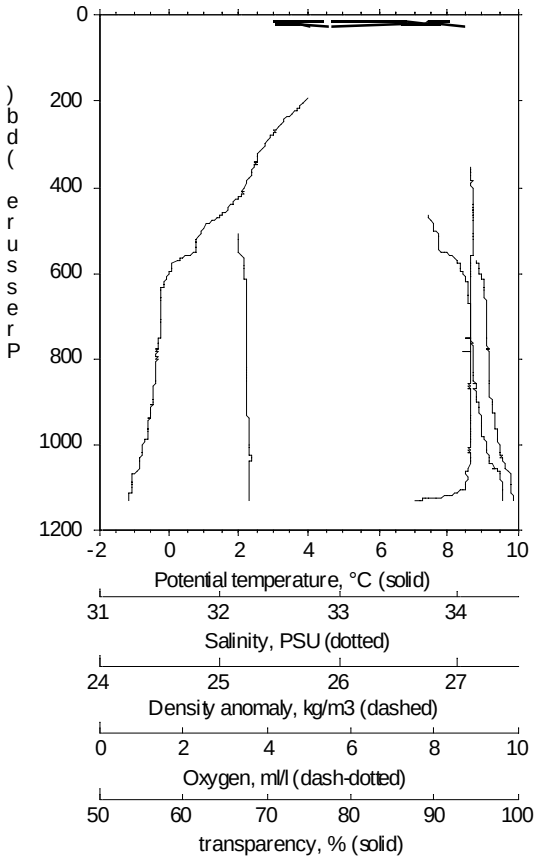

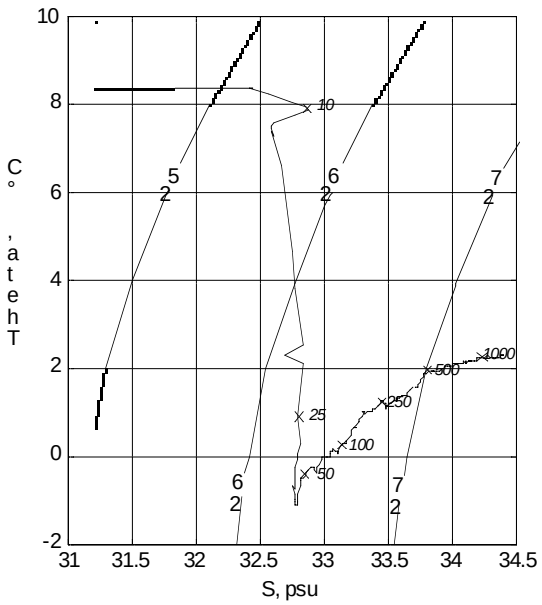

** Station: LV29-94/4
Time = Jul 12 2002 04:43:51
** Latitude: 54 53.530
** Longitude: 145 16.818
File : LV29-94D.CNV

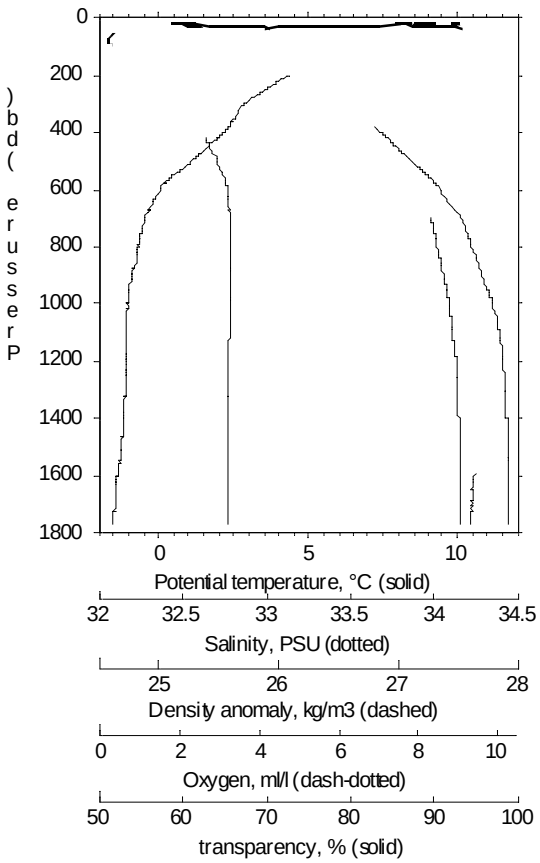

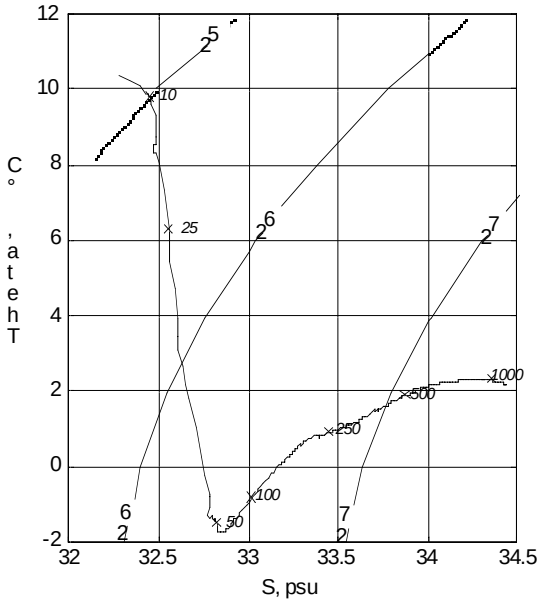

** Station: LV29-103/4
Time = Jul 14 2002 04:18:33
** Latitude: 53 25.802
** Longitude: 146 06.826
File : LV29103D.CNV

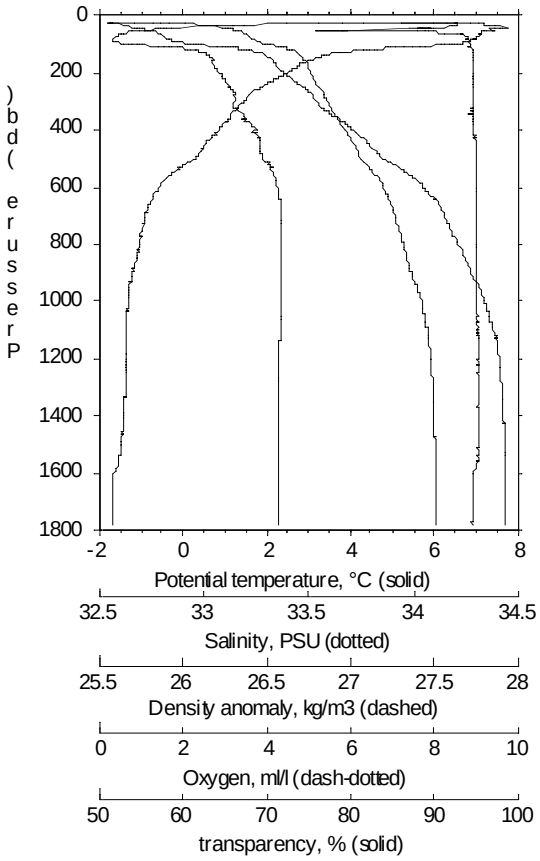

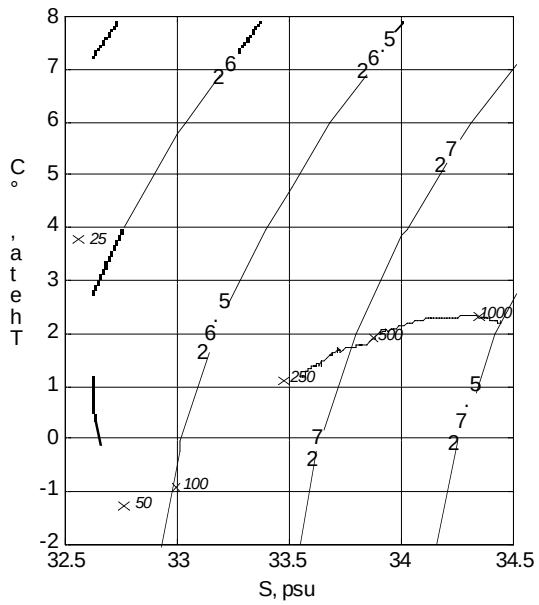

** Station: LV29-104/4
Time = Jul 14 2002 13:20:10
** Latitude: 53 13.150
** Longitude: 146 16.650
File : LV29104D.CNV

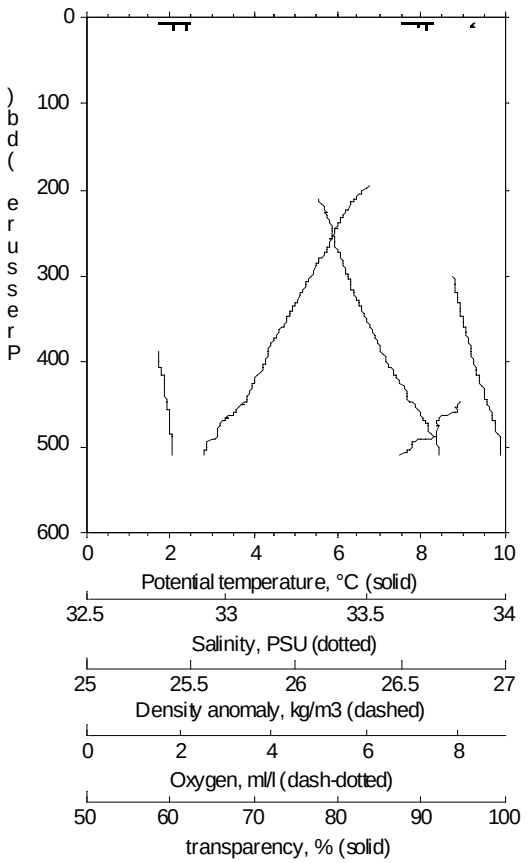

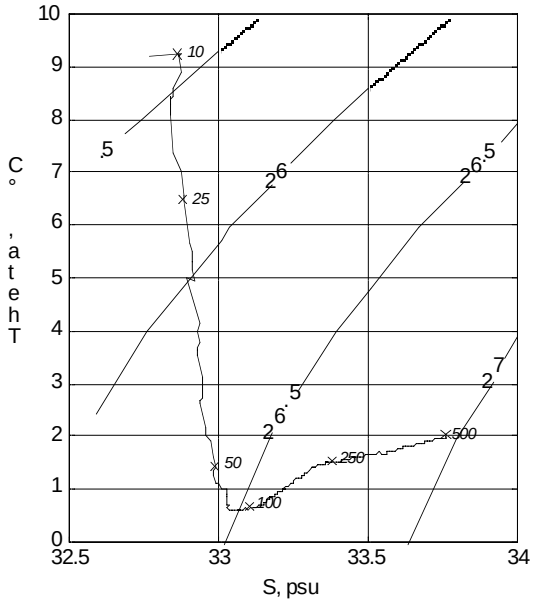

** Station: LV29-106/3
Time = Jul 16 2002 04:41:58
** Latitude: 51 59.825
** Longitude: 154 02.527
File : LV29106D.CNV

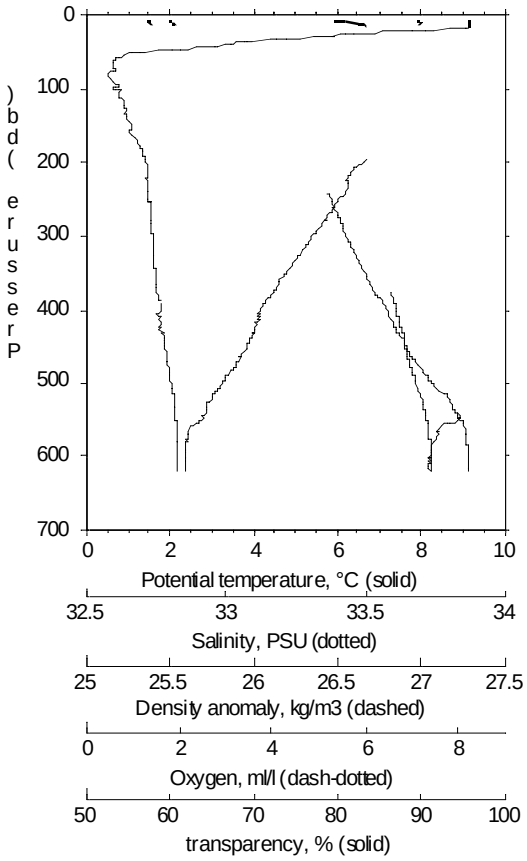

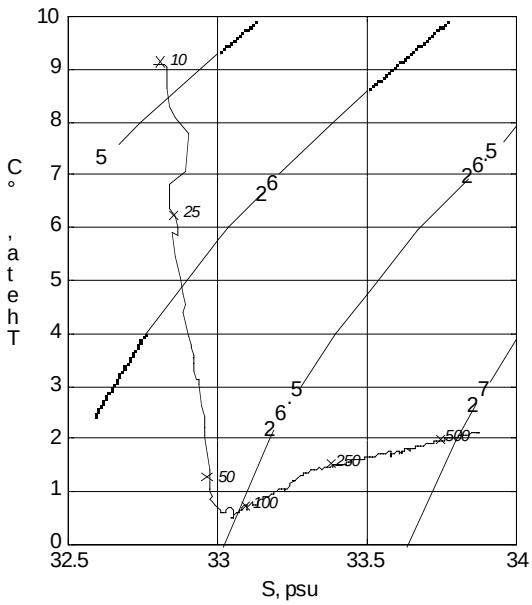

** Station: LV29-108/2
Time = Jul 16 2002 20:26:46
** Latitude: 52 01.639
** Longitude: 153 34.952
File : LV29108D.CNV

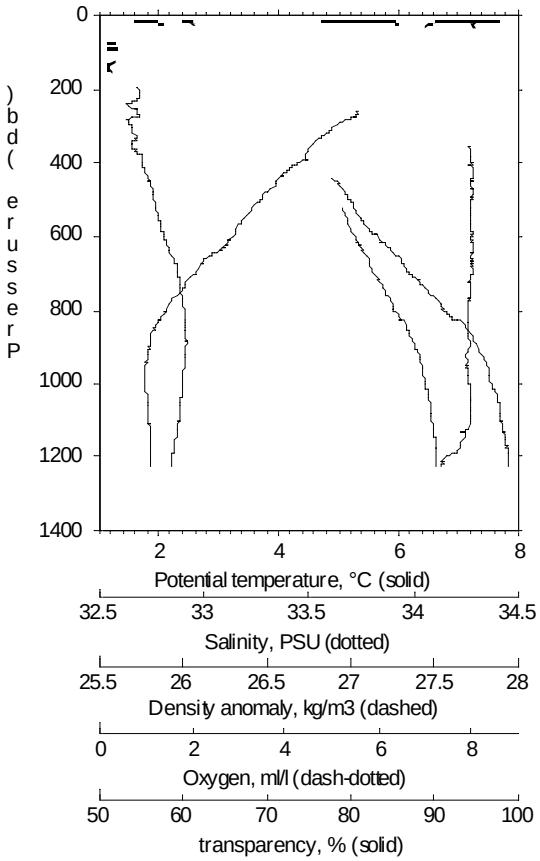

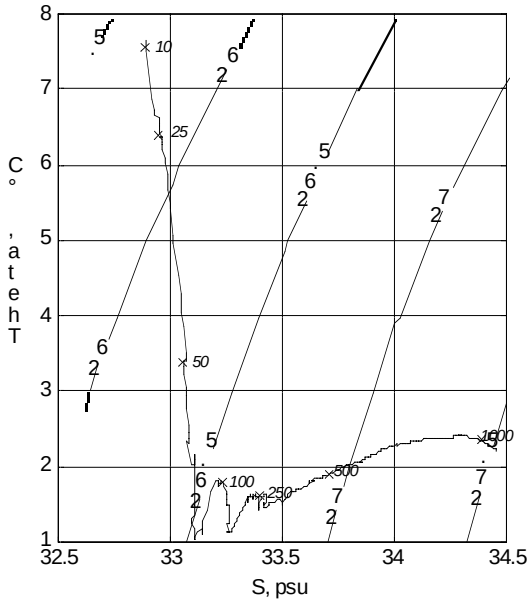

** Station: LV29-110/2
Time = Jul 18 2002 07:03:37
** Latitude: 50 27.042
** Longitude: 154 45.976
File : LV29110D.CNV

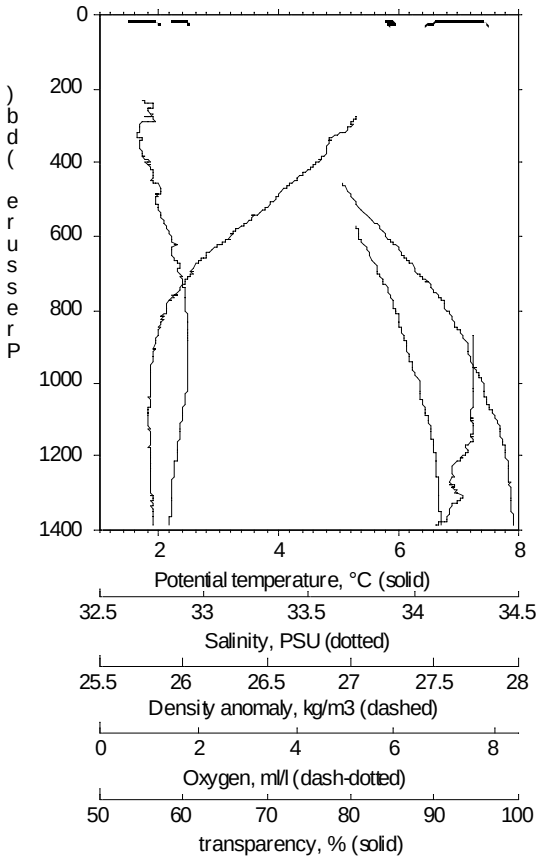

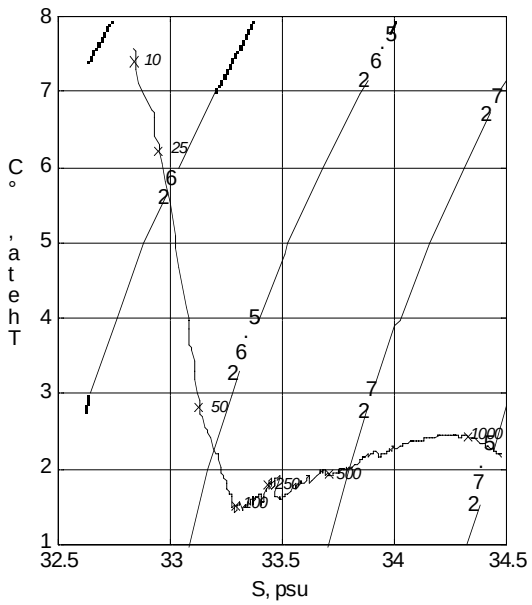

** Station: LV29-112/5
Time = Jul 19 2002 05:48:21
** Latitude: 50 12.683
** Longitude: 154 20.396
File : LV29112D.CNV

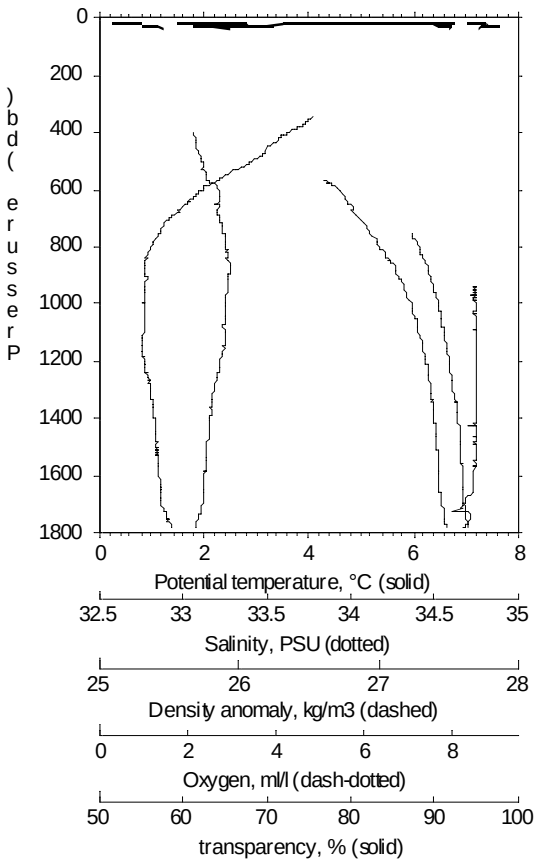

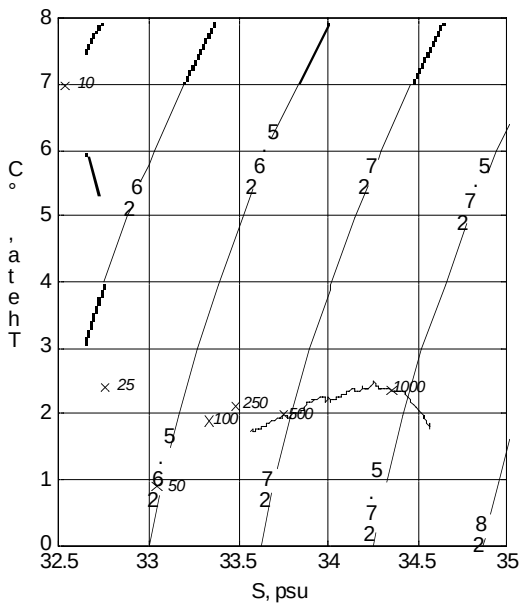

** Station: LV29-114/4
Time = Jul 20 2002 02:35:47
** Latitude: 49 22.617
** Longitude: 152 53.232
File : LV29114D.CNV

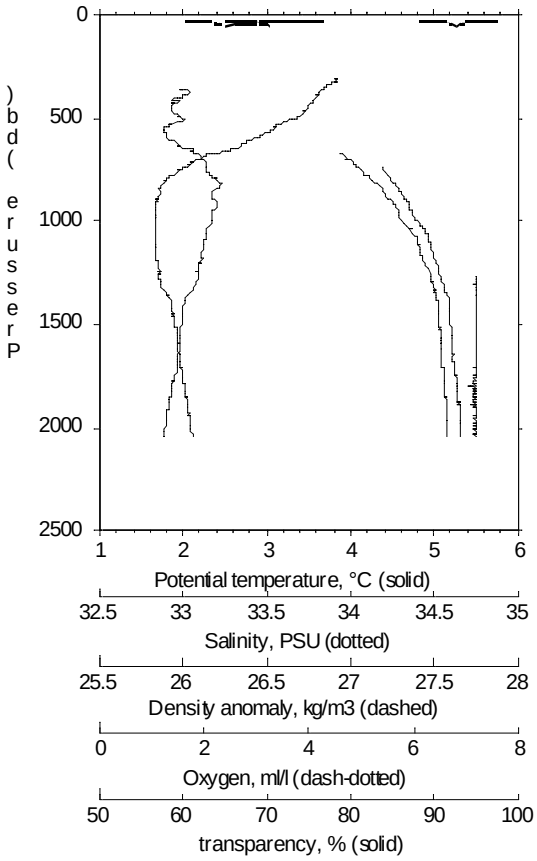

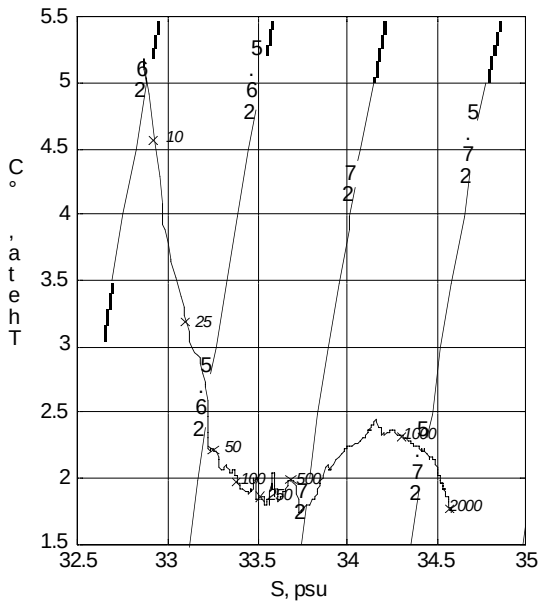

** Station: LV29-115/1
Time = Jul 20 2002 10:41:07
** Latitude: 48 35.603
** Longitude: 153 09.734
File : LV29115D.CNV

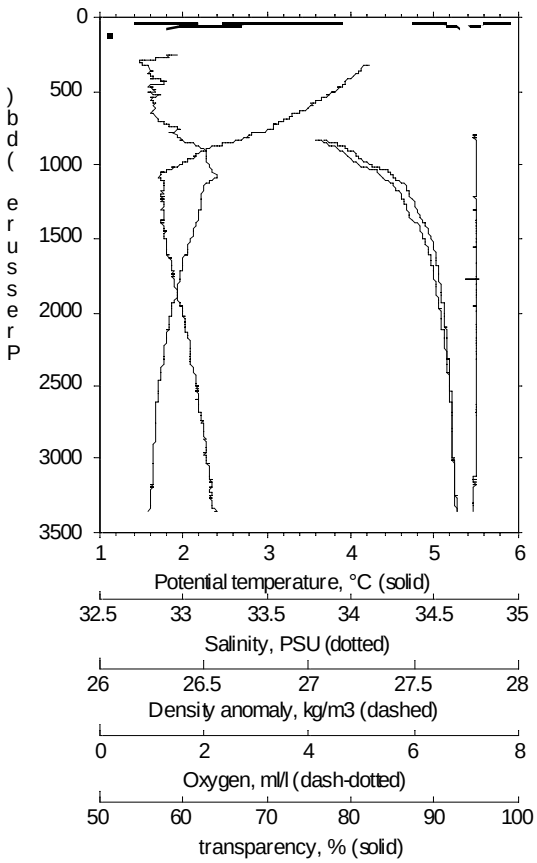

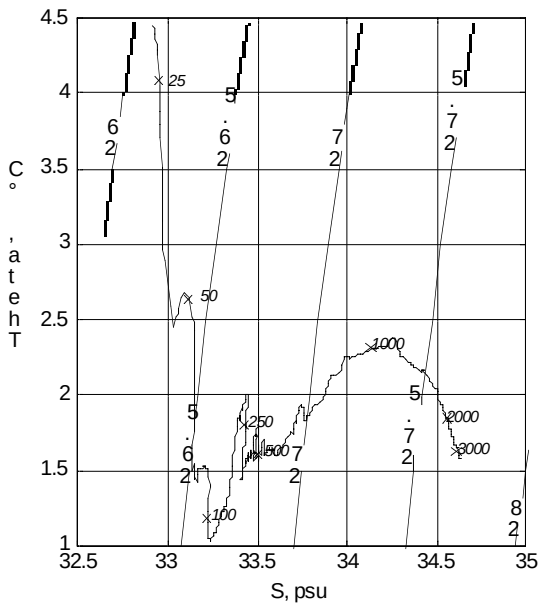

** Station: LV29-116/2
Time = Jul 20 2002 22:22:49
** Latitude: 47 56.889
** Longitude: 151 53.621
File : LV29116D.CNV

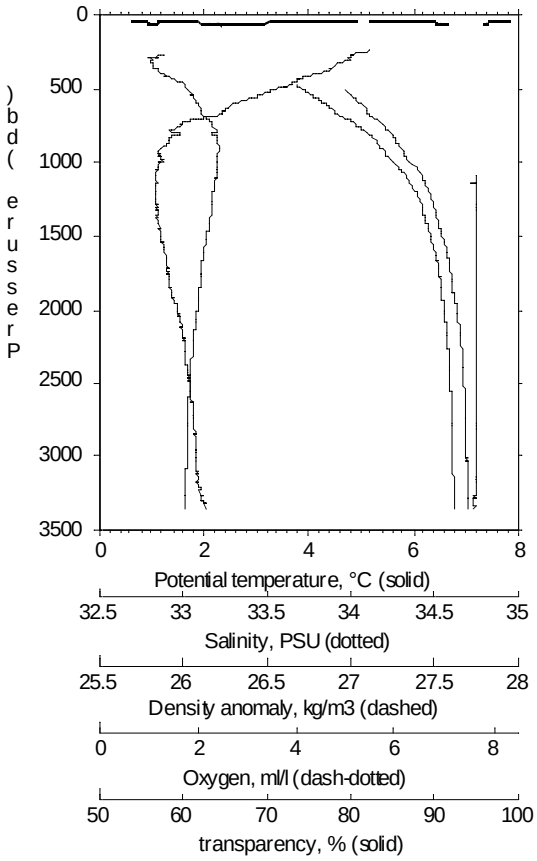

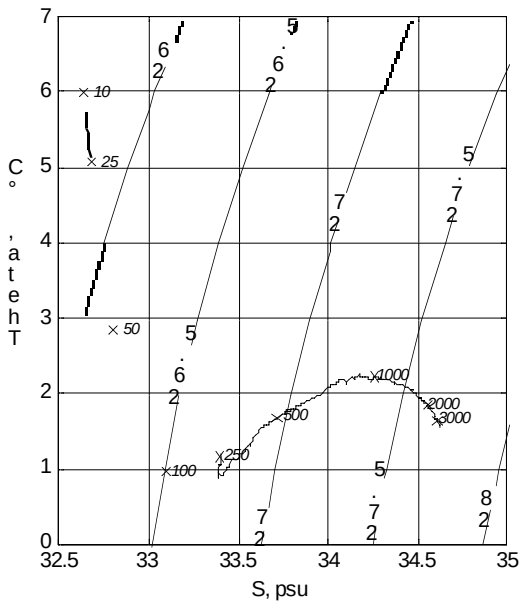

** Station: LV29-120/1
Time = Jul 22 2002 16:14:20
** Latitude: 47 03.138
** Longitude: 150 54.442
File : LV29120D.CNV

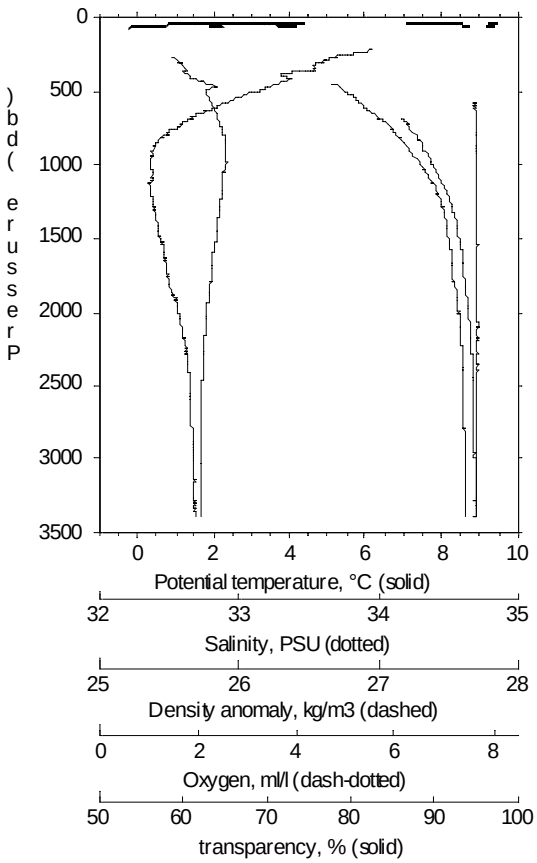

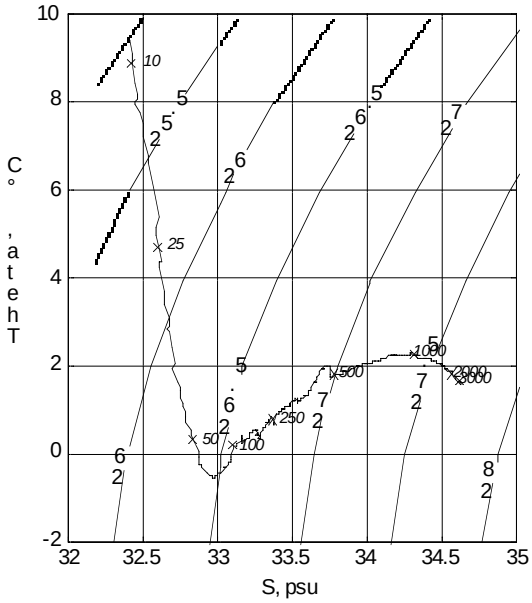

** Station: LV29-123/3
Time = Jul 23 2002 19:36:44
** Latitude: 47 40.315
** Longitude: 149 48.225
File : LV29123D.CNV

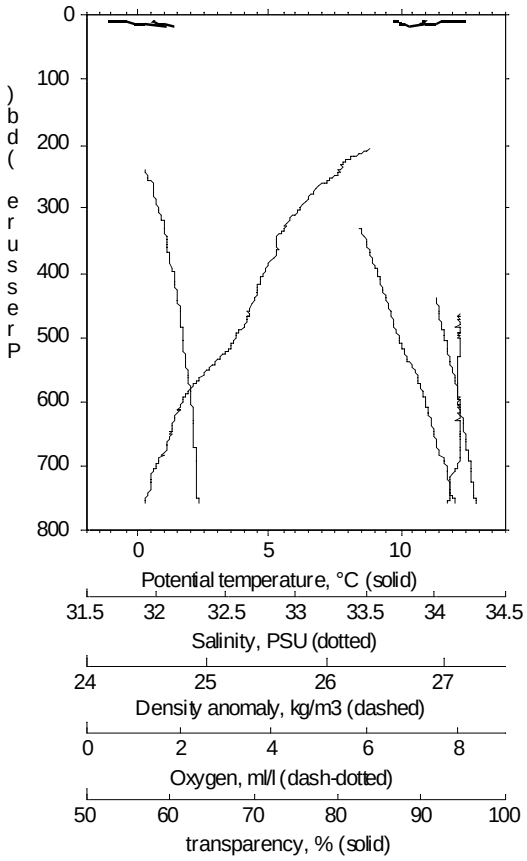

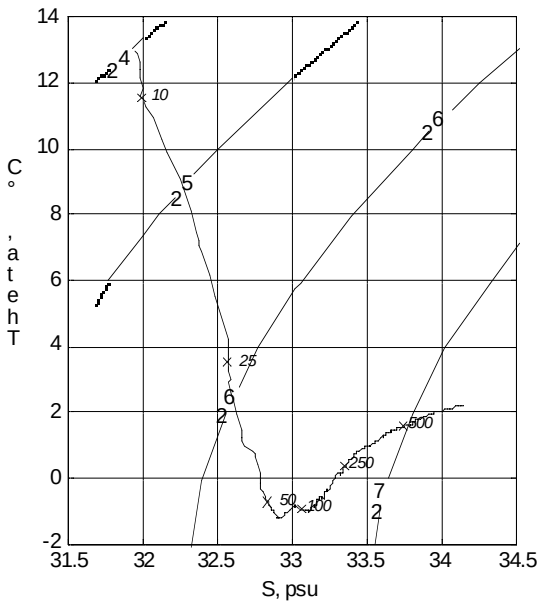

** Station: LV29-131/4
Time = Jul 30 2002 09:24:31
** Latitude: 45 32.704
** Longitude: 144 18.297
File : LV29131D.CNV

APPENDIX 4

Methane data

Methane distribution in the water column

Station	CH_4, nl/l	depth, m	Station	CH_4, nl/l	depth, m	Station	CH_4, nl/l	depth, m
LV29-69	73	3	LV29-81	91	4	LV29-88-5	142	3
	192	70		75	51		104	7
	48	171		175	100		81	11
	60	298		14640	199		102	16
	82	396		2916	298		69	21
	33	496		1728	358			
	49	594		1664	367	LV29-90-1	62	3
	143	692					35	7
	82	741	LV29-82	49	4		35	10
	78	793		60	64		34	20
	111	827		19	198		42	29
	103	837		47	386		52	45
				205	614		47	60
LV29-70	51	3		898	731			
	96	31		942	771	LV29-91-1	46	3
	197	89		916	787		55	8
	41	249					48	20
	40	496	LV29-84	33	4		60	36
	16	744		90	31		76	54
	16	990		25	59		90	80
	12	1237		20	110		97	102
	11	1484		31	199			
	21	1729		48	299	LV29-92-1	49	3
	13	1926		50	396		63	9
	7	1980		111	495		47	20
				73	596		81	40
LV29-72	46	3		223	694		438	59
	77	30		468	732		561	80
	86	60		341	745		528	91
	45	151						
	41	248	LV29-87	75	4	LV29-94-4	44	3
	34	347		276	10		46	46
	34	495		98	20		31	100
	25	645		128	30		15	249
	24	794		84	46		15	396
	23	941					13	545
	19	1062	LV29-88-2	123	3		31	695
	30	1113		440	10		57	842
				385	19		12	990
LV29-76	46	4		221	30		12	1067
	80	79		275	40		14	1102
	99	198		262	46		12	1115
	189	316						
	296	495	LV29-88-3	650	3	LV29-103-4	36	3
	672	609		930	6		43	69
	701	615		846	9		33	150
				135	22		34	297
LV29-79	61	4		44	31		17	496
	51	73		66	39		25	743
	42	247					16	990
	250	496	LV29-88-4	115	3		16	1237
	264	794		361	6		25	1482
	149	1005		525	10		70	1639
	241	1053		579	15		155	1719
				441	20		91	1740
				292	23			

Station	CH_4, nl/l	depth, m	Station	CH_4, nl/l	depth, m	Station	CH_4, nl/l	depth, m
LV29-104-4	37	3	LV29-114-4	57	3	LV29-123-3	131	3
	56	75		64	52		157	73
	27	198		58	99		50	198
	12	396		46	290		31	496
	17	694		36	390		6	951
	17	940		23	595		8	1047
	12	1187		19	842		9	1482
	23	1384		11	1138		6	1973
	31	1557		12	1384		4	2466
	8	1655		10	1627		5	2956
	7	1734		10	1733		5	3296
	7	1754		9	1756		8	3321
LV29-106-3	51	3	LV29-115-4	58	3	LV29-131-4	82	2
	44	29		63	51		200	30
	66	70		56	99		256	67
	73	198		42	297		184	99
	71	296		28	495		54	198
	44	396		9	742		85	297
	69	491		8	989		83	397
	62	502		6	1234		70	494
				5	1433		40	594
LV29-108-1	48	2		5	1728		433	692
	66	70		4	1925		433	731
	58	197		4	2011		225	749
	59	299						
	56	446	LV29-116-2	65	3			
	81	584		51	99			
	84	607		45	298			
				37	593			
LV29-110-2	58	3		11	987			
	54	30		7	1384			
	59	94		4	1776			
	54	140		5	2170			
	46	199		5	2564			
	42	347		4	2956			
	68	494		8	3265			
	91	692		10	3284			
	88	940						
	15	1088	LV29-120-1	92	3			
	21	1188		93	115			
	22	1207		57	297			
				13	744			
LV29-112-5	59	3		10	1138			
	53	49		8	1581			
	64	100		7	1975			
	50	199		8	2367			
	43	347		9	2760			
	36	496		15	3177			
	21	645		14	3249			
	16	843		11	3280			
	15	1039						
	21	1237						
	19	1345						
	22	1365						

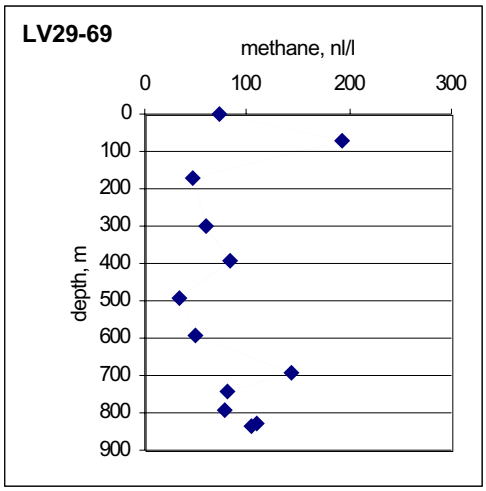
LV29-69
methane, nl/l
0
100
200
300
depth, m
0
100
200
300
400
500
600
700
800
900

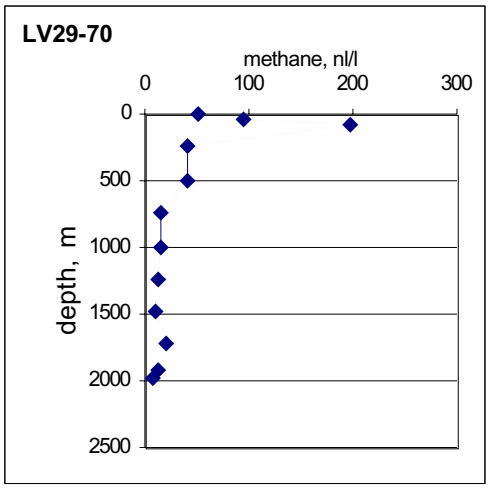
LV29-70
methane, nl/l
0
100
200
300
depth, m
0
500
1000
1500
2000
2500

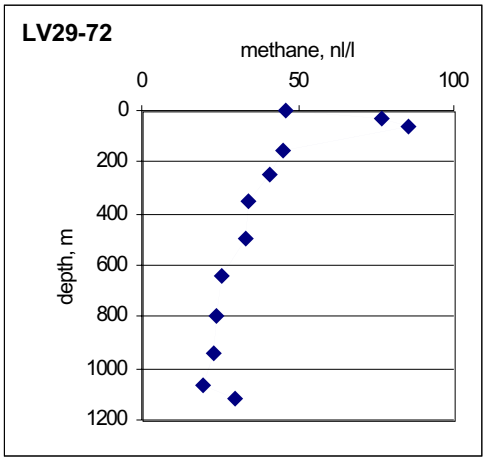
LV29-72
methane, nl/l
0
50
100
depth, m
0
200
400
600
800
1000
1200

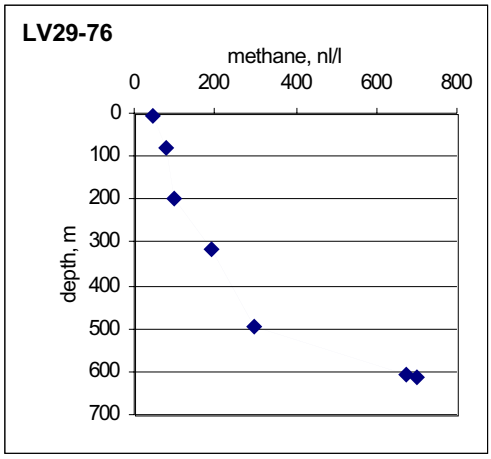
LV29-76
methane, nl/l
0
200
400
600
800
depth, m
0
100
200
300
400
500
600
700

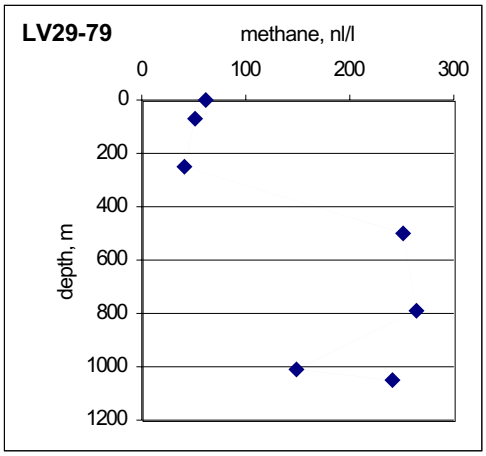
LV29-79
methane, nl/l
0
100
200
300
depth, m
0
200
400
600
800
1000
1200

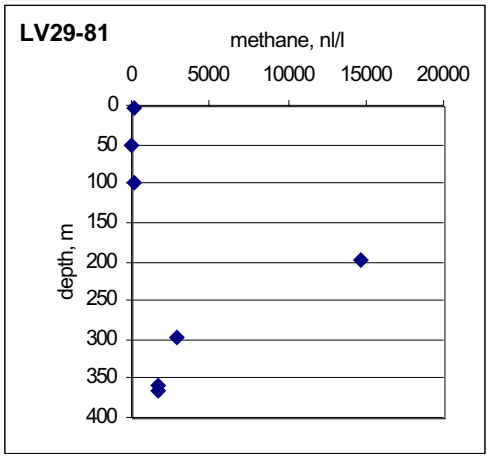
LV29-81
methane, nl/l
0
5000
10000
15000
20000
depth, m
0
50
100
150
200
250
300
350
400

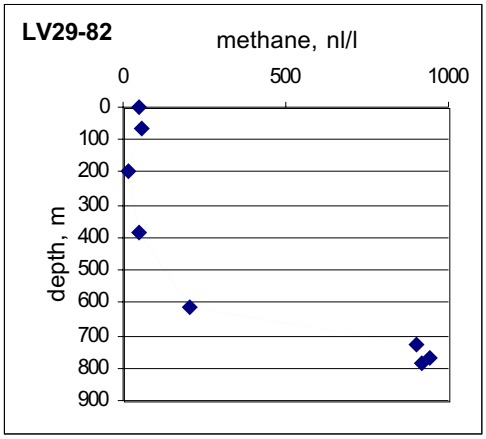
LV29-82
methane, nl/l
0
500
1000
depth, m
0
100
200
300
400
500
600
700
800
900

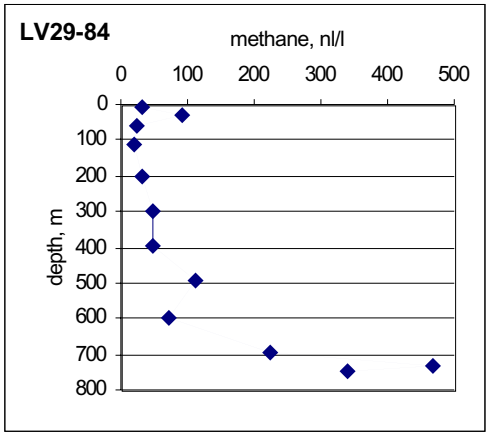
LV29-84
methane, nl/l
0
100
200
300
400
500
depth, m
0
100
200
300
400
500
600
700
800

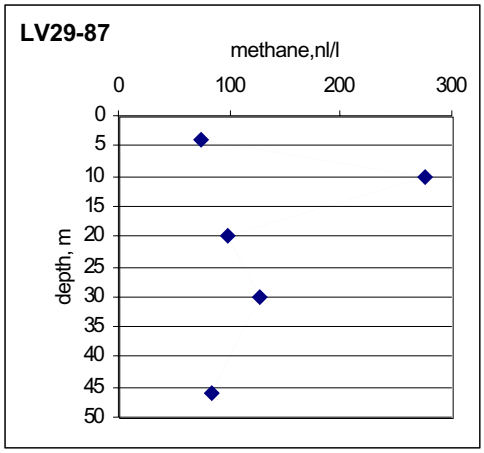
LV29-87
methane,nl/l
0
100
200
300
depth, m
0
5
10
15
20
25
30
35
40
45
50

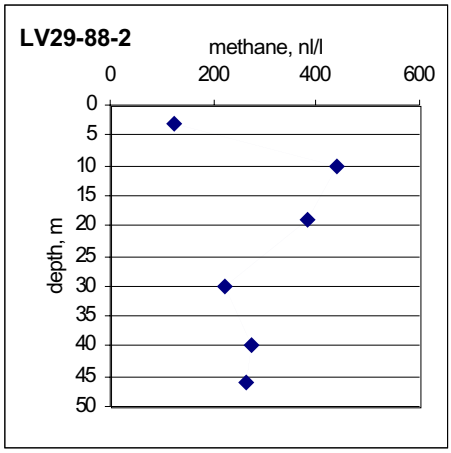
LV29-88-2
methane, nl/l
0
200
400
600
depth, m
0
5
10
15
20
25
30
35
40
45
50

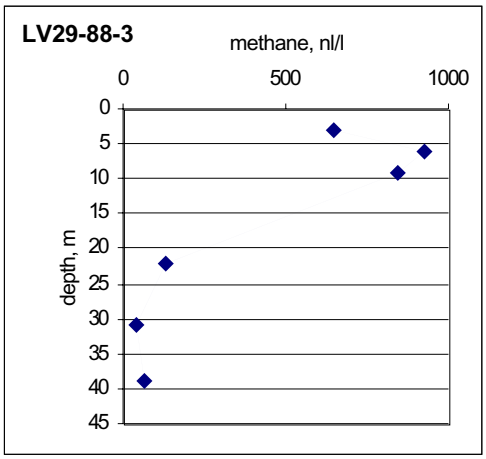
LV29-88-3
methane, nl/l
0
500
1000
depth, m
0
5
10
15
20
25
30
35
40
45

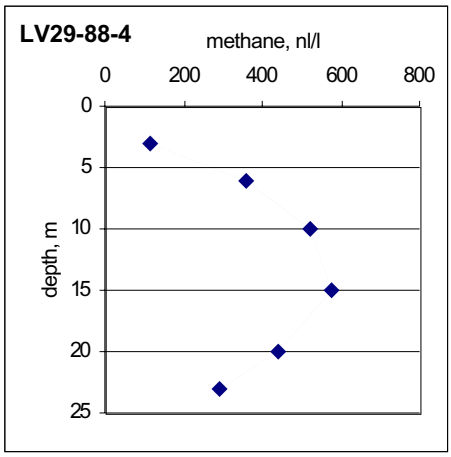
LV29-88-4
methane, nl/l
0
200
400
600
800
depth, m
0
5
10
15
20
25

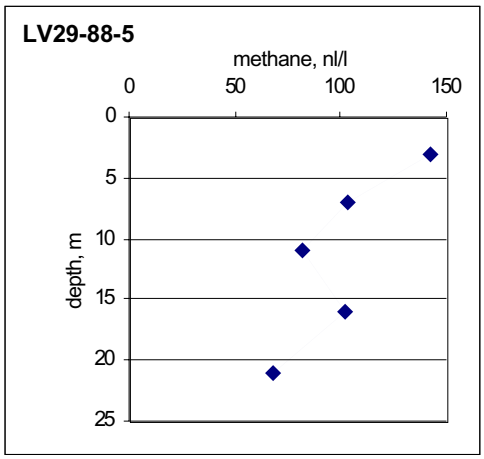
LV29-88-5
methane, nl/l
0
50
100
150
depth, m
0
5
10
15
20
25

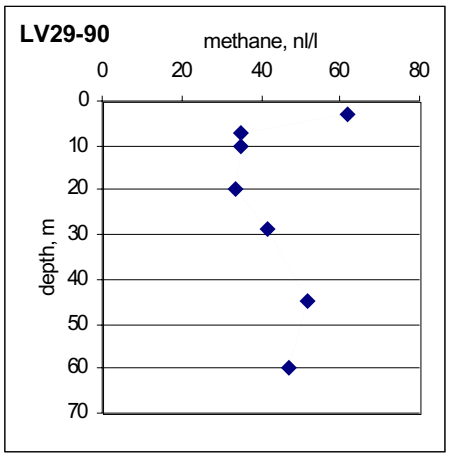
LV29-90
methane, nl/l
0
20
40
60
80
depth, m
0
10
20
30
40
50
60
70

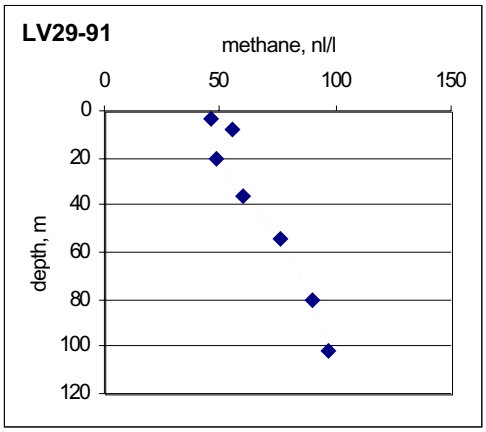
LV29-91
methane, nl/l
0
50
100
150
depth, m
0
20
40
60
80
100
120

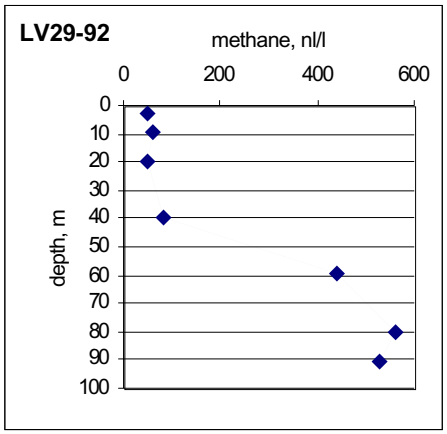
LV29-92
methane, nl/l
0
200
400
600
depth, m
0
10
20
30
40
50
60
70
80
90
100

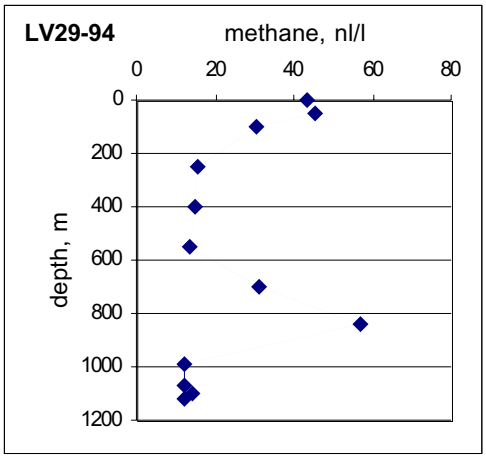
LV29-94
methane, nl/l
0
20
40
60
80
depth, m
0
200
400
600
800
1000
1200

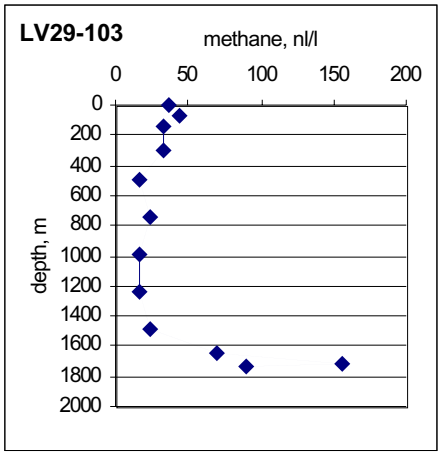
LV29-103
methane, nl/l
0
50
100
150
200
depth, m
0
200
400
600
800
1000
1200
1400
1600
1800
2000

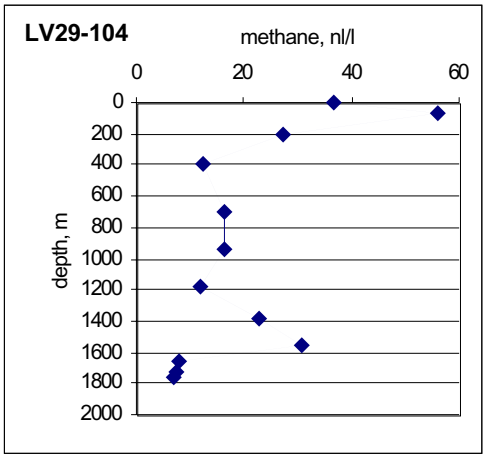
LV29-104
methane, nl/l
0
20
40
60
depth, m
0
200
400
600
800
1000
1200
1400
1600
1800
2000

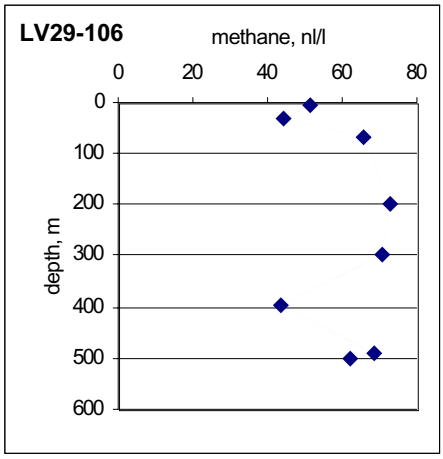
LV29-106
methane, nl/l
0
20
40
60
80
depth, m
0
100
200
300
400
500
600

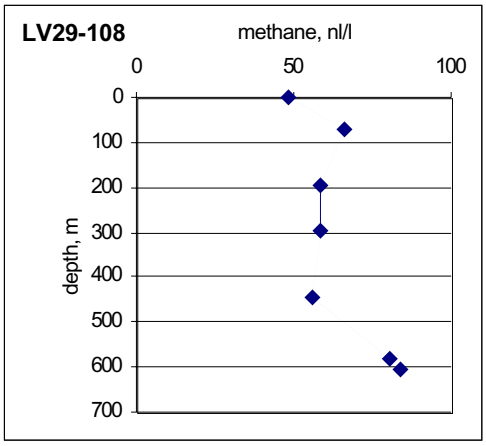
LV29-108
methane, nl/l
0
50
100
depth, m
0
100
200
300
400
500
600
700

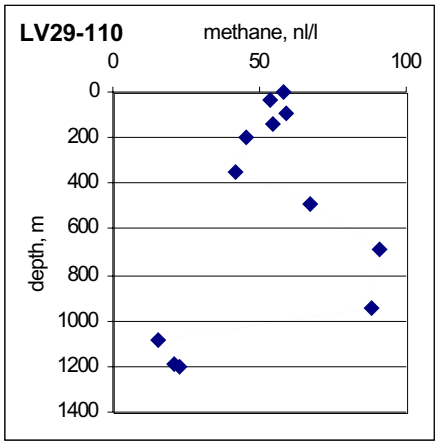
LV29-110
methane, nl/l
0
50
100
depth, m
0
200
400
600
800
1000
1200
1400

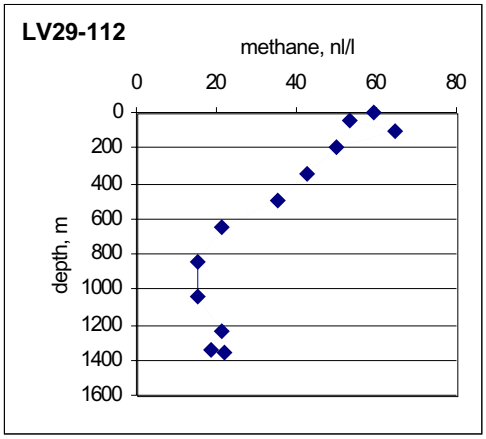
LV29-112
methane, nl/l
0
20
40
60
80
depth, m
0
200
400
600
800
1000
1200
1400
1600

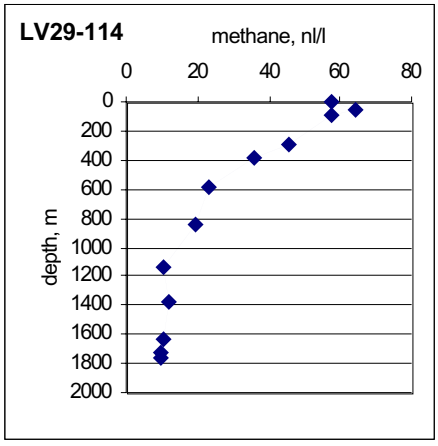
LV29-114
methane, nl/l
0
20
40
60
80
depth, m
0
200
400
600
800
1000
1200
1400
1600
1800
2000

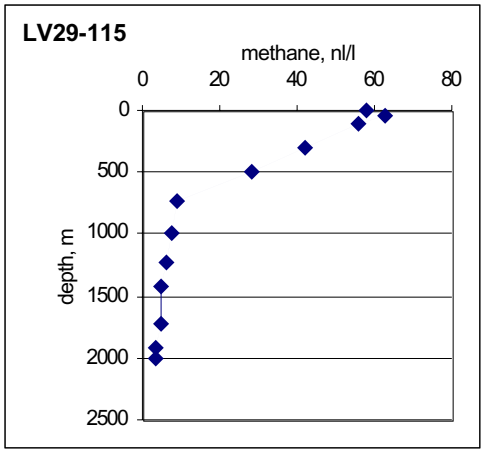
LV29-115
methane, nl/l
0
20
40
60
80
depth, m
0
500
1000
1500
2000
2500

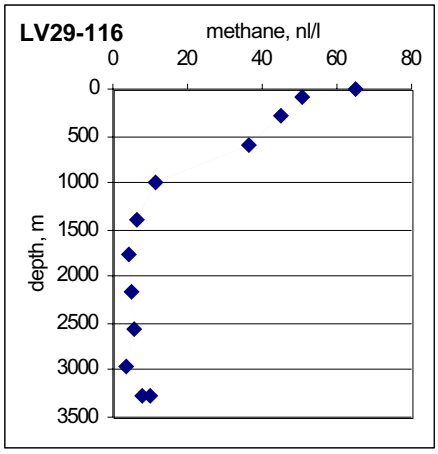
LV29-116
methane, nl/l
0
20
40
60
80
depth, m
0
500
1000
1500
2000
2500
3000
3500

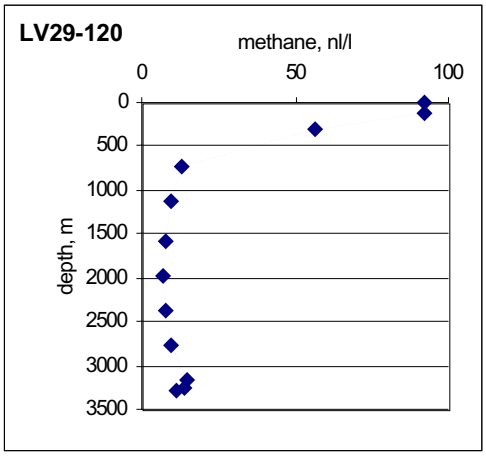
LV29-120
methane, nl/l
0
50
100
depth, m
0
500
1000
1500
2000
2500
3000
3500

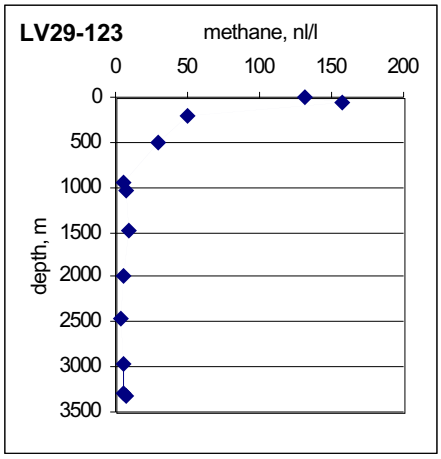
LV29-123
methane, nl/l
0
50
100
150
200
depth, m
0
500
1000
1500
2000
2500
3000
3500

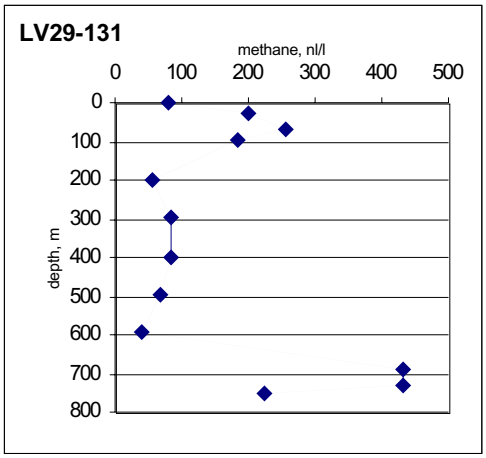
LV29-131
methane, nl/l
0
100
200
300
400
500
depth, m
0
100
200
300
400
500
600
700
800

Methane distribution in sediment cores

Station	Vgas, ml	level, cm	CH4, nl/kg	mM/kg	weight, g	K	CH4, ppm	cm
LV29-78	8	50	24713.28154	0.001103271	5.1	0.094339623	15.75471698	167
	8	200	46984.83167	0.002097537	5.1	0.235849057	29.95283019	127
	8	400	139104.6985	0.006210031	5.1	0.943396226	88.67924528	94
	8	600	739918.609	0.033032081	5.1	9.433962264	471.6981132	50
	8	800	13762486.13	0.614396702	5.1	94.33962264	8773.584906	93
LV29-104	8	200	61413.24454	0.002741663	5.1	0.471698113	39.1509434	83
	8	400	171661.1173	0.007663443	5.1	0.943396226	109.4339623	116
	8	600	9544950.055	0.426113842	5.1	47.16981132	6084.90566	129
	8	770	7103218.646	0.317107975	5.1	47.16981132	4528.301887	96
	8	870	12208657.05	0.545029332	5.1	47.16981132	7783.018868	165
LV29-112	8	470	11394746.58	0.508694044	5.1	47.16981132	7264.150943	154
	8	560	9914909.36	0.442629882	5.1	47.16981132	6320.754717	134
LV29-131	8	15	3847.576767	0.000171767	5.1	0.094339623	2.452830189	26
	8	50	9470.958195	0.000422811	5.1	0.094339623	6.037735849	64
	8	100	14354.42101	0.000640822	5.1	0.094339623	9.150943396	97
	8	160	31372.54902	0.00140056	5.1	0.094339623	20	212
	8	200	22197.55827	0.000990962	5.1	0.235849057	14.1509434	60
	8	250	177580.4661	0.007927699	5.1	0.943396226	113.2075472	120
	8	300	155382.9079	0.006936737	5.1	0.943396226	99.05660377	105
	8	350	78431.37255	0.003501401	5.1	0.943396226	50	53
	8	400	103588.6053	0.004624491	5.1	0.943396226	66.03773585	70
	8	450	113947.4658	0.00508694	5.1	0.943396226	72.64150943	77
	8	500	236773.9549	0.010570266	5.1	0.943396226	150.9433962	160
	8	550	260451.3504	0.011627292	5.1	0.943396226	166.0377358	176
	8	600	473547.9097	0.021140532	5.1	4.716981132	301.8867925	64
	8	670	1124676.286	0.050208763	5.1	4.716981132	716.9811321	152
	8	750	9914909.36	0.442629882	5.1	94.33962264	6320.754717	67
	8	830	17758046.61	0.792769938	5.1	94.33962264	11320.75472	120

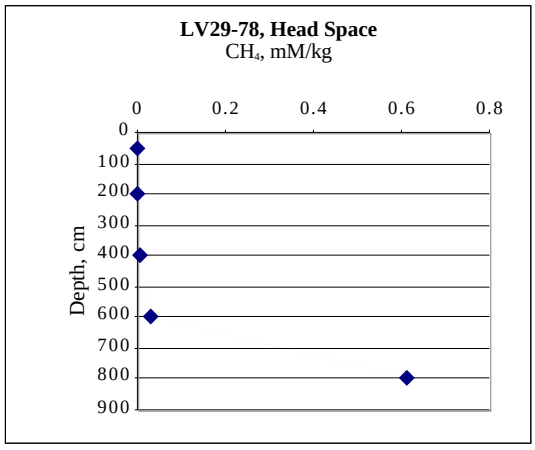
LV29-78, Head Space
CH4, mM/kg
0
0.2
0.4
0.6
0.8
Depth, cm
0
100
200
300
400
500
600
700
800
900

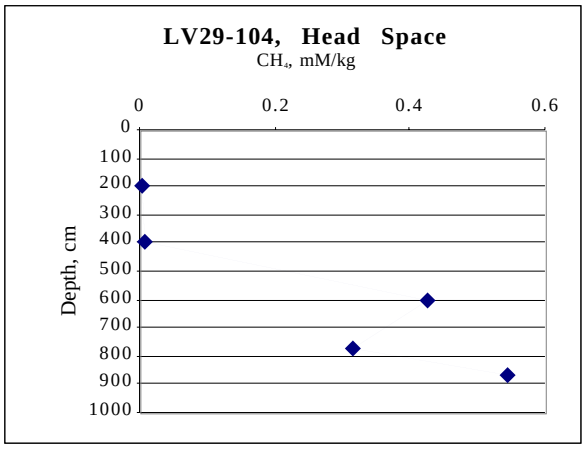
LV29-104, Head Space
CH4, mM/kg
0
0.2
0.4
0.6
Depth, cm
0
100
200
300
400
500
600
700
800
900
1000

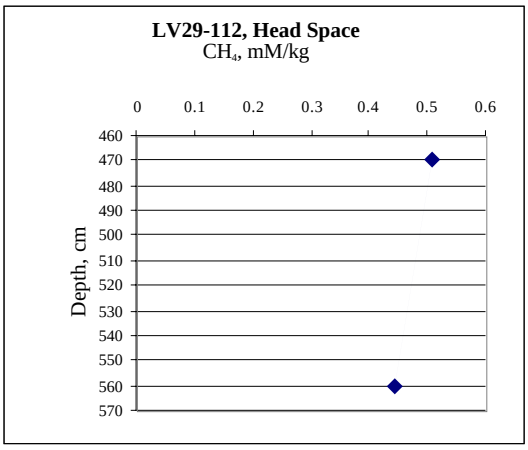
LV29-112, Head Space
CH4, mM/kg
0
0.1
0.2
0.3
0.4
0.5
0.6
Depth, cm
460
470
480
490
500
510
520
530
540
550
560
570

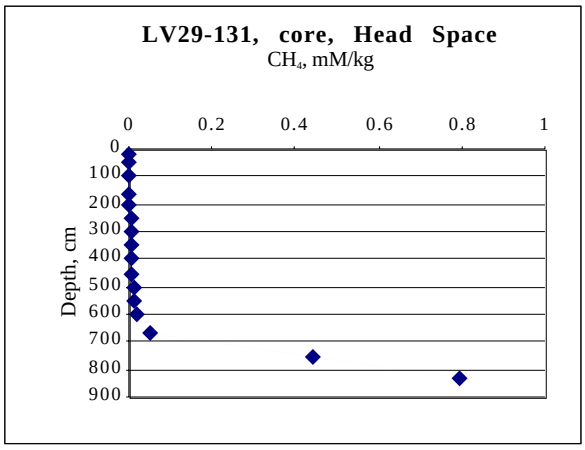
LV29-131, core, Head Space
CH4, mM/kg
0
0.2
0.4
0.6
0.8
1
Depth, cm
0
100
200
300
400
500
600
700
800
900

APPENDIX 5

Radiolarian data

Radiolarians in the Okhotsk Sea

Sample station	Latitude N	Longitude E	Water depth (m)	Net No	Depth interval (m)	F	S	V [m^3]
LV 29-69-6	45°27.087 /	144°04.157 /	849 / 839	5	0-50	11367	11262	78.75
	45°27.185	144°03.543		4	50-150	25641	25519	91.5
				3	150-200	21154	21057	72.25
				2	200-500	18000	17777	167.25
				1	500-800	18191	17735	342
LV 29-72-5	48°39.435 /	146°07.139 /	1118 / 1117	5	0-50	11523	11367	117
	48°39.976	146°06.913		4	50-150	25813	25641	129
				3	150-200	21284	21154	97.5
				2	200-500	18377	18000	282.75
				1	500-1000	19136	18191	708.75
LV 29-103-5	53°26.170 /	146°06.527 /	1750 / 1748	5	0-50	11712	11523	141.75
	53°26.893	146°05.638		4	50-150	26122	25813	231.75
				3	150-200	21490	21284	154.5
				2	200-500	18951	18377	430.5
				1	500-1000	20249	19136	834.75
LV 29-106-4	51°59.868 /	154°02.637 /	512 / 510	5	0-50	11937	11712	168.75
	51°59.967	154°02.804		4	50-150	26387	26122	198.75
				3	150-200	21677	21490	140.25
				2	200-300	19207	18951	192
				1	300-500	20866	20249	462.75
LV 29-108-1	52°01.077 /	153°34.755 /	624 / 626	5	0-50	12285	11937	261
	52°01.438	153°34.760		4	50-150	26776	26387	291.75
				3	150-200	21911	21677	175.5
				2	200-400	19787	19207	435
				1	400-600	21626	20866	570
LV 29-110-5	50°27.288 /	154°46.240 /	1218 / 1213	5	0-50	12591	12285	229.5
	50°25.736	154°48.721		4	50-150	27095	26776	239.25
				3	150-200	22192	21911	210.75
				2	200-500	20735	19787	711
				1	500-1000	22941	21626	986.25
LV 29-112-4	50°13.275 /	154°17.416 /	1312 / 1364	5	0-50	12740	12591	111.75
	50°12.804	154°19.327		4	50-150	27350	27095	191.25
				3	150-200	22373	22192	135.75
				2	200-500	21223	20735	366
				1	500-1000	24227	22941	964.5
LV 29-114-5	49°22.338 /	152°53.375 /	1770 / 1780	5	0-50	12843	12740	77.25
	49°21.598	152°53.328		4	50-150	27526	27350	132
				3	150-200	22475	22373	76.5
				2	200-500	21607	21223	288
				1	500-1000	24812	24227	438.75

Sample	Latitude N	Longitude E	Water depth (m)	Net No	depth interval (m)	F	S	V [m³]
LV 29-115-2	48°36.260 / 48°37.044	153°09.787 / 153°10.013	2126 / 2503	5	0-50	12923	12843	60
				4	50-150	27633	27526	80.25
				3	150-200	22549	22475	55.5
				2	200-500	21712	21607	78.75
				1	500-1000	25120	24812	231
LV 29-116-1	47°55.025 / 47°56.285	151°54.743 / 151°53.824	3278 / 3264	5	0-50	12997	12923	55.5
				4	50-150	27709	27633	57
				3	150-200	22604	22549	41.25
				2	200-500	21823	21712	83.25
				1	500-1000	25463	25120	257.25
LV 29-120-2	47°03263 / 47°02.061	150°55.809 / 150°56.143	3278 / 3273	5	0-800	14652	12997	1241.25
				4	800-1000	28024	27709	236.25
				3	1000-1200	22859	22604	191.25
				2	1200-1500	22226	21823	302.25
				1	1500-2000	26300	25463	627.75
LV 29-120-3	47°01.765 / 47°01.141	150°55.883 / 150°55.501	3273 / 3263	5	0-50	14784	14652	99
				4	50-150	28219	28024	146.25
				3	150-200	22962	22859	77.25
				2	200-500	22722	22226	372
				1	500-800	26937	26300	477.75
LV 29-123-1	47°41.453 / 47°41.239	149°52.929 / 149°50.728	3311 / 3312	5	0-600	15432	14784	486
				4	600-900	28504	28219	213.75
				3	900-1200	23121	22962	119.25
				2	1200-1500	23070	22722	261
				1	1500-2000	27631	26937	520.5
LV 29-123-2	47°40.826	149°49.224	3303	5	0-50	15535	15432	77.25
				4	50-150	28556	28504	39
				3	150-200	23192	23121	53.25
				2	200-400	23236	23070	124.5
				1	400-600	27888	27631	192.75

F = flowmeter final value
S = flowmeter start value
V = water volume flown through each net (m^3)

APPENDIX 6

Paleoceanology data

Physical core properties

Core	Depth (cm}	Weight water (%)	Volume Water (%)	Wot Density (g/cm^3)	Dry Density (g/cm^3)
LV29-53-2	48	44,96	69,60	1,55	0,85
LV29-53-2	78	42,68	67,00	1,57	0,90
LV29-53-2	132	49,56	73,20	1,48	0,75
LV29-53-2	170	52,85	75,60	1,43	0,67
LV29-53-2	207	55,21	77,60	1,41	0,63
LV29-53-2	310	50,54	74,60	1,48	0,73
LV29-53-2	350	48,65	66,60	1,37	0,70
LV29-53-2	390	47,14	70,80	1,50	0,79
LV29-53-2	445	47,38	70,20	1,48	0,78
LV29-53-2	490	49,81	72,40	1,45	0,73
LV29-56-2	22	37,47	61,70	1,65	1,03
LV29-56-2	48	46,99	71,00	1,51	0,80
LV29-59-2	30	34,83	56,00	1,61	1,05
LV29-59-2	73	32,01	52,40	1,64	1,11
LV29-59-2	135	29,30	49,60	1,69	1,20
LV29-59-2	175	37,42	60,20	1,61	1,01
LV29-59-2	238	31,34	55,00	1,76	1,21
LV29-59-2	280	36,57	59,20	1,62	1,03
LV29-59-2	315	31,11	50,00	1,61	1,11
LV29-59-2	360	32,67	51,00	1,56	1,05
LV29-59-2	395	38,61	68,10	1,76	1,08
LV29-59-2	451	31,17	48,60	1,56	1,07
LV29-59-2	498	23,43	39,30	1,68	1,28
LV29-59-2	537	21,81	38,60	1,77	1,38
LV29-63-2	15	49,02	72,50	1,48	0,75
LV29-63-2	50	43,70	69,70	1,60	0,90
LV29-63-2	85	45,68	71,30	1,56	0,85
LV29-63-2	130	51,06	75,30	1,47	0,72
LV29-63-2	170	54,63	75,90	1,39	0,63
LV29-63-2	210	44,93	69,80	1,55	0,86
LV29-63-2	252	49,80	74,20	1,49	0,75
LV29-63-2	290	44,61	69,10	1,55	0,86
LV29-63-2	330	37,06	61,40	1,66	1,04
LV29-63-2	370	40,45	66,90	1,65	0,99
LV29-63-2	412	40,35	65,30	1,62	0,97
LV29-63-2	448	43,95	69,00	1,57	0,88
LV29-69-2	50	61,62	82,20	1,33	0,51
LV29-69-2	100	60,36	80,40	1,33	0,53
LV29-69-2	150	59,29	78,80	1,33	0,54
LV29-69-2	200	59,60	79,80	1,34	0,54
LV29-69-2	250	58,01	78,90	1,36	0,57
LV29-69-2	300	57,47	78,80	1,37	0,58
LV29-69-2	350	57,75	79,00	1,37	0,58
LV29-69-2	400	54,51	77,00	1,41	0,64
LV29-69-2	450	52,70	75,50	1,43	0,68
LV29-69-2	500	51,50	74,00	1,44	0,70
LV29-69-2	550	48,41	71,40	1,48	0,76
LV29-69-2	600	45,86	69,20	1,51	0,82
LV29-69-2	625	46,93	71,80	1,53	0,81
LV29-69-2	675	45,11	68,80	1,53	0,84
LV29-69-2	700	44,75	68,20	1,52	0,84
LV29-69-2	740	45,87	69,80	1,52	0,82
LV29-70-2	50	65,35	84,60	1,29	0,45
LV29-70-2	100	56,23	79,00	1,41	0,62
LV29-70-2	150	55,13	76,60	1,39	0,62
LV29-70-2	200	54,36	76,60	1,41	0,64
LV29-70-2	250	52,27	75,40	1,44	0,69
LV29-70-2	300	54,85	77,40	1,41	0,64

Core	Depth (cm}	Weight water (%)	Volume Water (%)	Wot Density (g/cm^3)	Dry Density (g/cm^3)
LV29-70-2	350	57,15	79,50	1,39	0,60
LV29-70-2	400	52,46	75,80	1,44	0,69
LV29-70-2	450	48,05	71,40	1,49	0,77
LV29-70-2	500	48,49	72,40	1,49	0,77
LV29-70-2	550	49,35	73,40	1,49	0,75
LV29-70-2	600	49,67	73,80	1,49	0,75
LV29-70-2	650	56,23	77,20	1,37	0,60
LV29-70-2	700	54,13	77,40	1,43	0,66
LV29-70-2	750	53,66	76,60	1,43	0,66
LV29-70-2	800	52,07	75,60	1,45	0,70
LV29-70-2	850	52,79	73,80	1,40	0,66
LV29-72-2	45	70,99	92,30	1,30	0,38
LV29-72-2	100	70,35	89,20	1,27	0,38
LV29-72-2	150	69,53	89,60	1,29	0,39
LV29-72-2	200	69,49	87,20	1,25	0,38
LV29-72-2	250	67,95	84,60	1,25	0,40
LV29-72-2	300	66,66	84,50	1,27	0,42
LV29-72-2	350	57,27	80,00	1,40	0,60
LV29-72-2	400	55,09	77,40	1,41	0,63
LV29-72-2	450	55,58	78,20	1,41	0,63
LV29-72-2	500	54,06	77,30	1,43	0,66
LV29-72-2	550	56,06	78,60	1,40	0,62
LV29-72-2	600	57,25	79,00	1,38	0,59
LV29-72-2	650	54,55	77,30	1,42	0,64
LV29-72-2	700	53,82	77,40	1,44	0,66
LV29-72-2	750	55,39	78,10	1,41	0,63
LV29-72-2	800	47,88	72,40	1,51	0,79
LV29-72-2	850	47,46	71,90	1,52	0,80
LV29-78-2	65	64,27	84,20	1,31	0,47
LV29-78-2	100	59,72	82,00	1,37	0,55
LV29-78-2	150	60,26	82,20	1,36	0,54
LV29-78-2	200	61,04	82,20	1,35	0,52
LV29-78-2	250	64,38	86,20	1,34	0,48
LV29-78-2	300	61,02	84,50	1,38	0,54
LV29-78-2	350	60,17	85,00	1,41	0,56
LV29-78-2	400	59,67	83,30	1,40	0,56
LV29-78-2	450	58,37	79,80	1,37	0,57
LV29-78-2	500	59,08	78,40	1,33	0,54
LV29-78-2	550	56,78	76,60	1,35	0,58
LV29-78-2	600	56,44	78,40	1,39	0,61
LV29-78-2	650	58,37	77,80	1,33	0,55
LV29-78-2	700	57,10	78,60	1,38	0,59
LV29-78-2	750	57,12	75,80	1,33	0,57
LV29-78-2	790	57,03	73,80	1,29	0,56
LV29-79-2	50	67,44	86,70	1,29	0,42
LV29-79-2	100	67,95	88,40	1,30	0,42
LV29-79-2	150	66,26	85,20	1,29	0,43
LV29-79-2	200	68,03	88,40	1,30	0,42
LV29-79-2	250	66,41	86,60	1,30	0,44
LV29-79-2	300	67,10	87,80	1,31	0,43
LV29-79-2	350	65,07	88,20	1,36	0,47
LV29-79-2	400	64,60	86,40	1,34	0,47
LV29-79-2	450	59,44	80,60	1,36	0,55
LV29-79-2	500	58,59	83,20	1,42	0,59
LV29-79-2	550	60,32	82,40	1,37	0,54

Core	Depth (cm}	Weight water (%)	Volume Water (%)	Wot Density (g/cm^3)	Dry Density (g/cm^3)
LV29-94-2	50	53,19	77,00	1,45	0,68
LV29-94-2	100	51,14	75,10	1,47	0,72
LV29-94-2	150	49,47	74,00	1,50	0,76
LV29-94-2	200	47,88	72,40	1,51	0,79
LV29-94-2	250	50,83	76,40	1,50	0,74
LV29-94-2	300	46,77	71,60	1,53	0,82
LV29-94-2	350	50,47	74,40	1,47	0,73
LV29-94-2-	400	50,56	72,50	1,43	0,71
LV29-94-2	450	50,25	73,70	1,47	0,73
LV29-94-2	500	48,64	73,20	1,51	0,77
LV29-94-2	550	49,12	72,90	1,48	0,76
LV29-94-2	600	47,47	71,40	1,50	0,79
LV29-94-2	650	36,90	62,00	1,68	1,06
LV29-94-2	705	32,33	57,60	1,78	1,21
LV29-94-2	735	47,24	73,00	1,55	0,82
LV29-94-2	773	46,01	69,20	1,50	0,81
LV29-94-2	800	44,50	68,80	1,55	0,86
LV29-94-2	850	45,25	69,80	1,54	0,84
LV29-100-2	70	49,07	73,60	1,50	0,76
LV29-100-2	115	51,22	74,30	1,45	0,71
LV29-100-2	185	49,56	72,60	1,46	0,74
LV29-100-2	295	55,37	78,40	1,42	0,63
LV29-103-2	50	74,76	90,60	1,21	0,31
LV29-103-2	100	68,21	85,20	1,25	0,40
LV29-103-2	125	62,34	83,60	1,34	0,51
LV29-103-2	145	63,38	83,60	1,32	0,48
LV29-103-2	165	58,91	83,60	1,42	0,58
LV29-103-2	200	53,77	77,80	1,45	0,67
LV29-103-2	230	60,30	81,60	1,35	0,54
LV29-103-2	270	57,29	79,40	1,39	0,59
LV29-103-2	300	51,38	75,40	1,47	0,71
LV29-103-2	335	50,92	76,00	1,49	0,73
LV29-103-2	370	49,70	74,00	1,49	0,75
LV29-103-2	400	48,97	73,20	1,49	0,76
LV29-103-2	450	48,22	73,00	1,51	0,78
LV29-103-2	550	46,75	71,20	1,52	0,81
LV29-103-2	600	44,73	69,00	1,54	0,85
LV29-103-2	635	43,93	68,60	1,56	0,88
LV29-103-2	675	39,35	65,00	1,65	1,00
LV29-103-2	687	26,57	44,00	1,66	1,22
LV29-103-2	698	34,00	61,00	1,79	1,18
LV29-103-2	725	52,56	76,10	1,45	0,69
LV29-103-2	760	46,37	70,80	1,53	0,82
LV29-103-2	815	45,63	69,90	1,53	0,83
LV29-103-2	855	28,96	53,40	1,84	1,31
LV29-103-2	905	56,07	77,60	1,38	0,61
LV29-103-2	945	49,16	70,60	1,44	0,73
LV29-106-2	32	65,24	88,00	1,35	0,47
LV29-106-2	62	47,50	74,00	1,56	0,82
LV29-106-2	105	50,40	75,40	1,50	0,74
LV29-106-2	150	50,48	75,00	1,49	0,74
LV29-106-2	200	50,76	76,60	1,51	0,74
LV29-106-2	250	46,92	71,60	1,53	0,81
LV29-106-2	300	50,95	74,80	1,47	0,72
LV29-106-2	350	50,64	75,60	1,49	0,74

Core	Depth (cm}	Weight water (%)	Volume Water (%)	Wot Density (g/cm^3)	Dry Density (g/cm^3)
LV29-106-2	400	59,60	82,60	1,39	0,56
LV29-110-2	30	45,64	70,40	1,54	0,84
LV29-110-2	70	52,65	76,20	1,45	0,69
LV29-110-2	130	52,27	76,00	1,45	0,69
LV29-110-2	160	48,77	73,20	1,50	0,77
LV29-110-2	190	49,63	74,60	1,50	0,76
LV29-110-2	220	48,95	74,60	1,52	0,78
LV29-110-2	260	52,74	78,00	1,48	0,70
LV29-110-2	290	53,27	75,80	1,42	0,67
LV29-110-2	320	45,76	70,60	1,54	0,84
LV29-112-2	50	64,73	83,60	1,29	0,46
LV29-112-2	100	65,24	84,00	1,29	0,45
LV29-112-2	150	68,04	89,60	1,32	0,42
LV29-112-2	200	63,68	82,70	1,30	0,47
LV29-112-2	250	61,30	82,20	1,34	0,52
LV29-112-2	300	62,01	82,80	1,34	0,51
LV29-112-2	350	60,61	80,40	1,33	0,52
LV29-112-2	400	59,54	81,80	1,37	0,56
LV29-112-2	450	57,31	80,00	1,40	0,60
LV29-112-2	490	50,55	73,80	1,46	0,72
LV29-112-2	540	53,72	75,00	1,40	0,65
LV29-114-2	50	71,27	89,00	1,25	0,36
LV29-114-2	100	67,97	90,60	1,33	0,43
LV29-114-2	150	64,60	82,20	1,27	0,45
LV29-114-2	200	49,74	76,40	1,54	0,77
LV29-114-2	250	54,28	77,40	1,43	0,65
LV29-114-2	300	54,67	79,60	1,46	0,66
LV29-114-2	350	56,20	79,80	1,42	0,62
LV29-114-2	400	53,85	78,40	1,46	0,67
LV29-114-2	450	55,38	79,80	1,44	0,64
LV29-114-2	510	54,13	78,60	1,45	0,67
LV29-114-2	550	54,81	78,60	1,43	0,65
LV29-114-2	600	51,85	76,20	1,47	0,71
LV29-114-2	650	54,74	77,40	1,41	0,64
LV29-114-2	700	48,41	73,20	1,51	0,78
LV29-114-2	740	57,69	80,00	1,39	0,59
LV29-131-2	50	63,07	84,20	1,34	0,49
LV29-131-2	100	61,09	82,80	1,36	0,53
LV29-131-2	150	59,66	80,00	1,34	0,54
LV29-131-2	200	58,65	80,00	1,36	0,56
LV29-131-2	250	57,64	79,20	1,37	0,58
LV29-131-2	300	52,54	74,80	1,42	0,68
LV29-131-2	350	47,81	72,00	1,51	0,79
LV29-131-2	400	52,18	74,80	1,43	0,69
LV29-131-2	450	40,73	58,00	1,42	0,84
LV29-131-2	500	45,38	69,00	1,52	0,83
LV29-131-2	550	46,42	70,00	1,51	0,81
LV29-131-2	600	44,52	68,60	1,54	0,85
LV29-131-2	650	45,71	70,40	1,54	0,84
LV29-131-2	700	44,88	69,20	1,54	0,85
LV29-131-2	750	45,38	69,80	1,54	0,84
LV29-131-2	800	43,80	67,80	1,55	0,87
LV29-131-2	850	44,42	68,40	1,54	0,86

List of smear slides (intervals, cm) prepared from Russian cores

LV29-69-2	LV29-70-2	LV29-72-2	LV29-78-2	LV29-79-2	LV29-82-1	LV29-94-2		LV29-103-2			LV29-104-2			LV29-106-2	LV29-108-4	LV29-110-2	LV29-112-2	LV29-114-2	LV29-131-2	
0	0	0	0	0	0	0	450	0	340	755	0	410	920	0	0	0	0	0	0	630
20	15	20	20	20	20	5	460	5	350	760	5	420	930	10	20	20	20	20	20	640
40	35	40	40	40	40	10	470	10	360	765	10	430	940	20	40	40	40	40	40	650
60	55	60	60	60	60	15	480	15	370	770	15	440	950	30	60	60	60	60	60	650
80	75	80	80	80	80	20	490	20	380	775	20	450	960	40	80	80	80	80	80	670
100	95	100	100	100	100	25	500	25	400	780	25	460	970	50	100	100	100	100	100	680
120	115	120	120	120	120	30	510	30	410	785	30	470		60	120	120	120	120	120	690
140	135	140	140	140	140	35	520	35	420	790	35	480		70	140	140	140	140	140	700
160	155	160	160	160	160	40	530	40	430	795	40	490		80	160	160	160	160	160	710
180	175	180	180	180	180	45	540	45	440	800	45	500		90	180	180	180	180	180	720
200	195	200	200	200	200	50	550	50	450	810	50	510		100	200	200	200	200	200	730
220	215	220	220	220	220	55	560	55	460	820	55	520		120	220	220	220	220	220	740
240	235	240	240	240	240	60	570	60	470	830	60	530		140	240	240	240	240	240	750
260	255	260	260	260	260	70	580	65	480	840	65	540		160	260	260	260	260	250	760
280	275	280	280	280	280	80	590	70	490	850	70	550		180	280	280	280	280	260	770
300	295	300	300	300	300	90	600	75	500	855	75	560		200	300	300	300	300	270	780
320	315	320	320	320	320	100	610	80	510	860	80	570		220	320	320	320	320	280	790
340	335	340	340	340	340	110	620	85	520	865	85	580		240	340	340	340	340	290	800
360	355	360	360	360	360	120	630	90	530	870	90	590		260	360	360	360	360	300	810
380	375	380	380	380	380	130	640	95	540	875	95	600		280	380		380	380	310	820
400	395	400	400	400	400	140	650	100	550	879	100	610		300	400		400	400	320	830
420	415	420	420	420	420	150	650	105	560	880	110	620		320	420		420	420	330	840
440	435	440	440	440	440	160	670	110	570	885	120	630		340	440		440	440	340	850
460	455	460	460	460	460	170	680	115	580	890	130	640		360	460		460	460	350	860
480	475	480	480	480	480	180	690	120	590	895	140	650		380	480		480	480	360	870
500	495	500	500	500	500	190	700	125	600	900	150	650		400	500		500	500	370	
520	515	520	520	520	510	200	710	130	610	905	160	670		420	520		520	520	380	
540	535	540	540	540	520	210	720	135	620	910	170	680		440	540		540	540	390	
560	555	560	560	560	530	220	730	140	630	915	180	690			560		560	560	400	
580	575	580	580	570	540	230	740	145	640	920	190	700			580			580	410	
600	595	600	600	580	560	240	750	150	650	925	200	710			600			600	420	
610	615	620	620	590	580	250	760	155	665	930	210	720			620			620	430	
620	635	640	640	600	600	260	770	160	670	935	220	730			640			640	440	
630	655	660	660	610	620	270	780	165	675	940	230	740			660			660	450	
640	675	680	680	620	640	280	790	170	680	945	240	750			680			680	460	
650	695	700	700	630	660	290	800	180	685	950	250	760			700			700	470	
650	715	720	710	640	680	300	810	190	690	955	260	770			720			720	480	
670	735	740	720	660	700	310	820	200	695	960	270	780			740			740	490	
680	755	760	730	670	720	320	830	210	698	965	280	790			760			760	500	
690	775	780	740	676	740	330	840	220	700	970	290	800							510	
700	795	800	750	680	760	340	850	230	704	975	300	810							520	
710	815	820	760	690		350	860	240	705	980	310	820							530	
720	835	840	767	700		360	870	250	710		320	830							540	
730			770	710		370		260	715		330	840							550	
740			780	720		380		270	720		340	850							560	
750			790	730		390		280	725		350	860							570	
			800	740		400		290	730		360	870							580	
				750		410		300	735		370	880							590	
				760		420		310	740		380	890							600	
				770		430		320	745		390	900							610	
				788		440		330	750		400	910							620	

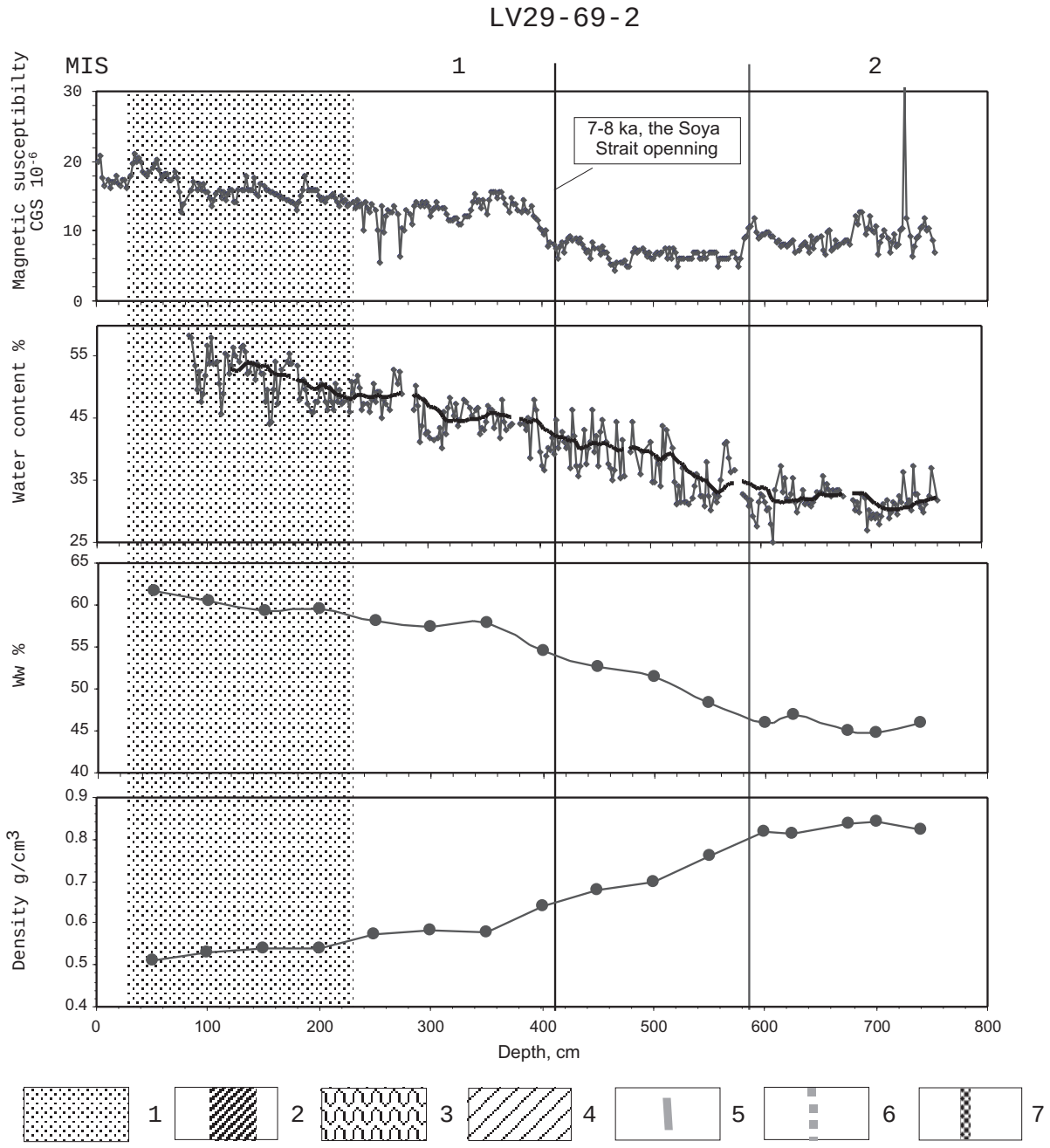

1 – diatom rich horizon with age 0-6 (8) ka; 2 – turbidite layers; 3 – diagenetic sulfide layer; 4 – diagenetic carbonate layers; 5 – volcanic ash layers; 6 – pumice layers; 7- top boundary of breccied sediment.

LV29-70-2

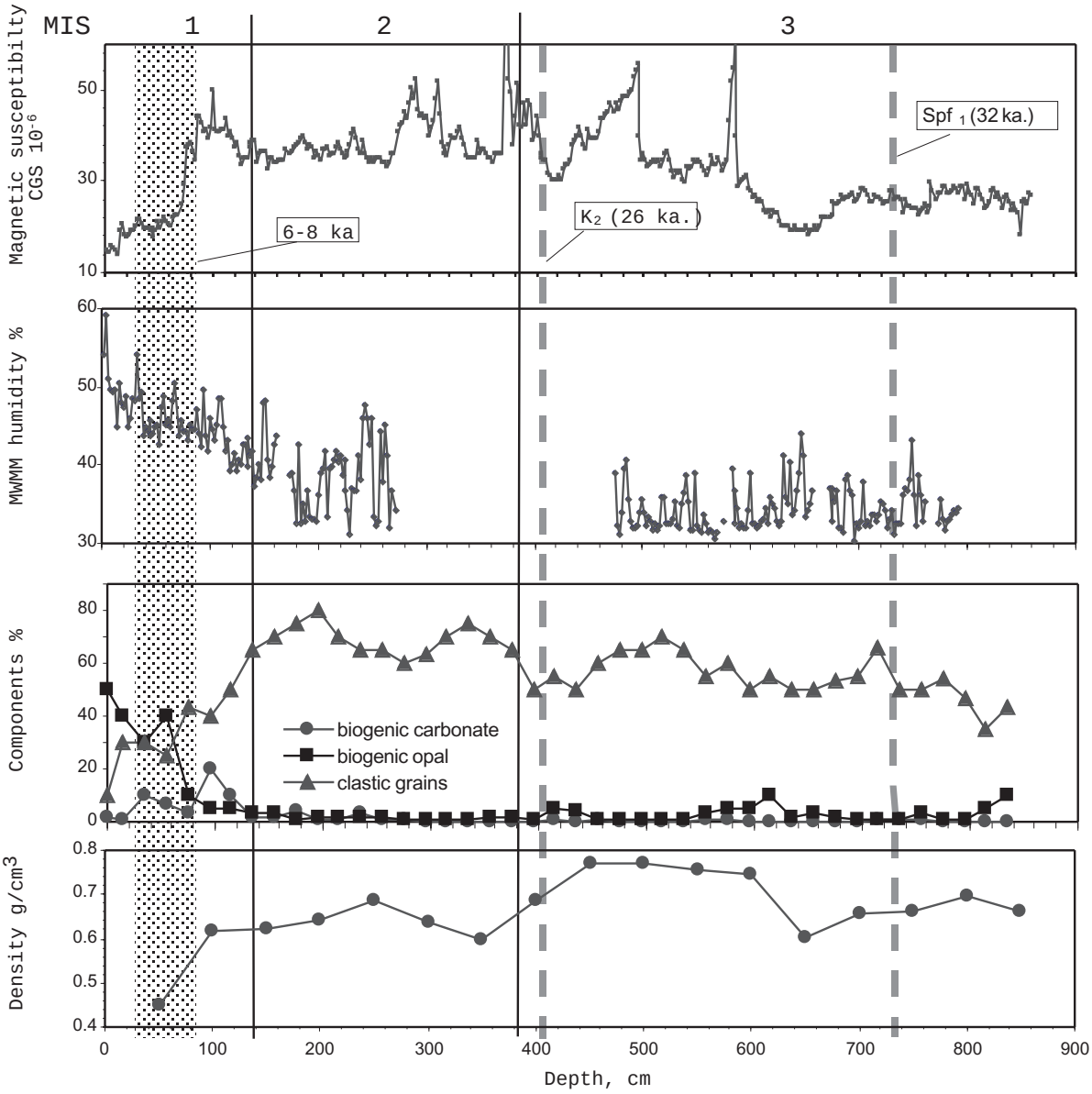
MIS
1
2
3
Magnetic susceptibility CGS 10-6
6-8 ka
K2 (26 ka.)
Spf 1 (32 ka.)
MWMM humidity %
Components %
biogenic carbonate
biogenic opal
clastic grains
Density g/cm3
Depth, cm

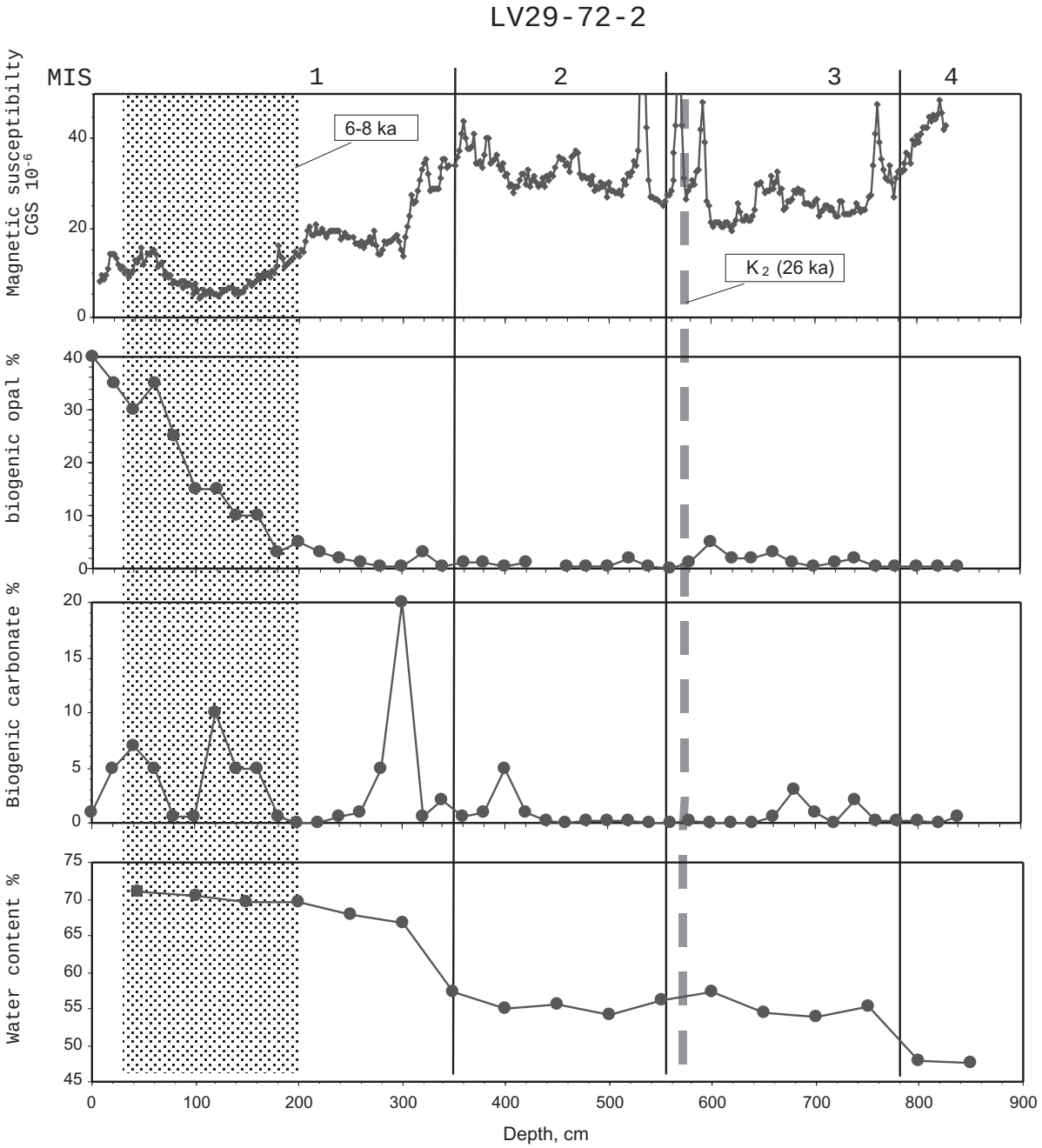
LV29-72-2
MIS
1
2
3
4
6-8 ka
K2 (26 ka)
Magnetic susceptibilty CGS 10-6
biogenic opal %
Biogenic carbonate %
Water content %
Depth, cm

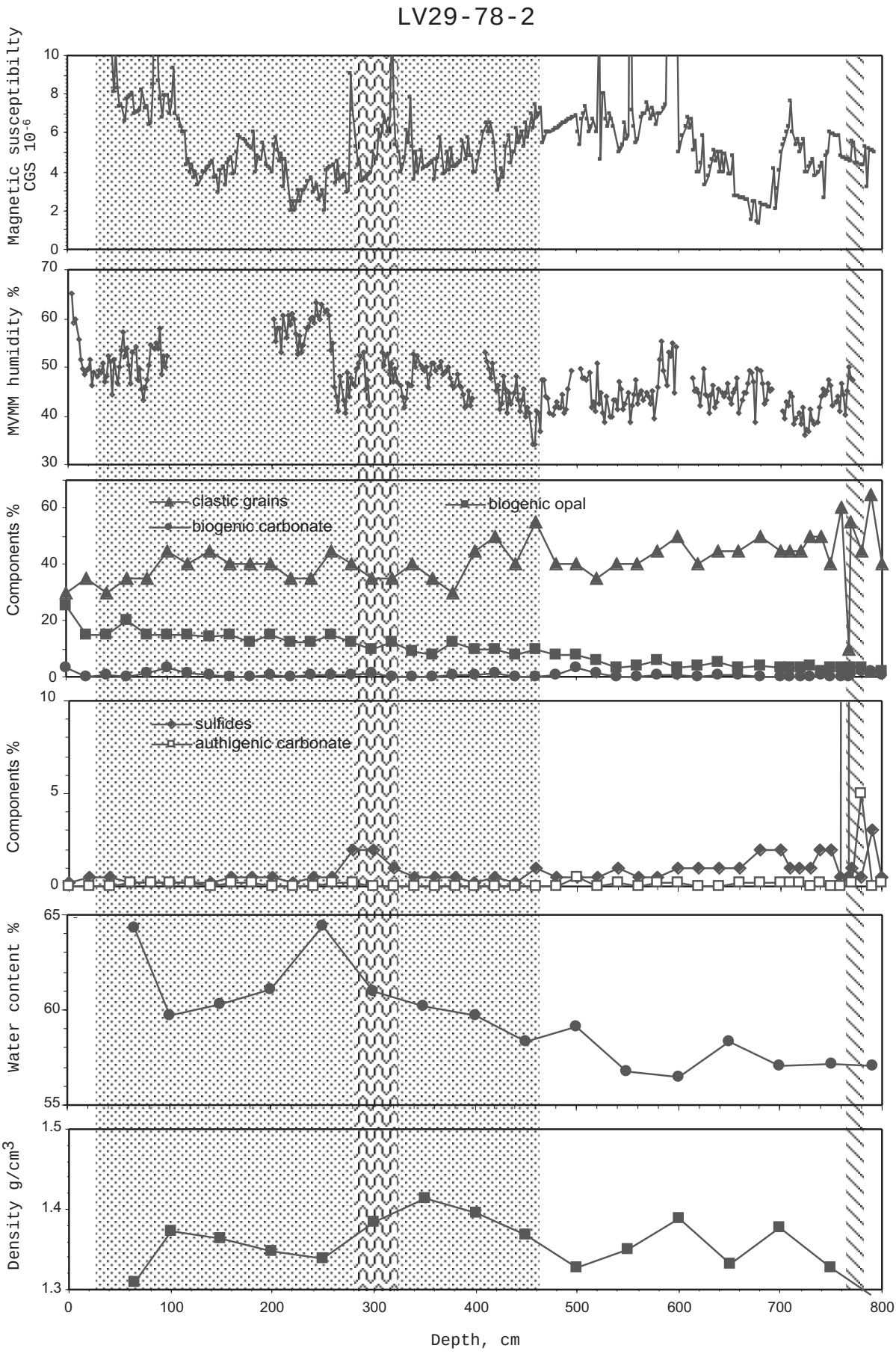
LV29-78-2
Magnetic susceptibilty CGS 10-6
MVMM humidity %
Components %
clastic grains
biogenic opal
biogenic carbonate
Components %
sulfides
authigenic carbonate
Water content %
Density g/cm3
Depth, cm

LV29-79-2

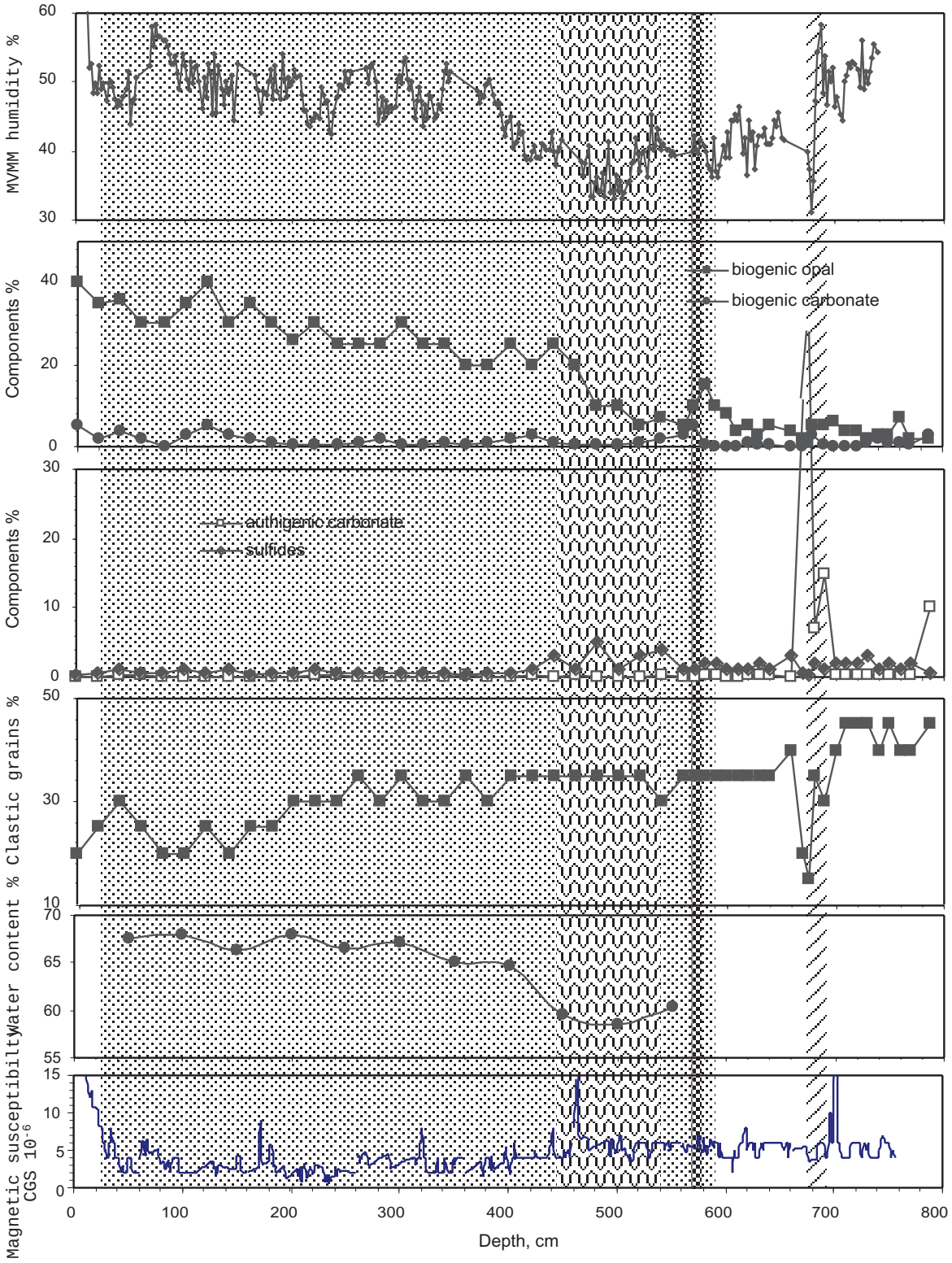
MVMM humidity %
Components %
biogenic opal
biogenic carbonate
authigenic carbonate
sulfides
Clastic grains %
Water content %
Magnetic susceptibility CGS 10^{-6}
Depth, cm

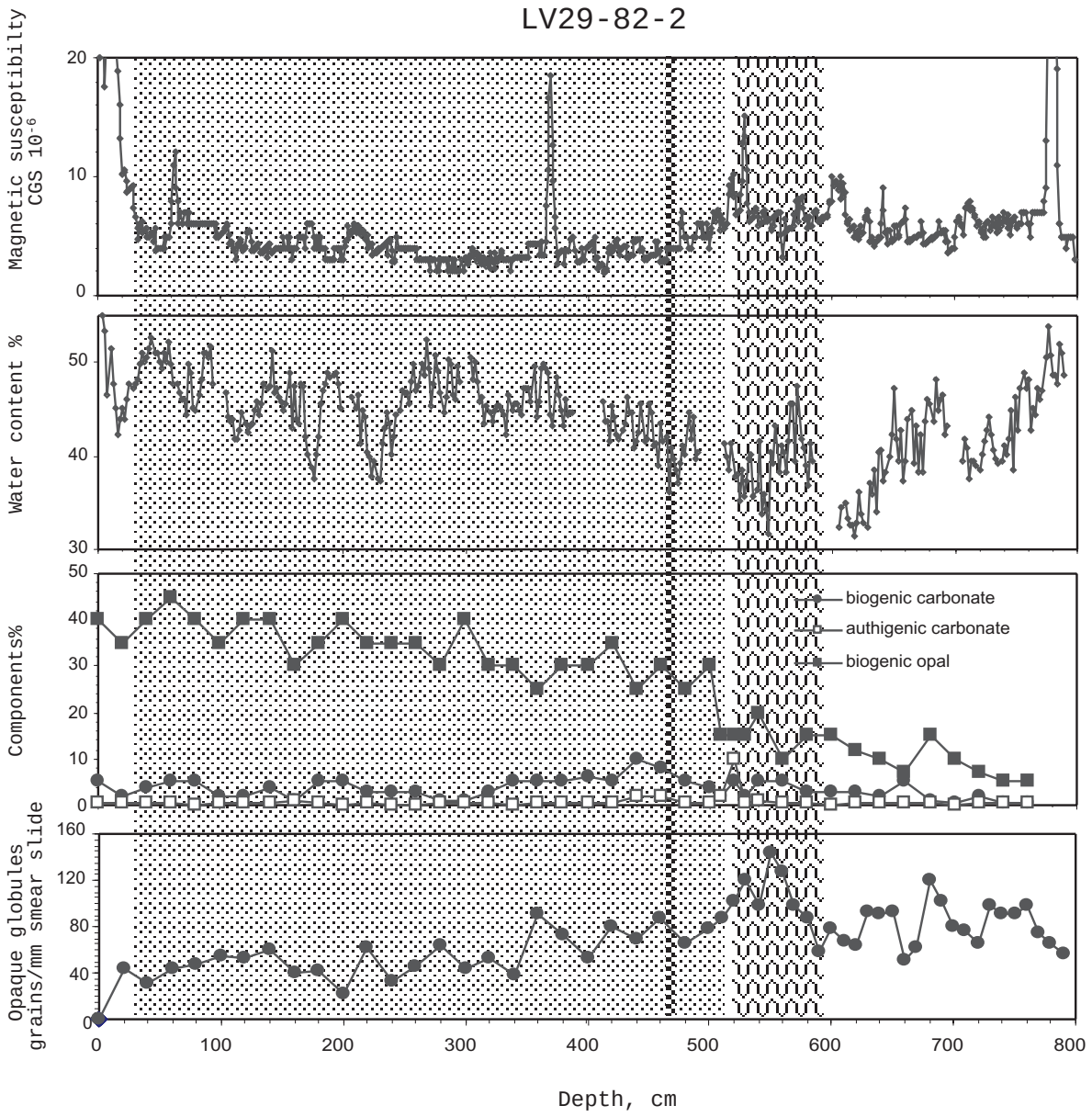
LV29-82-2
Magnetic susceptibilty
CGS 10-6
Water content %
Components%
biogenic carbonate
authigenic carbonate
biogenic opal
Opaque globules
grains/mm smear slide
Depth, cm

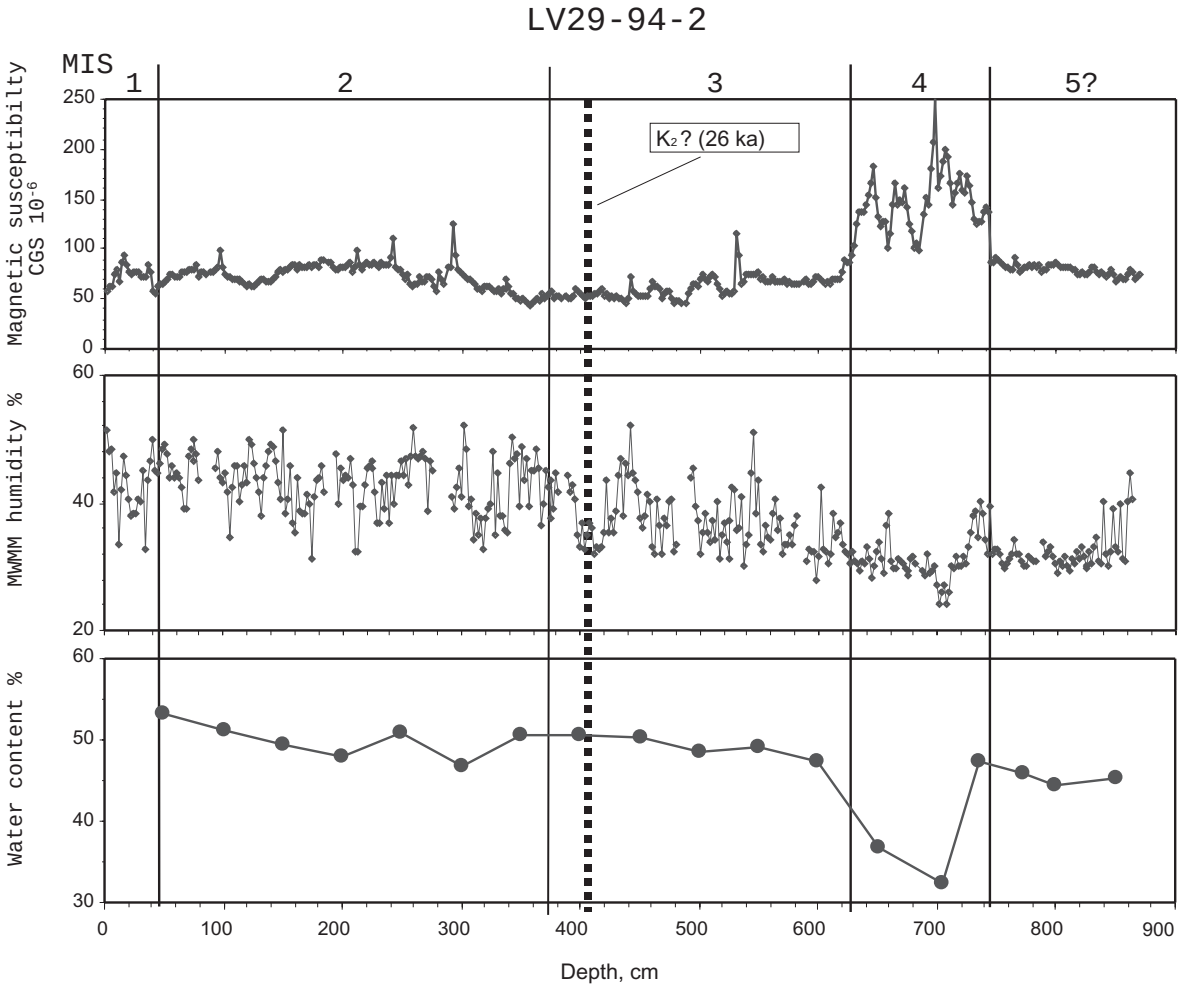
LV29-94-2
MIS
1
2
3
4
5?
K2? (26 ka)
Magnetic susceptibilty CGS 10-6
MWMM humidity %
Water content %
Depth, cm

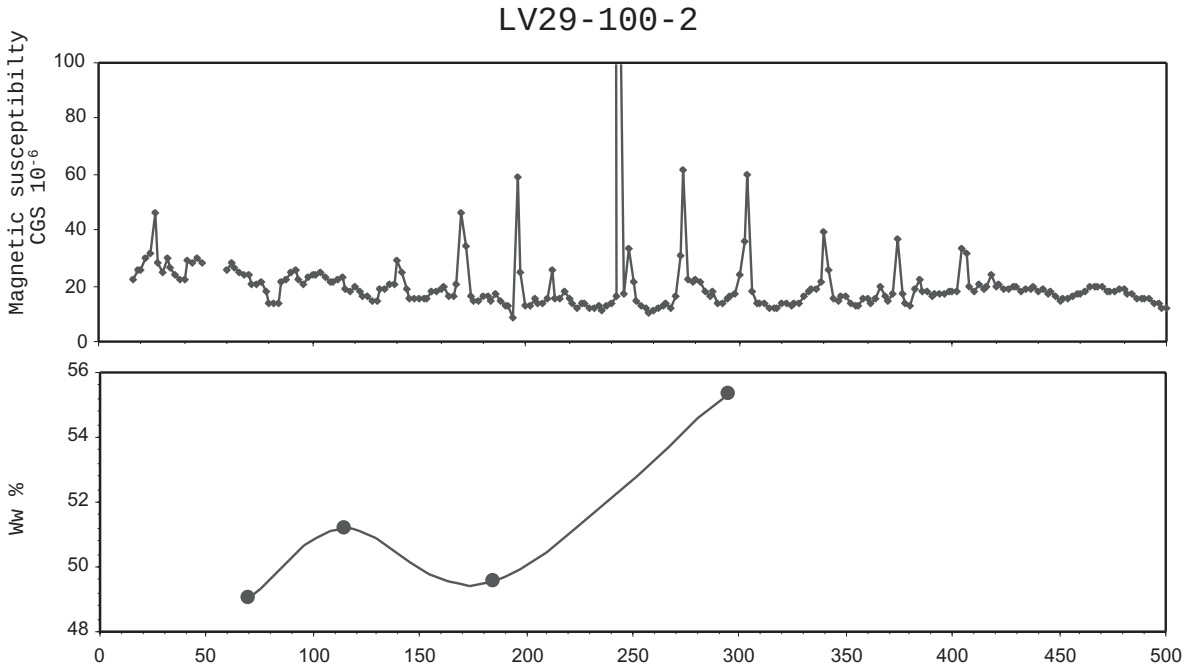
LV29-100-2
Magnetic susceptibilty CGS 10-6
Ww %

LV29-103-2

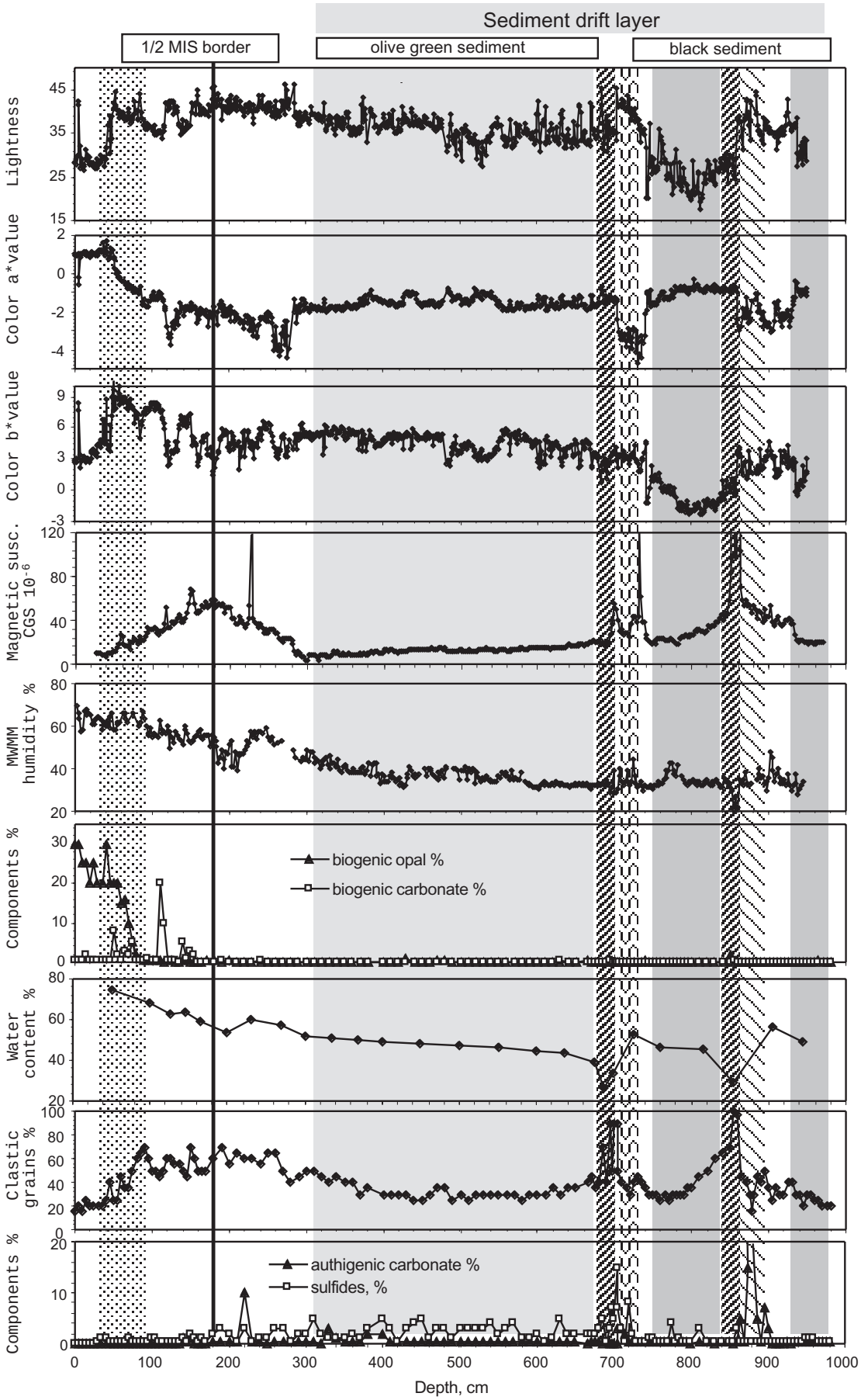
Sediment drift layer
1/2 MIS border
olive green sediment
black sediment
Lightness
Color a*value
Color b*value
Magnetic susc. CGS 10-6
MWMM humidity %
Components %
biogenic opal %
biogenic carbonate %
Water content %
Clastic grains %
Components %
authigenic carbonate %
sulfides, %
Depth, cm

LV29-104-2

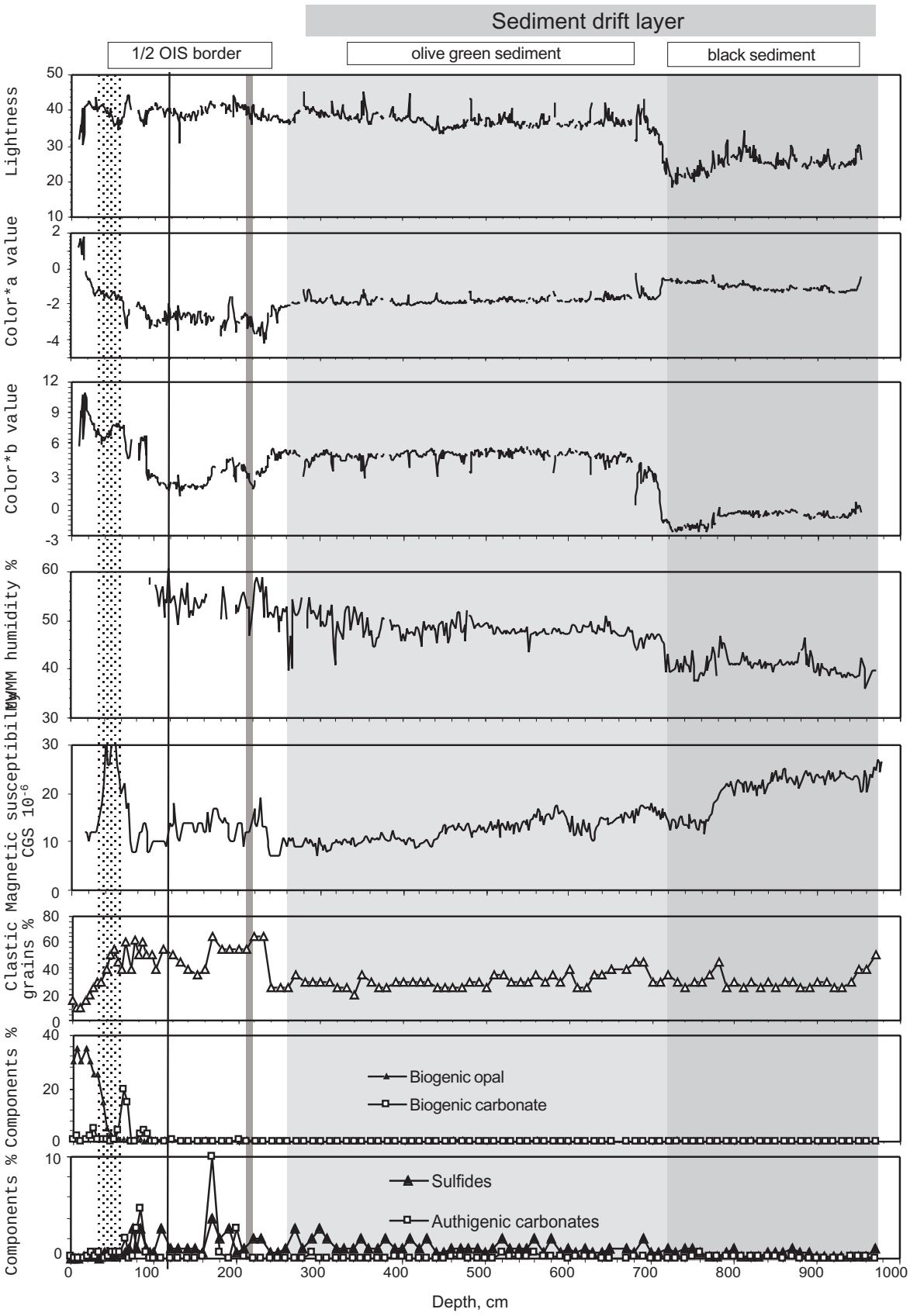
Sediment drift layer
1/2 OIS border
olive green sediment
black sediment
Lightness
Color*a value
Color*b value
MM humidity %
Magnetic susceptibility CGS 10-6
Clastic grains %
Components %
Components %
Biogenic opal
Biogenic carbonate
Sulfides
Authigenic carbonates
Depth, cm

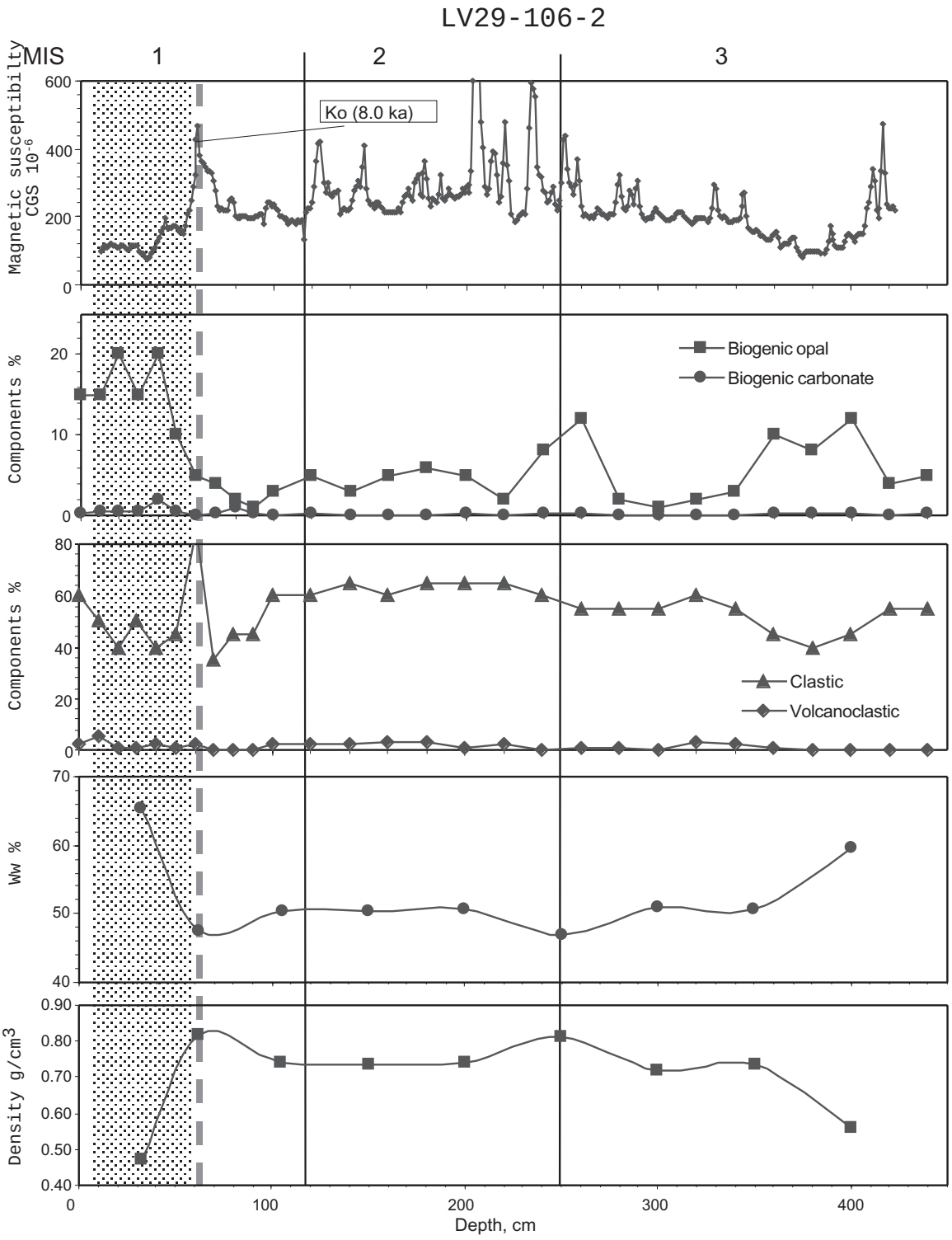
LV29-106-2
MIS
1
2
3
Magnetic susceptibility CGS 10-6
Ko (8.0 ka)
Components %
Biogenic opal
Biogenic carbonate
Components %
Clastic
Volcanoclastic
Ww %
Density g/cm3
Depth, cm

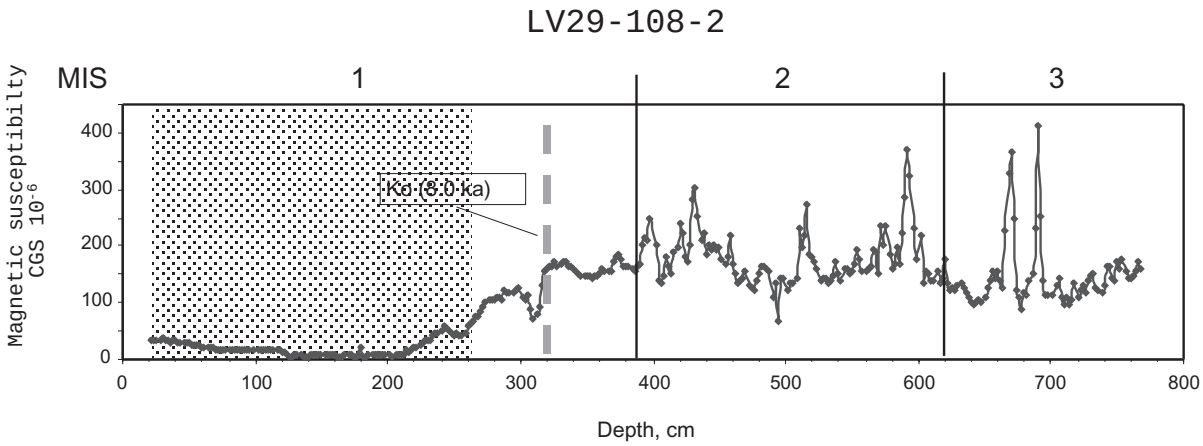
LV29-108-2
MIS
1
2
3
Ka (8.0 ka)
Magnetic susceptibilty
CGS 10-6
400
300
200
100
0
0
100
200
300
400
500
600
700
800
Depth, cm

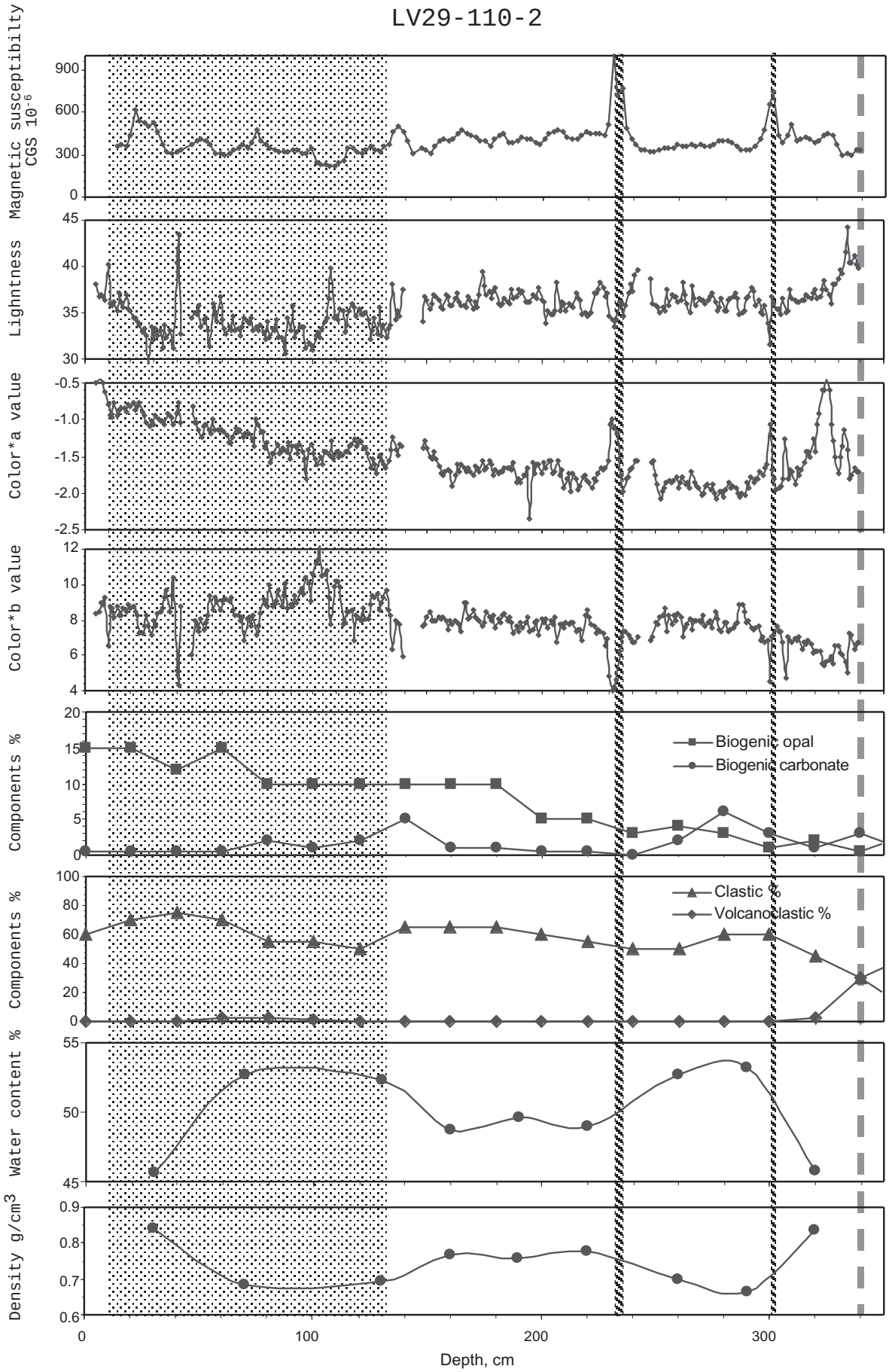
LV29-110-2
Magnetic susceptibilty CGS 10-6
Lighntness
Color*a value
Color*b value
Components %
Biogenic opal
Biogenic carbonate
Components %
Clastic %
Volcanoclastic %
Water content %
Density g/cm3
Depth, cm

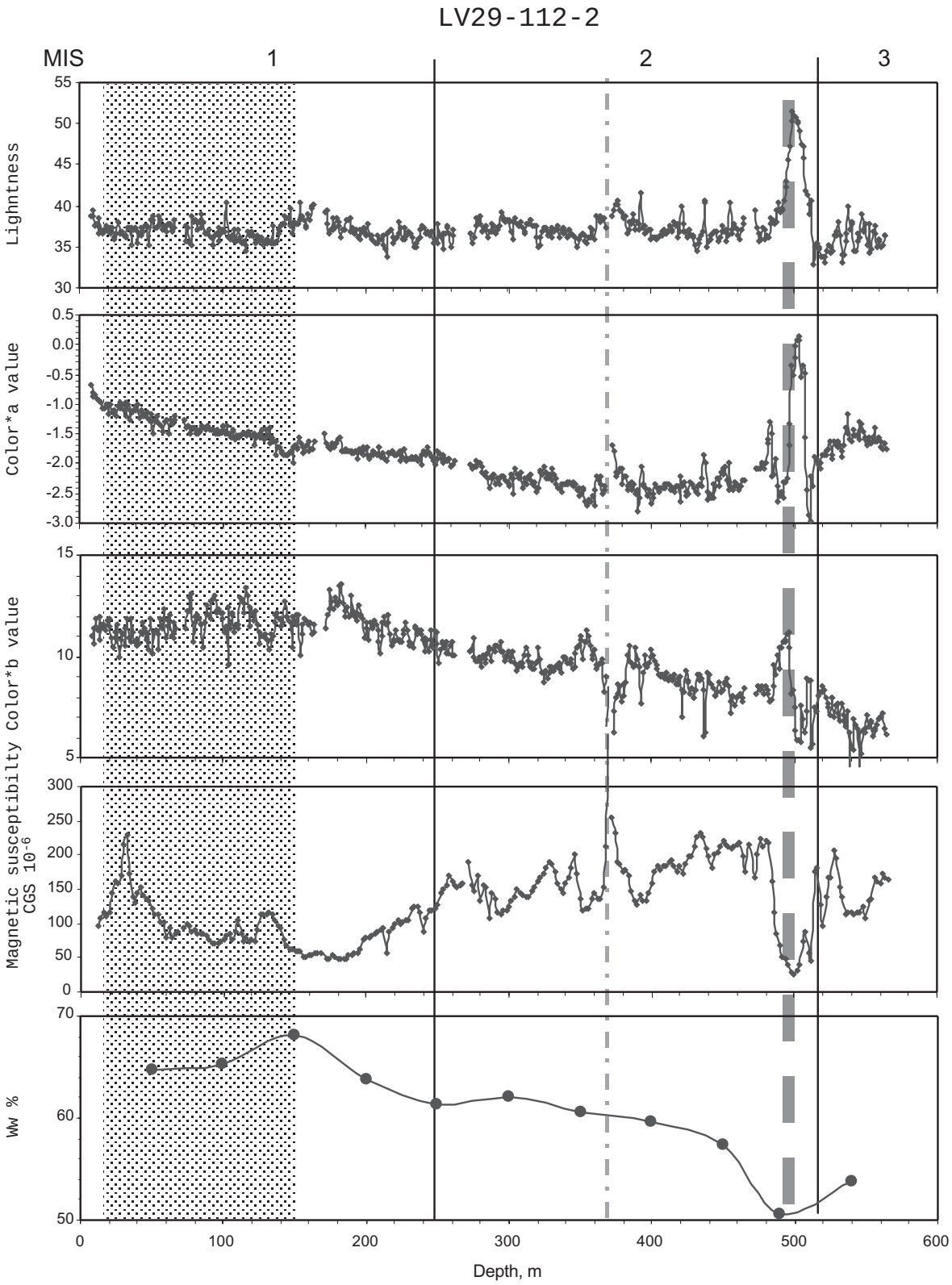
LV29-112-2
MIS
1
2
3
Lighntness
Color*a value
Color*b value
Magnetic susceptibility CGS 10-6
Ww %
Depth, m

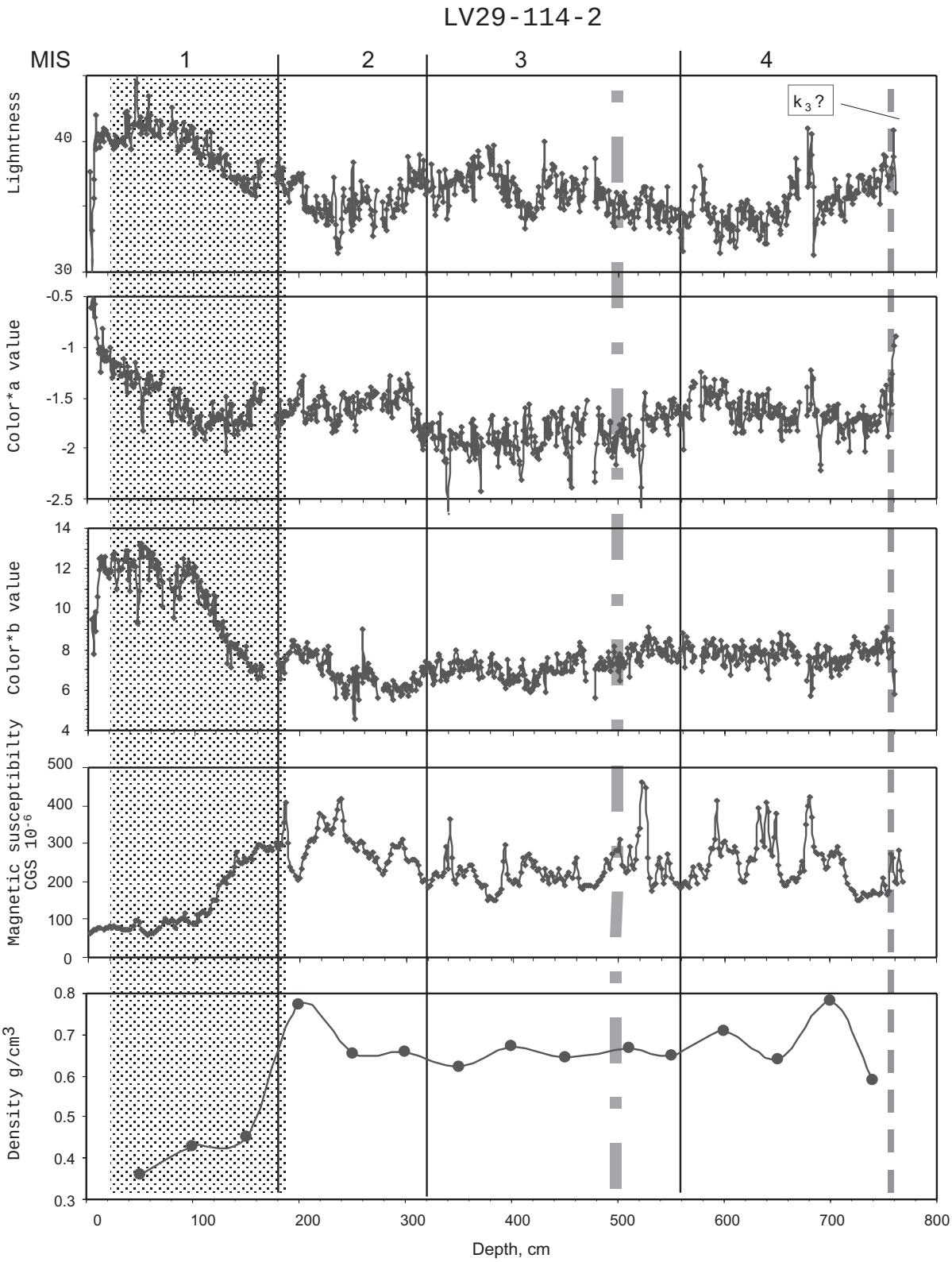
LV29-114-2
MIS
1
2
3
4
k3 ?
Lighntness
Color*a value
Color*b value
Magnetic susceptibilty CGS 10-6
Density g/cm3
Depth, cm

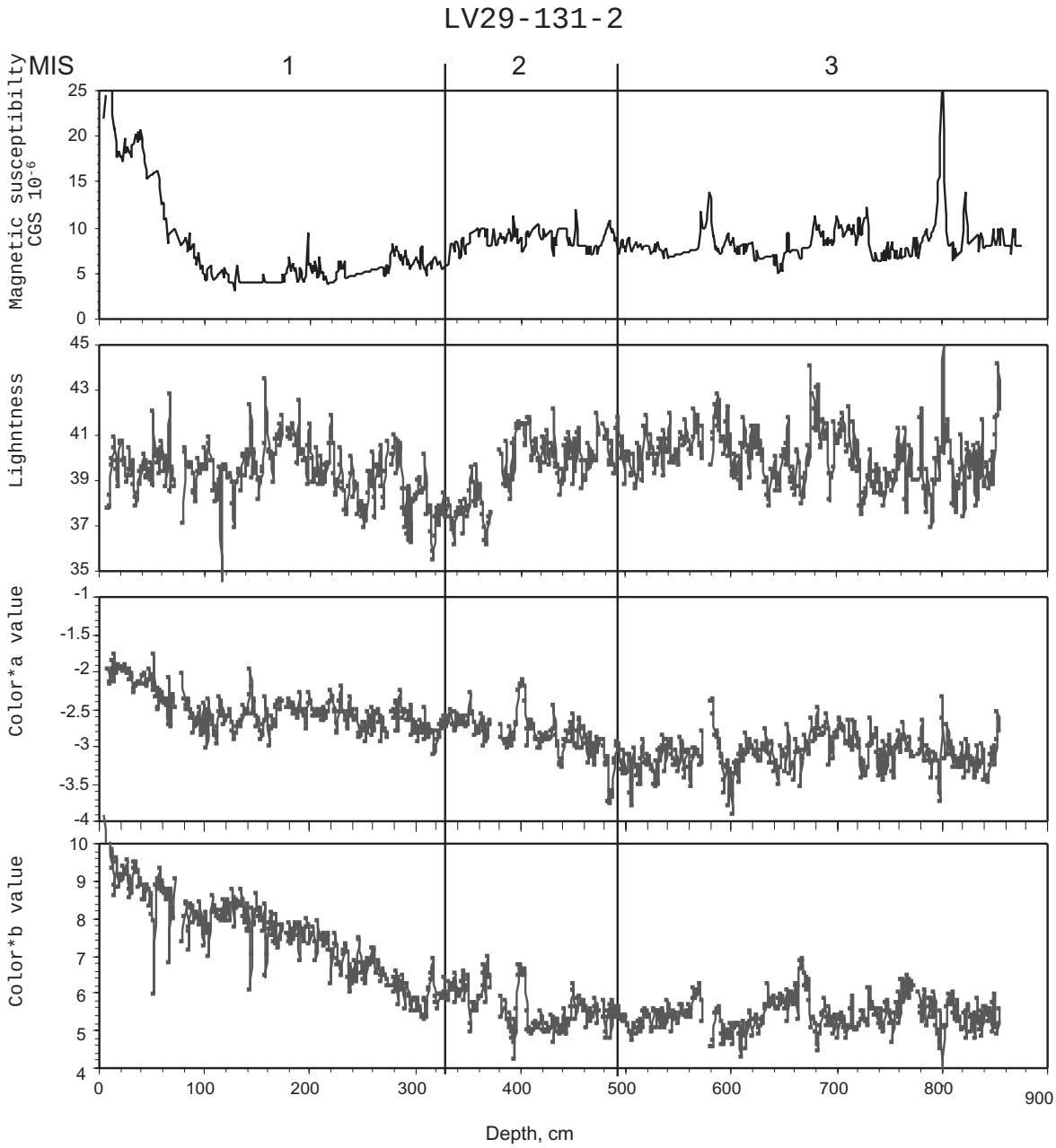
LV29-131-2
MIS
1
2
3
Magnetic susceptibility CGS 10-6
Lighntness
Color*a value
Color*b value
Depth, cm

LEGEND

LITHOLOGY

SAND	sandy silt	silty clay	sand with pebbles
silty sand	clayey silt	CLAY	volcanic ash
sand silt clay	DIATOM OOZE	clayey sand	gravel
SILT	gas saturated	sandy clay	

LITHOLOGIC ACCESSORIES

- sand laminae	- silt laminae	- clay lense
- sand lense	- black streaks	- black mottles
- ash layer	- ash lense	- breccied texture
Sul - sulfide, diagenetic	- diagenetic layer	SS - smearslide
Gl - glauconitic	- microcrystalline cement	Py - pyrite
- coal fragments	Wd - single Wood Fragments	- baryte crust
Pum. - pumice	H_2S - H2S	- sand agglomerate
- carb. concretion, nodule	- carbon. concretion, soft	- gas saturated texture
- hydrotroilite	- agglom. dropstones	- dropstone, single
- pebbles	- fining upward	- fining downward
- turbidite/contourite seq.	- void	- fissure
- laminae	- clay laminae	- Anoxic/black interval

FOSSILS

- wood fragment, large	- diatoms	- foraminifera (undiff.)
- foraminifera (pelagic)	- foraminifera (benthonic)	- shell fragment, undiff.
- gastropod	- pelecypod	- plant remains, debris
- radiolarians	Sp - spores, pollen	

BIOTURBATION

- Abundant
- Common
- Moderate
- Rare
- Barren

Nomenclature used for terrigenous fraction of mixed sediments

(modified after Shepherd, 1928)

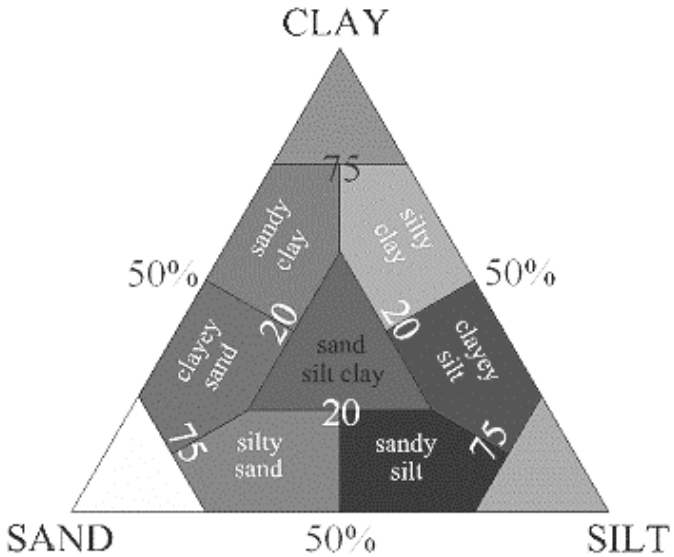

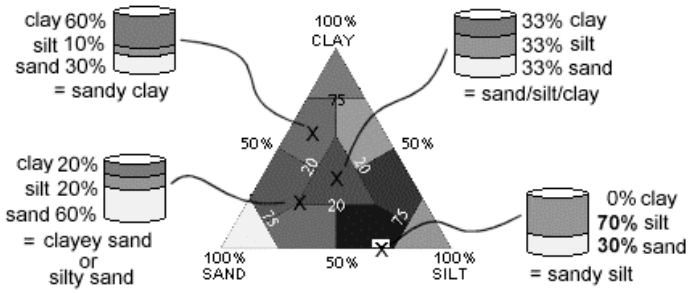

Columns in core descriptions

1 – core depth, metres
2 – section of core, no.
3 – graphic lithology
4 – graphic bioturbation
5 – lithological accessories
6 – fossils
7 – description

LV29-69-2 SL-R

45°26.447'N, 144°5.840'E

Date: July 1, 2002

Described by: Gorbarenko, S.A.; Astakhov, A.S. water depth: 868 m

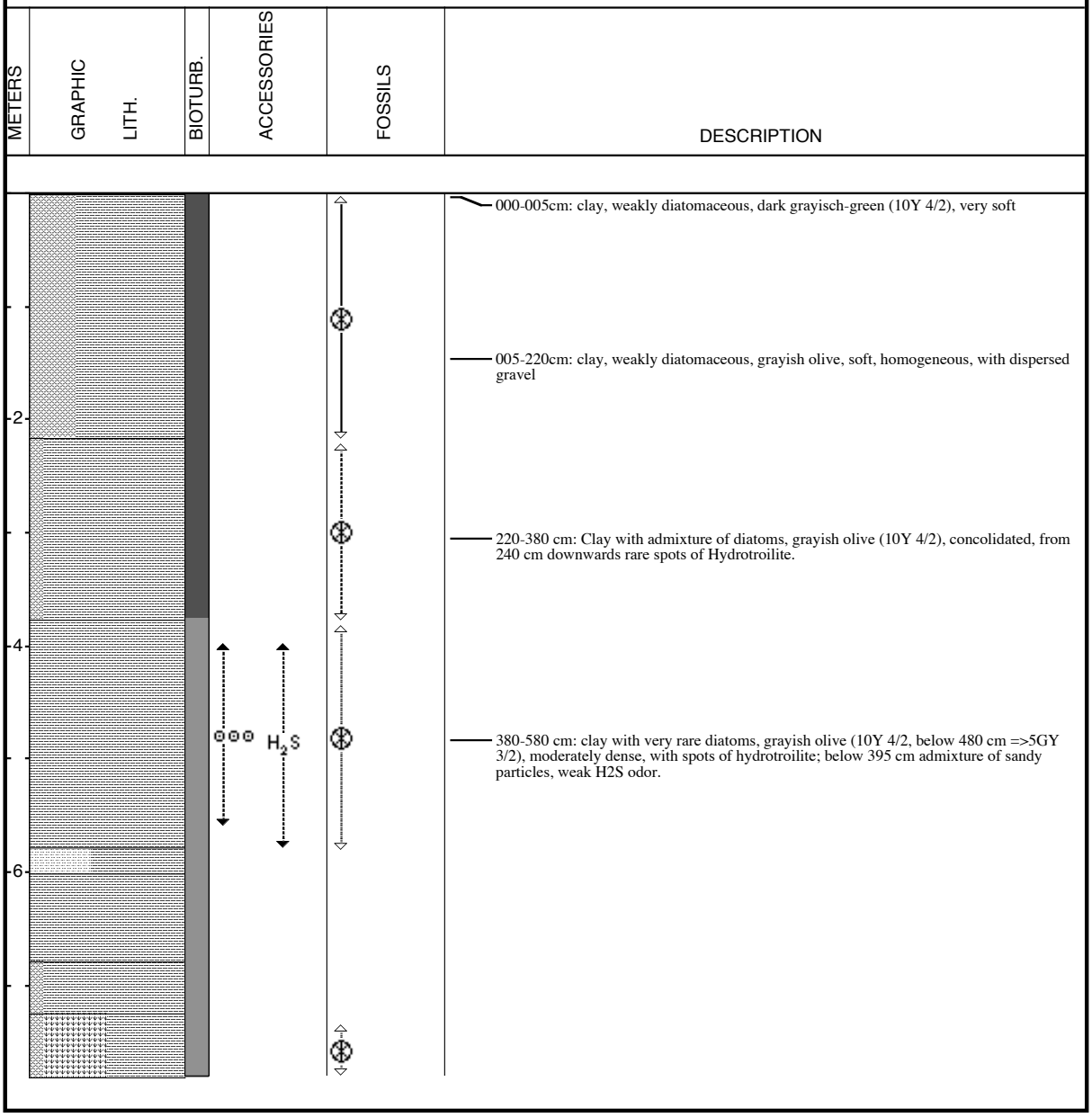

LV29-69-3 SL-G

45°26.602'N, 144°4.243'E

Date: July 02, 2002

Described by: Lembke, L. water depth: 841 m

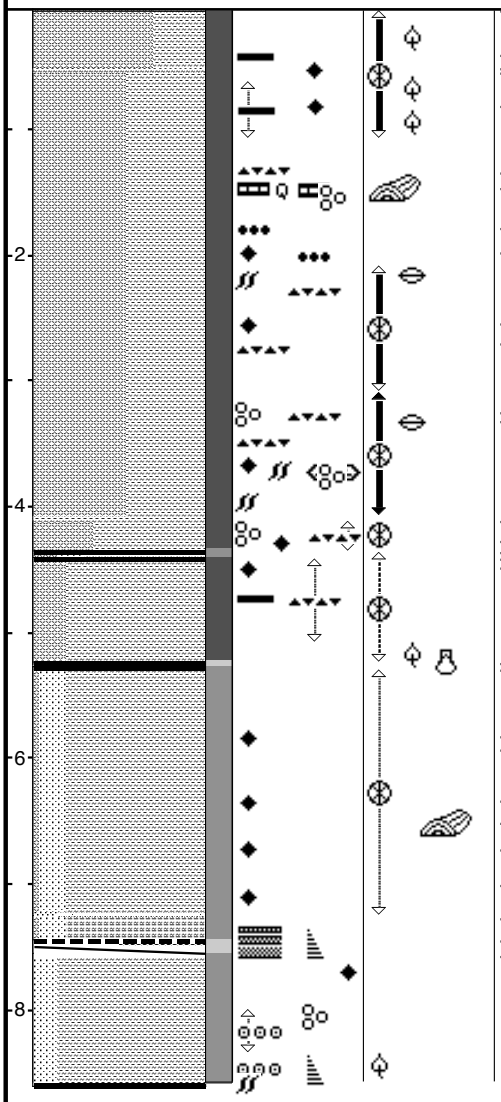

DESCRIPTION

005-055 cm: silty clayey diatomaceous ooze, soft, high water content, foraminifera , uniform sediment - moderate olive brown (5Y 4/4-4/2)

40.5cm: fine, 172 mm thick black streaks.

50.5 cm. DS, black, ø 7mm, rounded, subdiskoidal.

055-327: silty clayey diatomaceous ooze with fine sand - moderate olive brown (5Y 4/2), rare small plant fragments.

080 cm: DS, ø < 5 mm, weakly rounded, sperical.

132-135 cm: black streaks, non-continuous.

146.5 cm: wood fragment, 0.5 cm.
147-148 cm: interval with brighter colour (white dots), qz and ash particles.

179+191 cm: areas with small DS.

196.5 cm: DS, black, well rounded, subprismoidal.

253 cm: DS, covered.

268-281 cm: moderate black mottles.

324-334 cm: small degassing voids.

330-332 cm: small shell fragments.

380-410 cm: gradational decrease of diatom abundance towards diatomaceous silty clay, colour change to olive brown (5Y 4/2).

427 cm: DS, ø 3mm, covered.

435-438 cm: layer of sandy silt - sand silt clay with diatoms, at base 0,5 cm thick layer sand silt clay with middle/coarse sand, interval appears slightly darker (5Y 4/1,5).

439-524 cm: diatom-bearing silty clay, unchanged colour (olive brown, 5Y 4/2).

447 cm. DS, ø ~6mm, covered.

524-528.5 cm: two layers; silt-bearing fine sand with diatoms (upper), sand-bearing clayey silt (lower), sharp bottom boundaries, sharp (upper) and bioturbated (lower) top boundaries; detrital grains (amp, mic, pyr).

528-725 cm: very fine/fine sand-bearing silty clay with rare diatoms to silty clay with very fine/fine sand and rare diatoms.

582 cm: DS, black, weakly rounded, subdiskoidal.

593 cm: DS, small, covered.

634 cm: DS, well rounded, subprismoidal.

651 cm: wood fragment.

672 cm: DS, rounded, prismoidal, ø 5 mm.

699.5, 702, 704.5, 719 cm: small DS occur rarely, mostly small (ø 1-4 mm).

725-748 cm: change from silty clay to clayey silt with very fine/fine sand, slightly brighter colour (5Y 3.5-4/4).

748-751/54.5 cm: turbidite/contourite sequence, bottom boundary tilted and eroded, bottom layer: fine/middle sand. Upper section: cm-thick interbedding of silty clay-fine sand.

755-858 cm: facies ranging from silty clay with very fine/fine sand to sand-bearing silty clay.
755.5 cm: DS, rounded, black subdiskoidal, 3-5 mm.
765, 783 cm: small DS, covered.

LV29-70-2 SL-R

47°56.117'N, 146°10.209'E

Date: July 3, 2002

Described by: Gorbarenko, S.A.; Astakhov, A.S. water depth: 2325 m

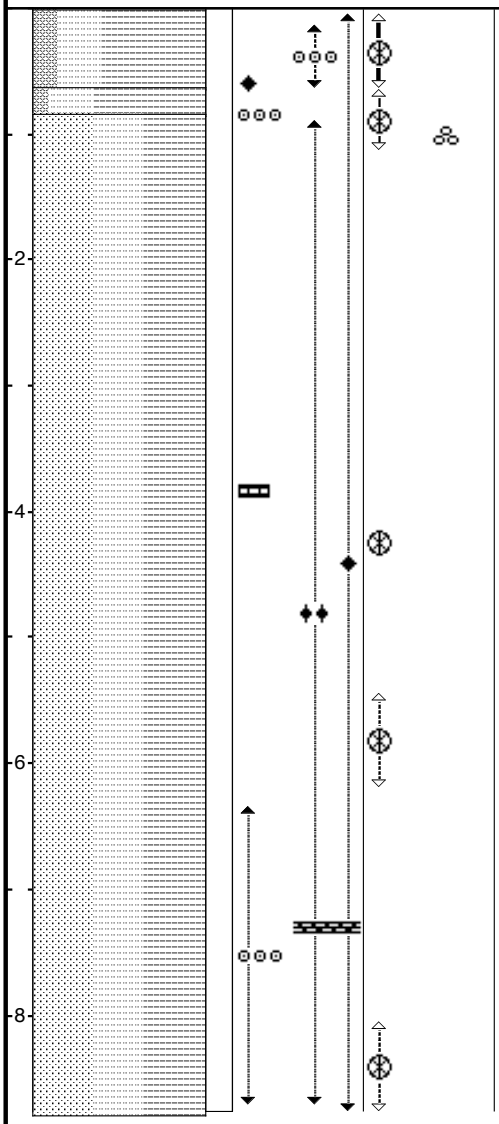

DESCRIPTION

000-065 cm: silty clay, diatomaceous, gray-green (0.5-10 cm - 10Y 472, below - 5GY 3/2), upper 0.5 cm is represented by a thin brown oxidized coat; at 0.5-10 cm - fluid, below - soft, consolidated.
10-65 cm: small admixture of sand
60 cm: DS

065-088 cm: silty clay, weakly diatomaceous, gray-green with small admixture of sand (more intense at 65-70 cm), soft

088-858 cm: sand-silt-clay, grayish olive-green, (5GY 3/2), below 470 cm - dusky yellow-green (5GY 5/2); with significant admixture of sand increasing below 603 cm; soft up to 170 cm, lower - moderately dense.

381-391, 395 cm: randomly oriented (bioturbated) small lenses of volcanic ash (K2)

410-440 cm,
540-620 cm,
800-878 cm: increased content of diatoms

727-727.6 cm: gray ash layer of silty size, hypothetically Spfa-1 layer.

640–650 cm: spots of greener sediment color (10GY 3/2)
785+832 cm: greenish diagenetic patterns and spots.

Dispersed DS in entire core

LV29-70-4 SL-G

48°0.086'N, 146°8.530'E

Date: July 3, 2002

Described by: Lembke, L. water depth: 2062 m

METERS	GRAPHIC LITH.	BIOTURB.	ACCESSORIES	FOSSILS	DESCRIPTION

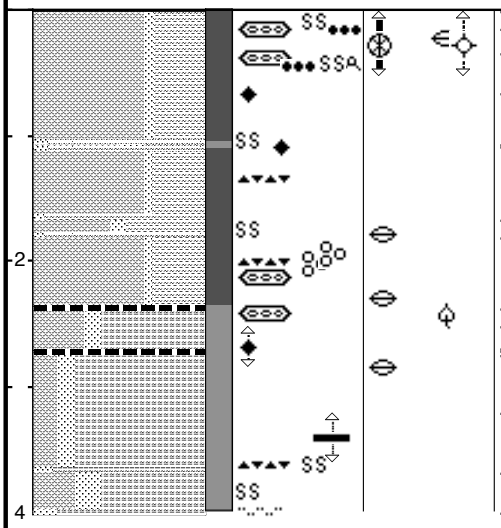

000-106 cm: silty clayey diatomaceous ooze with radiolaria and moderate fine sand. Dark yellowish brown (10YR 4/2).

014-016 cm: lense of fine sand and forams.
016-018 cm: DS's, black, rounded, subspherical.
023 cm: mm-large shell fragments.

034-036 cm: lenses with fine sand and forams, silty clay with sand, undulated boundaries.

066 cm: DS, ø 5 mm, weakly angular.

106-110 cm: section enriched in detrital grains - sand bearing silty clayey diatomaceous ooze.

109.5 cm: DS, ø 4 mm, weakly angular.

166-180 cm: fine sand-bearing silty clayey diatomaceous ooze, section with decreased diatom and increased clay content. Rare - moderate wooden fragments.
177-177 cm: white (shell?) fragments.

180-237 cm: return to silty clayey diatomaceous ooze with radiolarians and moderate - rare fine sand.

236-271 cm: change towards less diatoms and coarsening downward, diatom-bearing clayey silt with sand, forams rare. Section starts at top boundary as silty clay, no clear top and bottom boundaries.

250.5 cm: DS, ø 3 mm, covered.

267-268 cm: DS, ellipsoid, black, rounded, 1cm.

271-273 cm: section with mm-thin black layers, proposed boundary to lower section with decreased diatom content.

273-361 cm: diatom-bearing clayey silt, sometimes clayey silt with diatoms and sand. Unchanged colour. Terrigenous detrital grains and granule DS occur moderately - rarely.
278 cm: small plant/wood fragment, 2-4 mm.
283 cm: small shell fragment.
284 cm: DS, small, 0.4 cm.

319-359 cm: rare black mottles.
359-367 cm: black mottles more common.

366-439 cm: gradational change towards slightly higher diatom content, but still to be termed diatom-bearing clayey silt with sand.

399-402 cm: mm-thick slightly darker silty-fine sandy layers.

LV29-70-4 SL-G

48°0.086'N, 146°8.530'E

Date: July 3, 2002

Described by: Lembke, L. water depth: 2062 m

METERS | GRAPHIC LITH. | BIOTURB. | ACCESSORIES | FOSSILS | DESCRIPTION

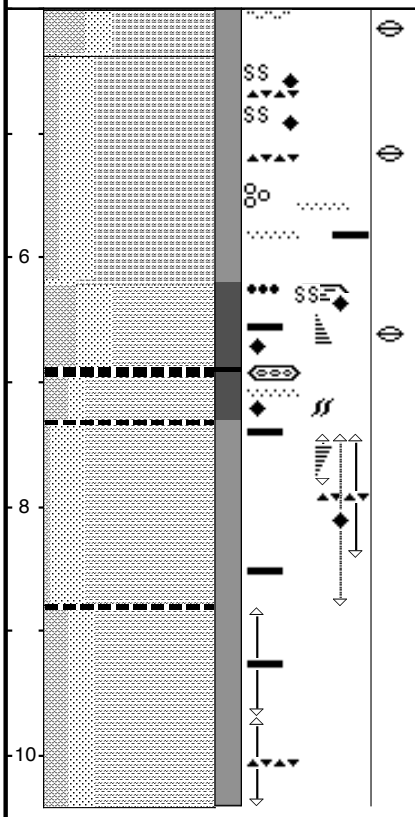

439-621 cm: heterogenous sediment, sand-bearing silty clay with diatoms, very rare forams (partially absent) and abundant dark detrital terrigenous grains (mostly fine sand, ranging from medium sand to coarser silt).
439-460 cm: mm-thick non-continuous layers, dark greyish-black (N3-N1), fine sand-coarse silt, increasing abundance in section downcore.
458.5-459.5 cm: DS, weakly rounded.
460-476 cm: area with enhanced black laminae and mottles.
480 cm: scaphopod fragment.
483.5 cm: cm-large lense of light greenish grey (5GY 8/1) to yellowish gray (5Y 8/1) sediment, fine sandy grain size, presumably ash lense.
490.5 cm: small DS, covered.
505, 512, 524.5 cm: mm-large calc. shell fragments.
514-523 cm: black laminae (non-continuous).
548 cm: deg. void, ø 1 cm.
557-559 cm: remains of darker interbedding, coarser grain size (medium sand), bioturbationally mixed.
580-581, 588-589 cm: dark greyish streaks and intercalations, mm thick, partially bioturbationally mixed.

621-690 cm: diatom-bearing sand-bearing silty clay, grayish olive (10Y 4/2), forams rare - absent.
627+628 cm: mud clasts, bioturbated.
632 cm: few, small DS.
643.5 cm: DS, rounded, ø 4 mm.
654-658.5 cm: prominent black streaks, bioturbated.
658.5 cm: granule shell fragment, ø 2mm.

690-693 cm: layer with increased diatom content; sand-bearing diatomaceous silty clay. Dark siliclastic grains (fine sand) abundant.

693-732 cm: sand-bearing to sandy silty clay with diatoms. No colour change. Small DS (coarse sand) occur moderately in entire section.
706.5 cm: 3mm thick sand-rich layer.
719 cm: DS, ø 1cm, fissure.

732-880 cm: decreased diatom content, silty clay with sand and rare, sometimes absent, diatoms, mostly fragments. Upper section fining downwards. No significant color cange. Black streaks and mottles increase downcore. Few DS (coarse sand) occur rarely.
752 cm: DS, covered.
851 cm: 2mm thick darker (dark gray) streak.
878-879 cm: residuals of fine sand-bearing layers, strongly bioturbated.

880-1041 cm: slightly increased diatom content, though mostly small fragments (fine silt), diatom-bearing sand bearing silty clay, perhaps clayey silt in some parts.
878-968 cm: lamina-like black streaks.
905-920 cm: intensest dark layers. Less bioturbated.
932 cm: DS, rounded-well rounded, ø 1-2 cm.
949.5-950 cm: slightly darker (0.5 value) finer grained layer, still silty clay, less sand.
968 cm-downcore: streaks turn into mottles. Non-continuous. Increased bioturbation.
1007.5 cm: DS, covered.

LV29-72-2 SL-R

48°37.701'N, 146°7.037'E

Date: July 4, 2002

Described by: Gorbarenko, S.A.; Astakhov, A.S. water depth: 1380 m

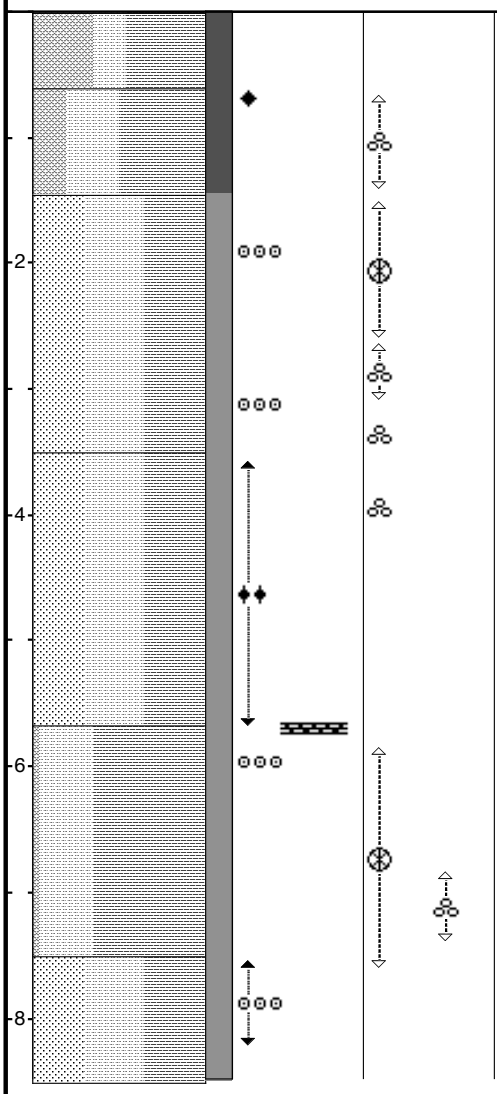

DESCRIPTION

000-065 cm: diatomaceous silty clay, upper 1st cm brown (oxidized layer), fluid.
001-020 cm: olive-green, below gray, soft.

065-150 cm: diatom-bearing silty clay, olive green, with admixture of foraminifera.
070, 080 cm: DS

150-350 cm: sand-silt-clay, gray-green (150-250 cm, 10Y 4/2), grayish olive-green (250-310 cm, 320-350 cm, 5GY 3/2), gray (310-320 cm, 5G 4/1); with admixture of diatoms in upper part and increased abundance of foraminifera at 260-310 cm, soft.
187-193 cm, 300-320 cm: admixture of sand.
Dispersed DS common.

350-569 cm: sand-silt-clay, greenish-gray (5GY 4/1), above 450 cm - soft, lower - moderately dense.
390-410 cm: admixture of foraminifers. Rare small lenses of hydrotroilite and dispersed dropstones occur.

569-570 cm: Volcanic ash layer K2, in form of lenses (0.5-0.6 cm in size).

570-750 cm: silty clay, interchange of grayer and greener sediment layers (5GY5/2, 5GY3/3, 5GY4/1, 10Y4/2); dense, viscous.
580-760 cm: increased content of diatoms,
680-740 cm: increased content of foraminifers.
585-602 cm: admixture of sand.

750-850 cm: sand-silt-clay, greenish-gray (10Y4/2)
750-822 cm: lighter, dense, with sand admixture.

LV29-72-3 SL-G

48°38.259'N, 146°7.098'E

Date: July 4, 2002

Described by: Lembke, L. water depth: 1142 m

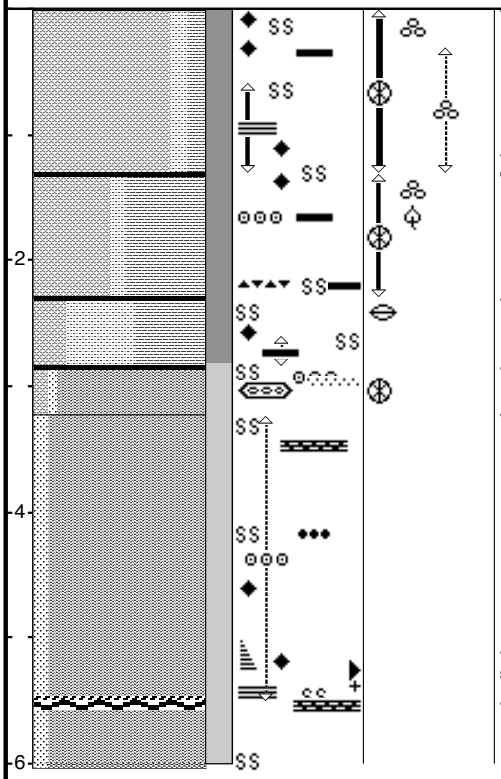

DESCRIPTION

000-131 cm: diatomaceous ooze with clay and rare terrigenous detrital grains of silty/fine sandy grain size, olive gray (5Y 3/2-3/1), very soft.
004 cm: DS, black, ø 2-3 mm, rounded.
000-040 cm: forams abundant, decreasing downcore.
015+016 cm: mm-thick glossy layers, diatomaceous.
033-040 cm: discontinuous dark laminae, 1/2 mm thickness.
030 cm: DS, elongated, 5x2 mm.
045 cm: DS, small, partly covered.
058-131 cm: laminations, darker layers are 0.2-1 mm thick, abundant.
063+064.5 cm: thicker, dark layers.
072 cm: small DS/IRD.
085.5 cm: shell fragment.
091.5 cm: plant fragment.
99, 99.5 cm: intense black lenses and layers.
100 cm: small DS within basal coarser grained layer.

114-116.5 cm: DS, well rounded, plutonite, dark, tilted.

130 cm: dark layer, maximum diatom abundance, mostly biosiliceous fragments.

131-229 cm: change towards diatomaceous clay with sandy silt, dark laminae and layers disappear, colour change towards olive gray-greyish olive (5-10Y 4/2).
133-135 cm: DS, rounded, grey-black.
152-154 cm: plant fragments, mm-size.
142-144 cm: forams abundant.
155-172 cm: dark gray - abundance of black detrital grains slightly higher.
176 cm: rare granule-sized plant fragments.

229.5-283 cm: decrease of diatom content downcore, sed. less soft; terrigenous grain size increases. Diatomaceous/diatom-bearing sandy silty clay. Slightly darker colour, olive gray - grayish olive green (5Y 3/2-5GY 3/2).
240, 246.5 cm: small (mm) shell fragments.
257-258 cm: DS, covered.
259-281 cm: black streaks and lenses, max. thickness 2-3 mm occur moderately (authig. minerals).

283-322 cm: diatom-bearing sand silt clay with medium sand in lenses and layers. Streaks are common. (Light) grayish olive (10Y 5-4/2).
297-322 cm: no streaks; sediment colour slightly darker, (mod.) olive gray (5Y 4-3/2).

322-629.5 cm: sand silt clay with occasional fine/medium sand, very rare diatoms. Black detrital grains abundant, mm-thick sand lenses and rare forams. Light olive gray (5Y 5/2).
345.5-350 cm: 0.5-1 cm thick layer, olive black (5Y 2/1), mostly medium sand. Suspected, previously unknown, ash layer.

510 cm: DS, pebble-sized.

526-529 cm: DS, black, rounded - well rounded, subprismoidal.

from 510/15 cm downcore: slightly coarsening downward, increased fine sand content.

550-555 cm: volcanic ash layer, pale red (5-10 R 6/2), variable thickness, bioturbated, forming nodules. Fine sand grain size, identified as K2 ash layer.

LV29-72-3 SL-G

48°38.259'N, 146°7.098'E

Date: July 4, 2002

Described by: Lembke, L. water depth: 1142 m

METERS	GRAPHIC LITH.	BIOTURB.	ACCESSORIES	FOSSILS	DESCRIPTION
8	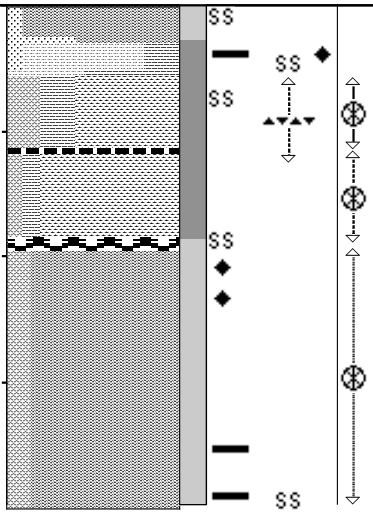				629-655 cm: change in grain size towards clay-bearing silt with sand. Colour remains unchanged. 635-638 cm: mm-thick dark streaks occur. 637-638 cm: DS, ø 1 cm, black. 655-724 cm: facies change towards diatom-bearing silty sand with clay, Light olive gray (5Y 5/2), slightly coarsening downward in upper section, black mottles occur moderately, forams not visible. 788-791 cm: interbedded clayey and sandy layers. 788-789 cm: medium- coarse sand layer with small DS. 790-791 cm: layer enriched in clay, olive grey (5Y 3/2). 790-791 cm: DS, ø 15 mm, weakly rounded, subdiskoidal. 791-998 cm: sand silt clay with diatoms (fragments), grayish olive (10Y 4/2). 806 cm: DS, covered. 830-831 cm: DS, covered, ø 1cm. 930-932 cm: slight colour change towards light olive gray (5Y 5/2), diatoms rare downcore. 942-958 cm: black streaks and mottles appear. 980-998 cm: black streaks denser and more common.

LV29-78-2 SL-R

52°40.244'N, 144°41.187'E

Date: July 6, 2002

Described by: Gorbarenko, S.A.; Astakhov, A.S. water depth: 655 m

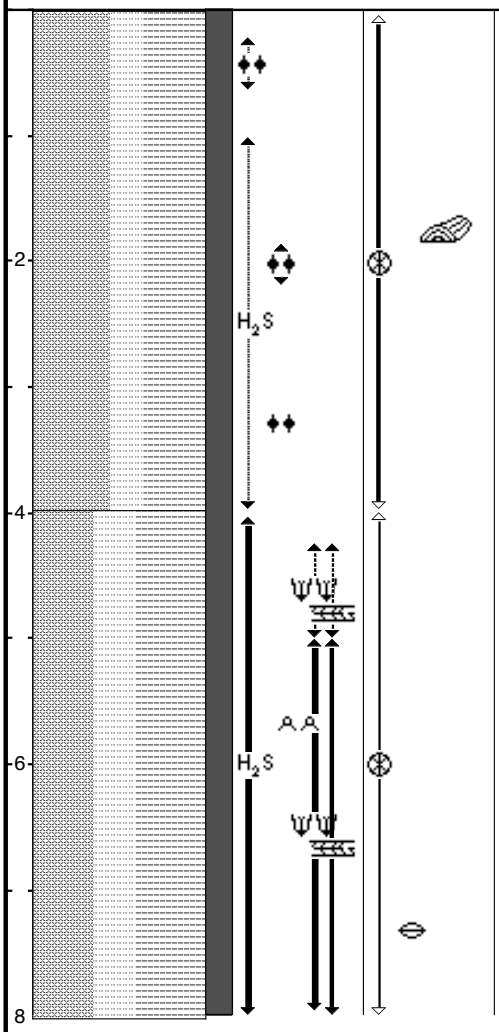

DESCRIPTION

0-400 cm: diatomaceous silty clay, olive green, down to 20 cm: very soft, below 20cm - soft, with rare small laminas of hydrotroilite.
100 cm downward: weak H2S odor.

400-800 cm: diatomaceous silty clay , olive green, soft.
From 420 cmdowncore: sediment becomes gas-saturated with pseudo-brecciated texture;
gas saturation increases down to 500 cm, and below sediment becomes strongly gas-saturated, lumpy.
732, 742 cm: small shell fragments.
765-773 cm: consolidated sediment lump (7x5 cm in size) consisting of carbonate (probably primary stage of carbonate concretion formation).
H2S odor in entire interval.

LV29-78-3 SL-G

52°40.388'N, 144°42.203'E

Date: July 7, 2002

Described by: Lembke, L. water depth: 673 m

METERS	GRAPHIC	LITH.	BIOTURB.	ACCESSORIES	FOSSILS	DESCRIPTION

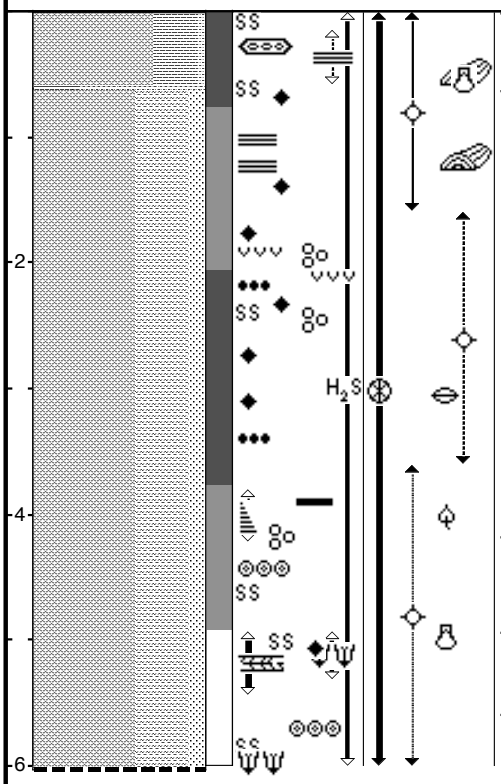

000-063 cm: silty clayey diatomaceous ooze, very soft, abundant forams, moderate - rare detrital dark grains, olive gray (5Y 3/2) - dark olive gray (5Y 2/2), very high water content.
014-059 cm: max. mm-thick diatomaceous/biosiliceous layers.
027.5-028 cm: silt/sand lense.
048.5 cm: wood fragment.
052 cm: shell (pelecypod) fragment, few mm.

063-604 cm: slighter decrease in biosiliceous content. Silty clayey diatomaceous ooze with fine sand. Forams abundant, occurrence of 1-4 mm large DS/detrital grains, mostly rounded-subangular. Olive gray (5Y 3-2/2). Bioturbated laminations moderately abundant in entire section.
068 cm: DS, ø 2-4 mm, subangular.
081-082 cm: interbedding, grayish olive (10Y 4/2).
090-114 cm: interval with clearly visible lamina structures, slightly darker color, finer grain size, 3-5 mm thick.
116.5 cm: layer of small plant fragments.
137 cm: DS, black, subangular, ø 5 mm.
149 cm: 4-5 DS, few mm each.
174 cm: DS, ø 4 mm, black angular.
186 cm: DS, few mm, covered.
191 cm: layer, 3 mm thick, darker greenish gray (5Gy 4/1) to olive gray (5Y 4/1), diagenetic alteration. Strong H2S odor.
199-220 cm: occasional irregular color changes (5Y 3/2 - 5Y 4/1), presumably diagenetic horizons.
218 cm: mm-large DS's.
231-233 cm: DS, height 2.5 cm, length 6 cm, separately sampled.
238 cm: 2-3 mm thick dark grayish layer, wavy. Strong H2S odor.
243 cm: DS, ø 0.5 cm.
below 245 cm: sediment increasingly homogenous.
260 cm: complete pelecypod shell, unfilled, in autochthonous position.
272 cm: DS, 3-4 mm, angular, black
303 cm: small pelecypod fragments (mm).
308-310 cm: DS, large, rounded, plutonite, appears in conjunction with several smaller DS (mm-large) in layer.

401.5 cm: small plant fragments, between ca. 395 and 420 cm grain size very slightly coarsening downward.
415-419: gas bubbles, small degassing voids.
442-447: carbonacious concretion (nodule), brownish nucleus consists of pelecypod shell.

491-543 cm: gas-saturated sediment, texture pervasively breccied, sedimentary structure strongly destroyed by degassing. Color changes between olive gray (5Y 3/2) and grayish olive green (5GY 3/2).
495-497 cm: fragments of single pelecypod shell.
505 cm: DS, black, well rounded, ø 6 mm.

558-563 cm: authig. carbonate concretion (chicken egg-size), sampled separately, grayish olive (10Y 3-4/2); nucleus consists of large piece of wood (sev. cm), sampled separately.
555-572 cm: numerous small concretions.

LV29-78-3 SL-G

52°40.388'N, 144°42.203'E

Date: July 7, 2002

Described by: Lembke, L. water depth: 673 m

METERS	GRAPHIC	LITH.	BIOTURB.	ACCESSORIES	FOSSILS	DESCRIPTION
8				H_2S		604-656 cm: transitional zone with decreased diatom content, change towards diatomaceous sand silt clay, no color change, uncertain top and bottom boundaries due to breccied structure and concretions in sediment. Foram. poor or devoid. Increase of fine sand grain size towards bottom boundary. 605-633 cm: partly breccied structure, degassing, numerous small carbonate concretions. 654-724 cm: further decrease of diatom content towards diatom-bearing sand-silt-clay, grayish olive (10Y 4/2) - grayish olive green (5Y 3/2). 665 cm: black streaks occur. 665-678 cm: enrichment of small wooden fragments and plant tissue. 668-690 cm: enrichment of medium/coarse sand particles. 680-690 cm: breccied structure, gas-saturated. 703-718 cm: 1/2 of core => breccied structure. 710 cm: small lense (1 cm) of brighter sediment, sandy. 708 cm downcore in section: occasional laminae, black. 724-29 cm: breccied structure. 710-ca. 740 cm: increase in foraminifera abundance. 744-750 cm: partially breccied structure. 759 cm: black mm-fine streaks. 760 cm: carbonaceous concretion, soft. 766 cm: 2 mm thick band, light olive gray (5Y 5/2), non-continuous, tilted. 770-774, 791, 795 cm: degassing void. 807-820 cm: laminae increasing into mm-thick longer sequences, black layer strata interbed with sediment. 809-814 cm: breccied structure. 808 cm: shell fragments, 3-4x 1-3 mm. 813 cm: scaphopod fragment, 4 mm. 822 cm: DS, black, rounded, partly covered by sediment. 829-830 cm: small shell fragment. Entire lower core section: heavily destroyed texture by degassing.

LV29-79-2 SL-R

52°47.447'N, 144°57.900'E

Date: July 7, 2002

Described by: Gorbarenko, S.A.; Astakhov, A.S. water depth: 1102 m

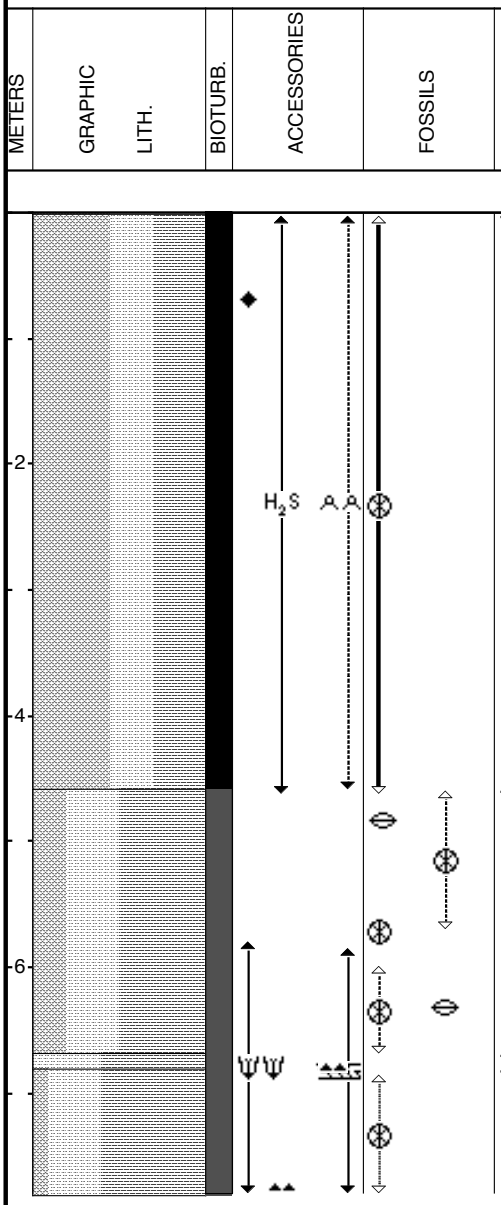

DESCRIPTION

0-460 cm: diatomaceous silty clay, olive-green, soft (0-3 cm - fluid), water-saturated. Small lenses and laminas of hydrotroilite are common.
70 cm: DS
H2S odor in entire interval.

460-669 cm: silty clay with increased content of diatoms (570-590 cm - weakly diatomceous), grayish-olive (460-500 cm - 10Y4/2), from soft to moderately dense.
575 cm downward: sediment becomes gas-saturated with specific pseudo-brecciated texture.
480, 630 cm: shell fragments.
570-575 cm: increased admixture of foraminifers.

669-681 cm: silty clay with microcrystalline carbonate cement. Denser precipitates with oval shape and light yellowish-green color occur, gradually turning into softer sediment (similar color).

681-780 cm: silty clay with small admixture of diatoms, gray-green, moderately dense, with vertical brecciated texture. Dense light interlayers with carbonate cement are marked at 686-688 and 778-780 cm.

LV29-79-3 SL-G

52°47.272'N, 144°57.318'E

Date: 07. July, 2002

Described by: Lembke, L. water depth: 1082 m

METERS	GRAPHIC	LITH.	BIOTURB.	ACCESSORIES	FOSSILS	DESCRIPTION

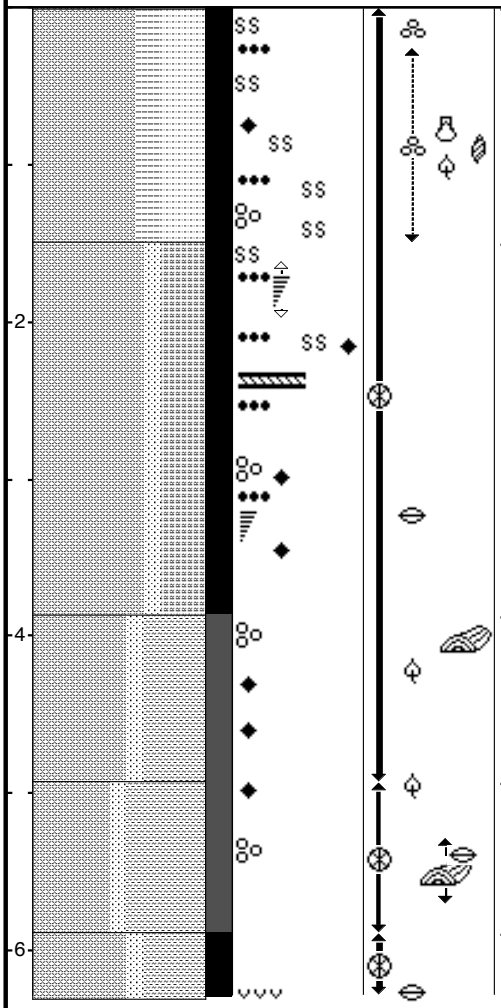

000-149.5 cm: sandy silty diatomaceous ooze with clay and forams. Grayish olive (10Y 4/2). Tiny detrital grains (terrigenous) occur moderately. Strong bioturbation.
026-027 cm: rare small DS, detrital grains (~1 mm).
046-049 cm: lighter ~5 mm thick striations occur, pale olive (10Y 6/2).
073 cm: DS, black, weakly rounded, subprismoidal, ø 6 mm.
077 cm: shell (pelecypod) fragment, partly dissolved/altered.
074-077 cm: very fluid texture, water saturated, with occasional black sandy grains (terrigenous, small DS).
074 cm: DS, subprismoidal, well rounded, < 1cm.
089-090 cm: gastropod shell, partly destroyed by early diagenetic carbonate dissolution.
088, 096, 098 cm: thin streaks, ca. 0.5 colour value darker than surrounding sediment, between upper two: increased abundance of forams and sand.
104-118 cm: step towards 0.5 val. darker sediment, increased abundance of mm DS/detrital grains and small plant fragments. Slightly weaker sorting.
114 cm: plant fragment, ø 2-3 mm.
130-139 cm: small degassing voids, encircled by thin rings of fine sand.

149-386 cm: clayey silty diatomaceous ooze, decreased sand content, 60-80% silt in terrigenous fraction, color change towards slightly darker values (0.5), darker grayish olive (10Y 3.5/2), small, black terrigenous granule grains occur.
171-172 cm: increased abundance of granule DS.
160-ca. 186 cm: fining downward section, sand => silt.
204 cm: degassing void, 1cm ø.
209 cm: layer with very coarse sandy-granule grains.
215 cm: DS, Brownish black (5YR 2/1), rounded, subdiskoidal.
207cm downward: color change dark grayish olive (10Y/3).
253 cm: several granule DS.
292+294 cm: marginal void.
297 cm: single granule DS.
311-316 cm: slight increase in very coarse sand terrigenous material.
322 cm: tiny shell fragment.
328-386 cm: fining downward section, silt => clay. Very gradual color change to grayish olive (10Y/4/2).
345 cm: void, 0.5 cm ø.

386-492 cm: transition to finer siliclastic fraction => clayey silty/silty clayey diatomaceous ooze with sand and rare wood/plant fragments. Patchy colour, mostly grayish olive (10Y 4/2). Diatom abundance decreases slightly downcore. Sediment less soft and very homogenous.
386-414 cm: transition from upper section, in lower part maximum of wood/plant fragments (est. up to 5%).
398 cm: layer of degassing voids.
421.5 cm: small piece of coal (?).
459.5 cm: DS, weakly rounded, black, subdiskoidal, pebble.

492-598 cm: decrease in diatom content, diatomaceous silty clay with sand.
494.5 cm: wood fragment.
497.5 cm: DS, rounded, subdiskoidal, small pebble grain size.
528-562 cm: abundant wood fragments and plant remains, adjusted horizontally (≈2-4 %), needle-shaped.
535 cm: void, ø 4.5 cm.
538.5 cm: partly dissolved shell fragment.
571 cm: small wood fragment, 3 mm.

598-630 cm: interval with higher diatom abundance => silty clayey diatomaceous ooze with fine sand. Minimum in terrestrial plant components. Color slightly darker. At base of interval, first diagenetic alterations occur. Uncertain basal boundary 628-640 cm (?).
628.5 cm: shell fragment.

LV29-79-3 SL-G

52°47.272'N, 144°57.318'E

Date: 07. July, 2002

Described by: Lembke, L. water depth: 1082 m

METERS	GRAPHIC LITH.	BIOTURB.	ACCESSORIES	FOSSILS	DESCRIPTION

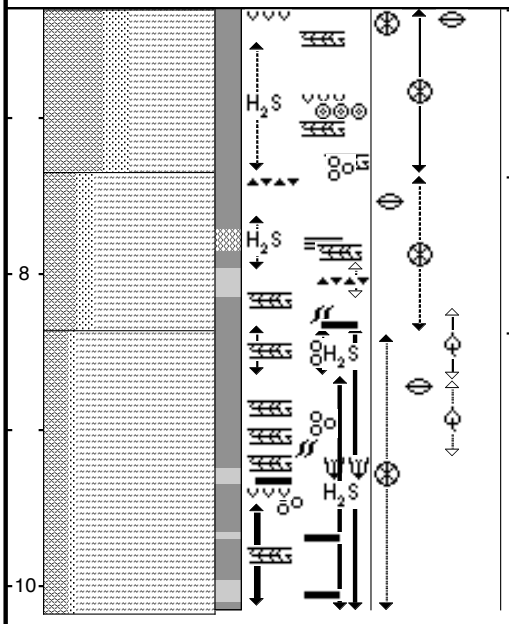

630-735 cm: transition to diatomaceous silty clay with sand and rare-moderate wood fragments of sandy/silty grain size. Interval is characterized by first occurences of of diagenetic carbonate layers, breccied structures and H2S odor.
631-635 cm: diagenetic horizon, silty clayey grain size, compacted, stiff sediment, dusky yellow green (5GY 5/2).
640-646 cm: breccied texture.
656-658 cm: breccied texture.
677-690 cm: unit of diagenetic layers, grayish yelloy green (5GY 5/6).
697-700 cm: weaker diagenetic carboante horizon. Dusky yellow green (5GY 5/6).
701-706 cm: breccied texture, forming nodules.
716-718, 723-726.5, 729-731 and 731-738 cm: small voids and diagenetic nodules.
734-745 cm: black streaks and mottles abundant.
735-46 cm: bottom boundary to lower facies.

735/745-830 cm: diatom-bearing silty clay with sand (in some sections diatom-bearing silty clay with sand and plant fragments). Texture increasingly gas-saturated and breccied, diagenetic alterations occur, voids and fissures increasingly common. In lower part: grayish olive (5Y 3/2) to grayish olive green (5GY 3/2).
741-745 cm: small degassing voids.
752.5 cm: small shell fragment.
760 cm: small void, tiny fragments of shells.
765-771 cm: degassing voids and breccied texture.
772.5-786 cm: laminated sediments, single laminae 1-2 mm thick (brown colour), laminae with increased abundance of biosiliceous material. More prominant layers at 774.5, 776.5, 777.4, 783, 784.5, 785 cm.
791-814 cm: black streaks and mottles.
806-808 cm: layer with black streaks.
820-827 cm: fissures, breccied texture.
832-865 cm: interval with pervasive breccied texture as nodules and degassing voids, ø 1-4 cm.
825-870 cm: interval with increased abundance of wood and plant fragments.

838-1017 cm: fining downward, sand < 10%, clay >60% of terrigenous fraction, decreased diatom content <20%. Diatom-bearing silty clay with rare sand - silty clay with diatoms and rare sand. Olive gray (5Y 3/2). Frequent degassing structures (voids, fissures) and strong H2S odour.
870 cm: small shell fragment.
885-887 cm: void, breccied texture, nodule.
902-904 cm: breccied texture, at 904 cm two black streaks,
908-913 cm. layer with voids and fissures, breccied.
from 920 cm downcore: increasing breccia in texture, in parts up to 60% of split surface.
927-937 cm: black streaks abundant.
968 cm: black lamina.

LV29-81-1 SL-G

53°59.558'N, 143°57.759'E

Date: July 8, 2002

Described by: Lembke, L. water depth: 356 m

METERS	SECTION		GRAPHIC LITH.	BIOTURB.	ACCESSORIES	FOSSILS	DESCRIPTION
2	1		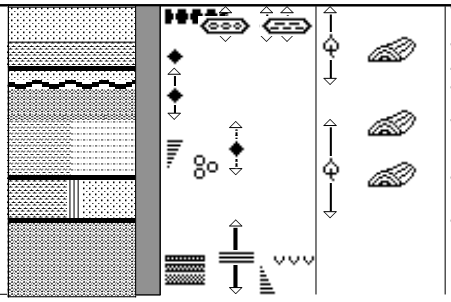				000-026.5 cm: middle-coarse sand, qz, dark clastic grains, amp, wood fragments, very weakly sorted, no graded bedding or synsedimentary structures, irregularly occuring lenses of fine sand, mud clasts, pebblesize DS occur. Patchy grayish olive green (5GY 3/2). 026.5-041 cm: silty sand, patchy color (5GY 3/2 - 5g 3/2). in brighter parts => sand silt clay, terrigenous debris abundant, wood fragments abundant, small (granule) DS, facies weakly-very weakly sorted, sharp bottom boundary. 030-033 cm: large (some cm) wood fragment, round. 041-055 cm: less well sorted facies, sand with abundant larger fragments of wood, very patchy colour => olive black (5Y 2/1) - grayish olive green (5GY 3/2). 048-049 cm: sandy carbonaceous concretion, very stiff. 055-078 cm: relatively homogenous sand silt clay (silt major comp.), wood/plant fragments abundant, DS (granule) abundant, well - less well sorted, abundant-pervasive black terrigenous detrital sandy grains. Olive gray (5Y 3/2) - light/moderate olive gray (5Y 5/2). 078-117 cm: sandy silt, in lower section change to smaller grain size. 078-084 cm: transitional zone, faces enriched in wood fragments and plant debris, decreasing DS and sand content. Change to laminated sediments, laminae 1-5 mm average thickness, color alterations olive gray (5Y 3/2) - grayish brown (5YR 2/2). 100-112 cm: fining downwards via sand silt clay to silty clay. Color changes (5Y 4/2-5Y3/2) with reddish tinge. 111 cm: large void. at basal boundary: abundant mm-large wood fragments. 117-147 cm: Interbedding of sand, dusky yellowish brown (10YR 2/2), and silty sand, dark yellowish brown (10YR 4/2). Coarser-grained layers with higher content of wood/plant debris and sandy siliciclastic grains. 121 cm: wood fragment, ø 1cm. 147-200 cm: facies entirely characterized by mm - sub-mm laminae, no interbedding. 147-176 cm: more homogenous section, area cloudy patchy => diagenetic alterations. 150-157 cm: fissures and voids, ø exceeding 1 cm. 175-176 cm: prominent diagenetic layer, grayish olive (10Y 4/2). 176-177 cm: condensed section, increased abundance of terrigenous detritus and plant fragments. 180-190.5 cm: contourite-like sequence. 187-190.5 cm: herein coarsening downward towards middle sand (matrix clayey silt). 191-200 cm: stiff, compacted sand/silt, olive gray (5Y 3/2).

LV29-82-1 SL-R

45°18.150'N, 144°10.795'E

Date: July 8, 2002

Described by: Gorbarenko, S.A.; Astakhov, A.S. water depth: 795 m

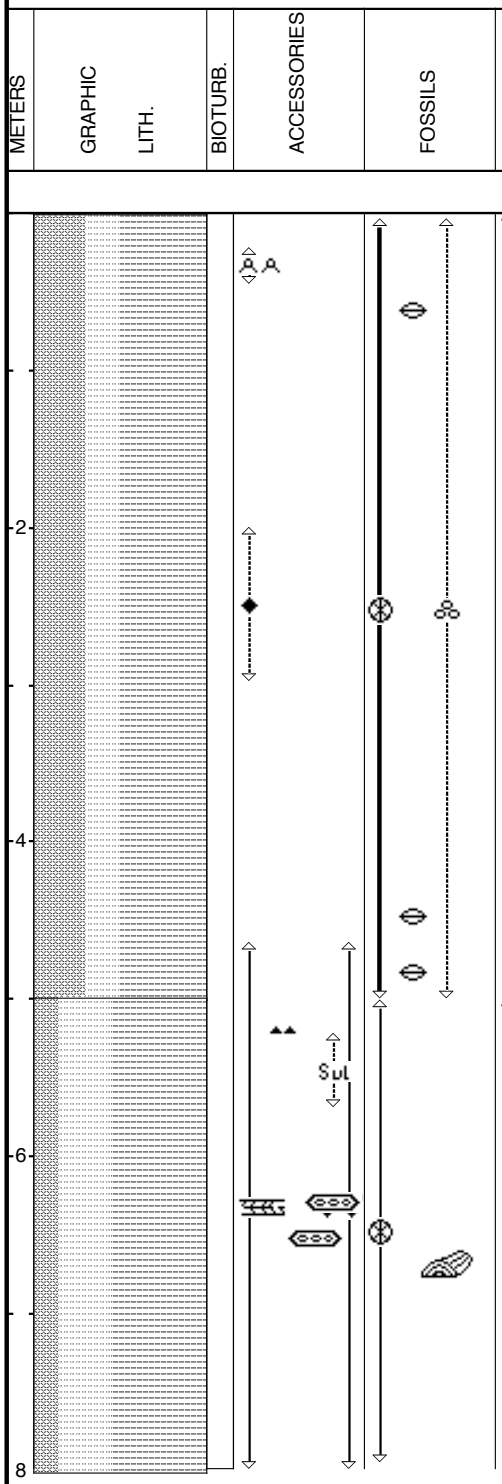

DESCRIPTION

000-500 cm: diatomaceous silty clay, with admixture of foraminifers (in particular at 430-470 cm), olive-green, with dark gray laminas of hydrotroilite in upper part (20-30, 45-50 cm), soft, upper part is fluid.
100-200 cm: layers of more dense clayey silt of olive gray colour (5GY3/2, 5Y3/2).
065, 448, 482 cm: fragments of decomposed shells.
460 cm downcore: sediment becomes gas-saturated with specific pseudo-brecciated texture.
200-300 cm: DS occur.
375, 490 cm: detritus.

500-800 cm: diatom-bearing silty clay, gray-green, soft, homogeneous. Down to base, the content of diatoms and foraminifers decreases.
628, 653 cm: sandy lenses.
668 cm: small (1 cm) wood fragment.
520 cm: diagenetic microcrystalline carbonate.
520-570 cm: diagenetic sulfides.
520, 539 cm: detritus.
A pseudo-brecciated texture is characteristic for entire interval.

LV29-84-2 SL-G

54°25.692'N, 144°7.436'E

Date: July 8, 2002

Described by: Lembke, L. water depth: 752 m

METERS	GRAPHIC LITH.	BIOTURB.	ACCESSORIES	FOSSILS	DESCRIPTION

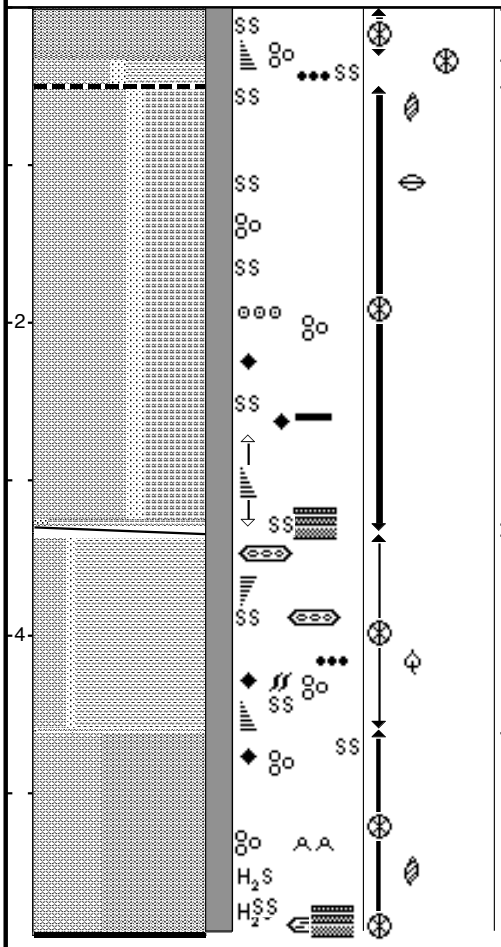

000-026/032 cm: sandy silty clayey diatomaceous ooze with forams and radiolarians. Moderate olive brown (5Y 4/4). Very soft with visible rare granule detrital grains.
028 cm: small degassing void.
026-032 cm: tranistional zone, less biosiliceous material.

032-049 cm: short interval of diatomaceous silty clay with sand. Increased abundance of terrigenous detrital grains.
43.5+44.5 cm: DS, granule size, black.

049-280 cm: clayey silty diatomaceous ooze with sand, no significant color change. At top gradual increase in diatom abundance. Sand fraction increases downcore (mostly fine sand). In upper part still considerably soft.
062 cm: gastropod shell, slightly damaged.
110 cm: small calcitic shell fragments occur.
137+147 cm: degassing voids, ø 0.5 cm.
191-193 cm: layer with slightly increased fine sand content.
202 cm: degassing void, ø 0.5 cm.
223 cm: DS, rounded, subprismoidal.
258.5 cm: 1 mm fine layer with increased diatom content and decreased sand grain size.
261 cm: DS, diskoidal, well roundend, ø 5mm.

280-335 cm: sandy silty clayey diatomaceous ooze, clay resembles ~50% of terrigenous fraction. Detrital grains (middle-coarser sand) occur. No significant color change. Diatom content decreases, at lowest part sand content increases to ~40-50 % of terrigenous fraction (=> contourite/turbidite?).
330 cm. 0.3-0.5 cm thick, slightly coarser layer.
330-332 cm: return to facies of upper part.
332-335 cm: coarsening downward, sediment darker, gradual top boundary at ~330 cm, sharp, inclined bottom boundary.

335-460 cm: diatom-bearing silty clay with sand/rare sand and rare forams. Small granule-size DS rarely occur in entire section. Grayish olive (10Y 4/2).
ca. 378-ca. 420 cm: fining downwards, decreasing sand content. Colour changes to light olive gray (5Y 5/2).
387 cm: lense, silty clay with wood fragments.
405-420 cm: granule-sized DS and plant fragments occur.
426-430 cm: small voids and fissures, < 0.5 cm.
427.5 cm: DS, weakly rounded, subprismoidal.
449-460 cm: slight gradual coarsening downward from silty clay towards sand-bearing silty clay. Slightly darker color (0.5 val.).

460-589 cm: diatomaceous sand silt clay, gradual facies change (increasing abundance of forams and coarsening of terrigenous fraction) from topmost unit. Unchanged color => grayish olive (10Y 4/2). Especially in lower part forams occur.
447.5 cm: DS, granule-sized, black.
477.5 cm: small void, ø 5mm.
487-497 cm: brighter channels and lenses, traces of bioturbation.
531, 537 and 538 cm: small concretions.
547-548 cm: fragments of destroyed gastropod, ≈ 1 cm.
584-589 cm: contourite-like structure, sediment contains mud clasts, shell's fragments, wood fragments, small granule DS, fine-scale interbedding of finer and coarser terrigenous layer, generally coarsening downward. Sharp bottom boundary with presumed erosional paleosurface.

LV29-84-2 SL-G

54°25.692'N, 144°7.436'E

Date: July 8, 2002

Described by: Lembke, L. water depth: 752 m

METERS	GRAPHIC	LITH.	BIOTURB.	ACCESSORIES	FOSSILS	DESCRIPTION
6				H_2S SS SS H_2S SS SS		589-630 cm: no major lithological change from upper unit, slightly decreased sand content => diatomaceous silty clay with sand. Increased abundance of forams. Color change to light olive gray (5Ý 5/2). No streaks or mottles in entire section. 599 cm: 1mm thick distinct sandy layer. 615 cm: small plant ragment, few mm. 618-630 cm: less sand. 620 cm: mm-scale calcitic shell fragments. 626-630 cm: water-saturated, softer sediment. Increased diatom content. 630/640-767 cm: gradual increase in terrigenous sand and biosiliceous content => sand-bearing silty clayey diatomaceous ooze. Forams moderately abundant. Slightly (0.5 val.) darker colour. 642 cm: mm-large shell fragments. 647 cm: DS, black, diskoidal, well rounded. 680 cm downcore: DS, granule sized, occur more frequently. 684.5-686.5 cm: void, fissure from carbonate concretions. 694-697 cm: breccied texture. Concretions with carbonate shell fragments inside as nucleoli. 703, 705,714 and 715 cm: breccied nodule texture. 734-767 cm: sediment texture is increasingly destroyed by intruded CC with large voids and fissures.

LV29-89-2 HYC

54°27.896'N, 141°57.988'E

Date: July 10, 2002

Described by: Gorbarenko, S.A.; Astakhov, A.S. water depth: 51 m

METERS	GRAPHIC LITH.	BIOTURB.	ACCESSORIES	FOSSILS	DESCRIPTION
					0-5 cm: medium-grained sand, olive-green (5Y4/4), well sorted, fluid, with admixture of pebble and gravel. 005-015 cm: silty sand, dark gray, moderately dense. 005-007 cm: abundance of gravel and pebble. Small shell fragments. Lenses of finer sediment are marked in lower part of horizon. 015-022 cm: oblique sandy lens with gravel. 022-047 cm: horizon of bedded dense sediments: interchange of interlayers (0,5-1,5 cm in thickness) with sandy silt (sometimes, silty sand) and clayey silt, dark gray color with slight greenish tone (5GY4/1 - 5GY2/1); enriched in mica. 020-025 cm: fragments of small wood branches

LV29-91-3 HYC

54°54.131'N, 141°58.236'E

Date: July 11, 2002

Described by: Gorbarenko, S.A.; Astakhov, A.S.

Water Depth: 108.00 m Rig Floor to Sea Level: 0.00 m

METERS	GRAPHIC LITH.	ACCESSORIES	FOSSILS	DESCRIPTION
	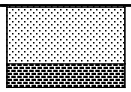			000-035 cm: medium-grained sand, greenish-gray, with admixture of gravel and pebble. Living worms occur. 035-050 cm: gravel-pebble deposits with sandy filler, probably representing Late Pleistocene (?) beach deposits.

LV29-94-2 SL-R

54°52.816'N, 145°16.554'E

Date: July 12, 2002

Described by: Gorbarenko, S.A.; Astakhov, A.S. water depth: 1442 m

METERS	GRAPHIC LITH.	BIOTURB.	ACCESSORIES	FOSSILS	DESCRIPTION

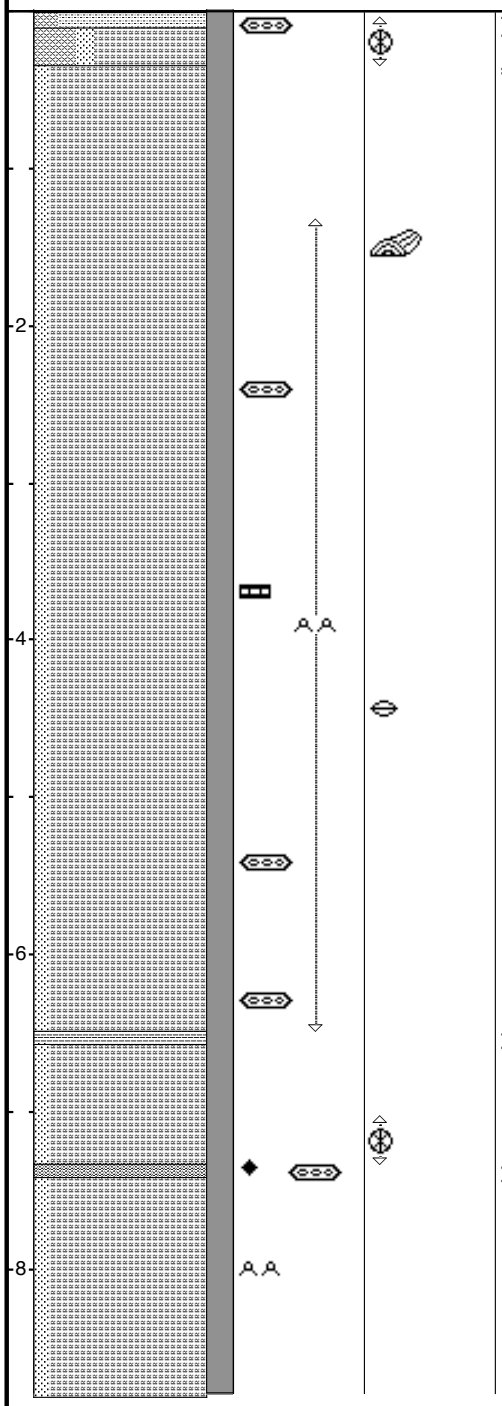

000-016 cm: sandy silt, weakly diatomaceous, grayish olive green, 0-5 cm - fluid, below - soft, with dispersed pebble; there are lenses enriched in sand.

016-037 cm: diatom-bearing clayey silt, dark gray (10Y4/2), with large admixture of sand, soft, bioturbated (numerous greenish-gray spots were observed).

37-38 cm: horizon enriched in sand with mica (5G4/1).

038-651 cm: sand-bearing clayey silt with, grey (5GY4/1, 86-386 cm - 5GY4/1-5G4/1), below 386 cm - olive-grey (5Y5/2-5Y3/2),
515-586 cm: with yellowish-green tone (5GY5/2); soft
186 cm downcore: moderately dense, homogeneous. An increased sand content is marked at 240-250, 543-544, 630 cm.
Below 130 cm: rare laminas of hydrotroilite.
370 cm: small lenses of white silty particles occur (probably, volcanic ash K2). At 150 cm - small wood fragment (1,5x0,5 cm in size).
442 cm: shell fragment. Dispersed dropstones are common.

651-659 cm: greenish-gray (10Y 4/2) clay, moderately dense.

659-734 cm: clayey silt with sand admixture, grayish-olive (10Y4/2) 700-734 cm: 10G 3/2; dense,
674-686 cm: very dense. Within lower part (700-734 cm) increased content of diatoms

734-743 cm: clay-silt-sand with lenses enriched in sand and gravel, with admixture of diatoms, greenish-gray (10Y4/2), some areas are greener.

743-880 cm: clayey silt with sand admixture, in upper part (743-750 cm) admixture of diatoms; gray (5G4/1), dense, with numerous traces of bioturbation.
786-880 cm: rare spots of hydrotroilite.
745 cm: large DS.

LV29-94-3 SL-G

54°53.095'N, 145°16.610'E

Date: July 12, 2002

Described by: Lembke, L. water depth: 1134 m

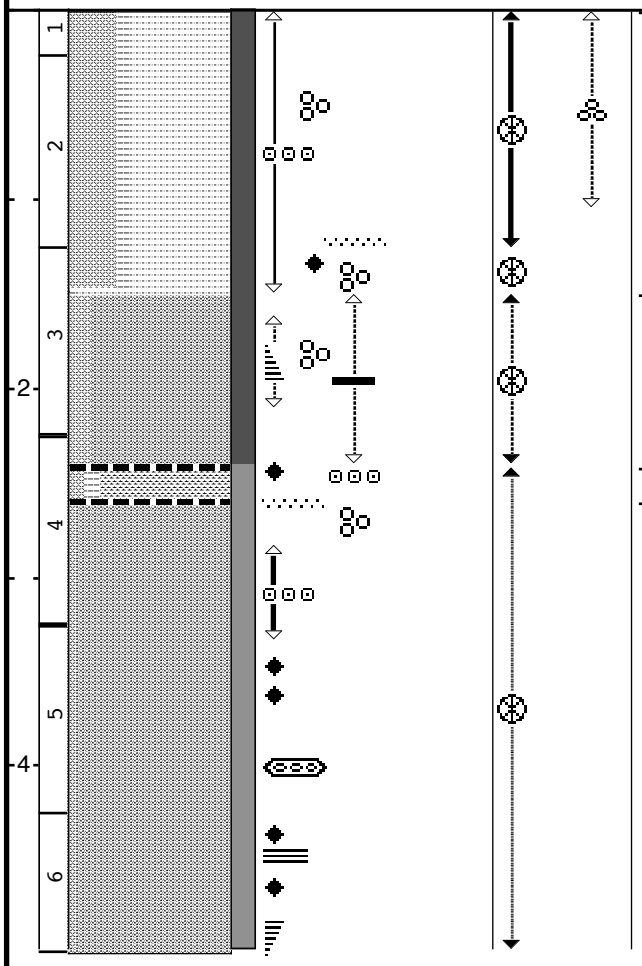

DESCRIPTION

000-150/160 cm: diatomaceous sandy silt with clay, downward gradually turning into diatom-bearing sandy silt with clay. Olive gray (5Y 3/2) changing downcore to grayish olive 5GY 3/2). Black detrital terrigenous grains and qz grains (middle sand) abundant. Upper ca. 50 cm very soft with high water content.
49-57 cm: gas-filled fissures and voids in sediment.
61-62 cm: voids.
66.5 cm: sandy silt lense.
74-76, 81-82, 84-85 cm: voids.
93 cm: agglomerated sandy parts, lenselike.
122.5 cm: thin sand layer (mm).
135 cm: DS, pebble, black, rounded, subdiskoidal.
140 cm: void, ø 1cm.

160-241 cm: diatom-bearing sand silt clay. Lighter olive gray (5-10Y 4/2). Moderately abundant dark streaks.
160-210 cm: gradual facies change from upper part, coarsening grain size.
180-190 cm: small voids.
200-218 cm: interval with increased abundance of terrigenous sand-granule debris.

241-259,5 cm: change to silty sand with clay and diatoms/rare diatoms.
241.5 cm: black layer, 2 mm thick, clay (?).
244-245 cm: terrigenous detrital grains abundant.
243 cm: forams, DS, ø 5 mm.
259.5 cm: basal sand layer, 1-2 mm thickness, with some non-continuous sand layers below.

260-493/498 cm: sand silt clay with rare diatoms. Olive gray (5Y 3/2).
269.5 cm: spherical voids.
281-282, 299-300 cm: coarse sand grains abundant.
320-323 cm: granule terrigenous debris abundant, DS's?
329-330 cm: coarse sand lenses.
345 cm: dark sand lamina, 2 mm thick.
347-348 cm: DS, subprismoidal, rounded, metam. or pluton.
362 cm: DS, covered.
399 cm: small sand lenses.
435-436.5 cm: DS, rounded, ø ca, 15 mm.
446 cm: dark laminae, DS.
462-7463 cm: DS, covered.
493-498 cm: transitional zone to lower facies, sediment color changes to grayish olive (10Y 4/2). Decreasing grain size/better sorted.

LV29-94-3 SL-G

54°53.095'N, 145°16.610'E

Date: July 12, 2002

Described by: Lembke, L. water depth: 1134 m

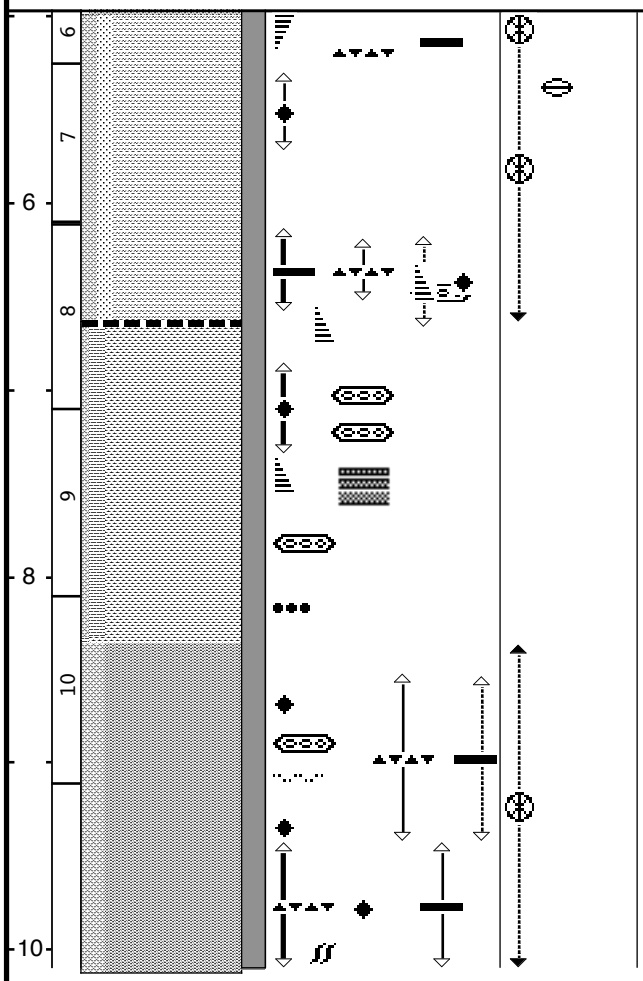

DESCRIPTION

498-663 cm: silty clay with sand and diatoms. Grayish olive (10Y 4/2), from 543 cm downcore less dark (10Y 5/2). Terrestrial debris moderately abundant. In lower part black streaks and mottles, coarsening downward, increased abundance of sand/silt.
512-525 cm: black streaks and mottles.
530.5-531.5 cm: DS, tilted, rounded - well rounded, ø 2 cm.
533-534 cm: DS, ø 2cm.
535.5 cm: shell fragment.
550, 561, 569-571.5 cm: DS's, covered.
638 cm: middle-coarse sand lense.
640-642 cm: DS, weakly angular, subprismoidal - prismoidal plutonite (?), ca. 4 cm.
647-648 cm: sand lenses.

663-830 cm: silty sand with clay and very rare diatoms. Frequent sand lenses, layers and clayey-silty nodules and lenses. Inhomogenous sediment. Mostly grayish olive green (5GY 3/2), grayish olive (10Y 4/2) in lower part.
663-681 cm: coarsening of grain size from upper facies.
684-685 cm: large DS.
700.5-703 cm: interval with inclined sand lenses and layers, granule DS's.
716, 723-726, 732-733 cm: large pebble/cobble-sized DS's.
732-733 cm: layer of coarse - very coarse sand.
747-757.5 cm: interval coarsening downwards, basal 5 cm very weakly sorted sand-gravel layer. Max. diameter ≈6cm, mostly well rounded and spherical. Contourite. Single lenses of same facies at 764 and 765 cm.
780-798 cm: frequent sand lenses.
817, 822 cm: small DS's.

830-1010 cm: sand silt clay with diatoms. Black streaks and mottles appear in facies, increasing downcore. Decreased abundance of DS and sand layers. No significant color change.
866, 881 cm: DS, covered.
887, 896-897 cm: sandy-silty lenses.
907 cm: clay-silt lamina.
933 cm: DS, covered.
959-962 cm: increased abundance of dark streaks.
977 cm: DS, granule.
991-995 cm: fissure, artefact.

LV29-100-1

53°58.810'N, 146°19.847'E

Date: July 13, 2002

Described by: Gorbarenko, S.A.; Astakhov, A.S. water depth: 1479 m

METERS	GRAPHIC LITH.	BIOTURB.	ACCESSORIES	FOSSILS	DESCRIPTION
2 4	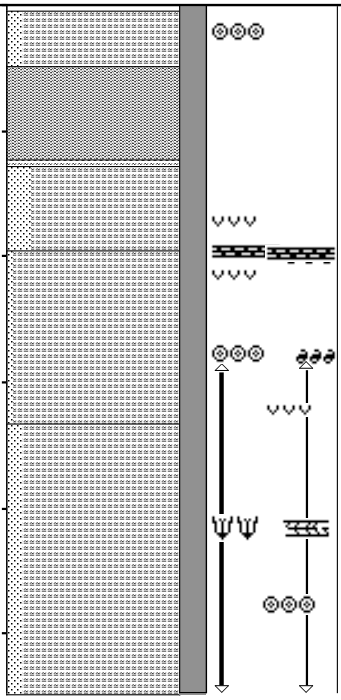				000-007 cm: upper part is washed out. 007-050 cm: clayey silt, beyond 20 cm with sand admixture, gray (5G4/1), soft. 010-015 cm: carbonate concretion 030 cm: carbonate concretions. 050-126 cm: sand-silt-clay, gray (5G4/1) 080-083 cm: with greenish tone, within lower part - blueish-gray; soft, homogeneous. 126-130 cm: oblique layer of silty clay with sand of slight greenish-brownish tone, soft. 130-197 cm: clayey silt with large sand admixture, olive-gray (5Y4/1), soft, homogeneous. 158-159, 169-170 cm: lumpy green diagenetic interlayers are marked. 197-198 cm: ash layer K2, silty size. 198-202 cm: horizon of carbonate concretions (up to 3-4 cm in size) 202-333 cm: clayey silt with sand admixtures; interchange of gray and greenish-gray sediment layers (10G4/2-5GY3/2); moderately dense. Below 282 cm: sediment is gas-saturated with pseudo-brecciated texture. 206, 215, 222, 323 cm: lumpy dense green diagenetic horizons. 274-282 cm: carbonate concretions up to 10 cm in size and barite crusts 333-547 cm: clayey silt with sand, steel-gray (5G5/2). Below 379 cm: greenish tone (5GY5/2), moderately dense (at 379-475 cm - diluted), gas-saturated, with typical pseudo-brecciated texture. 475 cm: carbonate concretion (4 cm in size).

Lv29-103-2 SI-R

53°26.151'N, 146°6.050'E

Date: July 14, 2002

Described by: Gorbarenko, S.A.; Astakhov, A.S. water depth: 1746 m

METERS	GRAPHIC LITH.	BIOTURB.	ACCESSORIES	FOSSILS	DESCRIPTION
	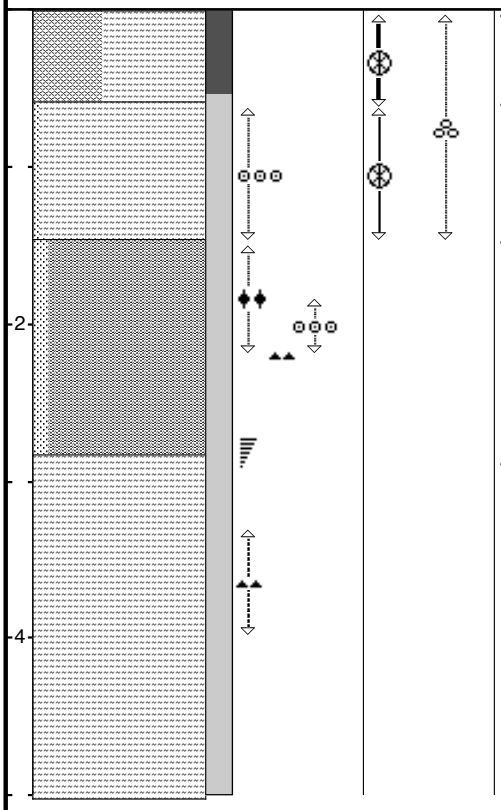				000-060 cm: diatomaceous silty clay, in upper part (0-32 cm) dark brown oxidized (10YR2/2), below (32-45 cm) - transitional from dark brown to greenish-gray, at 45-60 cm - greenish-gray 000-015 cm: fluid, lower - soft. An admixture of foraminifers is marked in entire interval (more intensive at 45-80 cm). 60-149 cm: silty clay with sand, diatoms and foraminifers. Grayish-green (10Y4/2) 116-133 cm: gray (10G4/2), soft. 107-115 cm: maximum content of foraminifers 105-113, 133-149 cm: thin (2-5 mm) bedded texture, interchange of dark and light interlayers. 119-122 cm: more dense and more dark diagenetically altered sediment 149-286 cm: sand-silt-clay with sand, gray (10G4/2), soft. 149-183 cm: micro-bedded texture (0,5-3 mm) similar to upper part, but less clear. 183-220 cm: increased content of sand 220 cm: admixture of microcrystalline diagenetic calcite 149-220 cm: rare spots of hydrotroilite 244, 257-259, 264, 266 cm: dense lumpy green diagenetic interlayers occur in entire interval, sediment in these places is more green (5G4/1) 280-286 cm: sediment develops into clay downwards 286-683 cm: silty clay, olive green (5GY3/2), soft, elastic, from 583 cm - moderately dense, with increased admixture of plant fragments, diagenetic pyrite and rare diatoms. 330-400 cm: horizons enriched in diagenetic microcrystalline carbonate below 600 cm: pseudo-bedded texture expressed in the interchange of dark and light interlayers 330-375 cm: lenses of more dark sediment enriched in organic substance

LV29-103-2 SI-R

53°26.151'N, 146°6.050'E

Date: July 14, 2002

Described by: Gorbarenko, S.A.; Astakhov, A.S. water depth: 1746 m

METERS	GRAPHIC	LITH.	BIOTURB.	ACCESSORIES	FOSSILS	DESCRIPTION
6				Py		683-703 cm: turbiditic sequence. Upper part (683-695 cm) thin-bedded sediment with interchange of more light silty clay and more dark clayey silt (685-687, 691-692, 693-695 cm), lower (695-697 cm) sorted silt occurs, clayey silt is distributed, in lower part reiteration of dark gray silt. Enrichment in plant fragments and diagenetic pyrite, especially in silty interlayers. Horizon is water-saturated. Bottom boundary very sharp, oblique (the angle of slope is ~ 10°). 703-723 cm: clayey silt with sand, greenish-gray (5GY4/1-5GY3/2), dense, lumpy, diagenetic alterations, microcrystalline diagenetic carbonate andframboidal pyrite. 723-745 cm: silty clay developing into clay, greenish-gray (transition from 10Y4/2 to 5GY5/2), dense. 734-735 cm: thin small lenses and layers of black sediment 745-783 cm: silty clay, dark gray (up to black), moderately dense. A large quantity of black amorphous substance (hydrotroilite?) was discovered under investigation of smear slides. Upper boundary is uneven, bioturbated. 783-846 cm: silty clay, black (continuation of upper interval), with increased content of silty clastic particles. 847-857 cm: turbidite sequence, base consists of dark-gray (up to black) water-saturated fine-grained sand. Gradational layers occur. Sharp boundary. 857-900 cm: sand-silt-clay with sand, grayish-green (5G5/2), dense, with diagenetic alterations: increased content of diagenetic microcrystalline carbonate (more intensive at 871-883 cm). 879 cm: lens of microcrystalline carbonate. Lenses of black sediment are common. 896 cm: DS 900-936 cm: silty clay, gray, dense, with rare laminas of hydrotroilite. 913, 927 cm: DS 936-983 cm: silty clay, black. Uneven upper boundary caused by bioturbation.
8						

LV29-103-3 SL-G

53°25.488'N, 146°6.461'E

Date: July 14, 2002

Described by: Lembke, L. water depth: 1748 m

METERS	GRAPHIC LITH.	BIOTURB.	ACCESSORIES	FOSSILS	DESCRIPTION
2	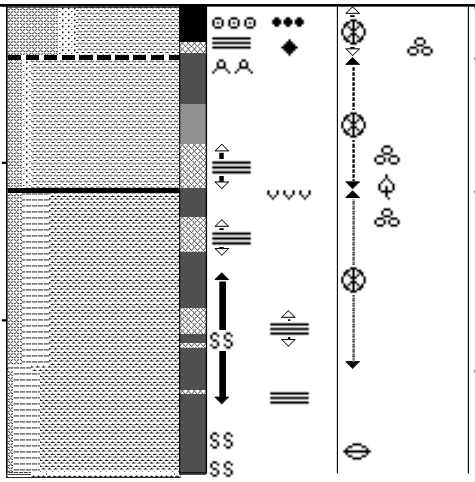				000-023 cm: diatomaceous silty clay with sand. Small granule DS and wooden fragments occur. Olive gray (5Y 4/1). Forams abundant. 023-118/122 cm: silty clay with diatoms and rare sand. Decreased foram abundance. Laminations occur in parts of this interval, mm-fine alterations between dark dusky yellowish brown (10YR 2/2) and and dark yellowish brown (10YR 4/2), differences in texture or matrix not clearly visible, from initial ss: slight differences in diatom/clay content. Sediment has partly undergone secondary colour changes (early diagenesis) towards greenish gray (5G 6/1), therein laminae are no longer visible, sediment composition remains unchanged. 026-033 cm: interval with abundant forams. 037-038 cm: relatively soft carbonaceous concretions. Dusky blue-yellow green (5GY 5/2-5BG 5/2). from 051-078 cm: subsequent color change from dark yellowish brown (10YR 4/2) towards olive gray (5Y 4/2). Texture appears better sorted, less plant debris and almost without granule-coarse sandy DS. Patchy color. 078-092 cm: occasional occurrence of granul DS. Color changes to grayish olive (10 Y 4/2). 092-118/122 cm: occurrence of laminations increases in interval towards bottom boundary, increasing abundance of forams (rich). 113+114 cm: wood/plant debris. 118-124 cm: carbonaceous concretions, stiff, hard. 118-122 cm: wavy and curved bottom boundary. 118/122-228/232 cm: silty sand with clay and rare diatoms, terrestrial plant debris and wooden fragments. Heterogenous interval. Grain size coarsens downward till app. 150-155 cm, fining downwards from there till bottom boundary. Forams rare-very rare. Terrigenous debris rare - common. 133-139 cm: color transition from diagenetically altered top boundary - pale olive (10Y 6/2) towards darker colour => light olive gray (5Y 5/2). 139-218/220cm: laminae 0.3-1mm thick, darker laminae: higher abundances of sand grain size, opaque minerals (pyrite, etc.) and plant debris/wood fragments, considerable (-1/2) less clayey grain size. 195.5, 196.3, 198.7, 200, 203.5, 210.5 and 216-218 cm: prominent laminae. 228/232-299/302 cm: silty sand with clay and rare diatoms, rare wooden fragments and overall very rare biogenic particles. Slightly coarsening downward. Grayish olive (10Y 4/2). 240-242 cm: moderate olive brown layer (5Y 4/2). Well - less well sorted. Very rare - absent forams. Terrigenous detrital grains (coarse - very coarse sand) occur. 282.5 cm: shell fragment. 299-302-302 cm: transitional zone/bottom boundary towards lower facies with slightly decreased diatom and clay content.

LV29-103-3 SL-G

53°25.488'N, 146°6.461'E

Date: July 14, 2002

Described by: Lembke, L. water depth: 1748 m

METERS	GRAPHIC LITH.	BIOTURB.	ACCESSORIES	FOSSILS	DESCRIPTION

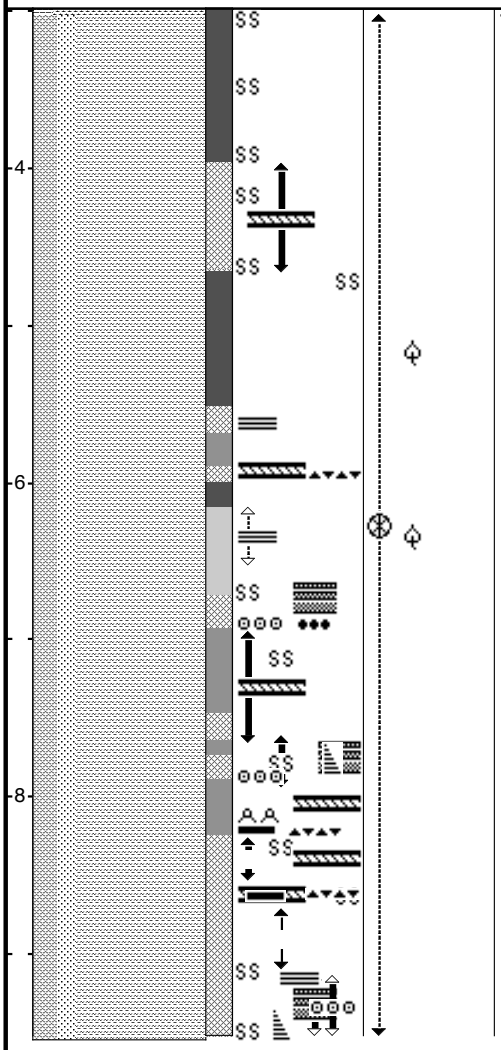

299/301-952 cm: silty clay with diatoms - diatom-bearing silty clay with sand particles and rare plant debris/wood fragments, very homogenous facies, forams absent. Dark yellowish brown (10YR 4/2).
within this facies, anoxic parts occur as denoted below.
395-398.5 cm: Tilted, but sharp boundary from previous sediment color towards dark olive - grey-olive black (5Y 1.5/1), almost black, sediment oxidizes quickly after opening of core sections.
465-466 cm: return to dark yellowish brown - moderate olive grey (10YR 4/2-5Y 4/2). No textural or lithological changes.
516 cm: wooden fragment, granule-sized.
553-569/71 cm: potentially residuals of former laminae, very regular, thin streaks.
590-599/601 cm: anoxic sediment, same characterisitcs as 395-465 cm, additionally => internal black mottles and streaks.
614-671 cm: residuals of laminations suspected, sub-mm thickness, sediments gets gradually darker to bottom.
633, 642 cm: wooden fragment, granule-sized.
671-693 cm: turbidite sequence as follows
671-678.5 cm: coarsening downward.
678.5-686 cm: diversely laminated intervals
686-686.5 cm: darker (0.5 val.) layer.
686.5-692/93 cm: lower part, basal turbidite layer, silty sand with granules, moderate yellow (5Y 7/6) clouds in grayish olive (10Y 4/2) matrix. Eroded bottom boundary. Sediment below basal layer unchanged from upper part. Silty clay with diatom fragments, rare diatoms and rare sand. Few mm below sediment surface => greyish black color (N2).
765-773 cm: grayish olive (10Y 4/2) interval with dark streaks and laminae, non continuous. Suspected top section of underlying turbidite as follows:
773-789 cm: turbiditic sequence, coarsening downward to medium sand size.
773-775 cm: intercalated laminated sections:
775-777 cm: graded bedding, coarsening downward.
783-785 cm: dark gray (N3) layer.
790/791 cm: Eroded, wavy, but sharp bottom boundary.
Below turbiditic sequence: unchanged general sediment composition (description see above). dark greenish gray - grayish olive color (5GY 4/1 - 10Y 4/2) with occasionally occurring intraclasts/diagenetic concretions in moderate yellowish brown-dark yellowish orange (10YR 5/4-10YR 6/6).
818-821 cm: black streaks and mottles.
823.5 cm: change to grayish black (N2) sediment colour, unchanged lithological characteristics. Sediment surface (ca. 3 mm deep) oxidizes shortly after opening to olive gray colour (5Y 4/1).
860-866.5 cm: dark streaks in core (russ.: "diagenetic layer").
910 cm: distinct top boundary of turbiditic sequence as follows:
910-916.5 cm: laminae/lenses mm-sub-mm thickness. Graded structure. Light olive gray-olive gray (5Y 5/2 - 5Y 3/2).
916.5-931 cm: graded structure, coarsening downward. streaks and single layers (0.3-0.6 cm thick) occur.
931-44.5 cm: coarser interval, coarsening downward from very fine/fine to middle sand. Well sorted.
944.5-951 cm: Layer of coarse-very coarse sand, dark gray-black (N3-N1).
CC got stuck in this turbiditic sequence.

LV29-104-2

53°12.850'N, 146°15.642'E

Date: July 14, 2002

Described by: Gorbarenko, S.A.; Astakhov, A.S. water depth: 1758 m

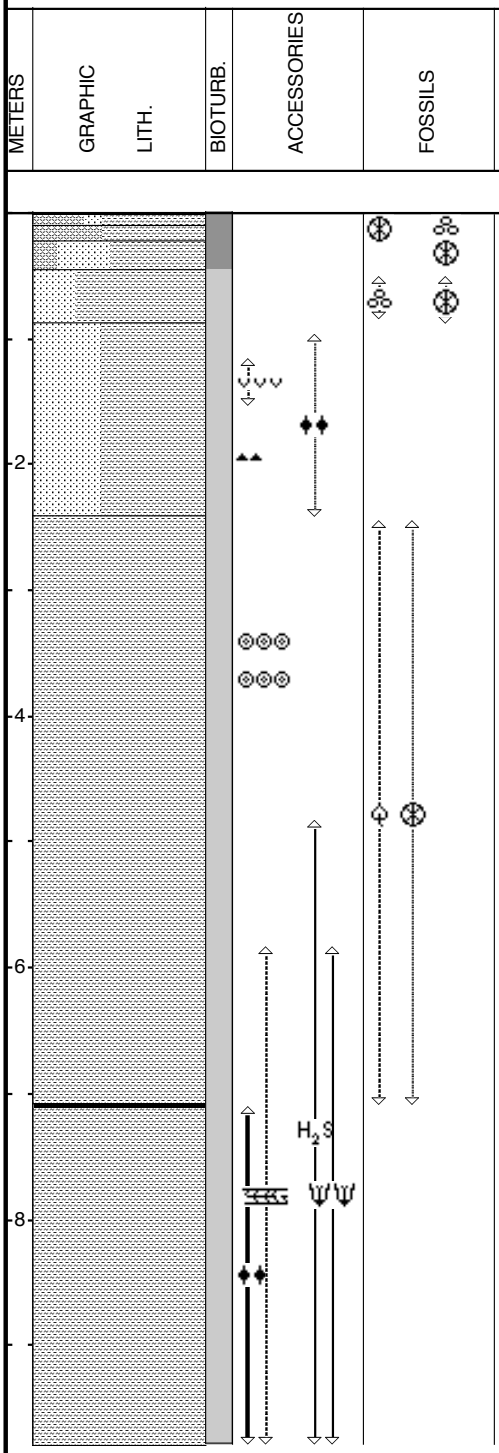

DESCRIPTION

000-012 cm: diatomaceous silty clay with sand and rare foraminifers, chocolate-brown (10YR2/2),
000-005 cm: fluid, lower - very soft.

012-025 cm: diatomaceous silty clay
025-047 cm: diatom-bearing sandy silty clay with sand and rare foraminifers, greenish-gray (10Y4/2), very soft.

047-090 cm: sand-bearing silty clay with foraminifers and rare diatoms, gray green (5GY5/2), below 67 cm - steel-gray (10G6/2), soft.
060-067 cm: enrichment of foraminifers.

090-242 cm: sand-bearing silty clay, 190-195 cm: silty clay; steel-gray
090-190 cm : 10Y4/2; 190-195 cm: 5GY5/2; 195-242 cm: 10G4/2
soft, homogeneous, with rare laminas of hydrotroilite.
116-155 cm: Dense greenish diagenetic interlayers (116, 129, 133, 154, 155 cm, 244-245 cm)
190-195 cm: diagenetic microcrystalline carbonate.

242-711 cm: silty clay, grayish olive-greenish (5GY5/2)
below 580 cm: dark greenish-gray (5GY4/1), soft beyond 480 cm, lower: moderately dense, homogeneous, with pseudo-bedded texture parallel to stratification.

339, 370 cm: microcrystalline white and yellowish carbonate aggregates (decomposed crystals of hydrocalcite?). Small plant fragments and rare diatoms are marked in entire interval.

below 480 cm: weak H2S odor

Below 580 cm: sediment gas-saturated with pseudo-brecciated texture.

711-980 cm: silty clay with characteristic black colour, analogous on composition to overlying sediment, gas-saturated with pseudo-brecciated texture. A large quantity of black amorphous substance (hydrotroilite?) was discovered under investigation of smear slides.

LV29-104-3 SL-G

53°12.740'N, 146°16.152'E

Date: 14 July 2002

Described by: Lembke, L. water depth: 1760 m

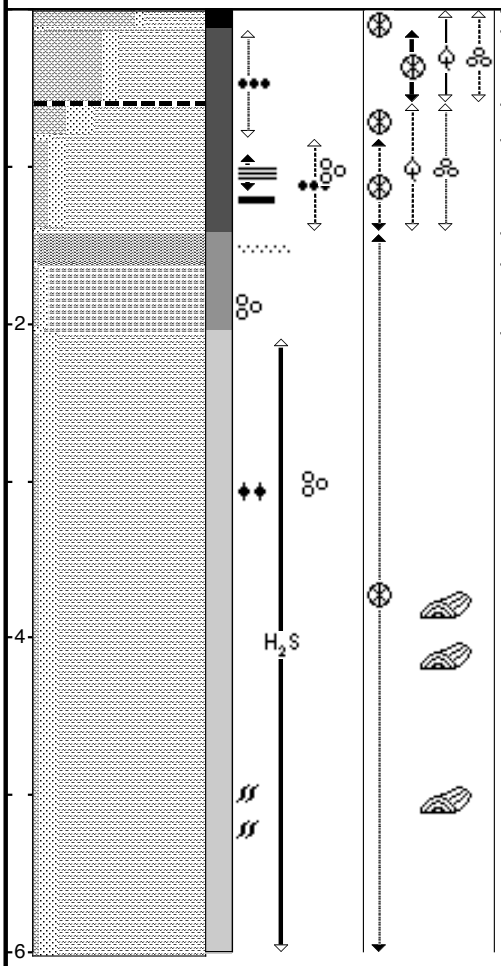

DESCRIPTION

000-013 cm: silty clayey diatomaceous ooze with sand, terrigenous organic matter and plant debris. Forams frequent - abundant. Dusky yellowish brown (10YR 2/2), very soft texture.

013-059 cm: diatomaceous silty clay with sand, some terrigenous organic matter, rare shell fragments and plant debris. Forams less frequent though increasing abundance to lower part. Occasionally granule-sized DS. Light olive gray (5Y 5/2) turning into grayish olive (10Y 4/2) downcore.

059-081 cm: diatom-bearing silty clay with sand, occasional small (granule) DS. Soft sediment, still high water content. Dark greenish gray (5GY 4/1). Margins disturbed (1 cm).

081-142 cm: silty clay with sand and rare diatoms. Slight increase in terrigenous detrital grains. Sediment more compacted and stiffer. Dark greenish gray (5GY 5/1).
091-116 cm: interval with intense laminae of greenish black (5GY 21/1) color. Darker laminae contain more sand, opaque minerals, plant remains and wood fragments.
102-104 cm: void, ø 2cm.
119, 123-124 cm: 0.5 cm thick dark layers, nearly black.
142-147 cm: transitional zone to lower facies.

142-162 cm: sand silt clay with rare diatoms and plant debris. Dark greenish gray (5GY 4/1!). Compact, stiff sediment.
151.5 cm: sand layer.
162-165 cm: color transition to lower facies.

162-204/207 cm: clayey silt with sand/rare sand, rare diatoms and plant debris. Dark detrital grains, granule-sized DS moderately abundant. Facies slightly coarsening downward. Olive gray (5Y 4/1), in lower part dusky yellow green (5GY 5/2).
187-189 cm: void.
202 cm: 0.5 cm-thick layer, no texture change, grayish olive green (5GY 3/2).
204-207 cm: transitional zone to lower facies.

204/207-640 cm: clayey silt with rare sand, diatoms and plant debris, dark greenish gray (5GY 4/1). Very homogenous section, very few detrital grains or larger (>1 mm) plant debris. Downcore in section strong H2S odor.
301-308 cm: void.
306 cm: diagenetic layer, 4 mm thick, crystallizations, needles, rhombic, hydrotroilite?
378 cm: small wood fragment, mm-large.
411 cm: small wood fragment.
498-499 cm: fissure.
502 cm: wood fragment, 2mm.
520-523 cm: fissure.

LV29-104-3 SL-G

53°12.740'N, 146°16.152'E

Date: 14 July 2002

Described by: Lembke, L. water depth: 1760 m

METERS	GRAPHIC LITH.	BIOTURB.	ACCESSORIES	FOSSILS	DESCRIPTION
8	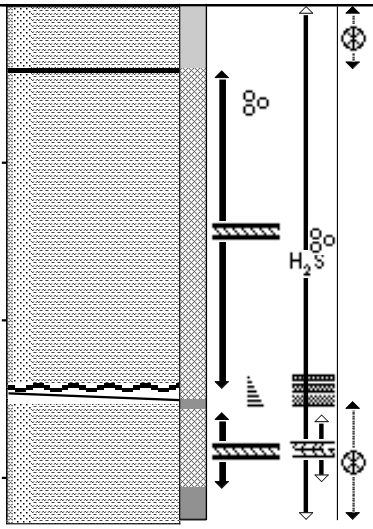				640-844 cm: lithology remains largely unchanged, but sharp color change to dark gray-black (N 0). Decreased silt content, more clay. Homogenous black color. 660-669 void, 0.5 cm deep. 748-752 cm: void. 844-849-851 cm: turbidite sequence. Sharp, tilted bottom contact with underlying sediment, eroded. middle - fine sand, fining upward. Relatively sharp, inclined top boundary. 851-928 cm: unchanged lithology from section beyond turbidite, but changes in color occur: 851-858 cm: grayish olive (10Y 4/2). 858-907 cm: change to black anoxic color. 907-928 cm: olive gray sediment color(5Y 3/2). 860-871 cm: pervasively breccied texture. 872-877 cm: spotty breccied texture. 879-904 cm: abundant-pervasive breccied texture. 916-928 cm: core partly disturbed by CC intrusion.

LV29-106-2 SL-R

51°59.849'N, 154°2.459'E

Date: July 16 , 2002

Described by: Gorbarenko, S.A.; Astakhov, A.S. water depth: 511 m

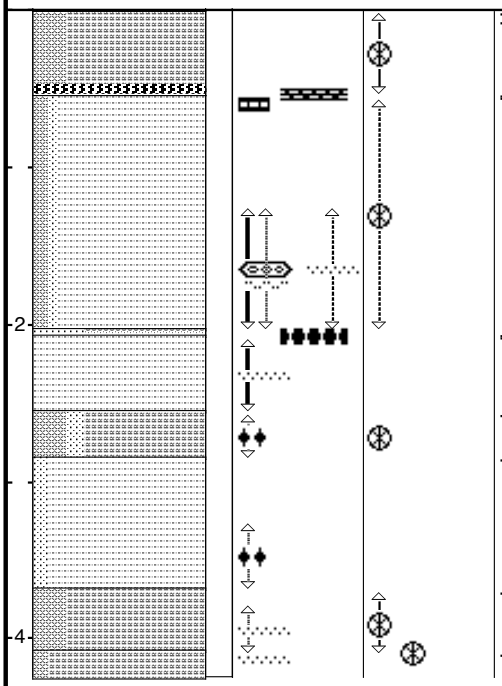

DESCRIPTION

000-008 cm: clayey silt weakly diatomaceous, greenish-gray, fluid.

008-054 cm: clayey silt weakly diatomaceous, olive green (5Y4/4), soft; below 44 cm: strongly bioturbated, with admixture of volcanic ash of underlying horizon.

054-056 cm: Ash layer, light gray (up to white), sandy-silt in size, shape of lenses due to bioturbation.

056-204 cm: sandy silt with diatoms and sand, gray-green (10Y4/2, 10Y3/2)
067-125 cm: gray (10G4/2); moderately dense. Filled by white volcanic ash burrows are traced up to 60 cm.
125-204 cm: Numerous lenses and interlayers of silty sand.

206-208 cm: interlayer of medium-grained sand with fine gravel and rounded pumice, dark gray.

208-257 cm: sandy silt, gray-green (10Y3/2), dense, with numerous lenses and interlayers of silty sand (sandy silt).
216(?), 219 cm: interlayers of black sand with pumice of about 1 cm in thickness.
254-255 cm: small interlayers of medium-grained black sand.

257-285 cm: diatom-bearing clayey silt with sand, greenish-gray (10Y4/2), homogeneous, with rare laminas of hydrotroilite.

285-368 cm: sandy silt with sand, greenish-gray beyond 325 cm (10GY3/2), lower - gray (5G4/1), homogeneous, moderately dense.
below 325 cm: Rare laminas of hydrotroilite

368-409 cm: diatom-bearing clayey silt, greenish-gray (5GY5/2), moderately dense, homogeneous. In lower part (378-409 cm) lenses of silty sand.

409-425 cm: clayey silt with diatoms, gray (5GY4/1).
409-410 cm: black interlayer
413-418 cm: admixture of sand with pumice.

LV29-106-5 SL-G

51°59.848'N, 154°2.854'E

Date: July 16, 2002

Described by: Lembke, L. water depth: 510 m

METERS	GRAPHIC	LITH.	BIOTURB.	ACCESSORIES	FOSSILS	DESCRIPTION

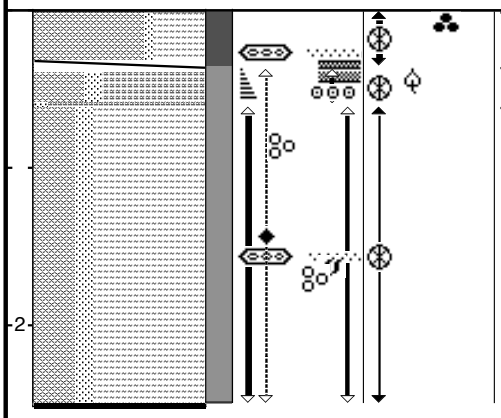

000-033/036 cm: silty clayey diatom ooze with sand. Moderate olive brown (5Y 4/4), below 011-013 cm turning into grayish olive (10Y 4/2). Very soft, high water content. Granule detrital grains and forams occur. Entire core exhibits moderate to frequent interpositions of sand lenses, intraclasts and turbidite-/contourite-like structures.
011-013 cm: sandy lense. Undulating top and bottom boundaries.
017-018, 021-032, 025 cm: lenses and layers, fine - medium size sand; qz, opx, cpx, rock fragments, mostly weakly rounded - subangular, weakly sorted.
033-036 cm: contourite-like structure, undulating top, sharp lense-like shaped inclined bottom boundary. clayey silt coarsening downward, devoid of biodetritus.

033/036-060 cm: diatomaceous clayey silt with sand. Detrital sand and granule DS occur. Moderate olive brown (5Y 4/4) to grayish olive (5Y 4/2) and slightly coarsening downward in basal part.
043.5 cm: granule-sized wood fragments and DS's.
047-051 cm: mudclast, silty clay, sharp, undulated boundaries with main facies.

060-254/255 cm: diatomaceous silty clay with sand, in parts increased abundance of terrigenous detrital grains. Grayish olive (10Y 4/2).
065-072 cm: fault zone with voids and fissures.
076-077 cm: layer with increased abundance of black detrital grains (sand size).
079-080 cm: small clouds of granule DS.
084 cm: void, ø 1cm. DS, ø 0.5 cm, rounded.
088.5 cm: several small DS's.
089-098 cm: marginal voids and fissure.
090-093 cm: three sand layers.
095 cm: sand lense.
100 cm: deep void.
105-118 cm: margins disturbed.
125-127 cm: hole from large DS.
129.5-134 cm: rectangular mud clast (?), sharp boundaries, olive gray (5Y 3/2).
134-136 cm: elongated sand nodule with dark rock fragments, also qz, fsp, weakly sorted, subangular.
149.5 cm: granule-sized DS's.
157-163 cm: sand lenses.
163 cm: fissure, 2 cm.
169 cm: void, ø 1cm.
185-252 cm: sediment becomes increasingly spotted with sand lenses/layers, matrix coarsening downward.
185-188 cm: layer with coarse-granule size DS, terrigenous debris.
188-190 cm: layer with (silty) clay.
190-191 cm: layer with sand, detritus.
199, 216 cm: sand lenses.
207-209 cm: inclined sand lense, varying thickness, sharp inclined bottom contact, fining upward.
217-222 cm: sand lense.
225-239 cm: frequent sandy intercalations and lenses, interrupted by voids and fissures.
254-255 cm: basal sand layer.

LV29-106-5 SL-G

51°59.848'N, 154°2.854'E

Date: July 16, 2002

Described by: Lembke, L. water depth: 510 m

METERS	GRAPHIC LITH.	BIOTURB.	ACCESSORIES	FOSSILS	DESCRIPTION
4	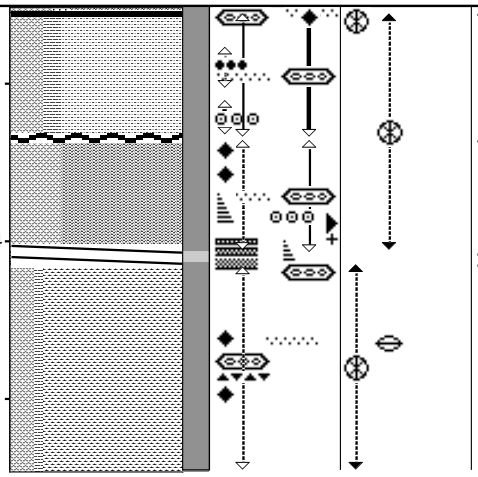				255-332/334 cm: diatom-bearing sandy silt with clay. Diatom abundance slightly decreases downward. Olive gray (5Y 3/2). Ocurrence of small DS, medium - very coarse sand in both matrix, frequent sand lenses and intercalations. 260 cm: shell fragment. 269 cm: DS, weakly rounded, white, subprismoidal, ø 4mm. 270, 272, 273 cm: undulating layers (mm-thick) of fine - middle sand. 275 cm: DS, rounded - weakly rounded, subdiskoidal, ø 4mm. 299 cm: DS, weakly rounded, subprismoidal, ø 5mm. 313.5-314.5 cm: layer with coarser grain size, DS. 322/323 cm: DS, weakly rounded, subdiskoidal - spherical, ø 15-20 mm. 332/334-403 cm: diatomaceous sand silt clay, ranging in sone intervals between sandy silt and clayey silt, sand lenses slightly less abundant than beyond. Undulated top boundary. Olive gray (5Y 3/2-2.5/2), sometimes a bit patchy. 339 cm: DS. 352 cm: calcitic shell fragment. 355 cm: DS, ø 5mm, weakly rounded, subspherical. 359 cm: some small granules, well rounded, spherical. 362.5-365 cm: interbedded clay and sandy layers, mm-thickness, lower layers weakly sorted. Dark olive gray (5Y 2/2). 371-378 cm: detrital fragments and grains. 378-382 cm: layer coarsening downward, lowest cm weakly sorted with granules and small pebbles. 386-388 cm: sand lense. 403/406-409/414 cm: contourite sequence. Tilted top and bottom boundaries. Coarsening downward with mm-thick lenses of silty clay intercalated. 409/414-545 cm: diatom-bearing silty sand, downcore gradually changing into sandy silt with diatoms. Light olive gray (5Y 4/2-5/2). Entire section relatively homogenous, less sand layers and lenses. Small black streaks and mottles occur in this section moderately. 418 cm: single sand lense. 442 cm: lense of black coarse sand, ø 1cm. 460 cm: DS, covered. 462 cm: tilted sand layer, 1mm thickness. 461+463 cm: calcitic shell fragments. 496 cm: DS, coarse sand, covered. 538 cm: end of undisturbed section, CC.

LV29-108-4 SL-R

52°1.311'N, 153°35.006'E

Date: July 16, 2002

Described by: Gorbarenko, S.A.; Astakhov, A.S. water depth: 625 m

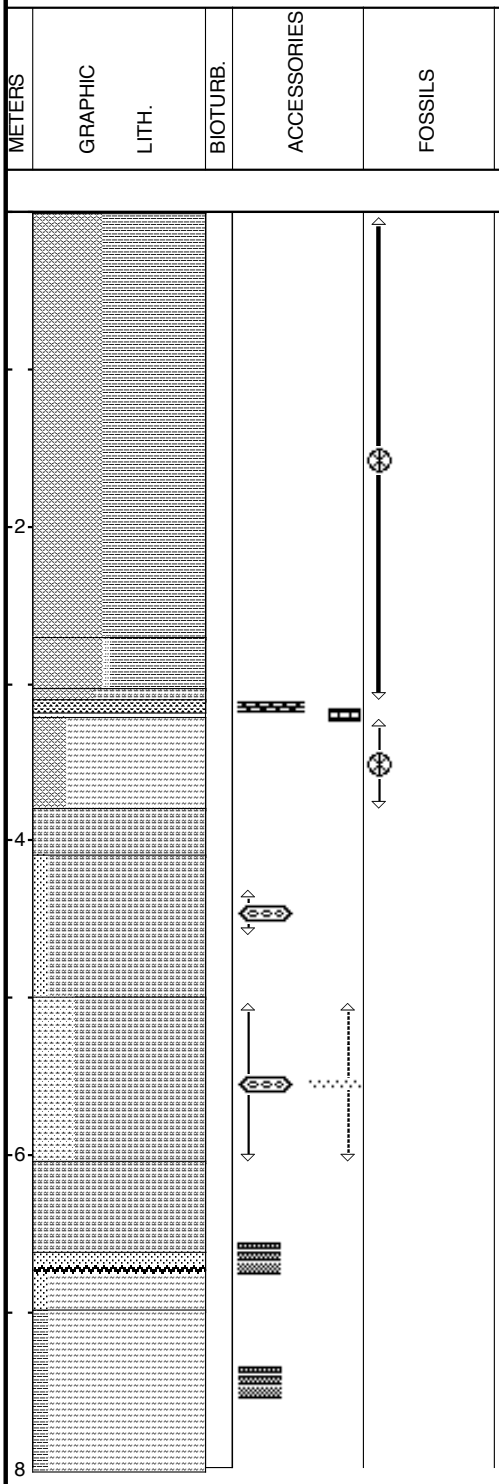

DESCRIPTION

000-272 cm: diatomaceous clay , olive green (10Y5/4),
beyond 15 cm: fluid, lower: very soft, water-saturated, homogeneous.

272-305 cm: diatomaceous clay , grayish-green (10Y4/2), soft; within lower part silty particles appear.

305-313 cm: diatomaceous clayey silt, light green, up to whitish (10Y6/2), with elongated spots and lenses of dark green sediment. The whitish tinge is caused by the admixture of large quantity of fine (silt-clay) light volcanic ash.

313-316 cm: ash layer, two horizons:
313-315 cm: light gray (up to white) volcanic ash of sand-silt in size;
315-316 cm: gray (5G6/1) volcanic ash of silt-sand in size. Strong bioturbation indicated by ash small lenses and interlayers between 316-322 cm.

316-382 cm: diatom-bearing silty clay , grayish-green (5GY5/2), homogeneous.

382-410 cm: clayey silt,
beyond 390 cm: greenish-gray (5G3/2), spotted
below 390 cm: dark gray (10Y4/2), homogeneous.

410-500 cm: clayey silt with sand
beyond 488 cm: gray (5G4/1)
below 488 cm: greenish-gray (10Y4/2); moderately dense.
430-460 cm: increased content of both sandy and silty sand lenses.

500-603 cm: clayey silt with lenses and thin interlayers of silty sand, moderately dense sediments, greenish-gray (10Y4/2)

603-663 cm: silty clay, grayish-green, moderately dense, with rare lenses of silty sand.

663-671 cm: turbiditic sequence lying on erosional sediment surface, homogeneous on colour and density.

671-700 cm: silty clay with sand, greenish-gray.
692 cm: turbiditic sequence, oblique interlayer of black silty sand of up to 0,5-0,7 cm thickness.

700-800 cm: silty clay – clay, greenish-gray, moderately dense, viscous,
743 cm: turbiditic sequence consisting of silty sand
745-760 cm: very dense

LV29-108-5 SL-G

52°1.330'N, 153°35.006'E

Date: July 16, 2002

Described by: Lembke, L. water depth: 627 m

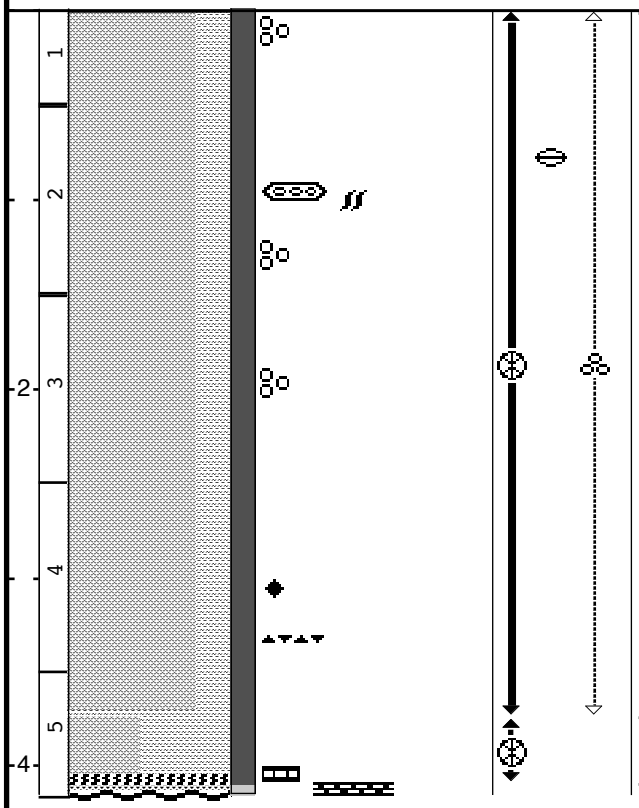

DESCRIPTION

000-373 cm: silty clayey diatom ooze with radiolarians and rare sand. Homogenous texture. Moderate olive brown (5Y 4/4). Forams abundant, terrigenous detritus rare.
000-050 cm: sediment very soft, almost fluid, high water content, section presumably slightly disturbed. Moderate dark olive brown (5Y 3/4).
010-028 cm: small voids.
067-082 cm: section with higher abundance of detrital rains (medium-coarse sand). Foram-rich.
076.5 cm: shell fragment, pelecypod, 3-4 mm.
094 cm: sand lense.
098-101 cm: fissure.
126 cm: layer of small voids.
191-200 cm: small voids, gas bubbles, ø 1-3 mm.
232 cm: void, ø 1cm.
300-301 cm: layer with pervasive whitish (biogenic?) detrital grains.
305 cm: small DS.
320 cm: small black mottles.
334-335 cm: black streaks.

373-420 cm: diatom content decreases slightly => diatomaceous silty clay with rads and rare sand.
373.5 cm: layer with pervasive abundance of biosiliceous components (diatoms and rads). 0.3-0.5 cm thick.
382-382.5 cm: lense/layer with coarser terrigenous and biogenic detritus (plant debris, forams, biosilica).
408-410 cm: decreasing abundance of biosiliceous components, transition to diatom-bearing silty clay with sand.

393-403.5 cm: intercalation of volcanic ash layer (=>K0, Gorbarenko), light olive gray (5Y 5/2-6/1) - yellowish gray (5Y 7/2).
382.5-395.5 cm: transitional zone, ash mixed with pelagic sediment by bioturbation.
393-394.5 cm: single ash nodule, ø 2cm.
395.5 cm: 2mm thick ash layer, continuous.
397-403.5 cm: large ash lense, deepest position of ash in core.

LV29-108-5 SL-G

52°1.330'N, 153°35.006'E

Date: July 16, 2002

Described by: Lembke, L. water depth: 627 m

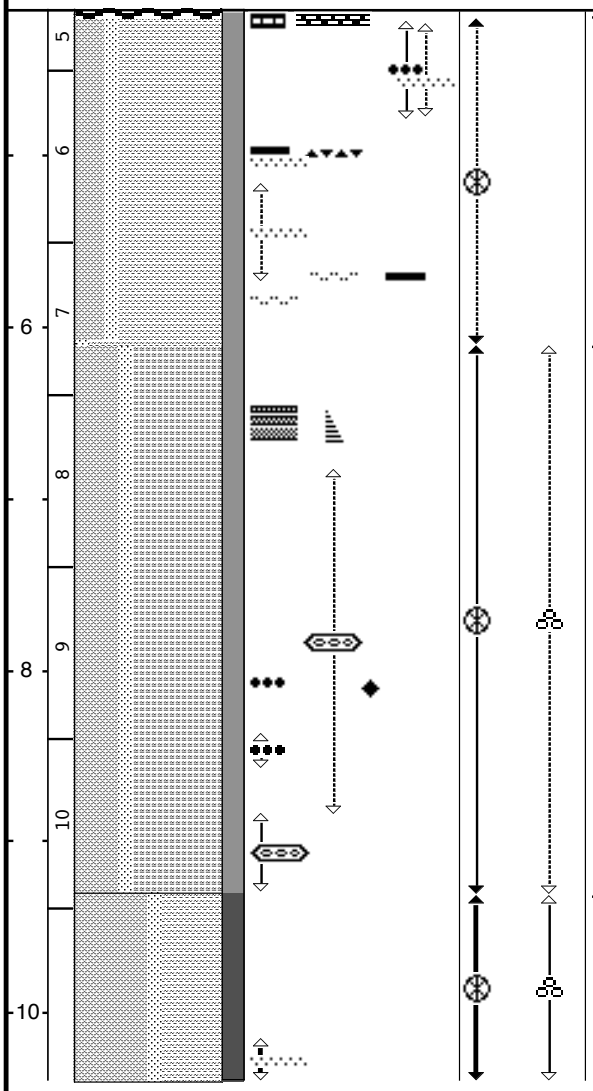

DESCRIPTION

420-610 cm: diatom-bearing silty clay with sand, grayish olive (10Y 4/2) changing into olive gray (5Y 3/2) in lower part. In upper part moderate - frequent intercalations of silty and sandy lenses and layers.
420-435 cm: coarsening downward to silty sand with clay and diatoms, inhomogenous facies.
428, 431-432 cm: increased abundance of granule-sized DS's.
434.5, 435, 444, 446 cm: sand layers.
455, 466 cm: dark lense of medium sand.
458 cm: DS's, ø 5mm.
470-479 cm: interval with increased abundance of granule DS's and detrital grains.
495.5-496.5, 497-500 cm: lense with black streaks and single DS.
502 cm: layer of silty sand.
514-516 cm: discordant layers of sand and silt detrital grains, microchannel structure (?).
539 cm: DS, covered and small shell fragment.
553, 557 cm: sand lenses.
561-568 cm: occasional black streaks, slightly finer grain size.
570-571 cm: layer of silty sand, 4 mm thick, sand lense below.

610-930 cm: coarsening grain size and decreasing diatom abundance to clayey silt with sand and diatoms, sometimes sand silt clay with diatoms. Brighter color (5Y 4/2), in lower part (≈740-930 cm) grayish olive (10Y 4/29), black mottles appear irregularly but increasingly downcore.
656/658-662/658 cm: lense-like intercalation of dark coarse - medium sand with discordant lower and inclined top boundary. Presumably contourite structure, extending down to 674.5 cm.
686 cm: small spheroidal sand lenses (ø 1-2 cm).
704 cm: irregularly shaped sand lenses.
711 cm. accumulation of granule DS's.
737-741 cm: lense of medium - coarse grained sand, dark olive black - greenish black (5Y 2/1-5GY 2/1).
747 cm: small sand lense.
755 cm: fissure.
794-797 cm: lenses of coarse sand, black.
799-801 cm: lense of silty clay.
805.5, 808.5 cm: DS's, granule-sized.
815.5 cm: DS, fissure.
826-833 cm: accumulations of granule-sized DS's.
845-854 cm: black streaks and mottles.
847.5 cm: DS's, well rounded, subspherical, granule - pebble.
862, 891 cm: sand lenses.
900-930 cm: increasing abundance of sandy/coarse silty layers and lenses, clayey matrix but higher fine sand content.
916 cm: sand layer.
919-921 cm: layer of DS's, 1 cm thickness.

930-1008 cm: gradual change towards silty clayey diatom ooze with sand. Olive gray (5Y 4/2-5Y 3/2). Forams visible. Terrigenous detrital grains, mostly weakly subangular - weakly rounded.
987 cm downcore: slightly darker color (0.5 value), increasing abundance of terrigenous debris in irregular lenses and streaks.
1008-1010 cm: coarse sand layer, sharp bottom boundary, fining upwards.
1020-1025 cm: interbedded strata of sandy silts and (darker) sands in layers of 1-3 mm, thickening upward.
1035-1039 cm: core section disturbed by CC.

LV29-110-2 SL-R

50°27.079'N, 154°46.165'E

Date: July 18, 2002

Described by: Gorbarenko, S.A.; Astakhov, A.S. water depth: 1218 m

METERS	GRAPHIC LITH.	BIOTURB.	ACCESSORIES	FOSSILS	DESCRIPTION
2	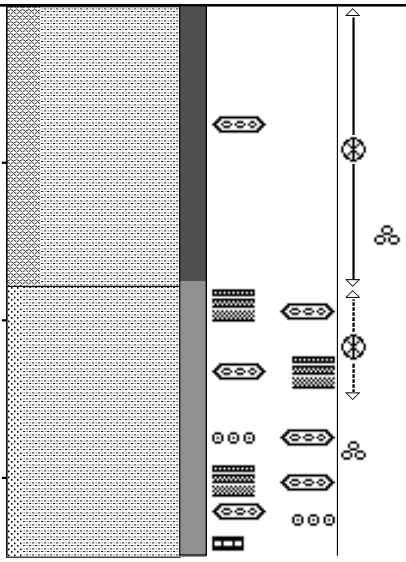				000-180 cm: diatom-bearing sandy silt , green (10Y4/2) 100-115 cm: light green (10Y5/4), moderately dense, homogeneous. 75 cm: lens of black sand. 135-155 cm: enrichment of foraminifera 180-350 cm: sandy silt with sand, 180-251 cm: green, lower - grayish-green and greenish-gray (10Y4/2), with diatoms 275-290 cm: foraminifer common. 194 cm, 231-233 cm: lenses of sorted dark gray silty sand and lenses of dark gray fine-grained sand. All lenses belong to turbidites. 265-280 cm: sandy lenses, sediment is more similar to silty sand. 301-302 cm: lense of dark gray sand, thickness 2.5-0.5 cm, turbiditic sequence. 320-330 cm: sandy lenses and small interlayers enriched in sand. 345-350 cm: numerous lenses of gray volcanic ash within lower part of the core; still unidentified.

Lv29-112-2 SL-R

50°13.497'N, 154°17.369'E

Date: July 19, 2002

Described by: Gorbarenko, S.A.; Astakhov; A.S. water depth: 1309 m

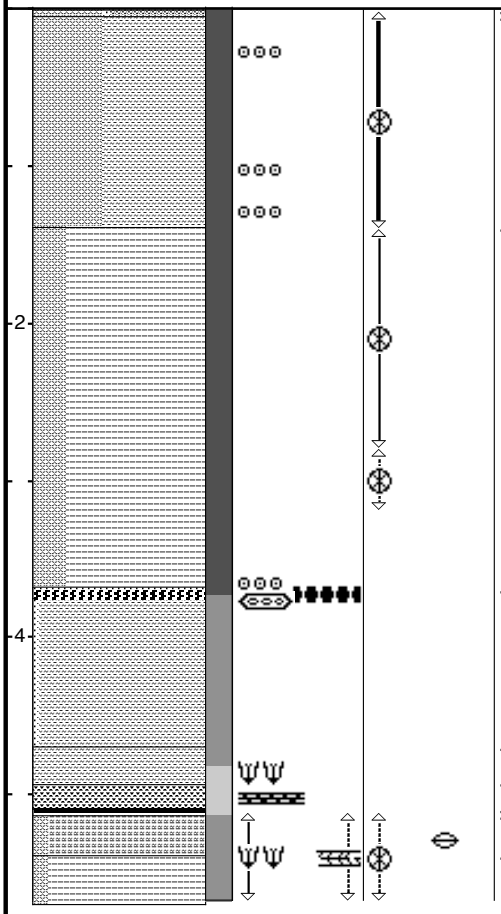

DESCRIPTION

000-007 cm: diatomaceous sand-silt-clay, olive green, fluid.

007-140 cm: diatomaceous silty clay, olive green, soft, homogeneous.
28-32, 97, 108, 129 cm: sediment is enriched in sand.

140-280 cm: diatom-bearing clay,
280-310 cm: clay with diatoms, olive green, soft, homogeneous
180-220 cm: spotted (bioturbated).
367-370 cm: sediment more coarse-grained - clayey silt with admixture of grayish-green sand.

372-470 cm: silty clay with rare sand, grayish-green, moderately dense, spotted (bioturbation).

470-494 cm: silty clay, grayish-green (5GY 3/2), downwards: greenish-gray (10Y4/2), moderately dense. Below 485 cm: first signs of gas-saturation appear (rare vertical cracks).

494-510 cm: massive volcanic ash layer (unidentified, 10Y5/4-10Y6/2-5Y6/1);
494-496.5 cm: clayey silt, light green whitish, in lower part - more light due to increased content of fine pyroclastics, bioturbated.
496.5-499 cm: fine silt, greenish-whitish, bioturbated.
499-500.5 cm: silt with gravel size pumice, light gray.
500.5-505 cm: coarse silt with rare gravel size pumice, light gray.
505-507.5 cm: sandy silt, light gray, thin interlayers of dark gray colour (due to enrichment of dark ore minerals).
507.5-510 cm: fine-grained sand with coarse silt, light gray; interlayers of darker colour; sharp bottom boundary. Lower part of this section is cleaved by thin vertical cracks caused by gas-saturation of underlying sediment.

510-513 cm: silty clay with diatoms, grayish-green, gas-saturated, pseudo-brecciated texture.

513-539 cm: clayey silt with diatoms, grayish-green, gas-saturated.
513-518 cm: dark sand lenses.
528 cm: shell fragments.

539-568 cm: clay with diatoms, grayish-green.

LV29-114-2 SL-R

49°22.465'N, 152°52.756'E

Date: July 19, 2002

Described by: Gorbarenko, S.A.; Astakhov, A.S. water depth: 1764 m

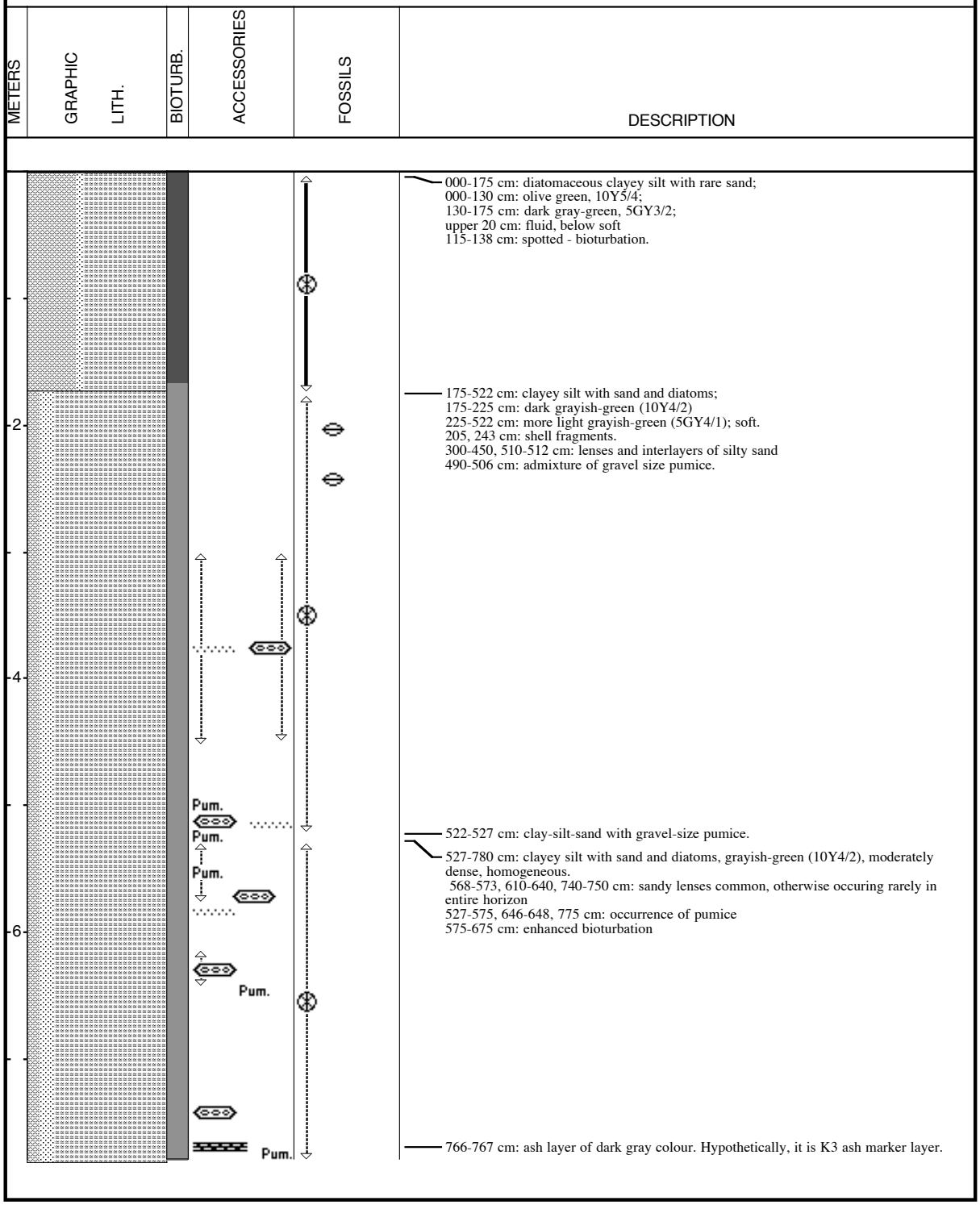

LV29-131-2

45°32.506'N, 144°18.002'E

Date: July 30, 2002

Described by: Gorbarenko, S.A.; Astakhov, A.S. water depth: 761 m

METERS	GRAPHIC LITH.	BIOTURB.	ACCESSORIES	FOSSILS	DESCRIPTION
	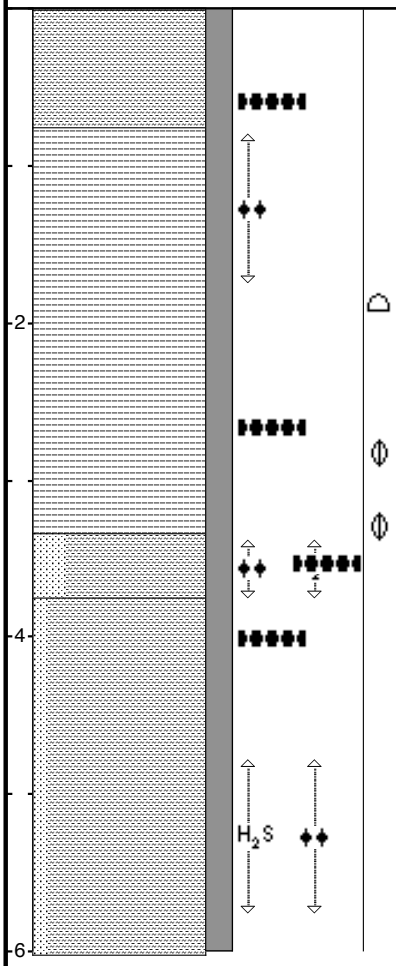				000-005 cm: silty clay, green, soft, fluid. 005-077 cm: silty clay, gray-green (10Y 4/2), soft. 060 cm: rare small pebble. 77-335 cm: clay, greenish-gray (10Y 4/2), soft, below 276 cm: slightly consolidated, homogeneous. 077-177 cm: rare laminas of hydrotroilite 188 cm: fragment of siliceous sponge 265 cm: rare pebble 285, 330 cm: coarse rare benthos foraminifers 335-376 cm: silty clay with sand, greenish-gray (10Y4/2), consolidated below 310 cm: bioturbated 345-350, 360-365 cm: rare gravel Small rare laminas of hydrotroilite and slight H2S odor are characteristic for entire interval. 376-721 cm: silty clay with rare sand, greenish-gray (5G5/2), consolidated, homogeneous, moderately bioturbated. 476-576 cm: small rare laminas of hydrotroilite and slight H2S odor 390, 402, 406, 630 cm: rare pebble 700, 704 cm: rare pumice 714-715 cm: sandy silt, grey, elongated lens (turbidites or ash interlayer?)

LV29-131-2

45°32.506'N, 144°18.002'E

Date: July 30, 2002

Described by: Gorbarenko, S.A.; Astakhov, A.S. water depth: 761 m

METERS	GRAPHIC LITH.	BIOTURB.	ACCESSORIES	FOSSILS	DESCRIPTION
8	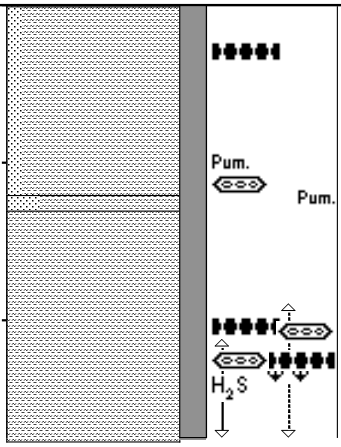				721-730 cm: silty clay enriched in dispersal pumice of coarse sand/gravel grain size. 730-876 cm: silty clay, greenish-gray (5GY 5/2), consolidated, homogeneous. 807, 823, 824 cm: lenses of gray sandy silt 806, 823 cm: rare gravel and pebble below 785 cm: gas-saturaterd sediment, increasing downcore. H2S odor.

APPENDIX 7

Foraminifera data

Foraminiferal percentages data for surface sediment samples

Planktic foraminifera	LV29-69-1 (0-1)		LV29-78-1 (0-1)		LV29-84-1 (0-0.5)		LV29-108-3 (0-1)		LV29-110-1 (0-1)		LV29-110-1 (1-2)		LV29-110-1 (2-3)		LV29-110-1 (3-4)		LV29-110-1 (4-5)		LV29-110-1 (5-6)		LV29-110-1 (7-8)	
N.pachyderma sin.	92.2		87.6		91.4		84.1		87.2		82.5		85.4		78.5		82.0		77.5		87.1	
N.pachyderma dex.	3.1				1.4		0.9		1.6		2.2		2.5		2.0		1.0		1.6		0.9	
G.bulloides	4.7		12.4		7.2		15		11.2		14.8		12.1		19.5		16.8		20.9		12.1	
T.quinqueloba											0.4						0.2					
No of planktonics counted	129		153		628		113		366		223		315		251		411		373		224	
No of planktonics/ cm^3	2		2		18		7		5		13		18		28		23		21		13	
Benthic foraminifera	living	dead	living	dead	living	dead	living	dead	living	dead	living	dead	living	dead	living	dead	living	dead	living	dead	living	dead
A.weddelensis	0.0	1.1	0.0	0.0	0.0	0.0	0.0	0.2	0.0	0.0	0.0	0.0	0.0	0.0	0.0	0.0	0.0	0.0	0.0	0.0	0.0	0.0
A.gallowayi	3.8	4.3	0.0	0.5	0.0	0.0	0.0	0.0	0.0	0.8	0.0	0.2	0.0	0.0	0.0	0.0	0.0	0.1	0.0	0.0	0.0	0.0
B.pseudoplicata	0.0	0.5	0.0	0.0	0.0	1.6	0.0	0.0	0.0	0.4	0.0	0.0	0.0	0.3	0.0	0.2	0.0	0.0	0.0	0.0	0.0	0.0
B.pacifica	0.0	0.5	8.1	4.9	23.2	18.6	0.3	1.5	0.6	0.8	5.1	1.0	4.9	2.2	1.6	0.5	3.9	0.6	5.0	0.4	0.0	0.2
B.subspinescens	2.6	1.6	0.0	4.1	0.0	0.0	0.3	1.0	0.0	0.0	0.0	0.0	0.0	0.0	0.0	0.0	0.0	0.1	0.0	0.0	0.0	0.0
B.spissa	0.0	0.0	0.0	0.0	0.0	0.0	0.0	0.0	0.0	0.4	0.0	0.0	0.0	0.0	0.0	0.0	0.0	0.0	0.0	0.0	0.0	0.0
B.tenerrima	7.7	5.4	0.0	0.5	1.9	0.8	0.3	0.2	0.0	0.0	0.0	0.2	0.0	0.0	0.0	0.0	0.0	0.0	0.0	0.0	0.0	0.0
Buccella spp.1	0.0	0.0	1.4	6.8	0.6	1.2	0.3	0.7	0.0	1.2	0.0	1.2	0.0	1.4	0.0	0.7	0.0	1.3	0.0	0.9	0.0	1.1
Bulimina spp.1	0.0	0.0	0.0	0.0	0.0	0.0	0.0	0.0	0.0	0.0	0.0	0.2	0.0	0.0	0.0	0.0	0.0	0.0	0.0	0.1	0.0	0.0
C.aff.laevigata	3.8	1.6	0.0	0.0	0.0	0.0	0.0	0.0	0.0	0.2	0.0	0.0	0.0	0.0	0.0	0.0	0.0	0.0	0.0	0.0	0.0	0.0
C.reniforme	7.7	1.1	0.0	5.1	1.9	10.4	0.3	0.0	0.0	0.2	0.0	0.7	0.0	1.4	0.0	0.5	0.0	0.4	0.0	0.0	0.0	0.2
Cassidulina spp.1	0.0	1.1	0.0	0.0	0.0	0.0	0.0	0.0	0.0	0.0	0.0	0.0	0.0	0.0	0.0	0.0	0.0	0.0	0.0	0.0	0.0	0.0
C.oolina	0.0	8.1	9.5	2.7	1.3	0.4	0.0	0.0	1.9	2.7	4.1	1.7	15.8	2.8	24.4	1.9	30.4	1.7	28.6	1.6	4.5	0.5
C.fimbriata	0.0	0.0	0.0	0.0	0.0	0.6	0.0	0.7	0.6	4.1	2.8	5.7	3.8	5.8	10.2	6.4	2.2	8.1	3.6	7.0	16.4	5.4
C.lobatulus	0.0	0.0	4.1	2.2	1.3	1.2	0.0	0.0	0.0	0.2	0.5	0.2	0.0	0.0	0.0	0.5	0.0	0.1	0.0	0.2	0.0	0.0
C.pseudoungerianus	0.0	0.0	6.8	0.5	1.9	1.0	0.3	0.0	0.6	0.6	0.5	0.2	0.0	0.0	0.8	0.5	0.0	0.0	0.7	0.4	0.0	0.3
Cibicides cf. spp.1	0.0	0.0	0.0	0.0	0.0	0.0	0.0	0.0	0.0	0.2	0.0	0.0	0.5	0.3	0.0	0.0	0.0	0.4	0.0	0.1	0.0	0.0
D.flobisherensis	1.3	0.0	0.0	0.0	0.0	0.0	0.0	0.0	0.0	0.0	0.0	0.0	0.0	0.0	0.0	0.0	0.0	0.0	0.0	0.0	0.0	0.0
D.ittai	0.0	0.5	0.0	0.3	0.0	0.0	0.0	0.0	0.0	0.0	0.0	0.0	0.0	0.0	0.0	0.0	0.0	0.0	0.0	0.0	0.0	0.0
D.pauperata	0.0	0.0	0.0	0.0	0.0	0.0	0.0	0.0	0.0	0.0	0.0	0.0	0.0	0.0	0.0	0.0	0.0	0.0	0.0	0.1	0.0	0.0
E.batialis	0.0	0.5	0.0	1.4	2.6	3.4	0.0	0.2	1.3	0.6	1.4	2.2	0.0	2.8	0.0	2.6	0.0	3.8	0.7	5.6	0.0	0.2
E.clavatum	0.0	0.0	1.4	1.9	0.0	0.4	0.6	0.0	0.0	2.5	0.0	2.0	1.1	0.8	0.0	0.7	0.0	1.7	0.7	1.8	3.0	0.9
E.aff. Incertum	0.0	0.0	0.0	6.2	0.0	0.2	0.0	1.5	0.6	7.9	0.0	6.4	0.5	5.6	0.0	8.8	0.0	6.6	0.0	4.7	1.5	7.9
E.subarcticum	0.0	0.5	0.0	1.9	0.0	0.0	0.0	0.0	0.0	0.0	0.0	0.2	0.0	0.3	0.0	0.2	0.0	0.1	0.0	0.2	0.0	0.8
E.tenuis	0.0	0.0	0.0	0.0	0.0	0.0	0.0	0.0	0.0	0.0	0.0	0.2	0.0	0.3	0.0	0.0	0.0	0.0	0.0	0.0	0.0	0.0
G.nipponica	0.0	1.1	0.0	0.0	0.0	0.0	0.0	0.0	0.0	0.0	0.0	0.0	0.0	0.0	0.0	0.0	0.0	0.0	0.0	0.0	0.0	0.0
G.arctica	0.0	3.8	0.0	0.0	2.6	1.2	0.0	0.0	0.0	0.0	1.4	0.2	2.2	0.0	3.1	0.0	5.5	0.4	5.7	0.5	7.5	0.8
G.elongata	0.0	0.0	14.9	2.7	0.0	0.6	0.0	0.5	0.0	0.4	0.0	0.0	0.0	0.0	0.0	0.0	0.0	0.0	0.0	0.0	0.0	0.0
I.californica	0.0	5.4	0.0	0.0	0.0	0.0	0.0	0.0	0.0	0.0	0.0	0.0	0.0	0.0	0.0	0.0	0.0	0.0	0.0	0.0	0.0	0.0
I.helenae	0.0	0.5	0.0	0.0	0.0	0.0	0.0	0.0	0.0	0.0	0.0	0.0	0.0	0.0	0.0	0.0	0.0	0.0	0.0	0.0	0.0	0.0
I.norcrossi	35.9	23.2	0.0	8.1	1.3	0.6	1.6	3.7	0.0	2.1	0.5	0.7	0.5	2.2	0.0	4.1	0.0	2.2	0.0	2.0	0.0	0.5
L.distoma	0.0	1.1	0.0	0.8	0.0	0.0	0.3	0.5	1.3	0.0	0.0	0.0	0.5	0.8	0.0	0.2	0.0	0.3	0.0	0.5	0.0	0.2
L.gracillima	0.0	0.0	0.0	0.3	0.0	0.0	0.0	0.0	1.3	0.0	0.0	0.0	0.0	0.0	0.0	0.0	0.0	0.0	0.7	0.0	0.0	0.0
L.nebulosa	0.0	0.0	0.0	0.0	0.0	0.0	0.0	0.0	0.0	0.4	0.0	0.5	0.0	0.3	0.8	0.0	0.0	0.1	0.0	0.0	0.0	0.0
L.semilineata	0.0	0.0	0.0	0.0	0.0	0.0	0.0	0.2	0.0	0.0	0.0	0.0	0.0	0.0	0.0	0.0	0.0	0.0	0.0	0.0	0.0	0.0
L.setigera	0.0	0.0	0.0	0.0	0.0	0.0	0.0	0.0	0.0	0.2	0.0	0.2	0.0	0.0	0.0	0.0	0.0	0.0	0.0	0.0	0.0	0.0
L.laevicostata	0.0	0.0	0.0	0.0	0.0	0.0	0.0	0.0	0.0	0.0	0.0	0.0	0.0	0.3	0.0	0.2	0.0	0.1	0.0	0.0	0.0	0.0
N.labradoricum	1.3	1.1	1.4	4.9	10.3	3.4	0.0	0.0	0.0	0.0	0.5	0.0	0.0	0.0	0.0	0.0	0.0	0.0	0.0	0.0	0.0	0.0
N.scaphum	0.0	0.0	0.0	1.9	3.9	2.8	5.6	7.3	25.0	22.6	49.8	19.1	32.1	20.8	30.7	25.3	11.6	22.1	7.9	21.8	3.0	23.8
N.grateloupi	0.0	0.0	0.0	1.9	0.0	1.8	0.0	0.2	0.0	0.0	0.0	0.2	0.0	0.0	0.0	0.2	0.0	0.0	0.0	0.0	0.0	0.0
N.digitata	0.0	0.5	1.4	11.7	7.7	14.0	4.3	60.2	0.0	6.2	4.1	11.4	4.9	8.3	7.1	5.7	3.3	7.4	4.3	5.9	10.4	6.4
N.irregularis	0.0	2.2	0.0	0.0	0.0	0.0	0.0	0.0	0.0	0.0	0.0	0.0	0.0	0.0	0.0	0.0	0.0	0.0	0.0	0.0	0.0	0.0
O.borealis	0.0	0.0	0.0	0.0	0.0	0.0	0.0	0.0	0.0	0.6	0.0	0.2	0.0	0.0	0.0	0.2	0.0	0.0	0.0	0.1	0.0	0.0
O.caudigera	0.0	0.0	0.0	0.0	0.0	0.0	0.0	0.0	0.0	0.0	0.0	0.0	0.0	0.0	0.0	0.0	0.0	0.0	0.0	0.1	0.0	0.0
O.lineata	0.0	0.0	0.0	0.0	0.0	0.0	0.0	0.0	0.0	0.0	0.0	0.0	0.0	0.0	0.0	0.0	0.6	0.0	0.0	0.0	0.0	0.0
O.melo	0.0	0.0	0.0	0.0	0.0	0.0	0.0	0.0	0.0	0.2	0.0	0.0	0.0	0.0	0.0	0.0	0.0	0.0	0.0	0.1	0.0	0.2
O.striatopunctata	0.0	0.0	0.0	0.0	0.0	0.0	0.0	0.2	0.0	0.0	0.0	0.0	0.0	0.0	0.0	0.0	0.0	0.0	0.0	0.0	0.0	0.0
O.tener	0.0	0.5	0.0	0.0	0.0	0.0	0.0	0.0	0.0	0.0	0.0	0.0	0.0	0.0	0.0	0.0	0.0	0.0	0.0	0.0	0.0	0.0
P.subcarinata	3.8	1.1	2.7	0.8	0.0	0.0	0.0	0.2	0.0	0.0	0.0	0.0	0.0	0.3	0.0	0.2	0.0	0.3	0.0	0.0	0.0	0.0
P.apertura	2.6	1.6	2.7	2.7	0.6	0.8	1.2	0.5	1.3	0.2	0.5	0.5	0.0	0.3	0.8	0.7	0.0	0.9	2.1	0.5	1.5	0.0
P.williamsoni	0.0	0.0	0.0	0.0	0.0	0.0	0.0	0.0	1.3	0.0	0.0	0.0	0.0	0.0	0.8	0.0	0.6	0.0	0.0	0.0	0.0	0.0

	LV29-69-1 (0-1)		LV29-78-1 (0-1)		LV29-84-1 (0-0.05)		LV29-108-3 (0-1)		LV29-110-1 (0-1)		LV29-110-1 (1-2)		LV29-110-1 (2-3)		LV29-110-1 (3-4)		LV29-110-1 (4-5)		LV29-110-1 (5-6)		LV29-110-1 (7-8)	
Benthic foraminifera	living	dead	living	dead	living	dead	living	dead	living	dead	living	dead	living	dead	living	dead	living	dead	living	dead	living	dead
T.tricarinata	1.3	0.0	0.0	0.0	0.0	0.0	0.0	0.0	0.0	0.0	0.0	0.0	0.0	0.0	0.0	0.0	0.0	0.0	0.0	0.0	0.0	0.0
T.frigida	6.4	0.5	0.0	0.0	0.6	0.0	0.0	0.0	0.0	0.2	0.0	0.0	0.0	0.0	0.0	0.0	0.0	0.0	0.0	0.0	0.0	0.0
Triloculina spp.1	0.0	0.5	0.0	0.0	0.0	0.0	0.0	0.0	0.0	0.0	0.0	0.0	0.0	0.0	0.0	0.0	0.0	0.0	0.0	0.0	0.0	0.0
U.auberiana	0.0	0.5	0.0	0.0	0.0	0.0	0.0	0.0	0.0	0.2	0.0	0.0	0.0	0.0	0.0	0.0	0.0	0.0	0.0	0.0	0.0	0.0
U.akitaensis	5.1	14.6	25.7	16.5	31.0	10.8	68.3	14.4	43.6	32.9	7.4	30.7	8.2	26.7	11.0	28.2	14.9	30.9	15.7	32.4	23.9	34.3
Uvigerina spp.1	1.3	5.9	0.0	0.0	0.0	0.0	0.0	0.0	0.0	0.4	0.0	0.0	0.0	0.3	0.0	0.2	0.0	0.0	0.0	0.1	0.0	0.2
V.sadonica	15.4	5.9	10.8	2.4	0.0	0.0	7.8	2.7	5.8	5.0	7.8	8.2	9.2	6.1	7.9	6.2	22.7	5.6	21.4	6.6	25.4	6.5
S.loeblichi	0.0	0.0	0.0	1.6	1.3	2.4	0.6	2.7	0.0	0.0	0.0	0.5	0.0	0.0	0.0	0.2	0.0	0.0	0.0	0.0	0.0	0.0
S.complanata	0.0	0.0	4.1	0.5	4.5	21.6	0.3	0.2	12.8	4.6	13.8	3.0	15.2	8.6	0.8	4.3	3.3	4.5	2.1	6.0	3.0	4.2
R.charlotensis	0.0	0.0	0.0	0.0	0.6	0.0	3.1	0.2	0.0	0.0	0.0	0.0	0.0	0.0	0.0	0.0	0.0	0.0	0.0	0.0	0.0	0.0
indetermined	1.3	0.0	0.0	2.2	0.0	0.2	0.0	0.0	0.0	0.8	0.0	1.2	0.0	0.0	0.0	0.2	1.1	0.0	0.7	0.1	0.0	0.3
no. of benthics counted	78	185	74	369	155	499	322	410	156	483	217	404	184	360	127	419	181	693	140	853	67	661
Total agglutinate foraminifera	41	295	55	139	49	56	121	100	143	46	23	34	9	36	1	11	1	32	2	6	3	21
no. of benthics/cm	2	7	2	7	6	16	25	29	4	7	14	25	11	22	14	49	10	41	8	48	4	39

Foraminiferal census data for surface sediment samples

Planktic foraminifera	LV29-69-1 (0-1)	LV29-78-1 (0-1)	LV29-84-1 (0-0.5)	LV29-108-3 (0-1)	LV29-110-1 (0-1)	LV29-110-1 (1-2)	LV29-110-1 (2-3)	LV29-110-1 (3-4)	LV29-110-1 (4-5)	LV29-110-1 (5-6)	LV29-110-1 (7-8)
N.pachyderma sin.	119	134	574	95	319	184	269	197	337	289	195
N.pachyderma dex.	4		9	1	6	5	8	5	4	6	2
G.bulloides	6	19	45	17	41	33	38	49	69	78	27
T.quinqueloba						1			1		
no. of planktonics counted	129	153	628	113	366	223	315	251	411	373	224
no. of planktonics/ cm^3	2	2	18	7	5	13	18	28	23	21	13

Benthic foraminifera	living	dead	living	dead	living	dead	living	dead	living	dead	living	dead	living	dead	living	dead	living	dead	living	dead	living	dead
A.weddelensis		2						1														
A.gallowayi	3	8		2						4		1						1				
B.pseudoplicata		1				8				2				1		1						
B.pacifica		1	6	18	36	93	1	6	1	4	11	4	9	8	2	2	7	4	7	3		1
B.subspinescens	2	3		15			1	4										1				
B.spissa										2												
B.tenerrima	6	10		2	3	4	1	1				1										
Buccella spp.1			1	25	1	6	1	3		6		5		5		3		9		8		7
Bulimina spp.1												1								1		
C.aff.laevigata	3	3								1												
C.reniforme	6	2		19	3	52	1			1		3		5		2		3				1
Cassidulina spp.1		2																				
C.oolina		15	7	10	2	2			3	13	9	7	29	10	31	8	55	12	40	14	3	3
C.fimbriata						3		3	1	20	6	23	7	21	13	27	4	56	5	60	11	36
C.lobatulus			3	8	2	6				1	1	1				2		1		2		
C.pseudoungerianus			5	2	3	5	1		1	3	1	1			1	2			1	3		2
Cibicides cf. spp.1										1			1	1				3		1		
D.flobisherensis	1																					
D.ittai		1		1																		
D.pauperata																				1		
E.batialis		1		5	4	17		1	2	3	3	9		10		11		26	1	48		1
E.clavatum			1	7		2	2			12		8	2	3		3		12	1	15	2	6
E.aff. Incertum				23		1		6	1	38		26	1	20		37		46		40	1	52
E.subarcticum		1		7								1		1		1		1		2		5
E.tenuis												1		1								
G.nipponica		2																				
G.arctica		7			4	6					3	1	4		4		10	3	8	4	5	5
G.elongata			11	10		3		2		2												
I.californica		10																				
I.helenae		1																				
I.norcrossi	28	43		30	2	3	5	15		10	1	3	1	8		17		15		17		3
L.distoma		2		3			1	2	2				1	3		1		2		4		1
L.gracillima				1					2										1			
L.nebulosa										2		2		1	1			1				
L.semilineata								1														
L.setigera										1		1										
L.laevicostata														1		1		1				
N.labradoricum	1	2	1	18	16	17					1											
N.scaphum				7	6	14	18	30	39	109	108	77	59	75	39	106	21	153	11	186	2	157
N.grateloupi				7		9		1				1				1						
N.digitata		1	1	43	12	70	14	247		30	9	46	9	30	9	24	6	51	6	50	7	42
N.irregularis		4																				
O.borealis										3		1				1				1		
O.caudigera																				1		
O.lineata																	1					
O.melo										1										1		1
O.striatopunctata								1														
O.tener		1																				
P.subcarinata	3	2	2	3				1						1		1		2				
P.apertura	2	3	2	10	1	4	4	2	2	1	1	2		1	1	3		6	3	4	1	
P.williamsoni									2						1		1					

	LV29-69-1 (0-1)		LV29-78-1 (0-1)		LV29-84-1 (0-0.5)		LV29-108-3 (0-1)		LV29-110-1 (0-1)		LV29-110-1 (1-2)		LV29-110-1 (2-3)		LV29-110-1 (3-4)		LV29-110-1 (4-5)		LV29-110-1 (5-6)		LV29-110-1 (7-8)	
Benthic foraminifera	living	dead	living	dead	living	dead	living	dead	living	dead	living	dead	living	dead	living	dead	living	dead	living	dead	living	dead
Quinqueloculina spp.1		4	4	9	1		14		3													35
T.angulosa		1										2	1	4						2		2
T.tricarinata	1																					
T.frigida	5	1			1					1												
Triloculina spp.1		1																				
U.auberiana		1								1												
U.akitaensis	4	27	19	61	48	54	220	59	68	159	16	124	15	96	14	118	27	214	22	276	16	227
Uvigerina spp.1	1	11								2				1		1				1		1
V.sadonica	12	11	8	9			25	11	9	24	17	33	17	22	10	26	41	39	30	56	17	43
S.loeblichi				6	2	12	2	11				2				1						
S.complanata			3	2	7	108	1	1	20	22	30	12	28	31	1	18	6	31	3	51	2	28
R.charlotensis					1		10	1														
indetermined	1			8		1				4		5				1	2		1	1		2
no. of benthics counted	78	185	74	369	155	499	322	410	156	483	217	404	184	360	127	419	181	693	140	853	67	661
Total agglutinated foraminife	41	295	55	139	49	56	121	100	143	46	23	34	9	36	1	11	1	32	2	6	3	21
no. of benthics/cm	1.7	6.8	1.8	7.2	5.8	16	25	29	4.2	7.5	14	25	11	22	14	49	10	41	8	48	4	39

List of benthic foraminifera found in surface sediments

Alabaminella weddelensis (Earland)	Ohkushi, et al., 2000, p.141, pl.3 , fig. 3.	*Lagena gracillima* (Seguenza)	Loeblich, Tappan, 1953, p. 60, pl. 11, figs. 1-4.
Astrononion gallowayi Loeblich & Tappan	Loeblich, Tappan, 1953, p. 90, pl. 17, figs. 4-7.	*Lagena nebulosa* Cushman	Ohkushi, et al., 2000, p.138, pl. 1 , figs. 10a-b.
Bolivina pseudoplicata Heron-Allen & Earland	Heron-Allen, Earland, 1930, p.81, pl.3, figs. 36-40.	*Lagena semilineata* Wright	Loeblich, Tappan, 1953, p. 65, pl. 11, figs. 14-22.
Bolivina pacifica Cushman & Mocculloch	Cushman, Mocculoch, 1942, p.185, pl. 21, figs. 2-3.	*Lagena setigera* Millett	Loeblich, Tappan, 1953, p. 66, pl. 11, figs. 23-24.
Bolivina subspinescens Cushman	Cushman, 1922, p. 48, pl. 7, fig. 5.	*Lagena sulcata laevicostata* Cushman & Gray	Feyling-Hanssen, et all,, 1971, p. 210, pl. 16, figs. 7-9.
Bolivina spissa Cushman	Cushman, 1926, p. 45, pl. 6, fig. 8.	*Nonion labradoricum* (Dawson)	Loeblich, Tappan, 1953, p. 86, pl. 17, figs. 1-2.
Buccella tenerrima (Bandy)	Feyling-Hanssen, et all, , 1971, p. 254, pl. 8, figs. 15-17.	*Nonion scaphum (* Fichtel et Moll)	Saidova, 1961, p. 73, pl. XXII, fig. 152.
Buccella spp.1	Not specifically determined species.	*Nonion grateloupi* (d'Orbigny)	Saidova, 1961, p. 73, pl. XXII, fig. 153.
Bulimina spp.1	Not specifically determined species.	*Nonionella digitata* (Norvang)	Mead, 1985, p. 240, pl. 6, figs. 1-2.
Cassidulina aff. laevidata d'Orbigny	Mackensen, Hald, 1988, c.17, pl.1, figs.1-7.	*Nummoloculina irregularis* (d'Orbigny)	Phliger et al., 1953, p. 28, pl. 5, figs. 19-20.
Cassidulina reniforme Norvang	Norvang, 1945, p.41, fig. 6.	*Oolina borealis* Loeblich & Tappan	Feyling-Hanssen, et all,, 1971, p. 223, pl. 17, figs. 2-4.
Cassidulina spp.1	Rare not specifically determined species.	*Oolina caudigera* (Weisner)	Feyling-Hanssen, et all,, 1971, p. 224, pl. 6, fig. 3.
Chilostomella oolina Schwager	Ohkushi, et al., 2000, p.139, pl. 2 , fig. 15.	*Oolina lineata* (Williamson)	Feyling-Hanssen, et all,, 1971, p. 225, pl. 17, figs. 7.
Chilostomellina fimbriata Cushman	Cushman, 1926, p.78, pl. 4, figs. 22a-c.	*Oolina melo* (d'Orbigny)	Loeblich, Tappan, 1953, p. 71, pl. 12, figs. 8-15.
Cibicides lobatulus (Walker &Jacob)	Mead, 1985., 242, pl. 6, figs. 6a-7b.	*Oolina striatopunctata* (Parker et Jacobs)	Loeblich, Tappan, 1953, p. 74, pl. 12, figs. 2-5.
Cibicides pseudoungerianus Cushman	*Truncatulina pseudoungeriana* Cushnan, 1922, p.97, pl. 20, fig.9 .	*Oridorsalis tener* (Brady)	Truncatulina tenera Brady, 1884, pl.V, figs. 6-8;
Cibicides cf. spp.	Not specifically determined species.	*Pullenia subcarinata* (d'Orbigny)	Mead, 1985., p. 236, pl. 4, figs. 9-10.
Dentalina flobisherensis Loeblich & Tappan	Loeblich, Tappan, 1953, p. 55, pl. 10, figs. 1-9.	*Pullenia apertura* Cushman	Cushman, 1927, p. 171, pl. 6, fig.10.
Dentalina ittai Loeblich & Tappan	Loeblich, Tappan, 1953, p. 56, pl. 10, figs. 10-12.	*Pyrgo williamsoni* (Silvestri)	Wollenburg, Mackensen, 1998, p.177, pl. III, figs. 1.
Dentalina pauperata d'Orbigny	Loeblich, Tappan, 1953, p. 57, pl. 9, figs. 7-9.	*Quinqueloculina spp.1*	Not specifically determined species.
Elphidium batialis Saidova	Saidova, 1975, p.751, pl. LX, fig.7.	*Trifarina angulosa* (Williamson)	Mead, 1985., 229, pl. 1, figs. 11-13.
Elphidium clavatum Cushman	Feyling-Hanssen, et all, 1971, 273, pl. 11, figs. 10-13.	*Triloculina tricarinata* d'Orbigny	Saidova, 1961, p. 54, pl. XVI, fig. 99.
Elphidium aff. incertum (Williamson)	Saidova, 1961, p.79, pl. XXIII, fig. 163.	*Triloculina frigida* Lagoe	Lagoe, 1977, pl.III, figs. 2-3.
Elphidium subarcticum Cushman	Loeblich, Tappan, 1953, p. 105, pl. 19, figs. 5-7.	*Triloculina sp.*	Not specifically determined species.
Evolvocassidulina tenuis (Phleger & Parker)	Phleger, Parker, 1951, p.27, pl. 14, figs. 14-17.	*Uvegerina auberiana* d'Orbigny	d'Orbigny, 1839, p. 106, pl. 2, figs. 23-24.
Glandulina nipponica Asano	Asano, 1951, c.14, figs. 71-72.	*Uvigerina akitaensis* Asano	Scott et all., 2000, figure 14, 261.
Globobulimina auriculata arctica Hoglund	Loeblich, Tappan, 1953, p. 110, pl. 20, figs. 8-9.	*Uvegerina spp.1*	Not specifically determined species.
Globobulimina auriculata elongata (Cushman)	Fursenko, et al., 1979, p.187, pl. 46, figs. 8-9.	*Valvulineria sadonica* Asano	Scott et all., 2000, figure 14, 271-273.
Islandiella californica (Cushman & Huges)	Cushman, Huges, 1925, p. 12, pl.2, fig. 1.	*Stainforthia loeblichi* (Feyling-Hanssen)	Feyling-Hanssen, et all, 1971, 1971, p. 238, pl. 7, figs. 1-5.
Islandiella helenae Feyling-Hanssen & Buzas	Feyling-Hanssen and Buzas, 1976, c.155, figs. 1-4.	*Stainforthia complanata* (Egger)	Ohkushi, et al., 2000, p.138, pl. 2 , fig. 10.
Islandiella norcrossi (Cushman)	Feyling-Hanssen, et all, 1971, p. 248, pl. 8, figs. 1-2.	*Robertinoides charlotensis* (Cushmam)	Loeblich, Tappan, 1953, p. 108, pl. 20, figs. 6-7.
Lagena distoma Parker & Jones	Parker, Jones, 1857, p. 467, pl. 11, fig. 24.		

APPENDIX 8

Seismic profiles

List of seismic profiles

Profile No	Start of profile				End of profile						
	Date	Time (UTC)	Latitude	Longitude	Date	Time (UTC)	Latitude	Longitude	Profile Duration	Distance (nm)	Distance (km)
Along SES-2000DS profiles											
1	01.07.02	19:00	45°25`70N	144°02`79E	01.07.02	21:00	45°26`73N	144°13`05E	2h 00min	7.60	14.09
2	03.07.02	15:15	48°55`37N	146°06`25E	03.07.02	21:20	48°35`39N	146°07`52E	6h 05min	20.64	38.27
3	04.07.02	20:50	51°03`05N	144°32`55E	05.07.02	05:17	51°08`31N	145°17`09E	8h 27min	30.03	55.68
4	05.07.02	08:00	51°09`60N	145°20`34E	05.07.02	14:38	51°29`44N	145°27`42E	6h 38min	23.98	44.46
8	08.07.02	09:40	54°29`55N	144°14`19E	08.07.02	19:50	54°26`49N	144°00`62E	10h 10min	34.52	64.00
9	11.07.02	17:45	54°53`00N	145°28`74E	11.07.02	22:43	55°01`55N	145°06`35E	4h 58min	19.79	36.69
10	12.07.02	18:33	54°22`46N	146°19`07E	12.07.02	21:00	54°16`13N	146°21`15E	2h 27min	8.81	16.33
11	15.07.02	19:00	51°59`99N	154°44`93E	16.07.02	01:23	52°00`01N	154°00`20E	6h 23min	28.59	53.00
12	16.07.02	07:50	52°00`04N	153°56`43E	16.07.02	14:29	52°00`01N	153°02`12E	6h 39min	34.47	63.91
13	17.07.02	21:23	50°33`08N	154°58`73E	18.07.02	02:47	50°20`09N	154°30`40E	5h 24min	22.95	42.55
14	18.07.02	12:50	50°19`00N	154°28`33E	18.07.02	20:51	49°56`40N	153°42`57E	8h 01min	38.00	70.45
Profiles in the Kurile Basin											
15	19.07.02	12:40	49°29`40N	153°04`88E	19.07.02	19:05	49°06`82N	152°37`46E	6h 25min	29.48	54.66
16	21.07.02	10:43	47°01`76N	150°14`03E	21.07.02	15:10	46°55`28N	150°05`51E	4h 27min	25.52	47.31
17	24.07.02	04:54	47°48`24N	148°37`13E	24.07.02	15:40	46°52`99N	147°18`69E	10h 46min	77.67	144.00
18	24.07.02	15:45	46°53`56N	147°17`93E	24.07.02	23:25	47°31`52N	148°02`27E	7h 40min	53.24	98.71

19	24.07.02	23:31	47°32`24N	148°01`53E	25.07.02	05:23	47°10`47N	147°20`28E	5h 52min	41.83	77.55
20	25.07.02	05:30	47°10`84N	147°19`33E	25.07.02	12:34	47°49`14N	148°02`76E	7h 04min	53.10	98.45
21	25.07.02	12:40	47°49`83N	148°02`58E	25.07.02	17:45	47°33`46N	147°24`96E	5h 05min	35.86	66.48
22	25.07.02	17:52	47°32`91N	147°25`51E	25.07.02	22:05	47°10`06N	147°51`87E	4h 13min	29.34	54.40
23	25.07.02	22:10	47°10`10N	147°52`56E	26.07.02	03:22	47°40`55N	147°28`90E	5h 12min	38.27	70.95
24	26.07.02	03:28	47°41`11N	147°29`41E	26.07.02	06:58	48°00`03N	147°55`61E	3h 30min	26.07	48.33
25	26.07.02	07:04	47°59`62N	147°56`41E	26.07.02	11:26	47°34`30N	148°29`76E	4h 22min	34.15	63.31
26	26.07.02	11:31	47°33`80N	148°29`44E	26.07.02	17:44	47°56`95N	147°45`03E	6h 13min	43.45	80.56
27	26.07.02	17:50	47°56`74N	147°44`44E	26.07.02	23:12	47°26`61N	148°16`59E	5h 22min	40.35	74.81
28	26.07.02	23:17	47°26`17N	148°16`16E	27.07.02	06:38	46°43`28N	147°55`83E	7h 21min	52.86	98.00
29	27.07.02	09:48	46°09`79N	147°59`79E	27.07.02	14:00	45°59`47N	148°04`86E	4h 12min	27.05	50.15
TOTAL									154h 58min	877.62	1627.10

APPENDIX 9

Participant list

List of participants

Scientists

1. Kulinich, Ruslan	chief scientist
2. Karp, Boris	co-chief scientist
3. Botsul, Anatoly	co-chief scientist
4. Obzhirov, Anatoly	scientist
5. Nikolayeva, Natalya	scientist
6. Derkachev, Alexander	scientist
7. Gorbarenko, Sergey	scientist
8. Salyuk, Anatoly	scientist
9. Karnaukh, Viktor	scientist
10. Lelikov, Yevgeny	scientist
11. Prokudin, Vladimir	scientist
12. Koptev, Andrey	scientist
13. Kraynikov, Gennady	scientific worker
14. Nepomiluyev, Gennady	scientific worker
15. Pavlova, Galina	scientist
16. Tararin, Igor	scientist
17. Sosnin, Valery	scientist
18. Baranov, Boris	scientist
19. Astakhov, Anatoly	scientist
20. Bubenshchikova, Natalya	scientist
21. Biebow, Nicole	co-chief scientist
22. Georgeleit, Katharina	foreign language assistant
23. Werner, Reinhard	scientist
24. Lembke Lester	scientist
25. Bohlmann, Harald	technician
26. Kozdon, Reinhard	student scientist
27. Fessler, Sebastian	technician
28. Pollak, Tanja	technician
29. Nöske, Carl-Ulrich	technician
30. Lüdmann, Thomas	scientist
31. Wunderlich, Jens	scientist

Ship`s crew

1.	Nikiforov, Valery	master
2.	Feshchenko, Oleg	chief mate
3.	Soleny, Konstantin	2nd mate
4.	Vashchenko, Vladimir	3rd mate
5.	Oblakov, Sergey	radio navigator
6.	Golublev, Vladimir	mate
7.	Khrapko, Yevgeny	chief engineer
8.	Khlynin, Vitaly	2nd engineer
9.	Tsimbalov, Igor	3rd engineer
10.	Vedernikov, Igor	3rd engineer
11.	Nagornov, Alexander	chief electric engineer
12.	Naydenov, Roman	2nd electric engineer
13.	Kucherov, Yevgeny	doctor
14.	Sychev, Andrey	boatswain
15.	Yurevich, Oleg	sailor
16.	Zeky, Yury	sailor
17.	Logachev, Igor	sailor
18.	Sobolev, Mikhail	sailor
19.	Yushkevich, Viktor	sailor
20.	Derkach, Vasily	sailor
21.	Kuchumov, Dmitry	motorman
22.	Alfeyev, Nikolay	motorman
23.	Barsukov, Gennady	motorman
24.	Goncharuk, Valery	motorman
25.	Timoshenko, Vasily	motorman
26.	Gubarev, Viktor	motorman
27.	Derkach, Alexander	electrician
28.	Konovalov, Alexander	cook
29.	Sheremetyeva, Yelena	cook
30.	Ovechkina, Marina	stewardess
31.	Golubkina, Lyudmila	stewardess
32.	Varfolomeyeva, Vera	stewardess
33.	Tsymbalova, Anzhelika	stewardess
34.	Timoshenko, Natalya	stewardess
35.	Kushch, Lyudmila	cook-mate